International Journal of Photoenergy

Advanced Oxidation Processes for Wastewater Treatment

Guest Editors: Meenakshisundaram Swaminathan, Manickavachagam Muruganandham, and Mika Sillanpaa

Advanced Oxidation Processes for Wastewater Treatment

International Journal of Photoenergy

Advanced Oxidation Processes for Wastewater Treatment

Guest Editors: Meenakshisundaram Swaminathan, Manickavachagam Muruganandham, and Mika Sillanpaa

Editorial Board

Contents

Contents

Hindawi Publishing Corporation
International Journal of Photoenergy
Volume 2013, Article ID 683682, 3 pages
http://dx.doi.org/10.1155/2013/683682

Editorial

Advanced Oxidation Processes for Wastewater Treatment

Meenakshisundaram Swaminathan,[1] Manickavachagam Muruganandham,[2] and Mika Sillanpaa[3]

[1] *Department of Chemistry, Annamalai University, Annamalainagar 608002, India*
[2] *Water and Environmental Technology (WET) Center, College of Engineering, Temple University, Philadelphia, PA 19122, USA*
[3] *Laboratory of Green Chemistry, Faculty of Technology, Lappeenranta University of Technology, 50130 Mikkeli, Finland*

Correspondence should be addressed to Meenakshisundaram Swaminathan; chemres50@gmail.com

Received 11 December 2012; Accepted 11 December 2012

Clean and nonpolluted water is one of the basic requirements for all living organisms including human beings. But its availability is a major problem nowadays. In the future, this problem will further increase due to global industrialization and population growth. Natural waters are being contaminated by the discharge of industrial, domestic, and agricultural wastes. Hence, at present it is very important to remove the pollutants and pathogens from wastewater to fulfill the needs for irrigation and industrial and domestic use. In the past years, conventional biological and physical treatment methods (adsorption, ultrafiltration, coagulation, etc.) have been used to remove the organic pollutants. These methods are not efficient and cost effective for wastewaters containing high concentration of more toxic pollutants. This requires some novel techniques to transfer the highly toxic pollutants chemically into benign species. Advanced oxidation processes (AOPs) are more efficient, cheap, and ecofriendly in the degradation of any kind of toxic pollutants. AOPs generate hydroxyl radical, a strong oxidant, which can completely degrade or mineralize the pollutants nonselectively into harmless products.

This special issue covered various AOPs used for the treatment of industrial wastewater, sewage, and landfill leachates. In 25 papers, authors have submitted original research articles in the following topics: (i) Fenton/photo-Fenton processes, (ii) UV/H_2O_2/ozone and sonolysis processes, (iii) Heterogeneous photocatalysis using TiO_2/ZnO and their modified forms, and (iv) Use of different photoreactors for treatment.

A review on recent development in AOPs for water and wastewater treatment provides the latest developments on heterogeneous photocatalysis, Fenton/photo-Fenton processes, and UV/H_2O_2/ozonation processes.

A brief outline of all the accepted papers is provided as the following. D. H. Tseng et al. studied the influences of oxygen and hydrogen peroxide (H_2O_2) on the degradation and mineralization of monochlorobenzene (MCB) in the UV/TiO_2 process. Their studies provided very useful information that the oxygen was a determining parameter for promoting the photocatalytic degradation.

N. R. Sanabria et al. reported development of pillared clays for wet hydrogen peroxide oxidation of phenol and its application in the posttreatment of coffee wastewater. From this study, they were able to conclude that catalytic wet hydrogen peroxide oxidation emerges as a viable alternative for posttreatment of coffee wastewater effluent.

Photo-Fenton and Fenton oxidation of recalcitrant industrial wastewater using nanoscale zero-valent iron was reported by H. Hansson et al., The highest removal of COD and TOC (80% and 60%, resp.) were achieved using photo-Fenton process.

W. S. Kuo and W. Y. Chen investigated Fresnel lens assisted by solar photocatalytic degradation of azo dye in aqueous TiO_2 suspension.

Tertiary wastewater treatment by using combined process of UV photolysis and ozonation with biological aerating filter was studied by Z. Jing and S. Cao. They concluded that the combination of UV/O_3 oxidation with biological aeration filter was quite efficient in the organic pollutants removal for tertiary wastewater treatment.

In "*Microbiological evaluation of the effectiveness of sewage sludge sanitization with solar drying technology*," authors estimated the sanitization effectiveness of the process of solar drying of sludge on technical scale in Poland, based on the inactivation kinetics of some test bacteria and parasite eggs.

C. D. Stan et al., investigated degradation of mepiquat chloride pesticide wastewaters by heterogeneous and homogeneous photocatalysis.

The oxidation degradation of Rhodamine B by using $UV/S_2O_8^{2-}$ treatment system was studied by X. Chen et al.

J. Naumczyk et al., studied the landfill leachates treatment by using the advanced oxidation processes (AOPs) such as H_2O_2/UV, O_3/H_2O_2, modified Fenton, and modified photo-Fenton methods. They concluded that modified photo-Fenton process was the most effective among the all AOPs investigated.

N. Kishimoto, E. Nakamura reported bromate formation from potassium bromide solution with or without 6.4 μM of 4-chlorobenzoic acid by using six physicochemical oxidation processes, such as UV irradiation, single addition of hydrogen peroxide, ozonation, UV irradiation with hydrogen peroxide addition (UV/H_2O_2), ozonation with hydrogen peroxide addition (O_3/H_2O_2), and ozonation with UV irradiation (O_3/UV).

M. Antonopoulou et al. studied the simultaneous photocatalytic reduction of Cr(VI) and oxidation of benzoic acid in aqueous suspensions using N-F-codoped TiO_2, and simulated solar irradiation in the present study. Chemometric optimization tools such as response surface methodology (RSM) and experimental design were used to model and optimize selected operational parameters of this simultaneous redox process.

In "*Energy effectiveness of direct UV and UV/H_2O_2 treatment of estrogenic chemicals in biologically treated sewage,*" the removal efficiency by direct UV and the UV/H_2O_2 treatment was investigated in biologically treated sewage for the parabens, industrial phenols, sunscreen chemicals, and steroid estrogens in wastewater in a thorough setup. Removal effectiveness was found to increase with H_2O_2 concentration up to 60 mg/L.

The electrochemical incineration of phenolic compounds using boron-doped diamond electrodes was studied by A. Medel et al. The results were compared to the photo-electro-Fenton process.

Z. Ding et al. have reported the preparation of a modified PTFE fibrous photo-Fenton catalyst and its optimization towards the degradation of organic dye. They found that increasing the Fe content or incorporation of Cu(II) ions could significantly improve the catalytic activity of the complexes.

The oxidation of landfill leachate by heterogeneous Fenton process using ceria-based catalysts was reported by E. Aneggi et al., They concluded from their studies that the heterogeneous Fenton technique could be effectively used for the treatment of landfill leachate.

S. Palmas et al. investigated the adsorption of glycerol at TiO_2, as well as its oxidative process during the contemporary water photo-electro-splitting for hydrogen production.

In "*Photocatalytic degradation of aniline using TiO_2 nanoparticles in a vertical circulating photocatalytic reactor*," photocatalytic degradation of aniline in the presence of titanium dioxide and ultraviolet illumination was performed in a vertical circulating photocatalytic reactor. The Langmuir-Hinshelwood kinetic model was successfully applied. The reactor was used successfully in the treatment of a real petroleum refinery wastewater.

The photocatalytic reduction of Cr(VI) ions in aqueous solutions by using UV/TiO_2 process was investigated by C. M. Ma et al. The influence of various experimental parameters on the photocatalytic reduction was studied.

In "*Photocatalytic treatment of shower water using a pilot scale reactor*," a pilot scale study of photocatalytic degradation of impurities in real shower water was performed using titanium dioxide as the photocatalyst in a continuous slurry recirculation mode. More than half of the total organic carbon (TOC) elimination was obtained after 6 hours of treatment. Importantly, photocatalysis was successfully transposed from bench scale to pilot scale.

In "*A new photocatalytic system using steel mesh and cold cathode fluorescent light for the decolorization of azo dye Orange G*," a new photocatalytic system was prepared by coating nanosized TiO_2 particles on steel mesh support and using cold cathode fluorescent light irradiation in a closed reactor for the oxidation of azo dye C.I. Orange G (OG). Efficient color removal of the OG azo dye by the photocatalytic system with TiO_2-coated temperature at 150°C was achieved at the optimal TiO_2 dosage 60 g m^{-2}. The TiO_2-coated steel mesh could be used repeatedly over 10 times without losing the photocatalytic efficiency.

R. Liu et al. reported the preparation of TiO_2 and Ag-TiO_2 by coprecipitation method. The synthesized photocatalysts were characterized by using suitable analytical techniques. The *E. coli* inactivation by using the synthesized photocatalyst was investigated.

R. M. Mohamed and M. A. Barakat synthesized the Pt-doped ZnO/SiO_2 photocatalysts and their photocatalytic activity was tested by using phenol as a model pollutant. The synthesized photocatalysts were characterized by using advanced analytical techniques.

V. Naddeo et al. studied the degradation of diclofenac by using various advanced oxidation processes such as ozonation (O_3) and sonolysis (US) and their combined application ($US+O_3$).

C. Y. Lee et al. studied methylene blue decomposition by using novel microwave/UV/DO/TiO_2 photocatalyst hybrid system. Authors discussed the effect of TiO_2 dosage, the influence of dissolved oxygen level, and the effect of microwave irradiation on the removal of methylene blue.

Q. Zhang et al. studied how the methylene blue dye degradation was affected by the high photon flux UV irradiation and results were compared with routine low photon flux photocatalytic process. Under the optimized conditions, the UV photocatalytic reaction 99% decolorization and 95% TOC removal of 20 mg L^{-1} methylene blue could be achieved in 30 s and 120 s of UV irradiation time, respectively.

Acknowledgments

We are much grateful to the scientific colleagues, who reviewed the paper by sparing their valuable time. We are thankful to the Editorial Board for giving us an opportunity to edit this special issue and for their suggestions and guidance.

Meenakshisundaram Swaminathan
Manickavachagam Muruganandham
Mika Sillanpaa

Hindawi Publishing Corporation
International Journal of Photoenergy
Volume 2012, Article ID 328526, 9 pages
doi:10.1155/2012/328526

Research Article

Effect of Oxygen and Hydrogen Peroxide on the Photocatalytic Degradation of Monochlorobenzene in TiO_2 Aqueous Suspension

Dyi-Hwa Tseng,[1] Lain-Chuen Juang,[2] and Hsin-Hsu Huang[1]

[1] *Graduate Institute of Environmental Engineering, National Central University, Jhongli 32001, Taiwan*
[2] *Department of Environmental Engineering and Green Environment R & D Center, Vanung University, Jhongli 32061, Taiwan*

Correspondence should be addressed to Lain-Chuen Juang, lcjuang@vnu.edu.tw

Received 1 June 2012; Accepted 21 August 2012

Academic Editor: Meenakshisundaram Swaminathan

The influences of oxygen and hydrogen peroxide (H_2O_2) on the degradation and mineralization of monochlorobenzene (MCB) during UV/TiO_2 process were investigated. Experimental results indicated that oxygen was a determining parameter for promoting the photocatalytic degradation. The presence of oxygen reduced the illumination time needed for the complete decay of MCB from 240 to 120 min. The photocatalytic degradation of MCB in UV/TiO_2/O_2 photocatalysis followed a simplified two-step consecutive kinetics. The rate constants of degradation (k_1) and mineralization (k_2) were increased from 0.016 to 0.046 min^{-1} and from 0.001 to 0.006 min^{-1}, respectively, as the initial concentration of dissolved oxygen (DO) was increased from 1.6 to 28.3 mg L^{-1}. Owing to the fact that H_2O_2 acted as an electron and hydroxyl radicals (·OH) scavenger, the addition of H_2O_2 should in a proper dosage range to enhance the degradation and mineralization of MCB. The optimal H_2O_2 dosage for MCB degradation was 22.5 mg L^{-1}, whereas the most efficient H_2O_2 dosage for MCB mineralization was 45.0 mg L^{-1}. In order to minimize the adverse effects of higher H_2O_2 dosage, including the capture of ·OH radicals and competitive adsorption, and to improve the photocatalytic degradation of MCB, the sequential replenishment of H_2O_2 was suggested. For the stepwise addition of a total H_2O_2 dosage of 45.0 mg L^{-1}, a complete destruction of MCB was observed within 120 min of irradiation. Additionally, the mineralization efficiency was about 87.4% after 240 min of illumination time.

1. Introduction

During last several decades, the control of organic pollutants has received much attention for its considerable amount and variety. However, the conventional biological, physical, and chemical technologies are ineffective and limitative toward the destruction of toxic and recalcitrant organic pollutants. Heterogeneous photocatalysis, one of the so-called Advanced Oxidation Processes (AOPs), offers an advanced oxidation capable of pollutant abatement [1, 2]. Many researchers have concluded that the UV/TiO_2 process is a promising technology for the degradation and mineralization of organic substrates to harmless final products in air and water media [3–6].

The mechanism of the UV/TiO_2 process has been discussed extensively in the literature [7–9]. When TiO_2 is irradiated with light energy equal to or higher than its band-gap, an electron (e^-) can be excited from the valence band to the conduction band and leaving a hole (h^+) in the valence band

$$TiO_2 + UV \longrightarrow h^+ + e^- \quad (1)$$

$$h^+ + OH^-/H_2O \longrightarrow \cdot OH/\cdot OH + H^+ \quad (2)$$

$$e^- + h^+ \longrightarrow \text{heat} \quad (3)$$

If charge separation is maintained, the paired e^--h^+ may migrate to the surface of the photocatalyst. In aqueous phase, the photoinduced h^+ is apparently able to oxidize surface hydroxyl groups or surface-bond water molecules to produce highly reactive and nonselective hydroxyl radicals (·OH) (2). The ·OH radicals are considered to be the dominant oxidizing species contributing to the photocatalytic degradation of organic substrates [10–12]. Nevertheless, the e^- can

recombine with the h^+ (3), causing a decrease in the availability of the photoinduced h^+ [13, 14]. Without electron acceptors, the limitation attributed to the recombination of e^--h^+ pairs would reduce the photocatalytic efficiency and cause radiation energy loss. Therefore, suppressing the recombination of e^--h^+ pairs is an important consideration in enhancing the performance of photocatalytic degradation.

In this study, both oxygen and hydrogen peroxide (H_2O_2) were selected as electron acceptors. Monochlorobenzene (MCB), one of the hydrophobic and volatile organic compounds (VOCs), was chosen as a model compound. The objectives of the present work were to evaluate the effect of oxygen and H_2O_2 on the photocatalytic degradation of MCB. The change in the concentration of MCB with various oxygen concentrations and H_2O_2 dosages was examined. Additionally, the extent of mineralization was also estimated by measuring the concentration of total organic carbon (TOC) in MCB solution.

2. Materials and Methods

2.1. Materials. Anatase TiO_2 powder with a specific BET surface area of $9.3\,m^2\,g^{-1}$ and a primary particle size of 150 nm was purchased from Acros Organics and used as received. Reagent grade MCB (C_6H_5Cl, MW = 112.56, density = $1.106\,g\,mL^{-1}$, vapor pressure = 12 mm Hg at 25°C, and water solubility = $494\,mg\,L^{-1}$ at 25°C) with a purity over 99% was obtained from Merck. H_2O_2 (30%) was obtained from Fluka Chemical. Other chemicals used for analysis, including acetonitrile, acetic acid, potassium hydrogen phthalate, phosphoric acid, and sodium peroxydisulfate were of analytical grade. Pure N_2 and O_2 gases and air were used to adjust the initial dissolved oxygen (DO) concentration to the desired levels. Deionized water was employed for solution preparation.

2.2. Experimental Apparatus and Procedure. A hollow cylindrical photoreactor with a working capacity of 2.5 l and equipped with a water jacket was used in this study. Cooling water from a thermostatic bath (TUNGTEC BL-20) was circulated through the photoreactor jacket to keep the temperature at 30°C. Irradiation was performed using a 15 W blacklight lamp (F15T8 BLB, UVP) with a maximum emission at 365 nm. The UV lamp was vertically immersed in a quartz tube placed in the center of the photoreactor. The light intensity inside the photoreactor, as measured by potassium ferrioxalate actinometry, was $5.68\,\mu$ Einstein s^{-1}. The reaction mixture was continuously agitated by a magnetic stirrer to keep the TiO_2 particles suspended.

Two series of experiments were carried out to examine the effects of oxygen and H_2O_2 on the photocatalytic degradation of MCB. Prior to MCB solution preparation, all deionized water was first purged by N_2 gas for 30 min to minimize the amount of DO. Subsequently, the deionized water was purged with either air or O_2 gas to obtain the predetermined DO concentration. The initial concentration of MCB was fixed at 0.1 mM and the TiO_2 dosage was $1.0\,g\,L^{-1}$ unless otherwise stated. The initial pH of solution was adjusted to 7 by adding an appropriate volume of dilute NaOH or HNO_3 solutions. After 30 min of premixing in the dark, the UV lamp was switched on to initiate the photocatalytic degradation.

The experimental procedure for the H_2O_2-assisted batch was similar to the oxygen-assisted batch. In this case, the MCB solution was prepared using deionized water that had been deoxygenated by N_2 gas. After TiO_2 powder was added into the solution, the solution pH was adjusted to 7 with dilute NaOH or HNO_3 solutions. Prior to irradiation, the suspension was magnetically stirred in the dark for 30 min. After the addition of H_2O_2 into the suspension, the UV lamp was turned on.

At given irradiation time intervals, samples were withdrawn from the irradiated suspension. These collected samples were immediately centrifuged and filtered through a $0.22\,\mu$m Millipore filter for further analysis.

2.3. Analytical Methods. The residual MCB measurement was carried out by HPLC (Biotronik HPLC BT 7900) equipped with a Linear UVIS 200 UV detector and an ODS2 C18 column (length 25 cm, inner diameter 4.6 mm). The mobile phase was composed of acetonitrile (70%), water (29%), and acetic acid (1%) and the flow rate was kept at 1.5 mL min^{-1}. The detection wavelength selected for detecting MCB was 265 nm. A TOC analyzer (O. I. Analytical Model 700) equipped with a nondispersive infrared detector (NDIR) was employed to monitor the concentration of TOC. The DO concentration was quantified by an oxygen membrane electrode (Oxi 320, WTW).

3. Results and Discussion

3.1. Direct Photolysis and H_2O_2-Assisted Photolysis. Two preliminary experiments were carried out to estimate the contribution of direct photolysis and H_2O_2-assisted photolysis for the removal of MCB. The variation in the MCB concentration during irradiation can be seen in Figure 1. For the direct photolysis, there was about 42.8% degradation of MCB after 240 min of illumination time. This result implied that the UV light had evident contribution on the degradation of MCB which was in agreement with the observation reported by other researcher [15]. The change in the MCB concentration fitted an exponential decay curve, suggesting the direct photolysis of MCB followed the pattern of pseudo first-order kinetics. A linear regression was obtained with natural logarithmic normalized concentration against illumination time. The degradation rate constant was calculated to be $0.002\,min^{-1}$.

In order to evaluate the degradation ability of H_2O_2-assisted photolysis, an irradiation experiment was conducted under the condition of H_2O_2 dosage equal to $22.5\,mg\,L^{-1}$. Corresponding to the obtained experimental result recorded in Figure 1, it was found that the concentration of MCB decreased gradually during the period of irradiation. The extent of MCB degradation in the H_2O_2-assisted photolysis within 240 min of irradiation was approximately 60.2% and the pseudo first-order degradation rate constant was

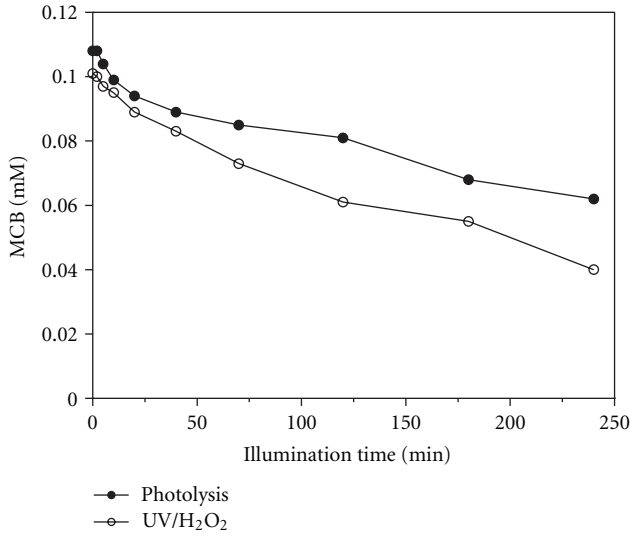

Figure 1: Direct photolysis and H_2O_2-assisted photolysis of MCB.

$0.004\,\text{min}^{-1}$. The typical time-dependent MCB concentration in the presence of both UV light and H_2O_2 was similar to that under the UV irradiation only. It was stated that H_2O_2 has an extremely low absorption at UV light of 365 nm [16], therefore, the generation of ·OH radicals due to the photolysis of H_2O_2 would be insignificant. As a result, the observable MCB decay can mainly be ascribed to the direct photolysis. Moreover, the additional MCB degradation can be explained by the oxidative ability of H_2O_2.

3.2. UV/TiO_2/O_2 Photocatalysis

3.2.1. Degradation of MCB. The dependency of the photocatalytic degradation of MCB on the initial DO concentration was studied in the range from 1.6 to 28.3 mg L^{-1}. Typical time-dependent MCB concentration during photocatalytic degradation is illustrated in Figure 2(a). As can be seen, when TiO_2 suspension was exposed to UV light, the MCB concentration decreased markedly with illumination time in comparison with the same experiment performed in the absence of TiO_2. The difference between direct photolysis and UV/TiO_2/O_2 photocatalysis revealed that UV light and TiO_2 photocatalyst together had a significant effect on the degradation of MCB. Since ·OH radicals were the key feature of UV/TiO_2 process, the degradation of MCB was primarily related to the generated ·OH radicals.

Referring to Figure 2(a), the presence of oxygen was contributed to the photocatalytic degradation. Complete destruction of MCB was observed after 240 min of irradiation when the experiment was performed under initial DO concentration equal to 1.6 mg L^{-1}. In addition, for the initial DO concentration of 28.3 mg L^{-1}, the illumination time required for complete decay of MCB was reduced to 120 min. The depletion of the DO concentration during irradiation, as recorded in Figure 2(b), confirmed that oxygen was involved in the photocatalytic degradation. Accordingly, the improvement of the degradation of MCB, which is related to the increasing initial DO concentration, can be attributed to the fact that oxygen acted as electron acceptor to trap the photoinduced e^- [17, 18]

$$O_2 + e^- \longrightarrow O_2\cdot^- \tag{4}$$

$$O_2\cdot^- + H^+ \longrightarrow HO_2\cdot \tag{5}$$

$$HO_2\cdot + HO_2\cdot \longrightarrow H_2O_2 + O_2 \tag{6}$$

$$O_2\cdot^- + HO_2\cdot + H^+ \longrightarrow H_2O_2 + O_2 \tag{7}$$

Through the reduction of oxygen with e^-, reactive superoxide radical anions ($O_2\cdot^-$) was produced (4). Simultaneously, the e^--h^+ pair recombination was restrained. Stabilizing the primary carrier led to promote the generation of ·OH radicals. Moreover, other oxidizing species such as $HO_2\cdot$ and H_2O_2 were also formed (5)–(7). It was believed that additional ·OH radicals would be generated through sequential reactions [11, 19–21]. Consequently, an increase in the DO concentration would accelerate the degradation of MCB.

3.2.2. Mineralization of MCB. The decay of TOC during photocatalytic degradation was monitored to evaluate the mineralization of MCB. From the plot shown in Figure 2(c), the improvement of the mineralization of MCB in the presence of oxygen was observed. The mineralization efficiency increased from 42.6 to 93.1% within 240 min of irradiation as initial DO concentration varied from 1.6 to 28.3 mg L^{-1}. Similar observations have been reported in the literature for other model compounds [22–24].

For the initial DO concentrations of 17.9 and 28.3 mg L^{-1}, there were still measurable DO concentrations after 240 min of illumination time. Since there was sufficient oxygen in the photocatalytic system, the TOC decreased abidingly during photocatalytic degradation. Moreover, besides the electron acceptor function, oxygen can also participate in the oxidative reaction to promote the mineralization of organic substrates and intermediates [25, 26]. Consequently, the depression of TOC decay was ascribed to the lack of oxygen involved in the photocatalytic degradation afterward in the case of lower initial DO concentration.

A comparison of Figures 2(a) and 2(c) indicated that the TOC decayed with illumination time in parallel with the MCB degradation. However, it should be noted that complete disappearance of MCB occurred within 120 to 240 min of irradiation under various initial DO concentrations, whereas residual TOC was still observed. This phenomenon implied that transient organic intermediates were likely to present in the photocatalytic system.

3.2.3. Two-Step Consecutive Kinetics. Based on the total organic carbon concentration in the photocatalytic system, the mass balance can be expressed as [27, 28]

$$[\text{TOC}]_t = [\text{MCB}]_{c,t} + [\text{Inter}\cdot]_{c,t}, \tag{8}$$

where $[\text{TOC}]_t$ is the total organic carbon concentration in the system, $[\text{MCB}]_{c,t}$ is the carbon concentration in the MCB

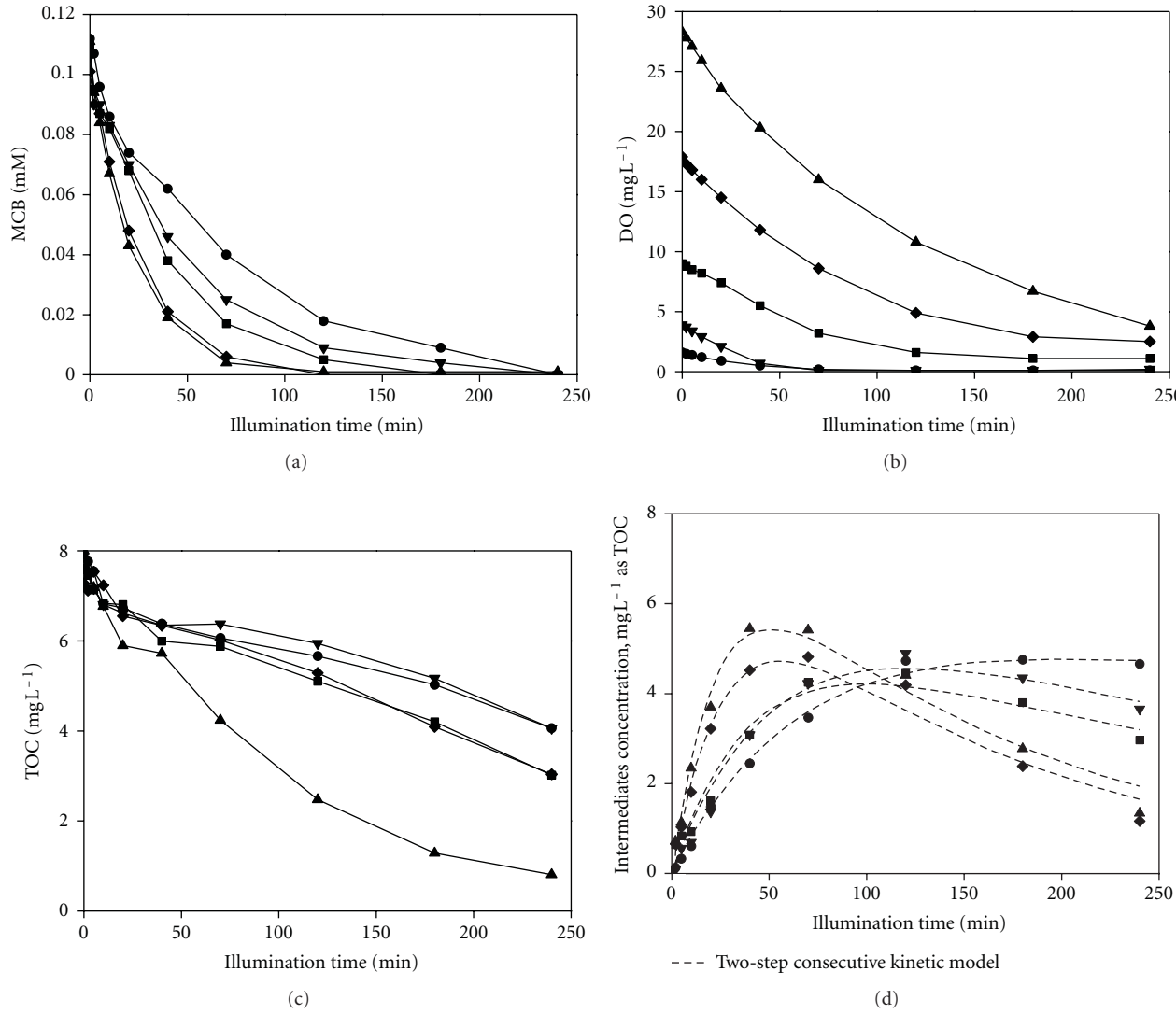

Figure 2: Concentration profiles of (a) MCB, (b) DO, (c) TOC, and (d) intermediates during photocatalytic degradation of MCB at various initial DO concentrations: (●) 1.6 mg L^{-1}, (▼) 3.9 mg L^{-1}, (■) 9.0 mg L^{-1}, (♦) 17.9 mg L^{-1}, and (▲) 28.3 mg L^{-1}.

at time t, and $[\text{Inter}\cdot]_{c,t}$ is the carbon concentration in the intermediates at time t. Correspondingly, the carbon concentration in the intermediates can be determined from the concentrations of MCB and TOC. Figure 2(d) illustrates the variation of carbon concentration in the intermediates for different initial DO concentration during the photocatalytic degradation of MCB. As can be seen, the intermediates accumulated first and decomposed thereafter.

Since the mineralization of MCB occurs through the intermediates, a simplified two-step consecutive kinetics can be used to describe the photocatalytic degradation [29, 30]

$$\text{MCB} \xrightarrow{k_1} \text{Intermediates} \xrightarrow{k_2} \text{ultimate product} \tag{9}$$

where k_1 is the degradation rate constant of MCB and k_2 is the mineralization rate constant of the intermediates. The ultimate product of the photocatalytic degradation can be CO_2, H_2O, and relevant inorganic ions. Each step in (9) is assumed to be a first-order and irreversible reaction. Applying the two-step consecutive kinetics, the carbon concentrations in the MCB and the intermediates can be expressed by

$$[\text{MCB}]_{c,t} = [\text{MCB}]_{c,o} e^{-k_1 t} \tag{10}$$

$$[\text{Inter}\cdot]_{c,t} = \frac{k_1 [\text{MCB}]_{c,o}}{k_2 - k_1} \left(e^{-k_1 t} - e^{-k_2 t}\right). \tag{11}$$

Accordingly, the two rate constants k_1 and k_2 can be derived from the disappearance of MCB and the intermediates.

As listed in Table 1, the increase in the value of k_1 was proportional to the initial DO concentration. The enhancement of k_1 was about 3 times higher when the initial DO concentration was 28.3 mg L^{-1} rather than 1.6 mg L^{-1}. Take the calculated k_1 and the determined $[\text{Inter}\cdot]_{c,t}$ into (11),

Table 1: Determination of the two-step consecutive kinetic constant for the photocatalytic degradation of MCB at different DO concentration.

DO concentration, mg L^{-1}	k_1, min^{-1}	R^2	k_2, min^{-1}	R^2
1.6	0.016	0.9915	0.001	0.9843
3.9	0.020	0.9884	0.003	0.9787
9.0	0.025	0.9940	0.003	0.9681
17.9	0.038	0.9975	0.007	0.9591
28.3	0.046	0.9977	0.006	0.9685

Table 2: Determination of the two-step consecutive kinetic constant for the photocatalytic degradation of MCB at different H_2O_2 dosage.

H_2O_2 dosage, mg L^{-1}	k_1, min^{-1}	R^2	k_2, min^{-1}	R^2
5.6	0.018	0.9966	0.002	0.9836
11.2	0.023	0.9932	0.002	0.9568
22.5	0.026	0.9956	0.002	0.8682
45.0	0.024	0.9872	0.001	0.8519
78.0	0.011	0.9972	<<0.001	0.9631

the value of mineralization rate constant k_2 was obtained. It was evident that the mineralization rate constant depended on the initial DO concentration. The value of k_2 increased with increasing initial DO concentration to a certain level and thereafter remained almost constant. The k_2 increased 8 times when the initial DO concentration was increased to 17.9 mg L^{-1} rather than 1.6 mg L^{-1}. Interestingly, the values of k_2 were lower than those of k_1, this revealed that the mineralization may be the rate-limiting step in the photocatalytic degradation of MCB. Therefore, prolonged illumination time would be reasonable for complete mineralization.

3.3. $UV/TiO_2/H_2O_2$ Photocatalysis

3.3.1. Degradation of MCB. According to its high oxidation potential and electrophilic, H_2O_2 is a stronger electron acceptor than oxygen [31–33]. A series of experiments were conducted with deoxygenated TiO_2 suspension in order to evaluate the effect of H_2O_2 dosage on the photocatalytic degradation of MCB. The examined range of H_2O_2 dosage was varied from 5.6 to 78.0 mg L^{-1}. From the typical temporal file exhibited in Figure 3(a), it can be seen that the degradation of MCB was sensitive to the variation of H_2O_2 dosage. A pseudo first-order kinetic model was provided to simulate the degradation of MCB. Table 2 summarizes the degradation rate constant k_1 derived from the gradient of the plot of the natural logarithm of the normalized MCB concentration against the illumination time. When the H_2O_2 dosage increased from 5.6 to 22.5 mg L^{-1} the value of k_1 increased from 0.018 to 0.026 min^{-1}. A further increase in the H_2O_2 dosage from 22.5 to 78.0 mg L^{-1}, however, led to a significant decline in the k_1 from 0.026 to 0.011 min^{-1}. The optimum H_2O_2 dosage for the degradation of MCB was around 22.5 mg L^{-1} which was similar to that observed by other researchers [20, 34–36].

The influence of H_2O_2 dosage on the degradation of MCB can be explained in terms of the number of generated ·OH radicals and the capture of ·OH radicals [36–39]. It is well known that H_2O_2 can trap photoinduced e^- to stabilize the paired e^--h^+

$$H_2O_2 + e^- \longrightarrow \cdot OH + OH^- \quad (12)$$

$$H_2O_2 + O_2\cdot^- \longrightarrow \cdot OH + OH^- + O_2 \quad (13)$$

$$H_2O_2 + \cdot OH \longrightarrow H_2O + OH_2^{\cdot} \quad (14)$$

$$HO_2 \cdot + \cdot OH \longrightarrow H_2O + O_2 \quad (15)$$

Additional ·OH radicals could be yielded via the reaction between H_2O_2 and e^- or $O_2\cdot^-$ (12) and (13). As a result, the addition of H_2O_2 into the photocatalytic system was expected to promote the degradation of MCB. Exceeding the optimum dosage, however, the excess H_2O_2 would trap the ·OH radicals to form weaker oxidant $HO_2\cdot$ radicals. Accordingly, the capture of ·OH radicals was occurred through (14) and (15). The decline in the ·OH radical concentration, trigged by the higher H_2O_2 dosage, restrained the degradation of MCB.

The variation of DO concentration during the $UV/TiO_2/H_2O_2$ photocatalysis for a variety of H_2O_2 dosage is illustrated in Figure 3(b). It was found that the DO concentration increased markedly with illumination time to reach a maximum value and decreased thereafter. The increase in the DO concentration was related to the decomposition of H_2O_2 [39, 40]

$$2H_2O_2 \longrightarrow H_2O + O_2. \quad (16)$$

Correspondingly, the addition of H_2O_2 seemed to act as an oxygen source. The later decrease in the DO concentration implied that the generated oxygen was involved in the mineralization.

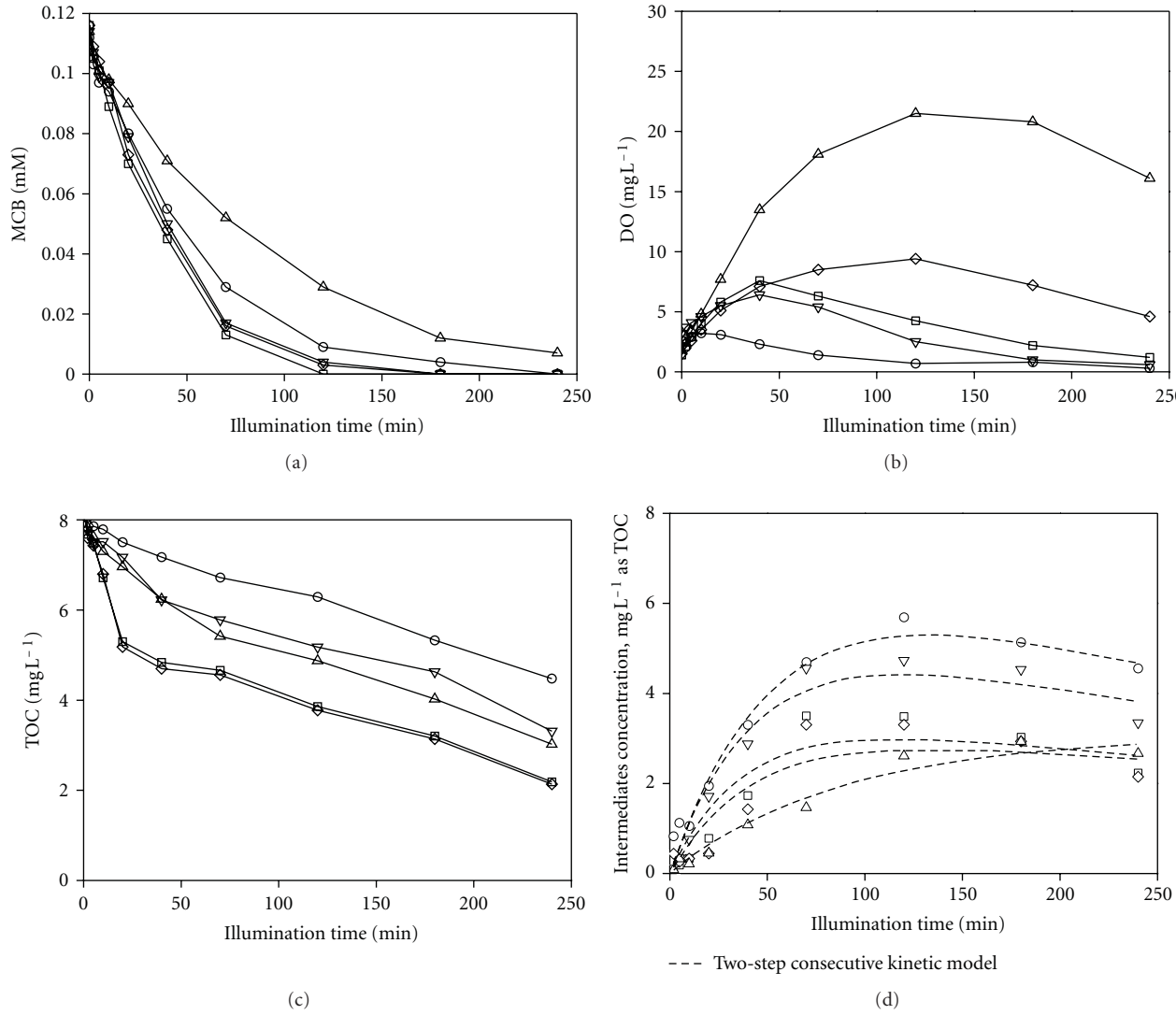

Figure 3: Concentration profiles for (a) MCB, (b) DO, (c) TOC, and (d) intermediates during photocatalytic degradation of MCB at various H_2O_2 dosages: (◯) 5.6 mg L^{-1}, (▽) 11.2 mg L^{-1}, (□) 22.5 mg L^{-1}, (◇) 45.0 mg L^{-1}, and (△) 78.0 mg L^{-1}.

3.3.2. Mineralization of MCB. Similar to the degradation of MCB, the mineralization of MCB also took place throughout the entire irradiation. Figure 3(c) shows the concentration of TOC as a function of illumination time under various H_2O_2 dosages. As can be seen, the extent of TOC decay increased from 44.4 to 74.1% with H_2O_2 dosage increased from 5.6 to 45.0 mg L^{-1} after 240 min of irradiation. At higher dosage, however, the mineralization efficiency decreased to 62.5%. Reviewing the result shown in Figure 3(a), there was still observable MCB throughout the entire irradiation period in the case of H_2O_2 dosage equal to 78.0 mg L^{-1}. This meant that the constraint on the mineralization efficiency may be ascribed to the competitive MCB.

Based on (8), the carbon concentration in the transient organic intermediates was determined as shown in Figure 3(d). Interestingly, the maximum value of intermediate concentration was decreased when the H_2O_2 dosage varied from 5.6 to 78.0 mg L^{-1}. When H_2O_2 dosage was 5.6 mg L^{-1}, the intermediates accumulated abidingly to its maximum value of 5.6 mg L^{-1} as TOC and then decreased. Similarly, the maximum values were 4.7, 3.5, 3.2, and 3.0 mg L^{-1} as TOC in the cases of H_2O_2 dosage equal to 11.2, 22.5, 45.0, and 78.0 mg L^{-1}, respectively. The decline in the maximum concentration of the intermediates revealed that some fraction of mineralization was occurred in parallel with the degradation of MCB.

Applying two-step consecutive kinetic model to the determined intermediate concentration, the mineralization rate constant k_2 was calculated as summarized in Table 2. It can be seen that the value of k_2 was decreased with increasing H_2O_2 dosage. The highest k_2 value was 0.002 min^{-1} under the experimental conditions of H_2O_2 dosage equal to 5.6, 11.2, and 22.5 mg L^{-1}. Notably, when the H_2O_2 dosage was 78.0 mg L^{-1}, the determined k_2 value was lower than

$0.001\,\text{min}^{-1}$. According to the principle of the two-step consecutive kinetics, the calculation of k_2 value was depend on the concentration of the intermediates and the value of k_1. Consequently, the decline of the maximum intermediates concentration as H_2O_2 dosage was increased led to a lower k_2 value.

3.4. Evaluation of Oxygen and H_2O_2 as Electron Acceptors. According to its characteristics as electron acceptor and oxidizing agent, the presence of oxygen in photocatalytic system was beneficial for the photocatalytic degradation of MCB. The experimental results confirmed that the photocatalytic degradation of MCB in the presence of oxygen followed a simplified two-step consecutive kinetics. For kinetic analysis, both degradation and mineralization rate constants had been demonstrated to increase with increasing DO concentration. However, this is an important consideration to bear in mind that the DO concentration in contaminated water may be limited and aeration would cause the stripping of volatile organic compound such as MCB.

It is preferential to use H_2O_2 where there is a limited availability of oxygen. Considering its hydrophilic property, the H_2O_2 would come into contact with the hydroxylated TiO_2 particles in aqueous solution and trap the photoinduced e^-. Furthermore, H_2O_2 could also serve as an oxygen source to improve the mineralization. Excess H_2O_2, however, could act as ·OH radical scavenger in the photocatalytic system. Moreover, the H_2O_2 may compete with MCB for the active sites of TiO_2 particle [32, 41–44] to suppress the photocatalytic degradation of MCB. To avoid the capture of ·OH radical and competitive adsorption under high H_2O_2 dosage, sequential replenishment of H_2O_2 into UV/TiO_2 system was suggested.

Referring to Figure 3, the most efficient degradation was observed where the H_2O_2 dosage was $22.5\,\text{mg L}^{-1}$, whereas the optimal H_2O_2 dosage for MCB mineralization was $45.0\,\text{mg L}^{-1}$. Accordingly, total dosage of H_2O_2 equal to $45.0\,\text{mg L}^{-1}$ was chosen for the evaluation of the photocatalytic degradation of MCB under various H_2O_2 addition sequences. In the experiment of stepwise addition of H_2O_2, $22.5\,\text{mg L}^{-1}$ of H_2O_2 was added into the TiO_2 suspension, once before irradiation and again after 40 min of illumination time. As the result illustrated in Figure 4(a), 120 min of irradiation was sufficient for complete elimination of MCB in the case when a two-step addition was made. On the contrary, 180 min of illumination time was needed for the one-time addition. The enhancement of the degradation efficiency was correlated to the higher degradation rate constant when the H_2O_2 dosage was $22.5\,\text{mg L}^{-1}$ rather than $45.0\,\text{mg L}^{-1}$. Moreover, the second addition of H_2O_2 was attributed to sustain the suppression of the e^--h^+ pair recombination.

Monitoring the variation of DO concentration during photocatalytic degradation, it was observed that the oxygen accumulated continuously within 120 min of illumination time then decreased thereafter for both cases (Figure 4(b)). The concentration of the intermediates showed a similar tendency as depicted in Figure 4(c). Oxygen generated as a result

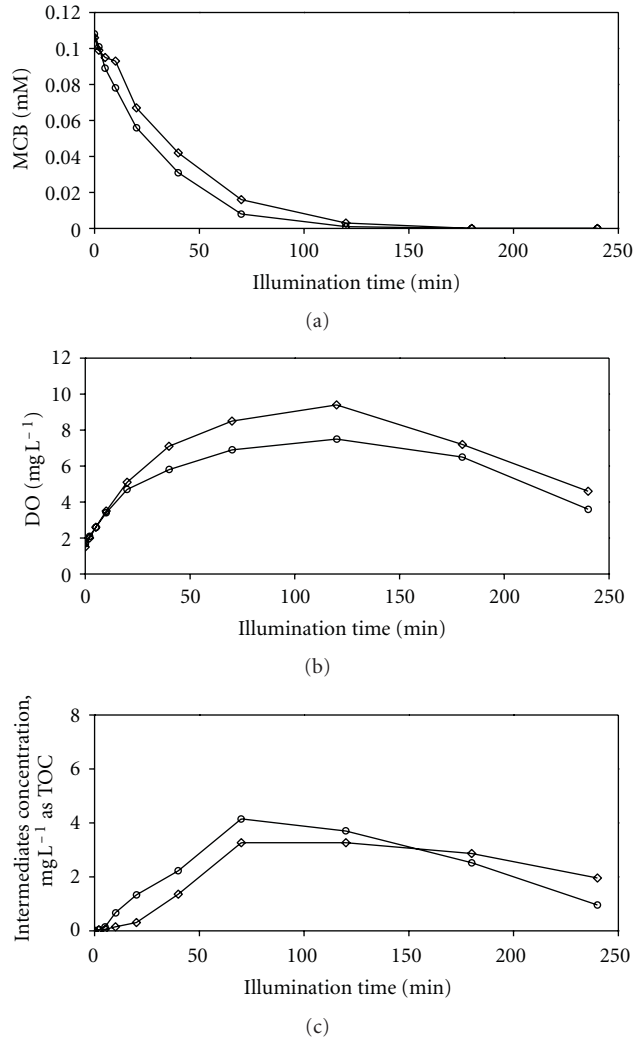

Figure 4: Comparison of the photocatalytic degradation of MCB under various H_2O_2: (◯) two-step addition and (◊) one-time addition.

of the decomposition of H_2O_2 whereas the accumulation of intermediates was due to the degradation of MCB. According to the effective degradation under the two-step addition of H_2O_2, the concentration of intermediates increased faster than that under one-time addition of H_2O_2. Furthermore, since oxygen would participate in the mineralization of MCB, both the concentrations of oxygen and intermediates declined afterward. A comparison of the experimental profiles shows that depletion of the intermediates concentration was shaper for the two-step addition of H_2O_2 than that for the one-time addition. Correspondingly, after 240 min of irradiation the mineralization efficiency of MCB in the case of two-step addition of H_2O_2 was 87.4% higher than the value of 74.1% in the case of one-time addition. The increment in the mineralization efficiency can be explained as due to the restraint of the capture of ·OH radicals, the additional ·OH radicals related with second dose of H_2O_2, and the participation of oxygen in photocatalytic degradation. Accordingly, it was evident that the sequential

replenishment of H_2O_2 into UV/TiO_2 system was advisable as a way to improve the efficiency of the photocatalytic degradation.

4. Conclusions

The direct photolysis and the oxidative potential of H_2O_2 were proven to have slight contribution on the degradation of MCB. Notably, UV light and TiO_2 together showed a marked effect. Increasing the DO concentration was beneficial for the photocatalytic degradation of MCB. Correspondingly, the degradation and mineralization rate constants increased with the DO concentration. Owing to the mineralization of MCB occurs through the intermediates, a simplified two-step consecutive kinetics can be used to describe the photocatalytic degradation in UV/TiO_2/O_2 photocatalysis. For the UV/TiO_2/H_2O_2 photocatalysis, H_2O_2 of lower dosage acted as electron acceptor to enhance the degradation efficiency. When the dosage was high, however, the degradation was suppressed due to the capture of ·OH radicals and the competitive adsorption of H_2O_2. In order to abate the disadvantages caused by using a higher H_2O_2 dosage, sequential replenishment of H_2O_2 into UV/TiO_2 system was performed. Experimental results demonstrated that both degradation and mineralization efficiencies were enhanced by the restraint of the capture of ·OH radicals, the additional ·OH radicals caused from the second stage addition of H_2O_2, and the participation of oxygen in photocatalytic degradation.

Acknowledgment

The authors would like to thank the National Science Council, R.O.C. for financial support of this study under Contract no. NSC 90-2211-E-238-003.

References

[1] U. G. Akpan and B. H. Hameed, "Parameters affecting the photocatalytic degradation of dyes using TiO_2-based photocatalysts: a review," *Journal of Hazardous Materials*, vol. 170, no. 2-3, pp. 520–529, 2009.

[2] J. M. Herrmann, "Heterogeneous photocatalysis: fundamentals and applications to the removal of various types of aqueous pollutants," *Catalysis Today*, vol. 53, no. 1, pp. 115–129, 1999.

[3] G. Balasubramanian, D. D. Dionysiou, M. T. Suidan, I. Baudin, and J. M. Laîné, "Evaluating the activities of immobilized TiO_2 powder films for the photocatalytic degradation of organic contaminants in water," *Applied Catalysis B*, vol. 47, no. 2, pp. 73–84, 2004.

[4] M. N. Chong, B. Jin, C. W. K. Chow, and C. Saint, "Recent developments in photocatalytic water treatment technology: a review," *Water Research*, vol. 44, no. 10, pp. 2997–3027, 2010.

[5] U. Stafford, K. A. Gray, and P. V. Kamat, "Photocatalytic degradation of organic contaminants: halophenols and related model compounds," *Heterogeneous Chemistry Reviews*, vol. 3, no. 2, pp. 77–104, 1996.

[6] T. Zhang, T. Oyama, S. Horikoshi, J. Zhao, N. Serpone, and H. Hidaka, "Photocatalytic decomposition of the sodium dodecylbenzene sulfonate surfactant in aqueous titania suspensions exposed to highly concentrated solar radiation and effects of additives," *Applied Catalysis B*, vol. 42, no. 1, pp. 13–24, 2003.

[7] M. R. Hoffmann, S. T. Martin, W. Choi, and D. W. Bahnemann, "Environmental applications of semiconductor photocatalysis," *Chemical Reviews*, vol. 95, no. 1, pp. 69–96, 1995.

[8] I. K. Konstantinou and T. A. Albanis, "Photocatalytic transformation of pesticides in aqueous titanium dioxide suspensions using artificial and solar light: intermediates and degradation pathways," *Applied Catalysis B*, vol. 42, no. 4, pp. 319–335, 2003.

[9] A. Sobczyński, L. Duczmal, and W. Zmudziński, "Phenol destruction by photocatalysis on TiO_2: an attempt to solve the reaction mechanism," *Journal of Molecular Catalysis A*, vol. 213, no. 2, pp. 225–230, 2004.

[10] K. Chhor, J. F. Bocquet, and C. Colbeau-Justin, "Comparative studies of phenol and salicylic acid photocatalytic degradation: influence of adsorbed oxygen," *Materials Chemistry and Physics*, vol. 86, no. 1, pp. 123–131, 2004.

[11] T. Hirakawa, K. Yawata, and Y. Nosaka, "Photocatalytic reactivity for $O_{2\cdot}^-$ and OH· radical formation in anatase and rutile TiO_2 suspension as the effect of H_2O_2 addition," *Applied Catalysis A*, vol. 325, no. 1, pp. 105–111, 2007.

[12] M. Qamar, M. Saquib, and M. Muneer, "Photocatalytic degradation of two selected dye derivatives, chromotrope 2B and amido black 10B, in aqueous suspensions of titanium dioxide," *Dyes and Pigments*, vol. 65, no. 1, pp. 1–9, 2005.

[13] D. D. Dionysiou, A. A. Burbano, M. T. Suidan, I. Baudin, and J. M. Laîné, "Effect of oxygen in a thin-film rotating disk photocatalytic reactor," *Environmental Science and Technology*, vol. 36, no. 17, pp. 3834–3843, 2002.

[14] C. H. Wu, "Comparison of azo dye degradation efficiency using UV/single semiconductor and UV/coupled semiconductor systems," *Chemosphere*, vol. 57, no. 7, pp. 601–608, 2004.

[15] D. S. Bhatkhande, S. B. Sawant, J. C. Schouten, and V. G. Pangarkar, "Photocatalytic degradation of chlorobenzene using solar and artificial UV radiation," *Journal of Chemical Technology and Biotechnology*, vol. 79, no. 4, pp. 354–360, 2004.

[16] W. Chu and C. C. Wong, "The photocatalytic degradation of dicamba in TiO_2 suspensions with the help of hydrogen peroxide by different near UV irradiations," *Water Research*, vol. 38, no. 4, pp. 1037–1043, 2004.

[17] D. Zhang, R. Qiu, L. Song, B. Eric, Y. Mo, and X. Huang, "Role of oxygen active species in the photocatalytic degradation of phenol using polymer sensitized TiO_2 under visible light irradiation," *Journal of Hazardous Materials*, vol. 163, no. 2-3, pp. 843–847, 2009.

[18] T. L. Villarreal, P. Bogdanoff, P. Salvador, and N. Alonso-Vante, "Photocatalytic oxidation on nanostructured chalcogenide modified titanium dioxide," *Solar Energy Materials and Solar Cells*, vol. 83, no. 4, pp. 347–362, 2004.

[19] O. Carp, C. L. Huisman, and A. Reller, "Photoinduced reactivity of titanium dioxide," *Progress in Solid State Chemistry*, vol. 32, no. 1-2, pp. 33–177, 2004.

[20] J. C. Garcia and K. Takashima, "Photocatalytic degradation of imazaquin in an aqueous suspension of titanium dioxide," *Journal of Photochemistry and Photobiology A*, vol. 155, no. 1–3, pp. 215–222, 2003.

[21] L. L. Lifongo, D. J. Bowden, and P. Brimblecombe, "Photodegradation of haloacetic acids in water," *Chemosphere*, vol. 55, no. 3, pp. 467–476, 2004.

[22] M. S. Dieckmann and K. A. Gray, "A comparison of the degradation of 4-nitrophenol via direct and sensitized photocatalysis in TiO_2 slurries," *Water Research*, vol. 30, no. 5, pp. 1169–1183, 1996.

[23] F. L. Palmer, B. R. Eggins, and H. M. Coleman, "The effect of operational parameters on the photocatalytic degradation of humic acid," *Journal of Photochemistry and Photobiology A*, vol. 148, no. 1–3, pp. 137–143, 2002.

[24] P. Wongkalasin, S. Chavadej, and T. Sreethawong, "Photocatalytic degradation of mixed azo dyes in aqueous wastewater using mesoporous-assembled TiO_2 nanocrystal synthesized by a modified sol-gel process," *Colloids and Surfaces A*, vol. 384, no. 1–3, pp. 519–528, 2011.

[25] Y. Wang and C. S. Hong, "TiO_2-mediated photomineralization of 2-chlorobiphenyl: the role of O_2," *Water Research*, vol. 34, no. 10, pp. 2791–2797, 2000.

[26] C. Adán, J. Carbajo, A. Bahamonde, and A. Martínez-Arias, "Phenol photodegradation with oxygen and hydrogen peroxide over TiO_2 and Fe-doped TiO_2," *Catalysis Today*, vol. 143, no. 3-4, pp. 247–252, 2009.

[27] L. Tatti, D. Niego, F. Rota et al., "Mathematical modelling of pilot-plant photomineralization of chlorophenols in aqueous solution, by photocatalytic membranes immobilizing titanium dioxide," *Chemosphere*, vol. 34, no. 1, pp. 41–49, 1997.

[28] K. H. Wang, Y. H. Hsieh, and L. J. Chen, "The heterogeneous photocatalytic degradation, intermediates and mineralization for the aqueous solution of cresols and nitrophenols," *Journal of Hazardous Materials*, vol. 59, no. 2-3, pp. 251–260, 1998.

[29] Y. Ku, R. M. Leu, and K. C. Lee, "Decomposition of 2-chlorophenol in aqueous solution by UV irradiation with the presence of titanium dioxide," *Water Research*, vol. 30, no. 11, pp. 2569–2578, 1996.

[30] F. Rota, M. Cavassi, D. Niego et al., "Mathematical modelling of photomineralization of phenols in aqueous solution, by photocatalytic membranes immobilizing titanium dioxide," *Chemosphere*, vol. 33, no. 11, pp. 2159–2173, 1996.

[31] N. Daneshvar, D. Salari, and A. R. Khataee, "Photocatalytic degradation of azo dye acid red 14 in water: investigation of the effect of operational parameters," *Journal of Photochemistry and Photobiology A*, vol. 157, no. 1, pp. 111–116, 2003.

[32] D. D. Dionysiou, M. T. Suidan, I. Baudin, and J. M. Laîné, "Effect of hydrogen peroxide on the destruction of organic contaminants-synergism and inhibition in a continuous-mode photocatalytic reactor," *Applied Catalysis B*, vol. 50, no. 4, pp. 259–269, 2004.

[33] I. Ilisz, Z. László, and A. Dombi, "Investigation of the photodecomposition of phenol in near-UV-irradiated aqueous TiO_2 suspensions—I: effect of charge-trapping species on the degradation kinetics," *Applied Catalysis A*, vol. 180, no. 1-2, pp. 25–33, 1999.

[34] I. Poulios, M. Kositzi, and A. Kouras, "Photocatalytic decomposition of triclopyr over aqueous semiconductor suspensions," *Journal of Photochemistry and Photobiology A*, vol. 115, no. 2, pp. 123–129, 1998.

[35] J. C. Yu, T. Y. Kwong, Q. Luo, and Z. Cai, "Photocatalytic oxidation of triclosan," *Chemosphere*, vol. 65, no. 3, pp. 390–399, 2006.

[36] V. K. Gupta, R. Jain, S. Agarwal, and M. Shrivastava, "Kinetics of photo-catalytic degradation of hazardous dye Tropaeoline 000 using UV/TiO_2 in a UV reactor," *Colloids and Surfaces A*, vol. 378, no. 1–3, pp. 22–26, 2011.

[37] E. R. Bandala, S. Gelover, M. T. Leal, C. Arancibia-Bulnes, A. Jimenez, and C. A. Estrada, "Solar photocatalytic degradation of Aldrin," *Catalysis Today*, vol. 76, no. 2–4, pp. 189–199, 2002.

[38] E. Bizani, K. Fytianos, I. Poulios, and V. Tsiridis, "Photocatalytic decolorization and degradation of dye solutions and wastewaters in the presence of titanium dioxide," *Journal of Hazardous Materials*, vol. 136, no. 1, pp. 85–94, 2006.

[39] J. Chen, M. Liu, J. Zhang, X. Ying, and L. Jin, "Photocatalytic degradation of organic wastes by electrochemically assisted TiO_2 photocatalytic system," *Journal of Environmental Management*, vol. 70, no. 1, pp. 43–47, 2004.

[40] T. Velegraki, I. Poulios, M. Charalabaki, N. Kalogerakis, P. Samaras, and D. Mantzavinos, "Photocatalytic and sonolytic oxidation of acid orange 7 in aqueous solution," *Applied Catalysis B*, vol. 62, no. 1-2, pp. 159–168, 2006.

[41] B. J. P. A. Cornish, L. A. Lawton, and P. K. J. Robertson, "Hydrogen peroxide enhanced photocatalytic oxidation of microcystin-lR using titanium dioxide," *Applied Catalysis B*, vol. 25, no. 1, pp. 59–67, 2000.

[42] T. Hirakawa and Y. Nosaka, "Properties of $O_2^{\cdot-}$ and $\cdot OH$ Formed in TiO_2 aqueous suspensions by photocatalytic reaction and the influence of H_2O_2 and some ions," *Langmuir*, vol. 18, no. 8, pp. 3247–3254, 2002.

[43] T. Sauer, G. Cesconeto Neto, H. J. José, and R. F. P. M. Moreira, "Kinetics of photocatalytic degradation of reactive dyes in a TiO_2 slurry reactor," *Journal of Photochemistry and Photobiology A*, vol. 149, no. 1–3, pp. 147–154, 2002.

[44] S. Lodha, A. Jain, and P. B. Punjabi, "A novel route for waste water treatment: photocatalytic degradation of rhodamine B," *Arabian Journal of Chemistry*, vol. 4, pp. 383–387, 2011.

Hindawi Publishing Corporation
International Journal of Photoenergy
Volume 2012, Article ID 864104, 17 pages
doi:10.1155/2012/864104

Review Article

Development of Pillared Clays for Wet Hydrogen Peroxide Oxidation of Phenol and Its Application in the Posttreatment of Coffee Wastewater

Nancy R. Sanabria, Rafael Molina, and Sonia Moreno

Estado Sólido y Catálisis Ambiental (ESCA), Departamento de Química, Universidad Nacional de Colombia, Carrera 30 No. 45-03, Bogotá, Colombia

Correspondence should be addressed to Sonia Moreno, smorenog@unal.edu.co

Received 29 May 2012; Accepted 26 September 2012

Academic Editor: Meenakshisundaram Swaminathan

This paper focuses on the use of pillared clays as catalysts for the Fenton-like advanced oxidation, specifically wet hydrogen peroxide catalytic oxidation (WHPCO). This paper discusses the limitations on the application of a homogeneous Fenton system, development of solid catalysts for the oxidation of phenol, advances in the synthesis of pillared clays, and their potential application as catalysts for phenol oxidation. Finally, it analyzes the use of pillared clays as heterogeneous Fenton-like catalysts for a real wastewater treatment, emphasizing the oxidation of phenolic compounds present in coffee wastewater. Typically, the wet hydrogen peroxide catalytic oxidation in a real effluent system is used as pretreatment, prior to biological treatment. In the specific case of coffee wet processing wastewater, catalytic oxidation with pillared bentonite with Al-Fe is performed to supplement the biological treatment, that is, as a posttreatment system. According to the results of catalytic activity of pillared bentonite with Al-Fe for oxidation of coffee processing wastewater (56% phenolic compounds conversion, 40% selectivity towards CO_2, and high stability of active phase), catalytic wet hydrogen peroxide oxidation emerges as a viable alternative for management of this type of effluent.

1. Introduction

1.1. Development of Heterogeneous Fenton-Like Catalysts. One of the most effective technologies to remove organic pollutants from aqueous solutions is the Fenton's reagent treatment [1]. Fenton's reagent was developed in the 1890s by Henry John Horstman Fenton and consists of a homogeneous solution of hydrogen peroxide and an iron salt [2]. The mechanism for producing free hydroxyl radicals in Fenton (Fe^{2+}/H_2O_2) and Fenton-like processes (Fe^{3+}/H_2O_2) is very complex and thought to occur in the following stages [3–7]:

$$Fe^{2+} + H_2O_2 \longrightarrow Fe^{3+} + HO^- + HO^\bullet \quad (1)$$

$$Fe^{3+} + H_2O_2 \longrightarrow Fe\text{–}OOH^{+2} + H^+ \quad (2)$$

$$Fe\text{–}OOH^{+2} \longrightarrow Fe^{2+} + HO_2^\bullet \quad (3)$$

$$Fe^{2+} + HO^\bullet \longrightarrow Fe^{3+} + HO^- \quad (4)$$

$$Fe^{3+} + H_2O_2 \longrightarrow Fe^{2+} + HO_2^\bullet + H^+ \quad (5)$$

$$HO^\bullet + H_2O_2 \longrightarrow H_2O + HO_2^\bullet \quad (6)$$

$$2Fe^{2+} + H_2O_2 + 2H^+ \longrightarrow 2Fe^{3+} + 2H_2O \quad (7)$$

$$Fe^{3+} + H_2O_2 \longrightarrow Fe^{2+} + HO_2^\bullet + H^+ \quad (8)$$

The success of Fenton processes for the oxidation of a variety of organic contaminants is attributed to the generation of hydroxyl radicals formed during the catalytic decomposition of hydrogen peroxide in acidic media, according to the above scheme [8–13]. This reaction is propagated by ferrous ion regeneration, which mainly occurs due to the reduction of the ferric species produced by hydrogen peroxide. However, in these reactions, the rate constant of (1) varies between 63 and 76 L/mol·s whereas the rate constant of (5) is in

the order of 0.01–0.02 L/mol·s [13–15]. This indicates that the consumption of ferrous ions is faster than regeneration. Therefore, during the process, the formation of a large amount of ferric hydroxide sludge occurs, which supposes additional separation [13, 16]. Both radicals $HO^{\bullet}$ and $HO_2^{\bullet}$ react indiscriminately with organic matter, being the second less reactive. In a Fenton oxidation, the hydroxyl radical reacts rapidly with most organic compounds by abstraction of carbon bound hydrogen and double bound addition, initiating a sequence of oxidative degradation reaction which may lead to mineralization of CO_2, H_2O, and the production of carboxylic acids [6, 17–19].

Catalytic oxidation reactions are almost exclusively limited to transition elements because these may exist in more than one state of oxidation, making the establishment of a repetitive oxidation-reduction cycle possible [20–22]. Therefore, these reactions also occur with transition metal ions such as Fe^{3+} or Cu^{2+} and are known as Fenton-type reactions [23] as follows

$$M^{n+} + H_2O_2 \longrightarrow M^{(n+1)+} + HO^- + HO^{\bullet}. \quad (9)$$

The application of a homogeneous Fenton system has as a disadvantage of the separation and reuse of the catalyst (Fe ions in solution). It is also necessary to control the pH solution so to avoid precipitation of iron hydroxide (pH > 5) [23]. To resolve some of the above drawbacks, a heterogeneous Fenton-like catalyst has been developed, that is, solids containing the cations of transition metals [24, 25]. This way, metals and the selected support directly affect the catalytic activity because they are determinant factors in the stability of the supported metal and its dispersion [26, 27].

A variety of solid catalysts among which are metal oxide (CuO and Cu/Al_2O_3) [28], Fe-clay [29], metal oxide impregnated activated carbon (Fe_2MO_4, M: Fe, and Mn) [30], iron molybdate $Fe_2(MoO_4)_3$ [31], CuFeZSM-5 zeolite [32], Fe exchanged/supported on zeolite [33–35], goethite [36], Fe^0/Fe_3O_4 composites [37, 38], nano magnetite [39], iron containing SBA-15 [40–42], and Al-Fe-pillared clays [43–45] have been evaluated in Fenton reactions. Some degraded organic compounds include dye (reactive blue 4 [29], methyl orange [30], acid orange II [31], rhodamine 6G [32], acid red 14 [33]), p-chlorophenol [28], 2-chlorophenol [36] and phenol [34, 40–42].

1.2. Heterogeneous Fenton-Like Catalysts for Phenol Oxidation. Phenol and its compounds are extremely toxic to the environment. These pollutants are released into the surface water bodies by oil refineries, pulp and paper, pharmaceutical and pesticide industries, and by several other chemical plants [74]. Phenol is toxic even at low concentrations, and its presence in natural waters can also lead to the formation of substituted compounds during disinfection and oxidation processes [75].

Phenol is also relevant in the field of environmental research because it has been chosen frequently as a model pollutant. Much data is available on its removal and destruction, in particular with respect to wastewater treatments [75]. The presence of phenol in the environment is acutely toxic to mankind; hence, treatment of phenolic pollutants is essential before disposal [76].

Widely studied methods for the removal of phenol include biological treatment [77], extraction [78], and wet oxidation [79]. However, advanced oxidation processes (AOPs) such as Fenton, photo-Fenton [80], ozone oxidation [81], and photo-catalytic oxidation [82] are successfully used for the removal of phenol [75]. There is an increasing interest in the use of wet hydrogen peroxide catalytic oxidation (WHPCO) for the disposal of phenolic compounds in water, because this method (in comparison, for example, with wet air oxidation) avoids the use of costly reactors, it can be selective towards the conversion of specific substrates, and it is easy to manage [69, 83].

Different solids are used in the wet hydrogen peroxide catalytic oxidation of phenol solutions, among which are pillared clays with Al-Cu [46, 58], Al-Fe [45, 46, 56], and Al-Ce-Fe [47, 51, 56] Fe-exchanged pillared beidellite [59], polymer-supported metal complexes [84], iron species supported on silica-based mesoporous molecular sieves of the MCM-41 and HMS-types [85], commercial CuO/alumina [86], Fe_2O_3/CeO_2 and WO_3/CeO_2 [87], CuO/CeO_2 [88], crystalline hematite particles embedded into a mesostructured SBA-15 matrix [89], Fe/activated carbon [90–93], Cu/ZSM-5 [94], iron-based mesoporous silica [41], CuO/SBA-15 [95], and Cu-Ni-Al hydrotalcite [96]. The effect of temperature, catalyst load, hydrogen peroxide concentration, dosage strategies on phenol mineralization, hydrogen peroxide consumption efficiencies, and catalyst stability were studied [13, 59, 86, 87].

One of the most popular catalysts for the oxidation of phenol with H_2O_2 is zeolite Fe-ZSM-5, which has been found to be very active but shows diffusion limitations due to the relatively small sized pores [97]. Transition metals containing mesoporous materials, such as MCM-41 and SBA-15, have been appropriate for the oxidation of phenols due to a larger pore size that is expected to enhance diffusion of reagents in comparison with microporous materials. However, these materials are not stable in the reaction medium and go through destruction of mesoporosity and high leaching of the active phase [75].

In the search for other iron containing heterogeneous Fenton-type catalysts that have a low leaching of the active phase at pH 3-4, where the phenol oxidation with H_2O_2 is maximal [75], a new class of catalysts with a bidimensional open structure called pillared interlayered clays (PILCs) was developed. PILCs result from the intercalation of inorganic polycations into the interlayer space of clays to form rigid cross-linked material of uniform microporosity [98]. Due to a high surface area and permanent porosity, they are very attractive solids for use in catalysis [99]. The use of pillared clays as catalytically active supports for phases (mainly Fe and Cu) has the advantage that these transition metals show low leaching into a WHPCO reaction [46, 56, 58, 60, 100].

1.3. Developments in the Synthesis of Pillared Clays. Barrer and MacLeod first introduced the concept of transforming a lamellar solid into a porous structure by inserting laterally spaced molecular props between the layers of a smectite

clay mineral [101]. A pillaring agent is any compound which can be intercalated between adjacent layers of a layered compound, maintaining the spacing between adjacent layers upon removal of the solvent, and inducing an experimentally observable pore structure between the layers [102]. When montmorillonites pillared with hydroxyl-aluminium oligomer $[Al_{13}O_4(OH)_{24}(H_2O)_{12}]^{7+}$, are heated in air at 500°C, the Keggin ions lose their water ligands forming shorter Al_{13} blocks (0.84 nm in height) that become the structure supporting pillars [103, 104]. Although the pillaring cation is the main Al_{13}, the addition of a second inorganic cation can improve the thermal, adsorptive and catalytic properties of the pillared clays [99].

The classical pillaring method involves two steps: first, the addition of the precursor polymer solution (pillaring agent) into the diluted clay mineral dispersion (intercalation). A second step is the thermal treatment of the intercalated clay mineral [99]. A wide variety of factors can influence the intercalation/pillaring process. This variation makes it difficult to compare the results obtained by different authors, and also good reproducibility becomes hard to achieve. The factors influencing this process include the nature of the raw clay used as parent material, nature of the metallic cations, the hydrolysis conditions (concentration, time, and ageing), intercalation time, temperature of synthesis and, finally, the washing, drying and calcination processes [105].

Variants of the traditional method have been researched in order to decrease the water volume and timing of the synthesis. Thus, it has become possible to decrease the volume of water by the use of concentrated suspensions, both clay and the pillaring agent [106–111]. Also, the time of intercalation of montmorillonite with chlorhydrol has been reduced through the use of ultrasound, having led to the obtaining of Al-PILC with a high thermal stability and textural properties superior to those of clay modified with an exchange time of 24 h. In overall, during the intercalation, treatment with ultrasound [51, 112, 113] and microwaves [107, 114–116] has been proved to be an adequate method for reducing the contact time between clay and the pillaring agent [57].

Although, in the past 30 years, several studies highlighting some applications of industrial pillared clays have been published, such materials have not been used as commercial catalysts primarily due to the difficulty of extending the laboratory synthesis to an industrial scale [57]. However, in 2005, a procedure for pillaring clays with aluminum, which minimizes the processing time and the amount of water used, allowing its extension to an industrial level was developed. To simplify the synthesis of Al-PILC, nonpurified clay and the pillaring agent in a solid state are used, so that clay powder and solid Al_{13} nitrate are placed together in a dialysis membrane [117].

A diversity of raw clays has been used for the preparation of these pillared materials, around 80% corresponding to bentonite-montmorillonite [118]. In pursuing the use and valorization of Colombian clay minerals, a series of systematic studies were carried out modifying, via pillaring of bentonite, clays from Valle del Cauca. One of the largest companies in Colombia exploiting and marketing bentonite is located in that Colombian region. The purpose of using such clays was to obtain catalysts (pillared bentonite) for removal of phenolic compounds in an aqueous solution by a heterogeneous Fenton system, in which the iron and/or cerium species were supported on bentonite. Table 1 summarizes results of the research conducted.

The first pillared bentonites with Al-Fe and Al-Ce-Fe were synthesized using the conventional method of diluted pillaring solution and diluted suspension of clay (2 wt%), which involves the use of large volumes of water and long synthesis times. The pillared clays were very efficient catalysts in the reaction of a phenol oxidation in diluted aqueous media under mild experimental conditions (25°C and atmospheric pressure), as well as in the elimination of different intermediary compounds of the reaction, reaching high-mineralization levels. The catalysts showed high stability in the reaction media due to the strong interaction between the iron species and the catalyst support. The incorporation of cerium showed a favorable effect in pillaring of the materials, allowing the increase of the basal spacing and enhancing the catalytic activity of the catalysts [47–50]. Carriazo et al. performed the characterization of pillaring species of Al-Ce-Fe, finding three different crystalline structures (boehmite, α-Fe_2O_3, and CeO_2) into the solid synthesized from the Al-Ce-Fe polyhydroxocationic solution. The EPR analysis confirmed the formation of iron oxide particles and the likely inclusion of isolated Fe^{3+} species into the alumina matrix [50].

To expand the pillaring process to an industrial scale, it was necessary to simplify procedures and optimization of the unit operations involved, particularly to decrease the volume of water and synthesis times. In this regard, Pérez et al. used ultrasound for aging and intercalating of pillared bentonite with Al-Ce and Al-Ce-Fe. The use of ultrasound showed a clear effect in the synthesis of this type of solids allowing the synthesis in a shorter time and preserving the physical-chemical characteristics as well as catalytic activity in the oxidation reactions [51]. Olaya et al. used microwaves and ultrasound, both in the formation of the polymeric precursor and in the stage of intercalation in concentrated suspensions of clay, finding that this type of radiation improves the formation of pillars and promotes the catalytic activity of the final solid [53–55].

With a procedure similar to that developed by Aouad et al. [117], Sanabria et al. propose a new methodology for the synthesis of clays pillared with mixed Al-Fe and Al-Ce-Fe systems, using minimal volumes of water and reducing intercalation times. This methodology involves the synthesis of the solid polymeric precursor and its use as a pillaring agent. The use of powdered clay and a solid pillaring agent, contained in a dialysis membrane, considerably reduces the amount of water used in the conventional synthesis. The intercalation of the polymeric precursor in clay is favored by the use of ultrasound, reducing long contact times required in conventional synthesis into diluted suspensions [52, 56, 57].

Table 1: Bentonite-based catalysts for oxidation of phenol using Fenton-like AOPs.

Pillared bentonite	Year	Synthesis condition	Development	Reference
B-Fe[50] B-Fe[100]	2003	Pillaring solution: dilute Suspension clay: 2 wt% Time intercalation: 48 h	This is the first work using natural bentonite from Valle del Cauca.	[46]
Al-Fe (10%) Al-Ce-Fe (10%) Al-Ce-Fe (5%) Al-Ce-Fe (1%)	2005 2007	Pillaring solution: dilute Suspension clay: 2 wt% Time intercalation: 24 h	Addition of Ce during the synthesis of the catalysts show favorable results in phenol oxidation.	[47–49]
B-AlCe(10)Fe(10)	2008	Pillaring solution: dilute Suspension clay: 2 wt% Time intercalation: 24 h	The clay pillared with the Al-Ce-Fe mixed solution is a very active and selective catalyst in the phenol oxidation.	[50]
AlCe24US AlCeUS24 AlCeFe24US AlCeFeUS24 AlCeFe2424	2008	Pillaring solution: dilute Aging: 24 h or 10 min ultrasound (50 kHz) Suspension clay: 2 wt% Time intercalation: 24 h or 10 min US	Ultrasound considerably reduces the modification time of the pillared clays. The catalysts show physical-chemical and catalytic properties similar to those when synthesizing by the conventional method.	[51]
B1-AlFe B2-AlFe B3-AlFe	2008	Pillaring agent: solid Clay: powder Intercalation: dialysis membrane Time intercalation: 60 h	Using powdered clay and a solid pillaring agent, the water volume needed in the synthesis of pillared clays was reduced.	[52]
AlCe (10%) MAl-Fe UAl-Fe AlCeFe (10%) MAl-Fe-Ce UAl-Fe-Ce	2009	Pillaring agent: solid Aging and intercalation: microwaves (160 W, 10 min) or ultrasound (50 kHz, 30 min) Clay: powder Intercalation: dialysis membrane	The use of microwaves and ultrasound significantly reduces the synthesis time of pillared clays.	[53]
MAlFe(1), MAlFe(10) UAlFe(1) UAlFe(10) MAlCeFe(1-1) MAlCeFe(5-1) MAlCeFe(10-10) UAlCeFe(1-1) UAlCeFe(5-1) UAlCeFe(10-10)	2009	Pillaring solution: dilute Aging and intercalation: microwaves (160 W, 10 min) or ultrasound (50 kHz, 30 min) Clay: powder	The use of microwaves and ultrasound significantly reduces the synthesis time of pillared clays.	[54]
B2R, BT21 B21, B22 B301, B302 BD1, BD2	2009	Pillaring solution: dilute Aging and intercalation: microwaves (160 W, 10 min) OH/metal: 2.0 Suspension clay: 2%, 3%, and 100%	The use of microwaves significantly reduces the synthesis time. Additionally, the use of a clay suspension (30%) and dry clay reduces the amount of water used in the synthesis.	[55]
B-Al US B-AlFe(2) US B-AlFe(5) US B-AlFe(10) US B-AlFe B-AlCeFe	2009	Pillaring agent: Solid Clay: powder Intercalation: dialysis membrane Time intercalation: 30 min (ultrasound, 50 kHz)	With the methodology here used, the volume of water needed and the synthesis time of pillared clays were reduced.	[56, 57]

The synthesis of pillared clays by mixed systems Al-Fe and Al-Ce-Fe in a concentrated medium allows a 90%–95% decrease in the volume of water and a reduction in the intercalation times between 70% and 93% with respect to the conventional synthesis. The pillared clays using this new methodology show a catalytic activity and selectivity comparable to those of solids synthesized by the conventional method in a dilute medium [56, 119]. An important aspect is that the Fe introduced into the clays is preferentially associated with the alumina pillars and not with surface Fe oxides (cluster). This is explained by the high stability of the active phase in the reaction medium [57].

The commercial use of PILCs based catalysts not only depends on the optimization of the synthesis, but also on the ability to shape the powder material into pellets, agglomerates, and so forth. These materials should keep their chemical properties, reactivity, and stability in the reaction medium. The manufacture of pellets, Raschig rings and monoliths, that involve pillared montmorillonites has basically been accomplished by the use of extrusion techniques [120].

With the developments in the synthesis of pillared clays in a concentrated medium, the manufacture of extruded materials with Al-Fe Al-Ce-Fe pillared bentonites was achieved. We found that the most adequate composition of the mixture of poly(hydroxo metal) bentonite/binder/water for the manufacture of extrudates with B-AlFe and B-AlCeFe was 42/28/30. The use of poly(hydroxo metal) bentonite (dried at 60°C) and not the pillared bentonite (after calcination at 400°C) considerably improved the mechanical stability of the extrudates. The mechanical resistance of B-AlFe and B-AlCeFe based extrudates depended on the calcination temperature. At 500°C, good mechanical strength and sufficient stability to immersion in water were achieved. The extrudates largely preserved the structural and textural properties of Al-Fe and Al-Ce-Fe-PILC and retained the catalytic properties of powdered pillared clays [27, 61].

1.4. Wet Hydrogen Peroxide Catalytic Oxidation (WHCPO) of Phenol Using Pillared Clay. Advanced oxidation processes (AOPs) are based on physical and chemical processes capable of fundamental changes in the chemical structure of contaminants, as they involve the generation and use of transitory species with a high oxidation power, mainly the hydroxyl radical ($OH^{\bullet}$) [6]. Among advanced oxidation processes, the activation of hydrogen peroxide by means of a solid catalyst (wet hydrogen peroxide catalytic oxidation, WHPCO) has turned out to be the most promising process for the oxidation of phenol and phenol-like compounds and application in the treatment of wastewater [23, 83, 118].

Oxidation processes using hydrogen peroxide as oxidant have turned out to be a viable alternative for the wastewater treatments of medium-high total organic carbon concentrations. Furthermore, iron is an abundant and nontoxic element; hydrogen peroxide does not give origin to any harmful by-products and it is a nontoxic and ecological reactant [6, 121].

Among the different materials used as support for oxidation reaction in a liquid phase, pillared clays represent around 7% in the existing literature. However, the interest for pillared clays has increased substantially in the last decade, given their use in different oxidation processes such as WHPCO and photocatalytic oxidation [118]. The properties of pillared clays-based catalysts have been mainly studied in the wet hydrogen peroxide oxidation of phenolic compounds as model molecules, among them are phenol [44, 45, 48, 57, 58, 62, 65, 68], 4-nitrophenol [122, 123], tyrosol [70], and p-coumaric and p-hydroxybenzoic acids [69].

Pillared clays with Al-Fe and Al-Cu are promissory catalysts for wet hydrogen peroxide oxidation of phenol, because they combine a porous support and active sites for the adsorption of organic compounds in the activation of H_2O_2 [68]. The use of pillared clays with copper in a Fenton reaction would be important since the optimal pH of that reaction is close to 6, while for AlFe-PILC, the optimum pH ranges between 3.5 and 4.0 [46, 62, 100]. The properties of AlCu-PILC were compared with those of analogous iron-based clays (AlFe-PILC) in the wet hydrogen peroxide catalytic oxidation of model phenolic compounds. These two catalysts have comparable performances in all these reactions, although they showed some differences in the rates of the various steps of the reaction. In particular, AlCu-PILC showed a lower formation of oxalic acid (main intermediate reaction) with respect to Fe-PILC [69]. Among the metals studied as active phase in oxidation processes with pillared clays-supported catalysts, iron is the most frequently used metal, followed by titanium, copper, and chromium [118]; hence, some of the most studied are the pillared clays with Al-Fe.

In general, pillared clays with Al-Fe are efficient in phenol elimination under mild experimental conditions (atmospheric pressure and room temperature) without considerable leaching of metal ions [44, 46, 56, 60]. AlFe-PILC achieved high conversions of phenol and TOC thus showing to be very selective towards the formation of CO_2, as shown in Table 2.

Cerium (Ce) was introduced into pillared clays with Al and Al-Fe, improving the metallic dispersion properties, increasing the pillars resistance [124–126], and favoring the redox properties of the active metallic phase [48, 127]. The catalysts obtained by the pillaring of Colombian bentonite with Al-Fe or Al-Ce-Fe are highly efficient for the reaction of phenol oxidation in diluted aqueous media in moderate conditions of temperature and pressure (25°C and atmospheric pressure). The low iron leaching indicate that the active phase of these catalysts is strongly fixed to the clay support and pillars, and that it is highly stable under oxidizing conditions of the reaction medium [47, 48].

Most research on the use of pillared clays for the oxidation of phenol was conducted with the powdered catalyst and a few with pellets of Al-Fe pillared clay [27, 61, 66–68]. Therefore, the development of catalysts based on pillared clays not only depends on the optimization of the synthesis, but also on the ability to shape the powder material into structured shapes (e.g., pellets, Raschig rings, and monoliths) that retain the chemical properties and reactivity of the active phase and can be used in fixed bed reactors [27].

Table 2: Some examples of pillared clays-based catalysts for wet hydrogen peroxide oxidation of phenol.

Clay catalyst	Operation conditions	Best performances reached	Reference
Fe-Al pillared clays	$T = 28^{\circ}C$ Phenol 200 mL, 13–38 mg/L Catalyst = 0.1–0.7 g, pH = 4.0, time = 1–3 h	$X_{phenol} = 100\%$ Fe leaching < 0.5 ppm	[44]
(Al-Cu)-pillared clays	$T = 20^{\circ}C$ Phenol 100 mL, 5×10^{-5} M Catalyst = 0.5 g, pH = 4.0-5.0, time = 18 h	$X_{TOC} = 20\%–60\%$	[58]
B-AlFe	$T = 25^{\circ}C$ Phenol 100 mL, 5×10^{-4} M Catalyst = 0.5 g, pH = 3.7	$X_{phenol} = 100\%$ $X_{TOC} = 48\%$ Fe leaching < 0.2 ppm	[56]
B-AlCeFe	As above	$X_{phenol} = 100\%$ $X_{TOC} = 58\%$ Fe leaching < 0.2 ppm	[56]
AlCe24US AlCeUS24	As above	$X_{phenol} = 100\%$ $X_{TOC} = 42\%$	[51]
AlCeFe24US AlCeFeUS24 AlCeFe2424	As above	$X_{phenol} = 100\%$ $X_{TOC} = 50\%$	[51]
Fe/Al-PILC	$T = 50^{\circ}C$ Phenol 100 mL, 250 mg/L Catalyst = 0.05–0.1 g, pH = 5.0–5.5, time = 3 h	$X_{phenol} = 89\%–100\%$ $X_{COD} = 65\%–89\%$ Fe leaching < 2.0 ppm	[59]
B-Fe[50] B-Fe[100]	$T = 20^{\circ}C$ Phenol 100 mL, 5×10^{-4} M Catalyst = 0.5 g, H_2O_2 excess, time = 4 h	$X_{phenol} = 96\%–100\%$ $X_{TOC} = 45\%–70\%$ Fe leaching < 0.6 ppm	[46]
B-Cu[10]	As above pH = 5.0–5.5	$X_{phenol} = 37\%–70\%$ $X_{TOC} = 96\%–100\%$ Cu leaching < 0.4 ppm	[46]
(Al-Fe)-pillared clays (FAZA)	$T = 25$, 40, and $70^{\circ}C$ Phenol 100 mL, 5×10^{-4} M Catalyst = 0.5–1.0 g, pH = 3.5–4.0, time = 0.5–4.0 h	$X_{phenol} = 100\%$ $X_{TOC} = 63\%–78\%$ Fe leaching 0.4–0.8 ppm	[60]
B-AlFe extruded	$T = 25^{\circ}C$ Phenol 250 mL, 5×10^{-4} M Catalyst = 2.08 g, pH = 3.7, time = 8-9 h	$X_{phenol} = 100\%$ $X_{TOC} = 36–50\%$ Fe leaching < 0.2 ppm	[27, 61]
B-AlCeFe extruded	As above	$X_{phenol} = 100\%$ $X_{TOC} = 42\%–55\%$ Fe leaching < 0.2 ppm	[27, 61]
FAZA (Al-Fe)	$T = 25–70^{\circ}C$ Phenol 100 mL, 5×10^{-4} M Catalyst = 0.1–1.0 g, pH = 3.5–3.7 , time = 1.0–4.0 h	$X_{phenol} = 83\%–100\%$ $X_{TOC} = 21\%–78\%$ Fe leaching 0.1–0.8 ppm	[62]
Al-Fe (10%)	$T = 25^{\circ}C$ Phenol 100 mL, 5×10^{-4} M Catalyst = 0.5 g, pH = 3.7, time = 4 h	$X_{phenol} = 100\%$ $X_{TOC} = 50\%$ Fe leaching 0.21 ppm	[47, 48]
Al-Ce-Fe (10%) Al-Ce-Fe (5%) Al-Ce-Fe (1%)	As above	$X_{phenol} = 100\%$ $X_{TOC} = 52\%–55\%$ Fe leaching 0.25–0.34 ppm	[47, 48]
FAZA-1 FAZA-2	$T = 18–70^{\circ}C$ Phenol 100 mL, 5×10^{-4} M Catalyst = 0.5–1.0 g, pH = 3.7, time = 4 h	$X_{phenol} = 100\%$ $X_{TOC} = 51\%–80\%$ Fe leaching < 0.6 ppm	[63]
Al/Fe-PILC	$T = 25^{\circ}C$ Phenol 125 mL, 2000 mg/L pH = 3.0–3.5, Time = 6 h	$X_{phenol} = 100\%$ $X_{TOC} = 65\%$ Fe leaching < 2.0 ppm	[45]

Table 2: Continued.

Clay catalyst	Operation conditions	Best performances reached	Reference
MAlFe(1) MAlFe(10) UAlFe(1) UAlFe(10)	$T = 25°C$ Phenol 100 mL, 5×10^{-4} M Catalyst = 0.5 g, pH = 3.7, time = 4 h	$X_{phenol} = 100\%$ $X_{TOC} = 54\%–60\%$	[53, 54]
MAlCeFe(1-1) MAlCeFe(5-1) MAlCeFe(10-10) UAlCeFe(1-1) UAlCeFe(5-1) UAlCeFe(10-10)	As above	$X_{phenol} = 100\%$ $X_{TOC} = 50\%–57\%$	[53, 54]
B1-AlFe B2-AlFe B3-AlFe	As Above	$X_{phenol} = 100\%$ $X_{TOC} = 49\%–52\%$ Fe leaching < 0.4 ppm	[52]
$Fe_{0.8}Al_{12.2}$-PILC $Fe_{6.5}Al_{6.5}$-PILC	$T = 30–60°C$ Phenol : H_2O_2 = 1 : 14 mol/mol (20 ml, 30 wt% in water) Catalyst = 0.25–1.5 g, time = 1–7 h	$X_{phenol} = 50\%–100\%$ Fe leaching < 0.01wt%–20 wt%	[64]
Al-Fe-PILC	$T = 25°C$ 5–50 mg phenol/L H_2O Catalyst = 0.25–1.5 g, pH = 3.5–4.0, time = 1–4 h	$X_{phenol} = 38\%–100\%$	[65]
Extrudates Al-Fe pillared clay	$T = 25–90°C$ 100–2000 mg phenol/L H_2O Catalyst = 0.0–10 g, pH = 3.8–6.0, time = 1–4 h	$X_{phenol} = 100\%$ $X_{TOC} = 35\%–55\%$ Fe leaching < 0.4 ppm	[66]
FAZA powder FAZA extrudates	$T = 20°C$ Ultrasound assisted Phenol 100 mL, 5×10^{-4} M Catalyst = 0.5 g, pH = 3.5–4.0, time = 4 h	$X_{phenol} = 100\%$	[67]
FAZA	$T = 25°C$ Phenol 100 mL, 5×10^{-4} M Catalyst = 0.5–1.0 g, pH = 3.7, time = 4 h	$X_{phenol} = 100\%$ $X_{TOC} = 65\%$ Fe leaching < 0.2 ppm	[68]

Extrudates of an Al-Fe pillared clay catalyst suitable for packed-bed operations are evaluated for oxidation of phenol using hydrogen peroxide as the oxidant. The reaction was processed in a semibatch basket reactor under rather mild conditions. Operational parameters were studied under the following conditions: temperature from 25 to 90°C, atmospheric pressure, initial phenol concentration from 100 to 2000 ppm of the liquid phase, catalyst loading from 0 to 10 g/L, and input H_2O_2 concentration from 0.15 to 0.6 mol/L. Under these conditions, the Al-Fe pillared clay catalyst achieves a total elimination of phenol and significant total organic carbon (TOC) removal. This catalyst can be used several times without any change in its catalytic properties, and, hence, it would be a promising catalyst for industrial wastewater treatment [66].

Extrudates manufactured with pillared bentonites were also employed in phenol oxidation at 25°C and atmospheric pressure. Extrudates with B-AlFe and B-AlCeFe reached 100% conversion of phenol and TOC conversion between 30% and 62%, after 9 h of reaction. Once the reaction was completed (9 h), the catalyst was removed and the leachate was recovered and analyzed, showing Fe values in the range of 0.11–0.14 ppm. The outstanding differences in time for the phenol conversion and TOC of extruded materials compared to the powdered materials were a consequence of the agglomeration process and the inherent diffusional limitations [61]. The extruded catalyst retained its catalytic activity during at least 10 consecutive tests (80 h), and only a loss of mechanical stability was observed for the series containing B-AlFe as the active phase. This result proved the importance of cerium in the synthesis of pillared clays with mixed systems because it not only increased the catalytic activity due to its oxygen storage capacity, but also increased the mechanical stability of extruded catalysts in the reaction medium [27].

2. Fenton Oxidation with Pillared Clays for Wastewater Treatment

The interest for pillared clays has dramatically increased in the last years, in great part due to their potential applications as catalysts. Metals incorporated in the pillared clay structure are crucial and make them suitable for a number of different

applications, most of them belonging to the so-called "green chemistry" [118]. This way, pillared clays have been tested as catalysts in different oxidation processes. Distribution of the pollutants studied in the literature corresponds mainly to phenol (22%), orange II and other dyes (23%), and only 5% to industrial effluents [118].

Table 3 summarizes the research related to the use of pillared clays in wet hydrogen peroxide catalytic oxidation (WHPCO) of industry wastewater. The studies have basically focused on real olive oil milling wastewater (OMW). The reason for studying an olive oil mill wastewater effluent is because it constitutes a critical environmental problem in the Mediterranean area that accounts for 95% of the world olive oil production [128] and generates 30 million m^3 of OMW every year [129].

Most treatment studies of OMW are focused on aerobic biodegradation or anaerobic digestion of that material [130]. Unfortunately, due to the effluents' high toxicity and biodegradability, no satisfactory results were obtained by these treatments. Indeed, in order to remove the organic compounds and reduce the methanogenic bacteria inhibition of the OMW, the WHPCO as pretreatment has been researched [83, 131].

Tyrosol, p-coumaric, and p-hydroxybenzoic acids have also deserved the attention of some researchers because they are representative compounds of the polyphenolic fraction typically found in olive processing wastewater [69, 70]. The polyphenolic compounds conversion in OMW using Cu-PILC and Fe-PILC is about 45% and similar for the two catalysts. Therefore, the rate of polyphenolic conversion is around two to three times higher than the rate of TOC abatement, indicating a preferential reduction of these toxic compounds with respect to TOC abatement, in agreement with the goal of toxicity reduction, to improve biodegradability and to minimize as much as possible TOC reduction, because the OMW after WHPCO should go through a biological treatment [69].

3. Environmental Problems Associated with Coffee Wet Processing in Colombia

Coffee is one of the largest agricultural-based products sold in international markets and has become the second best-marketed product worldwide, surpassed only by oil [132]. Colombian coffee has become a benchmark for the rest of the world due to the country unique weather and topography, wet processing, and programs to guarantee the coffee's origin. Colombia, the largest producer of washed Arabica coffee worldwide, counts an estimated average coffee production rate of 11 million bags per year (1 bag equals 60 kg of dried coffee beans), with coffee grown by a total of 553,000 families covering an area of 914,000 hectares [133].

The coffee fruit consists of a coloured exocarp (skin), a fleshy, yellowish-white mesocarp (pulp), mucilage layers (covering the two beans) and two coats (the first, a thin, fibrous parchment and the second, a fine membrane, silver skin) [134]. Primary coffee processing refers to the processing of the coffee fruit to obtain coffee beans (also called green coffee beans at this stage). Coffee beans are extracted using one of three different methods: dry processing, wet processing, or semidry processing [135]. Although all methods aim at removing the fruit flesh of the coffee cherry, each method removes the flesh in different ways [136]. In the wet method process, which requires the use of specific equipment and substantial amounts of water, the pulp is eliminated using a pulper, followed by the mucilage's removal by natural fermentation. When fermentation is complete, the wet processed seeds are washed and dried, and the final product is "washed" or "parchment" coffee. Coffee processed using the wet method typically increases the market value of the beans because of its ability to add a soft acidity, good body, and better flavour [135, 136].

The mucilage, a by-product of coffee wet processing, is primarily composed by pectin, sugars, water [136, 137], and minor compounds such as tannins, caffeine, and phenols [138]. It is estimated that for every 1×10^6 parchment bags, approximately 55.5×10^6 kg of fresh mucilage is generated, resulting in highly polluted nearby tributary water sources where the waste is discharged [139]. For this reason, the National Coffee Research Center—Cenicafé has developed modular anaerobic treatment systems (SMTA, the Spanish acronym) using hydrolytic acidogenic and methanogenic reactors to treat coffee processing wastewater prior to its release, reducing the chemical oxygen demand (COD) by approximately 87%. The remaining 13% of the COD in the effluent is nondegrading and corresponds to recalcitrant compounds, including phenolic compounds [140]. Treatment of coffee wastewater in a UASB (upflow anaerobic sludge blanket) reactor showed similar results: between 14% and 44% of phenolic compounds were removed during anaerobic digestion and, on average, 8% of the COD remained in the effluent and was not degraded [138]. Because the SMTA effluent still poses toxic consequences for aquatic life, the effluent must go through posttreatment before being discharged into any water source.

To determine the biological impact generated by coffee wet processing wastewater, the National Coffee Research Center of Colombia—Cenicafé conducted bioassays using *Chlorella vulgaris* (algae), *Daphnia pulex* (microcrustacean), and *Lebistes reticulatus* (fish). It was found that the effluent from coffee wastewater can be toxic to the ecosystem at concentrations above 300 ppm of COD, inflicting a 50% mortality of fish, 43% of microcrustaceans, and 40% of algae, a negative impact on the aquatic ecosystem [141].

To complement the biological treatment, an integrated biosystem that uses macrophytes for posttreatment for coffee wet processing wastewater has been proposed, in order to generate the least negative impact on the coffee aquatic ecosystem [139]. However, the biomass produced in these aquatic systems should be properly utilized in other processes such as the production of fertilizers, animal feed, and mushroom growing.

Considering that coffee wastewater is highly biodegradable, biological treatments have been widely used [142–144]. In Colombia, a posttreatment for coffee wastewater is usually not performed because the elimination of 80% of the initial

Table 3: Some examples of WPHCO of water pollutants (model molecules) or real effluents, using a Fenton reaction catalyzed by pillared clays.

Clay catalyst	Organic pollutant	Performances reached	Reference
Al/Fe-PILC	Treatment of municipal leachate from landfill by catalytic wet peroxide oxidation using an Al/Fe-pillared montmorillonite	$T = 18 \pm 2°C$ $X_{COD} = 50\%$ This advanced oxidation process has enhanced the biodegradability index of the leachate from 0.135 to 0.321 in 4 h	[43]
Cu-PILC Fe-PILC	Phenolic compounds (p-coumaric and p-hydroxybenzoic acids) and real olive oil milling wastewater (OMW)	$T = 70°C$ $X_{\text{p-coumaric acid}} = 100\%$, $X_{\text{p-hydroxybenzoic acid}} = 100\%$, X_{TOC}: 74–80% Olive oil milling wastewater $X_{\text{polyphenols}} = 46–48\%$, X_{TOC}: 18–22%	[69]
Cu/Al-PILC	Tyrosol, major compound of the polyphenolic fraction present in olive oil mill wastewaters	$T = 25–80°C$ $X_{\text{Tyrosol}} = 100\%$, $X_{TOC} \sim 80\%$ Without significant leaching of copper ions	[70]
(Al-Fe)PILC	Polyphenols in olive mill wastewater (OMW)	$T = 25–70°C$ $X_{COD} = 37–69\%$, $X_{\text{polyphenols}} = 54–100\%$ Pretreated OMW reduced considerably the COD and total phenolic contents	[71]
Cu-PILC	Real wastewaters from agro-food production (Citrus juice production and olive oil milling wastewater)	Citrus juice production wastewater $T = 80°C$, $X_{\text{polyphenols}} = 65–98\%$ $X_{TOC} = 20–52\%$ Cu leaching = 0.21–0.64 ppm Olive oil milling wastewater $T = 80°C$, $X_{\text{polyphenols}} = 18–39\%$, $X_{TOC} = 7–30\%$	[72]
Cu-AZA	Wet hydrogen peroxide catalytic oxidation of olive oil mill wastewaters using a Cu-pillared clay catalyst	$T = 80°C$ $X_{\text{polyphenols}} = 45\%$, $X_{TOC} = 13.5\%$ No copper leaching during the oxidation reactions	[73]

COD in wastewater that is required by Colombian legislation can be achieved with the SMTA developed by Cenicafé [145].

3.1. WHPCO with AlFe-PILC as a Posttreatment System for Coffee Wet Processing Wastewater. The effluent from the anaerobic biological treatment of coffee wet processing wastewater (CWPW) developed in the National Coffee Research Center-Cenicafé still contains a nonbiodegradable compound that must be treated before it is discharged into a water source. It was found that chlorogenic acid, caffeic acid and tannins are toxic compounds because they inhibit the process of methanogenesis and limit the biodegradability of water during anaerobic digestion [138]. In the research group of "Solid State and Environmental Catalysis," the CWHPO using pillared clays with Al-Fe as catalysts was tested as a possible posttreatment system for coffee wet processing wastewater.

The physical chemical characterisation of the CWPW is detailed in Table 4. In general, with the use of the SMTA developed at Cenicafé, many of the contaminants present in wastewater as a result of the coffee wet processing were eliminated. However, the effluent of SMTA still retained an organic load that generated negative ecological impacts when deposited in the water bodies of the Colombian coffee zone, making posttreatment systems necessary.

A preliminary analysis of the phenolic compounds in CWPW was performed by HPLC-ESI-MS^n (high-performance liquid chromatography/electrospray ionization multiple mass spectrometry) by using a Shimadzu Liquid Chromatograph-Ion Trap-Time of Flight Mass Spectrometer (LCMS-IT-TOF, Kyoto, Japan). To conduct the analysis, 100 mL of WPCW were filtered through Millipore filters (0.45 μm), and phenolic compounds were selectively obtained through successive extractions with 10 mL of ethyl acetate. Separation was performed in a Zorbax-SB C18 column (250 $\times$ 4.6 mm i.d., 5 μm, Phenomenex, USA). CWPW analysis (pos-biological treatment and precatalytic oxidation) using HPLC-ESI-MS^n permitted a preliminary identification of compounds in the sample to compare with the values of *m/z* (molecular ion and fragments) reported in the literature [146, 147]. The results showed that the CWPW contains mainly chlorogenic and hydroxycinnamic acids: 3-*O*-p-coumaroylquinic acid (3-pCoQA), 4-*O*-p-coumaroylquinic acid (4-pCoQA), and 5-*O*-p-coumaroylquinic acid (5-pCoQA), and caffeic and ferulic acids. These compounds have also been found in green coffee beans [146].

Considering the results of the analysis of phenolic compounds in CWPW, the catalytic activity of the pillared bentonite with Al-Fe was evaluated in the oxidation reaction of three phenolic acids which were used as model molecules,

Table 4: Physicochemical parameters of coffee wet processing wastewater before and after biological treatment in SMTA.

Parameters	Water characteristics	
	Before[a]	After[b]
pH	4.2	6.5
BOD_5 (mg O_2/L)	2,990	284
COD (mg O_2/L)	6,580	551
COD/BOD	2.2	1.9
Total suspended solids (mg/L)	435	904
Acidity (mg/L)	413	72
Total phenols (mg/L)	ND	165

[a]Analysis conducted at Cenicafé.
[b]Analysis after biological treatment in hydrolytic acidogenic and methanogenic reactors (SMTA).
ND: Not determined because the sample contained a large amount of reducing sugars that generated interference and overestimated the total phenols content.

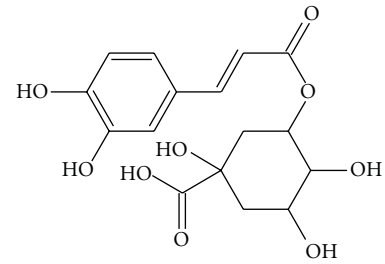

Chlorogenic acid (3-CQA)

3-(3, 4-dihydroxycinnamoyl)quinic acid

(a)

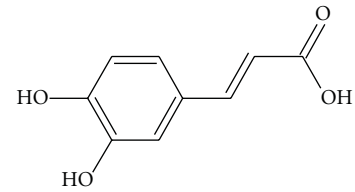

Caffeic acid

3, 4-dihydroxy-cinnamic acid

(b)

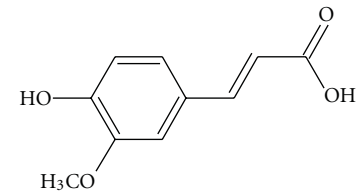

Ferulic acid

3-methoxy-4-hydroxycinnamic acid

(c)

Figure 1: Structure of phenolic acids.

using a similar procedure as that reported in previous studies for phenol [46, 49, 56, 57]. The phenolic acids used were chlorogenic (3-caffeoylquinic or 3-CQA), caffeic, and ferulic acids (Figure 1) at the following concentrations: 100 mg/L for 3-CQA and 40 mg/L for both caffeic and ferulic acids.

Traditionally, the tests with phenol as a model system are performed with 40 mg/L but, for 3-CQA, a higher concentration was used, given that 3-CQA is one of the most abundant compounds in the CWPW [138]. Monitoring of the phenolic acid conversion over time was conducted by high performance liquid chromatography (HPLC) using a Hitachi D-7000 (LaChrom) instrument equipped with a LiChrospher 60 Select B column, absorbance detector UV-vis L-7400, and, as a mobile phase, using a mixture of H_2O, H_3PO_4, and CH_3OH. The retention times for chlorogenic, caffeic, and ferulic acids were 9.3, 9.9 and 11.0 min, respectively. Selectivity of the catalysts toward CO_2 and H_2O was evaluated using the analysis of total organic carbon (TOC) by an AnaTOC equipment.

Wet hydrogen peroxide catalytic oxidation tests of Al-Fe-PILC with chlorogenic (3-CQA), caffeic, and ferulic acids showed a beneficial effect when incorporating Fe in the bentonite, both with respect to the phenolic acids conversion (Figure 2) and total organic carbon, TOC (Figure 3). The conversion of phenolic compounds using the catalyst Al-Fe-PILC was higher for the chlorogenic acid (91%), followed by caffeic acid (87%) and ferulic acid (78%) after 4 h. Although a complete oxidation of these acids was not achieved, conversions higher than 78% are considered to be very good considering the complex structure of these compounds and the fact that the reaction was performed at 25°C. Selectivity of the Al-Fe-PILC towards CO_2 and H_2O was higher for the chlorogenic acid (49%), followed by the caffeic acid (37%) and ferulic acid (34%). These results are associated with differences in chemical structure. It was also found that the reactivity of phenolic compounds can be drastically affected by the electronic nature of substituents and by their positions in the aromatic ring [148, 149].

The high conversion of chlorogenic acid can be explained by the presence of two electron-donating groups (as caffeic acid) and by three additional hydroxyl groups in the ester moiety. An example of the relationship between the chemical structure and its reactivity with hydroxyl radical would be the wet hydrogen peroxide photo-oxidation of p-coumaric, vanillic, ferulic, and caffeic acids when catalysed by (Al-Fe)-PILC, in which the degradation of phenolic compounds was 28%, 50%, 58%, and 86%, respectively [148]. Because the hydroxyl radicals generated by the catalytic decomposition of H_2O_2 are both reactive and nonselective, the attack position in the aromatic ring can be located anywhere on the ring [150]. Therefore, the catalytic degradability of some phenolic compounds has been correlated by the Hammett constant (σ), explaining the effect that different substituents have on the electronic character of a given aromatic system (electron-withdrawing or electron-donating groups) [148, 150].

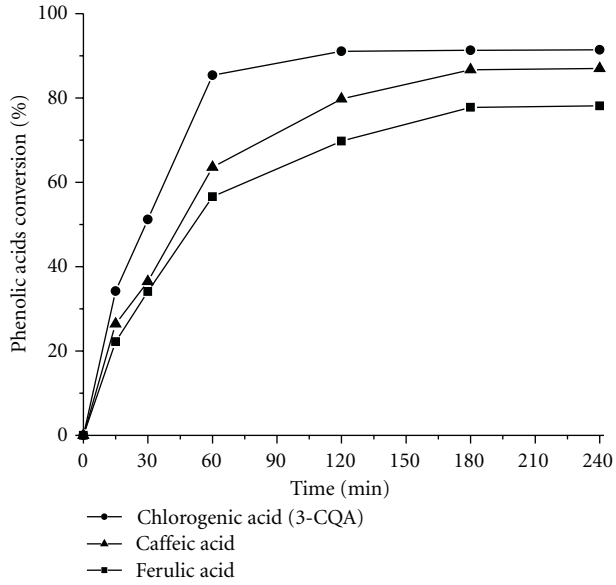

Figure 2: Phenolic acids conversion with AlFe-PILC.

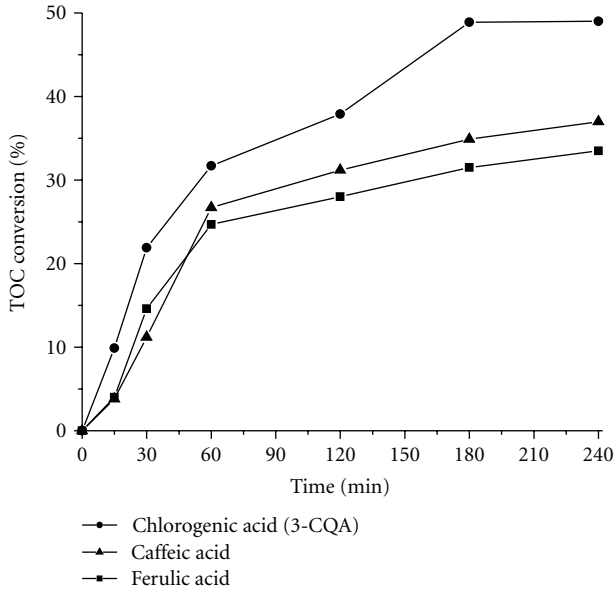

Figure 3: Total organic carbon (TOC) conversion with AlFe-PILC.

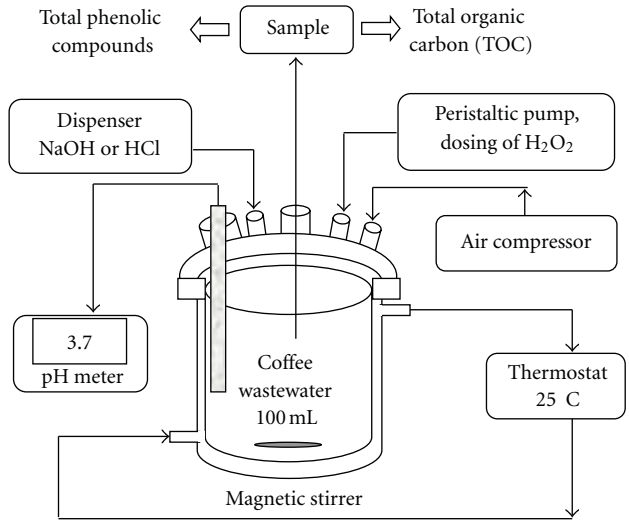

Figure 4: Diagram of the reaction system.

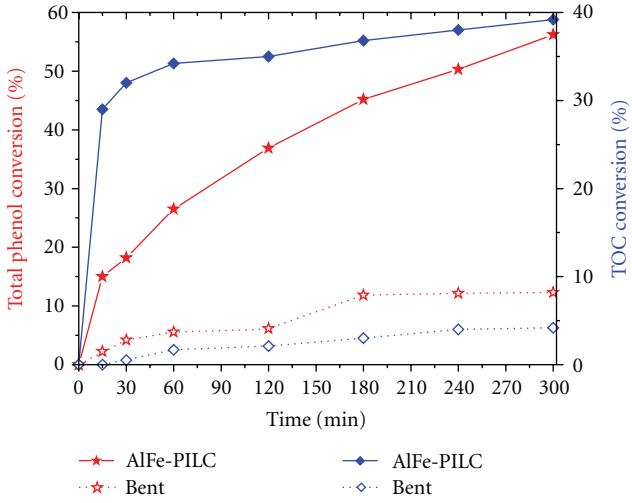

Figure 5: Catalytic oxidation of coffee wastewater with AlFe-PILC (continuous line) and Bent (dotted line). Total phenols conversion (star) and TOC conversion (diamond).

The reaction scheme for evaluating the catalytic activity of AlFe-PILC in the oxidation of the CWPW was described in Figure 4. For testing, the semibatch reactor thermostated at 25°C was loaded with 100 mL of coffee wastewater, 0.5 g of the catalyst, 0.1 M hydrogen peroxide solution (10 mL, 2 mL/h), bubbling air at a constant flow (2 L/h), and brought to a pH of 3.7 with 0.1 M NaOH or HCl. The total phenol conversion in CWPW was performed using the Folin-Ciocalteu colorimetric method [151, 152]. Selectivity of the catalysts toward CO_2 and H_2O or grade of mineralization was evaluated using the analysis of total organic carbon (TOC) with an AnaTOC equipment.

The AlFe-PILC achieved a high conversion rate of total phenolic compounds (56%) and mineralization towards CO_2 and H_2O (40%) after 5 h reaction time (Figure 5). The starting bentonite (Bent) used as a reaction target achieved a conversion rate of phenolic compounds of 8% and selectivity to CO_2 and H_2O of 4%, values attributed to the activity of iron in the starting clay (8.2% Fe_2O_3). The chemical oxygen demand (COD) of coffee processing wastewater after wet hydrogen peroxide catalytic oxidation was reduced in 60%. In terms of stability of the active phase, an average concentration of leached iron was <0.22 ppm.

The combination of the two treatment methods, biological (developed by Cenicafé) and catalytic oxidation with AlFe-PILC, achieved a 96.7% reduction of COD in CWPW. These results are higher than those obtained when

coffee processing wastewater was treated by coagulation-flocculation in combination with advanced oxidation processes ($UV/H_2O_2/O_3$), where a COD reduction of 87% was achieved [153]. Therefore, the WHPCO using AlFe-PILC catalysts is a viable alternative for the posttreatment of coffee processing wastewater.

4. Conclusions

The pillared clays have received considerable attention in the last decade as catalysts for wet hydrogen peroxide oxidation of phenolic compounds because of their high activity (conversion of phenolic compound and degree of mineralization) and environmental compatibility (low cost, easy recovery of the catalyst, are reusable catalysts, oxidation that can be carried out at room temperature and atmospheric pressure, and that they show high stability of the active phase in the reaction medium). With the developments in the synthesis of pillared clays, it has been possible to reduce the water volume and synthesis times, and technical requirements for these materials can be useful at industrial level.

Given the excellent properties of pillared clays in the WHPCO for phenol and other model molecules, as well as real wastewater treatment, this advanced oxidation process can be integrated with biological process, as a pre- or post-treatment, depending on the physicochemical characteristics of the wastewater.

The high conversion of phenolic compounds, the selectivity to CO_2 and H_2O, and stability of the active phase in the pillared bentonite with Al-Fe in the WHPCO of coffee wastewater show the potentiality of this catalyst for posttreatment for this type of effluent. The combination of the two treatment methods, biological and catalytic oxidation with AlFe-PILC, achieved a 96.7% reduction of chemical oxygen demand in coffee wet processing wastewater.

Acknowledgments

The authors are grateful for the financial support provided by CSIC-COLCIENCIAS and DIB of Universidad Nacional de Colombia, Bogotá, for the development of several research projects conducted over the past 10 years. The authors also appreciate the cooperation received from the National Coffee Research Center—Cenicafé.

References

[1] R. J. Bigda, "Consider Fenton chemistry for waste-water treatment," *Chemical Engineering Progress*, vol. 91, no. 12, pp. 62–66, 1995.

[2] H. J. H. Fenton, "LXXIII.—oxidation of tartaric acid in presence of iron," *Journal of the Chemical Society, Transactions*, vol. 65, pp. 899–910, 1894.

[3] C. Walling, "Fenton's reagent revisited," *Accounts of Chemical Research*, vol. 8, no. 4, pp. 125–131, 1975.

[4] S. S. Lin and M. D. Gurol, "Catalytic decomposition of hydrogen peroxide on iron oxide: kinetics, mechanism, and implications," *Environmental Science and Technology*, vol. 32, no. 10, pp. 1417–1423, 1998.

[5] J. Beltran De Heredia, J. Torregrosa, J. R. Dominguez, and J. A. Peres, "Kinetic model for phenolic compound oxidation by Fenton's reagent," *Chemosphere*, vol. 45, no. 1, pp. 85–90, 2001.

[6] A. Safarzadeh-Amiri, J. R. Bolton, and S. R. Cater, "The use of iron in advanced oxidation processes," *Journal of Advanced Oxidation Technologies*, vol. 1, no. 1, pp. 18–26, 1996.

[7] G. Zelmanov and R. Semiat, "Phenol oxidation kinetics in water solution using iron(3)-oxide-based nano-catalysts," *Water Research*, vol. 42, no. 14, pp. 3848–3856, 2008.

[8] F. Haber and J. Weiss, "The catalytic decomposition of hydrogen peroxide by iron salts," *Proceedings of the Royal Society of London A*, vol. 147, no. 861, pp. 332–351, 1934.

[9] C. Walling, G. M. El-Taliawi, and R. A. Johnson, "Fenton's reagent. IV. Structure and reactivity relations in the reactions of hydroxyl radicals and the redox reactions of radicals," *Journal of the American Chemical Society*, vol. 96, no. 1, pp. 133–139, 1974.

[10] E. Chamarro, A. Marco, and S. Esplugas, "Use of Fenton reagent to improve organic chemical biodegradability," *Water Research*, vol. 35, no. 4, pp. 1047–1051, 2001.

[11] C. K. Duesterberg and T. D. Waite, "Process optimization of fenton oxidation using kinetic modeling," *Environmental Science and Technology*, vol. 40, no. 13, pp. 4189–4195, 2006.

[12] W. P. Ting, M. C. Lu, and Y. H. Huang, "The reactor design and comparison of Fenton, electro-Fenton and photoelectro-Fenton processes for mineralization of benzene sulfonic acid (BSA)," *Journal of Hazardous Materials*, vol. 156, no. 1–3, pp. 421–427, 2008.

[13] A. Babuponnusami and K. Muthukumar, "Advanced oxidation of phenol: a comparison between Fenton, electro-Fenton, sono-electro-Fenton and photo-electro-Fenton processes," *Chemical Engineering Journal*, vol. 183, pp. 1–9, 2012.

[14] H. Kušić, N. Koprivanac, A. L. Božić, and I. Selanec, "Photo-assisted Fenton type processes for the degradation of phenol: a kinetic study," *Journal of Hazardous Materials*, vol. 136, no. 3, pp. 632–644, 2006.

[15] N. Kang, D. S. Lee, and J. Yoon, "Kinetic modeling of Fenton oxidation of phenol and monochlorophenols," *Chemosphere*, vol. 47, no. 9, pp. 915–924, 2002.

[16] S. Chou, Y. H. Huang, S. N. Lee, G. H. Huang, and C. Huang, "Treatment of high strength hexamine-containing wastewater by Electro-Fenton method," *Water Research*, vol. 33, no. 3, pp. 751–759, 1999.

[17] D. F. Bishop, G. Stern, M. Fleischman, and L. S. Marshall, "Hydrogen peroxide catalytic oxidation of refractory organics in municipal waste waters," *IandEC Process Design and Development*, vol. 7, no. 1, pp. 110–117, 1968.

[18] E. S. Henle and S. Linn, "Formation, prevention, and repair of DNA damage by iron/hydrogen peroxide," *Journal of Biological Chemistry*, vol. 272, no. 31, pp. 19095–19098, 1997.

[19] E. Neyens and J. Baeyens, "A review of classic Fenton's peroxidation as an advanced oxidation technique," *Journal of Hazardous Materials*, vol. 98, no. 1–3, pp. 33–50, 2003.

[20] K. H. Kim, J. R. Kim, and S. K. Ihm, "Wet oxidation of phenol over transition metal oxide catalysts supported on $Ce_{0.65}Zr_{0.35}O_2$ prepared by continuous hydrothermal synthesis in supercritical water," *Journal of Hazardous Materials*, vol. 167, no. 1–3, pp. 1158–1162, 2009.

[21] K. H. Kim and S. K. Ihm, "Heterogeneous catalytic wet air oxidation of refractory organic pollutants in industrial

wastewaters: a review," *Journal of Hazardous Materials*, vol. 186, no. 1, pp. 16–34, 2011.

[22] F. Arena, C. Italiano, A. Raneri, and C. Saja, "Mechanistic and kinetic insights into the wet air oxidation of phenol with oxygen (CWAO) by homogeneous and heterogeneous transition-metal catalysts," *Applied Catalysis B*, vol. 99, no. 1-2, pp. 321–328, 2010.

[23] X. Domènech, W. F. Jardim, and M. I. Litter, "Procesos avanzados de oxidación para la eliminación de contaminantes," in *Eliminación de contaminantes por fotocatálisis heterogénea*, M. Blesa, Ed., pp. 3–26, CYTED, La Plata, Argentina, 2001.

[24] A. N. Soon and B. H. Hameed, "Heterogeneous catalytic treatment of synthetic dyes in aqueous media using Fenton and photo-assisted Fenton process," *Desalination*, vol. 269, no. 1–3, pp. 1–16, 2011.

[25] S. Moreno, N. Sanabria, and R. Molina, "Chapter 4. Recent tendences in the synthesis of pillared clays for phenol oxidation," in *Focus on Water Resource Research*, E. Heikkine, Ed., pp. 185–209, Nova Science Publischer, New York, NY, USA, 2008.

[26] T. S. R. Prasada Rao and G. Murali Dhar, *Recent Advanced in Basic and Applied Aspects of Industrial Catalysis*, Elsevier Science B. V., Amsterdam, The Netherlands, 1998.

[27] N. R. Sanabria, R. Molina, and S. Moreno, "Raschig rings based on pillared clays: efficient reusable catalysts for oxidation of phenol," *Journal of Advanced Oxidation Technologies*, vol. 15, no. 1, pp. 117–124, 2012.

[28] J. K. Kim, F. Martinez, and I. S. Metcalfe, "The beneficial role of use of ultrasound in heterogeneous Fenton-like system over supported copper catalysts for degradation of p-chlorophenol," *Catalysis Today*, vol. 124, no. 3-4, pp. 224–231, 2007.

[29] H. Hassan and B. H. Hameed, "Fe-clay as effective heterogeneous Fenton catalyst for the decolorization of Reactive Blue 4," *Chemical Engineering Journal*, vol. 171, no. 3, pp. 912–918, 2011.

[30] T. D. Nguyen, N. H. Phan, M. H. Do, and K. T. Ngo, "Magnetic Fe_2MO_4 (M:Fe, Mn) activated carbons: fabrication, characterization and heterogeneous Fenton oxidation of methyl orange," *Journal of Hazardous Materials*, vol. 185, no. 2-3, pp. 653–661, 2011.

[31] S. H. Tian, Y. T. Tu, D. S. Chen, X. Chen, and Y. Xiong, "Degradation of Acid Orange II at neutral pH using $Fe_2(MoO_4)_3$ as a heterogeneous Fenton-like catalyst," *Chemical Engineering Journal*, vol. 169, no. 1–3, pp. 31–37, 2011.

[32] M. Dükkanci, G. Gündüz, S. Yilmaz, and R. V. Prihod'ko, "Heterogeneous Fenton-like degradation of Rhodamine 6G in water using CuFeZSM-5 zeolite catalyst prepared by hydrothermal synthesis," *Journal of Hazardous Materials*, vol. 181, no. 1–3, pp. 343–350, 2010.

[33] R. Idel-aouad, M. Valiente, A. Yaacoubi, B. Tanouti, and M. López-Mesas, "Rapid decolourization and mineralization of the azo dye C.I. Acid Red 14 by heterogeneous Fenton reaction," *Journal of Hazardous Materials*, vol. 186, no. 1, pp. 745–750, 2011.

[34] H. Kušić, N. Koprivanac, and I. Selanec, "Fe-exchanged zeolite as the effective heterogeneous Fenton-type catalyst for the organic pollutant minimization: UV irradiation assistance," *Chemosphere*, vol. 65, no. 1, pp. 65–73, 2006.

[35] E. V. Kuznetsova, E. N. Savinov, L. A. Vostrikova, and V. N. Parmon, "Heterogeneous catalysis in the Fenton-type system FeZSM-5/H_2O_2," *Applied Catalysis B*, vol. 51, no. 3, pp. 165–170, 2004.

[36] G. B. Ortiz de la Plata, O. M. Alfano, and A. E. Cassano, "Decomposition of 2-chlorophenol employing goethite as Fenton catalyst II: reaction kinetics of the heterogeneous Fenton and photo-Fenton mechanisms," *Applied Catalysis B*, vol. 95, no. 1-2, pp. 14–25, 2010.

[37] R. C. C. Costa, F. C. C. Moura, J. D. Ardisson, J. D. Fabris, and R. M. Lago, "Highly active heterogeneous Fenton-like systems based on Fe^0/Fe_3O_4 composites prepared by controlled reduction of iron oxides," *Applied Catalysis B*, vol. 83, no. 1-2, pp. 131–139, 2008.

[38] F. C. C. Moura, M. H. Araujo, R. C. C. Costa et al., "Efficient use of Fe metal as an electron transfer agent in a heterogeneous Fenton system based on Fe^0/Fe_3O_4 composites," *Chemosphere*, vol. 60, no. 8, pp. 1118–1123, 2005.

[39] S.-P. Sun and A. T. Lemley, "P-Nitrophenol degradation by a heterogeneous Fenton-like reaction on nano-magnetite: process optimization, kinetics, and degradation pathways," *Journal of Molecular Catalysis A*, vol. 349, no. 1-2, pp. 71–79, 2011.

[40] F. Martínez, G. Calleja, J. A. Melero, and R. Molina, "Heterogeneous photo-Fenton degradation of phenolic aqueous solutions over iron-containing SBA-15 catalyst," *Applied Catalysis B*, vol. 60, no. 3-4, pp. 181–190, 2005.

[41] R. Molina, F. Martínez, J. A. Melero, D. H. Bremner, and A. G. Chakinala, "Mineralization of phenol by a heterogeneous ultrasound/Fe-SBA-15/H_2O_2 process: multivariate study by factorial design of experiments," *Applied Catalysis B*, vol. 66, no. 3-4, pp. 198–207, 2006.

[42] P. Shukla, S. Wang, H. Sun, H. M. Ang, and M. Tadé, "Adsorption and heterogeneous advanced oxidation of phenolic contaminants using Fe loaded mesoporous SBA-15 and H_2O_2," *Chemical Engineering Journal*, vol. 164, no. 1, pp. 255–260, 2010.

[43] L. A. Galeano, M. Á. Vicente, and A. Gil, "Treatment of municipal leachate of landfill by fenton-like heterogeneous catalytic wet peroxide oxidation using an Al/Fe-pillared montmorillonite as active catalyst," *Chemical Engineering Journal*, vol. 178, pp. 146–153, 2011.

[44] M. Luo, D. Bowden, and P. Brimblecombe, "Catalytic property of Fe-Al pillared clay for Fenton oxidation of phenol by H_2O_2," *Applied Catalysis B*, vol. 85, no. 3-4, pp. 201–206, 2009.

[45] C. B. Molina, J. A. Casas, J. A. Zazo, and J. J. Rodríguez, "A comparison of Al-Fe and Zr-Fe pillared clays for catalytic wet peroxide oxidation," *Chemical Engineering Journal*, vol. 118, no. 1-2, pp. 29–35, 2006.

[46] J. G. Carriazo, E. Guelou, J. Barrault, J. M. Tatibouët, and S. Moreno, "Catalytic wet peroxide oxidation of phenol over Al-Cu or Al-Fe modified clays," *Applied Clay Science*, vol. 22, no. 6, pp. 303–308, 2003.

[47] J. Carriazo, E. Guélou, J. Barrault, J. M. Tatibouët, R. Molina, and S. Moreno, "Catalytic wet peroxide oxidation of phenol by pillared clays containing Al-Ce-Fe," *Water Research*, vol. 39, no. 16, pp. 3891–3899, 2005.

[48] J. Carriazo, E. Guélou, J. Barrault, J. M. Tatibouët, R. Molina, and S. Moreno, "Synthesis of pillared clays containing Al, Al-Fe or Al-Ce-Fe from a bentonite: characterization and catalytic activity," *Catalysis Today*, vol. 107-108, pp. 126–132, 2005.

[49] J. G. Carriazo, M. A. Centeno, J. A. Odriozola, S. Moreno, and R. Molina, "Effect of Fe and Ce on Al-pillared bentonite and their performance in catalytic oxidation reactions," *Applied Catalysis A*, vol. 317, no. 1, pp. 120–128, 2007.

[50] J. G. Carriazo, R. Molina, and S. Moreno, "A study on Al and Al-Ce-Fe pillaring species and their catalytic potential as they are supported on a bentonite," *Applied Catalysis A*, vol. 334, no. 1-2, pp. 168–172, 2008.

[51] A. Pérez, M. A. Centeno, J. A. Odriozola, R. Molina, and S. Moreno, "The effect of ultrasound in the synthesis of clays used as catalysts in oxidation reactions," *Catalysis Today*, vol. 133-135, no. 1–4, pp. 526–529, 2008.

[52] N. Sanabria, A. Álvarez, R. Molina, and S. Moreno, "Synthesis of pillared bentonite starting from the Al-Fe polymeric precursor in solid state, and its catalytic evaluation in the phenol oxidation reaction," *Catalysis Today*, vol. 133-135, no. 1–4, pp. 530–533, 2008.

[53] A. Olaya, S. Moreno, and R. Molina, "Synthesis of pillared clays with Al_{13}-Fe and Al_{13}-Fe-Ce polymers in solid state assisted by microwave and ultrasound: characterization and catalytic activity," *Applied Catalysis A*, vol. 370, no. 1-2, pp. 7–15, 2009.

[54] A. Olaya, G. Blanco, S. Bernal, S. Moreno, and R. Molina, "Synthesis of pillared clays with Al-Fe and Al-Fe-Ce starting from concentrated suspensions of clay using microwaves or ultrasound, and their catalytic activity in the phenol oxidation reaction," *Applied Catalysis B*, vol. 93, no. 1-2, pp. 56–65, 2009.

[55] A. Olaya, S. Moreno, and R. Molina, "Synthesis of pillared clays with aluminum by means of concentrated suspensions and microwave radiation," *Catalysis Communications*, vol. 10, no. 5, pp. 697–701, 2009.

[56] N. R. Sanabria, M. A. Centeno, R. Molina, and S. Moreno, "Pillared clays with Al-Fe and Al-Ce-Fe in concentrated medium: synthesis and catalytic activity," *Applied Catalysis A*, vol. 356, no. 2, pp. 243–249, 2009.

[57] N. R. Sanabria, R. Molina, and S. Moreno, "Effect of ultrasound on the structural and textural properties of Al-Fe pillared clays in a concentrated medium," *Catalysis Letters*, vol. 130, no. 3-4, pp. 664–671, 2009.

[58] J. Barrault, C. Bouchoule, K. Echachoui, N. Frini-Srasra, M. Trabelsi, and F. Bergaya, "Catalytic wet peroxide oxidation (CWPO) of phenol over mixed (Al-Cu)-pillared clays," *Applied Catalysis B*, vol. 15, no. 3-4, pp. 269–274, 1998.

[59] C. Catrinescu, C. Teodosiu, M. Macoveanu, J. Miehe-Brendlé, and R. Le Dred, "Catalytic wet peroxide oxidation of phenol over Fe-exchanged pillared beidellite," *Water Research*, vol. 37, no. 5, pp. 1154–1160, 2003.

[60] J. Barrault, M. Abdellaoui, C. Bouchoule et al., "Catalytic wet peroxide oxidation over mixed (Al-Fe) pillared clays," *Applied Catalysis B*, vol. 27, no. 4, pp. L225–L230, 2000.

[61] N. R. Sanabria, P. Ávila, M. Yates, S. B. Rasmussen, R. Molina, and S. Moreno, "Mechanical and textural properties of extruded materials manufactured with AlFe and AlCeFe pillared bentonites," *Applied Clay Science*, vol. 47, no. 3-4, pp. 283–289, 2010.

[62] J. Barrault, J. M. Tatibouët, and N. Papayannakos, "Catalytic wet peroxide oxidation of phenol over pillared clays containing iron or copper species," *Comptes Rendus de l'Academie des Sciences*, vol. 3, no. 10, pp. 777–783, 2000.

[63] E. Guélou, J. Barrault, J. Fournier, and J. M. Tatibouët, "Active iron species in the catalytic wet peroxide oxidation of phenol over pillared clays containing iron," *Applied Catalysis B*, vol. 44, no. 1, pp. 1–8, 2003.

[64] M. N. Timofeeva, S. T. Khankhasaeva, S. V. Badmaeva et al., "Synthesis, characterization and catalytic application for wet oxidation of phenol of iron-containing clays," *Applied Catalysis B*, vol. 59, no. 3-4, pp. 243–248, 2005.

[65] E. E. Kiss, M. M. Lazic, and G. C. Boskovic, "AlFe-pillared clay catalyst for phenol oxidation in aqueous solution," *Reaction Kinetics and Catalysis Letters*, vol. 83, no. 2, pp. 221–227, 2004.

[66] J. Guo and M. Al-Dahhan, "Catalytic wet oxidation of phenol by hydrogen peroxide over pillared clay catalyst," *Industrial and Engineering Chemistry Research*, vol. 42, no. 12, pp. 2450–2460, 2003.

[67] A. N. Nikolopoulos, O. Igglessi-Markopoulou, and N. Papayannakos, "Ultrasound assisted catalytic wet peroxide oxidation of phenol: kinetics and intraparticle diffusion effects," *Ultrasonics Sonochemistry*, vol. 13, no. 1, pp. 92–97, 2006.

[68] J. M. Tatibouët, E. Guélou, and J. Fournier, "Catalytic oxidation of phenol by hydrogen peroxide over a pillared clay containing iron. Active species and pH effect," *Topics in Catalysis*, vol. 33, no. 1–4, pp. 225–232, 2005.

[69] S. Caudo, G. Centi, C. Genovese, and S. Perathoner, "Copper- and iron-pillared clay catalysts for the WHPCO of model and real wastewater streams from olive oil milling production," *Applied Catalysis B*, vol. 70, no. 1–4, pp. 437–446, 2007.

[70] R. B. Achma, A. Ghorbel, A. Dafinov, and F. Medina, "Copper-supported pillared clay catalysts for the wet hydrogen peroxide catalytic oxidation of model pollutant tyrosol," *Applied Catalysis A*, vol. 349, no. 1-2, pp. 20–28, 2008.

[71] S. Azabou, W. Najjar, M. Bouaziz, A. Ghorbel, and S. Sayadi, "A compact process for the treatment of olive mill wastewater by combining wet hydrogen peroxide catalytic oxidation and biological techniques," *Journal of Hazardous Materials*, vol. 183, no. 1–3, pp. 62–69, 2010.

[72] S. Caudo, C. Genovese, S. Perathoner, and G. Centi, "Copper-pillared clays (Cu-PILC) for agro-food wastewater purification with H_2O_2," *Microporous and Mesoporous Materials*, vol. 107, no. 1-2, pp. 46–57, 2008.

[73] G. Giordano, S. Perathoner, G. Centi et al., "Wet hydrogen peroxide catalytic oxidation of olive oil mill wastewaters using Cu-zeolite and Cu-pillared clay catalysts," *Catalysis Today*, vol. 124, no. 3-4, pp. 240–246, 2007.

[74] M. Pimentel, N. Oturan, M. Dezotti, and M. A. Oturan, "Phenol degradation by advanced electrochemical oxidation process electro-Fenton using a carbon felt cathode," *Applied Catalysis B*, vol. 83, no. 1-2, pp. 140–149, 2008.

[75] G. Busca, S. Berardinelli, C. Resini, and L. Arrighi, "Technologies for the removal of phenol from fluid streams: a short review of recent developments," *Journal of Hazardous Materials*, vol. 160, no. 2-3, pp. 265–288, 2008.

[76] H. Ma, X. Zhang, Q. Ma, and B. Wang, "Electrochemical catalytic treatment of phenol wastewater," *Journal of Hazardous Materials*, vol. 165, no. 1–3, pp. 475–480, 2009.

[77] H. H. P. Fang, D. W. Liang, T. Zhang, and Y. Liu, "Anaerobic treatment of phenol in wastewater under thermophilic condition," *Water Research*, vol. 40, no. 3, pp. 427–434, 2006.

[78] W. Kujawski, A. Warszawski, W. Ratajczak, T. Porębski, W. Capała, and I. Ostrowska, "Removal of phenol from wastewater by different separation techniques," *Desalination*, vol. 163, no. 1–3, pp. 287–296, 2004.

[79] A. Santos, P. Yustos, S. Gomis, G. Ruiz, and F. Garcia-Ochoa, "Reaction network and kinetic modeling of wet oxidation of phenol catalyzed by activated carbon," *Chemical Engineering Science*, vol. 61, no. 8, pp. 2457–2467, 2006.

[80] M. Pérez, F. Torrades, J. A. García-Hortal, X. Domènech, and J. Peral, "Removal of organic contaminants in paper

pulp treatment effluents under Fenton and photo-Fenton conditions," *Applied Catalysis B*, vol. 36, no. 1, pp. 63–74, 2002.

[81] M. G. Joshi and R. L. Shambaugh, "The kinetics of ozone-phenol reaction in aqueous solutions," *Water Research*, vol. 16, no. 6, pp. 933–938, 1982.

[82] A. M. Amat, A. Arques, F. López, and M. A. Miranda, "Solar photo-catalysis to remove paper mill wastewater pollutants," *Solar Energy*, vol. 79, no. 4, pp. 393–401, 2005.

[83] S. Perathoner and G. Centi, "Wet hydrogen peroxide catalytic oxidation (WHPCO) of organic waste in agro-food and industrial streams," *Topics in Catalysis*, vol. 33, pp. 207–224, 2005.

[84] I. U. Castro, D. C. Sherrington, A. Fortuny et al., "Synthesis of polymer-supported copper complexes and their evaluation in catalytic phenol oxidation," *Catalysis Today*, vol. 157, no. 1–4, pp. 66–70, 2010.

[85] N. Crowther and F. Larachi, "Iron-containing silicalites for phenol catalytic wet peroxidation," *Applied Catalysis B*, vol. 46, no. 2, pp. 293–305, 2003.

[86] N. Inchaurrondo, J. Cechini, J. Font, and P. Haure, "Strategies for enhanced CWPO of phenol solutions," *Applied Catalysis B*, vol. 111-112, pp. 641–648, 2012.

[87] P. Massa, A. Dafinov, F. M. Cabello, and R. Fenoglio, "Catalytic wet peroxide oxidation of phenolic solutions over Fe_2O_3/CeO_2 and WO_3/CeO_2 catalyst systems," *Catalysis Communications*, vol. 9, no. 7, pp. 1533–1538, 2008.

[88] P. Massa, F. Ivorra, P. Haure, and R. Fenoglio, "Catalytic wet peroxide oxidation of phenol solutions over CuO/CeO_2 systems," *Journal of Hazardous Materials*, vol. 190, no. 1–3, pp. 1068–1073, 2011.

[89] G. Calleja, J. A. Melero, F. Martínez, and R. Molina, "Activity and resistance of iron-containing amorphous, zeolitic and mesostructured materials for wet peroxide oxidation of phenol," *Water Research*, vol. 39, no. 9, pp. 1741–1750, 2005.

[90] A. Quintanilla, A. F. Fraile, J. A. Casas, and J. J. Rodríguez, "Phenol oxidation by a sequential CWPO-CWAO treatment with a Fe/AC catalyst," *Journal of Hazardous Materials*, vol. 146, no. 3, pp. 582–588, 2007.

[91] A. Rey, J. Carbajo, C. Adán et al., "Improved mineralization by combined advanced oxidation processes," *Chemical Engineering Journal*, vol. 174, no. 1, pp. 134–142, 2011.

[92] A. Rey, M. Faraldos, J. A. Casas, J. A. Zazo, A. Bahamonde, and J. J. Rodríguez, "Catalytic wet peroxide oxidation of phenol over Fe/AC catalysts: influence of iron precursor and activated carbon surface," *Applied Catalysis B*, vol. 86, no. 1-2, pp. 69–77, 2009.

[93] J. A. Zazo, J. A. Casas, A. F. Mohedano, and J. J. Rodríguez, "Catalytic wet peroxide oxidation of phenol with a Fe/active carbon catalyst," *Applied Catalysis B*, vol. 65, no. 3-4, pp. 261–268, 2006.

[94] K. M. Valkaj, A. Katovic, and S. Zrnčević, "Investigation of the catalytic wet peroxide oxidation of phenol over different types of Cu/ZSM-5 catalyst," *Journal of Hazardous Materials*, vol. 144, no. 3, pp. 663–667, 2007.

[95] X. Zhong, J. Barbier, D. Duprez, H. Zhang, and S. Royer, "Modulating the copper oxide morphology and accessibility by using micro-/mesoporous SBA-15 structures as host support: effect on the activity for the CWPO of phenol reaction," *Applied Catalysis B*, vol. 121-122, pp. 123–134, 2012.

[96] S. Zhou, Z. Qian, T. Sun, J. Xu, and C. Xia, "Catalytic wet peroxide oxidation of phenol over Cu-Ni-Al hydrotalcite," *Applied Clay Science*, vol. 53, no. 4, pp. 627–633, 2011.

[97] E. V. Parkhomchuk, M. P. Vanina, and S. Preis, "The activation of heterogeneous Fenton-type catalyst Fe-MFI," *Catalysis Communications*, vol. 9, no. 3, pp. 381–385, 2008.

[98] D. Tabet, M. Saidi, M. Houari, P. Pichat, and H. Khalaf, "Fe-pillared clay as a Fenton-type heterogeneous catalyst for cinnamic acid degradation," *Journal of Environmental Management*, vol. 80, no. 4, pp. 342–346, 2006.

[99] F. Bergaya, A. Aouad, and T. Mandalia, "Chapter 7.5 Pillared clays and clay minerals. Developments in clay science," in *Handbook of Clay Science*, pp. 393–421, Elsevier, Amsterdam, The Netherlands, 2006.

[100] J. Barrault, C. Bouchoule, J. M. Tatibouët et al., "Catalytic wet peroxide oxidation over mixed (Al-Fe) pillared clays," in *Studies in Surface Science and Catalysis*, A. Corma, F. V. Melo, S. Mendioroz, and J. L. Fierro, Eds., pp. 749–754, Elsevier, Amsterdam, The Netherlands, 2000.

[101] R. M. Barrer and D. M. Macleod, "Activation of montmorillonite by ion exchange and sorption complexes of tetra-alkyl ammonium montmorillonites," *Transactions of the Faraday Society*, vol. 51, pp. 1290–1300, 1955.

[102] R. A. Schoonheydt, T. Pinnavaia, G. Lagaly, and N. Gangas, "Pillared clays and pillared layered solids," *Pure and Applied Chemistry*, vol. 71, no. 12, pp. 2368–2371, 1999.

[103] M. L. Occelli, J. A. Bertrand, S. A. C. Gould, and J. M. Dominguez, "Physicochemical characterization of a Texas montmorillonite pillared with polyoxocations of aluminum Part I: the microporous structure," *Microporous and Mesoporous Materials*, vol. 34, no. 2, pp. 195–206, 2000.

[104] J. P. Olivier and M. L. Occelli, "Surface area and microporosity of pillared rectorite catalysts from a hybrid density functional theory method," *Microporous and Mesoporous Materials*, vol. 57, no. 3, pp. 291–296, 2003.

[105] J. L. Valverde, A. Romero, R. Romero, P. B. García, M. L. Sánchez, and I. Asencio, "Preparation and characterization of Fe-PILCS. Influence of the synthesis parameters," *Clays and Clay Minerals*, vol. 53, no. 6, pp. 613–621, 2005.

[106] W. Diano, R. Rubino, and M. Sergio, "Al-pillared montmorillonite: preparation from concentrated slurries of homoionic Ca clay, characterization and thermal stability," *Microporous Materials*, vol. 2, no. 3, pp. 179–184, 1994.

[107] G. Fetter, G. Heredia, L. A. Velázquez, A. M. Maubert, and P. Bosch, "Synthesis of aluminum-pillared montmorillonites using highly concentrated clay suspensions," *Applied Catalysis A*, vol. 162, no. 1-2, pp. 41–45, 1997.

[108] R. Molina, A. Vieira-Coelho, and G. Poncelet, "Hydroxy-Al pillaring of concentrated clay suspensions," *Clays and Clay Minerals*, vol. 40, no. 4, pp. 480–482, 1992.

[109] P. Salerno and S. Mendioroz, "Preparation of Al-pillared montmorillonite from concentrated dispersions," *Applied Clay Science*, vol. 22, no. 3, pp. 115–123, 2002.

[110] A. Sánchez and M. Montes, "Influence of the preparation parameters (particle size and aluminium concentration) on the textural properties of Al-pillared clays for a scale-up process," *Microporous and Mesoporous Materials*, vol. 21, no. 1–3, pp. 117–125, 1998.

[111] L. Storaro, M. Lenarda, M. Perissinotto, V. Lucchini, and R. Ganzerla, "Hydroxy-Al pillaring of concentrated suspensions of smectite clays," *Microporous and Mesoporous Materials*, vol. 20, no. 4–6, pp. 317–331, 1998.

[112] S. P. Katdare, V. Ramaswamy, and A. V. Ramaswamy, "Ultrasonication: a competitive method of intercalation for the preparation of alumina pillared montmorillonite catalyst," *Catalysis Today*, vol. 49, no. 1–3, pp. 313–320, 1999.

[113] S. P. Katdare, V. Ramaswamy, and A. V. Ramaswamy, "Factors affecting the preparation of alumina pillared montmorillonite employing ultrasonics," *Microporous and Mesoporous Materials*, vol. 37, no. 3, pp. 329–336, 2000.

[114] V. Singh, V. Sapehiyia, and G. L. Kad, "Ultrasound and microwave activated preparation of ZrO_2-pillared clay composite: catalytic activity for selective, solventless acylation of 1,n-diols," *Journal of Molecular Catalysis A*, vol. 210, no. 1-2, pp. 119–124, 2004.

[115] G. Fetter, V. Hernández, V. Rodríguez, M. A. Valenzuela, V. H. Lara, and P. Bosch, "Effect of microwave irradiation time on the synthesis of zirconia-pillared clays," *Materials Letters*, vol. 57, no. 5-6, pp. 1220–1223, 2003.

[116] A. M. De Andrés, J. Merino, J. C. Galván, and E. Ruiz-Hitzky, "Synthesis of pillared clays assisted by microwaves," *Materials Research Bulletin*, vol. 34, no. 4, pp. 641–651, 1999.

[117] A. Aouad, T. Mandalia, and F. Bergaya, "A novel method of Al-pillared montmorillonite preparation for potential industrial up-scaling," *Applied Clay Science*, vol. 28, no. 1–4, pp. 175–182, 2005.

[118] C. B. Molina, J. A. Casas, A. H. Pizarro, and J. J. Rodriguez, "Pillared Clays as green chemistry catalysts: application to wastewater treatment," in *Clay: Types, Properties and Uses*, J. P. Humphrey and D. E. Boyd, Eds., pp. 435–474, Nova Science, New York, NY, USA, 2011.

[119] S. Moreno-Guáqueta, R. Molina-Gallego, N. R. Sanabria-González, and A. J. Olaya-Avendaño, "Procedimiento para la modificación de arcilla con el sistema mixto Al-Fe o Al-Ce-Fe," Patente IPC C 01 B 033/020, Superintendencia de Industria y Comercio, Colombia, 2007.

[120] F. Mohino, A. B. Martin, P. Salerno, A. Bahamonde, and S. Mendioroz, "High surface area monoliths based on pillared clay materials as carriers for catalytic processes," *Applied Clay Science*, vol. 29, no. 2, pp. 125–136, 2005.

[121] L. F. Liotta, M. Gruttadauria, G. Di Carlo, G. Perrini, and V. Librando, "Heterogeneous catalytic degradation of phenolic substrates: catalysts activity," *Journal of Hazardous Materials*, vol. 162, no. 2-3, pp. 588–606, 2009.

[122] C. Catrinescu, D. Arsene, and C. Teodosiu, "Catalytic wet hydrogen peroxide oxidation of para-chlorophenol over Al/Fe pillared clays (AlFePILCs) prepared from different host clays," *Applied Catalysis B*, vol. 101, no. 3-4, pp. 451–460, 2011.

[123] L. Chirchi and A. Ghorbel, "Use of various Fe-modified montmorillonite samples for 4-nitrophenol degradation by H_2O_2," *Applied Clay Science*, vol. 21, no. 5-6, pp. 271–276, 2002.

[124] M. J. Hernando, C. Pesquera, C. Blanco, and F. González, "Synthesis, characterization, and catalytic properties of pillared montmorillonite with aluminum/cerium polyoxycations," *Chemistry of Materials*, vol. 13, no. 6, pp. 2154–2159, 2001.

[125] M. J. Hernando, C. Pesquera, C. Blanco, and F. González, "Increase in thermal stability of the texture in montmorillonites pillared with aluminum/cerium polyoxocations," *Langmuir*, vol. 18, no. 14, pp. 5633–5636, 2002.

[126] G. Fetter, P. Salas, L. A. Velazquez, and P. Bosch, "Ce-Al-pillared clays: synthesis, characterization, and catalytic performance," *Industrial and Engineering Chemistry Research*, vol. 39, no. 6, pp. 1944–1949, 2000.

[127] S. K. Kim and S. K. Ihm, "Effects of Ce addition and Pt precursor on the activity of Pt/Al_2O_3 catalysts for wet oxidation of phenol," *Industrial and Engineering Chemistry Research*, vol. 41, no. 8, pp. 1967–1972, 2002.

[128] K. Al-Malah, M. O. J. Azzam, and N. I. Abu-Lail, "Olive mills effluent (OME) wastewater post-treatment using activated clay," *Separation and Purification Technology*, vol. 20, no. 2-3, pp. 225–234, 2000.

[129] J. Herney-Ramirez, M. A. Vicente, and L. M. Madeira, "Heterogeneous photo-Fenton oxidation with pillared clay-based catalysts for wastewater treatment: a review," *Applied Catalysis B*, vol. 98, no. 1-2, pp. 10–26, 2010.

[130] C. Pulgarin, M. Invernizzi, S. Parra, V. Sarria, R. Polania, and P. Péringer, "Strategy for the coupling of photochemical and biological flow reactors useful in mineralization of biorecalcitrant industrial pollutants," *Catalysis Today*, vol. 54, no. 2-3, pp. 341–352, 1999.

[131] R. Ben Achma, A. Ghorbel, S. Sayadi, A. Dafinov, and F. Medina, "A novel method of copper-exchanged aluminum-pillared clay preparation for olive oil mill wastewater treatment," *Journal of Physics and Chemistry of Solids*, vol. 69, no. 5-6, pp. 1116–1120, 2008.

[132] R. L. Lucier, *The International Political Economy of Coffee: From Juan Valdez to Yank's Diner*, Praeger Publishers, New York, NY, USA, 1988.

[133] FNC, "Federación Nacional de Cafeteros de Colombia. Colombia es café," 2012, http://www.federaciondecafeteros.org/algrano-fnc-es/index.php/comments/colombia_es_cafe.

[134] H. N. Chanakya and A. A. P. De Alwis, "Environmental issues and management in primary coffee processing," *Process Safety and Environmental Protection*, vol. 82, no. 4 B, pp. 291–300, 2004.

[135] J. N. Wintgens and C. H. J. Brando, "Harvesting and green coffee processing," in *Coffee: Growing, Processing, Sustainable Production: A Guidebook for Growers, Processors, Traders, and Researchers*, J. N. Wintgens, Ed., pp. 610–723, Wiley-VCH, Weinheim, Germany, 2009.

[136] G. S. Duarte, A. A. Pereira, and A. Farah, "Chlorogenic acids and other relevant compounds in Brazilian coffees processed by semi-dry and wet post-harvesting methods," *Food Chemistry*, vol. 118, no. 3, pp. 851–855, 2010.

[137] N. Rodríguez-Valencia and D. A. Zambrano-Franco, "Los subproductos del café: fuente de energía renovable," *Avances Técnicos Cenicafé*, no. 393, pp. 1–8, 2010.

[138] J. Field, "Aguas residuales del café," in *Arranque y operación de sistemas de flujo ascedente con mato de lodos—UASB*, pp. H1–H11, Universidad del Valle-CVC, Santiago de Calí, Colombia, 1987.

[139] N. Rodríguez-Valencia, *Estudio de un biosistema integrado para el postratamiento de las aguas residuales del café utilizando macrófitas acuáticas [Ph.D. thesis]*, Universidad Politécnica de Valencia, Valencia, Spain, 2009.

[140] D. A. Zambrano-Franco, N. Rodríguez-Valencia, U. López-Posada, P. A. Orozco-Restrepo, and A. J. Zambrano-Giraldo, "Tratamiento anaerobio de las aguas mieles del café," *Boletin Técnico Cenicafé*, vol. 29, pp. 1–28, 2006.

[141] V. Matuk-Velasco, N. Rodríguez-Valencia, and G. I. Puerta-Quintero, "El impacto biológico de los efluentes del beneficio húmedo de café," *Cenicafé*, vol. 48, no. 4, pp. 234–252, 1997.

[142] R. Bello-Mendoza and M. F. Castillo-Rivera, "Start-up of an anaerobic hybrid (UASB/filter) reactor treating wastewater from a coffee processing plant," *Anaerobe*, vol. 4, no. 5, pp. 219–225, 1998.

[143] F. R. L. Fia, A. T. Matos, A. C. Borges, R. Fia, and P. R. Cecon, "Treatment of wastewater from coffee bean processing in anaerobic fixed bed reactors with different support materials:

performance and kinetic modeling," *Journal of Environmental Management*, vol. 108, pp. 14–21, 2012.

[144] M. Selvamurugan, P. Doraisamy, and M. Maheswari, "An integrated treatment system for coffee processing wastewater using anaerobic and aerobic process," *Ecological Engineering*, vol. 36, no. 12, pp. 1686–1690, 2010.

[145] "Decreto 1594 del 26 de junio de 1984, por el cual se reglamenta parcialmente el Título 1 de la Ley 9 de 1979, así como el Capítulo II del Título VI -Parte III- Libro II y el Título III de la Parte 111 -Libro I-del Decreto—Ley 2811 de 1974 en cuanto a usos del agua y residuos líquidos," Ministerio de Agricultura de Colombia, Bogotá DC, Colombia, 1984.

[146] M. N. Clifford, S. Knight, B. Surucu, and N. Kuhnert, "Characterization by LC-MS^n of four new classes of chlorogenic acids in green coffee beans: dimethoxycinnamoylquinic acids, diferuloylquinic acids, caffeoyl-dimethoxycinnamoylquinic acids, and feruloyl- dimethoxycinnamoylquinic acids," *Journal of Agricultural and Food Chemistry*, vol. 54, no. 6, pp. 1957–1969, 2006.

[147] R. Jaiswal, M. A. Patras, P. J. Eravuchira, and N. Kuhnert, "Profile and characterization of the chlorogenic acids in green Robusta coffee beans by LC-MS^n: identification of seven new classes of compounds," *Journal of Agricultural and Food Chemistry*, vol. 58, no. 15, pp. 8722–8737, 2010.

[148] S. Azabou, W. Najjar, A. Gargoubi, A. Ghorbel, and S. Sayadi, "Catalytic wet peroxide photo-oxidation of phenolic olive oil mill wastewater contaminants. Part II. Degradation and detoxification of low-molecular mass phenolic compounds in model and real effluent," *Applied Catalysis B*, vol. 77, no. 1-2, pp. 166–174, 2007.

[149] S. Parra, J. Olivero, L. Pacheco, and C. Pulgarin, "Structural properties and photoreactivity relationships of substituted phenols in TiO_2 suspensions," *Applied Catalysis B*, vol. 43, no. 3, pp. 293–301, 2003.

[150] J. A. Peres, J. R. Domínguez, and J. Beltran-Heredia, "Reaction of phenolic acids with Fenton-generated hydroxyl radicals: hammett correlation," *Desalination*, vol. 252, no. 1–3, pp. 167–171, 2010.

[151] V. L. Singleton and J. A. Rossi, "Colorimetry of total phenolics with phosphomolybdicphosphotungstic acid reagents," *American Journal of Enology and Viticulture*, vol. 16, no. 3, pp. 144–158, 1965.

[152] V. L. Singleton, R. Orthofer, and R. M. Lamuela-Raventós, "Analysis of total phenols and other oxidation substrates and antioxidants by means of folin-ciocalteu reagent," *Methods in Enzymology*, vol. 299, pp. 152–178, 1998.

[153] T. Zayas Pérez, G. Geissler, and F. Hernandez, "Chemical oxygen demand reduction in coffee wastewater through chemical flocculation and advanced oxidation processes," *Journal of Environmental Sciences*, vol. 19, no. 3, pp. 300–305, 2007.

Hindawi Publishing Corporation
International Journal of Photoenergy
Volume 2012, Article ID 531076, 11 pages
doi:10.1155/2012/531076

Research Article

Photo-Fenton and Fenton Oxidation of Recalcitrant Industrial Wastewater Using Nanoscale Zero-Valent Iron

Henrik Hansson,[1] Fabio Kaczala,[1] Marcia Marques,[1,2] and William Hogland[1]

[1] *School of Natural Sciences, Linnaeus University (LNU), Landgången 3, 392 82 Kalmar, Sweden*
[2] *Department of Sanitary and Environmental Engineering, Rio de Janeiro State University (UERJ), São Francisco Xavier 524, 20551-013 Rio de Janeiro, RJ, Brazil*

Correspondence should be addressed to Marcia Marques, marcia.marques@lnu.se

Received 1 June 2012; Revised 20 August 2012; Accepted 7 September 2012

Academic Editor: Manickavachagam Muruganandham

There is a need for the development of on-site wastewater treatment technologies suitable for "dry-process industries," such as the wood-floor sector. Due to the nature of their activities, these industries generate lower volumes of highly polluted wastewaters after cleaning activities. Advanced oxidation processes such as Fenton and photo-Fenton, are potentially feasible options for treatment of these wastewaters. One of the disadvantages of the Fenton process is the formation of large amounts of ferrous iron sludge, a constraint that might be overcome with the use of nanoscale zero-valent iron (nZVI) powder. Wastewater from a wood-floor industry with initial COD of 4956 mg/L and TOC of 2730 mg/L was treated with dark-Fenton (nZVI/H_2O_2) and photo-Fenton (nZVI/H_2O_2/UV) applying a 2-level full-factorial experimental design. The highest removal of COD and TOC (80% and 60%, resp.) was achieved using photo-Fenton. The supply of the reactants in more than one dose during the reaction time had significant and positive effects on the treatment efficiency. According to the results, Fenton and mostly photo-Fenton are promising treatment options for these highly recalcitrant wastewaters. Future investigations should focus on optimizing treatment processes and assessing toxic effects that residual pollutants and the nZVI might have. The feasibility of combining advanced oxidation processes with biological treatment is also recommended.

1. Introduction

The discharge of industrial wastewaters into either municipal sewerage system or directly into recipient water bodies has raised serious concerns during decades, leading to intensive research and development of on-site treatment technologies for industrial wastewater. However, whereas investigations have been focusing on industrial sectors that have water as an important input to their manufacturing processes, "dry-process industries" such as wood-floor and wood-furniture industries that have no water requirement in their production processes have been neglected [1, 2]. These industries generate wastewaters during cleaning and washing of machinery, surfaces, and floors and regardless of their relatively low volumes these cleaning wastewaters have very high chemical oxygen demand (COD) that varies from 3200 to 50,000 mg L^{-1} and the presence of recalcitrant organic compounds is a limiting factor for biological treatment in conventional centralized treatment plants. Dilution of 50 times or more with drinking water has been a common practice before discharging these wastewaters into the sewage system, which is not a sustainable strategy for the 21st century. The treatment of wastewaters from the timber industry using chemical methods has shown limited efficiency [3]. The use of biological treatment [1] and sorption/filtration processes [2] has also shown limitations when the main purpose is to comply with established standards for discharges into recipient water bodies. Advanced oxidation processes (AOPs) have previously been used to treat complex wastewaters in combinations with biological and/or chemical treatment. These studies have used AOP either after biological treatments to handle the most recalcitrant substances [4, 5] or before with the purpose of reducing toxicity, when the wastewater is too toxic for biological

treatment [6, 7]. The Fenton reaction was first observed by H. J. Fenton in 1894 and is described as the enhanced oxidative power of H_2O_2 when using iron (Fe) as a catalyst under acidic conditions. It was later found that this enhancement was due to the generation of hydroxyl radical ($HO^\bullet$) [8] that is one of the strongest oxidants (E = 2.73 V), and it is nonselective and capable of quickly oxidizing a broad range of organic pollutants [9]. AOPs are based on the generation of these very reactive species, which are the main oxidizing species in the Fenton process [10]. The Fenton's reagent alone or in combination has proven to be an effective way to degrade organic pollutants [11–13] and it has been used for the treatment of a wide variety of industrial wastewaters [14–16]. The Fenton process is a relatively economical method since it requires no additional energy when compared to many other AOPs. Furthermore, both iron and hydrogen peroxide are relatively cheap and safe. In the Fenton process, there is no mass transfer limitation, except during coagulation when high dose of the activator ferrous salt is needed [17]. The Fenton process is well known [18]. Iron (Fe) will in aqueous solution under acidic conditions oxidize to Fe^{2+} [19], which initiates the Fenton reaction:

$$2Fe^0 + 2H_2O \longrightarrow Fe^{2+} + H_2 + 2OH^- \quad (1)$$

The Fenton reaction is characterized by the catalytic decomposition of H_2O_2 as described below [20]:

$$Fe^{2+} + H_2O_2 \longrightarrow Fe^{3+} + OH^- + OH^\bullet \quad (2)$$

The hydroxyl radicals created by the process can be scavenged by excess Fe^{2+} [20]:

$$OH^\bullet + Fe^{2+} \longrightarrow OH^- + Fe^{3+} \quad (3)$$

This conventional Fenton process may be positively assisted by the application of UV-light [20]:

$$Fe^{3+} + H_2O + h\nu \longrightarrow OH^\bullet + Fe^{2+} + H^+ \quad (4)$$

Photo-Fenton oxidation in the presence of short UV light (UV-C, 180–290 nm) [21] gives a faster oxidation as a consequence of the higher quantum yields [12]. When applying UV-C light, H_2O_2 can also be hydrolysed contributing to the $HO^\bullet$ formation [8]. The disadvantages of the Fenton process include (i) the formation of a high concentration of anions in the treated wastewater and (ii) large amounts of ferrous iron sludge [22]. Recent studies have attempted to overcome these drawbacks by applying nZVI together with H_2O_2 for industrial wastewater treatment [19, 23]. This alternative process could overcome the disadvantages associated with Fe^{2+}-based AOPs by using the solid form of iron instead of Fe^{2+} as iron salts. During the last decade there has been a widespread development of nanomaterials for both industrial and domestic use. When the dimensions of a piece of solid material become very small, its physical and chemical properties become very different from those of the same material in larger bulk form [24]. Nanoparticles as a subset of nanomaterial is currently defined by consensus as single particles with a diameter < 100 nm [24]. The small particle size increases the proportion of atoms located at the surface increasing the possibility for the atoms to adsorb, interact, and react with other atoms and molecules [25]. The particles have also the capacity to remain in suspension [25] and, hence, aqueous slurries containing nZVI can easily be pumped and injected where needed. The nZVI has been mostly used for groundwater remediation and treatment of specific pollutants [25]. Additionally, the treatment of industrial wastewater using nZVI in Fenton and other processes has also been reported recently [26, 27].

Table 1: Wastewater characterization ($n = 3$).

Parameter	Value	Mixture*
pH	2.3 ± 0.5	2.2
Conductivity (mS/cm)	6.3 ± 0.6	5.9
COD (mg/L)	5102 ± 513	4956
TOC (mg/L)	2,801 ± 287	2730

* Wastewater obtained from a mixture of these three characterized samples.

The main objective of this investigation was two-folded: (i) to verify the technical feasibility of treating wastewaters generated in the wood-floor industry sector using Fenton with nZVI compared to photo-Fenton with nZVI and (ii) to verify the effects of the selected variables (H_2O_2/COD ratio, H_2O_2/nZVI ratio and dosing mode) on the treatment efficiency.

2. Materials and Methods

2.1. Wastewater Samples. The wastewater used in the current investigation was a mixture of different streams of real industrial wastewater generated during cleaning procedures in a wood-floor industry in Nybro, Sweden. The quality and quantity of these wastewaters vary in time, as they are manually and intermittently generated as a consequence of different manufacturing processes such as wood gluing, wood filling, cleaning of floors, blade sharpening, and others. These wastewaters are characterized by the presence of formaldehyde, nitrogen [1], metals [28] detergents, and, phenols [29]. At the factory, the wastewater mixture is kept in a full-scale on-site settling/sedimentation tank from where the samples for lab studies were taken. Wastewater samples were obtained at three different occasions and transported to the laboratory where they were stored at −20°C.

In order to obtain an average composition of the wastewater, a mixture of similar proportion of the three samples stored in the lab (1 : 1 : 1) was prepared. This mixture was then filtered with a Munktell OOR grade filter paper with a pore size >10 μm to homogenize the wastewater. The characteristics of the wastewater used in the experiments are shown in Table 1. Proxy indicators such as TOC and COD were considered suitable to monitor treatability studies of this wastewater, since it is well known that these variables as well as the ratio between them are appropriate to evaluate the efficiency of treatment options [30, 31].

Table 2: Variable levels applied in the 2-level factorial design.

Variables	Symbol	−1	0	+1
H_2O_2 : COD	χ_1	2 : 1	3.5 : 1	5 : 1
H_2O_2 : nZVI	χ_2	2 : 1	8.5 : 1	15 : 1
Dosing mode	χ_3	1	2	3

Notations: +1(high level); 0 (centre point); −1 (lower level).

2.2. Experimental Design. To have a better understanding on which independent variables play important roles on the treatment efficiency measured as percentage reduction of COD and TOC (dependent variables), it was applied a two-level full-factorial design with triplicates of the central points with the following selected independent variables or factors: (1) H_2O_2 : COD ratio; (2) H_2O_2 : nZVI ratio and; (3) the dosing mode. By dosing mode one means the procedure of adding equal aliquots of the oxidizing agent (H_2O_2) and the catalyst (nZVI) at different times throughout the experiment or adding it at once. The levels used for each factor in this investigation (Table 2) were selected according to the literature.

The AOS (average oxidation state) value was calculated using the COD and TOC data obtained by the above-described experimental design. The AOS value can attain a value between +4, for CO_2, and −4, for CH_4, the most oxidized and the most reduced state of carbon (C). The AOS value is a rough parameter to estimate the degree of oxidation in a mixed wastewater and was calculated according to the following [31]:

$$\mathrm{AOS} = \frac{4(\mathrm{TOC} - \mathrm{COD})}{\mathrm{TOC}}, \tag{5}$$

where COD and TOC values are expressed in mol O_2/L and C/L, respectively.

The statistical software Minitab 16 was used to setup the full factorial design. For statistical analysis Minitab 16 and GraphPad Prism 5 were used.

2.3. Experimental Setup. Two variations of Fenton treatment were investigated: dark-Fenton (nZVI/H_2O_2) and photo-Fenton (nZVI/H_2O_2/UV), using, in both cases, commercial nZVI. The commercial nZVI powder consisted of Fe^0 surface stabilized nanoparticles coated with a thin inorganic surface layer, which makes it possible long-term storage as the manufacturer delivers it. The material had particle sizes ranging between 20–100 nm with an average of 50 nm according to the manufacturer (Nano Iron, s.r.o., Czech Republic). The photo-Fenton studies were carried out in a glass-jacket immersion-type UV-reactor (UV-Consulting Peschl Mainz, Germany) with a volume of 0.7 L (Figure 1). The distance between the UV-lamp and the liquid phase was 15 mm. The reactor was cooled down with distilled water to keep the liquid phase at room temperature of around 22°C. The UV-light was emitted at a 150 W in wavelengths ranging between 250 and 580 nm with the highest peaks at 310, 360, 400, 440, 550, and 580 nm.

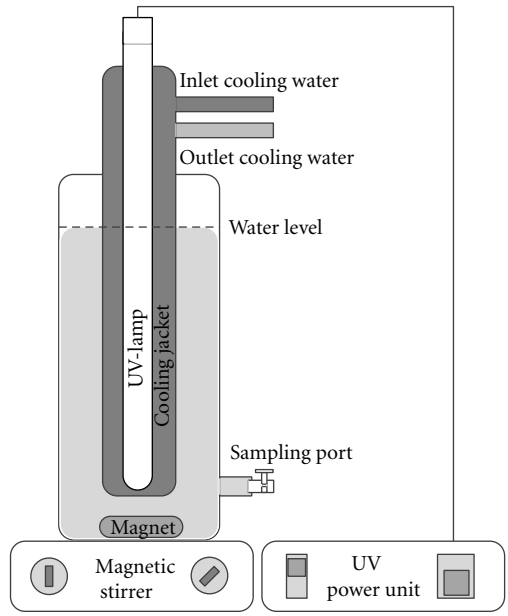

Figure 1: Schematic view of the UV-reactor used in the photo-Fenton experiments.

The dark-Fenton studies were conducted in 1 L glass beakers. The difference between standard glass beaker and the UV-reactor with the light in the off-mode was considered negligible according to the literature [32, 33]. Air purging was not considered in this study in order to keep treatment operational costs as low as possible. All glassware was carefully washed before each experiment.

2.4. Experimental Procedure. All runs were conducted with a volume of 0.5 L of wastewater that was agitated during 120 min by a magnetic stirrer at 400 rpm. The pH was adjusted at the beginning of each run to be kept between 2.95 and 3.05. Since this pH range has been reported to be the optimum for Fenton oxidation [13, 34], every 15 min throughout the 120 min of reaction time the pH was readjusted if needed. All pH adjustments were done with analytical grade sodium hydroxide (NaOH) and hydrochloric acid (HCl). The total amounts of nZVI and H_2O_2 were added either at the beginning of each run or in similar aliquots, at different time intervals (Table 3). The nZVI was added as slurry formed by 1 : 4 nZVI powder and water, after being stirred in a high speed sheerer for 5 min, according to the manufacturer's instructions.

During the photo-Fenton treatment, the wastewater was exposed to UV-light during the treatment time of 120 min. After both Fenton and photo-Fenton treatments of 120 min, the pH of the wastewater was adjusted to 6.5 and agitated for 5 min at 400 rpm to quench the Fenton reaction [35]. In a sequence, 5 min after the agitation was stopped, the pH was raised to 8.5 to form iron precipitates [35]. The supernatant was then heated to 50°C and slowly shaken in a water bath for 30 min to expel any remaining H_2O_2. The water was then

Table 3: Dosing modes (the way the H_2O_2 and nZVI were added during the runs).

Sample number*	Total amount of H_2O_2 (g/L)	Total amount of nZVI (g/L)	Number of equal doses	0 min		40 min		60 min		80 min		120 min
				H_2O_2 (g/L)	nZVI (g/L)	H_2O_2 (g/L)	nZVI(g/L)	H_2O_2 (g/L)	nZVI (g/L)	H_2O_2 (g/L)	nZVI (g/L)	
1.1; 2.1; 3.1; 4.1	24,8	1,7	1	24,8	1,7	—	—	—	—	—	—	
1.2; 2.2; 3.2; 4.2	9,9	0,7	1	9,9	0,7	—	—	—	—	—	—	
1.3; 2.3; 3.3; 4.3	17,3	2,0	2	8,7	1,0	—	—	8,7	1,0	—	—	
1.4; 2.4; 3.4; 4.4	17,3	2,0	2	8,7	1,0	—	—	8,7	1,0	—	—	
1.5; 2.5; 3.5; 4.5	9,9	0,7	3	3,3	0,2	3,3	0,2	—	—	3,3	0,2	
1.6; 2.6; 3.6; 4.6	9,9	5,0	3	3,3	1,7	3,3	1,7	—	—	3,3	1,7	Full treatment time
1.7; 2.7; 3,7; 4.7	17,3	2,0	2	8,7	1,0	—	—	8,7	1,0	—	—	
1.8; 2.8; 3.8; 4.8	24,8	1,7	3	8,3	0,6	8,3	0,6	—	—	8,3	0,6	
1.9; 2.9; 3.9; 4.9	24,8	12,4	3	8,3	4,1	8,3	4,1	—	—	8,3	4,1	
1.10; 2.10; 3.10; 4.10	24,8	12,4	1	24,8	12,4	—	—	—	—	—	—	
1.11; 2.11; 3.11; 4.11	9,9	5,0	1	9,9	5,0	—	—	—	—	—	—	

* Treatments from 1.1 to 1.11: dark-Fenton; from 2.1 to 2.11: Photo-Fenton.

Table 4: COD and TOC reductions (%) with dark-Fenton and photo-Fenton experiments.

Coded variables			Dark-Fenton			Photo-Fenton		
χ_1	χ_2	χ_3	Run	% COD reduction	% TOC reduction	Run	% COD reduction	% TOC reduction
+1	+1	−1	1.1	42.6	21.4	2.1	78.4	59.4
−1	+1	−1	1.2	34.6	17.3	2.2	70.6	50.0
0	0	0	1.3	42.0	21.4	2.3	80.5	57.8
0	0	0	1.4	39.3	19.9	2.4	78.2	56.7
−1	+1	+1	1.5	35.6	19.0	2.5	77.6	56.0
−1	−1	+1	1.6	35.1	18.9	2.6	76.1	53.9
0	0	0	1.7	38.4	24.2	2.7	61.3	61.7
+1	+1	+1	1.8	43.5	23.0	2.8	60.3	61.7
+1	−1	+1	1.9	77.5	50.3	2.9	81.6	61.6
+1	−1	−1	1.10	49.2	34.9	2.10	78.5	58.0
−1	−1	−1	1.11	38.3	24.7	2.11	70.9	53.6

centrifuged at 614 g for 15 min. After this, the supernatant was separated and all samples were frozen before analysis.

2.5. Analytical Methods. COD and TOC in the wastewater samples were analysed spectrophotometrically using Hach Lange cuvette tests (Hach Lange, Dusseldorf) and measured with a Hach Lange DR 5000 spectrophotometer (Hach Lange, Dusseldorf). The pH and conductivity were measured with an HQ40d multiparameter meter.

3. Results and Discussion

3.1. Comparison between Fenton and Photo-Fenton

3.1.1. nZVI Fenton Treatment. The treatments based on dark-Fenton (Table 4 and Figures 2(a) and 2(b)) showed large variation in the responses measured as the COD and TOC removal percentages. As observed in Table 4, the removal of COD and TOC varied from 34% to 77% and from 17% to 50%, respectively, depending on the run indicating that the ranges of H_2O_2 : COD; H_2O_2 : nZVI and dosing modes combined in different ways have played an important role on the COD and TOC removal. There was a significant difference between COD and TOC reduction % within the dark-Fenton and photo-Fenton processes (paired t-test, $P < 0.05$) as illustrated in Table 4.

The highest reductions for both COD and TOC were achieved with a setup using high H_2O_2 : COD ratios and low H_2O_2 : nZVI ratio (run 1.9 in Table 4 and 9 in Figure 2(a)), indicating that higher concentrations of the oxidizing agent (H_2O_2) and the catalyst were able to oxidize a higher amount of COD and TOC, despite the fact that high concentrations of nZVI will possibly scavenge hydroxyl radicals. The stoichiometric ratio for the reduction of COD by H_2O_2 is 2.125 which is calculated assuming the complete oxidation of COD [36]:

$$\begin{aligned} 1\,\text{g COD} &= 1\,\text{g } O_2 = 0.03125\,\text{mol } O_2 \\ &= 0.0625\,\text{mol } H_2O_2 = 2.125\,\text{g } H_2O_2, \end{aligned} \quad (6)$$

(see [36]).

The results have shown that the amount of H_2O_2 to achieve the best treatment efficiency was twice as much the amounts stoichiometrically required. However such occurrences can be due to several factors that need to be further investigated. An important aspect regarding the Fenton treatment is the reduction of Fe^{3+} to Fe^{2+} making crucial the presence of reaction intermediates able to reduce Fe^{3+} and regenerate the catalyst. However, there are reaction intermediates that instead of reducing the Fe^{3+} remove it from the Fe^{2+}/Fe^{3+} cycle, due to the generation of iron complexes, delaying and/or inhibiting the oxidation process [18]. Regardless the use of higher amounts of H_2O_2 in comparison to the stoichiometric need, the H_2O_2 : COD ratio of 5 : 1 was in a range similar to that reported as being effective in previous studies [14, 18]. On the other hand the H_2O_2 : nZVI ratio of 2 : 1 was lower than the values found in literature [12, 18, 37].

When analysing the amount of oxidizing agent H_2O_2 per unit of COD removed (g H_2O_2/g COD removed) used in different treatments in Figure 2(b), other treatments can be considered economically more feasible (runs 1.2, 1.5, 1.6, and 1.11 in Table 4; respectively 2, 5, 6, and 11 in Figure 2(b)). But run 1.9 was much more efficient in terms of COD removal and it was not considerably worse than the others above mentioned regarding g H_2O_2/g COD removed.

3.1.2. nZVI Photo-Fenton Treatment. The results regarding COD and TOC removals with photo-Fenton have shown that the addition of the UV energy has significantly increased the treatment efficiency compared to dark-Fenton (paired t-test, $P < 0.05$) (Figures 3(a) and 3(b)). Furthermore, it was observed that during the photo-Fenton process, the reductions of COD and TOC were more homogenous in comparison to those observed for the dark-Fenton treatment (Table 4; Figures 2(c) and 2(d)).

The increase of TOC reduction was significantly higher than the increase of COD reduction by photo-Fenton (Figure 3(c)). A significant difference was observed between the reductions (in %) of COD and TOC with photo-Fenton treatment (paired t-test, $P < 0.05$).

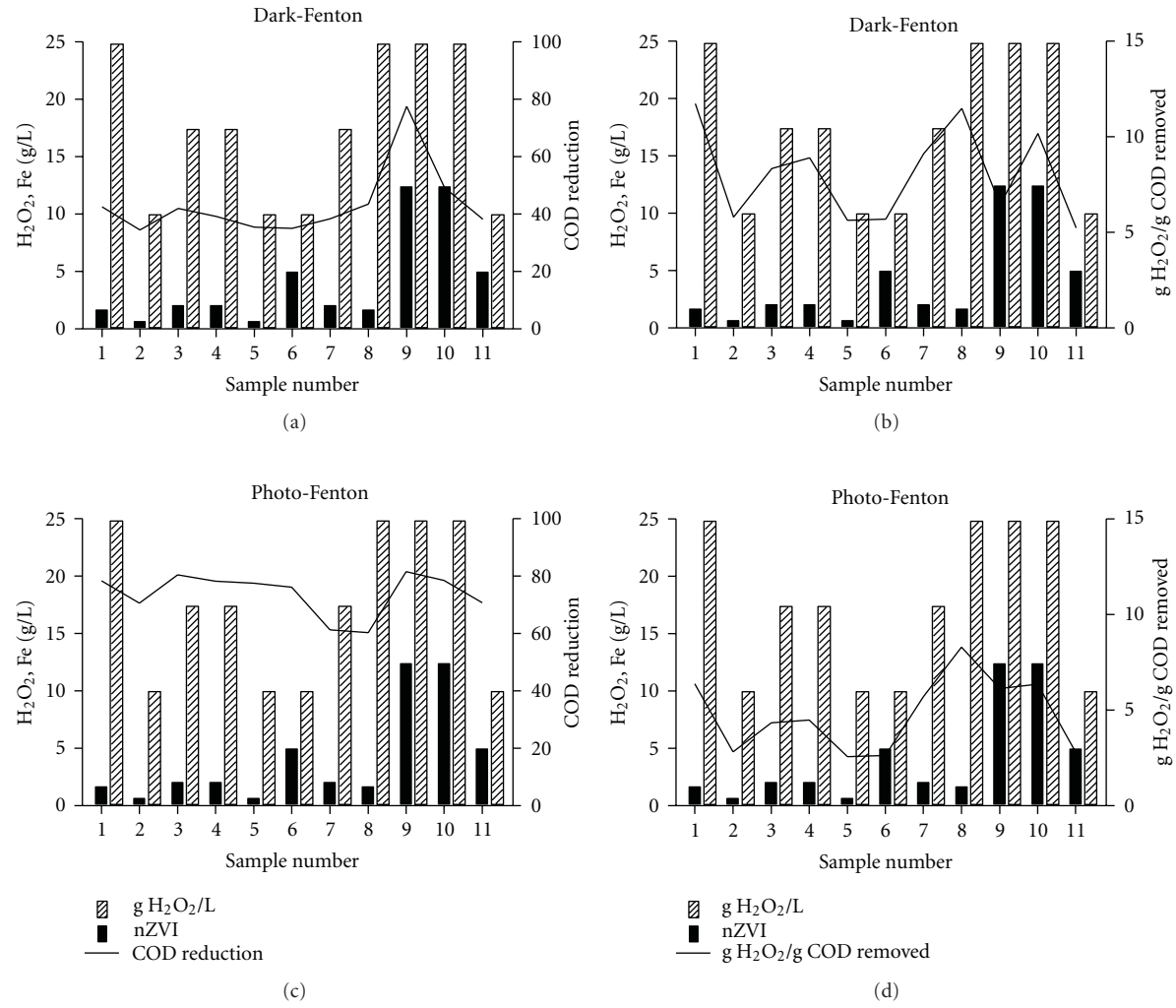

Figure 2: Results from dark-Fenton (a) and (b) and photo-Fenton (c) and (d) experiments using nZVI in 11 runs each. (a) and (c) Amounts of reagents (g/L) and COD removal (%); (b) and (d) amounts of reagents (g/L) and g H_2O_2 consumed per g COD removed.

Run 2.9 in Table 4 (equivalent to 9 in Figure 2(c)) promoted the highest removal of COD and TOC in %. However, when taking into account the amount of oxidizing agent used per amount of COD removed (g H_2O_2/g COD removed), another treatment was economically more effective (run 2.5 in Table 4, equivalent to run 5 in Figure 2(d)). In Figure 2, both runs 5 and 6 performed satisfactorily and with low amounts of H_2O_2 promoted COD removals of around 80%, indicating the crucial role played by the UV energy in terms of treatment efficiency. The efficiency in using the UV in combination with the Fenton reaction is confirmed in Figures 2(c) and 2(d), which illustrate that despite using a H_2O_2 : COD ratio as high as 5 : 1 in run 2.9 (Table 4), only a small increase in COD removal in % was observed compared to runs 2.5 and 2.6 (Table 4) where a H_2O_2 : COD ratio of only 2 : 1 was used. COD and TOC reductions over 75% and 55%, respectively, were achieved in runs 2.5 and 2.6 (Table 4), respectively, which corresponded to less than half of the amount of H_2O_2 applied in run 2.9 (COD and TOC reductions of 82% and 61%, resp.). Similar results were reported [38] where an increase of H_2O_2 : COD ratio above the range of 1–3 did not improve the COD reduction related to the presence of antibiotics in the water. Furthermore, the use of high concentrations of nZVI in runs 2.6 and 2.9 (H_2O_2 : nZVI of 2 : 1, Table 4) did not result in a increased efficiency, in comparison to run 2.5 (H_2O_2 : nZVI of 15 : 1). As discussed previously, one important event for the Fenton process is the reduction of Fe^{3+} to Fe^{2+} and such reduction is enhanced when using photo-Fenton [20]. This is likely one of the reasons for the much larger reductions in general achieved with photo-Fenton, being another reason for the fact that significantly lower concentrations of nZVI can be used. It is worth noting that in all these setups the reactants were added in three doses along the treatment, reducing the risk for scavenging between the reactants. Figure 2(d) shows that when 94% less nZVI was used, only 6% less COD and TOC reductions were observed in the presence of UV. Such a large reduction of iron reduces the costs with this catalyst and the amount of spent iron that needs to be handled (see the discussion Cost Effectiveness in this paper).

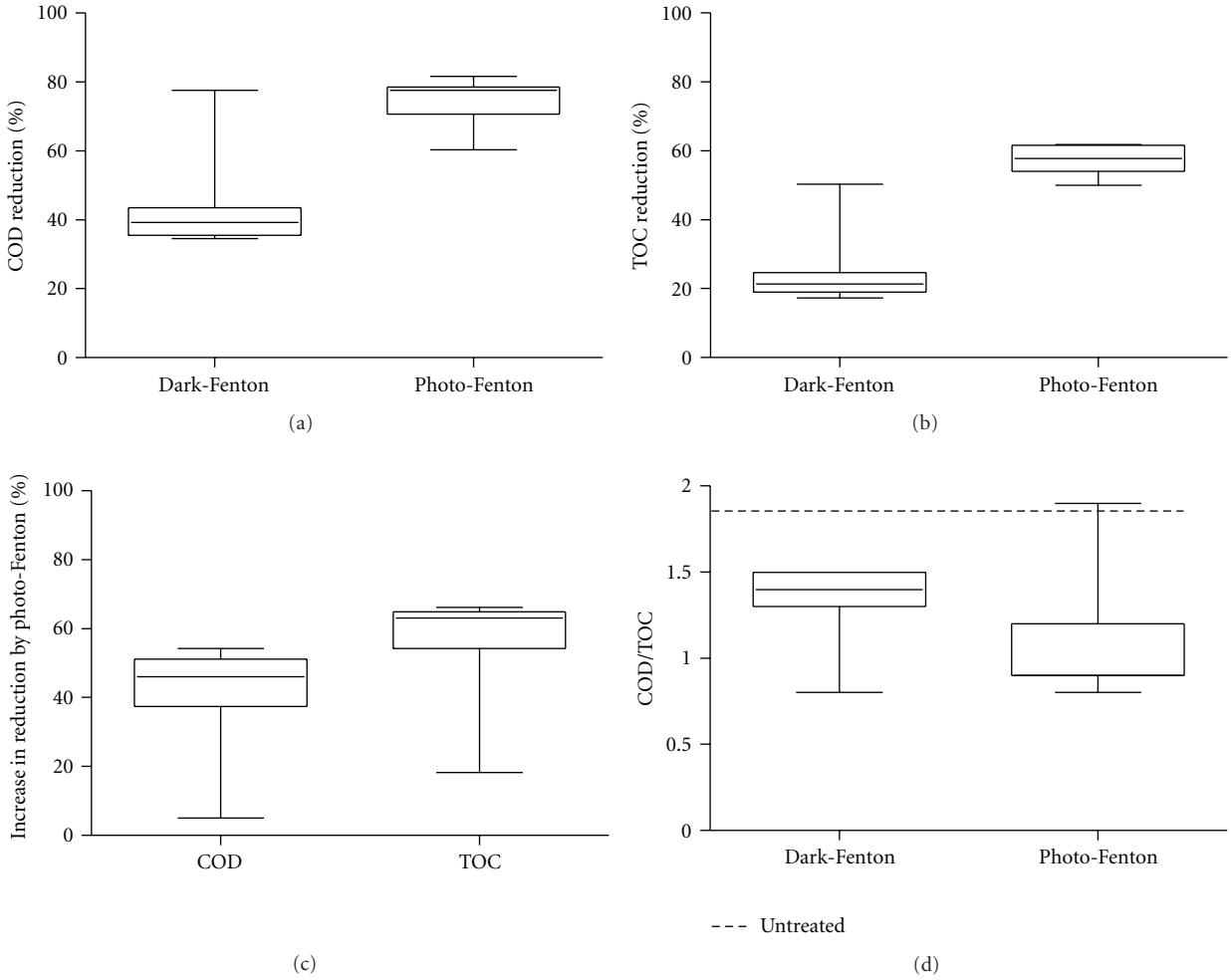

Figure 3: Boxplots built up with data from COD and TOC values obtained with dark-Fenton and photo-Fenton treatments. (a) COD reduction (in %) with both treatments; (b) TOC reduction (in %) with both treatments; (c) increase (in %) in the percentage of COD and TOC reduction by photo-Fenton compared to dark-Fenton; (d) changes in COD/TOC ratio due to different treatments.

3.1.3. Oxidation and Mineralisation. The results have shown that the COD and TOC values after both dark- and photo-Fenton treatments were considerably different as indicated by the COD/TOC ratios (Figure 3(d)). There was no significant difference in COD/TOC ratios when comparing photo-Fenton and dark-Fenton; however, COD/TOC ratios decreased after treatment. As illustrated in Figure 4, whereas negative correlations were found between COD and TOC reduction (in %) and COD/TOC ratio (R^2 = 0.86 and 0.62, resp.) for the dark-Fenton experiments, only COD removal (in %) was correlated with COD/TOC ratio (R^2 = 0.92) in the photo-Fenton investigation. The correlation between TOC removal (in %) and COD/TOC for photo-Fenton had coefficient of determination as low as R^2 = 0.18. These results suggest that the remaining organic compounds measured as TOC were very recalcitrant and difficult to degrade as indicated by very low COD/TOC ratios after these treatments, and even with higher reductions of COD, the TOC value was not lowered. Previous studies have reported that a COD/TOC ratio below 1.3 indicates that that residual organic carbon was mostly related to refractory organic compounds [16].

Unlike the COD value that is related to organically-bound and inorganic constituents [39], TOC is independent of the oxidation state of the organic matter and only measures organic carbon converted to CO_2 [40], suggesting that changes observed in the COD/TOC ratio can be related to the degree of changes in the structure of the organic compounds after oxidation. Figure 5 shows the AOS values before and after the treatment with dark-Fenton and photo-Fenton. It was found that by the end of the photo-Fenton treatment, the oxidation states were higher in comparison to those after the dark-Fenton treatment, confirming the stronger oxidation (higher reduction efficiency for COD and TOC) with photo-Fenton and suggesting the yield of different end products. Regarding the oxidation states in the dark-Fenton, the AOS value in the run 1.9 was considerably higher in comparison to the raw wastewater and to other dark-Fenton treatments reaching AOS value approximately as high as those obtained after the photo-Fenton process.

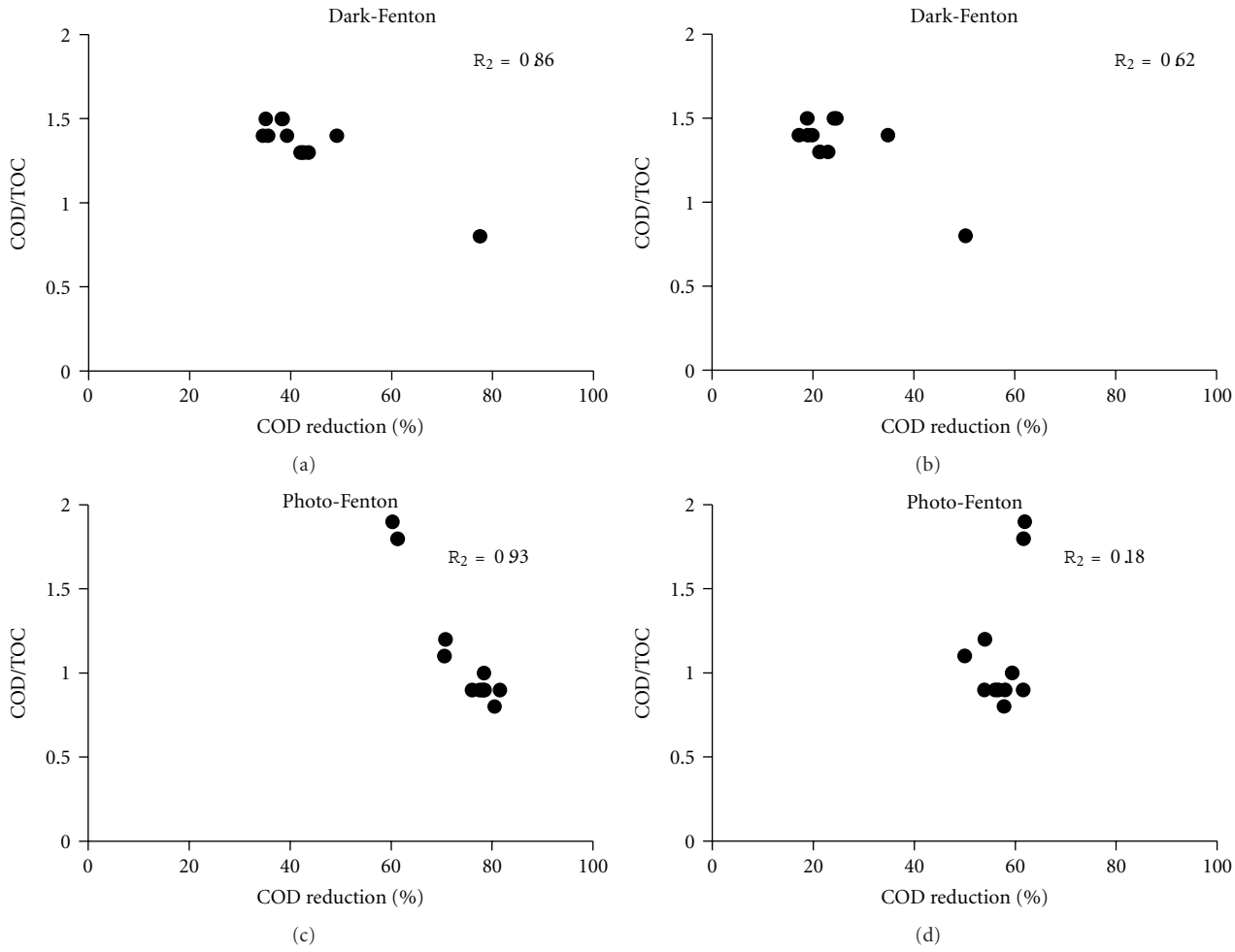

Figure 4: Correlation between COD and TOC reductions (in %) and COD/TOC ratios obtained with different dark- and photo-Fenton treatment setups.

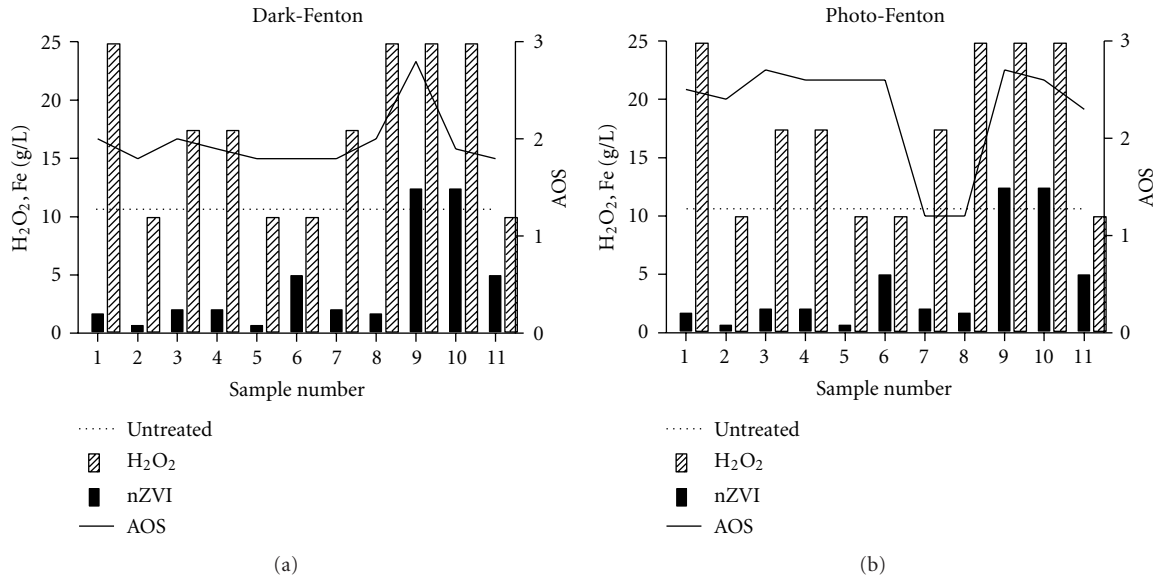

Figure 5: Amounts of reagents (g/L) and the AOS values obtained after each run/treatment.

Table 5: Results of statistical analyses of independent variables.

	Dark-Fenton				Photo-Fenton			
	COD reduction		TOC reduction		COD reduction		TOC reduction	
Term	Effect	P	Effect	P	Effect	P	Effect	P
Constant		0.00		0.00		0.00		0
H_2O_2 : COD Ratio	17.3	0.01	12.4	0.02	0.9	0.91	6.8	0.07
H_2O_2 : nZVI Ratio	−11.0	0.02	−12.0	0.02	−5.0	0.57	0.0	0.99
Doses	6.8	0.04	3.3	0.12	−0.7	0.94	3.0	0.24
H_2O_2 : COD Ratio ∗ H_2O_2 : nZVI Ratio	−9.3	0.02	−8.4	0.03	−5.7	0.52	0.9	0.68
H_2O_2 : COD Ratio ∗ Dose	7.8	0.03	5.2	0.08	−6.8	0.46	0.0	0.99
H_2O_2 : nZVI Ratio ∗ Dose	−5.8	0.05	−1.6	0.40	−4.9	0.58	1.2	0.57
H_2O_2 : COD Ratio ∗ H_2O_2 : nZVI Ratio∗Dose	−8.0	0.02	−5.3	0.07	−5.7	0.52	−1.8	0.43
Ct Pt		0.07		0.01		0.91		0.39

According to Figure 5, with the exception of runs 2.7 and 2.8, AOS values after the photo-Fenton treatments were approximately +3 in all remaining runs suggesting that the oxidised chemical nature of most of the photo-Fenton treatments reached a stable AOS value and even though the treatment was to be continued, intermediates with higher oxidation state would not be formed. At the moment that AOS stabilizes, the chemical treatment is only mineralizing organic contaminants, but with no partial oxidation [41]. This together with the fact that the difference between the COD and TOC after treatment was considerably reduced by the photo-Fenton treatment (paired t-test, $P < 0.05$) indicates that a more complete reduction of the organic material was achieved when applying the photo-Fenton process. An increase in AOS during the treatment as observed in the current study, particularly for the photo-Fenton treatments, has been related to an increase in biodegradability [41] and reduction of toxicity [38].

This was confirmed by the fact that the reduction (in %) obtained with photo-Fenton is greater for TOC than for COD (paired t-test, $P < 0.05$), (Figure 3(c)). UV irradiation might have been responsible, for instance, for breaking down large aromatic molecules into aliphatic carbon chains, besides its effect on recycling Fe^{3+} back to Fe^{2+} [20].

3.1.4. Cost Effectiveness. Even though economic feasibility was not the focus of this investigation, one can mention that the main costs involved in the studied processes are related to the nZVI, the oxidizing agent H_2O_2, and the energy consumption of the UV-lamp. Photo-Fenton is reasonably more expensive than dark-Fenton treatment due to the use of a UV-lamp. However, the results have shown that when considering the overall treatment efficiency of both Fenton and photo-Fenton, the additional costs related to the UV-lamp could be compensated by the less amounts of nZVI to achieve high COD and TOC reduction %. Furthermore, the use of UV energy has brought advantages since it widened the range of reactant concentrations that could be used and still achieve very satisfactory treatment performances, making reasonable to state that is the less the amount of reactants, the more economically feasible the treatment becomes. Such advantage becomes very important in a full scale plant, where the concentration of pollutants in the raw wastewater can vary, which would require the use of different concentrations of reactants. A clear example is the run 2.5 (Table 4), which had the most satisfactory performance observed with the photo-Fenton treatment. In run 2.5 with the lowest reactant concentrations, COD and TOC reductions of 78% and 56%, respectively, were achieved, making this the most economically feasible option in this study.

3.2. Effect of Independent Variables. The effects of the independent variables (H_2O_2 : COD; H_2O_2 : nZVI and dosing mode) and the interaction among them on the COD and TOC removal (in %) were obtained based on the data from the full-factorial design as shown in Table 5. Whereas all factors and respective two-way and three-way interactions had significant effects on the COD and TOC removal efficiency with dark-Fenton process ($P < 0.05$), no significance was found in the case of photo-Fenton (Table 5). Reasonably, H_2O_2 : COD and H_2O_2 : nZVI ratios were the factors that played the most important roles considering dark-Fenton treatment. Reasonably, negative values were obtained for the effects caused by the H_2O_2 : nZVI ratios on COD and TOC reduction in % with dark-Fenton, since the lower the ratio is, the higher the treatment efficiency will be as previously discussed. The results have shown that by reducing the H_2O_2 : nZVI ratio from 15 : 1 down to 2 : 1, the reductions (in %) of COD and TOC could be increased by 11% and 12%, respectively. The significant effect of the dosing mode on both COD and TOC reductions suggests that when large amounts of reactants are added at once, the treatment performance was not increased due to scavenging [37, 42]. On the other hand, by splitting the doses of the reactants into several steps, scavenging was avoided, an effect that has been described only very few previous studies [42, 43]. The results have shown that the studied factors and levels applied did not play any significant role in the case of photo-Fenton experiments. These results suggest that the long UV-exposure time has eliminated large differences in the results or by combining chemical oxidation and UV irradiation other factors might be involved.

4. Conclusions

The following conclusions can be withdrawn from this investigation:

a. COD and TOC can effectively be reduced by at least 80% and 60%, respectively, from recalcitrant industrial wastewater from the wood industry using photo-Fenton;

b. the most effective treatment setup for dark-Fenton was achieved with H_2O_2 : COD ratio of 5 : 1, H_2O_2 : nZVI ratio of 2 : 1 and with a dose mode that supplies the reactants in 3 equal aliquots added at equal time intervals;

c. the most effective treatment setup for photo-Fenton was obtained with H_2O_2 : COD ratio of 5 : 1, H_2O_2 : nZVI ratio of 2 : 1, supplying the reactants in 3 equal aliquots added at equal time intervals; however, treatments close to the stoichiometry value (2.125) preformed almost as good;

d. there was a significant increase in the mineralization when combining UV with Fenton (photo-Fenton).

Acknowledgments

The financial support to the research project from the Swedish Knowledge Foundation (KK-Stiftelsen), the European Regional Development Fund, and the industry AB Gustaf Kähr is acknowledged.

References

[1] F. Kaczala, M. Marques, and W. Hogland, "Biotreatability of wastewater generated during machinery washing in a wood-based industry: COD, formaldehyde and nitrogen removal," *Bioresource Technology*, vol. 101, no. 23, pp. 8975–8983, 2010.

[2] S. Laohaprapanon, M. Marques, and W. Hogland, "Removal of organic pollutants from wastewater using wood fly ash as a low-cost sorbent," *Clean*, vol. 38, no. 11, pp. 1055–1061, 2010.

[3] M. Krzemieniewski, M. Debowski, A. Dobrzynska, and M. Zielinski, "Chemical oxygen demand reduction of various wastewater types using magnetic field-assisted fenton reaction," *Water Environment Research*, vol. 76, no. 4, pp. 301–309, 2004.

[4] A. Kyriacou, K. E. Lasaridi, M. Kotsou, C. Balis, and G. Pilidis, "Combined bioremediation and advanced oxidation of green table olive processing wastewater," *Process Biochemistry*, vol. 40, no. 3-4, pp. 1401–1408, 2005.

[5] D. Suryaman, K. Hasegawa, and S. Kagaya, "Combined biological and photocatalytic treatment for the mineralization of phenol in water," *Chemosphere*, vol. 65, no. 11, pp. 2502–2506, 2006.

[6] I. Oller, S. Malato, J. A. Sánchez-Pérez, M. I. Maldonado, and R. Gassó, "Detoxification of wastewater containing five common pesticides by solar AOPs-biological coupled system," *Catalysis Today*, vol. 129, no. 1-2, pp. 69–78, 2007.

[7] W. K. Lafi, B. Shannak, M. Al-Shannag, Z. Al-Anber, and M. Al-Hasan, "Treatment of olive mill wastewater by combined advanced oxidation and biodegradation," *Separation and Purification Technology*, vol. 70, no. 2, pp. 141–146, 2009.

[8] O. Tunay et al., *Chemical Oxidation Applications for Industrial Wastewaters*, IWA, 2010.

[9] F. Torrades, S. Saiz, and J. A. García-Hortal, "Using central composite experimental design to optimize the degradation of black liquor by Fenton reagent," *Desalination*, vol. 268, no. 1–3, pp. 97–102, 2011.

[10] K. Choi and W. Lee, "Enhanced degradation of trichloroethylene in nano-scale zero-valent iron Fenton system with Cu(II)," *Journal of Hazardous Materials*, vol. 211-212, pp. 146–153, 2012.

[11] M. I. Badawy, M. Y. Ghaly, and T. A. Gad-Allah, "Advanced oxidation processes for the removal of organophosphorus pesticides from wastewater," *Desalination*, vol. 194, no. 1–3, pp. 166–175, 2006.

[12] I. Arslan-Alaton Idil, A. B. Yalabik, and T. Olmez-Hanci, "Development of experimental design models to predict Photo-Fenton oxidation of a commercially important naphthalene sulfonate and its organic carbon content," *Chemical Engineering Journal*, vol. 165, no. 2, pp. 597–606, 2010.

[13] K. V. Padoley, S. N. Mudliar, S. K. Banerjee, S. C. Deshmukh, and R. A. Pandey, "Fenton oxidation: a pretreatment option for improved biological treatment of pyridine and 3-cyanopyridine plant wastewater," *Chemical Engineering Journal*, vol. 166, no. 1, pp. 1–9, 2011.

[14] D. Hermosilla, N. Merayo, R. Ordóñez, and A. Blanco, "Optimization of conventional Fenton and ultraviolet-assisted oxidation processes for the treatment of reverse osmosis retentate from a paper mill," *Waste Management*, vol. 32, no. 6, pp. 1236–1243, 2012.

[15] P. Bautista, A. F. Mohedano, M. A. Gilarranz, J. A. Casas, and J. J. Rodriguez, "Application of Fenton oxidation to cosmetic wastewaters treatment," *Journal of Hazardous Materials*, vol. 143, no. 1-2, pp. 128–134, 2007.

[16] A. M. F. M. Guedes, L. M. P. Madeira, R. A. R. Boaventura, and C. A. V. Costa, "Fenton oxidation of cork cooking wastewater—overall kinetic analysis," *Water Research*, vol. 37, no. 13, pp. 3061–3069, 2003.

[17] M. Umar, H. A. Aziz, and M. S. Yusoff, "Trends in the use of Fenton, electro-Fenton and photo-Fenton for the treatment of landfill leachate," *Waste Management*, vol. 30, no. 11, pp. 2113–2121, 2010.

[18] P. Bautista, A. F. Mohedano, J. A. Casas, J. A. Zazo, and J. J. Rodriguez, "An overview of the application of Fenton oxidation to industrial wastewaters treatment," *Journal of Chemical Technology and Biotechnology*, vol. 83, no. 10, pp. 1323–1338, 2008.

[19] W. Z. Tang and R. Z. Chen, "Decolorization kinetics and mechanisms of commercial dyes by H_2O_2/iron powder system," *Chemosphere*, vol. 32, no. 5, pp. 947–958, 1996.

[20] M. Tamimi, S. Qourzal, N. Barka, A. Assabbane, and Y. Ait-Ichou, "Methomyl degradation in aqueous solutions by Fenton's reagent and the photo-Fenton system," *Separation and Purification Technology*, vol. 61, no. 1, pp. 103–108, 2008.

[21] I. Arslan and I. A. Balcioglu, "Advanced oxidation of raw and biotreated textile industry wastewater with O3, H_2O_2/UV-C and their sequential application," *Journal of Chemical Technology & Biotechnology*, vol. 76, no. 1, pp. 53–60, 2001.

[22] B.-H. Moon, Y.-B. Park, and K.-H. Park, "Fenton oxidation of Orange II by pre-reduction using nanoscale zero-valent iron," *Desalination*, vol. 268, no. 1–3, pp. 249–252, 2011.

[23] M. Barreto-Rodrigues, F. T. Silva, and T. C. B. Paiva, "Combined zero-valent iron and fenton processes for the treatment of Brazilian TNT industry wastewater," *Journal of Hazardous Materials*, vol. 165, no. 1–3, pp. 1224–1228, 2009.

[24] P. J. A. Borm, D. Robbins, S. Haubold et al., "The potential risks of nanomaterials: a review carried out for ECETOC," *Particle and Fibre Toxicology*, vol. 3, no. 1, article 11, 2006.

[25] R. A. Crane and T. B. Scott, "Nanoscale zero-valent iron: future prospects for an emerging water treatment technology," *Journal of Hazardous Materials*, vol. 211-212, pp. 112–125, 2012.

[26] S. Jagadevan, M. Jayamurthy, P. Dobson, and I. P. Thompson, "A novel hybrid nano zerovalent iron initiated oxidation—biological degradation approach for remediation of recalcitrant waste metalworking fluids," *Water Research*, vol. 46, no. 7, pp. 2395–2404, 2012.

[27] Q. J. Rasheed, K. Pandian, and K. Muthukumar, "Treatment of petroleum refinery wastewater by ultrasound-dispersed nanoscale zero-valent iron particles," *Ultrasonics Sonochemistry*, vol. 18, no. 5, pp. 1138–1142, 2011.

[28] F. Kaczala, M. Marques, and W. Hogland, "Lead and vanadium removal from a real industrial wastewater by gravitational settling/sedimentation and sorption onto Pinus sylvestris sawdust," *Bioresource Technology*, vol. 100, no. 1, pp. 235–243, 2009.

[29] S. Laohaprapanon, F. Kaczalaa, P. S. Salomonbc, M. Marquesad, and W. Hoglanda, "Wastewater generated during cleaning/washing procedures in a wood-floor industry: toxicity on the microalgae *Desmodesmus subspicatus*," *Environmental Technology*. In press.

[30] Z. Shiyun, Z. Xuesong, and L. Daotang, "Ozonation of naphthalene sulfonic acids in aqueous solutions. Part I: elimination of COD, TOC and increase of their biodegradability," *Water Research*, vol. 36, no. 5, pp. 1237–1243, 2002.

[31] V. Sarria, S. Kenfack, O. Guillod, and C. Pulgarin, "An innovative coupled solar-biological system at field pilot scale for the treatment of biorecalcitrant pollutants," *Journal of Photochemistry and Photobiology A*, vol. 159, no. 1, pp. 89–99, 2003.

[32] F. J. Benitez, F. J. Real, J. L. Acero, C. Garcia, and E. M. Llanos, "Kinetics of phenylurea herbicides oxidation by Fenton and photo-Fenton processes," *Journal of Chemical Technology and Biotechnology*, vol. 82, no. 1, pp. 65–73, 2007.

[33] H. Kusic, N. Koprivanac, and L. Srsan, "Azo dye degradation using Fenton type processes assisted by UV irradiation: a kinetic study," *Journal of Photochemistry and Photobiology A*, vol. 181, no. 2-3, pp. 195–202, 2006.

[34] C.-C. Su, M. Pukdee-Asab, C. Ratanatamskulb, and M.-C. Lu, "Effect of operating parameters on decolorization and COD removal of three reactive dyes by Fenton's reagent using fluidized-bed reactor," *Desalination*, vol. 278, no. 1–3, pp. 211–218, 2011.

[35] X. Zhu, J. Tian, R. Liu, and L. Chen, "Optimization of Fenton and electro-Fenton oxidation of biologically treated coking wastewater using response surface methodology," *Separation and Purification Technology*, vol. 81, no. 3, pp. 444–450, 2011.

[36] M. S. Lucas and J. A. Peres, "Removal of COD from olive mill wastewater by Fenton's reagent: kinetic study," *Journal of Hazardous Materials*, vol. 168, no. 2-3, pp. 1253–1259, 2009.

[37] C. T. Benatti, C. R. G. Tavares, and T. A. Guedes, "Optimization of Fenton's oxidation of chemical laboratory wastewaters using the response surface methodology," *Journal of Environmental Management*, vol. 80, no. 1, pp. 66–74, 2006.

[38] E. Elmolla and M. Chaudhuri, "Optimization of Fenton process for treatment of amoxicillin, ampicillin and cloxacillin antibiotics in aqueous solution," *Journal of Hazardous Materials*, vol. 170, no. 2-3, pp. 666–672, 2009.

[39] H. Zhang, J. C. Heung, and C. P. Huang, "Optimization of Fenton process for the treatment of landfill leachate," *Journal of Hazardous Materials*, vol. 125, no. 1–3, pp. 166–174, 2005.

[40] D. R. Medley and E. L. Stover, "Effects of ozone on the biodegradability of biorefractory pollutants," *Journal of the Water Pollution Control Federation*, vol. 55, no. 5, pp. 489–494, 1983.

[41] C. Sirtori, A. Zapata, I. Oller, W. Gernjak, A. Agüera, and S. Malato, "Decontamination industrial pharmaceutical wastewater by combining solar photo-Fenton and biological treatment," *Water Research*, vol. 43, no. 3, pp. 661–668, 2009.

[42] Y. Deng and J. D. Englehardt, "Treatment of landfill leachate by the Fenton process," *Water Research*, vol. 40, no. 20, pp. 3683–3694, 2006.

[43] R. C. Martins, A. F. Rossi, and R. M. Quinta-Ferreira, "Fenton's oxidation process for phenolic wastewater remediation and biodegradability enhancement," *Journal of Hazardous Materials*, vol. 180, no. 1–3, pp. 716–721, 2010.

Hindawi Publishing Corporation
International Journal of Photoenergy
Volume 2012, Article ID 303586, 7 pages
doi:10.1155/2012/303586

Research Article

Solar Photocatalytic Degradation of Azo Dye in Aqueous TiO_2 Suspension Assisted by Fresnel Lens

Wen-Shiuh Kuo and Wen-Yu Chen

Department of Safety, Health and Environmental Engineering, National United University, Miaoi 360, Taiwan

Correspondence should be addressed to Wen-Shiuh Kuo, wsk@nuu.edu.tw

Received 29 May 2012; Accepted 24 August 2012

Academic Editor: Meenakshisundaram Swaminathan

Solar TiO_2 photocatalytic process assisted by a Fresnel lens was investigated for treating an azo dye wastewater of Acid Orange 10 (AO10). Response surface methodology (RSM) was employed to assess the effect of critical process parameters (including initial pH of wastewater, concentration of TiO_2, and reaction time) on treatment performance in terms of COD and TOC degradation efficiency. Optimized reaction conditions based on the analysis of RSM were established under an initial pH of 6.0, a concentration of TiO_2 of 1 g/L, and a reaction time of 2 h for reaching a 90% COD and TOC degradation of AO10 wastewater. With the assistance of Fresnel lens, the TOC degradation rate of AO10 wastewater increased significantly from 0.606 h^{-1} and 0.289 h^{-1} to 1.477 h^{-1} and 0.866 h^{-1} in summer (June) season ($UV_{280–400\,nm}$ nm: 39.9–44.8 W/m^2) and winter (December) season ($UV_{280–400\,nm}$ nm: 23.9–26.9 W/m^2), respectively. This could be mainly due to the concentrating effect of Fresnel lens for solar energy, resulting in an increase of 2∼2.5 times of solar light intensity and a raising heat irradiation in terms of 10∼15 °C of wastewater temperature. These results revealed that solar energy could be concentrated effectively by using Fresnel lens and showed a significant promoting effect on the TiO_2 photocatalytic degradation of dye wastewater.

1. Introduction

Over 100,000 different types of dyes are commercially available and 700,000 tons are produced yearly all over the world. Nearly 50% of these dyes are azo-type dyes [1]. Azo dyes, aromatic moieties linked together by azo (–N=N–) chromophores, represent the largest class of dyes used in textile processing and other industries. The release of these compounds into the environment is undesirable, because the color matters and their toxic breakdown products can be mutagenic [2]. In addition, due to the complex aromatic structure and stability of the azo-dyes, conventional biological treatments are ineffective for degradation and mineralization of the dye molecules [3]. Instead, activated carbon adsorption or coagulation is commonly used. However, new environmental laws may consider the spent adsorbents or sludge as hazardous waste and require further treatment. Consequently, intensive research for novel technologies with higher efficiency and less amount of waste generated has been stimulated. Advanced oxidation processes (AOPs) have been previously described as a promising option to remove persistent pollutants from contaminated water [4]. AOPs are able to produce a highly reactive, nonspecific oxidant, mainly hydroxyl radicals ($^{\bullet}OH$). The hydroxyl radical possesses inherent properties that enable it to attack refractory organic pollutants in water to achieve a complete mineralization. However, the production of photons with artificial light sources requires significant electrical energy demand and UV lamp consumption, leading to a high operation cost in AOPs [5]. Alternatively, solar energy is essentially unlimited and its utilization is ecologically benign. In the wastewater treatment sector, solar technology has been extensively used as an alternative to UV lamps to reduce the operation cost in AOPs [6]. In particularly, TiO_2 photocatalysis (1)–(3) using solar irradiation has been used as an economically viable process and has attracted great interest in recent years [7]. However, solar TiO_2 photocatalysis was usually carried out by using solar irradiation directly, resulting in a lower

absorption and utilization of solar energy [8]. To improve the efficiency of solar TiO_2 photocatalysis, it is necessary to maximize the absorption of solar energy.

$$TiO_2 \xrightarrow{h\nu(\lambda < 382\,\text{nm})} h^+_{vb} + e^-_{cb} \quad (1)$$

$$h^+_{vb} + H_2O \longrightarrow {}^\bullet OH + H^+ \quad (2)$$

$$h^+_{vb} + OH- \longrightarrow {}^\bullet OH \quad (3)$$

In this study, treatment of an azo dye-Acid Orange 10 (AO10) wastewater towards highly mineralization using solar TiO_2 photocatalysis enhanced by high-concentrating Fresnel lens was investigated. Response surface methodology (RSM) was employed to obtain the optimal reaction conditions of critical process parameters (including initial pH of wastewater, TiO_2 concentration, and reaction time) to reach a 90% of COD and TOC degradation of dye wastewater. Moreover, the effect of Fresnel lens on treatment performance in terms of color, COD, and TOC degradation efficiency of AO10 dye wastewater was examined.

2. Materials and Methods

2.1. Materials. AO10 ($C_{16}H_{10}N_2O_7S_2Na_2$) with a purity of 84% was purchased from the Sigma-Aldrich Co. (USA) and used without further purification. The chemical properties of AO10 are shown in Table 1. An initial AO10 concentration of 50 mg/L was prepared for all experimental runs. TiO_2 powder P25 (mainly anatase form, with a mean particle size of 30 nm and a BET surface area of $50 \pm 15\,m^2/g$) from Degussa Co. (Frankfurt, Germany) was used in this study. All other chemicals used in this study were analytical grade and used as received.

2.2. Procedures. All experiments were carried out in a batch mode. A 1 L glass beaker containing 200 mL of AO10 solution was used. The initial pH of the solution was adjusted to the desired pH by adding 1 N H_2SO_4 or 1 N NaOH. In this study, a 3-factor * 3-level experimental design with three replicates at center point according to the methodology of response surface [9] as shown in Table 2 was applied to investigate the influence of three factors (namely, initial pH, TiO_2 concentration and reaction time) for COD and TOC degradation efficiency of AO10 wastewater. At the RSM runs, the prepared dye solution was placed into the photoreactor and irradiated by a 1500 W Xe lamp in an Atlas Suntest CPS+ solar simulator (Atlas Co., USA) emitting artificial solar light with a spectral distribution resembling the solar spectrum (300–800 nm) in which the $UV_{280-400\,nm}$ intensity is around $67 \pm 0.5\,W/m^2$. In addition, the AO10 solution was maintained at $25 \pm 0.5°C$ in a water bath. During the experiments, the pH of the solution was monitored using a pH meter (SP-701LI 120, Suntex Co., Taiwan) equipped with a glass electrode. Samples were withdrawn from the reactor at preset time intervals and then stored at 4°C for the following ADMI, COD, TOC, and IC analysis.

As the optimal values of the process parameters were developed on the basis of RSM application and related equations, a Fresnel lens made of PMMA (thickness: 2 mm, pitch: 0.5 mm, facet depth: 0.2 mm, and Fresnel circles: 395) was added into solar TiO_2 photocatalytic system with a distance of 16 cm above the level of wastewater. To investigate the effect of Fresnel lens in summer (June) and winter (December) seasons, a similar reactor without Fresnel lens was also performed under the same natural solar irradiation using the experimental conditions obtained from RSM runs. A schematic diagram of the photoreactor using Fresnel lens is shown in Figure 1. In addition, two blank experiments including direct photolysis reaction and adsorption on TiO_2 only under the experimental conditions of this study were performed. The result indicated that the mineralization efficiency of AO10 solution was less than 2%, which implied that the mineralization of AO10 solution due to these effects was slight in this study.

2.3. Analysis

2.3.1. American Dye Manufacturing Institute (ADMI) Measurement. The color of AO10 solution was determined with a DR 4000 photometer (HACH Co., USA) for ADMI measurement. The efficiency of decolorization was calculated on the basis of ADMI reduction of solution.

2.3.2. Chemical Oxygen Demand (COD) Measurement. COD of solution via a DR 4000 photometer (Hach Co., USA) by using a $K_2Cr_2O_7$ as the reacting reagent was measured in order to understand the changes in the degree of oxidation for AO10 wastewater.

2.3.3. Total Organic Carbon (TOC) Measurement. TOC of solution was measured by using a Shimadzu VCPH analyzer (Shimadzu Co., Japan) in order to know the amount of AO10 molecules degraded to CO_2 during oxidation.

2.3.4. Ion Chromatography (IC) Analysis. To quantify the degradation product—oxalate ($C_2O_4^{2-}$) and acetate (CH_3COO^-)—an ion-chromatographic system (Dionex ICS-1000) equipped with an IonPac AS12A column (L: 200 mm, ID: 4.0 mm) was used. Aqueous solutions of 2.7 mM Na_2CO_3 and 0.3 mM $NaHCO_3$ were used as eluents. Analysis was performed under a flow rate of 1.5 mL/min and operated on an isocratic mode.

3. Results and Discussion

3.1. Optimization of Solar Photocatalytic Treatment of AO10 Wastewater. Figure 2 displays the three-dimensional response surface plots for percent of COD and TOC degradation efficiencies of AO10 wastewater as a function of initial pH and concentration of TiO_2. As shown in Figure 2, when the pH of AO10 wastewater was varied from 5 ($X_1 = -1$) to 9 ($X_1 = 1$), the degradation efficiency reached a maximum at pHs 5.5–6.5 followed by a decrease of COD and TOC degradation efficiency in the range 6.5–9.0 in all the TiO_2 concentration ranges studied. This phenomenon can be explained by the surface charge of TiO_2 as a function

Table 1: Chemical characteristics of alizarin violet AO10.

Dye	Chemical structure	λ_{max} (nm)	MW, g/mol	Category
Acid Orange 10 ($C_{16}H_{10}N_2O_7S_2Na_2$) (C.I. number 16230)	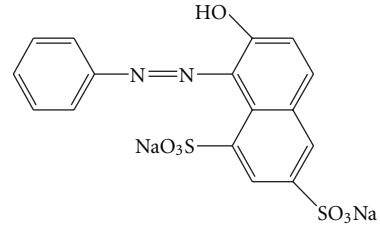	478	452.37	Azo

Table 2: Experimental range and levels of the process independent variables in this study.

Independent variable	Factor	Range and level		
		−1	0	+1
Initial pH	X_1	5.0	7.0	9.0
TiO_2, g/L	X_2	0.5	1.0	1.5
Reaction time, hr	X_3	1.0	1.5	2.0
Y (response)—COD or TOC degradation, %				

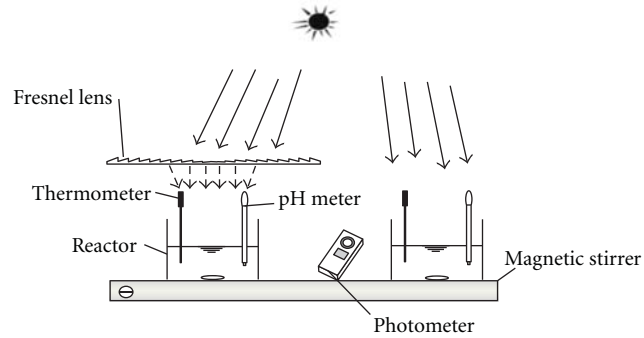

Figure 1: Schematic diagram of the solar photocatalytic reactor with and without Fresnel lens.

of pH. The zero point of charge (ZPC) for TiO_2-P25 is around pH 6.3–6.8 [10]. Therefore, at more acidic pH environment ($pH < pH_{ZPC}$), the TiO_2 surface is positively charged as expressed by (4), and at alkaline pH, the surface ($pH > pH_{ZPC}$) is negatively charged as expressed by (5) [11]. AO10 in water is negatively charged because the two sodium sulfonate group is hydrolyzed to form dye anion and sodium ions as expressed by (6). At pH values below 6.3, the adsorption of AO10 is favorable due to the electrostatic attraction between the fully ionized sulfonic group and positively charged TiO_2 on the surface. Above pH 6.8, AO10 is subjected to electrostatic repulsion between itself and the negative surface of TiO_2. Hence, the adsorption of the AO10 dye is less and the degradation efficiency decreased. Similar result was also observed in the photocatalytic degradation of Acid Orange 7 [12]. However, the effect of initial pH of dye solution was not significant because of some carboxyl acid intermediates such as acetate and oxalate were produced, leading to a gradually decreased pH of solution, and then the reaction of (4) may be dominant.

$$\mathrm{TiOH} + \mathrm{H^+} \longrightarrow \mathrm{TiOH_2^+}, \quad \mathrm{pK_{a1}} = 4.95 \tag{4}$$

$$\mathrm{TiOH} + \mathrm{OH^-} \longrightarrow \mathrm{TiO^-} + \mathrm{H_2O}, \quad \mathrm{pK_{a2}} = 7.80 \tag{5}$$

$$\text{dye-}(\mathrm{SO_3Na})_2 \longrightarrow \text{dye-}\left(\mathrm{SO_3^-}\right)_2 + 2\mathrm{Na^+}. \tag{6}$$

On the other hand, as shown in Figure 2, the effect of TiO_2 concentration was much more considerable than that of initial pH on the COD and TOC degradation of AO10 wastewater. In general, more catalysts will substantially result in generation of more hydroxyl radicals until an optimum catalyst concentration is achieved. Hence, the results showed that, within the pH range studied (5–9), the increase of catalyst concentration from 0.5 to 1.0 g/L increased the degradation efficiency. This fact may be due to the increase in the number of dye molecules adsorbed and more oxidation of dye [13]. Above this value, no obvious improvement is obtained by increasing the concentration of catalyst. This may be due to an increased opacity of the suspension and the shielding effect of light with an excess of TiO_2 particles, consequently leading to a decrease in the formation of $^{\bullet}OH$ radicals. Accordingly, the optimum concentration of the catalyst for efficient solar photodegradation of AO10 would be around 1.0 g/L. This result was consistent with those reported in the literature [14] for the TiO_2 photocatalytic degradation of Remazol Red dye.

On the basis of RSM application, the empirical relationship between the dye degradation efficiency (Y) and the independent variables is developed and listed in Table 3. The regression model had a high value of coefficient of determination ($r^2 > 0.97$). This implies that the process efficiency could be predicted well by the second-order polynomial regression equations under the conditions studied.

Based on the model equations in Table 3, the optimal values of the process parameters were established as an initial pH of 6.0, an initial concentration of TiO_2 of 1 g/L, and a reaction time of 2 h for reaching a 90% COD and TOC degradation of AO10 wastewater. In order to confirm the optimum conditions of AO10 degradation, a five-replicate and t-test analyses were performed. The results showed that the average COD and TOC degradation efficiency were 90.5% and 90.4%, respectively, and the 95% of confidence intervals for COD and TOC degradation efficiency were 89.7~91.3% and 89.4~90.8%, respectively. Consequently,

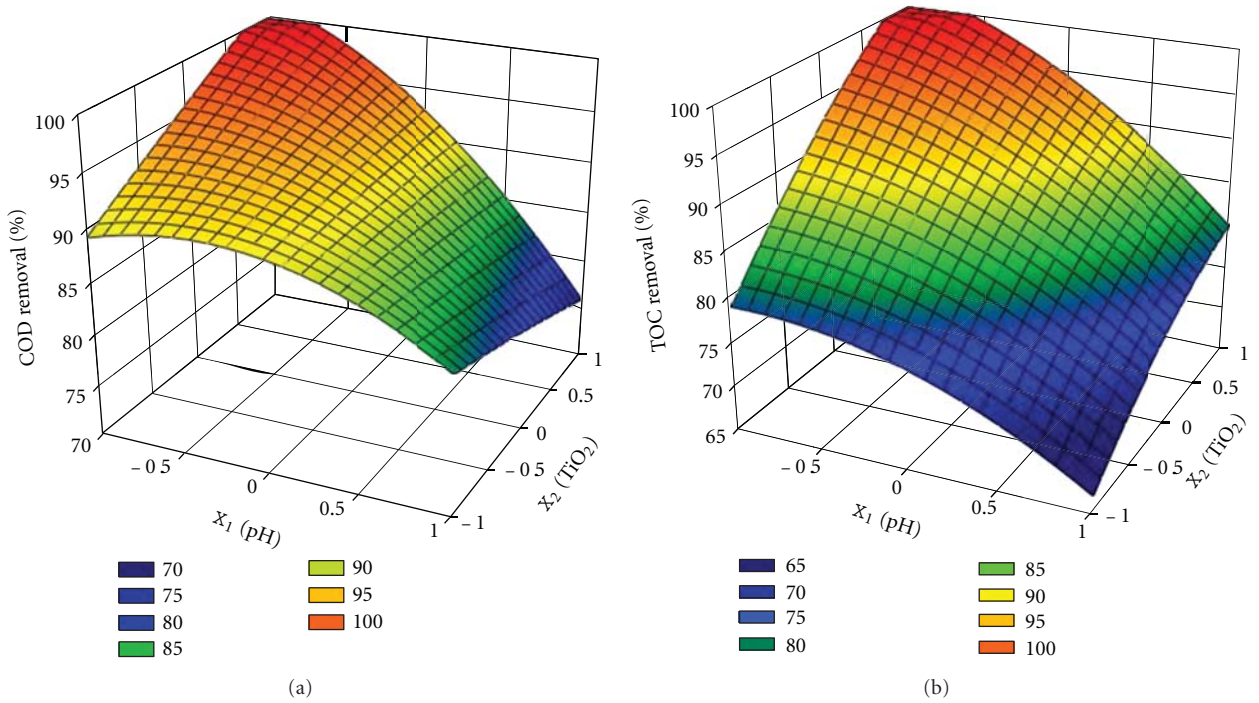

Figure 2: Response surface for (a) COD and (b) TOC degradation efficiency of AO10 wastewater as a function of initial pH and TiO_2 concentration. (Reaction time: 2 h, light intensity ($UV_{280–400\,nm}$: 66.5 W/m^2, water temperature: 25 ± 0.5°C).

Table 3: Polynomial regression equation of AO10 degradation on the basis of COD and TOC removal.

Polynomial regression equation	r^2
[a] $Y_{COD} = 81.0 + X_1 + 9.7X_2 + 15.3X_3 - 3.9\,X_1{}^2 - 0.2\,X_2{}^2 - 4.6\,X_3{}^2 - 5X_1X_2 - 6.9X_1X_3 - 8.3X_2X_3$	0.971
[a] $Y_{TOC} = 74.1 - 5X_1 + 10.5X_2 + 18.7X_3 - 3.2X_1{}^2 - 2\,X_2{}^2 - 5.7\,X_3{}^2 - 2.6X_1X_2 - 3.7X_1X_3 - 1.3X_2X_3$	0.997

[a] Y_{COD}: the COD degradation efficiency of AO10 wastewater.
[b] Y_{TOC}: the TOC degradation efficiency of AO10 wastewater.

the credibility of the optimal conditions obtained in this study was acceptable.

3.2. Effect of Fresnel Lens on the Degradation Efficiency of AO10 Wastewater. To investigate the effect of Fresnel lens, photocatalytic oxidation of AO10 wastewater with or without Fresnel lens was performed simultaneously under natual solar irradiation using the optimal experimental conditions obtained from RSM runs.

Basically, it was found that the concentrating effect of Fresnel lens for solar energy could result in an increase of 2.2~2.5 and 1.8~2.0 times of solar light irradiation in summer (June) and winter (December) seasons, respectively, as shown in Table 4. Also, a raising heat irradiation in terms of 10~15°C of wastewater temperature was observed in this study. Figures 3 and 4 showed the effect of Fresnel lens on the COD, TOC degradation, and decolorization efficiency of AO10 wastewater in summer (June) and winter (Dec.) season, respectively. As shown in Figure 3, a 99% of COD and a 94% of TOC degradation of AO10 wastewater were achieved with the assistance of Fresnel lens, in contrast to a 94% of COD and a 74% of TOC degradation in solar photocatalytic process without Fresnel lens observed within a reaction of 2 h. The decolorization efficiency of AO10 wastewater was also increased 29% as using Fresnel lens for a reaction of 1 h only. Moreover, it was found that the degradation efficiency of AO10 wastewater with the aid of Fresnel lens at a reaction of 1 h was close to that without the assistance of Fresnel lens at a reaction time of 2 h. This could be due to a higher light irradiation and water temperature that increased the rate of generation of oxidizing species such as •OH radical. This result implied that the higher the solar light irradiation applied, the higher the generation of electron-hole pairs and •OH radicals. A similar phenomenon was observed in the study of Liu et al. [15]. Their result indicated that the TOC degradation efficiency of Acid Yellow 17 solution increased from 5.1% to 53.2% as the intensity of UV light increased from 12.4 to 31.5 W/m^2, indicating a positive effect of increasing light irradiation. In addition, the results of Lin and Lee [16] indicated that the degradation efficiency of MX-5B dye wastewater improved 15% while the temperature of water was increased from 22°C to 40°C in TiO_2 photocatalytic process. This is due to a higher

Table 4: Effect of Fresnel lens on the degradation rate constant of AO10 wastewater.

Solar photocatalytic process*	[a]k_{COD}, h^{-1}	[b]k_{TOC}, h^{-1}	$UV_{280–400\,nm}$, W/m^2	[c]ΔT, °C
Without fresnel lens	0.792	0.606	39.9–44.8 (June)	8 ~ 10
	0.438	0.289	23.9–26.9 (Dec.)	6 ~ 8
With fresnel lens	2.307	1.477	96.8–112.1 (June)	14 ~ 15
	1.799	0.866	48.5–53.8 (Dec.)	14 ~ 16

*Operation condition: pH_0: 6.0, $[TiO_2]_0$ = 1.0 g/L; reaction time: 2 h;
[a]k_{COD}: pseudo-first order rate constant based on the degradation of COD in solution;
[b]k_{TOC}: pseudo-first order rate constant based on the degradation of TOC in solution;
[c]ΔT: final solution temperature—initial solution temperature.

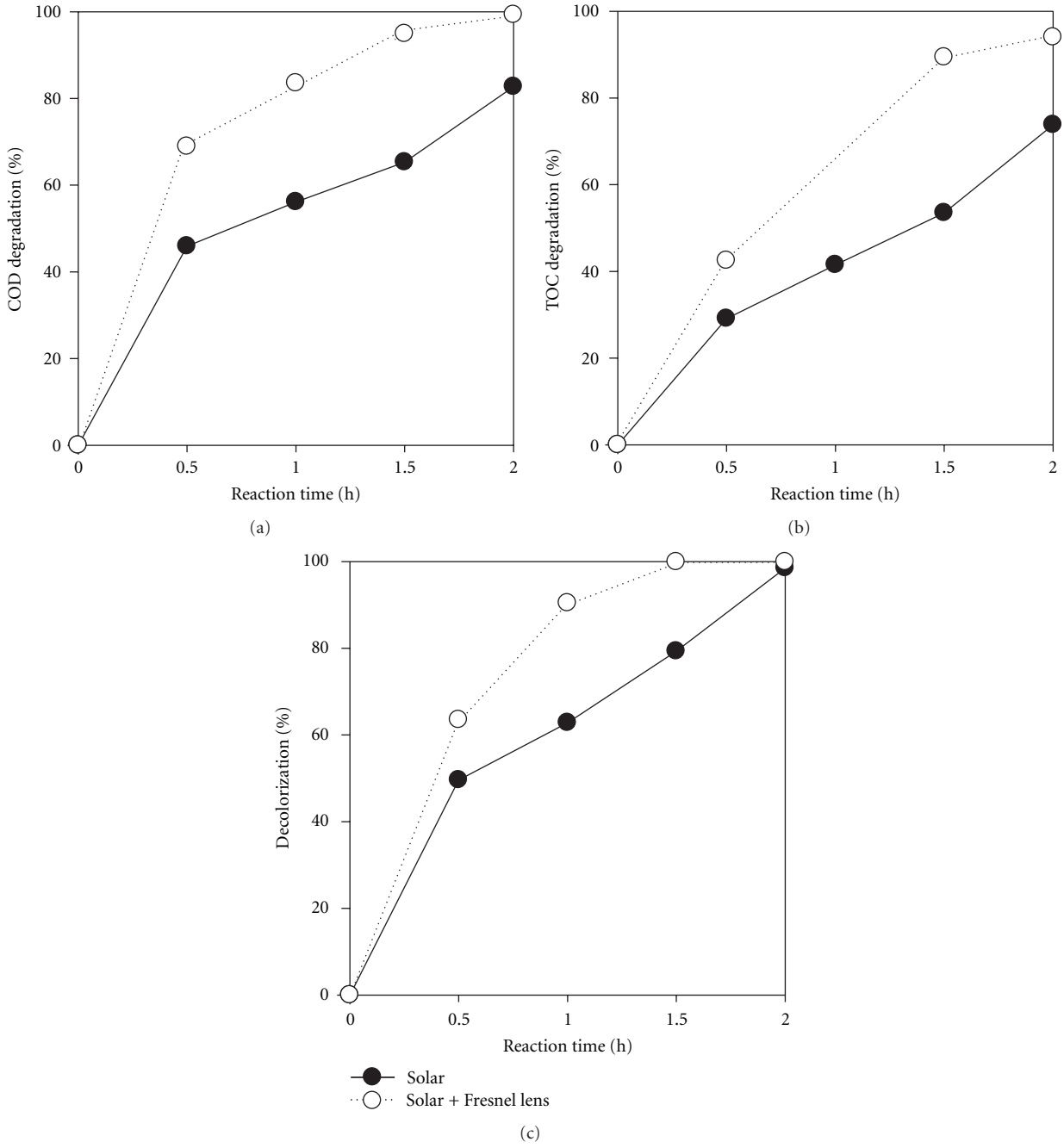

Figure 3: Effect of Fresnel lens on the degradation efficiency of AO10 dye wastewater in summer season (June).

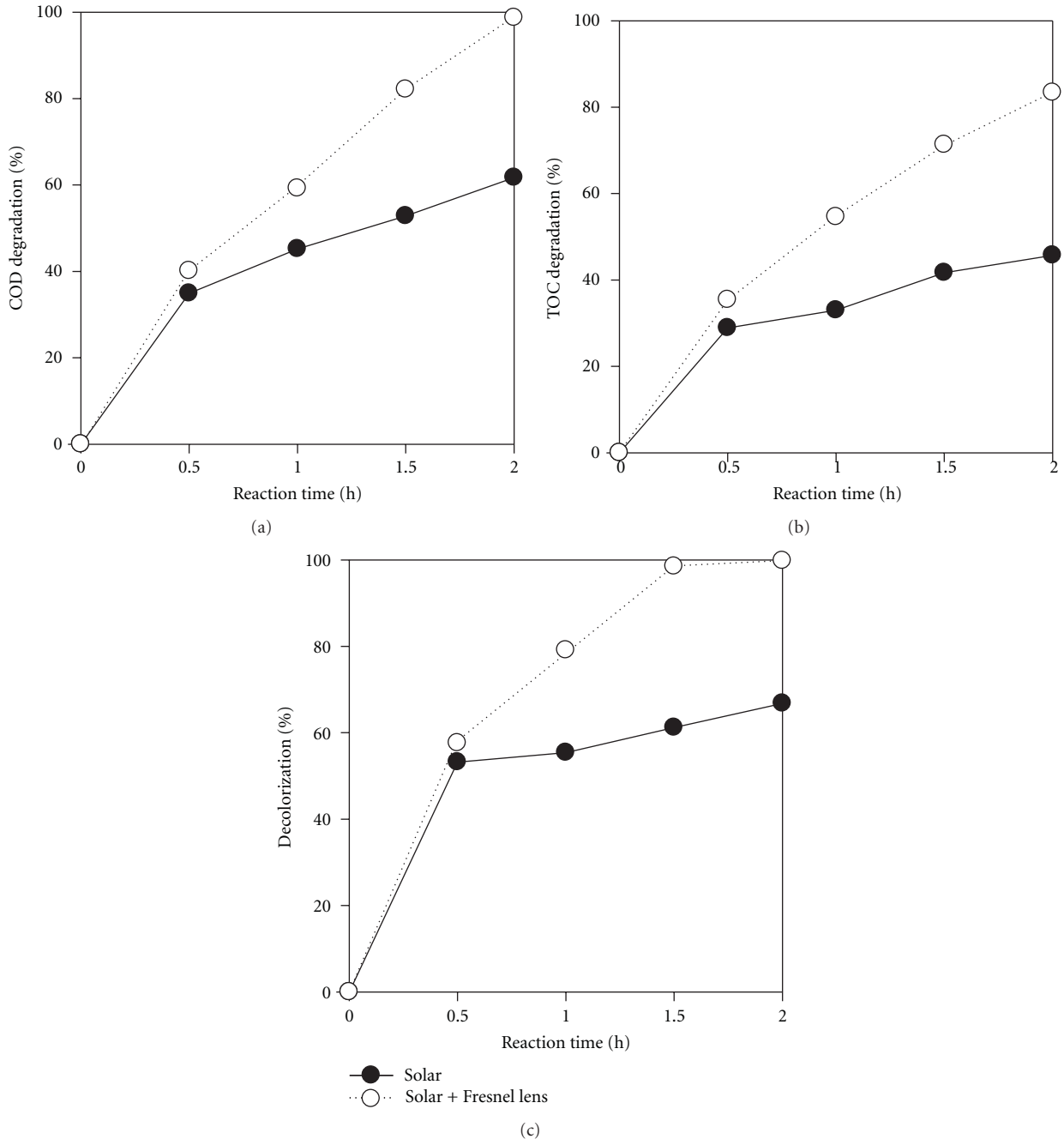

Figure 4: Effect of Fresnel lens on the degradation efficiency of AO10 dye wastewater in winter season (December).

water temperature that increased the reaction rate between $^{\bullet}$OH and organic molecules. Accordingly, two promotion effects were found with the assistance of Fresnel lens. First, the increase of solar light irradiation could enhance the excitation of electron hole and hence persistent promotion of $^{\bullet}$OH production. Second, the raise of water temperature would be higher due to the effect of solar heat irradiation, which renders additional positive effect on the performance of solar photocatalytic process.

To quantitatively analyze the effect of Fresnel lens on the degradation of AO10 wastewater, a pseudo-first-order model was applied to obtain the rate constants. It was found that both the COD and TOC degradation efficiencies of AO10 wastewater, with or without Fresnel lens, followed the pseudo-first-order reaction kinetics as indicated by high correlation coefficients ($r^2 > 0.90$). It was obvious that a significant enhancement for the degradation rate of AO10 wastewater was achieved by using Fresnel lens. As the rate constant shown in Table 4, the COD and TOC degradation rate of AO10 wastewater increased a factor of 2.9 and 2.4, respectively, in summer (June) season and a factor of 4.1 and 3.0, respectively, in winter (December)

season. The promotion effect of Fresnel lens was more significant in winter season. This may be due to a lower solar irradiation (23.9~26.9 W/m^2) and a lower initial water temperature (15~18°C) in winter season, leading to a much lower production of $^{\bullet}$OH radicals in the solar photocatalytic process without the assistance of Fresnel lens.

4. Conclusions

Optimized reaction conditions based on the application of RSM were established as an initial pH of 6.0, a TiO_2 concentration of 1.0 g/L, and a reaction time of 2 h for more than a 90% of COD and TOC degradation of AO10 wastewater in solar TiO_2 photocatalytic process. Solar energy could be concentrated efficiently by using Fresnel lens and had a significant effect on the increasing of $UV_{280–400\,nm}$ light intensity of solar irradiation and the temperature of wastewater, leading to a positive effect on the performance of solar photocatalytic process. Consequently, the solar TiO_2 photocatalytic process with the use of a low cost of PMMA Fresnel lens can offer an economical and practical alternative for the treatment of dye wastewater.

Acknowledgment

Many thanks are due to the kind sponsorship of the National Science Council, Taiwan (Project no. NSC 99-2221-E-239-011), without which this work would not have been possible.

References

[1] I. D. Mall, V. C. Srivastava, N. K. Agarwal, and I. M. Mishra, "Removal of congo red from aqueous solution by bagasse fly ash and activated carbon: kinetic study and equilibrium isotherm analyses," *Chemosphere*, vol. 61, no. 4, pp. 492–501, 2005.

[2] C. Bauer, P. Jacques, and A. Kalt, "Photooxidation of an azo dye induced by visible light incident on the surface of TiO_2 ," *Journal of Photochemistry and Photobiology A*, vol. 140, no. 1, pp. 87–92, 2001.

[3] Z. Zhang and H. Zheng, "Optimization for decolorization of azo dye acid green 20 by ultrasound and H_2O_2 using response surface methodology," *Journal of Hazardous Materials*, vol. 172, no. 2-3, pp. 1388–1393, 2009.

[4] F. Al Momani, "Impact of photo-oxidation technology on the aqueous solutions of nitrobenzene: degradation efficiency and biodegradability enhancement," *Journal of Photochemistry and Photobiology A*, vol. 179, no. 1-2, pp. 184–192, 2006.

[5] L. A. Pérez-Estrada, S. Malato, A. Agüera, and A. R. Fernández-Alba, "Degradation of dipyrone and its main intermediates by solar AOPs. Identification of intermediate products and toxicity assessment," *Catalysis Today*, vol. 129, no. 1-2, pp. 207–214, 2007.

[6] M. I. Maldonado, P. C. Passarinho, I. Oller et al., "Photocatalytic degradation of EU priority substances: a comparison between TiO_2 and Fenton plus photo-Fenton in a solar pilot plant," *Journal of Photochemistry and Photobiology A*, vol. 185, no. 2-3, pp. 354–363, 2007.

[7] S. Malato, P. Fernández-Ibáñez, M. I. Maldonado, J. Blanco, and W. Gernjak, "Decontamination and disinfection of water by solar photocatalysis: recent overview and trends," *Catalysis Today*, vol. 147, no. 1, pp. 1–59, 2009.

[8] A. Durán and J. M. Monteagudo, "Solar photocatalytic degradation of reactive blue 4 using a Fresnel lens," *Water Research*, vol. 41, no. 3, pp. 690–698, 2007.

[9] G. E. P. Box, W. G. Hunter, and J. S. Hunter, *Statistics for Experimenters: An Introduction to Design. Data Analysis and Model Building*, Wiley, New York, NY, USA, 1st edition, 1978.

[10] E. Evgenidou, K. Fytianos, and I. Poulios, "Semiconductor-sensitized photodegradation of dichlorvos in water using TiO_2 and ZnO as catalysts," *Applied Catalysis B*, vol. 59, no. 1-2, pp. 81–89, 2005.

[11] S. Lakshmi, R. Renganathan, and S. Fujita, "Study on TiO_2-mediated photocatalytic degradation of methylene blue," *Journal of Photochemistry and Photobiology A*, vol. 88, no. 2-3, pp. 163–167, 1995.

[12] P. Bansal, D. Singh, and D. Sud, "Photocatalytic degradation of azo dye in aqueous TiO_2 suspension: reaction pathway and identification of intermediates products by LC/MS," *Separation and Purification Technology*, vol. 72, no. 3, pp. 357–365, 2010.

[13] M. S. T. Gonçalves, A. M. F. Oliveira-Campos, E. M. M. S. Pinto, P. M. S. Plasência, and M. J. R. P. Queiroz, "Photochemical treatment of solutions of azo dyes containing TiO_2," *Chemosphere*, vol. 39, no. 5, pp. 781–786, 1999.

[14] K. Soutsas, V. Karayannis, I. Poulios et al., "Decolorization and degradation of reactive azo dyes via heterogeneous photocatalytic processes," *Desalination*, vol. 250, no. 1, pp. 345–350, 2010.

[15] C. C. Liu, Y. H. Hsieh, P. F. Lai, C. H. Li, and C. L. Kao, "Photodegradation treatment of azo dye wastewater by UV/TiO_2 process," *Dyes and Pigments*, vol. 68, no. 2-3, pp. 191–195, 2006.

[16] Y. C. Lin and H. S. Lee, "Effects of TiO_2 coating dosage and operational parameters on a TiO_2/Ag photocatalysis system for decolorizing procion red MX-5B," *Journal of Hazardous Materials*, vol. 179, no. 1–3, pp. 462–470, 2010.

Hindawi Publishing Corporation
International Journal of Photoenergy
Volume 2012, Article ID 140605, 6 pages
doi:10.1155/2012/140605

Research Article

Combined Application of UV Photolysis and Ozonation with Biological Aerating Filter in Tertiary Wastewater Treatment

Zhaoqian Jing and Shiwei Cao

College of Civil Engineering, Nanjing Forestry University, Nanjing 210037, China

Correspondence should be addressed to Zhaoqian Jing, carljing@163.com

Received 13 May 2012; Accepted 26 September 2012

Academic Editor: Meenakshisundaram Swaminathan

To enhance the biodegradability of residual organic pollutants in secondary effluent of wastewater treatment plants, UV photolysis and ozonation were used in combination as pretreatment before a biological aerating filter (BAF). The results indicated that UV photolysis could not remove much COD (chemical oxygen demand), and the performance of ozonation was better than the former. With UV photolysis combined with ozonation (UV/O_3), COD removal was much higher than the sum of that with UV photolysis and ozonation alone, which indicated that UV photolysis could efficiently promote COD removal during ozonation. This pretreatment also improved molecular weight distribution (MWD) and biodegradability greatly. Proportion of organic compounds with molecular weight (MW) <3 kDalton was increased from 51.9% to 85.9%. COD removal rates with BAF and O_3/BAF were only about 25% and 38%, respectively. When UV/O_3 oxidation was combined with BAF, the average COD removal rate reached above 61%, which was about 2.5 times of that with BAF alone. With influent COD ranging from 65 to 84 mg/L, the effluent COD was stably in the scope of 23–31 mg/L. The combination of UV/O_3 oxidation with BAF was quite efficient in organic pollutants removal for tertiary wastewater treatment.

1. Introduction

In recent years, contamination of surface and subsurface water by organic pollutants has received much attention. Wastewater treatment plants (WWTPs) play important roles in such pollutants removal. In China, more and more WWTPs have been built not only in large cities, but also in small towns and counties. To meet the national discharge standard for municipal WWTPs, most of them have been built with secondary treatment processes, which usually comprise physical interception, precipitation, and biological treatment. Although the secondary treatment processes are efficient in bulk and soluble pollutants removal, there are still some residual organic compounds, nitrogen, phosphorus, and pathogenic bacteria in the effluent. Some researchers have found that there are more than 200 organic micropollutants in the secondary effluent of municipal WWTPs [1, 2]. Most of these organic pollutants are refractory and difficult to be further degraded, and therefore their discharge in water may cause long-term environmental effects to aquatic and terrestrial organisms [3, 4].

In late May, 2007, a drinking water crisis took place in Wuxi, Jiangsu Province, China, owing to the large scale growth of algae bloom in Wuxi's drinking water source—Taihu Lake. This crisis has made nearly 170 WWTPs being required to be upgraded with deep treatment or tertiary treatment to relieve the pollution load to Taihu Lake. Coagulation and filtration have been usually applied in tertiary treatment for residual suspended solids and partial colloid substances removal. However, most refractory and volatile organic compounds cannot be eliminated by these processes [5]. Owing to the low biodegradability of residual organic compounds, it is difficult to treat the secondary effluent directly with further biological processes. Appropriate processes should be found for refractory pollutants removal in tertiary wastewater treatment.

Many advanced oxidation processes (AOPs) can be used for destruction of refractory and high molecular organic compounds in wastewater, such as ozonation, ultraviolet (UV) photolysis, hydrogen peroxide (H_2O_2) oxidation, and Fenton oxidation. These AOPs can be used alone or in combination. During these processes, hydroxyl radicals

with redox potential of 2.8 V are usually generated as the basic oxidants for pollutants removal [6]. Hydroxyl radicals are highly reactive and consequently short-lived. In the application of these AOPs, it is vital to provide appropriate reaction conditions and produce enough hydroxyl radicals. Fenton oxidation is usually accomplished in acid conditions, resulting in large quantities of acid and base consumption [7]. It can be used in small scale industrial wastewater treatment or special pollutants removal. Ozone is a strong oxidant that decomposes in water to form hydroxyl radicals which are stronger oxidizing agents than ozone itself. The use of ozonation for refractory and complex organic pollutants oxidation is very popular in water and wastewater treatment [8, 9]. During ozonation, the high molecular pollutants are decomposed into small molecular compounds, which are readily to be biodegraded [10]. Ozonation can also reduce the toxic effects of some micropollutants, but does not decrease the viability of bacteria [11]. Therefore, it is feasible to apply ozonation with biological processes in wastewater treatment. UV light is often used in water and wastewater disinfection. UV photolysis can selectively reduce some organic compounds, but it alone is not efficient enough for pollutants removal. However, many researchers have found UV photolysis can enhance the oxidation potential of some oxidation processes. When UV is used with H_2O_2, a strong oxidant whose photolytic dissociation yields hydroxyl radicals [12, 13], many recalcitrant pollutants such as pharmaceuticals and pesticides can be oxidized [14]. When UV photolysis is combined with ozonation (UV/O_3 oxidation), more hydroxyl radicals are produced via the photolysis of reaction intermediates such as H_2O_2 [15], and the organic pollutants are decomposed more completely. UV/O_3 oxidation has been used in pharmaceuticals, drinking water and industrial wastewater treatment [16–18]. In WWTPs, UV/O_3 oxidation can be used as pretreatment for biological process, in which complex pollutants are decomposed into more biodegradable substances. Therefore, more organic compounds can be removed in the subsequent biological treatment process.

As described above, although there are many studies on UV/O_3 oxidation in organic pollutants removal from water and wastewater, there are few studies in the application of UV/O_3 oxidation with biological processes in tertiary wastewater treatment. In this study, UV/O_3 oxidation was combined with a biological aerating filter (BAF) to treat the secondary effluent from a WWTP. The application of UV/O_3 oxidation in combination with BAF could achieve high organic pollutants removal with low cost [19]. The characteristics of the secondary effluent were evaluated. COD (chemical oxygen demand) removal performance and molecular weight distribution (MWD) changes during UV photolysis, ozonation, and their combination were investigated. Contrast experiments were also carried out to study the performances of COD removal with BAF, O_3/BAF and UV/O_3/BAF.

2. Materials and Methods

2.1. Reactors. A pilot system shown in Figure 1 was built in a WWTP in Nanjing, Jiangsu Province of China. UV/O_3 oxidation was carried out in a cylinder glass reactor with diameter of 300 mm and effective volume of 4 L. A 10 W low-pressure mercury UV lamp with main wavelength of 254 nm was installed in the center of the reactor. Ozone was produced with an ozone generator (CF-G-3-2.5 g, Qingdao Guolin Industry Co., Ltd, China) with dry air. Ozone dosage was controlled with a flowmeter.

The wastewater after pretreatment with UV photolysis and ozonation was pumped into a BAF, an organic glass cylinder reactor with diameter of 100 mm. Clay ceramisites with diameter of 10 mm were used as filling material with depth of 1.5 m. This BAF was operated with hydraulic load of 1.5 m^3/m^2 h and gas/water ratio of 5 : 1.

2.2. Analytical Methods. The samples from the influent, oxidation reactor, and final effluent of BAF were taken regularly and the concentrations of COD, BOD_5 (5-day biological oxygen demand) and NH_4^+-N (ammonia) were analyzed according to the standard methods (APHA, 1999). MWD was measured using ultrafiltration membrane filters with cutoff sizes of 1–100 kDalton. DOC (dissolved organic carbon) after membrane filtration with different cutoff sizes was measured using a Shimadzu TOC-V instrument. pH, dissolved oxygen, ozone concentration, and temperature were monitored regularly.

2.3. Influent Characteristics. The effluent from the secondary clarifiers in the WWTP was directly used as influent of the combined process. This WWTP was run with an A^2/O (anaerobic/anoxic and oxic) process, which had removed most soluble organic compounds and nitrogen. The main indexes of influent during this study were as follows: COD 63.2–91.4 mg/L, BOD_5 9–23 mg/L, NH_4^+-N 5.3–8.6 mg/L, pH 7.1–7.4, and water temperature 19–25°C.

3. Results and Discussion

3.1. Evaluation of Secondary Effluent. COD and BOD_5 in the effluent from the secondary clarifiers of the WWTP in 2009 are shown in Figure 2. COD in the effluent ranged from 63.2 mg/L to 91.4 mg/L while BOD_5 was in the scope of 9–23 mg/L. According to the national discharge standard for municipal wastewater treatment plant in China, when the effluent from a WWTP is discharged into an enclosed watershed, COD and BOD_5 in the effluent are required below 50 mg/L and 10 mg/L, respectively. It is obvious that the effluent could not meet the national discharge standard. This WWTP was run with A^2/O process, in which most biodegradable organic compounds had been degraded. The ratio of BOD_5/COD (B/C) was low, ranging from 0.17 to 0.25, which indicated that most of the residual organic substances in the effluent were difficult to be biodegraded.

3.2. COD Removal with UV Photolysis, Ozonation, and UV/O_3 Oxidation. Figure 3 shows COD variation in the oxidation reactor with time under UV photolysis, ozonation, and UV/O_3 oxidation. It can be seen that COD removal with UV photolysis alone was low. In 30 min contacting

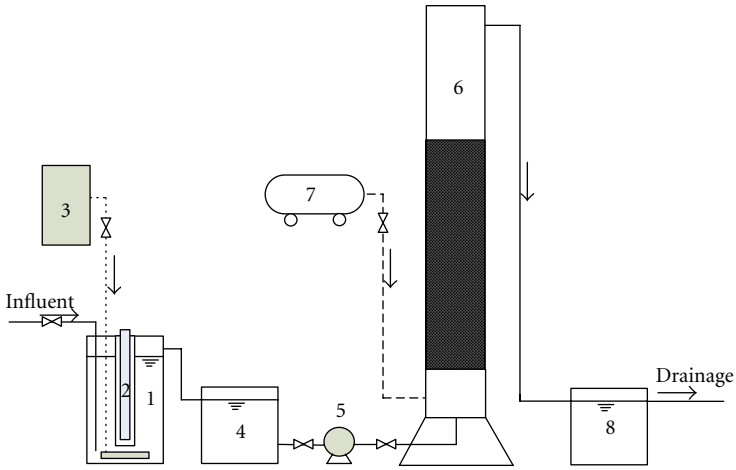

Figure 1: Schematic diagram for UV/O_3 oxidation combined with BAF, (1) UV/O_3 oxidation reactor, (2) UV lamp, (3) ozone generator, (4) medium water tank, (5) pump, (6) BAF, (7) aerator, (8) final water tank.

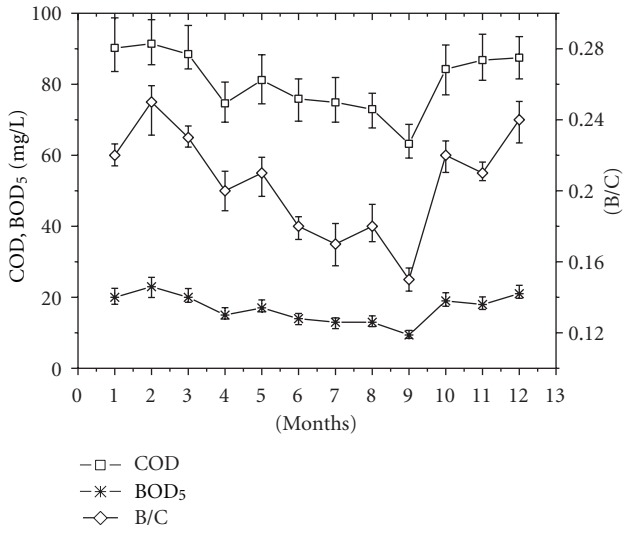

Figure 2: COD, BOD_5, and B/C changes in the effluent from the secondary clarifiers.

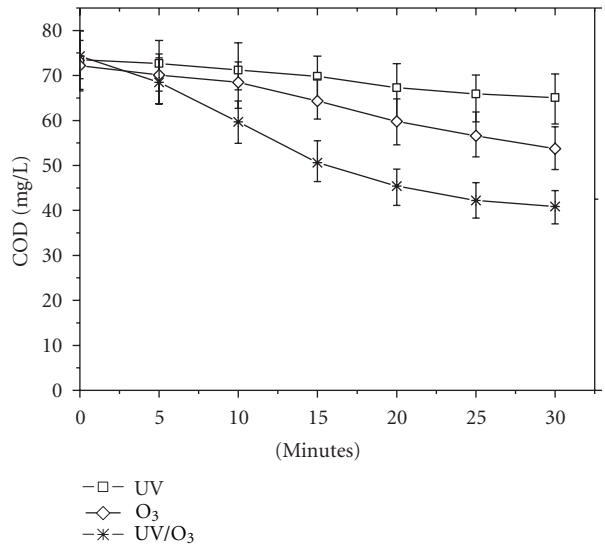

Figure 3: COD changes with time under UV photolysis, ozonation, and UV/O_3 oxidation (O_3 dosage 8 mg/L, temperature 21°C, pH 7.2).

time, COD only declined from 73.5 mg/L to 65.1 mg/L. The performance of ozonation was much better compared with UV photolysis. After 30 min ozonation, COD decreased from 72.2 mg/L to 53.7 mg/L. More than 25% of COD was removed during ozonation. The combination of UV photolysis and ozonation led to significant improvement of COD removal compared with UV photolysis and ozonation alone. In 30 min, COD reduced from 74.3 mg/L to 40.9 mg/L. The removal rate of COD attained about 45%, which was much higher than the sum of COD removal rates with UV photolysis and ozonation alone. The results indicated that UV photolysis could greatly improve COD removal during ozonation [20].

It can also be observed that COD concentration decreased with contact time rise. During UV/O_3 oxidation, COD decreased from the original 74.3 mg/L to 59.7, 45.4, and 40.9 mg/L at contact time of 10, 20, and 30 min, respectively. The extension of contact time was beneficial for COD removal. Nevertheless, the reactor volume needed to be amplified with contact time extension. More construction investment and operation cost would be required. It can be seen that contact time influence on COD removal was relieved with contact time exceeding 20 min. Therefore the subsequent experiments were done with contact time of 20 min.

3.3. Influence of O_3 Dosages on UV/O_3 Oxidation. A series of experiments of UV/O_3 oxidation was done at different ozone dosages in the range of 0–12 mg/L. Results of COD variation with ozone dosages are shown in Figure 4. It can

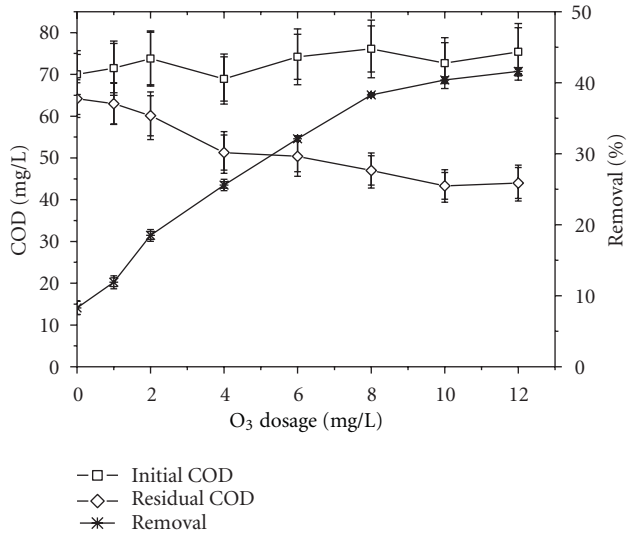

Figure 4: Influence of O_3 dosage on COD removal in UV/O_3 oxidation (contact time 20 min, temperature 20°C, pH 7.2).

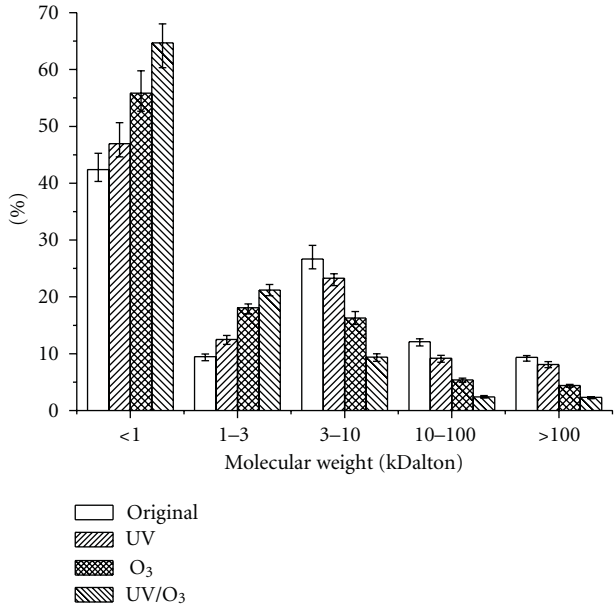

Figure 5: Molecular weight distribution under UV photolysis, ozonation, and UV/O_3 oxidation (contact time 20 min, O_3 dosage 8 mg/L, temperature 21°C, pH 7.2).

be seen that COD removal rose with ozone dosage increase. COD removal increased from 8.3% to 41.6% with dosage ranging from 0 to 12 mg/L, while residual COD decreased from 64.2 mg/L to 44 mg/L. It can also be noticed that when ozone dosage was under 2 mg/L, COD removal was low. When ozone dosage was increased from 2 to 8 mg/L, COD removal was enhanced greatly. These results indicated that ozone dosage was an important factor of UV/O_3 oxidation. However, COD changed little when ozone dosage was above 8 mg/L. This indicated that there were still some organic compounds which were difficult to be degraded with UV/O_3 oxidation, and excessive ozone dosage could not make further COD removal.

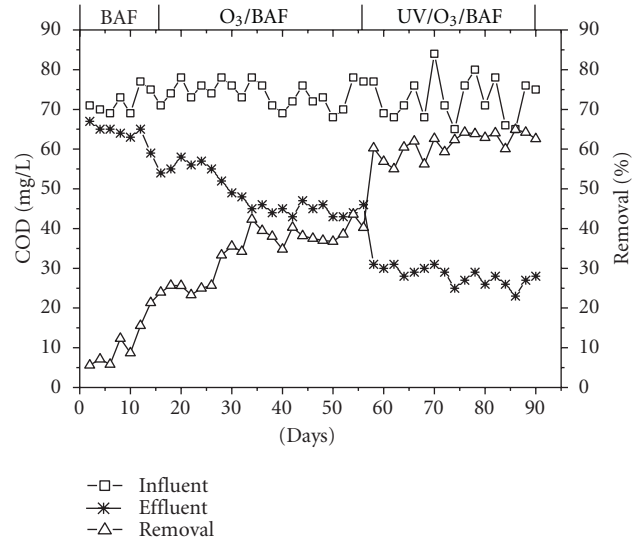

Figure 6: COD removal contrast with BAF, O_3/BAF, and UV/O_3/BAF (oxidation contact time 20 min, O_3 dosage 8 mg/L).

3.4. Molecular Weight Distributions under UV Photolysis, Ozonation, and UV/O_3 Oxidation. MWD under different operations is shown in Figure 5. In the effluent from the secondary clarifiers, organics with molecular weight (MW) <1 kDalton were 42.4%. After UV photolysis, there was a minor increase of organics with MW <3 kDalton. After ozonation, the proportions of organics with MW <1 kDalton and 1–3 kDalton were increased obviously. Organics with MW <3 kDalton attained about 74%, which was much higher than 51.9% in the original influent. The combination of UV photolysis and ozonation changed MWD more greatly. Organics with MW <1 kDalton and 1–3 kDalton reached 64.7% and 21.2%, respectively. The proportion of organics >10 kDalton decreased from the original 21.5% to 4.7%. UV/O_3 oxidation improved MWD of organics greatly and produced more biodegradable substances [21]. Consequently, the wastewater after UV/O_3 oxidation was more appropriate for further biological treatment.

3.5. Performance of UV/O_3 Oxidation Combined with BAF. Figure 6 shows COD removal with BAF alone (1–26 d), O_3/BAF (27–56 d), and UV/O_3/BAF (57–90 d). At the beginning, the BAF was started with the activated sludge of this WWTP as inoculum. COD removal increased gradually with time as more biofilm grew on the ceramisites. At the end of Day 16, COD removal rate attained about 24%. Subsequently, COD removal rate was maintained around 25%. Owing to the low biodegradability of organics in the influent, BAF alone could not remove more COD. COD in the effluent from the BAF was still above 50 mg/L, exceeding the standard limit for WWTPs in China.

In the second phase (27–56 d), ozonation was combined with BAF, and there was an obvious increase in

COD removal. The combination of ozonation and BAF could remove 33%–44% COD. The average removal rate reached 38%. Ozonation had decomposed partial organic compounds into biodegradable substances, which could be readily biodegraded in subsequent BAF.

When UV photolysis and ozonation were combined with BAF (UV/O_3/BAF, from Day 57 to Day 90), there was further improvement of COD removal. The average COD removal rate was above 61%, which was 2.5 and 1.6 times of that in BAF and O_3/BAF, respectively. With influent COD ranging from 65 mg/L to 84 mg/L, the effluent COD was stably maintained in the scope of 23–31 mg/L. These results indicated that the combination of UV/O_3 oxidation with BAF was an appropriate process for low biodegradable wastewater treatment. UV/O_3 oxidation could not only remove partial organic pollutants, but also efficiently enhance wastewater biodegradability [22]. With UV/O_3 oxidation combined with BAF, most organics were removed from the wastewater with the comprehensive activities of physicochemical decomposition and biodegradation.

4. Conclusion

The effluent from the secondary clarifiers of the WWTP comprises many refractory organic pollutants, most of which are difficult to be biodegraded. Direct treatment with further biological processes cannot make satisfactory performance. AOPs are usually efficient in refractory pollutants removal, and can be combined with biological processes in low biodegradable wastewater treatment. In this study, UV/O_3 oxidation was combined with BAF in tertiary treatment. The results indicated that although UV photolysis alone was not quite efficient for COD removal, it could improve the performance of ozonation. When UV photolysis was combined with ozonation, 45% of COD in the wastewater from the secondary effluent was removed, and more biodegradable organic compounds were produced. It was really feasible to combine UV/O_3 oxidation with BAF to improve COD removal in tertiary wastewater treatment. The combination of UV/O_3 oxidation with BAF could remove more than 61% of COD in the wastewater from the second clarifiers, which was nearly 2.5 and 1.6 times of that in BAF and O_3/BAF, respectively.

Acknowledgments

This research was supported by the project of the priority academic program development of Jiangsu Higher Education Institutions (2011-6), and science and technology project of China Housing and Urban-Rural Development Ministry (2010-K7-10).

References

[1] J. Hollender, S. G. Zimmermann, S. Koepke et al., "Elimination of organic micropollutants in a municipal wastewater treatment plant upgraded with a full-scale post-ozonation followed by sand filtration," *Environmental Science and Technology*, vol. 43, no. 20, pp. 7862–7869, 2009.

[2] V. J. P. Vilar, A. I. E. Gomes, V. M. Ramos, M. I. Maldonado, and R. A. R. Boaventura, "Solar photocatalysis of a recalcitrant coloured effluent from a wastewater treatment plant," *Photochemical and Photobiological Sciences*, vol. 8, no. 5, pp. 691–698, 2009.

[3] J. Gong, Y. Liu, and X. Sun, "O_3 and UV/O_3 oxidation of organic constituents of biotreated municipal wastewater," *Water Research*, vol. 42, no. 4-5, pp. 1238–1244, 2008.

[4] M. Bundschuh, R. Pierstorf, W. H. Schreiber, and R. Schulz, "Positive effects of wastewater ozonation displayed by in situ bioassays in the receiving stream," *Environmental Science and Technology*, vol. 45, no. 8, pp. 3774–3780, 2011.

[5] M. Petala, V. Tsiridis, P. Samaras, A. Zouboulis, and G. P. Sakellaropoulos, "Wastewater reclamation by advanced treatment of secondary effluents," *Desalination*, vol. 195, no. 1–3, pp. 109–118, 2006.

[6] F. J. Beltrán, M. González, and J. F. González, "Industrial wastewater advanced oxidation. part 1. UV radiation in the presence and absence of hydrogen peroxide," *Water Research*, vol. 31, no. 10, pp. 2405–2414, 1997.

[7] S. Kenfack, V. Sarria, J. Wéthé et al., "From laboratory studies to the field applications of advanced oxidation processes: a case study of technology transfer from Switzerland to burkina faso on the field of photochemical detoxification of biorecalcitrant chemical pollutants in water," *International Journal of Photoenergy*, vol. 2009, Article ID 104281, 8 pages, 2009.

[8] R. G. Rice, "Applications of ozone for industrial wastewater treatment—a review," *Ozone*, vol. 18, no. 6, pp. 477–515, 1997.

[9] K. Ikehata and M. G. El-Din, "Aqueous pesticide degradation by ozonation and ozone-based advanced oxidation processes: a review (part II)," *Ozone*, vol. 27, no. 3, pp. 173–202, 2005.

[10] F. J. Beltràn, J. F. García-Araya, and P. M. Alvarez, "Wine distillery wastewater degradation. 1. Oxidative treatment using ozone and its effect on the wastewater biodegradability," *Journal of Agricultural and Food Chemistry*, vol. 47, no. 9, pp. 3911–3918, 1999.

[11] M. Mišík, S. Knasmueller, F. Ferk et al., "Impact of ozonation on the genotoxic activity of tertiary treated municipal wastewater," *Water Research*, vol. 45, no. 12, pp. 3681–3691, 2011.

[12] A. Mandal, K. Ojha, A. K. De, and S. Bhattacharjee, "Removal of catechol from aqueous solution by advanced photooxidation process," *Chemical Engineering Journal*, vol. 102, no. 2, pp. 203–208, 2004.

[13] K. J. Friesen, T. M. El-Morsi, and A. S. Abd-El-Aziz, "Photochemical oxidation of short-chain polychlorinated n-alkane mixtures using H_2O_2/UV and the photo-fenton reaction," *International Journal of Photoenergy*, vol. 6, no. 2, pp. 81–88, 2004.

[14] M. Klavarioti, D. Mantzavinos, and D. Kassinos, "Removal of residual pharmaceuticals from aqueous systems by advanced oxidation processes," *Environment International*, vol. 35, no. 2, pp. 402–417, 2009.

[15] W. Zhao, Q. Liao, J. Zhang, Y. Yang, J. Dai, and D. Zhao, "Oxidation of cationic red X-GRL by ozonation combined with UV radiation in aqueous solution: degradation, kinetics, and modeling," *Chemical Engineering Journal*, vol. 171, no. 2, pp. 628–639, 2011.

[16] F. J. Beltrán, J. M. Encinar, and J. F. González, "Industrial wastewater advanced oxidation. Part 2. Ozone combined with hydrogen peroxide or UV radiation," *Water Research*, vol. 31, no. 10, pp. 2415–2428, 1997.

[17] C. Hofl, G. Sigl, O. Specht, I. Wurdack, and D. Wabner, "Oxidative degradation of AOX and COD by different

advanced oxidation processes: a comparative study with two samples of a pharmaceutical wastewater," *Water Science and Technology*, vol. 35, no. 4, pp. 257–264, 1997.

[18] W. K. Lafi, M. Al-Anber, Z. A. Al-Anber, M. Al-Shannag, and A. Khalil, "Coagulation and advanced oxidation processes in the treatment of olive mill wastewater (OMW)," *Desalination and Water Treatment*, vol. 24, no. 1–3, pp. 251–256, 2010.

[19] A. S. Stasinakis, "Use of selected advanced oxidation processes (AOPs) for wastewater treatment—a mini review," *Global NEST Journal*, vol. 10, no. 3, pp. 376–385, 2008.

[20] W. S. Kuo, "Synergistic effects of combination of photolysis and ozonation on destruction of chlorophenols in water," *Chemosphere*, vol. 39, no. 11, pp. 1853–1860, 1999.

[21] J. Chung and J. O. Kim, "Application of advanced oxidation processes to remove refractory compounds from dye wastewater," *Desalination and Water Treatment*, vol. 25, no. 1–3, pp. 233–240, 2011.

[22] K. Ito, W. Jian, W. Nishijima, A. U. Baes, E. Shoto, and M. Okada, "Comparison of ozonation and AOPs combined with biodegradation for removal of THM precursors in treated sewage effluents," *Water Science and Technology*, vol. 38, no. 7, pp. 179–186, 1998.

Hindawi Publishing Corporation
International Journal of Photoenergy
Volume 2012, Article ID 341592, 11 pages
doi:10.1155/2012/341592

Research Article

Microbiological Evaluation of the Effectiveness of Sewage Sludge Sanitization with Solar Drying Technology

Zbigniew Paluszak,[1] Krzysztof Skowron,[1,2] Małgorzata Sypuła,[1] and Karolina Jadwiga Skowron[1]

[1] *Department of Microbiology, Faculty of Agriculture and Biotechnology, University of Technology and Life Sciences in Bydgoszcz, Bernardyńska 6-8, 85-029 Bydgoszcz, Poland*
[2] *Department of Microbiology, Faculty of Pharmacy, Nicolaus Copernicus University in Toruń, Collegium Medicum of L. Rydygier in Bydgoszcz, M. Skłodowskiej-Curie 9, 85-094 Bydgoszcz, Poland*

Correspondence should be addressed to Zbigniew Paluszak, paluszak@utp.edu.pl

Received 28 May 2012; Accepted 4 September 2012

Academic Editor: Manickavachagam Muruganandham

The aim of study was to estimate the sanitization effectiveness of the sludge solar drying process carried out on technical scale in Poland based on the inactivation of bacteria and parasite eggs. Sewage sludge samples inoculated with *Escherichia coli*, *Salmonella* Senftenberg W_{775} and enterococci and perlon bags containing *Ascaris suum* eggs were placed inside the carriers fixed in the dried sludge pile and on the shovels and frame of the sludge turner. The number of reisolated microorganisms was determined with MPN method and the percentage of invasive *A. suum* eggs—with the microscope counting. On the basis of regression equations, the theoretical survivability and elimination rate of bacteria and parasite eggs were calculated. Experiment showed low hygienization efficiency of solar drying method. The theoretical survival time was 46–104 days in summer and 90–98 days in winter for *S.* Senftenberg W_{775} and, respectively 42–55 and 71–148 days for *E. coli*, depending on the carriers location. Enterococci were able to survive for 52–168 days in summer and in winter its number increased. The decrease in the percentage of invasive *A. suum* eggs was almost not observed. Results indicated that solar drying is a technology, which does not guarantee biosafety of product.

1. Introduction

Growing effectiveness of sewage treatment technologies results in a considerable increase in generated sewage sludge [1]. The dry matter of stabilized municipal sewage sludge is expected to amount to 662,000 Mg in Poland in 2015.

A considerable number of viruses, bacteria, and intestinal parasites may be present in sewage derived from hospitals, slaughter houses, and animal farms [2–5].

According to Bień [6], Sahlström [7], Pepper et al. [8], and Sun et al. [9], bacteria of the genera: *Salmonella* (about 1,700 types), *Shigella* (4 species), *Escherichia coli*, *Vibrio cholerae*, *Mycobacterium tuberculosis*, *Pseudomonas aeruginosa*, *Clostridium perfringens*, *Bacillus anthracis*, *Listeria monocytogenes, Streptococcus faecalis*, and *Proteus vulgaris* and viruses of the genera Enterovirus (67 types), Rotavirus, Parvovirus, and Adenovirus (31 types) are frequently isolated from sewage sludge.

Of various methods of sewage treatment in Poland, those consisting in physicochemical processing, including drying, are developing dynamically. Conventional drying allows considerable reduction in the mass and volume of produced sludge, but it generates high costs resulting from the facility operation and causes a substantial emission of gaseous pollutions to the atmosphere.

The unconventional, low-temperature technology of solar drying of sewage sludge is prospective from the economic and ecological point of view [10].

Due to sanitary and epidemiological reasons, it is necessary to establish biological and microbiological methods which allow constant monitoring of sewage sludge sanitization effectiveness in solar drying process.

The aim of this study was to estimate the sanitization effectiveness of the sludge's solar drying process conducted on technical scale in Poland, based on the inactivation kinetics of indicator bacteria and selected parasite eggs.

Figure 1: Solar drying plant in Iława.

Figure 2: Heating floor system in drying hall.

2. Material and Methods

The study was carried out in a solar drying plant of sewage sludge in north Poland in 2 research cycles, in summer and winter.

2.1. Description of the Examined Technology of Sludge Drying. The solar drying plant is a system used commercially and it works in full scale at the waste water treatment plant in Iława. This sewage sludge drying installation consists of drying halls similar to green houses with gable roof (Figure 1). The construction of the drying hall is made of zinc-coated steel and covered with polycarbonate plates. The dimensions of the drying hall are 120 m length, 12 m width, and 6 m height.

The described solar drying plant is a hybrid installation. The main principle of the drying operation is the solar effect, but also the heating floor system (Figure 2) is exploited for water evaporation from sewage sludge. The heating floor additionally supports the drying process and the heat necessary for its functioning is made by a heating pump which recovers energy from the treated sewage through the collector in secondary clarifier.

The solar drying plant is located next to the building of mechanical sludge dewatering station, from where dehydrated sludge is transported into the hall by the transporter system. Inside the drying hall mechanically dewatered sludge is spread with an even layer on the concrete floor and then transported, aerated, granulated and moved to the end of the hall by the nave turning sludge device (Figure 3). The

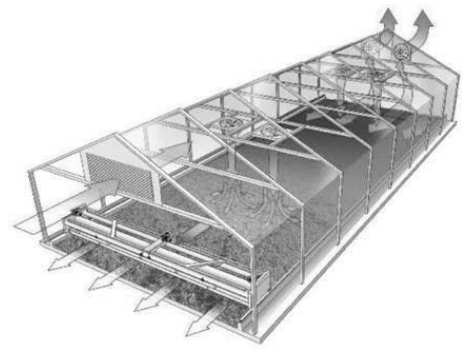

Figure 3: Scheme of solar drying plant with nave turning sludge device (http://www.huber.de/).

automatic ventilation system, which consists of mechanical ventilators inside the hall and the automatically opened window at the top of the roof, ensures and improves water evaporation and humidity removal outside the drying hall.

The annual plant capacity is 3,500 t of sewage sludge whose dry matter content at the beginning of the process is up to 20% and after drying 85–90%. The studies conducted so far show that under the climatic conditions prevailing in Iława, using solar energy allows to evaporate on average 988 kg of water from 1 m^2 of active surface of the dryer within a year. The drying hall with a total drying area of 1,440 m^2 provides evaporation of about 1,422 tons of water.

Solar sludge drying is currently the cheapest method of getting rid of water from the sludge. For example, 1 tone of water evaporation in the solar drying system requires using about 20–30 kWh, while in conventional drying system based on traditional fuels above 800 kWh.

2.2. Material for the Study. The material for the study was sewage sludge after mechanical dewatering to a dry matter content of 10% to 20%. The presence of native *Salmonella*, bacteria *E. coli*, and enterococci was examined in collected sludge samples. Also the proportion of dry matter and dry organic matter, pH, and the content of basic macroelements and heavy metals were determined in the sludge.

2.3. Experimental Design. The study was conducted in 2 cycles, summer and winter. In each cycle, 3 replications were made for each location of the carrier.

The experiment was carried out using carriers in the form of perforated cylinder with a threaded lock.

Samples of municipal sludge with a weight of 25 g were contaminated with 1 mL of the suspension of *Escherichia coli*, bacilli *Salmonella* Senftenberg W_{775} and enterococci and placed in the carriers. Also perlon bags containing live eggs of *Ascaris suum* were placed inside the carriers. Then they were closed and fixed in selected points (in the pile of dried sludge at the end of the hall, as well as on shovels and frame of the sludge turner).

From each location, 3 carriers were collected for the study after 7, 14, 21, and 28 days, respectively.

Table 1: Applicable reference methods of municipal sewage sludge research [11].

Number	Parameter	Method
(1)	pH	Electrometric determination in water solution
(2)	Dry matter content	Drying at 105°C, weighing
(3)	Organic substance content	Roasting at 600°C, weighing
(4)	Total nitrogen content	Mineralization in acid pH with addition of catalyst
(5)	Ammonium nitrogen content	Distillation of ammonia and determination with spectrophotometric method
(6)	Total phosphorus content	Mineralization to phosphorus (V) and determination with spectrophotometry
(7)	Calcium and magnesium content	Mineralization with acid mixture and determination with atomic spectrometry
(8)	Heavy metal content: lead, cadmium, mercury, nickel, zinc, copper and chromium	Atomic absorption spectroscopy after mineralization in aqua regia or concentrated acids

2.4. Monitoring of Climatic Conditions. During the experiment, the following parameters were monitored: humidity and temperature in the drying plant (with the use of the hygrothermometer), the temperature in the pile (with the use of the in-pile thermometer), the intensity of diffuse solar radiation coming to the horizontal plane of the drying plant roof (with the use of pyranometer), and the outside microclimatic conditions (the climatic station data). Monitoring was conducted according the methods commonly applied in meteorology.

2.5. Physicochemical Analyses. The physicochemical analysis of the dried sludge parameters was made at each sampling time. It involved the assessment of dry matter and organic dry matter content, pH, the content of fertilizer components (total and ammonium nitrogen, total phosphorus, calcium, and magnesium), and heavy metals (lead, cadmium, mercury, nickel, zinc, copper, and chromium).

Physicochemical analyses of the sludge were carried out using the referential methods described in Appendix 5 to the ordinance of the Ministry of the Environment of 13rd July 2010 on municipal sewage sludge (Dz.U. 2010 nr 137 poz. 924) [11]. The applied methods are presented in Table 1.

2.6. Microbiological Analyses. For contamination of the experimental material, suspension of *Salmonella* Senftenberg W_{775}, bacteria *E. coli*, and enterococci were used.

From 24-hour pure cultures of the tested microorganisms on nutrient agar, bacterial suspensions in 0.90% physiological salt solution with a density of 10 McF ($\sim 3.0 \times 10^9$ cfu $\times$ cm^{-3}) were prepared.

The number of microorganisms isolated from the carriers submitted to solar drying process at successive times was determined based on the MPN method in the three-tube design.

In the process of *Salmonella* isolation, 1% buffered peptonic water was used for initial multiplication (incubation for 24 hours at 37°C). Selective enrichment was conducted on the Rappaport medium (incubation for 24 hours at 43°C). BPLS agar was used as the solid growing medium (incubation for 24 hours at 37°C). Final identification was carried out using the PCR reaction for detecting the fragment *invA* [12]. To 5 μL of isolated DNA 20 μL mastermix was added, composed of distilled water (8.85 μL), 10x PCR buffer (2.5 μL; Bioline, cat. no. BIO-37030), magnesium chloride (1.50 μL–25 mM; Bio-Rad, cat. no. 170-8872), dNTP's (5 μL–1 mM; Bio-Rad, cat. no. 170-8874), primer 139 (5′ GTGAAATTATCGCCACGTTCGGGCAA 3′ 1 μL–10 μM), primer 141 (5′ TCATCGCACCGTCAAAGGAACC 3′ 1 μL–10 μM), and *Taq* polymerase (0.15 μL–5 U/μL; Bio-Rad, cat. no. 170-8870). The initial denaturation of DNA was conducted at 95°C for 1 minute. Then 38 cycles were comprising of denaturation (30 seconds at 95°C), annealing (30 seconds at 64°C), and elongation (30 seconds at 72°C). The last stage of the PCR reaction was the final elongation carried out for 4 minutes at 72°C. Electrophoresis was carried out in 1.8% agarose gel (Bio-Rad, cat. no. 151-0450) at the voltage 5 V $\times$ cm^{-1} for 60 minutes and dyed with ethidium bromide (Bio-Rad, cat. no. 161-0433).

To determine *E. coli* number, the MacConkey liquid medium was used (incubation for 24 at 43°C). Then the material was sieved on the solid medium ENDO agar (incubation for 24 hours at 43°C). The final identification was carried out based on the set of biochemical tests API 20E.

Enterococci determination was carried out using broth with glucose and azide (incubation for 24 hours at 37°C) and agar with kanamycin (incubation for 24 hours at 37°C). The final identification was carried out based on the Phadebact D—Strep Test.

2.7. Parasitological Investigation. Ascaris suum eggs were obtained from uteruses of sexually mature females and placed on Petri dishes filled with saline solution. Suspension in volume of 1 mL with a density from 1.0×10^3 to 6.0×10^3 eggs $\times$ cm^{-3} was introduced to each perlon bag and used for experiment. The bags collected during the study were opened and placed on Petri dishes with tap water. Incubation lasted for 28 days at 28°C. The percentage of invasive eggs was determined with the microscope counting method.

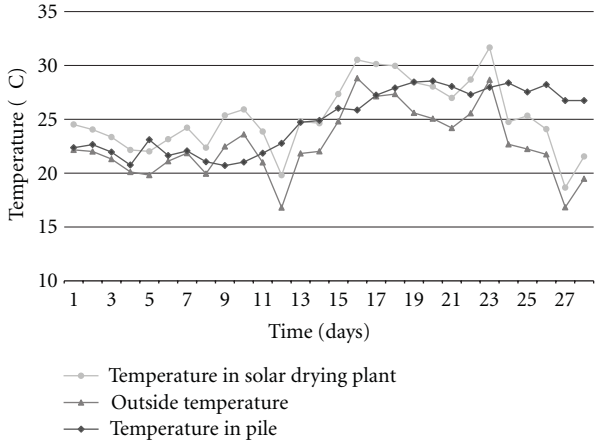

Figure 4: The course of temperature during the summer cycle (July).

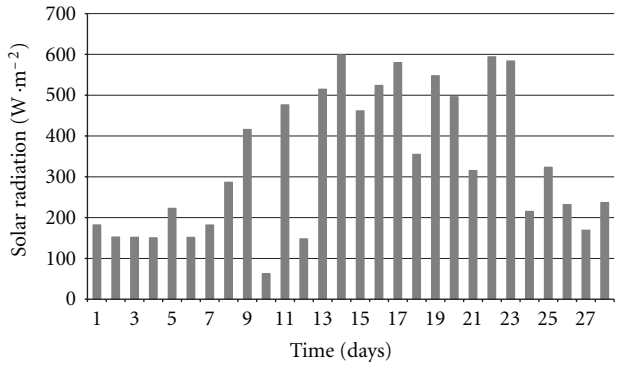

Figure 5: The course of insolation during the summer cycle (July).

2.8. The Statistical Analysis of the Results. The obtained results were analyzed statistically in the program SAS 9.2 PL. On the basis of regression equations, the theoretical times of survival and elimination rates of the studied bacteria and parasite eggs were determined. The significance of differences between the theoretical survival rate of individual microorganisms in respect of the season and the location of the carrier was estimated based on Tukey's test at the significance levels $P \leq 0.05$ and $P \leq 0.01$.

3. Results and Discussion

3.1. Climatic Conditions. The effectiveness of sludge drying in solar drying plants is very closely connected with climatic conditions.

The detailed course of the analyzed indexes of microclimate in the summer cycle was presented in Figures 4, 5, and 6.

In the summer cycle, the temperature in the pile of dried sludge remained above 20°C and its gradual increase during the experiment was recorded up to a value of above 28°C. The air temperature inside the drying plant hall was changing and ranged from 18°C to 32°C, with the average value of 25.2°C. The mean difference between the inside temperature

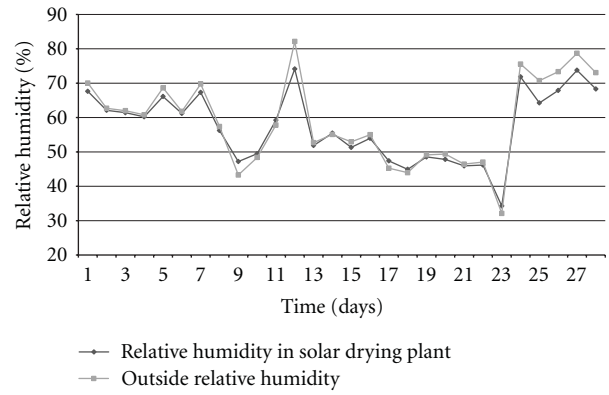

Figure 6: The course of relative humidity during the summer cycle (July).

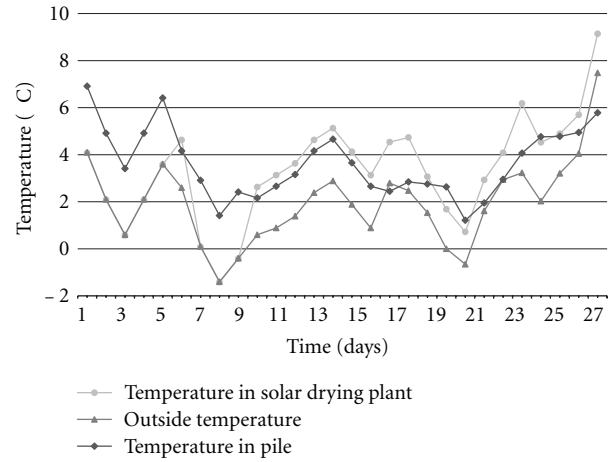

Figure 7: The course of temperature during the winter cycle (December).

in the drying plant and the outside temperature was on average 3.0°C (Figure 4).

The average daily level of solar radiation during the summer cycle was 327.8 W × m^{-2}, and the maximal radiation recorded reached the value of 598.4 W × m^{-2} (Figure 5).

The course of the relative humidity inside the drying plant hall was dependent on the air humidity outside and in both cases it showed considerable fluctuations. The lowest observed value of relative humidity inside the hall was 34%, whereas the highest was 74%, on average 58% (Figure 6).

A detailed course of the analyzed indexes of microclimate in the winter cycle was presented in Figures 7, 8, and 9.

The temperatures recorded in the winter period were definitely lower. The average temperature in the pile remained at 3.6°C, whereas the air temperature inside and outside the drying hall was 3.4°C and 2.0°C, respectively, (Figure 7).

Also the solar radiation intensity reached considerably the lowest level in comparison with the summer cycle. The maximal value of radiation exceeded 72.0 W × m^{-2}, whereas the minimal value did not fall below 6.3 W × m^{-2}, giving an average of 27.7 W × m^{-2} (Figure 8). Thus the measured daily

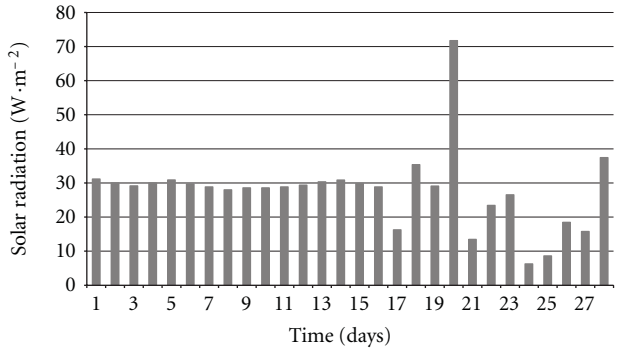

Figure 8: The course of insolation during the winter cycle (December).

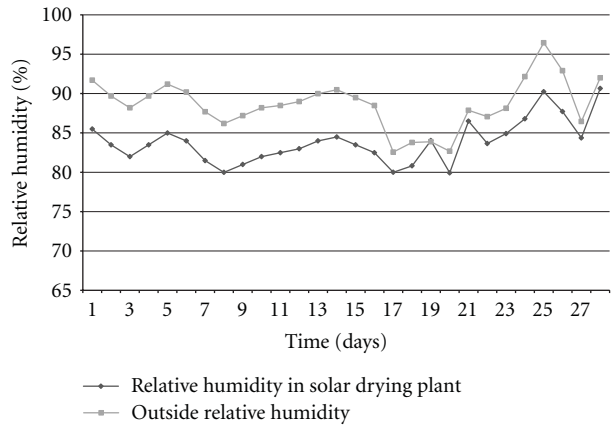

Figure 9: The course of relative humidity during the winter cycle (December).

intensity of solar radiation was insufficient for the effective drying by means of radiation [13].

The monitored air humidity in the winter cycle remained at the definitely higher level compared with the summer. Average values of the relative humidity inside the drying hall amounted to about 84%, whereas outside this was 89% (Figure 9). Such a level of the air humidity made convective drying of sludge considerably more difficult [13].

The distribution of insolation and air temperature may vary in different regions of Poland. The total yearly solar radiation intensity in the studied location stays within the range 996–1022 kWh $\times$ $(m^2 \times year)^{-1}$ [14].

The average long-time relative humidity of the air in Poland expressed in percent during the year is 76%, with the monthly average ranging from 71% in May to 88% in December. Large fluctuations occur in the daily cycle, irrespective of the season [15].

3.2. Physicochemical Analyses of Sewage Sludge. The average results of physicochemical analyses of sewage sludge in the summer cycle were presented in Table 2.

The dry matter of mechanically dewatered sludge processed in the drying plant reached the value 16.22%. The pH value was close to neutral and amounted to pH 6.69. The content of organic substances in the sludge was 66.9% (Table 2).

The proportion of fertilizer components, phosphorus, calcium, and magnesium, was on the average level of the values for municipal sewage sludge, and the concentration of seven tested heavy metals was low, qualifying the sludge for use in agriculture (Table 2).

In the summer cycle, an increase in the sludge dry matter was clearly visible. On 7th day of the study, it grew on average to more than 40%, and on 28th day of the cycle, sludge in the pile contained on average 86.4% dry matter. There was a decrease in organic substance proportion on 28th day of the study, as well as in total and ammonium nitrogen in dried sludge (Table 2). The other studied indexes were at the same level (Table 2).

Average results of physicochemical analyses of sewage sludge in the winter cycle were presented in Table 3.

Mechanically dewatered sludge processed in the drying plant in the winter cycle contained an average 13.86% dry matter, thus slightly less than in the summer period. The pH value had a marginally higher level than that in the summer cycle (pH 6.90), but it was also close to neutral. The content of organic substances in the sludge was on average 64.2% and was slightly lower than in the summer cycle (Table 3).

Just as in the material intended for drying in the summer, the proportion of fertilizer components, phosphorus, calcium, and magnesium, was characteristic of municipal sewage sludge, and the content of seven studied heavy metals was low, qualifying sludge for use in agriculture (Table 3). It is worthy of note that the mercury content in sewage sludge subjected to solar drying in the winter cycle (Table 3) is much lower than in summer (Table 2). This difference probably results from a slightly different chemical composition of sewage (higher content of mercury) directed to the sewage treatment plant during the particular period, which directly influenced the physicochemical parameters of sewage sludge.

During the winter research cycle, a small increase in the sludge dry matter was visible, considerably smaller than in the summer. On 7th day of the study, it grew to more than 18.9%. On 28th day of the study, the sludge in the pile contained 24.54% D.M (Table 3).

Just as in the summer, also in the winter cycle a decrease in organic substance in the dried sludge from 64.2% to 62.4% was observed. Contrary to the summer period, a distinct decrease in the total nitrogen content during sludge drying did not occur. The other studied indexes were not changed (Table 3).

The humidity of raw material has a substantial effect on the final level of sewage sludge drying in the solar drying plant. In the present study, the average dry matter content in sludge after centrifuge was 16.22% in the summer cycle and 13.86% in the winter cycle (Tables 2 and 3) and did not differ significantly from that given by other authors [16–18], where it was in the range 13.80–28.00%. In the summer cycle, the average proportion of dry matter in the sludge dried material after 28 days of the process increased to 86.4% and was similar to that observed by Bux et al. [16] during 21 days of solar drying. Slightly better effects of drying were reported

Table 2: Average results of physicochemical analyses of sewage sludge in summer cycles.

Parameter	Unit	Average results for summer cycles (replications number = 3) Sampling terms for the research (days)				
		0	7	14	21	28
Dry matter of sludge after centrifuge	%	16.22 (±0.16)*	—	—	—	—
Dry matter of sludge in the pile	%	—	40.30 (±4.00)	47.20 (±10.68)	69.90 (±10.81)	86.40 (±13.01)
Organic substance	% D.M.	66.90 (±0.71)	67.00 (±0.71)	66.60 (±0.90)	65.70 (±1.45)	65.30 (±1.71)
pH	—	6.70 (±0.16)	6.70 (±0.16)	6.69 (±0.13)	6.70 (±0.16)	6.70 (±0.18)
Total nitrogen content	% D.M.	4.08 (±1.27)	4.05 (±1.28)	3.60 (±1.19)	3.30 (±1.04)	3.20 (±1.04)
Ammonium nitrogen content	% D.M.	0.19 (±0.09)	0.16 (±0.10)	0.17 (±0.06)	0.15 (±0.02)	0.15 (±0.02)
Total phosphorus	% D.M.	2.14 (±0.99)	2.12 (±0.98)	2.12 (±0.98)	2.05 (±0.94)	2.12 (±0.98)
Calcium content (Ca)	% D.M.	1.13 (±0.14)	1.12 (±0.15)	1.12 (±0.15)	1.13 (±0.14)	1.13 (±0.14)
Magnesium content (Mg)	% D.M.	0.43 (±0.03)	0.43 (±0.03)	0.43 (±0.03)	0.43 (±0.03)	0.43 (±0.03)
Heavy metals						
Lead (Pb)	mg/kg D.M.	31.50 (±0.58)	31.50 (±0.58)	31.50 (±0.58)	31.50 (±0.58)	31.51 (±0.53)
Cadmium (Cd)	mg/kg D.M.	2.41 (±0.09)	2.42 (±0.07)	2.40 (±0.11)	2.41 (±0.09)	2.41 (±0.09)
Mercury (Hg)	mg/kg D.M.	1.03 (±0.60)	1.00 (±0.57)	1.00 (±0.57)	1.00 (±0.57)	1.00 (±0.57)
Nickel (Ni)	mg/kg D.M.	16.30 (±3.90)	16.31 (±3.76)	16.30 (±3.90)	16.30 (±3.90)	16.31 (±3.75)
Zinc (Zn)	mg/kg D.M.	1100.00 (±84.97)	1100.00 (±84.97)	1100.00 (±84.97)	1100.00 (±84.97)	1100.00 (±84.97)
Copper (Cu)	mg/kg D.M.	240.50 (±19.05)	240.50 (±19.05)	240.52 (±20.17)	240.51 (±20.15)	240.50 (±19.05)
Chromium (Cr)	mg/kg D.M.	38.37 (±23.56)	38.30 (±23.58)	38.37 (±23.56)	38.36 (±23.55)	38.37 (±23.56)

* Standard deviation.

Table 3: Average results of physicochemical analyses of sewage sludge in winter cycles.

Parameter	Unit	Average results for winter cycles (replications number = 3) Sampling terms for the research (days)				
		0	7	14	21	28
Sludge dry matter after centrifuge	%	13.86 (±0.62)*	—	—	—	—
Sludge dry matter in the pile	%	—	18.90 (±3.21)	21.43 (±4.33)	25.12 (±3.93)	24.54 (±4.84)
Organic substance	% D.M.	64.20 (±2.17)	65.50 (±2.04)	64.20 (±2.65)	63.40 (±2.87)	62.40 (±3.50)
pH	—	6.90 (±0.06)	6.90 (±0.06)	7.00 (±0.11)	6.98 (±0.10)	6.90 (±0.06)
Total nitrogen content	% D.M.	2.10 (±0.15)	2.12 (±0.17)	2.00 (±0.06)	2.12 (±0.17)	2.09 (±0.23)
Ammonium nitrogen content	% D.M.	0.10 (±0.06)	0.10 (±0.06)	0.11 (±0.04)	0.09 (±0.03)	0.15 (±0.01)
Total phosphorus	% D.M.	2.20 (±0.12)	2.22 (±0.13)	2.21 (±0.11)	2.20 (±0.12)	2.20 (±0.12)
Calcium content (Ca)	% D.M.	1.15 (±0.03)	1.13 (±0.03)	1.12 (±0.02)	1.15 (±0.03)	1.15 (±0.03)
Magnesium content (Mg)	% D.M.	0.23 (±0.04)	0.23 (±0.04)	0.23 (±0.04)	0.34 (±0.05)	0.23 (±0.03)
Heavy metals						
Lead (Pb)	mg/kg D.M.	22.23 (±2.79)	22.20 (±2.76)	22.20 (±2.76)	22.20 (±2.76)	22.20 (±2.76)
Cadmium (Cd)	mg/kg D.M.	1.98 (±0.26)	1.97 (±0.21)	1.89 (±0.20)	1.89 (±0.20)	1.87 (±0.18)
Mercury (Hg)	mg/kg D.M.	0.05 (±0.03)	0.05 (±0.03)	0.05 (±0.03)	0.00 (—)	0.05 (±0.03)
Nickel (Ni)	mg/kg D.M.	19.50 (±1.94)	19.50 (±2.12)	19.50 (±1.94)	19.50 (±1.94)	19.50 (±1.94)
Zinc (Zn)	mg/kg D.M.	1248.00 (±131.15)	1248.00 (±131.15)	1248.00 (±131.15)	1249.00 (±125.87)	1250.00 (±126.26)
Copper (Cu)	mg/kg D.M.	220.70 (±17.43)	220.70 (±17.43)	220.70 (±17.43)	220.70 (±17.50)	220.70 (±17.43)
Chromium (Cr)	mg/kg D.M.	27.64 (±2.08)	27.64 (±2.08)	27.64 (±2.08)	27.64 (±2.08)	27.64 (±2.08)

* Standard deviation.

Table 4: Number of indicator bacteria in particular determination times.

Cycle	Bacteria number [MPN × g^{-1}]	Drying time (days)				
		0	7	14	21	28
Sludge from carriers placed on the turner frame						
Summer	*Salmonella* Senftenberg W_{775}	4.5×10^7	3.83×10^6	9.97×10^7	4.83×10^5	2.8×10^5
	Escherichia coli	4.33×10^7	6.83×10^6	3.17×10^4	6.83×10^3	4.5×10^3
	Enterococci	6.13×10^7	5.5×10^6	4.15×10^7	2.13×10^5	1.87×10^5
Winter	*Salmonella* Senftenberg W_{775}	2.13×10^9	3.83×10^8	1.38×10^9	1.73×10^7	3.83×10^6
	Escherichia coli	3.83×10^7	3.83×10^7	1.51×10^8	6.17×10^4	1.83×10^5
	Enterococci	9.0×10^7	1.82×10^9	1.25×10^9	1.07×10^9	3.25×10^8
Sludge from carriers placed on the turner shovels						
Summer	*Salmonella* Senftenberg W_{775}	4.5×10^7	6.5×10^6	2.86×10^5	4.9×10^3	4.67×10^2
	Escherichia coli	4.33×10^7	4.33×10^5	7.83×10^6	2.65×10^4	7.65×10^3
	Enterococci	6.13×10^7	2.15×10^8	4.37×10^8	5.17×10^6	5.5×10^6
Winter	*Salmonella* Senftenberg W_{775}	2.13×10^9	1.38×10^9	1.73×10^8	2.83×10^6	1.72×10^7
	Escherichia coli	3.83×10^7	7.17×10^7	9.67×10^5	9.33×10^4	1.55×10^5
	Enterococci	9.0×10^7	6.17×10^8	2.38×10^8	3.17×10^8	1.07×10^9
Sudge from carriers placed in the sludge pile						
Summer	*Salmonella* Senftenberg W_{775}	4.5×10^7	3.17×10^6	1.77×10^6	6.17×10^5	3.17×10^5
	Escherichia coli	4.33×10^7	2.84×10^7	3.8×10^5	3.26×10^4	7.17×10^2
	Enterococci	6.13×10^7	3.75×10^8	2.48×10^7	5.98×10^4	7.17×10^3
Winter	*Salmonella* Senftenberg W_{775}	2.13×10^9	2.13×10^9	5.58×10^8	7.83×10^6	6.83×10^6
	Escherichia coli	3.83×10^7	2.5×10^7	7.83×10^5	1.2×10^6	3.17×10^6
	Enterococci	9.0×10^7	9.17×10^8	1.67×10^8	1.13×10^9	1.67×10^9

by Hertwig [19], as after 20 days of the process sewage sludge contained 94% dry matter.

3.3. Microbiological Analyses. In the sludge after centrifuging collected to the analyses, no bacilli of the genus *Salmonella* were isolated, and the number of isolated *E. coli* and enterococci was on average 10^5 and 10^4 NPL × g^{-1}, respectively.

Using the PCR technique, it was found that the bacteria reisolated from carriers and cultured on BPLS agar belonged to the genus *Salmonella*. Their presence was proved by the product of 284 bp corresponding to the fragment *invA* (Figure 10).

The results of API 20E tests for the microorganisms grown on ENDO agar determined the code 5144572, typical of *E. coli*. The final identification of bacteria grown on agar with kanamycin and azide based on the Phadebact D-Strep Test confirmed the presence of enterococci.

During sewage sludge solar drying in the summer cycle, a partial elimination of all the studied bacteria was observed (Table 4). This was dependent on the kind of carriers and their location. The population of *Salmonella* Senftenberg W_{775} decreased during 28 days of the process on average by about 2 log in sludge from the carriers placed on the frame of the turner and from carriers placed in the pile (Table 4).

In the carriers placed on the shovels of the turner, a reduction in their population was on average as much as

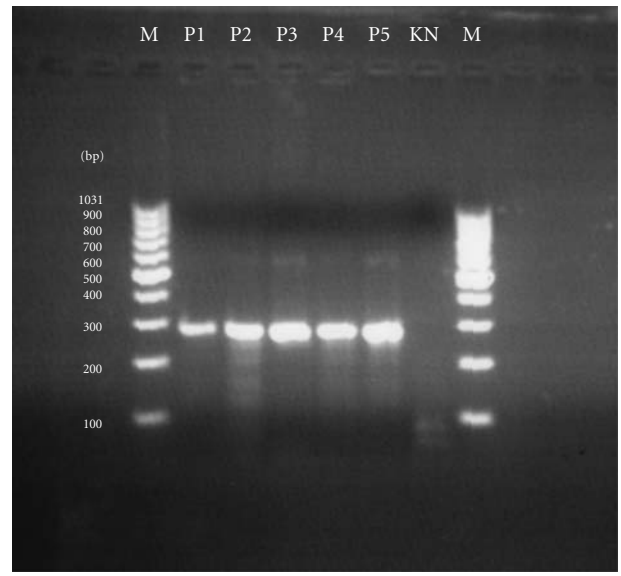

Figure 10: The PCR test confirming the presence of bacilli in the studied material (M: the size marker, P1: a sample from the carrier placed on the frame of the turner, P2: a sample from the carrier placed on the shovels of the turner; P3: a sample from the carrier placed in the sludge pile, P4: *Salmonella* Agona, P5: *Salmonella* Braenderup H9812 (P4 and P5: positive control), KN: negative control).

Table 5: Results of statistical analysis of obtained microbiological data.

Cycle	Bacteria	Regression equation	R^2 (%)	Theoretical time of survival (days)	Elimination rate (log MPN × day^{-1})
Sludge from carriers placed on the turner frame					
Summer	Salmonella Senftenberg W775	$y = -0.075x + 7.57$	61.11	104A,a,c,j	0.08A,G,a,e,f,j,n
	Escherichia coli	$y = -0.157x + 7.43$	88.93	$47^{B,a,c,j}$	$0.16^{B,D,a,d,j,n}$
	Enterococci	$y = -0.089x + 7.68$	68.95	$89^{A,D,a,d,j}$	$0.09^{A,D,G,c,e,f,g}$
Winter	*Salmonella* Senftenberg W_{775}	$y = -0.103x + 9.48$	77.69	$94^{A,E,a,e,j,g}$	$0.10^{A,D,G,I,b,e,h}$
	Escherichia coli	$y = -0.106x + 7.85$	65.97	$75^{A,B,b,d,f,g}$	$0.11^{A,D,G,I,b,e,h}$
	Enterococci	$y = 0.012x + 8.46$	6.26	—	$0.01^{C,E,a,e,i,m}$
Sludge from carriers placed on turner shovels					
Summer	*Salmonella* Senftenberg W_{775}	$y = -0.192x + 7.72$	96.57	$40^{B,a,c,j}$	$0.19^{B,F,a,e,j,n}$
	Escherichia coli	$y = -0.139x + 7.51$	74.77	$55^{B,D,E,c,h,k}$	$0.14^{A,D,F,H,I,b,d,i,k,l}$
	Enterococci	$y = -0.050x + 8.23$	38.99	$168^{C,F,G,a,c,f,h}$	$0.05^{E,G,f,j,k}$
Winter	*Salmonella* Senftenberg W_{775}	$y = -0.096x + 9.29$	70.46	$98^{A,a,c,j}$	$0.10^{A,D,G,I,e,l,m}$
	Escherichia coli	$y = -0.111x + 7.78$	77.03	$71^{A,B,E,b,d,h,l,k}$	$0.11^{A,D,G,I,c,e,l,o}$
	Enterococci	$y = 0.030x + 8.01$	36.67	—	$-0.03^{C,a,e,j,l,n}$
Sludge from carriers placed in a sludge pile					
Summer	*Salmonella* Senftenberg W_{775}	$y = -0.070x + 7.28$	91.29	$104^{A,a,c,j}$	$0.07^{A,G,a,e,j,n}$
	Escherichia coli	$y = -0.187x + 7.84$	92.09	$42^{B,a,c,j}$	$0.19^{B,H,a,e,j,n}$
	Enterococci	$y = -0.165x + 8.57$	79.27	$52^{B,D,c,e,k}$	$0.17^{B,I,a,g,k,n}$
Winter	*Salmonella* Senftenberg W_{775}	$y = -0.107x + 9.60$	81.05	$90^{A,D,a,f,i,j,k}$	$0.11^{A,D,G,I,c,e,l,p}$
	Escherichia coli	$y = 0.051x + 7.37$	50.05	$148^{C,F,G,g,j,k}$	$0.05^{E,G,g,k,n}$
	Enterococci	$y = 0.035x + 7.99$	40.77	—	$0.04^{C,a,g,h,j,k,o,p,m}$

$^{A, B, C,\cdots}$ Highly statistically significant differences ($P \leq 0.01$).
$^{a, b, c,\cdots}$ Statistically significant differences ($P \leq 0.05$).

5 log. The mean theoretical time of survival of *Salmonella* Sanftenberg W_{775} in the summer cycle, calculated based on the regression equations, was 104 days in dried sludge from the carriers placed on the frame of the turner and in the pile. This time was highly statistically significantly longer than that in the sludge from carriers on the shovels of the turner (40 days) (Table 5). The elimination rate of the bacteria on the shovels was highly significantly higher (0.19 log MPN × day^{-1}) in relation to the other samples (0.08 and 0.07 log MPN × day^{-1}) (Table 5).

At the same time, the number of *E. coli* isolated from carriers located on the frame and shovels of the turner decreased on average by about 4 log, whereas in the pile by about 5 log (Table 4). The mean theoretical times of survival ranged from 42 to 55 days (Table 5).

In the summer cycle, the highest average decrease in the number of enterococci, amounting to 4 log, was observed in the sludge from carriers placed in the pile, whereas the lowest, about 1 log, was observed in the material from carriers on the turner shovels (Table 4). In the sludge subjected to solar drying in the summer cycle, enterococci were theoretically able to survive on average from 52 days in the material from carriers placed in the pile to 168 days in samples from the turner shovels, at the elimination rate ranging from 0.05 to 0.17 log MPN × day^{-1} (Table 5). Highly statistically significant differences in the theoretical survival rates of enterococci were found between the material from the pile and the sludge from the other two locations, and statistically significant differences between samples from the turner frame and those from the pile (Table 5).

The available literature data shows that solar drying does not provide the complete sanitization of sewage sludge even in the summer cycles. The study by Bux et al. [16] conducted on technical scale in sludge solar drying plants working with charging method indicated that during the cycle lasting 21 days a reduction in the number of fecal coliform bacteria by 3 $\log_{10}$ was obtained. Also in experiments conducted in Australia [20], despite more favorable climatic conditions, a considerable smaller decrease in the number of *E. coli* was found in comparison with the present study, amounting to 1 $\log_{10}$. Also in the pilot study conducted in Turkey by Ögleni and Özdemir [21], the number of fecal coliform bacteria in sludge after 12 weeks of solar drying did not fall below 1.0×10^3 MPN × g^{-1} D.M., just as during its

storage. Mathioudakis et al. [22], in spite of very high temperatures, from 35 to 40°C, and large sun exposure from 950 to 1000 W $\times$ m^{-2}, obtained only a slight reduction in the number of coliform bacteria from 4 $\times$ 10^6 to 2 $\times$ 10^4 MPN $\times$ g^{--} D.M. and of fecal coliform bacteria from 3 $\times$ 10^5 to 10^3 MPN $\times$ g^{-1} D.M. in the dried sludge. Different results were obtained by Cota et al. [17] studying sludge at the pilot sludge drying plant in Mexico. The elimination of the studied pathogens proceeded in a very fast rate there. At the beginning of the research cycle, the number of fecal coliform bacteria amounted to 3.87 $\times$ 10^6 MPN $\times$ g^{-1} D.M. After 4 days (98 h), a decrease in the number up to 7.74 $\times$ 10^4 MPN $\times$ g^{-1} D.M. was obtained, whereas after 11 days (269 h) only up to 1.6 $\times$ 10^0 MPN $\times$ g^{-1} D.M. were isolated.

During the winter cycle of sludge solar drying, the number of *Salmonella* Senftenberg W_{775} decreased on average by 2-3 log, depending on the location (Table 4). The average theoretical time of survival calculated based on the regression line equation ranged from 90 to 98 days, at the elimination rate from 0.11 to 0.10 log MPN $\times$ day^{-1}, respectively (Table 5). The above values did not differ significantly (Table 5). In the sludge from carriers located on the turner frame and in the pile, bacilli of *Salmonella* Senftenberg W_{775} theoretically survived slightly shorter in the winter cycle as compared with the summer, whereas in the samples from the turner shovels the reverse tendency occurred, and the differences in the survival time and elimination rate were highly statistically significant (Table 5).

A decrease in the number of *E. coli* in the winter period was very low and ranged between 1 and 2 log (Table 4). The average theoretical time of survival of *E. coli* in the winter cycle ranged from 75 to 148 days at the elimination rate within the range 0.05–0.11 log MPN $\times$ day^{-1} (Table 5). Differences in the theoretical survival time between microorganisms isolated from the carriers placed in the pile and those obtained from samples collected at the other two locations were highly statistically significant, and those in the elimination rate were statistically significant (Table 5). Bacilli of *E. coli* survived longer in the winter cycle than in summer, and the observed differences in the theoretical survivability and elimination rate resulting from the season were highly statistically significant for the microorganisms isolated from the carriers placed in the pile and statistically significant for the bacilli from the carriers located on the frame of the turner (Table 5).

A low effectiveness of the method of sewage sludge solar drying in the winter cycle is particularly noticeable on the example of the dynamics of changes in enterococci population count. Conditions prevailing in the drying plant during winter did not cause the elimination of those bacteria, but contributed to their unexpected multiplication. During 28 days of the process, the count of enterococci in sludge from the carriers placed on the turner frame increased on average by about 1 log, whereas at the other two locations the increase was at a level of 2 log (Table 4).

A very low sanitization effectiveness of drying process in the winter cycle observed in the present study confirms the results obtained by Mathioudakis et al. [22], who did not report a significant reduction in the microorganism

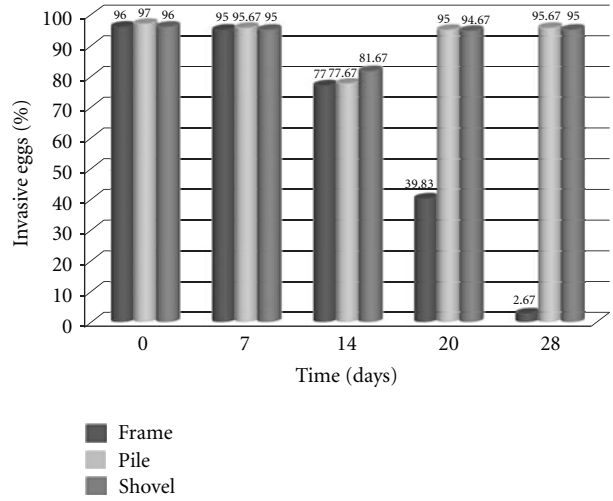

Figure 11: The course of inactivation of *Ascaris suum* eggs in summer cycle (July).

quantity in winter. The amount of *E. coli* they found in dried wastes was high and ranged from 8 $\times$ $10^5$to 2 $\times$ 10^6 MPN $\times$ g^{-1} D.M. Also Ögleni and Özdamir [21] under autumn and winter conditions obtained a low degree of elimination of faecal coliforms, not exceeding 1 $\log_{10}$. Bux et al. [16] obtained different results. The authors observed a reduction in faecal coliforms from 2.4 $\times$ $10^5$to 9.3 $\times$ 10^1 MPN $\times$ g^{-1} D.M. after 49 days.

3.4. Parasitological Analyses. The results of the study obtained in the summer cycle indicated that waste solar drying resulted in a small inactivation of parasite eggs (Figure 11). However, during the experiment, clear fluctuations in the percentage of invasive eggs in individual carriers could be observed (Figure 11), which may indicate the lack of uniform conditions during the drying process and its poor sanitization potential.

The environmental impact on retaining invasiveness by *Ascaris suum* eggs was largely dependent on location of the carriers. After 28 days of the process, on average 93.33% decrease in live parasite eggs was obtained in the carrier located on the frame (Figure 11). However, a slight reduction, that is, from 1.0% to 1.33%, was obtained in the research material placed on the shovel of the turner and in the waste pile (Figure 11). Such considerable reduction in the percentage of invasive eggs in the carrier on the frame may result from the fact that material placed inside had the smallest contact with the mass of dried sludge. Therefore it was more susceptible to drying and the effect of higher temperature, that is, factors facilitating the elimination of *Ascaris suum* eggs, which are very sensitive to moisture deficit.

During the winter cycle, similarly to the summer period, slight fluctuations in the percentage of *Ascaris suum* eggs were observed in the material collected from the carriers, which indicated the lack of proper waste sanitization (Figure 12). In the winter cycle a considerable decrease in

Table 6: Values of parameters that determine the way of using sewage sludge [11].

Number	Parameter	Type of reuse		
		Reuse in agriculture and agricultural land reclamation	Reuse for nonagricultural land reclamation	Reuse for the cultivation of plants destined for compost production; reuse for the cultivation of plants which are not destined for consumption and fodder production
1	Cadmium Cd [mg × kg^{-1} DM]	20	25	50
2	Copper Cu [mg × kg^{-1} DM]	1000	1200	2000
3	Nickel Ni [mg × kg^{-1} DM]	300	400	500
4	Lead Pb [mg × kg^{-1} DM]	750	1000	1500
5	Zinc Zn [mg × kg^{-1} DM]	2500	3500	5000
6	Mercury Hg [mg × kg^{-1} DM]	16	20	25
7	Chromium Cr [mg × kg^{-1} DM]	500	1000	2500
8	Number of Salmonella [cfu × 100 g^{-1}]	0	u*	u
9	ATT [egg × kg^{-1} DM]	0	≤300	≤300

* Undefined.

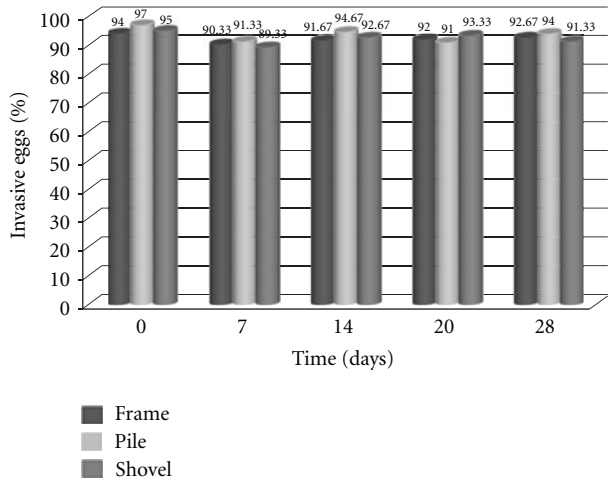

Figure 12: The course of inactivation of *Ascaris suum* eggs in winter cycle (December).

percentage of invasive *A. suum* eggs in the carrier on the frame was not observed, since temperature inside the hall was lower and air humidity was higher than in the summer season.

Different results were obtained by Shanahan et al. [23] who, while conducting a study of a system with an aisle turner in south-east Queensland, observed a reduction in the number of invasive eggs of *Ascaris* sp. and *Taenia* sp. during waste solar drying to the level below 1 egg per 4 g of dry matter.

Hertwig [19] proves that the main factor limiting a development of helminth eggs in wastes is a decrease in water activity index (a_w) below 0.65. Obtaining an increase in dry matter to 94% after 20 days of intensive waste drying, he observed the complete elimination of *Ascaris suum* eggs. A similar phenomenon was observed by Cota et al. [17] who proved that an increase in the proportion of waste dry matter during solar drying up to 93.33% resulted in the effective inactivation of the eggs of *Ascaris lumbricoides* and *Hymenolepis*.

The obtained results of microbiological and parasitological analyses show that the process of sewage sludge solar drying does not provide sufficient hygienization, and in some cases it favors multiplying microorganisms in dried material. Therefore it is essential to show possibilities for management of the final product generated in described facility. The basic Polish legal act laying down guidelines of sewage sludge management depending on its properties is the Regulation of the Minister of Environment of 13 July 2010 on municipal sewage sludge (Dz.U. of 2010 no. 137 item 924) [11]. This regulation is in accordance with international regulations, including the following:

(i) Regulation (EC) no. 1774/2002 of the European Parliament and of the Council of 3 October 2002 laying down health rules concerning animal by-products not intended for human consumption,

(ii) Directive 98/34/EC of the European Parliament and of the Council of 22 June 1998 laying down a procedure for the provision of information in the field of technical standards,

(iii) and Council Directive 86/278/EEC of 12 June 1986 on the protection of the environment, and in particular of the soil, when sewage sludge is used in agriculture.

The above mentioned regulation [11] includes values of parameters determining the way of sewage sludge management (Table 6). It is notable that in most cases sludge subjected to drying is relatively safe in microbiological and parasitological terms and contain normative amount of heavy metals. Consequently, the product obtained after solar

drying can be used as a fertilizer. However, in the case of occurrence of pathogenic bacteria and eggs of gastrointestinal parasites in the batch material, as it was in the described experiment, the hygienization potential of solar drying plant is insufficient. In such situation, sludge after drying can be used for nonagricultural land reclamation, cultivation of plants destined for compost production and cultivation of plants which are not destined for consumption and fodder production, or constitute an energy substrate in the process of burning or coburning.

During the operation of sludge solar drying plant, constant microbiological and parasitological monitoring of both watered and dried sludge making its final product is of utmost importance. Only obtaining such results, it is possible to choose the optimal way of managing processed sludge.

4. Conclusions

Based on the obtained results, it may be concluded that waste solar drying is a technology that does not guarantee obtaining of stable, biologically safe material for agricultural purposes. The lack of explicit positive results of elimination of harmful microflora in both seasons of the year in drying plants located under various climatic conditions confirms that solar drying technology cannot be regarded as an effective technology of waste sanitization. In this respect, it is much less effective than other biological (e.g., composing), chemical (e.g., liming), and physical (e.g., pasteurization) methods of waste processing. To obtain sanitary clean wastes, the vast majority of the authors report the need for additional sanitization treatments. Subjecting waste dried material to pelletization may guarantee obtaining its proper sanitization.

References

[1] J. A. Oleszkiewicz, *Gospodarka osadami ściekowymi, Poradnik decydenta*, LEM s.c., Kraków, Poland, 1998.

[2] F. O. Kocaer, U. Alkan, and H. S. Başkaya, "The effect of alkaline-stabilized-sludge application on the microbiological quality of soil and leachate," *Journal of Plant Nutrition and Soil Science*, vol. 167, no. 6, pp. 704–712, 2004.

[3] M. Michałkiewicz, "Podstawowe testy biologiczne stosowane w eksploatacji oczyszczalni ścieków," in *Proceedings of the Eksploatatora Forum*, no. 1, 2002.

[4] B. Nørrung and S. Buncic, "Microbial safety of meat in the European Union," *Meat Science*, vol. 78, no. 1-2, pp. 14–24, 2008.

[5] J. Zamorska, "Organizmy patogenne w osadach ściekowych," *Zeszyty Naukowe PTIE i PTG Oddziału w Rzeszowie*, vol. 9, 2007.

[6] J. Bień, *Osady ŚcIekowe TeorIa I Praktyka*, Wydawnictwo Politechniki Częstochowskiej, Częstochowa, Poland, 2002.

[7] L. Sahlström, "A review of survival of pathogenic bacteria in organic waste used in biogas plants," *Bioresource Technology*, vol. 87, no. 2, pp. 161–166, 2003.

[8] I. L. Pepper, J. P. Brooks, and C. P. Gerba, "Pathogens in Biosolids," *Advances in Agronomy*, vol. 90, pp. 1–41, 2006.

[9] Y. H. Sun, Y. M. Luo, L. H. Wu, Z. G. Li, J. Song, and P. Christie, "Survival of faecal coliforms and hygiene risks in soils treated with municipal sewage sludges," *Environmental Geochemistry and Health*, vol. 28, no. 1-2, pp. 97–101, 2006.

[10] R. Sobczyk, "Gospodarka komunalnymi osadami ściekowymi teoria a praktyka," in *Proceedings of the 6th Konferencja Naukowo-Techniczna Woda-Człowiek-Środowisko*, Licheń, Poland, 2007.

[11] "Rozporządzenie Ministra Środowiska z dnia 13 lipca 2010 r. w sprawie komunalnych osadów ściekowych," *Dziennik Ustaw*, no. 137, p. 924, 2010.

[12] K. Rahn, S. A. De Grandis, R. C. Clarke et al., "Amplification of an *invA* gene sequence of *Salmonella* typhimurium by polymerase chain reaction as a specific method of detection of *Salmonella*," *Molecular and Cellular Probes*, vol. 6, no. 4, pp. 271–279, 1992.

[13] R. Sobczyk and P. Kabus, "Słoneczne suszarnie osadów," in *Forum Eksploatatora*, no. 03, Wydawnictwo Seidel-Przywecki, 2006.

[14] http://www.neostar.com.pl/.

[15] J. Szczygieł and P. Krawczyk, "Uwarunkowania słonecznego suszenia osadów ściekowych," *Gaz, Woda I TechnIka SanItarna*, no. 3, pp. 30–44, 2006.

[16] M. Bux, R. Baumann, W. Philipp, T. Conrad, and W. Mühlbauer, "Class—a by solar drying recent experiences in Europe," in *Proceedings of the Water Environment Federation (WEFTEC'01)*, pp. 309–317, Atlanta, Ga, USA, 2001, session 45.

[17] A. D. Cota, C. Figueroa, E. Espinoza et al., "Active Solar Drying of Wastewater Sludge: Physicochemical, Toxicological, and Nutrimental Characterization," México, http://www.uacj.mx/docentes/juflores/Documents/, 2007.

[18] S. Nathan and B. Clarke, *SolarMix—Innovation in Drying Technology*, CabWater Caboolture Shire Council, Arkwood Organic Recycling Pty, Mixwell Specialized Transport Pty, 2004.

[19] P. K. Hertwig, *Seuchenhygienische Untersuchungen bei der Trocknung und Pelletierung von Klärschlamm. [Diplomarbait]*, Universität Hohenheim, 2004.

[20] K. Barr, M. Bux, S. Horn, and J. McLellan, "Accelerated air-drying of sewage sludge using a climate-controlled solar drying hall," http://www.thermo-system.com/, 2002.

[21] N. Ögleni and S. Özdemir, "Pathogen reduction effects of solar drying and soil application in sewage sludge," *Turkish Journal of Agriculture and Forestry*, vol. 34, pp. 509–515, 2010.

[22] V. L. Mathioudakis, A. G. Kapagiannidis, E. Athanasoulia, V. I. Diamantis, P. Melidis, and A. Aivasidis, "Extended dewatering of sewage sludge in solar drying plants," *Desalination*, vol. 248, no. 1–3, pp. 733–739, 2009.

[23] E. F. Shanahan, A. Roiko, N. W. Tindale, M. P. Thomas, R. Walpole, and D. Ipek Kurtböke, "Evaluation of pathogen removal in a solar sludge drying facility using microbial indicators," *International Journal of Environmental Research and Public Health*, vol. 7, no. 2, pp. 565–582, 2010.

Hindawi Publishing Corporation
International Journal of Photoenergy
Volume 2012, Article ID 194823, 6 pages
doi:10.1155/2012/194823

Research Article

Treatment of Pesticides in Wastewater by Heterogeneous and Homogeneous Photocatalysis

Catalina Daniela Stan,[1] Igor Cretescu,[2] Cristina Pastravanu,[3] Ioannis Poulios,[4] and Maria Drăgan[1]

[1] *Department of Drug Industry and Pharmaceutical Biotechnology, Grigore T. Popa University of Medicine and Pharmacy, 16 Universitatii Street, 700115 Iasi, Romania*
[2] *Department of Environmental Engineering and Management, Faculty of Chemical Engineering and Environmental Protection, Gheorghe Asachi Technical University of Iasi, 73 Professor D. Mangeron Street, 700050 Iasi, Romania*
[3] *Department of Materials Chemistry, "Al. I. Cuza" University of Iasi, 11 Carol I Boulvard, 700506 Iasi, Romania*
[4] *Department of Chemistry, Aristotle University of Thessaloniki, 54124 Thessaloniki, Greece*

Correspondence should be addressed to Igor Cretescu, icre@tuiasi.ro

Received 1 June 2012; Revised 10 August 2012; Accepted 21 August 2012

Academic Editor: Meenakshisundaram Swaminathan

The effect of different heterogeneous and homogeneous photocatalytic systems on the oxidative degradation of mepiquat chloride in aqueous solutions was investigated. In the case of heterogeneous reactions, the influence of five factors was studied: the type of catalyst, photocatalyst concentration, pH, pesticide concentration, and the presence of H_2O_2 and/or Fe^{3+}. For homogeneous catalysis, other factors were studied: the oxidising agent and the light source. Nearly complete degradation of mepiquat chloride was obtained after about 180 minutes in the presence of an acid medium (pH3) using a UV-A lamp and TiO_2P-25 catalyst (0.5 g/L), for an initial pesticide concentration of 10 ppm. Degradation rates corresponding to homogeneous photocatalysis were lower compared to those corresponding to the use of TiO_2 as the photocatalyst.

1. Introduction

Removing refractory organic pollutants from wastewaters is an important issue given the fact that most of them are toxic, mutagenic, and/or carcinogenic, even in low concentrations, and are a real health threat to humans, animals, as well as to the environment [1]. Heterogeneous and homogeneous solar photocatalytic detoxification methods (TiO_2/H_2O_2, Fe^{+3}/H_2O_2) have recently shown great promise for the treatment of industrial wastewater, groundwater, and contaminated air [2].

Mepiquat chloride or 1,1-dimethylpiperidine chloride, also known as DPC, is a new plant growth regulator that can be used on a variety of crops and exerts a variety of effects. It works by inhibiting gibberellic acid synthesis, reduces internode length, hastens maturity, and retards abscission [3]. In addition, DPC is used to prevent the lodging of winter wheat; for apples, it can increase calcium absorption, reduced by depression disease; for citrus, it can increase the sugar content. In agrochemical products, it is formulated as an emulsifiable concentrate, a water dispersible granulate and as a technical product. This pesticide was first registered in the USA in 1980 to be used as a growth regulator of cotton, and in 1997 it was reregistered by the Environmental Protection Agency (EPA) for its use in the USA [4]. Currently, it is formulated as an emulsifiable concentrate at concentrations lower than 5% (w/v) [5].

Mepiquat chloride has the molecular formula $C_7H_{16}ClN$ and a molecular weight of 149.66 g/mol. Figure 1 presents the structural formula of 1,1-dimethylpiperidine chloride.

Mepiquat chloride is labelled as a potential groundwater contaminant by the DPR (Department of Pesticide Regulation), because it has the potential to move into groundwater based on its water solubility, ability to bind to soils (K_{oc}),

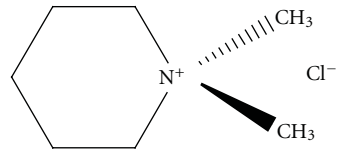

Figure 1: Structural formula of 1,1-dimethylpiperidine chloride.

and half-life. Its acute toxicity is classified as moderate by the IRIS (Integrated Risk Information System) of the US Environmental Protection Agency.

In recent years, new and more severe regulations coupled with enforcement against wastewater discharges have been established in most industrially developed countries [6]. This is why various technologies have been developed for the advanced treatment of wastewater containing pollutants that cannot be removed by conventional treatment processes. Destructive oxidation methods such as heterogeneous photocatalysis (TiO_2/UV-A), ozonation, H_2O_2/UVB, photo-Fenton, and sonolysis are considered very attractive since they transform hazardous pollutants into compounds with a reduced impact on the environment [7]. Also, among advanced oxidation processes, homogeneous and heterogeneous photochemical oxidation processes have proven their efficiency in the degradation of refractory organic pollutants [8].

Photocatalysis implies the acceleration of a photoinduced reaction by the presence of a catalyst [9]. Photoinduced reactions are activated by the absorption of a photon with sufficient energy, that is, equal to or higher than the band-gap energy (E_{bg}) of the catalyst [10]. The absorption leads to a charge separation due to the promotion of an electron (e^-) from the valence band of the semiconductor catalyst to the conduction band, thus generating a hole (h^+) in the valence band.

The activation equation can be written as:

$$TiO_2 + h\nu \longrightarrow h^+ + e^- \quad (1)$$

In this reaction, h^+ and e^- are powerful oxidising and reducing agents, respectively. The oxidation and reduction reactions can be expressed as:

$$\text{oxidation reaction: } h^+ + OH^- \longrightarrow OH^\bullet \quad (2)$$

$$\text{reduction reaction: } e^- + O_{2ads} \longrightarrow O_{2ads}{}^- \quad (3)$$

In order to sustain a photocatalysed reaction, e^--h^+ recombination subsequent to the initial charge separation must be prevented as much as possible [11].

Heterogeneous photocatalysis may be considered a viable alternative for the removal of refractory organics due to several important advantages such as: complete mineralization or formation of more readily biodegradable intermediates when complex organic compunds are treated, no need of auxiliary chemicals, no residual formation, easily operation and maintenance of the equipment [12].

Heterogeneous photocatalysis leads to the mineralisation of organic carbon using a semiconductor catalyst in suspension or as a thin film. One advantage of the photocatalytic process is its mild operating conditions and the fact that it can be powered by sunlight, thus significantly reducing the amount of electric power required and therefore the operating costs [13]. Heterogeneous photocatalysis is influenced by catalyst loading, initial pollutant concentration, pH, radiant flux, aeration, the presence of other substances or impurities, and photoreactor geometry [14].

The most widely used semiconductor catalyst in photoinduced processes is titanium dioxide (TiO_2), because it is chemically and biologically inert, photocatalytically stable, relatively easy to produce and to use, able to efficiently catalyse reactions, cheap, and without risks to the environment or humans [15].

Homogeneous photocatalysis uses UV radiation in combination with chemical oxidising agents such as hydrogen peroxide or ozone.

2. Experimental

2.1. Light Sources. For the photocatalytic degradation of mepiquat chloride, a G23 Radium Ralutec UVA lamp (9W/78, 350–400 nm, $I = 1.3517$ ein/min) and a Radium Ralutec VIS lamp (9W/71, $I = 0.5898$ ein/min) were used.

Actinometry was used to determine the exact radiation intensity of both lamps within the vessels. The radiation intensities obtained for the UVA and the VIS lamp were 1.3517 ein/min and 0.3517 ein/min, respectively. After 10–15 uses of the lamps, it was necessary to repeat the actinometric determinations to check that the lamp intensity remained constant.

2.2. Vessels and Reagents. For the photocatalytic experiments, a solution of mepiquat chloride pesticide was used. As catalysts, TiO_2P-25, TiO_2UV-100, TiO_2-A, TiONa, and ZnO were studied.

A photochemical reactor (Figure 2) with volume of 500 mL was used to carry out the experimental tests. The reactor was covered with a black cloth to avoid interactions with ambient light.

2.3. Procedures and Analyses. In the initial 300 mL aqueous solution of the pesticide ($C = 10$ mg/L), different quantities of catalysts were added. The reaction solutions were magnetically stirred in the dark for 30 min until adsorption/desorption equilibrium was reached. The solutions were then irradiated under UV light with continuous magnetic stirring. A fixed quantity of each mepiquat chloride solution was taken at regular time intervals during the illumination period and filtered through a syringe filter to analyse the amount of pesticide remaining in the solution. DPC concentrations during the experiments were monitored by a Total Organic Carbon Analyzer (Shimadzu), in order to measure the mineralisation of the pesticide.

3. Results and Discussion

3.1. Mepiquat Chloride Degradation by Heterogeneous Photocatalysis. The influence of five experimental factors was

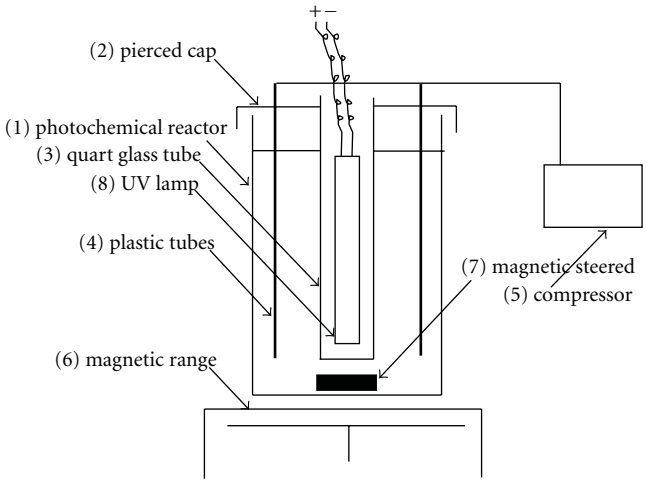

Figure 2: Photocatalysis experimental setup ((1) photochemical reactor, (2) pierced cap, (3) quart glass tube, (4) plastic tubes, (5) compressor, (6) magnetic range, (7) magnetic steered, (8) UV lamp).

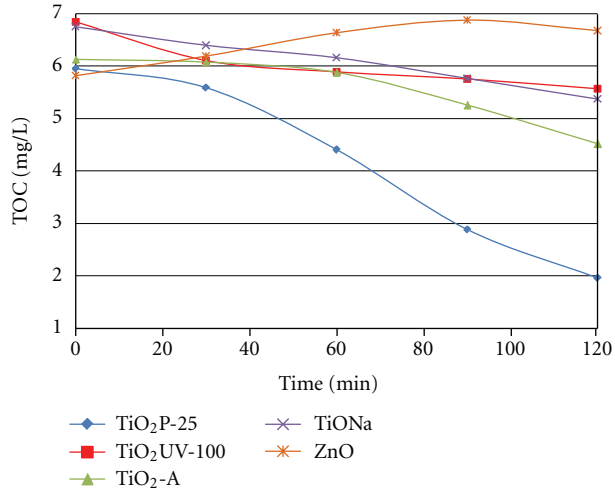

Figure 3: Pesticide degradation by heterogeneous photocatalysis using different catalysts (initial conditions: 10 ppm mepiquat chloride, 0.5 g/L catalyst, UV-A lamp).

studied: the type of catalyst, photocatalyst concentration, pH, pesticide concentration, and the presence of H_2O_2 and/or Fe^{3+}. The experiments were conducted by varying one factor and keeping the others constant.

3.1.1. Influence of the Type of Catalyst. Five types of catalysts were investigated in this study: TiO_2P-25, TiO_2 UV-100, TiO_2-A, TiONa, and ZnO; the results are plotted in Figure 3.

The corresponding amounts of catalyst were added to 10 ppm solutions of mepiquat chloride in order to obtain a dose of 0.5 g catalyst/L and then irradiated with UV-A light. From Figure 3, it can be seen that the TiO_2P-25 catalyst exhibited the best behaviour in the degradation of mepiquat chloride and was thus considered the reference catalyst. The increase of the TOC values in the case of the ZnO catalyst might be assigned to the desorption of the pesticide from the ZnO surface, taking into consideration that the adsorption of mepiquat chloride on this material is less intense in comparison with the other photocatalysts.

3.1.2. Influence of Catalyst Concentration. The influence of catalyst concentration was studied for the TiO_2P-25 catalyst, which was chosen as the reference.

The degradation experiments were conducted using the same pesticide concentration (10 ppm), the same UV-A lamp, and different concentrations of the same photocatalyst. The results are depicted in Figure 4.

As expected, Figure 4 shows that the most advanced pesticide degradation occurred when heterogeneous photocatalysis was conducted with a higher dose of the catalyst (TiO_2P-25).

3.1.3. Influence of pH. The influence of the pH of the solution was studied by conducting the photocatalyst experiments with 0.5 g/L TiO_2P-25 catalyst in 10 ppm mepiquat chloride solution, using the UV-A lamp but adjusting the solution pH

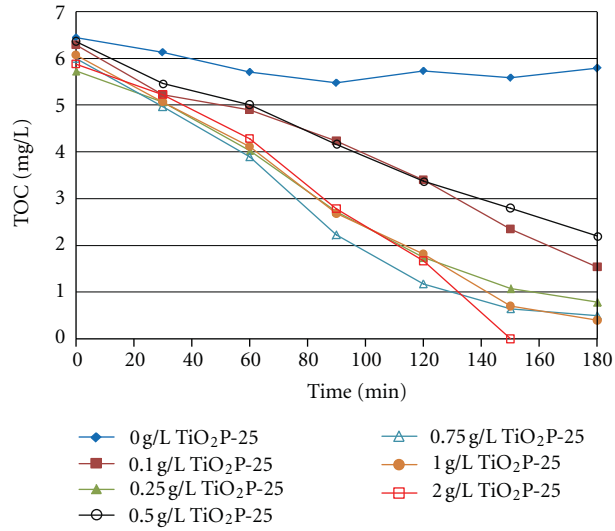

Figure 4: The TiO_2P-25 dose influence on the degradation of mepiquat chloride (initial conditions: 10 ppm mepiquat chloride, 0.5 g/L TiO_2P-25, UV-A lamp).

from acidic values (pH3, 4, and 5) to basic values (pH8, 9, and 11)

Figure 5 illustrates the variation in TOC/TOC(0) values over time at different pH values. The positive effect of acidic pH on pesticide degradation noted in the figure can be assigned to the fact that the TiO_2 surface is positively charged when the solution pH is lower than 6.8, thus facilitating the photocatalytic process [9].

3.1.4. Influence of the Mepiquat Chloride Concentration. The influence of the mepiquat chloride concentration on the photocatalytic process was studied using the TiO_2P-25 catalyst. The degradation experiments were conducted using pesticide solutions of various initial concentrations, the same

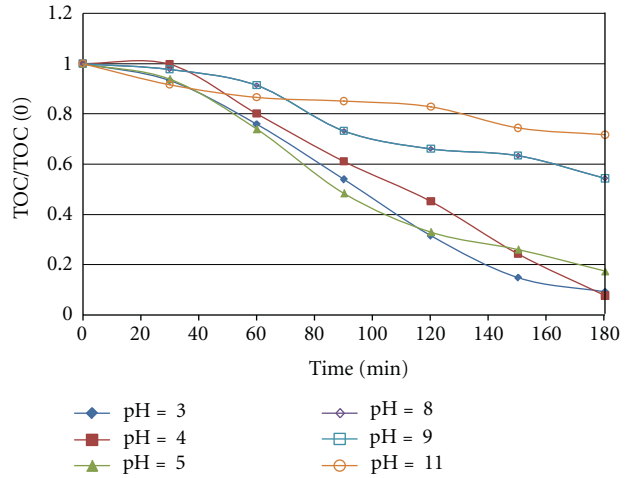

Figure 5: Pesticide degradation over time at different pH values of the initial solution (initial conditions: 10 ppm mepiquat chloride, 0.5 g/L TiO_2P-25, UV-A lamp).

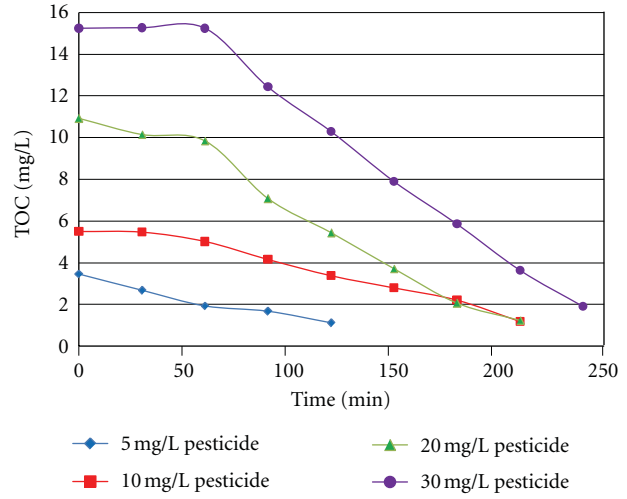

Figure 6: Behaviour of different concentrations pesticide solutions during heterogeneous photocatalysis using UV-A light and 0.5 g/L TiO_2P-25 as the catalyst.

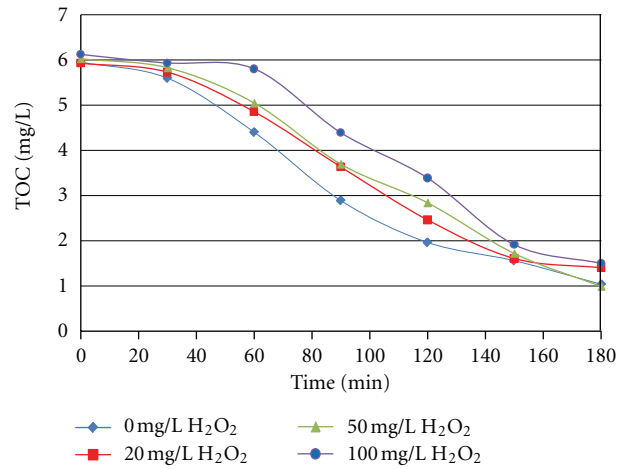

Figure 7: Heterogeneous photocatalysis of mepiquat chloride in the presence of TiO_2P-25 and H_2O_2 (initial conditions: 10 ppm mepiquat chloride, 0.5 g/L TiO_2P-25, UV-A lamp).

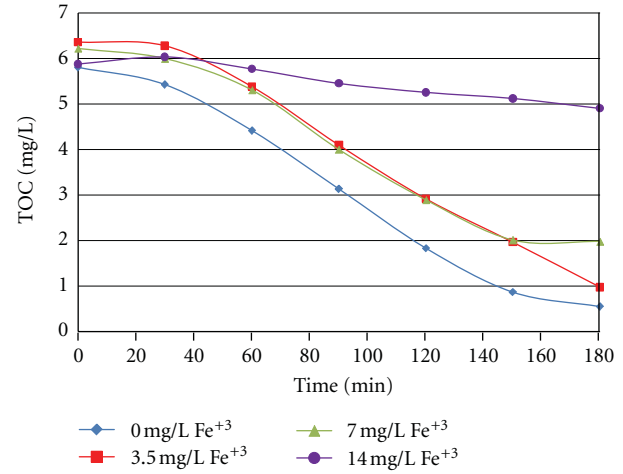

Figure 8: Heterogeneous photocatalysis of mepiquat chloride in the presence of TiO_2P-25 and Fe^{+3} (initial conditions: 10 ppm mepiquat chloride, 0.5 g/L TiO_2P-25, UV-A lamp).

UV-A lamp, and the same photocatalyst concentration (0.5 g/L). The results are shown in Figure 6.

3.1.5. The Influence of H_2O_2 or Fe^{+3}. The next step of this study focused on enhancing the photocatalysis reaction by adding H_2O_2 or Fe^{+3} in different concentrations to the initial solution.

Figures 7 and 8 show pesticide degradation during photocatalysis with TiO_2P-25, facilitated by H_2O_2 and Fe^{+3}, respectively. The best degradation rate was obtained when the TiO_2P-25 photocatalysis was used alone. It was noted that no enhancement was obtained by adding H_2O_2 or Fe^{+3} at any dose.

3.2. Mepiquat Chloride Degradation by Homogeneous Photocatalysis. Homogeneous photocatalytic oxidation of the pesticide was also tested using two oxidising agents: a photo-Fenton agent (H_2O_2 + Fe^{+3}) and a ferrioxalate agent (potassium oxalate + H_2O_2+Fe^{+3}) in various concentrations. The influence of light was also studied using UV-A and VIS lamps, respectively. The results are depicted in Figures 9 and 10, respectively.

In the case of the photo-Fenton reagent, the best results were obtained when less oxidant was used: 50 ppm H_2O_2 and 3.5 ppm Fe^{+3}. When more photo-Fenton agent was used, lower values for pesticide decontamination were obtained.

With the ferrioxalate reagent, an excellent degradation rate was obtained when visible light was used, as can be seen in Figure 11, this being economically reliable. When using the UV-A lamp, photodegradation results were comparable with those achieved for photo-Fenton homogeneous catalysis.

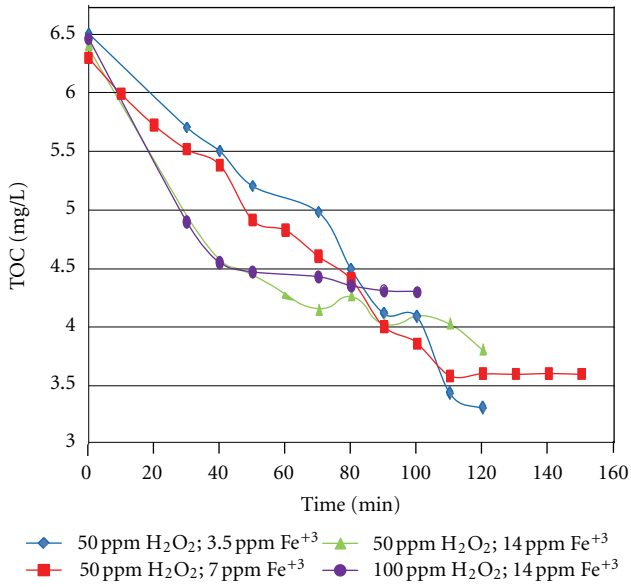

Figure 9: Homogeneous photocatalysis of mepiquat chloride using the photo-Fenton agent (initial conditions: 10 ppm mepiquat chloride, UV-A lamp).

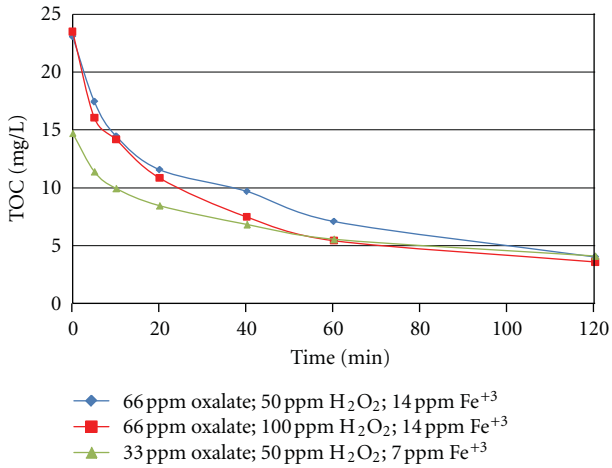

Figure 10: Homogeneous photocatalysis of mepiquat chloride using the ferrioxalate agent (initial conditions: 10 ppm mepiquat chloride, 0.5 g/L TiO_2P-25, UV-A lamp).

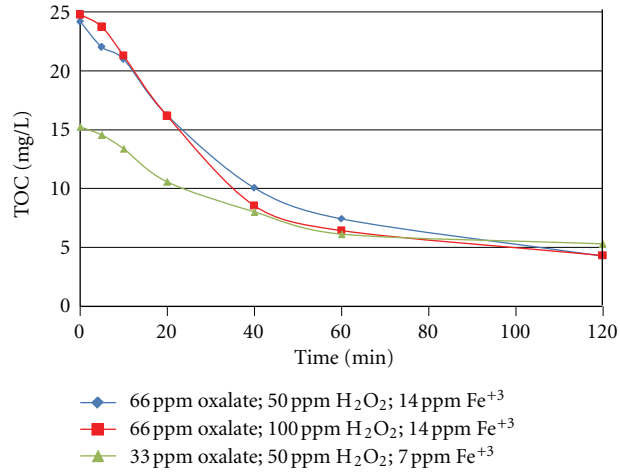

Figure 11: Homogeneous photocatalysis of mepiquat chloride using the ferrioxalate agent (initial conditions: 10 ppm mepiquat chloride, VIS lamp).

4. Conclusions

(i) The present study demonstrated the possibility of oxidative degradation of persistent organic pesticides by heterogeneous photocatalysis.

(ii) Nearly complete degradation of mepiquat chloride was obtained after about 180 minutes in the presence of an acid medium (pH3) using a UV-A lamp and the TiO_2P-25 catalyst (0.5 g/L), for an initial pesticide concentration of 10 ppm.

(iii) The remnant pesticide concentrations were higher when homogeneous photocatalytic oxidation was involved, in comparison with levels obtained in a heterogeneous photocatalytic degradation process based on TiO_2.

(iv) Degradation rates corresponding to homogeneous photocatalysis were lower compared to those corresponding to the use of TiO_2 as the photocatalyst. In this way, the remnant concentrations of mepiquat chloride were below the drinking water level of comparison for acute and chronic risk range for infants and children (6 ppm), but as a consequence of the heterogeneous photocatalysis degradation process, this remnant concentration was about 10 times lower than the abovementioned level (0.54 ppm for 0.5 g/L TiO_2P-25, C_i = 10 ppm pesticide).

(v) Moreover, we tested the possibility of reusing TiO_2P-25 three times and found comparable photocatalytic activity for the solids with each use. The TiO_2 Degussa was recovered by simple washing, providing an economic advantage to this process.

(vi) Our study succeeded in achieving the task of finding a suitable photocatalytic system to provide a mepiquat chloride remnant concentration in accordance with EPA standards.

References

[1] I. Poulios, E. Micropoulou, R. Panou, and E. Kostopoulou, "Photooxidation of eosin Y in the presence of semiconducting oxides," *Applied Catalysis B*, vol. 41, no. 4, pp. 345–355, 2003.

[2] G. D. Suditu, M. Secula, C. G. Piuleac, S. Curteanu, and I. Poulios, "Genetic algorithms and neural networks based optimization applied to the wastewater decolorization by photocatalytic reaction," *Revista de Chimie*, vol. 59, no. 7, pp. 816–825, 2008.

[3] 2012, http://chemyq.com/.

[4] 2012, http://www.epa.gov/oppsrrd1/REDs/factsheets/.

[5] G. Quintás, S. Garrigues, A. Pastor, and M. de la Guardia, "FT-Raman determination of Mepiquat chloride in agrochemical

products," *Vibrational Spectroscopy*, vol. 36, no. 1, pp. 41–46, 2004.

[6] M. S. Secula, G. D. Suditu, I. Poulios, C. Cojocaru, and I. Cretescu, "Response surface optimization of the photocatalytic decolorization of a simulated dyestuff effluent," *Chemical Engineering Journal*, vol. 141, no. 1–3, pp. 18–26, 2008.

[7] A. F. Caliman, C. Cojocaru, A. Antoniadis, and I. Poulios, "Optimized photocatalytic degradation of Alcian Blue 8 GX in the presence of TiO_2 suspensions," *Journal of Hazardous Materials*, vol. 144, no. 1-2, pp. 265–273, 2007.

[8] S. Kaniou, K. Pitarakis, I. Barlagianni, and I. Poulios, "Photocatalytic oxidation of sulfamethazine," *Chemosphere*, vol. 60, no. 3, pp. 372–380, 2005.

[9] A. Mills and S. Le Hunte, "An overview of semiconductor photocatalysis," *Journal of Photochemistry and Photobiology A*, vol. 108, no. 1, pp. 1–35, 1997.

[10] O. Carp, C. L. Huisman, and A. Reller, "Photoinduced reactivity of titanium dioxide," *Progress in Solid State Chemistry*, vol. 32, no. 1-2, pp. 33–177, 2004.

[11] I. Poulios, M. Kositzi, K. Pitarakis, S. Beltsios, and I. Oikonomou, "Photocatalytic oxidation of methomyl in the presence of semiconducting oxides," *International Journal of Environment and Pollution*, vol. 28, no. 1-2, pp. 33–44, 2006.

[12] A. F. Caliman, C. Teodosiu, and I. Balasanian, "Aplications of heterogeneous photocatalysis for industrial wastewater treatment," *Environmental Engeneering and Management Journal*, vol. 1, pp. 187–196, 2002.

[13] I. Poulios, A. Avranas, E. Rekliti, and A. Zouboulis, "Photocatalytic oxidation of Auramine O in the presence of semiconducting oxides," *Journal of Chemical Technology and Biotechnology*, vol. 75, no. 3, pp. 205–212, 2000.

[14] C. Betianu, F. A. Caliman, M. Gavrilescu, I. Cretescu, C. Cojocaru, and I. Poulios, "Response surface methodology applied for Orange II photocatalytic degradation in TiO_2 aqueous suspensions," *Journal of Chemical Technology and Biotechnology*, vol. 83, no. 11, pp. 1454–1465, 2008.

[15] C. Pastravanu, I. Poulios, E. Popovici, and I. Cretescu, "A case study of textile wastewater treatment by heterogeneous photocatalytic degradation," *The Annals of the "Dunarea de Jos" University of Galati Fascicle II—Mathematics, Physics, Chemistry, Informatics*, vol. 32, pp. 31–38, 2009.

Hindawi Publishing Corporation
International Journal of Photoenergy
Volume 2012, Article ID 754691, 5 pages
doi:10.1155/2012/754691

Research Article

Oxidation Degradation of Rhodamine B in Aqueous by UV/$S_2O_8^{2-}$ Treatment System

Xiaoyang Chen, Zhiyong Xue, Yanlai Yao, Weiping Wang, Fengxiang Zhu, and Chunlai Hong

Institute of Environmental Resource and Soil Fertilizer, Zhejiang Academy of Agricultural Sciences, Hangzhou 310021, China

Correspondence should be addressed to Chunlai Hong, spring76212@yahoo.com.cn

Received 31 May 2012; Revised 23 August 2012; Accepted 27 August 2012

Academic Editor: Manickavachagam Muruganandham

The UV photolysis of persulfate ($S_2O_8^{2-}$) is a novel advanced oxidation technologies (AOTs), which leads to the formation of strong oxidizing radicals, sulfate radicals ($SO_4^{\bullet-}$). The effect of oxidant $S_2O_8^{2-}$ concentration, initial dye concentration, initial pH of solution, and various inorganic anions (Cl^-, $H_2PO_4^-$, and HCO_3^-) were investigated using Rhodamine B (RhB), a kind of xanthene dye, as a model pollutant. With the increase of oxidant $S_2O_8^{2-}$, more $SO_4^{\bullet-}$ produced to attack RhB molecules and result in the increase of RhB degradation. While the improvement was not sustained above a critical value, beyond which degradation rate does not increase. Initial pH of solution had great effect on the RhB degradation rate during UV/$S_2O_8^{2-}$ system. $SO_4^{\bullet-}$ is rather stable in acidic solutions, while increasing system pH results in the transformation of $SO_4^{\bullet-}$ to $^{\bullet}OH$. The effects of three inorganic anions (Cl^-, $H_2PO_4^-$, and HCO_3^-) all had some negative effect on the degradation of RhB. Based on the RhB solution changes of the UV-vis absorption intensity during the UV/$S_2O_8^{2-}$ treatment, decolorization of RhB accompanied the destruction of aromatic ring structures of RhB molecules.

1. Introduction

Dyes are widely used in textile, leather, pharmaceutical, plastic, paint, and food industries [1].

Nearly more than 800,000 tons dye are produced per year, and over 15% of the synthetic textile dyes used are lost during manufacturing or processing operations and released as effluents [2, 3]. The effluents will produce adverse effects on the ecoenvironments due to their nonbiodegradability, toxicity, potential carcinogenic and mutagenic nature [3, 4]. For the treatment of dye-containing wastewater, traditional physicochemical techniques such as adsorption on activated carbon, membrane separation and coagulation have difficulties in the complete destruction of dye pollutants [5].

Advanced oxidation technologies (AOTs) are attractive alternatives to nondestructive physical water treatment processes because they are able to mineralize organic contaminants. AOTs, such as Fenton reagent, photo-Fenton, UV/O_3, UV/H_2O_2, and TiO_2-mediated photocatalysis processes based on the generation reactive hydroxyl radicals ($^{\bullet}OH$), have emerged to be promising alternatives for dye-off wastewaters [6–9].

In recently, sulfate radicals-based AOTs have come forth for the degradation of nonbiodegradable compounds [10–14]. The rapid destruction of organic contaminants by sulfate radicals ($SO_4^{\bullet-}$) at a near diffusion-controlled rate ($10^9\ M^{-1}\cdot s^{-1}$) has gained great interest among practitioners as a potential method for on-site hazardous waste remediation [15]. Compared to $^{\bullet}OH$, $SO_4^{\bullet-}$ demonstrate higher reduction potential at neutral pH and are more selective for oxidizing organic pollutants [16]. In general, $SO_4^{\bullet-}$ can be generated by scission of peroxide bond by radiolytic, photolytic, and thermal activation of persulfate ($S_2O_8^{2-}$), or electron transfer by transition-metal activation of $S_2O_8^{2-}$ or peroxymonosulfate [17–20]. Among them, UV-mediated decomposition of persulfate ($UV/S_2O_8^{2-}$) is an efficient oxidative system that can form $SO_4^{\bullet-}$ as major oxidizing species. Similar to H_2O_2, $S_2O_8^{2-}$ shows significant photochemical activity under the UV irradiation. $S_2O_8^{2-}$ is the most important oxidant used as $SO_4^{\bullet-}$-based oxidants

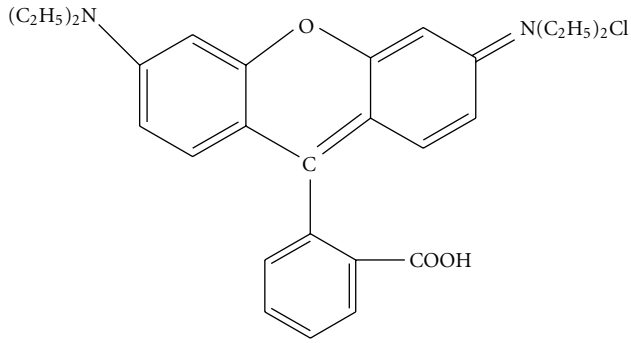

Figure 1: Structure of Rhodamine B.

and thus has drawn increasing attention as an alternative oxidant in the chemical oxidation of contaminants [11–15, 19–21]. The use of $S_2O_8^{2-}$ has several advantages. $S_2O_8^{2-}$ itself is a strong oxidant with a standard oxidation potential of 2.01 V comparable to O_3 (2.07 V), nonselectively reactive, and relatively stable at room temperature [10, 19–21]. Moreover, a low cost of $S_2O_8^{2-}$ facilitates $SO_4^{\bullet-}$-based AOTs for potential application in wastewater treatment.

In this work, a model refractory organic dye pollutant Rhodamine B (RhB), which contains four N-ethyl groups at either side of the xanthene ring, was chosen as the target pollutant to examine the degradation behavior of the UV/$S_2O_8^{2-}$ system. RhB is an important representative of xanthene dye, widely used as a colorant in textiles and food stuffs, and is also a well-known water tracer fluorescent, which has the property of carcinogenicity, reproductive and developmental toxicity, neurotoxicity, and chronic toxicity towards humans and animals [6, 22]. The objective of this work was to investigate the factors that influence the degradation rate of RhB in UV/$S_2O_8^{2-}$ treatment system such as oxidant doses, initial dye concentration, and the effects of anions (Cl^-, $H_2PO_4^-$, and HCO_3^-) that are ubiquitous coexistent in waters on the degradation of RhB with the UV/$S_2O_8^{2-}$ system.

2. Experimental

2.1. Chemicals. RhB (Figure 1) was purchased from Alfa Aesar, A Johnson Matthey Company. $K_2S_2O_8$ was purchased from Tianjing Guangfu Company, China. All other chemicals were analytical grade and used as received without further purification. For pH adjustment, 0.1 M sulfuric acid and 0.1 M sodium hydroxide were used, and all the experiments were conducted in an air-conditioned room at 25 ± 2°C. Milli-Q water was used throughout this study. Triplicate ($n = 3$) experiments were conducted under the identical condition.

2.2. Photoreactor and Light Source. The photodegradation experiments were performed in an XPA-7 merry-go-round photochemical reactor (Xujiang Electromechanical Plant, Nanjing, China) with quartz tubes containing the reaction solutions. A 300 W high-pressure mercury lamp used for the photodegradation experiment under UV-vis irradiation immersed inside water-cooled quartz well. The light source irradiance spectra (Figure 2) were measured with a monochromator (Acton, SP-300). The light intensity (200–420 nm) in the center of the reactive solutions was 4.10 mW/cm^2 for the mercury lamp.

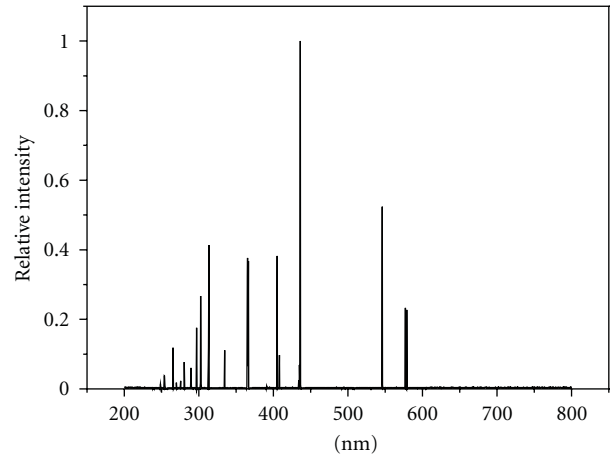

Figure 2: Irradiance spectra of the high-pressure mercury lamp light sources.

2.3. Experimental Procedure and Analysis. At specific intervals, samples were removed from exposure for UV-vis spectra measurement. The RhB degradation was characterized by measuring absorbency at 554 nm, the peak wavelength of RhB in the visible region. UV-vis spectra variations were recorded between 190 and 800 nm employing a Shimaduz 1700 UV-vis spectrometer.

3. Results and Discussion

3.1. Effect of Oxidants $K_2S_2O_8$ on the Photodegradation of RhB. The effect of oxidant $K_2S_2O_8$ on the degradation of RhB was investigated at natural pH, and the results were shown in Figure 3. Initially, control experiments were carried out in the absence and presence of either UV light or $K_2S_2O_8$ alone. Results showed that mere $K_2S_2O_8$ was not sufficient for the degradation of RhB. There was no observable color loss in the absence of UV irradiation. Only UV light irradiation, there was about 35% degradation of RhB with 60 min reaction time, while there was 85% with UV/$K_2S_2O_8$ ([$K_2S_2O_8$] = 0.2 mM) treatment system at the same reaction time, which is indicating that UV/$K_2S_2O_8$ was superior to UV alone in terms of the dye removal efficiency. The RhB degradation rate increased with the increasing of concentration of oxidant $K_2S_2O_8$ from 0.2 mM to 0.8 mM. While the improvement was not sustained above a critical value ([$K_2S_2O_8$] = 1.0 mM), beyond which the reaction rate decreased. This is mainly because that oxidant $K_2S_2O_8$ has two opposing effects [23, 24]. As the concentration of oxidant $K_2S_2O_8$ is increased, more $SO_4^{\bullet-}$ will be available to attack RhB molecules. Therefore, the rate of reaction increases. On the other hand, when $K_2S_2O_8$ is used in

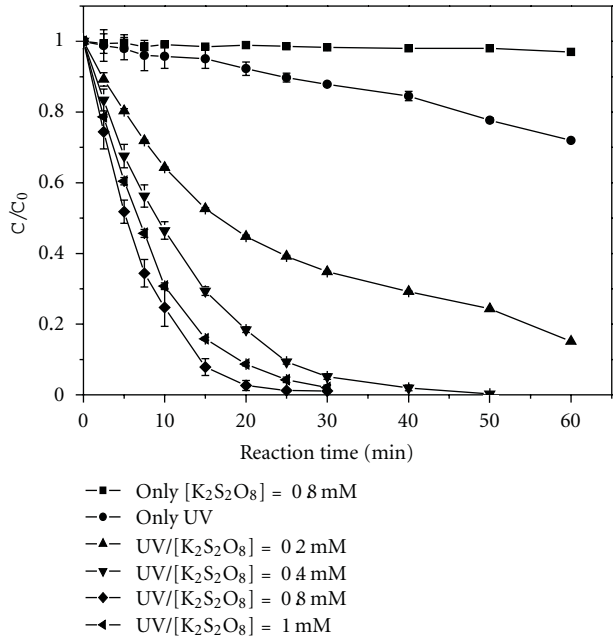

Figure 3: RhB degradation rate during UV/$K_2S_2O_8$ treatment system at different oxidant concentration. Conditions: [RhB] = 0.02 mM, no pH adjustment.

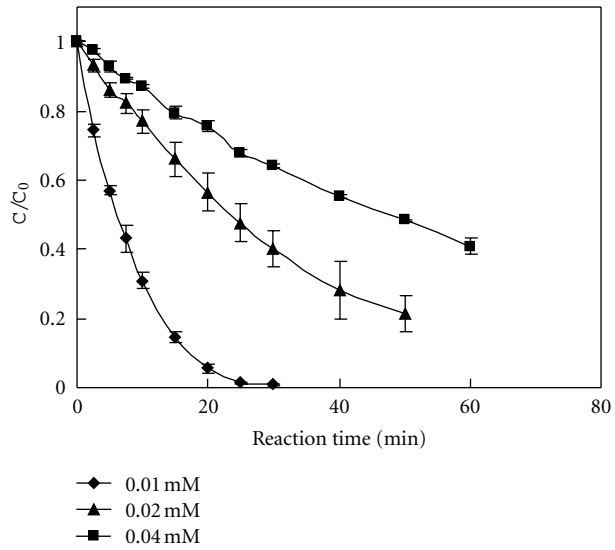

Figure 4: RhB degradation rate during the UV/$K_2S_2O_8$ treatment system at different dye initial concentration. Conditions: [$K_2S_2O_8$] = 0.4 mM, no pH adjustment.

excess, $SO_4^{\bullet-}$ efficiently reacts with $K_2S_2O_8$ produce to $S_2O_8^{\bullet-}$, and $SO_4^{\bullet-}$ with $SO_4^{\bullet-}$ can dimerize to generate $S_2O_8^{2-}$.

3.2. Effect of the Initial RhB Concentration. The effect of dye initial concentration on the degradation efficiency was monitored, and the results were presented in Figure 4. It can be seen that photooxidation efficiency decreased as initial dye concentration is increased when the concentration of $K_2S_2O_8$ is constant. At high concentration of RhB, the penetration of photons entering into the solution decreases, so that an inner filter effect is induced, and hence the solution becomes more and more impermeable to UV radiation, consequently $SO_4^{\bullet-}$ concentration decreases. On the other hand, since the oxidant $K_2S_2O_8$ is constant and high concentration of RhB would consume more $SO_4^{\bullet-}$, the degradation rate would be decrease with the increase of the initial RhB concentration.

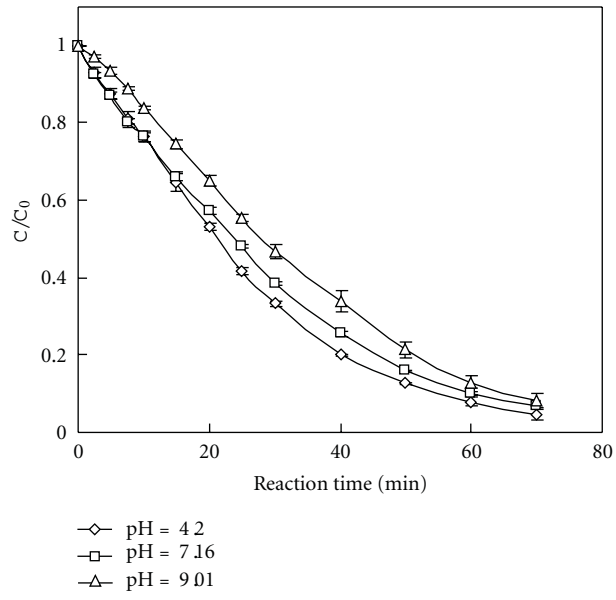

Figure 5: Effect of initial pH on the RhB degradation rate during the UV/$K_2S_2O_8$ treatment system. Conditions: [RhB] = 0.02 mM, [$K_2S_2O_8$] = 0.4 mM, no pH adjustment.

3.3. Effect of the Initial pH. To illustrate the effect of pH in the UV/$K_2S_2O_8$ treatment, the pH was adjusted to 4.20, 7.16, and 9.01, respectively. The results of pH dependency on the RhB degradation rate during UV/$K_2S_2O_8$ system at various initial pH were presented in Figure 5. When the initial pH was 4.21 and 9.01, the degradation efficiency was ~67.7% and 55.5% at 30 min, respectively. From the results, we can observe that acid initial pH has slightly positive effect on the RhB degradation during the UV/$K_2S_2O_8$ system. That is perhaps mainly because that $SO_4^{\bullet-}$ start to decompose and transform into $^{\bullet}OH$ rapidly with the pH increase [20, 25]. On the contrary, $SO_4^{\bullet-}$ are rather stable in acidic solutions. At low pH, the dominant active species is $SO_4^{\bullet-}$. In general, different pH values have not significant effect on the degradation of UV/$K_2S_2O_8$ system. Hence, the application of the combined UV/$K_2S_2O_8$ system will be of great significance because dye wastewater is usually in a broad range of pH.

3.4. Effect of Inorganic Ions. This study also examined the effect of anions on the decolorization of RhB such as Cl^-, $H_2PO_4^-$, and HCO_3^-, which are usually found in textile waste streams. The effect of three typical inorganic anion on the degradation of RhB with UV/$K_2S_2O_8$ was illustrated in Figure 6. It can be seen that all the anions used in this

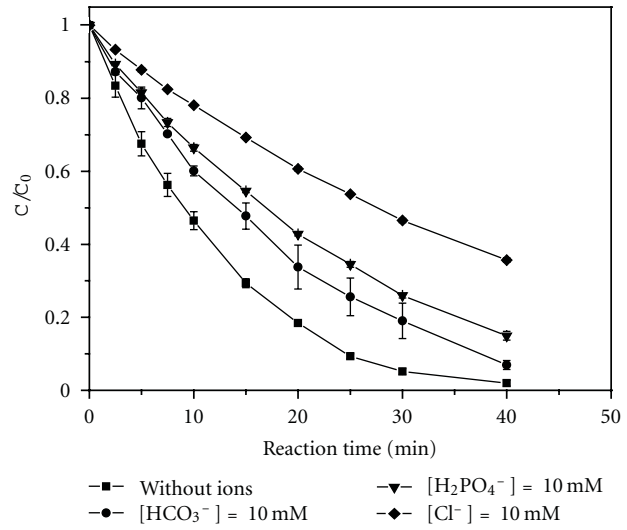

Figure 6: Influence of Cl^-, $H_2PO_4^-$ and HCO_3^- anions on the degradation of with UV/$K_2S_2O_8$ system. Conditions: [RhB] = 0.02 mM, [$K_2S_2O_8$] = 0.4 mM.

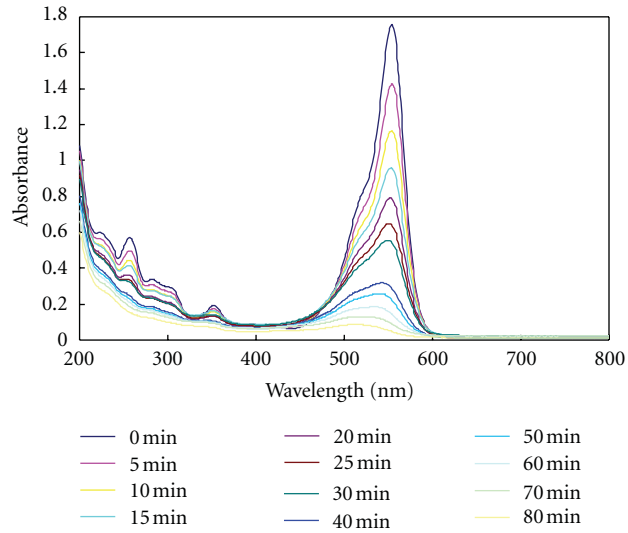

Figure 7: UV/Vis spectral changes of RhB with UV/$K_2S_2O_8$ treatment system. Conditions: [RhB] = 0.02 mmol/L, [$K_2S_2O_8$] = 0.4 mmol/L, no pH adjustment.

work inhibited the RhB degradation. It is well known that $SO_4^{\bullet-}$ can directly oxidize Cl^-, $H_2PO_4^-$, and HCO_3^- vis electron transfer reactions to produce less-active species [13, 26–28]. It is well known that $SO_4^{\bullet-}$ can directly oxidize Cl^-, $H_2PO_4^-$ and HCO_3^- vis electron transfer reactions to produce less-active species [13, 26–28]. The reaction rate constants for the reactions of $SO_4^{\bullet-}$ with HCO_3^-, $H_2PO_4^-$, and Cl^- are $\sim 10^6$ L/mol·s, $\sim 10^5$ L/mol·s and $\sim 10^8$ L/mol·s, respectively [28, 29]. The reaction rate constants of $SO_4^{\bullet-}$ with HCO_3^- and $H_2PO_4^-$ are less than that of Cl^- with $SO_4^{\bullet-}$. Hence, the inhibiting effect on RhB degradation of Cl^- is more obvious than HCO_3^- and $H_2PO_4^- \cdot SO_4^{\bullet-}$ were the dominant oxidative species in the UV/$K_2S_2O_8$ process, these anions were able to compete with RhB for $SO_4^{\bullet-}$ at various rate and thus led to the decrease of degradation of RhB.

3.5. The UV-Visible Absorption Spectra Analysis. In order to investigate the change in the molecule of RhB with the reaction time, UV-visible absorption spectra changes in the dye solution were observed, and the corresponding spectra are shown in Figure 7. It can be seen that there are two main characteristic absorption bands of RhB solution. One is UV region (259 nm), and another is in the visible region (554 nm). The UV band absorbance of dye solution at 554 nm ($n \rightarrow \pi$ transition of C=N, C=O groups) is due to the color of the dye solution, and it is used to monitor the decolorization of dye. Absorbance at 259 nm represents the aromatic content of RB, and the decrease of absorbance at this band indicates the degradation of aromatic part of dye [30]. During the UV/$K_2S_2O_8$ treatment system, absorption intensity of RhB in solution became weaker along with the reaction time. It can be explained that the aromatic ring structures of RhB molecules were destructed with reaction process.

4. Conclusion

In this study, application of the UV/$K_2S_2O_8$ treatment processes to the aqueous degradation of RhB was investigated. The efficiency of the UV/$K_2S_2O_8$ system was investigated in terms of RhB decay. The effects of oxidants doses, initial RhB concentration anions, initial pH, and three kinds of anions (Cl^-, $H_2PO_4^-$ and HCO_3^-) on the degradation rate in the UV/$K_2S_2O_8$ system were investigated. The RhB degradation rate increased with the increasing of concentration of oxidant $K_2S_2O_8$ from 0.2 mM to 0.8 mM. While the improvement was not sustained above a critical value ([$K_2S_2O_8$] = 1.0 mM), photooxidation efficiency decreased as initial dye concentration increased at the same concentration of $K_2S_2O_8$. Acid initial pH facilitated the RhB degradation during the UV/$K_2S_2O_8$ system because that $SO_4^{\bullet-}$ are the dominant active species in this pH value area. In the UV/$K_2S_2O_8$ system, the observed adverse effects of inorganic anions could be the result of competitive with dye and the inhibiting effect followed the order of $Cl^- < H_2PO_4^- < HCO_3^-$. During the UV/$K_2S_2O_8$ treatment system, absorption intensity of RhB in solution became weaker along with the reaction time, which can be explained that the aromatic ring structures of RhB molecules were destructed with reaction process.

Acknowledgment

The study was supported by Zhejiang Provincial Natural Science Foundation (no. Y5110338) and the National Natural Science Foundation (no. 20907045) of China.

References

[1] M. A. Behnajady and N. Modirshahla, "Evaluation of electrical energy per order (E_{EO}) with kinetic modeling on photooxidative degradation of C. I. Acid orange 7 in a tubular

continuous-flow photoreactor," *Industrial and Engineering Chemistry Research*, vol. 45, no. 2, pp. 553–557, 2006.

[2] J. W. Lee, S. P. Choi, R. Thiruvenkatachari, W. G. Shim, and H. Moon, "Evaluation of the performance of adsorption and coagulation processes for the maximum removal of reactive dyes," *Dyes and Pigments*, vol. 69, no. 3, pp. 196–203, 2006.

[3] S. Wang, "A Comparative study of Fenton and Fenton-like reaction kinetics in decolourisation of wastewater," *Dyes and Pigments*, vol. 76, no. 3, pp. 714–720, 2008.

[4] S. K. Ling, S. Wang, and Y. Peng, "Oxidative degradation of dyes in water using Co^{2+}/H_2O_2 and Co^{2+}/peroxymonosulfate," *Journal of Hazardous Materials*, vol. 178, no. 1–3, pp. 385–389, 2010.

[5] I. Arslan-Alaton and J. L. Ferry, "Application of polyoxotungstates as environmental catalysts: wet air oxidation of acid dye Orange II," *Dyes and Pigments*, vol. 54, no. 1, pp. 25–36, 2002.

[6] F. H. AlHamedi, M. A. Rauf, and S. S. Ashraf, "Degradation studies of Rhodamine B in the presence of UV/H_2O_2," *Desalination*, vol. 238, no. 1–3, pp. 159–166, 2009.

[7] Z. He, S. Yang, Y. Ju, and C. Sun, "Microwave photocatalytic degradation of Rhodamine B using TiO_2 supported on activated carbon: mechanism implication," *Journal of Environmental Sciences*, vol. 21, no. 2, pp. 268–272, 2009.

[8] M. Cheng, W. Ma, J. Li et al., "Visible-light-assisted degradation of dye pollutants over Fe(III)-loaded resin in the presence of H_2O_2 at neutral pH values," *Environmental Science and Technology*, vol. 38, no. 5, pp. 1569–1575, 2004.

[9] P. Shukla, I. Fatimah, S. Wang, H. M. Ang, and M. O. Tadé, "Photocatalytic generation of sulphate and hydroxyl radicals using zinc oxide under low-power UV to oxidise phenolic contaminants in wastewater," *Catalysis Today*, vol. 157, no. 1–4, pp. 410–414, 2010.

[10] Y. Deng and C. M. Ezyske, "Sulfate radical-advanced oxidation process (SR-AOP) for simultaneous removal of refractory organic contaminants and ammonia in landfill leachate," *Water Research*, vol. 45, no. 18, pp. 6189–6194, 2011.

[11] P. Nfodzo and H. Choi, "Triclosan decomposition by sulfate radicals: effects of oxidant and metal doses," *Chemical Engineering Journal*, vol. 174, no. 2-3, pp. 629–634, 2011.

[12] J. Criquet and N. K. V. Leitner, "Degradation of acetic acid with sulfate radical generated by persulfate ions photolysis," *Chemosphere*, vol. 77, no. 2, pp. 194–200, 2009.

[13] R. H. Waldemer, P. G. Tratnyek, R. L. Johnson, and J. T. Nurmi, "Oxidation of chlorinated ethenes by heat-activated persulfate: kinetics and products," *Environmental Science and Technology*, vol. 41, no. 3, pp. 1010–1015, 2007.

[14] G. P. Anipsitakis and D. D. Dionysiou, "Radical generation by the interaction of transition metals with common oxidants," *Environmental Science and Technology*, vol. 38, no. 13, pp. 3705–3712, 2004.

[15] C. Liang, Y. J. Chen, and K. J. Chang, "Evaluation of persulfate oxidative wet scrubber for removing BTEX gases," *Journal of Hazardous Materials*, vol. 164, no. 2-3, pp. 571–579, 2009.

[16] P. Neta, V. Madhavan, H. Zemel, and R. W. Fessenden, "Rate constants and mechanism of reaction of so4·- with aromatic compounds," *Journal of the American Chemical Society*, vol. 99, no. 1, pp. 163–164, 1977.

[17] A. Rastogi, S. R. Al-Abed, and D. D. Dionysiou, "Sulfate radical-based ferrous-peroxymonosulfate oxidative system for PCBs degradation in aqueous and sediment systems," *Applied Catalysis B*, vol. 85, no. 3-4, pp. 171–179, 2009.

[18] S. K. Kuriechen, S. Murugesan, S. P. Raj, and P. Maruthamuthu, "Visible light assisted photocatalytic mineralization of Reactive Red 180 using colloidal TiO_2 and oxone," *Chemical Engineering Journal*, vol. 174, no. 2-3, pp. 530–538, 2011.

[19] P. Wang, S. Yang, L. Shan, R. Niu, and X. Shao, "Involvements of chloride ion in decolorization of Acid Orange 7 by activated peroxydisulfate or peroxymonosulfate oxidation," *Journal of Environmental Sciences*, vol. 23, no. 11, pp. 1799–1807, 2011.

[20] Y. F. Huang and Y. H. Huang, "Identification of produced powerful radicals involved in the mineralization of bisphenol A using a novel UV-$Na_2S_2O_8/H_2O_2$-Fe(II,III) two-stage oxidation process," *Journal of Hazardous Materials*, vol. 162, no. 2-3, pp. 1211–1216, 2009.

[21] D. Salari, A. Niaei, S. Aber, and M. H. Rasoulifard, "The photooxidative destruction of C.I. Basic Yellow 2 using $UV/S_2O_8^{2-}$ process in a rectangular continuous photoreactor," *Journal of Hazardous Materials*, vol. 166, no. 1, pp. 61–66, 2009.

[22] S. Merouani, O. Hamdaoui, F. Saoudi, M. Chiha, and C. Pétrier, "Influence of bicarbonate and carbonate ions on sonochemical degradation of Rhodamine B in aqueous phase," *Journal of Hazardous Materials*, vol. 175, no. 1–3, pp. 593–599, 2010.

[23] E. Hayon, A. Treinin, and J. Wilf, "Electronic spectra, photochemistry, and autoxidation mechanism of the sulfite-bisulfite-pyrosulfite systems. The SO_2^-, SO_3^-, SO_4^-, and SO_5^- radicals," *Journal of the American Chemical Society*, vol. 94, no. 1, pp. 47–57, 1972.

[24] H. Herrmann, B. Ervens, H. W. Jacobi, R. Wolke, P. Nowacki, and R. Zellner, "CAPRAM2.3: a chemical aqueous phase radical mechanism for tropospheric chemistry," *Journal of Atmospheric Chemistry*, vol. 36, no. 3, pp. 231–284, 2000.

[25] L. Dogliotti and E. Hayon, "Flash photolysis of persulfate ions in aqueous solutions. Study of the sulfate and ozonide radical allions," *Journal of Physical Chemistry*, vol. 71, no. 8, pp. 2511–2516, 1967.

[26] S. Canonica, T. Kohn, M. Mac, F. J. Real, J. Wirz, and U. Von Gunten, "Photosensitizer method to determine rate constants for the reaction of carbonate radical with organic compounds," *Environmental Science and Technology*, vol. 39, no. 23, pp. 9182–9188, 2005.

[27] R. E. Huie and C. L. Clifton, "Temperature dependence of the rate constants for reactions of the sulfate radical, $SO_4^{\bullet-}$, with anions," *Journal of Physical Chemistry*, vol. 94, no. 23, pp. 8561–8567, 1990.

[28] B. Ouyang, H. J. Fang, C. Z. Zhu, W. B. Dong, and H. Q. Hou, "Reactions between the $SO_4^{\bullet-}$ radical and some common anions in atmospheric aqueous droplets," *Journal of Environmental Sciences*, vol. 17, no. 5, pp. 786–788, 2005.

[29] X. Y. Vu, Z. C. Bao, and J. R. Barker, "Free radical reactions involving $Cl^{\bullet}$, $Cl_2^{-\bullet}$, and $SO_4^{\bullet-}$ in the 248 nm photolysis of aqueous solutions containing $S_2O_8^{2-}$ and Cl^-," *Journal of Physical Chemistry A*, vol. 108, no. 2, pp. 295–308, 2004.

[30] B. Cuiping, X. Xianfeng, G. Wenqi et al., "Removal of rhodamine B by ozone-based advanced oxidation process," *Desalination*, vol. 278, no. 1–3, pp. 84–90, 2011.

Hindawi Publishing Corporation
International Journal of Photoenergy
Volume 2012, Article ID 909157, 9 pages
doi:10.1155/2012/909157

Research Article

Landfill Leachates Treatment by H_2O_2/UV, O_3/H_2O_2, Modified Fenton, and Modified Photo-Fenton Methods

Jeremi Naumczyk, Izabela Prokurat, and Piotr Marcinowski

Faculty of Environmental Engineering, Warsaw University of Technology, Nowowiejska 20, 00-653 Warsaw, Poland

Correspondence should be addressed to Jeremi Naumczyk, jeremi.naumczyk@is.pw.edu.pl

Received 31 May 2012; Revised 8 August 2012; Accepted 11 August 2012

Academic Editor: Manickavachagam Muruganandham

Advanced oxidation processes (AOPs) such as H_2O_2/UV, O_3/H_2O_2, modified Fenton, and modified photo-Fenton processes have been investigated in terms of the treatment of landfill leachate with ratio of BOD_5/COD in the range of 0.22 to 0.24. The modification of Fenton and photo-Fenton processes consisted in the inclusion of precipitation and separation of humic substances at pH 3. Due to the precipitation, the value of COD decreased by 39% and BOD_5 by 7.1%. The modification of the processes allowed us to improve the efficiency and to decrease the doses of reagents necessary to continue the process. Modified photo-Fenton process proved to be the most effective (92.7% COD removal) of all processes investigated. Additionally, modified-Fenton process was much more effective than the other two processes when compared up to 120 min, while after longer times it gave the least satisfactory results. After 30 min of modified-Fenton process BOD_5/COD ratio increased to 0.43. The parameter referred to as "efficiency of oxidants" was used to estimate the efficiency of all the processes—its value varied from 178 to 239%. Various substances including phthalates, hydrocarbons, silanes, and siloxanes were identified in raw and treated leachate.

1. Introduction

In advanced oxidation processes (AOPs) the hydroxyl radical $HO^{\bullet}$ characterized by high redox potential (2,8 V) is produced. The chain reaction evoked by $HO^{\bullet}$ leads to an effective organic pollutants degradation identified by decreased COD value [1]. The use of AOPs in landfill leachate treatment has been the subject of numerous publications, including reviews [1–3]. Despite that it is still difficult to order different methods in terms of their efficiency to oxidize organic compounds. Additionally, the number of studies referring to more than two methods is limited. Another reason is a wide range of concentrations of organics in leachate varying from a few hundreds to more than ten thousand mg/L COD [1]. According to the review published by Kurniawan et al. [1] photo-Fenton and H_2O_2/O_3/UV processes are the most effective. The efficiency of O_3/H_2O_2 and H_2O_2/UV processes is comparable, while Fenton and O_3/OH^- processes are less effective. In one of the recently published papers [4] O_3/OH^-, O_3/H_2O_2, and Fenton processes have been compared. It has been shown that Fenton process yielding 46% COD removal is far less effective than the two remaining processes, in which efficiency is approximately 72%. Primo et al. [5] investigated the efficiency of the treatment of landfill leachate by means of different AOPs. They also classified the methods according to their efficiency in the following order: photo-Fenton, Fenton-like > Fenton > H_2O_2/UV > UV.

Another interesting method among AOPs is oxone/Co^{2+} process. According to the results of the studies carried out by Sun et al. [6] the efficiency of this method is higher that the efficiency of Fenton one. Sulfate radical oxidation process (SR-AOP) [7] is another method worth mentioning. In this method persulfate ($S_2O_8^{2-}$) is activated by heating to produce $SO_4^{\bullet -}$ radical, which is a strong oxidant (E^0 = 2,4 V). At pH 4 and 50°C COD removal is estimated to be 91% and additionally it is possible to remove ammoniacal nitrogen.

Significant differences observed in COD values are caused by different age of landfills. Young landfill leachate shows higher COD values and BOD_5/COD ratio equal to or higher than 0.4, which is typical of domestic wastewaters. Old

landfill leachate (stabilized) exhibits lower values of COD; its organics are difficult to biodegrade and the BOD_5/COD ratio is below 0.10. The humic acids with molecular mass between 10 and 100 kD dominate in old landfill leachate [8]. Additionally, the degree of humification increases with the increasing age of the landfill [9]. Differences in BOD_5/COD ratio cause different susceptibility of organics to chemical oxidation [1], which leads to a decrease in the concentration of high molecular weight organics (>10 kDa) [10]. Within a certain period of chemical oxidation BOD_5/COD ratio increases, which results in better biodegradability. Therefore, AOPs are often used as a pretreatment step before a biological process. Fenton process has been the most widely used process of all the AOPs [1, 3]. It is also the most common pretreatment method applied before biological treatment. In contrast, photo-Fenton method is one of the least studied. Fenton process has a few modifications. One of them consists in the separation of the sediment of humic substances precipitating after pH decrease (preliminary coagulation), which is a necessary step in this process. According to the results of our studies [9] sediment formation is an instant process. However, the amount of the sediment increases in time and depends on the pH value: the lower the pH value, the greater amount of the sediment. After the separation of sediment the process is continued.

Fenton process after Fe^{2+} and H_2O_2 application continues according to the reactions given below [1].

Initial reactions:

$$Fe^{2+} + H_2O_2 + H^+ \longrightarrow Fe^{3+} + HO^\bullet + H_2O \quad (1)$$

$$Fe^{3+} + H_2O_2 \longrightarrow Fe(OOH)^{2+} + H^+ \longleftrightarrow Fe^{2+} + HO_2^\bullet + H^+ \quad (2)$$

Propagation:

$$H_2O_2 + HO^\bullet \longrightarrow HO_2^\bullet + H_2O \quad (3)$$

$$H_2O_2 + HO_2^\bullet \longrightarrow HO^\bullet + O_2 + H_2O \quad (4)$$

Termination:

$$Fe^{2+} + HO^\bullet \longrightarrow Fe^{3+} + HO^- \quad (5)$$

$$Fe^{3+} + HO_2^\bullet \longrightarrow Fe^{2+} + H^+ + O_2 \quad (6)$$

$$HO^\bullet + HO_2^\bullet \longrightarrow H_2O + O_2 \quad (7)$$

$$HO^\bullet + HO^\bullet \longrightarrow H_2O_2 \quad (8)$$

Photo-Fenton process is based on the same reagents as Fenton process but the solution is additionally exposed to UV radiation. As a result, the higher concentration of hydroxyl radicals is obtained. This is due to the fact that ferric complex ion formed in the Fenton reaction ((1), (5)) may be reduced to Fe^{2+} by near UV, according to the following reaction in acidic solution [11]:

$$Fe(OH)^{2+} + h\nu \longrightarrow Fe^{2+} + HO^\bullet \quad (9)$$

In the presence of hydrogen peroxide, Fe^{2+} can be oxidized according to (1).

In the H_2O_2/UV process $HO^\bullet$ radicals are generated according to the following reaction:

$$H_2O_2 + h\nu(UV) \longrightarrow 2HO^\bullet \quad (10)$$

Additionally, the application of UV light leads to the situation in which organic compounds become more reactive due to the changes in their molecular structure.

Propagation reactions in H_2O_2/UV process are exactly the same as in Fenton and photo-Fenton processes ((3), (4)). Termination reaction follows according to (7) and (8).

AOP employing O_3/H_2O_2 method involves the synergistic action of the two reagents. As a result, hydroxyl radicals are formed according to the following reactions:

$$O_3 + HO^- \longrightarrow HO_2^\bullet + O_2^{\bullet -} \quad (11)$$

$$H_2O_2 \longrightarrow HO_2^- + H^+ \quad (12)$$

$$O_3 + HO_2^- \longrightarrow HO^\bullet + O_2^{\bullet -} + O_2 \quad (13)$$

$$O_3 + O_2^{\bullet -} \longrightarrow O_3^{\bullet -} + O_2 \quad (14)$$

$$O_3^{\bullet -} + H_2O \longrightarrow HO^\bullet + HO^- + O_2 \quad (15)$$

Oxidation of organic matter in landfill leachates treated by O_3/H_2O_2 takes place faster than if only one of the above-mentioned oxidants is used. Efficiency expressed as the rate of COD or TOC decrease depends on the ozone dose per mg of COD as well as on the $H_2O_2 : O_3$ ratio. Haapea et al. [12] achieved the highest ratio of TOC decrease for landfill leachates while using ozone dose of 0.5 mg O_3/mg COD and $H_2O_2 : O_3$ ratio equal to 1 : 2. Application of other ratios of reagents (1 : 4 and 3 : 2) while maintaining the same ozone dose produced less satisfactory results.

The aim of this study was to compare efficiency of four AOPs in leachate treatment—modified Fenton and modified photo-Fenton process (m-Fenton, m-photo-Fenton), as well as H_2O_2/UV and O_3/H_2O_2process. The leachate used in this study can be described as medium stabilized and can be characterized by the values of BOD_5/COD in the range of 0.1–0.4. Such type of leachate has not been very often used in the studies reported in the literature. Additionally, the effectiveness of oxidation of anthropogenic nonbiodegradable pollutants present in the leachate was also investigated.

2. Methods

The paper was conducted on leachate from a landfill site in Lubna near Warsaw. Before the tests samples were subject to 30 min of preliminary sedimentation to separate easily settleable solids.

2.1. Analysis of Raw and Treated Landfill Leachate. The determination of COD, total solids (TS), conductivity, total Kjeldhal nitrogen (TKN), ammonia (N_{NH_4}), chlorides (Cl^-), pH, H_2O_2, and alkalinity was carried out according to the European Standards. BOD_5 was determined using Selutec

Table 1: Characteristics of leachate.

Parameter	pH (—)	Conductivity (μS/cm)	Chlorides (mg/L)	Ammonia (mg/L)	TKN (mg/L)	COD (mg/L)	BOD_5 (mg/L)	BOD_5/COD (—)
Minimum value	7.8	17600	2400	160	700	4960	1080	0.22
Maximum value	8.7	23000	4000	480	940	6100	1486	0.24
Average	—	20443	2951	339	797	5678	1315	0.23

BSBdigiO_2 respirometer. H_2O_2 was determined by iodometric method. The analysis of raw and treated landfill leachate was also carried out using GC/MS (Finnigan GCQ Mat). The 1L sample was extracted three times using hexane. Collected organic fractions were dried with anhydrous Na_2SO_4 and evaporated using Heidolph VV-micro vacuum rotary evaporator. In the next step, the evaporated extract passed through glass column filled with silica gel. The purified extract was evaporated to the volume of 2 mL using the Kuderna-Danish apparatus (Supelco) and analyzed. Separation was achieved using an RTX-5MS Restek Corporation column of 60 m length $\times$ 0.32 mm i.d. $\times$ 0.25 μm film thickness. The GC operated at an injector temperature of 280°C with an initial column temperature of 60°C held for 3 min. The temperature was programmed to step up with the speed of 3°C/min until it reached 300°C, which was held for 5 min. The mass spectrometer operated in EI (70 eV) full scan mode, with ion source temperature of 185°C. Mass spectra were compared to the NIST 98.L published spectra. Xcalibur Qual Browser v.1.2 was used for data acquisition and handling.

For sediment precipitated at pH 3.0 and leachate after 0, 5, 10, 15, and 30 min of Fenton reaction, GC-MS analysis was also performed. The separated sediment was then chemically dried by adding small amounts of anhydrous $MgSO_4$. In the next step the extraction with dichloromethane in Soxhlet apparatus was carried out. The extract was then evaporated in rotary evaporator using *n*-hexane as a solvent to obtain the volume of 5 cm^3. Subsequently, it was cleaned up in a column with florisil. Further GC/MS analysis was carried out in the same conditions as the ones used to analyze raw leachate.

2.2. Experiment. M-photo-Fenton process was conducted in 1 L glass cylindrical Heraeus Noblelight photoreactor equipped with a cooling jacket. UV radiation in m-photo-Fenton method was provided by a medium-pressure mercury lamp TQ (150 W), immersed in the sleeve. H_2O_2/UV process was carried out in 1 L Heraeus Noblelight with low-pressure mercury lamp (15 W). The leachate was stirred with a magnetic stirrer. In O_3/H_2O_2 method a self-constructed 1 L cylindrical Plexiglas reactor with the diameter of 8 cm was used along with Sander ozone generator. Ozone was introduced through a porous-fritted diffuser, with the dosage of 500–1000 mg/h. M-Fenton process was carried out in 2 L cylindrical reactor equipped with a magnetic stirrer.

After acidifying with 1 M H_2SO_4 to pH 3.0, the leachate became turbid and humic substances started to precipitate. Full clarification was obtained after 5 h and then the sediment was separated. This process is referred to as a preliminary coagulation. When the separation of the sediment had been finished, 35% H_2O_2 and 10% $FeSO_4$ solutions were added and m-Fenton and m-photo-Fenton processes were continued. After a certain reaction period the leachate was neutralized with 10% NaOH and after 30 min of flocculation and sedimentation the supernatant was examined.

During 5 h of sedimentation of raw leachate some fine solids precipitated. Therefore, H_2O_2/UV and O_3/H_2O_2 treatments were also preceded by 5 h of sedimentation in order to enable better comparison of all results.

After reaction periods of 0, 15, 30, 60, 120, 240, and 360 min, COD, BOD_5 (only in m-Fenton process), pH, and H_2O_2 concentrations were determined. Before COD analysis, the remaining H_2O_2 was removed with catalase. All tests were conducted for 6 different samples of leachate and the results were calculated to obtain average values.

3. Results and Discussion

3.1. Raw Leachates. The composition characteristic of the landfill leachates is given in Table 1. It can be noticed that the leachates are rich in organic substances (COD 4960–6100 mg/L), ammonium ions, and chlorides. Due to the fact that the leachates come from an old, medium-stabilized landfill site, they have BOD_5/COD values of 0.22–0.24. Since this ratio is far below 0.4, the leachates can be classified as refractory to biological treatment.

3.2. AOPs Results

3.2.1. Modified Fenton Process. Changes of COD during the process are shown in Figure 1. Preliminary coagulation at pH 3.0 and 5 h of sedimentation led to the average decrease in COD by 39.3% (Figure 1, time "0"). COD value was decreasing relatively fast until 60 min. After that the process started to slow down. Figure 1 proves that the optimal effect of treatment was obtained for H_2O_2/Fe (II) doses 3500/500 and 3000/1000 mg/L. Application of doses 4000/500 and 4000/1000 resulted in slightly worse effect. For the two optimal doses the value of COD decreased by approximately 75% after preliminary coagulation and 60 min of Fenton reaction. For Fenton reaction periods of 15, 120, 240, and 360 min these values were 53.6, 77.9, 82.2, and 87.5%, respectively. BOD_5 value also decreased during Fenton process. Preliminary coagulation at pH 3.0 led to the increase in BOD_5/COD ratio to 0.33–0.35. For the above-mentioned optimal doses and after Fenton reaction period of 15 min the ratio increased to 0.42–0.45. After that time the ratio started to decrease, reaching the average values of 0.36, 0.33, 0.30, and 0.26 after 30, 60, 120, and 480 min of reaction,

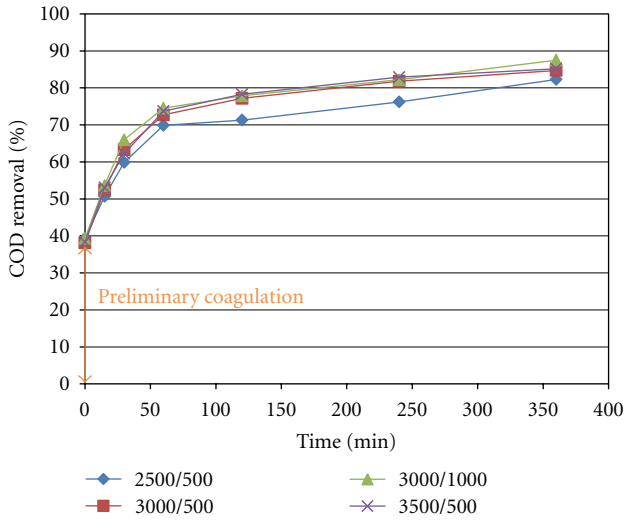

Figure 1: COD removal as a function of time for m-Fenton process and different doses of H_2O_2/Fe (II).

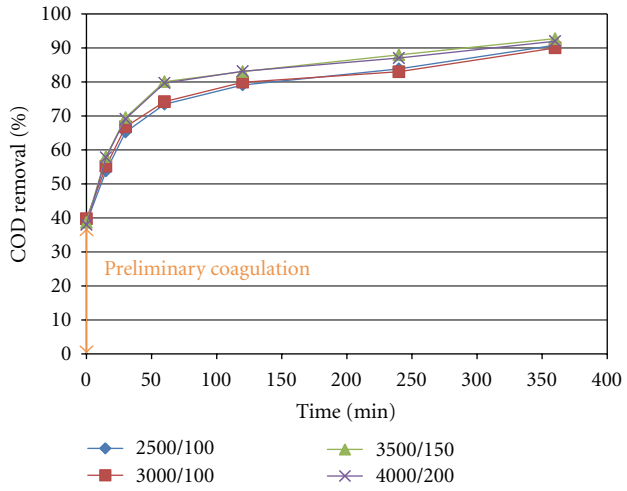

Figure 2: COD removal as a function of time for m-photo-Fenton process and different doses of H_2O_2/Fe (II).

respectively. The same ratio was obtained after 20 min if smaller reagent doses were used (2500/500).

3.2.2. Modified Photo-Fenton Process. Changes of COD during the process are shown in Figure 2. Similarly to m-Fenton process, a fast drop of COD occurred until 60 min. After that the process started to slow down. Optimal dose of H_2O_2/Fe (II) was estimated to be 3500/150 mg/L. After reaction periods of 60, 120, 240, and 360 min, COD value decreased by 80.1, 83.0, 88.0, and 92.7%, respectively. Doses of 4000/150 and 4000/200 led to only slightly better results. For doses 4000/100, 4000/150, and 4500/200 (data not shown in the picture to ensure its clarity), the effect was less pronounced. For doses of 3500/100 the effect was a little better than that for 3000/100.

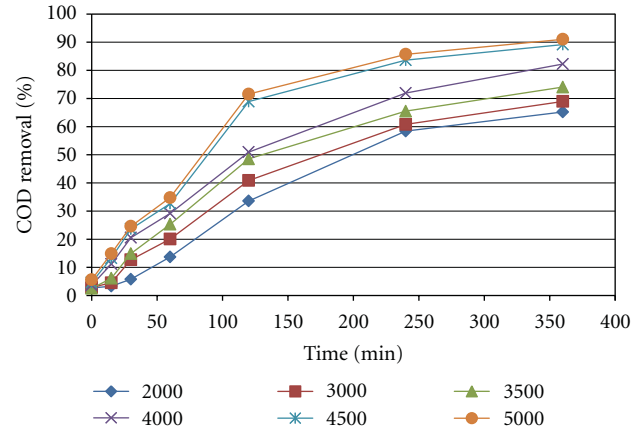

Figure 3: COD removal as a function of time for H_2O_2/UV process and different doses of H_2O_2.

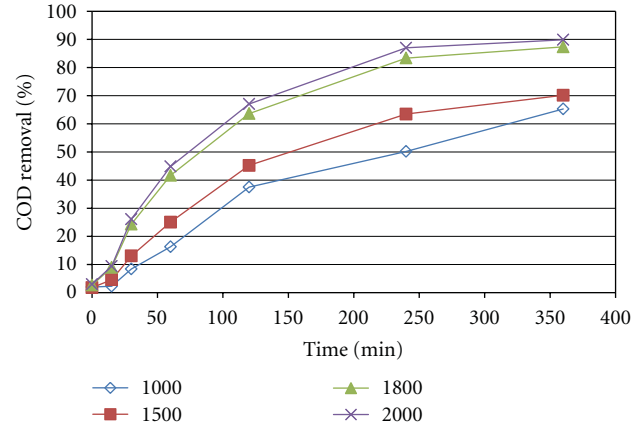

Figure 4: COD removal as a function of time for O_3/H_2O_2 process and different doses of H_2O_2.

3.2.3. H_2O_2/UV. Figure 3 shows changes in COD values for different doses of H_2O_2 (2000–6000 mg/L). Five hours of preliminary sedimentation resulted in 4.6% COD removal. The effect of the process for each sample increased considerably when H_2O_2 dose was increased to 4500 mg/L. Therefore, this dose can be considered as optimal. The resulted decrease in COD after 60, 120, 240, and 360 min was equal to 32.7, 68.9, 83.6, and 89.2%, respectively. The dose of 5000 mg/L slightly improved the process efficiency—91.0% after 360 min. For doses 5500 and 6000 mg/L the efficiency was approximately the same or slightly lower.

3.2.4. O_3/H_2O_2. The COD values for H_2O_2 doses varying from 1000 to 2000 mg/L and O_3 dose of 750 mg/h are shown in Figure 4. The 3.0% of COD removal due to sedimentation was taken into account as above. The efficiency of the process increased when H_2O_2 dose was increased up to 2000 mg/L. For higher doses (to 3000 mg/L) the efficiency was approximately the same. For the dose of 2000 mg/L, considered as optimal, the decrease in COD value after 60,120, 240, and 360 min was equal to 44.8, 67.1, 87.0, and 89.9%, respectively.

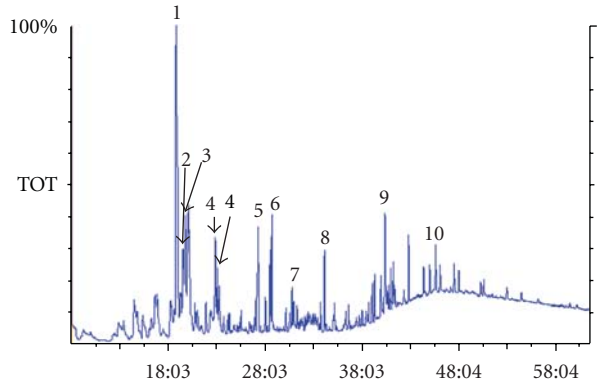

(1) Bicyclo[2.2.1]heptan-2-one, 5,5,6-trimethyl-
(2) Cyclopentane, 1-methyl-1-(2-methyl-2-propenyl)-
(3) Benzenemethanol, 4-trimethyl-
(4) Phenol, m-tert-butyl-
(4) Phenol, 2,3,5,6-tetramethyl-
(5) 3,4-undecadiene-2,10-dione, 6,6-dimethyl-
(6) o-hydroxybiphenyl
(7) Benzophenone
(8) 2-cyclopropen-1-one, 2,3-diphenyl-
(9) Phenanthrene, 1-methyl-7-(1-methylethyl)-
(10) Phthalate, di-isooctyl

Figure 5: Chromatogram of raw leachate.

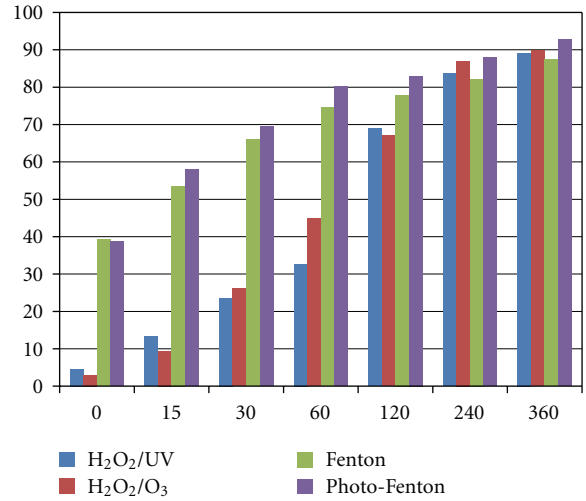

Figure 6: COD removal as a function of time for all process.

Decreasing the O_3 dose to 500 mg/L caused a considerable decrease in the efficiency of the process—COD removal related to 2000 mg/L H_2O_2 was similar to the value obtained for the higher dose of O_3 and 1000 mg/L H_2O_2. An increase in O_3 dose to 1000 mg/L did not improve the efficiency of the process even when lower doses of H_2O_2 were applied.

3.3. GC-MS Analysis. Figure 5 depicts GC-MS chromatograms obtained for raw leachates. Peaks corresponding to the main identified substances are indicated in the figure.

Substances which were either the main pollutants in raw leachates (Figure 5) were detected in leachates treated by AOPs in significantly lower concentrations or were not detected at all. They were oxidized to simple compounds, which cannot be detected by GC/MS method. Due to the matrix complexity it is impossible to derive the sample and unequivocally identify the products of the oxidation. Simple compounds present in raw leachates were removed and have not been detected either in treated leachates or in the resulting sediment. The major identified compound in treated leachates was di-n-butyl phthalate. Similar amounts of this compound were identified both in sediment after preliminary coagulation at pH 3.0 and in remaining leachate. A small part of the total amount of the compound was oxidized—after 30 min 70% of di-n-butyl phthalate remained in leachate. Moreover, the presence of aliphatic hydrocarbons C26-C40 was reported, 70–80% of which precipitated at pH 3. The remaining amount was oxidized in 90% after 30 min. The list of compounds detected in the greatest amount in raw and treated leachates is given in Table 2. The table also includes the degree of the decrease in the compounds' content after preliminary coagulation and Fenton process.

Additionally, small amount of the following substances has been detected in raw leachates:

(i) tricosanoic acid methyl ester and dodecanoic acid methyl ester,

(ii) hasuban-9-ol, 7,8-didehydro-4,5-epoxy-3-methoxy-17-methyl (5-alpha),

(iii) benzene, 1-chloro-3,5-bis(1,1-dimethylethyl)-2-(2-propenyloxy),

(iv) diazene, diphenyl-[E],

(v) cyclopentasiloxane, decamethyl,

(vi) hexa-T-butylthiatrisiletane.

4. Discussion

Figure 6 presents the efficiency of the treatment using the four methods described in this study, for the doses of reagents considered as optimal. For the process periods up to 120 min the methods can be ordered with respect to their oxidation efficiency as follows: m-photo-Fenton > m-Fenton > H_2O_2/UV ~ O_3/H_2O_2. After reaction period of 360 min the highest COD removal was obtained for m-photo-Fenton method and the lowest for m-Fenton method. However, the values after this period did not vary significantly. For short reaction periods the prevalence of m-Fenton and m-photo-Fenton methods is evident. It results from considerable COD removal obtained in coagulation at pH 3, which preceded the Fenton reaction. This advantage is observed until 60 min of the process. With the progress of m-Fenton and m-photo-Fenton processes, the contribution from the preliminary coagulation at pH 3.0 to the overall effect of the processes decreases. Preliminary coagulation does not completely eliminate the contribution from the final coagulation to COD removal. This contribution is significantly smaller and decreases with the increasing time of the process duration

Table 2: Main compounds detected in raw leachates and after Fenton process and the corresponding degree of removal.

Compounds	Preliminary coagulation (%)	Fenton (15 min) (%)	Fenton (30 min) (%)
Bicyclo[2.2.1]heptan-2-one, 5,5,6-trimethyl-	61	99	n.d.
Cyclopentane, 1-methyl-1-(2-methyl-2-propenyl)-	66	99	n.d.
Benzenemethanol, 4-trimethyl-	53	n.d.	n.d.
Phenol, m-tert-butyl-	45	n.d.	n.d.
Phenol, 2,3,5,6-tetramethyl-	45	n.d.	n.d.
3,4-undecadiene-2,10-dione, 6,6-dimethyl-	50	n.d.	n.d.
o-Hydroxybiphenyl	55	n.d.	n.d.
Benzophenone	50	n.d.	n.d.
2-Cyclopropen-1-one, 2,3-diphenyl-	64	n.d.	n.d.
Phenanthrene, 1-methyl-7-(1-methylethyl)-	81	n.d.	n.d.
Phthalate, di-butyl	26	30	30
Phthalate, di-isooctyl	50	56	60
Aliphatic hydrocarbons C26–C40	70–80	90–95	n.d.
2,4,6 (1H,3H,5H)-pyrimidinetrione, 5-ethyl-5-(3-methylbutyl)-1,3-bis(trimethylsilyl)	80–90	95	n.d.
1,3,5,7,9-Penthaethylbicyclo[5, 3, 1] pentasiloxane	50	70	90
Benzeneacetic acid, alpha,3,4-tris[(trimethylsilyl)oxy]-methyl ester	90	n.d.	n.d.
Ent-3a,10-dihydroxy-13-iodomethyl-16-oxo-8,13-epi-17,20-dinogibberell-1	90	n.d.	n.d.
3,4-Dihydroxymandelic acid, ethyl ester, tri-TMS	89	97	98
2H-1,4-Benzodiazepin-2-one, 7-chloro-1,3-dihydro-5-phenyl-1-(trimethylsilyl)	50	n.d.	n.d

[9]. At the same time, after 60 min of the process the rate of Fenton reaction clearly decreases. This decrease in the reaction rate can be explained by the inhibition of Fe (II) ions generation, according to the reactions (2) and (6). Much higher rate of H_2O_2/UV and O_3/H_2O_2 processes compared to Fenton reaction results not only from greater production of $OH^{\bullet}$ radicals but also from higher organics' concentration. Very high and similar values of COD removal (87.5–92.7%) for all processes after 360 min (Figure 6) show that products of the final oxidation are also similar and resistant to further oxidation by $OH^{\bullet}$ radicals.

We have recently showed [9] that the modification of photo-Fenton process results in the higher increase in the efficiency compared to the classic process than in case of the modification of Fenton process. This observation and high photo-Fenton reaction rate caused by the regeneration of $OH^{\bullet}$ radicals (9) lead to very high value of COD removal (92.7%) obtained in this study.

Results of comparative studies conducted by other researchers [1, 13] proved that the efficiency of Fenton process is lower than the efficiency of H_2O_2/UV and O_3/H_2O_2 processes. Only Primo et al. [5] reported that Fenton process was more effective than H_2O_2/UV process. Higher efficiency of m-Fenton process obtained in this study for shorter reaction periods proves the need for conducting such research in the modified way, including coagulation at pH 3.0, separation of the precipitate, and continuation of the process by adding other reagents. Precipitation of humic substances at pH 2.0–4.0 was studied by Rivas et al. [8]. The obtained value of COD removal was equal to 25%. After separating the precipitate, the next stages of the process included coagulation with $FeCl_3$ at pH 3.5 and finally Fenton reaction. Overall COD removal was nearly 90%. Other researchers who studied Fenton reaction did not consider coagulation of humic substances. There is one more advantage of initial coagulation. As a result, Fenton reaction itself is conducted in leachate with much lower COD value, which requires lower reagents doses.

Schulte et al. [13] conducted similar research with stabilized leachate (COD 780 mg/L) using the same three processes, apart from photo-Fenton process. It was shown that Fenton process allowed reducing COD only by 60%. H_2O_2/UV process gave the result of 90% reduction and O_3/H_2O_2 was only slightly more effective. The results of our paper on modified Fenton process can be compared to the research of Lopez et al. [14]. They gained similar results during the treatment of leachate and obtained similar COD/BOD_5 ratio 10540/2300 (4.6) for H_2O_2/Fe (II) doses of 1000/830 mg/L—COD removal was equal to 60%. The presented results are similar to those of Calli et al. [15]. For not stabilized leachate with COD/BOD_5 ratio equal to 5850/2860, it was possible to obtain COD removal by 87%. Similar efficiency was gained by Zhang et al. [16, 17]—approximately 70 and 89% COD removal. Lower value of COD removal for stabilized leachate (61%) was reported by Deng [18].

The results obtained for modified photo-Fenton process were much better than the ones obtained by other researchers in "classic" photo-Fenton process and better than ever obtained for any AOPs [1]. de Morais and Zamora [19] achieved 58% of COD removal for leachate having similar

values of COD and BOD_5. Kim et al. [11] while studying stabilized leachate (COD/BOD_5 1150/5) reported the value of COD removal equal to 70%. In this study the used H_2O_2 dose was similar to COD value and mass ratio of H_2O_2/Fe (II) was approximately 15.

The results shown in Figure 6 do not explicitly point out which method is more effective—H_2O_2/UV or O_3/H_2O_2. The advantage of one method over the other is very small and the difference in the efficiency of the two methods is within the experimental error. The efficiency obtained in this study is similar to that reported by Schulte et al. [13] and Steensen [20], who also achieved COD removal by 90% for stabilized leachate with COD value of 1200 mg/L. de Morais and Zamora [19] obtained the value of 56%, Ince [21] 54%, and Shu et al. [22] 65% of COD removal. The results obtained by O_3/H_2O_2 method were also similar to the results published by Schulte et al. [13] and much higher than those of Haapea et al. [12], who reported only 50% COD removal.

In order to estimate the efficiency of Fenton process, a parameter referred to as "efficiency of hydrogen peroxide" was recommended by Kang and Hwang [23]. However, we suggest some modifications of this parameter. The parameter referred to as "efficiency of oxidants" will allow one to estimate the efficiency of both oxidants,

$$\eta(\%) = \frac{\Delta\text{COD}}{0.4706 \cdot [H_2O_2] + 0.333 \cdot [O_3]} \cdot 100\%, \quad (16)$$

where $\triangle$COD—COD removed, mg/L, $[H_2O_2]$, $[O_3]$—doses of H_2O_2 and O_3, mg/L,

0.4706- factor—COD theoretically removed (mg) by 1 mg H_2O_2,

0.333- factor—COD theoretically removed (mg) by 1 mg O_3.

The values of this parameter for particular processes, without taking into account the results of sedimentation and coagulation at pH 3, for reagent doses considered as optimal, were equal to 184.6%, 239.8%, 178.3%, and 238.0% for H_2O_2/UV, O_3/H_2O_2, m-Fenton, and m-photo-Fenton processed, respectively. Very high values of this parameter prove that the role of oxygen is significant in oxidation processes, since it reacts with organic radicals generated in the reaction of organic compounds with hydroxyl radical and later reactions [1].

$$HO^\bullet + RH \longrightarrow R^\bullet + H_2O \quad (17)$$

$$R^\bullet + O_2 \longrightarrow RO_2^\bullet \quad (18)$$

The organic radical ($R^\bullet$) reacts with oxygen to yield peroxyl radical ($RO_2^\bullet$), which initiates subsequent chain and oxidation reactions.

It is worth noticing that after 360 min of the process several dozen mg/L of H_2O_2 still remains in the leachate (the amount which has not reacted). Moreover, 30% of ozone leaves the reaction environment and some oxidants are lost during the processes. Therefore, the role of oxygen in oxidation process may be even twice higher than the participation of $OH^\bullet$ radicals.

It should be also noted that O_3/H_2O_2 process is characterized by the high efficiency of oxidants, which is much higher than in H_2O_2/UV process. In the same time, the efficiency of COD removal is similar for the two processes. Additionally, it is also comparable to the value typical for a more effective m-photo-Fenton process. In O_3/H_2O_2 process the dose of H_2O_2 is more than twice lower than in case of H_2O_2/UV process. In the O_3/H_2O_2 process much higher contribution of oxygen into the oxidation results from its high dose supplied together with ozone and from its in situ generation, according to the reaction (13). In the H_2O_2/UV process conducted in the photoreactor, the oxygen is supplied in much smaller quantities. Additionally, H_2O_2/UV process is more sensitive to the scavenging effect of H_2O_2 [1]. Due to this effect, high H_2O_2 concentration slows down the oxidation rate, while at low H_2O_2 concentration the generation of $HO^\bullet$ radicals is insufficient.

The results of GC-MS analysis are also interesting. The presence of hydrocarbons and phthalates was expected. O-phthalic acid diesters have been detected in many landfill leachates [24]. They are widely used in many materials (PVC, other resins, paints, adhesives), which after their service life are landfilled. However, the presence of silicon derivatives silyl ethers, siloxanes, silanes, and siletanes was unexpected. Similarly to phthalates, they are also used as plastic additives, in cosmetics, defoamers, soaps, deodorants, lubricants, and other materials. Most of organics detected in landfill leachates in our studies were not reported by other researches. Most of them are probably the products of the conversions taking place in the landfill.

4.1. Kinetics of m-Fenton and m-photo-Fenton Process. The reaction rate of Fenton process causes problems in its description. In order to describe the process of Fenton kinetics pseudofirst and second order equations were employed by Wu et al. [25]. Godala and Nowicki [26] used a fractional-order equation to describe dihydroxyphenols oxidation kinetics in relation to the concentration of oxidized substances and H_2O_2. Wu et al. [25] recognized that Fenton process kinetics cannot be described by a simple equation and suggested an elaborated model, considering reaction rate constants for the ones described by (1)–(8). The same authors [27] suggested a two-stage model consisting of a "rapid reaction stage" followed by a "stagnant stage" for leachate. An attempt to apply these models in this study did not give satisfactory results. The process seems to be too complex and assumptions taken by other authors do not consider factors such as coagulation or reaction of organic radicals with oxygen. Reference [9] revealed that an empirical model can be successfully employed to describe Fenton reaction rate as a change of COD values in time according to the following equation:

$$\frac{d[\text{COD}]}{dt} = -at^m[\text{COD}], \quad (19)$$

where "t" time and "a" and "m" constants are dependent on the initial concentration of reagents.

Table 3: The values of the constants and correlation coefficients for m-Fenton and m-photo-Fenton processes.

	$a*10^{-2}$ (—)	$-m$ (—)	R^2 (—)
m-Fenton 2500/500	3.36	0.496	0.920
m-Fenton 3000/500	4.20	0.503	0.927
m-Fenton 3000/1000	4.48	0.503	0.919
m-Fenton 3500/500	4.23	0.494	0.933
m-photo-Fenton 2500/100	4.03	0.430	0.966
m-photo-Fenton 3000/100	4.18	0.436	0.940
m-photo-Fenton 3500/150	5.41	0.456	0.948
m-photo-Fenton 4000/200	4.84	0.4506	0.963

After integration and applying double logarithm the following formula is obtained:

$$\ln \ln \frac{[\mathrm{COD}_0]}{[\mathrm{COD}]} = n \ln t + \ln k, \tag{20}$$

where $[\mathrm{COD}]_0$ initial COD, $n = m + 1$, $k = a/n$.

In the present study the same empirical model has been used to describe m-Fenton and m-photo-Fenton processes involving oxidation reactions as well as final coagulation and sedimentation. High values of correlation coefficient (from 0.919 to 0.966) prove that the above-mentioned equation may be successfully used to describe the kinetics of the decrease in COD value in m-Fenton and m-photo-Fenton processes. The values of the constants and correlation coefficients for the processes determined in relation to the reagent dose have been included in Table 3.

Constant "a" has the highest values for the individual processes when the reagent dose is optimal. Comparing the values of "m" constant, which is the exponent in the equation, it can be stated that the decrease rate in COD value during m-photo-Fenton process depends on time to the higher extent than in case of m-Fenton process.

5. Conclusions

Adjusting pH to 3.0, which is a necessary step to conduct m-Fenton process, leads to a slow precipitation of humic substances. However, the separation of the sediment before adding next reagents significantly decreases both COD value and $\mathrm{COD/BOD_5}$ ratio. The continuation of m-Fenton or m-photo-Fenton processes results in higher COD removal and the values obtained in the studied leachate correspond to 87.5% and 92.7%, respectively. The reported efficiency of 120 min of m-Fenton process was higher than the efficiency obtained for either O_3/H_2O_2 or H_2O_2/UV processes, for which the values of efficiency were similar. After longer reaction periods the value of the efficiency of m-Fenton process was slightly lower than values observed for the other two processes. Based on the obtained results, it can be stated that m-photo-Fenton process was definitely the most effective of the all processes studied, regardless of the reaction period. Additionally, the "efficiency of oxidants" parameter is recommended to be used to assess the efficiency of AOPs. Its value allows to estimate the approximate amount of oxygen used in the oxidation process.

References

[1] T. A. Kurniawan, W. H. Lo, and G. Y. S. Chan, "Radicals-catalyzed oxidation reactions for degradation of recalcitrant compounds from landfill leachate," *Chemical Engineering Journal*, vol. 125, no. 1, pp. 35–57, 2006.

[2] E. Neyens and J. Baeyens, "A review of classic Fenton's peroxidation as an advanced oxidation technique," *Journal of Hazardous Materials*, vol. 98, no. 1–3, pp. 33–50, 2003.

[3] Y. Deng and J. D. Englehardt, "Treatment of landfill leachate by the Fenton process," *Water Research*, vol. 40, no. 20, pp. 3683–3694, 2006.

[4] S. Cortez, P. Teixeira, R. Oliveira, and M. Mota, "Evaluation of Fenton and ozone-based advanced oxidation processes as mature landfill leachate pre-treatments," *Journal of Environmental Management*, vol. 92, no. 3, pp. 749–755, 2011.

[5] O. Primo, M. J. Rivero, and I. Ortiz, "Photo-Fenton process as an efficient alternative to the treatment of landfill leachates," *Journal of Hazardous Materials*, vol. 153, no. 1-2, pp. 834–842, 2008.

[6] J. Sun, X. Li, J. Feng, and X. Tian, "Oxone/Co^{2+} oxidation as an advanced oxidation process: comparison with traditional Fenton oxidation for treatment of landfill leachate," *Water Research*, vol. 43, no. 17, pp. 4363–4369, 2009.

[7] Y. Deng and C. M. Ezyske, "Sulfate radical-advanced oxidation process (SR-AOP) for simultaneous removal of refractory organic contaminants and ammonia in landfill leachate," *Water Research*, vol. 45, no. 18, pp. 6189–6194, 2011.

[8] F. J. Rivas, F. Beltrán, F. Carvalho, B. Acedo, and O. Gimeno, "Stabilized leachates: sequential coagulation-flocculation + chemical oxidation process," *Journal of Hazardous Materials*, vol. 116, no. 1-2, pp. 95–102, 2004.

[9] A. Krzysztoszek and J. Naumczyk, "Landfill leachate treatment by Fenton, photo-Fenton processes and their modification," *Journal of Advanced Oxidation Technologies*, vol. 15, no. 1, pp. 53–63, 2012.

[10] J. J. Wu, C. C. Wu, H. W. Ma, and C. C. Chang, "Treatment of landfill leachate by ozone-based advanced oxidation processes," *Chemosphere*, vol. 54, no. 7, pp. 997–1003, 2004.

[11] S. M. Kim, S. U. Geissen, and A. Vogelpohl, "Landfill leachate treatment by a photoassisted Fenton reaction," *Water Science and Technology*, vol. 35, no. 4, pp. 239–248, 1997.

[12] P. Haapea, S. Korhonen, and T. Tuhkanen, "Treatment of industrial landfill leachates by chemical and biological methods: ozonation, ozonation + hydrogen peroxide, hydrogen peroxide and biological post-treatment for ozonated water," *Ozone: Science and Engineering*, vol. 24, no. 5, pp. 369–378, 2002.

[13] P. Schulte, A. Bayer, F. Kuhn, T. Luy, and M. Volkmer, "H_2O_2/O_3, H_2O_2/UV and H_2O_2/Fe^{2+} processes for the oxidation of hazardous waste," *Ozone: Science and Engineering*, vol. 17, no. 2, pp. 119–134, 1995.

[14] A. Lopez, M. Pagano, A. Volpe, and A. C. Di Pinto, "Fenton's pre-treatment of mature landfill leachate," *Chemosphere*, vol. 54, no. 7, pp. 1005–1010, 2004.

[15] B. Calli, B. Mertoglu, and B. Inanc, "Landfill leachate management in Istanbul: applications and alternatives," *Chemosphere*, vol. 59, no. 6, pp. 819–829, 2005.

[16] H. Zhang, J. C. Heung, and C. P. Huang, "Optimization of Fenton process for the treatment of landfill leachate," *Journal of Hazardous Materials*, vol. 125, no. 1–3, pp. 166–174, 2005.

[17] H. Zhang, H. J. Choi, and C. P. Huang, "Treatment of landfill leachate by Fenton's reagent in a continuous stirred tank reactor," *Journal of Hazardous Materials*, vol. 136, no. 3, pp. 618–623, 2006.

[18] Y. Deng, "Physical and oxidative removal of organics during Fenton treatment of mature municipal landfill leachate," *Journal of Hazardous Materials*, vol. 146, no. 1-2, pp. 334–340, 2007.

[19] J. L. de Morais and P. P. Zamora, "Use of advanced oxidation processes to improve the biodegradability of mature landfill leachates," *Journal of Hazardous Materials*, vol. 123, no. 1–3, pp. 181–186, 2005.

[20] M. Steensen, "Chemical oxidation for the treatment of leachate—process comparison and results from full-scale plants," *Water Science and Technology*, vol. 35, no. 4, pp. 249–256, 1997.

[21] N. H. Ince, "Light-enhanced chemical oxidation for tertiary treatment of municipal landfill leachate," *Water Environment Research*, vol. 70, no. 6, pp. 1161–1169, 1998.

[22] H. Y. Shu, H. J. Fan, M. C. Chang, and W. P. Hsieh, "Treatment of MSW landfill leachate by a thin gap annular UV/H_2O_2 photoreactor with multi-UV lamps," *Journal of Hazardous Materials*, vol. 129, no. 1–3, pp. 73–79, 2006.

[23] Y. W. Kang and K. Y. Hwang, "Effects of reaction conditions on the oxidation efficiency in the Fenton process," *Water Research*, vol. 34, no. 10, pp. 2786–2790, 2000.

[24] S. Jonsson, J. Ejlertsson, A. Ledin, I. Mersiowsky, and B. H. Svensson, "Mono- and diesters from o-phthalic acid in leachates from different European landfills," *Water Research*, vol. 37, no. 3, pp. 609–617, 2003.

[25] Y. Wu, S. Zhou, F. Qin, K. Zheng, and X. Ye, "Modeling the oxidation kinetics of Fenton's process on the degradation of humic acid," *Journal of Hazardous Materials*, vol. 179, no. 1–3, pp. 533–539, 2010.

[26] M. Godala and L. Nowicki, "Kinetics of dihydroxyphenols oxidation by Fenton reagent," *Ecological Chemistry and Engineering*, vol. 9, no. 1, pp. 43–52, 2002.

[27] Y. Wu, S. Zhou, K. Zheng, X. Ye, and F. Qin, "Mathematical model analysis of Fenton oxidation of landfill leachate," *Waste Management*, vol. 31, no. 3, pp. 468–474, 2011.

Hindawi Publishing Corporation
International Journal of Photoenergy
Volume 2012, Article ID 107293, 10 pages
doi:10.1155/2012/107293

Research Article

Bromate Formation Characteristics of UV Irradiation, Hydrogen Peroxide Addition, Ozonation, and Their Combination Processes

Naoyuki Kishimoto[1] and Eri Nakamura[2]

[1] *Faculty of Science and Technology, Ryukoku University, 1-5 Yokotani, Setaoe-cho, Otsu 520-2194, Japan*
[2] *Graduate School of Science and Technology, Ryukoku University, 1-5 Yokotani, Setaoe-cho, Otsu 520-2194, Japan*

Correspondence should be addressed to Naoyuki Kishimoto, naoyuki@rins.ryukoku.ac.jp

Received 28 May 2012; Revised 8 August 2012; Accepted 8 August 2012

Academic Editor: Manickavachagam Muruganandham

Bromate formation characteristics of six-physicochemical oxidation processes, UV irradiation, single addition of hydrogen peroxide, ozonation, UV irradiation with hydrogen peroxide addition (UV/H_2O_2), ozonation with hydrogen peroxide addition (O_3/H_2O_2), and ozonation with UV irradiation (O_3/UV) were investigated using 1.88 μM of potassium bromide solution with or without 6.4 μM of 4-chlorobenzoic acid. Bromate was not detected during UV irradiation, single addition of H_2O_2, and UV/H_2O_2, whereas ozone-based treatments produced BrO_3^-. Hydroxyl radicals played more important role in bromate formation than molecular ozone. Acidification and addition of radical scavengers such as 4-chlorobenzoic acid were effective in inhibiting bromate formation during the ozone-based treatments because of inhibition of hydroxyl radical generation and consumption of hydroxyl radicals, respectively. The H_2O_2 addition was unable to decompose 4-chlorobenzoic acid, though O_3/UV and O_3/H_2O_2 showed the rapid degradation, and UV irradiation and UV/H_2O_2 showed the slow degradation. Consequently, if the concentration of organic contaminants is low, the UV irradiation and/or UV/H_2O_2 are applicable to organic contaminants removal without bromate formation. However, if the concentration of organic contaminants is high, O_3/H_2O_2 and O_3/UV should be discussed as advanced oxidation processes because of their high organic removal efficiency and low bromate formation potential at the optimum condition.

1. Introduction

Nowadays, the world demand for water is growing because of the rapid population growth. Furthermore, pollution of freshwater resources proceeds in all over the world. For instance, China encounters severe water pollution caused by industrial chemicals, heavy metals, and algal toxin with an extraordinary economic growth [1]. Gadgil [2] reported that about half the population in the developing world is suffering from one or more of the six main diseases, diarrhea, ascaris dracunculisis, hookworm, schistosomiasis, and trachoma, which are associated with water supply and sanitation. In the industrialized countries, micropollutants like pharmaceuticals gather much concern as potential contaminants in drinking water [3] and surface water [4]. As a result of this situation, water supply section has made efforts to supply a plenty of safe drinking water. In this context, various advanced water treatment like UV disinfection, ozonation, and adsorption processes [5–7] have been introduced to water purification plants.

UV irradiation and ozone-based chemical oxidation are widely used as advanced water purification processes. These processes can achieve higher level of disinfection and organic pollutants removal [9, 10]. However, bromate (BrO_3^-) formation in these chemical oxidation processes may bring a potential health risk, because BrO_3^- is a possibly carcinogenic to human [11]. Therefore, it is important to understand BrO_3^- formation potential in these processes.

Various knowledge of the BrO_3^- formation during UV and ozone-based chemical oxidation processes has been accumulated for past a few decades. For instance, ozonation of bromide-containing water produces BrO_3^- via ozone and

hydroxyl radical pathways [8], but pH depression [12] and ammonia addition [12, 13] successfully decrease BrO_3^- formation. The pH depression decreased 50–63% in BrO_3^- formation per a decline in one-pH-unit [12] because of a depression of hydroxyl radical generation and a decrease in hypobromite (BrO^-), which is a key intermediate of BrO_3^- formation. The inhibition effect of ammonia addition on BrO_3^- formation is caused by bromamines formation from the reaction of HOBr with ammonia [14]. The effective ammonia dose for BrO_3^- depression was limited to 200 μg/L and further increase in ammonia addition did not enhance the BrO_3^- minimization [14]. Effect of hydrogen peroxide (H_2O_2) in ozonation on BrO_3^- formation is complicated. As H_2O_2 can reduce BrO^- into bromide (Br^-) [15], it seems to be useful to depress the BrO_3^- formation. However, ozone reacts with hydroperoxide anion (HO_2^-) and produces hydroxyl radicals ($^\bullet$OH) [16], which promotes oxidation of Br^- [8]. Ozekin et al. [13] reported that an increase in H_2O_2 dose in ozonized water enhanced BrO_3^- formation at pH 6.5, though the BrO_3^- formation at pH 8.5 did not depended on the H_2O_2 dose and was smaller than that of ozone alone. Kim et al. [17] pointed out the importance of molar ratio of H_2O_2/O_3 for BrO_3^- formation during ozonation with H_2O_2 addition; the molar ratio of H_2O_2/O_3 above 0.5 and the dissolved ozone concentration below 0.1 mg/L successfully depress the BrO_3^- formation. The inconsistent results between Ozekin et al. [13] and Kim et al. [17] may be caused by the difference in their experimental designs: H_2O_2 was injected during ozonation [17] or after ozonation [13]. But, both research groups suggested that the $^\bullet$OH generation under a certain concentration of dissolved ozone enhanced the BrO_3^- formation during ozone/H_2O_2 treatment [13, 17]. UV light is known to decompose BrO_3^- into BrO^- and/or Br^- [18]. As the result, Collivignarelli and Sorlini [19] reported that BrO_3^- formation during ozonation with UV 254 nm irradiation (O_3/UV) was about 40% lower than that during conventional ozonation. However, Ratpukdi et al. [20] showed that the BrO_3^- formation potential of O_3/UV was similar to ozonation alone, though ozonation combined with vacuum UV irradiation could decrease the BrO_3^- formation. Thus, the BrO_3^- formation mechanisms of UV and ozone-based chemical oxidation processes have been explored extensively. However, each research was performed using different reactors, different procedures, and different water matrices. Therefore, it is not easy to judge which process should be selected for BrO_3^- control.

In this study, BrO_3^- formation in UV irradiation, H_2O_2 addition, ozonation, and their combination processes, UV irradiation with H_2O_2 addition (UV/H_2O_2), ozonation with H_2O_2 addition (O_3/H_2O_2), and ozonation with UV irradiation (O_3/UV), were discussed using the same reactor and the same water matrix to provide comparable information of their features of BrO_3^- formation and its control.

2. Experimental

2.1. Material and Experimental Conditions. A low-pressure mercury vapor lamp (20W, UVL20PH-6, Sen Lights, Japan) was used as a UV light source. Ozone gas was generated from analytical grade oxygen gas with a silent discharge ozonizer (ED-OG-R3Lt, Eco Design, Japan). Hydrogen peroxide was purchased from Nacalai Tesque, Japan as about 35% aqueous solution (extra pure grade) and used without further purification. The accurate H_2O_2 concentration was checked just before an experiment and final concentration was set at 10, 100, or 1,000 μM. Figure 1 shows the experimental setup. The reactor was made of glass with a volume of 1.9 L. The UV lamp in a duplex quartz jacket was installed in the center of the reactor. Ozone was injected through two gas diffusers made of glass at the injection rate of about 20 mg/min. Inlet and outlet ozone gas concentration was monitored with two ozone monitors (EG-600, Ebara Jitsugyo, Japan). The exhaust ozone gas was dried with a gas dryer (DH106-1, Komatsu Electronics, Japan) before ozone monitoring, because water vapor biases the ozone concentration. Oxygen gas flow rate was regulated with a mass flow controller (CMQ9200, Yamatake, Japan) at 500 mL/min. Test solution was 1.9 L of 1.88 μM potassium bromide (KBr, Nacalai Tesque, Japan) solution with or without 6.4 μM of 4-chlorobenzoic acid (4-CBA, Wako Chemicals, Japan). The 4-CBA was used as a model compound of organic scavengers of hydroxyl radical ($^\bullet$OH), because it was unreactive with ozone [21]. The solution pH was adjusted by addition of sulfuric acid or sodium hydroxide at around 2.5 or 7. An experimental run continued for 10 or 30 minutes and solution in the reactor was sampled every two or five minutes for chemical analyses of BrO_3^-, bromide ion (Br^-), dissolved ozone, H_2O_2, 4-CBA, and pH.

2.2. Chemical Analysis. The Br^- concentration was analyzed using an ion chromatography system with a conductivity detector (DX-500, Dionex, USA). Analytical conditions were as follows. Column: Dionex IonPac AS12A with a suppressor (Dionex ASRS-ULTRA 4 mm); mobile phase: aqueous solution with 2.7 mM sodium carbonate and 0.3 mM sodium bicarbonate; flow rate: 1.0 mL/min; sample injection volume: 100 μL; oven temperature: 40°C. The BrO_3^- concentration was determined by the ion chromatography coupled with a postcolumn system (Dionex BRS-500) [22]. Reaction conditions were as follows, reactant A: 1.5 M potassium bromide and 1.0 M sulfuric acid; reactant B: 1.2 mM sodium nitrite; flow rate: 0.4 mL/min for reactant A and 0.2 mL/min for reactant B; reaction temperature: 40°C; detection: absorbance at 268 nm. The determination limit was estimated to be 0.050 μM. Dissolved ozone and H_2O_2 were analyzed by indigo-colorimetric method [23] and DMP method [24], respectively. The 4-CBA concentration was determined by the high-performance liquid chromatography (LV-10ADVP, Shimadzu, Japan) [21]. Analytical conditions were as follows: column: ODS-80TM (4.6 × 250 mm, Tosoh, Japan); mobile phase: acetonitrile (70%) and 0.1% phosphoric acid (30%); flow rate: 1.0 mL/min; sample injection volume: 200 μL; oven temperature: 40°C; detection: absorbance at 234 nm. The solution pH was measured with a pH meter (Twin pH B-212, Horiba, Japan).

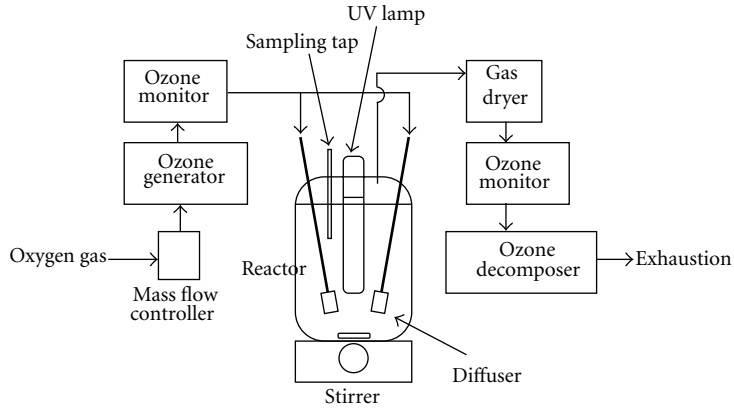

Figure 1: Experimental setup.

3. Results and Discussion

3.1. UV Irradiation, H_2O_2 Addition, and UV/H_2O_2 Process. The H_2O_2 addition did not change concentrations of BrO_3^-, Br^-, and 4-CBA under both acid and neutral pH conditions (data not shown). Although H_2O_2 is an oxidant, H_2O_2 is nucleophilic too. Therefore, H_2O_2 can oxidize Br^- into bromine (Br_2), but Br_2 is reduced into Br^- by H_2O_2 as follows [25]:

$$\begin{aligned} 2Br^- + H_2O_2 + 2H^+ &\longrightarrow Br_2 + 2H_2O \\ Br_2 + H_2O_2 &\longrightarrow 2H^+ + 2Br^- + O_2 \end{aligned} \quad (1)$$

Accordingly, Br^- concentration did not change because of the catalytic behavior of Br^- as shown in reactions (1). On the reactivity of 4-CBA with H_2O_2, Dionysiou et al. [26] also observed that H_2O_2 did not decompose 4-CBA under the dark condition. Since the standard electrode potential of H_2O_2 (1.736 V versus standard hydrogen electrode (SHE)) is lower than that of ozone (2.07 V versus SHE) and $^\bullet$OH (2.38 V versus SHE) [25], the low oxidation potential of H_2O_2 may be responsible for the low reactivity with 4-CBA.

Figure 2 shows the time-course changes in Br^-, BrO_3^-, and 4-CBA concentrations during UV irradiation and UV/H_2O_2 at neutral pH. The concentration changes at acidic condition were almost the same at neutral pH, though the H_2O_2 accumulation was enhanced at acidic condition. The low-pressure mercury vapor lamp emits vacuum UV light of 185 nm, which can photolyze water molecules into hydrogen atoms and $^\bullet$OH [27]. Therefore, H_2O_2 accumulation was caused by H_2O_2 production via the combination of two $^\bullet$OH [28]. The concentrations of Br^- and 4-CBA declined during the UV irradiation and UV/H_2O_2, though BrO_3^- was not generated (Figure 2). No BrO_3^- formation during UV irradiation and UV/H_2O_2 was also reported by Kruithof et al. [29]. The H_2O_2 concentration in the both treatment increased with the passage of time, and the final concentration in UV irradiation reached over 10 μM, which was the initial concentration in UV/H_2O_2. The 4-CBA degradation in UV irradiation slightly delayed in comparison with that in UV/H_2O_2, but the degradation was enhanced with the accumulation of H_2O_2. Accordingly, $^\bullet$OH generation via UV photolysis of H_2O_2 [27] was believed to contribute to the 4-CBA degradation during the UV irradiation and UV/H_2O_2. The decline in Br^- concentration without BrO_3^- accumulation indicates the formation of intermediates. Von Gunten and Oliveras [8] reported that ozone and $^\bullet$OH oxidized Br^- to BrO_3^- (Figure 3). In this mechanism, hypobromite ion (BrO^-) and bromite ion (BrO_2^-) are the critical intermediates, which participate in all BrO_3^- formation pathways. Accordingly, UV irradiation and UV/H_2O_2 were thought to produce BrO^- and/or BrO_2^-. The H_2O_2 can reduce hypobromous acid (HOBr) and BrO^- as follows [15]:

$$\begin{aligned} BrO^- + H_2O_2 &\longrightarrow Br^- + H_2O + O_2 \\ k &= 1.3 \times 10^6\,M^{-1}\,s^{-1}, \\ HOBr + HO_2^- &\longrightarrow Br^- + H_2O + O_2 \\ k &= 7.6 \times 10^8\,M^{-1}\,s^{-1}, \\ HOBr + H_2O_2 &\longrightarrow Br^- + H^+ + H_2O + O_2 \\ k &= 1.5 \times 10^4\,M^{-1}s^{-1}. \end{aligned} \quad (2)$$

Therefore, the accumulation of H_2O_2 was inferred to contribute partly to the prevention of BrO_3^- formation in UV irradiation and UV/H_2O_2. Phillip et al. [30] reported that low-pressure mercury vapor lamps decayed free bromine into Br^- (major) and BrO_3^- (minor). Thus, the photo-degradation of HOBr/BrO^- might conduce to the prevention of BrO_3^- formation too.

3.2. Ozonation. In ozonation, BrO_3^- formation was correspondent to a decrement in Br^- at neutral pH without 4-CBA. However, the BrO_3^- formation was much lower than Br^- removal at acidic pH or coexistence of 4-CBA (Figure 4). Although both ozone and $^\bullet$OH promote the oxidation of Br^- to BrO_3^- via BrO^- and BrO_2^- (Figure 3), our experimental results shown in Figure 4 indicated that contribution of $^\bullet$OH to BrO_3^- evolution was relatively large. Because acidic pH restrains $^\bullet$OH generation via self-decomposition of ozone [31], and 4-CBA is a $^\bullet$OH radical scavenger with low reactivity with ozone [21]. Since HOBr has a pKa of 8.8–9.0 [32],

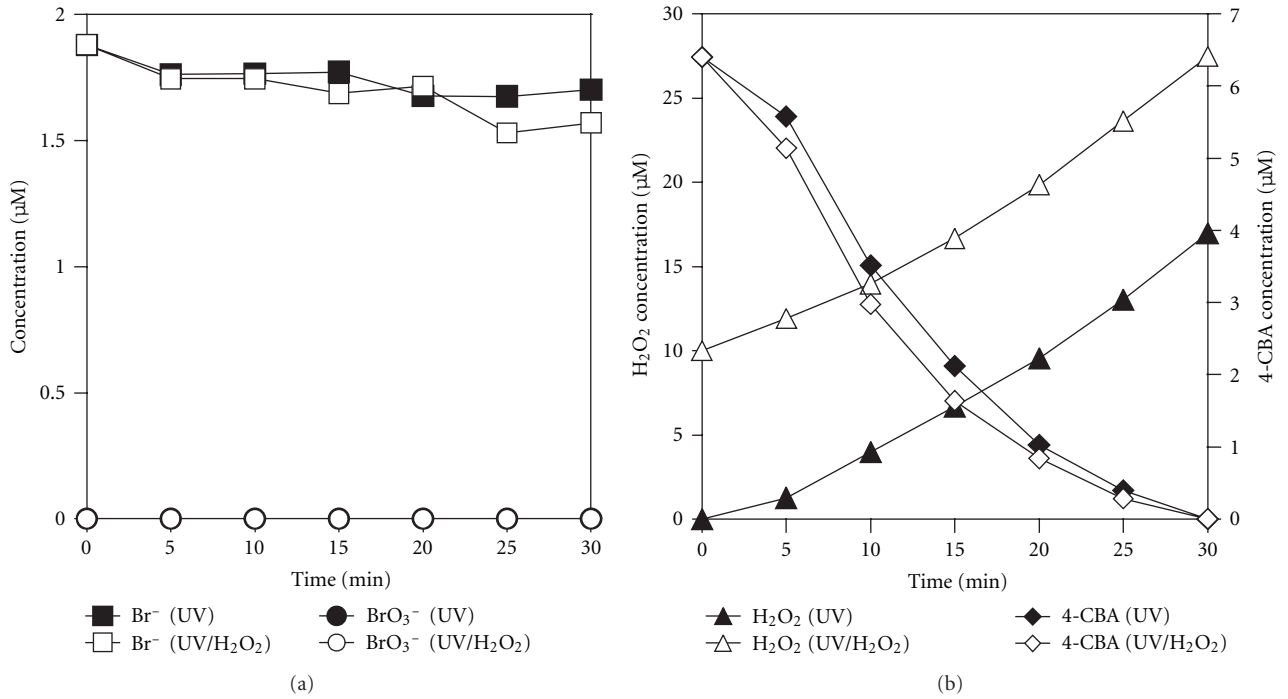

Figure 2: Changes in concentrations of Br^-, BrO_3^-, H_2O_2, and 4-CBA during UV irradiation (UV) and UV/H_2O_2 treatment at neutral pH. The initial H_2O_2 concentration for UV/H_2O_2 was 10 μM.

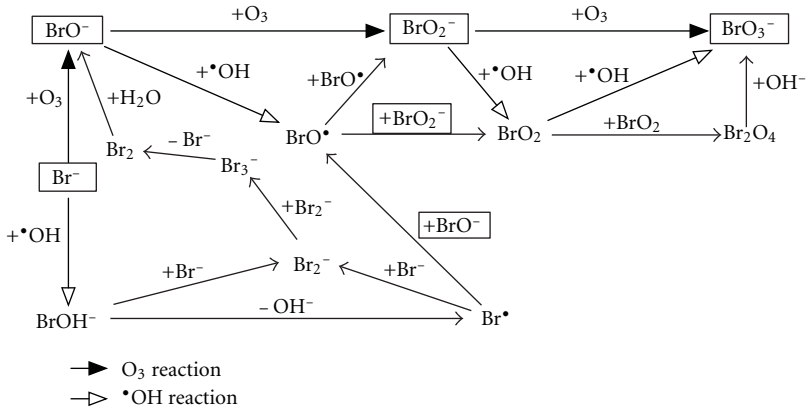

Figure 3: BrO_3^- formation pathways illustrated on the basis of Von Gunten and Oliveras [8].

acidification decreases the percentage of BrO^-. The decrease in BrO^- at acidic pH also contributed to the decrease in BrO_3^- formation [33]. In addition, the discordance of a decrement in Br^- and an increment in BrO_3^- at acidic pH in Figure 4 suggested the accumulation of HOBr.

3.3. O_3/H_2O_2. Figure 5 shows the changes in concentrations of Br^-, BrO_3^-, and 4-CBA during O_3/H_2O_2 at various H_2O_2 doses and pHs. The O_3/H_2O_2 processes showed additional effect on lowering BrO_3^- formation, especially at higher H_2O_2 dose. Bromate ion was not detected in O_3/H_2O_2 at the H_2O_2 dose of 1,000 μM. When the H_2O_2 dose was lowered to 100 or 10 μM, rapid BrO_3^- formation was observed (Figure 5). As H_2O_2 can reduce HOBr/BrO^- into Br^-, the excess H_2O_2 was believed to restrain BrO_3^- formation. The behavior of BrO_3^- formation in O_3/H_2O_2 at the H_2O_2 dose of 10 μM (Figure 5) was similar to that in ozonation (Figure 4), since H_2O_2 concentration in ozonation increased to around 10 μM, which was nearly equal to H_2O_2 concentration in O_3/H_2O_2 at the H_2O_2 dose of 10 μM (Figure 6). Thus, the initial H_2O_2 dose of 10 μM was too low to restrain the BrO_3^- formation in this study.

When acidification was applied, BrO_3^- was not detected in O_3/H_2O_2 at the H_2O_2 dose of 100 μM or higher. This effect was caused by both the HOBr/BrO^- reduction by H_2O_2

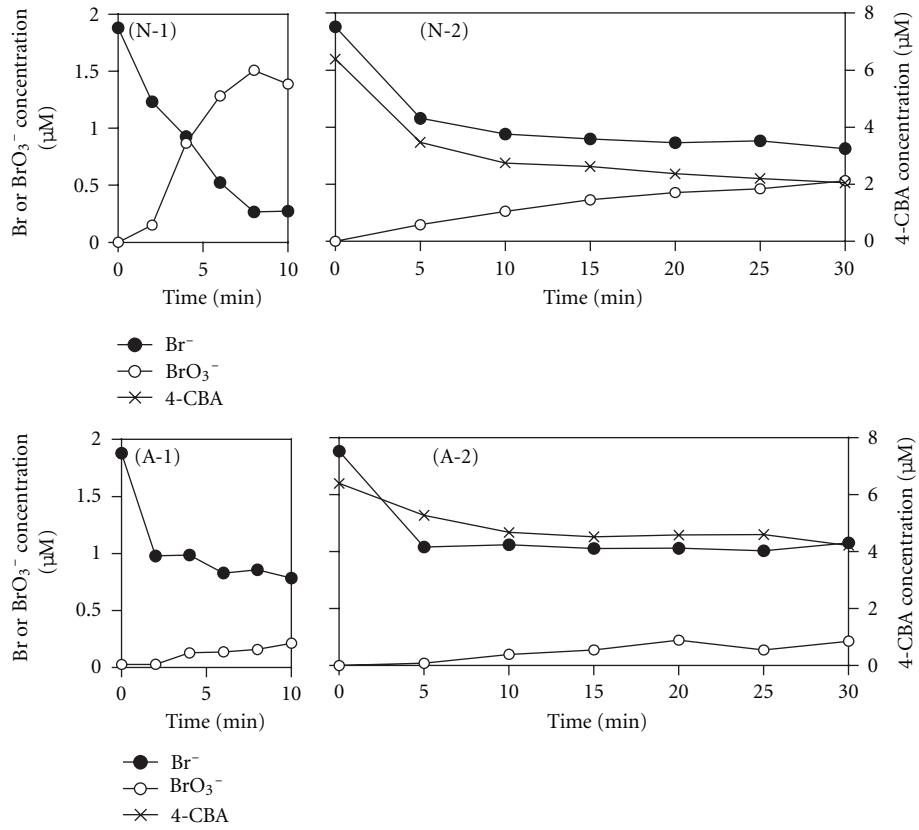

Figure 4: Changes in concentrations of Br^-, BrO_3^-, and 4-CBA during ozonation at neutral pH without 4-CBA (N-1), ozonation at neutral pH with 4-CBA (N-2), ozonation at acidic pH without 4-CBA (A-1), and ozonation at acidic pH with 4-CBA (A-2).

and inhibition of $^\bullet OH$ generation in O_3/H_2O_2. Because $^\bullet OH$ generation in O_3/H_2O_2 is expressed by the following reactions [16] and the acidification inhibits the dissociation of H_2O_2 and HO_2 (reactions (3) and (5)) as follows:

$$H_2O_2 \longleftrightarrow H^+ + HO_2^- \quad (3)$$

$$O_3 + HO_2^- \longrightarrow {}^\bullet O_3^- + HO_2^\bullet \quad (4)$$

$$HO_2^\bullet \longleftrightarrow H^+ + {}^\bullet O_2^- \quad (5)$$

$$O_3 + {}^\bullet O_2^- \longrightarrow {}^\bullet O_3^- + O_2 \quad (6)$$

$$^\bullet O_3^- + H^+ \longleftrightarrow HO_3 \rightarrow O_2 + {}^\bullet OH \quad (7)$$

The inhibition of $^\bullet OH$ generation in O_3/H_2O_2 was also confirmed by a slow decrease in 4-CBA at acidic pH (Figure 5).

3.4. O_3/UV. Figure 7 shows changes in Br^-, BrO_3^-, and 4-CBA concentrations during O_3/UV. The O_3/UV increased BrO_3^- concentration rapidly, even at the acidic pH. However, the addition of 4-CBA successfully decreased the BrO_3^- formation regardless of the pH condition. Collivignarelli and Sorlini [19] also observed lower BrO_3^- formation in O_3/UV than that in ozonation. As mentioned in the Section 3.2, the acidification decreases BrO_3^- formation by the inhibition of $^\bullet OH$ generation via the self-decomposition of ozone. Accordingly, it was thought that $^\bullet OH$ generated by the self-decomposition of ozone did not contribute to BrO_3^- formation very much in O_3/UV. This discussion was supported by the lower concentration of dissolved ozone in O_3/UV (Figure 8). The low dissolved ozone concentration also brought the negligible contribution of molecular ozone to BrO_3^- formation. The decrease in BrO_3^- formation by the addition of 4-CBA indicated the contribution of $^\bullet OH$ to BrO_3^- formation. Accordingly, it is suggested that the main oxidant in O_3/UV was $^\bullet OH$, which mainly generated via UV photolysis of ozone [16]. The first step of $^\bullet OH$ generation in O_3/UV is the production of H_2O_2 [16]. Then the H_2O_2 generates $^\bullet OH$ through UV photolysis [16] and the same reactions as O_3/H_2O_2 (reactions (3)–(7)). As the coexistence of dissolved ozone and $^\bullet OH$ favors BrO_3^- formation [13, 17], low dissolved ozone concentration in O_3/UV was thought to be advantageous to the depression of BrO_3^- formation. Moreover, strong H_2O_2 accumulation was observed during O_3/UV (Figure 9). Therefore, the reduction of intermediates by H_2O_2 [15] and UV photolysis [30] was also inferred to contribute to the decline in the BrO_3^- formation potential.

3.5. Strategy for Organic Contaminants Removal with Preventing BrO_3^- Formation. The aim of advanced oxidation processes is organic contaminants removal from a water stream. Therefore, it is important to remove organic contaminants without BrO_3^- formation. In this context, H_2O_2 addition

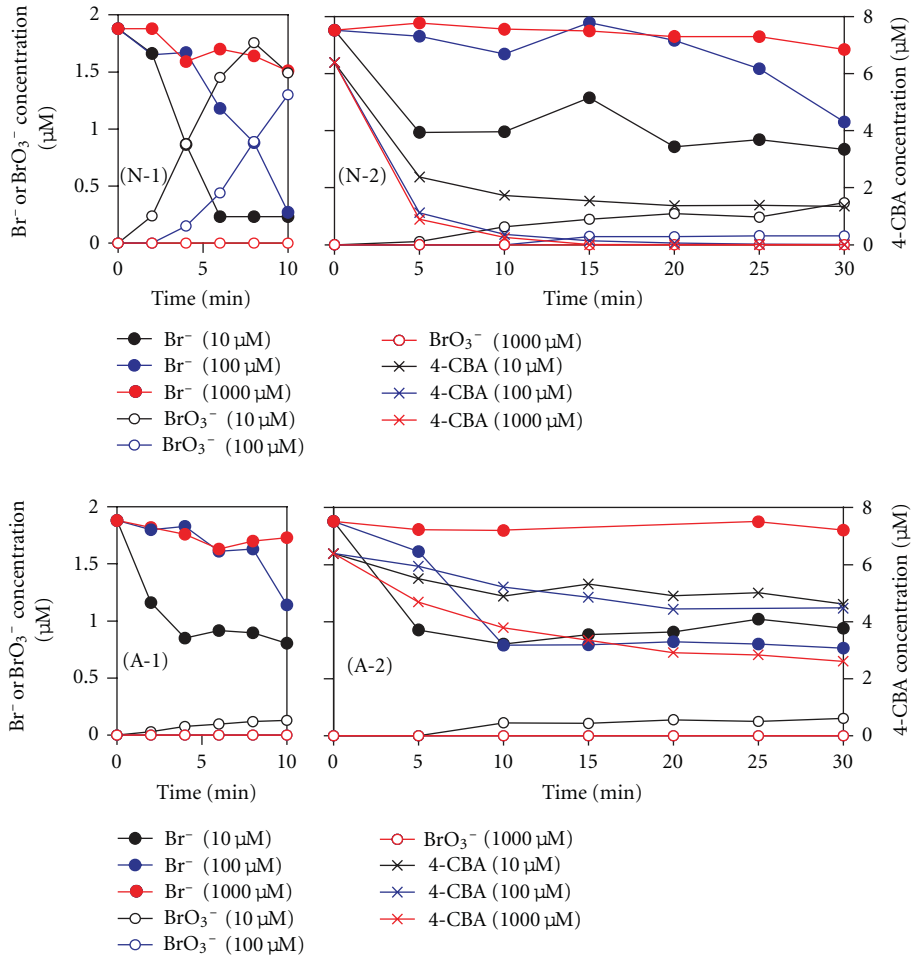

Figure 5: Changes in concentrations of Br^-, BrO_3^-, and 4-CBA during O_3/H_2O_2 at various H_2O_2 doses. The concentrations in the legend mean the H_2O_2 dose. The symbols in the bracket mean O_3/H_2O_2 at neutral pH without 4-CBA (N-1), O_3/H_2O_2 at neutral pH with 4-CBA (N-2), O_3/H_2O_2 at acidic pH without 4-CBA (A-1), and O_3/H_2O_2 at acidic pH with 4-CBA (A-2).

is inapplicable to advanced water treatment, because it is not effective to degrade refractory organic matters like 4-CBA. Ozonation is also difficult to apply to the organic contaminants removal, because it has higher BrO_3^- formation potential at the neutral pH than at the acidic pH as shown in Figure 4. Although the acidification successfully decreases the BrO_3^- formation potential of ozonation, it decreases the removal rate of organic contaminants too.

Contrary to H_2O_2 addition and ozonation, UV-based processes and O_3/H_2O_2 are potentially applicable to advanced water treatment with inhibiting BrO_3^- formation. The UV irradiation and UV/H_2O_2 successfully decompose organic contaminants without BrO_3^- formation. But their degradation rate of organic contaminants is not high, and H_2O_2 dose of 10 μM is too low to enhance the degradation rate of UV irradiation. The O_3/H_2O_2 is characterized by rapid degradation of organic contaminants and low BrO_3^- formation rate at high H_2O_2 dose. Although the acidification effectuates further decrease in BrO_3^- formation, it spoils the degradation of organic contaminants. Therefore, the acidification should not apply to O_3/H_2O_2. The feature of O_3/UV is rapid degradation of organic contaminants, low dissolved ozone concentration, and much H_2O_2 accumulation. As the BrO_3^- formation in O_3/UV is restrained under the coexistence of organic contaminants, the O_3/UV is applicable, if water contains sufficient quantity of organic contaminants. Figure 10 shows the relationship between BrO_3^- concentration and cumulative ozone consumption. Figure 10 demonstrates that O_3/UV and O_3/H_2O_2 at the H_2O_2 doses of 100 and 1,000 μM were significantly decreased BrO_3^- formation per ozone consumption in comparison with ozonation and O_3/H_2O_2 at the H_2O_2 dose of 10 μM. Kim et al. [17] reported that BrO_3^- concentration in O_3/H_2O_2 remained less than 10 μg/L, when the molar ratio of H_2O_2 to ozone was above 0.5. In our study of O_3/H_2O_2 at the H_2O_2 dose of 100 μM, BrO_3^- was not produced at ozone consumption less than 250 μM. Thus, our result approximately accorded with the research by Kim et al. [17].

Consequently, if the concentration of organic contaminants is low, the UV irradiation and/or UV/H_2O_2 are applicable to organic contaminants removal without BrO_3^- formation, though it is necessary to beware nitrite formation

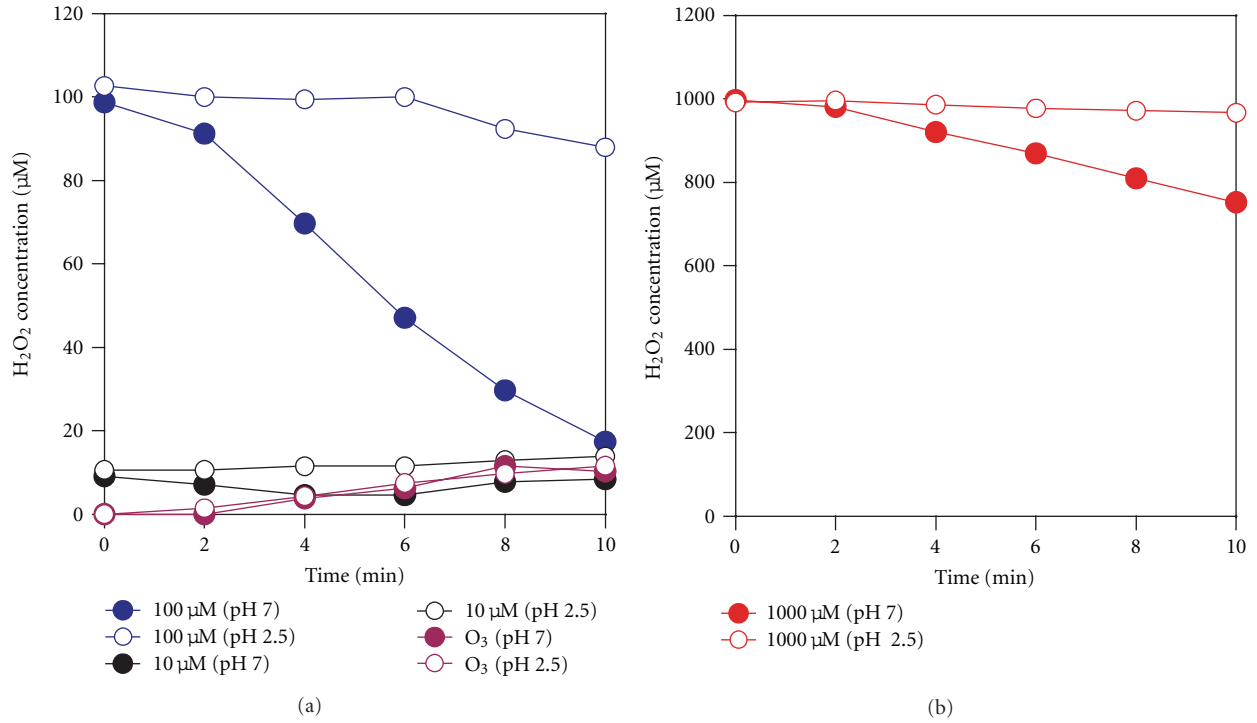

FIGURE 6: Changes in H_2O_2 concentrations during O_3/H_2O_2 and ozonation without 4-CBA. The concentrations in the legend mean the H_2O_2 dose in O_3/H_2O_2.

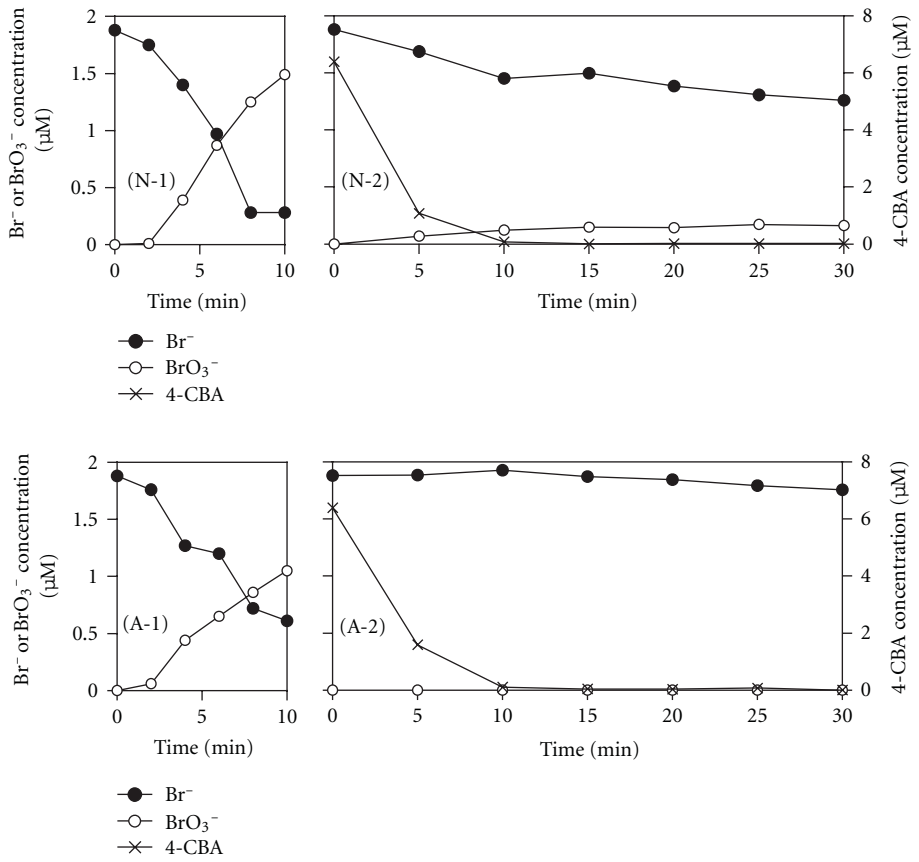

FIGURE 7: Changes in concentrations of Br^-, BrO_3^-, and 4-CBA during O_3/UV at neutral pH without 4-CBA (N-1), O_3/UV at neutral pH with 4-CBA (N-2), O_3/UV at acidic pH without 4-CBA (A-1), and O_3/UV at acidic pH with 4-CBA (A-2).

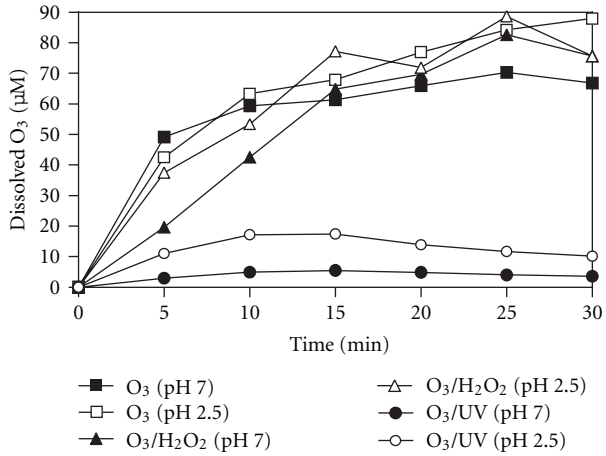

Figure 8: Changes in dissolved ozone concentrations during ozonation, O_3/H_2O_2 (the H_2O_2 dose of 100 μM), and O_3/UV with the addition of 4-CBA.

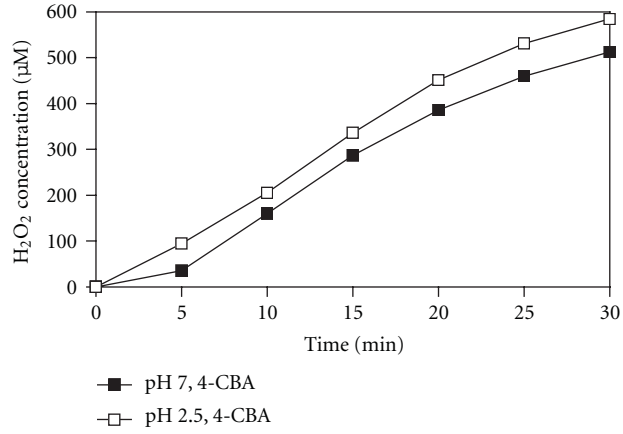

Figure 9: Changes in H_2O_2 concentrations during O_3/UV with 4-CBA.

during the treatment [34]. However, if the concentration of organic contaminants is high, O_3/H_2O_2 and O_3/UV should be discussed as advanced oxidation processes. When O_3/H_2O_2 is applied, the H_2O_2 dose should be more than the half of ozone consumption, because low H_2O_2 dose is ineffective for BrO_3^- control. When O_3/UV is applied, the reaction time should be optimized, because extended reaction time increases the BrO_3^- formation potential. The real-time monitoring of UV absorbance of organic contaminants in water [35] may be effective in the optimum control of the reaction time of O_3/UV without BrO_3^- formation.

4. Conclusion

In this research, BrO_3^- formation potential of UV irradiation, H_2O_2 addition, ozonation, UV/H_2O_2, O_3/H_2O_2, and O_3/UV treatment were discussed for organic contaminants

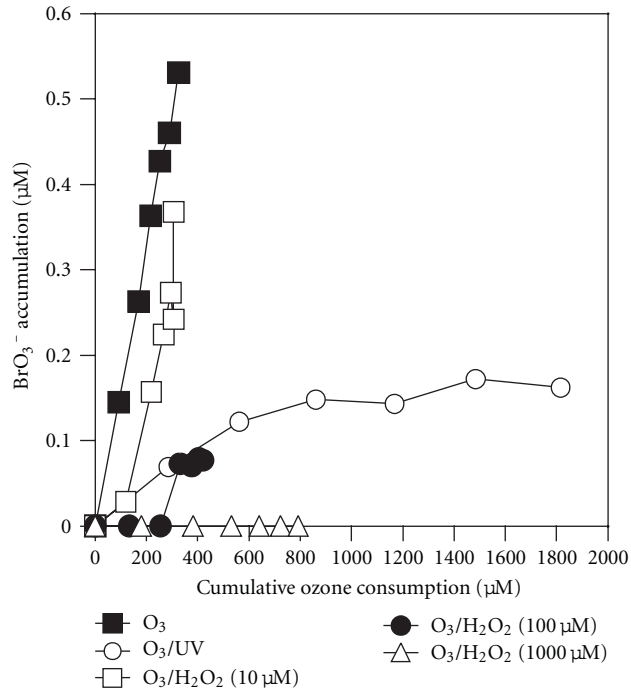

Figure 10: Relationship between cumulative ozone consumption and BrO_3^- accumulation during each treatment with 4-CBA addition at neutral pH. Each treatment continued 30 minutes.

removal with restraining BrO_3^- formation using KBr solution with 4-CBA as a model refractory organic contaminant.

The UV irradiation, H_2O_2 addition, and UV/H_2O_2 prevented BrO_3^- formation completely. However, H_2O_2 addition was inapplicable as advanced water treatment because of its weak oxidation ability. The UV irradiation and UV/H_2O_2 could decompose the organic contaminant moderately. Ozonation produced the most BrO_3^- at neutral pH. Although acidification could decrease the BrO_3^- formation, it also deteriorated the oxidation ability of ozonation. Therefore, it was thought to be difficult to apply ozonation to organic contaminants removal with restraining BrO_3^- formation. The O_3/H_2O_2 successfully decreased BrO_3^- formation at the H_2O_2 doses of 100 μM or higher. The degradation rate of 4-CBA was larger than the UV irradiation and UV/H_2O_2. However, the behavior of BrO_3^- formation in the O_3/H_2O_2 at the H_2O_2 dose of 10 μM was similar to that in ozonation because of a deficiency of H_2O_2. The O_3/UV also showed rapid degradation of 4-CBA. Although it produced much BrO_3^- under the absence of 4-CBA, the BrO_3^- formation was strongly inhibited by the coexistence of 4-CBA. Consequently, if the concentration of organic contaminants is low, the UV irradiation and/or UV/H_2O_2 are applicable to organic contaminants removal without BrO_3^- formation. However, if the concentration of organic contaminants is high, O_3/H_2O_2 and O_3/UV should be discussed as advanced oxidation processes because of their higher organic removal efficiency.

References

[1] C. Wu, C. Maurer, Y. Wang, S. Xue, and D. L. Davis, "Water pollution and human health in China," *Environmental Health Perspectives*, vol. 107, no. 4, pp. 251–256, 1999.

[2] A. Gadgil, "Drinking water in developing countries," *Annual Review of Energy and the Environment*, vol. 23, no. 1, pp. 253–286, 1998.

[3] O. A. Jones, J. N. Lester, and N. Voulvoulis, "Pharmaceuticals: a threat to drinking water?" *Trends in Biotechnology*, vol. 23, no. 4, pp. 163–167, 2005.

[4] R. Takanami, H. Ozaki, R. R. Giri, S. Taniguchi, and S. Hayashi, "Antiviral drugs zanamivir and oseltamivir found in wastewater and surface water in Osaka, Japan," *Journal of Water and Environment Technology*, vol. 10, pp. 57–68, 2012.

[5] D. Dotson, C. E. Rodoriquez, and K. G. Linden, "UV disinfection implementation status in US water treatment plants," *Journal AWWA*, vol. 104, pp. 77–78, 2012.

[6] B. L. Loeb, C. M. Thompson, J. Drago, H. Takahara, and S. Baig, "Worldwide ozone capacity for treatment of drinking water and wastewater: a review," *Ozone: Science & Engineering*, vol. 34, pp. 64–77, 2012.

[7] I. Ali and V. K. Gupta, "Advances in water treatment by adsorption technology," *Nature Protocols*, vol. 1, no. 6, pp. 2661–2667, 2007.

[8] U. Von Gunten and Y. Oliveras, "Advanced oxidation of bromide-containig waters: bromate formation mechanisms," *Environmental Science and Technology*, vol. 32, no. 1, pp. 63–70, 1998.

[9] D. Gerrity and S. Snyder, "Review of ozone for water reuse applications: toxicity, regulations, and trace organic contaminant oxidation," *Ozone: Science and Engineering*, vol. 33, no. 4, pp. 253–266, 2011.

[10] B. A. Wols and C. H. M. Hofman-Caris, "Review of photochemical reaction constants of organic micropollutants required for UV advanced oxidation processes in water," *Water Research*, vol. 46, pp. 2815–2827, 2012.

[11] *IARC Monographs on the Evaluation of Carcinogenic Risks to Humans*, vol. 73, International Agency for Research on Cancer, Lyon, France, 1999.

[12] M. S. Siddiqui and G. L. Amy, "Factors affecting DBP formation during ozone-bromide reactions," *Journal of American Water Works Association*, vol. 85, no. 1, pp. 63–72, 1993.

[13] K. Ozekin, P. Westerhoff, G. L. Amy, and M. Siddiqui, "Molecular ozone and radical pathways of bromate formation during ozonation," *Journal of Environmental Engineering*, vol. 124, no. 5, pp. 456–462, 1998.

[14] U. Pinkernell and U. von Gunten, "Bromate minimization during ozonation: mechanistic considerations," *Environmental Science and Technology*, vol. 35, no. 12, pp. 2525–2531, 2001.

[15] U. Von Gunten and Y. Oliveras, "Kinetics of the reaction between hydrogen peroxide and hypobromous acid: implication on water treatment and natural systems," *Water Research*, vol. 31, no. 4, pp. 900–906, 1997.

[16] W. H. Glaze, J. Kang, and D. H. Chapin, "The chemistry of water treatment processes involving ozone, hydrogen peroxide and ultraviolet radiation," *Ozone: Science & Engineering*, vol. 9, pp. 335–352, 1987.

[17] H. S. Kim, H. Yamada, and H. Tsuno, "The control of brominated by-products and the removal of organic pollutants during the ozone/hydrogen peroxide treatment of secondary effluent," *Ozone: Science and Engineering*, vol. 29, no. 1, pp. 23–30, 2007.

[18] M. S. Siddiqui, G. L. Amy, and L. J. McCollum, "Bromate destruction by UV irradiation and electric arc discharge," *Ozone: Science and Engineering*, vol. 18, no. 3, pp. 271–290, 1996.

[19] C. Collivignarelli and S. Sorlini, "AOPs with ozone and UV radiation in drinking water: contaminants removal and effects on disinfection byproducts formation," *Water Science and Technology*, vol. 49, no. 4, pp. 51–56, 2004.

[20] T. Ratpukdi, F. Casey, T. Desutter, and E. Khan, "Bromate formation by ozone-VUV in comparison with ozone and ozone-UV: effects of pH, ozone dose, and VUV power," *Journal of Environmental Engineering*, vol. 137, no. 3, pp. 187–195, 2011.

[21] N. Kishimoto, Y. Morita, H. Tsuno, T. Oomura, and H. Mizutani, "Advanced oxidation effect of ozonation combined with electrolysis," *Water Research*, vol. 39, no. 19, pp. 4661–4672, 2005.

[22] N. Kishimoto, A. Kishimoto, and A. Nakayama, "Rapid removal of bromate ion from water streams with an electrolytic flow cell," *Journal of Water Supply: Research and Technology-AQUA*, vol. 61, pp. 103–110, 2012.

[23] *Standard Methods for the Examination of Water & Wastewater*, American Public Health Association, Washington, DC, USA, 22nd edition, 2012.

[24] A. N. Baga, G. R. A. Johnson, N. B. Nazhat, and R. A. Saadalla-Nazhat, "A simple spectrophotometric determination of hydrogen peroxide at low concentrations in aqueous solution," *Analytica Chimica Acta*, vol. 204, pp. 349–353, 1988.

[25] J. P. Hoare, "4. Oxygen," in *Standard Potentials in Aqueous Solution*, A. J. Bard, R. Parsons, and J. Jordan, Eds., pp. 49–66, Mercel Dekker, New York, NY, USA, 1985.

[26] D. D. Dionysiou, M. T. Suidan, E. Bekou, I. Baudin, and J. M. Laîné, "Effect of ionic strength and hydrogen peroxide on the photocatalytic degradation of 4-chlorobenzoic acid in water," *Applied Catalysis B*, vol. 26, no. 3, pp. 153–171, 2000.

[27] N. Kishimoto, I. Somiya, and Y. Morita, "Dependence of hydroxyl radical production in UV/H_2O_2 photo-oxidation on UV energy absorbed by aqueous solution," *Advances in Asian Environmental Engineering*, vol. 2, no. 2, pp. 8–17, 2002.

[28] J. Staehelin, R. E. Bühler, and J. Hoigné, "Ozone decomposition in water studied by pulse radiolysis. OH and HO_4 as chain intermediates," *Journal of Physical Chemistry*, vol. 88, no. 24, pp. 5999–6004, 1984.

[29] J. C. Kruithof, P. C. Kamp, and M. Belosevic, "UV/H_2O_2-treatment: the ultimate solution for pesticide control and disinfection," *Water Science and Technology: Water Supply*, vol. 2, no. 1, pp. 113–122, 2002.

[30] N. H. Phillip, E. Gürten, and V. Diyamandoğlu, "Transformation of bromine species during decomposition of bromate under UV light from low pressure mercury vapor lamps," *Ozone: Science and Engineering*, vol. 28, no. 4, pp. 217–228, 2006.

[31] M. S. Elovitz, U. Von Gunten, and H. P. Kaiser, "Hydroxyl radical/ozone ratios during ozonation processes. II. The effect of temperature, pH, alkalinity, and DOM properties," *Ozone: Science and Engineering*, vol. 22, no. 2, pp. 123–150, 2000.

[32] W. R. Haag and J. Holgné, "Ozonation of bromide-containing waters: kinetics of formation of hypobromous acid and bromate," *Environmental Science and Technology*, vol. 17, no. 5, pp. 261–267, 1983.

[33] L. Xie and C. Shang, "A review on bromate occurrence and removal strategies in water supply," *Water Science and Technology: Water Supply*, vol. 6, no. 6, pp. 131–136, 2006.

[34] A. J. Martijn and J. C. Kruithof, "UV and UV/H_2O_2 treatment: the silver bullet for by-product and genotoxicity formation in water production," *Ozone: Science & Engineering*, vol. 34, pp. 92–100, 2012.

[35] R. A. Dobbs, R. H. Wise, and R. B. Dean, "The use of ultra-violet absorbance for monitoring the total organic carbon content of water and wastewater," *Water Research*, vol. 6, no. 10, pp. 1173–1180, 1972.

Hindawi Publishing Corporation
International Journal of Photoenergy
Volume 2012, Article ID 520123, 10 pages
doi:10.1155/2012/520123

Research Article

Simultaneous Photocatalytic Reduction of Cr(VI) and Oxidation of Benzoic Acid in Aqueous N-F-Codoped TiO_2 Suspensions: Optimization and Modeling Using the Response Surface Methodology

Maria Antonopoulou, Aris Giannakas, and Ioannis Konstantinou

Department of Environmental and Natural Resources Management, University of Western Greece, 30100 Agrinio, Greece

Correspondence should be addressed to Ioannis Konstantinou, iokonst@cc.uoi.gr

Received 1 June 2012; Accepted 29 July 2012

Academic Editor: Manickavachagam Muruganandham

The simultaneous photocatalytic reduction of Cr(VI) and oxidation of benzoic acid (BA) in aqueous suspensions using N-F-codoped TiO_2 and simulated solar irradiation were investigated in the present study. Chemometric optimization tools such as response surface methodology (RSM) and experimental design were used to model and optimize selected operational parameters of the simultaneous photocatalytic reduction of Cr(VI) and oxidation of BA. RSM was developed by considering a central composite design with three input variables, that are, N-F-codoped TiO_2 mass, ratio of Cr/BA, and pH. The removal of Cr(VI) and BA in binary systems, containing both Cr(VI) and BA, showed a synergistic photocatalytic decontamination as BA significantly facilitated Cr(VI) reduction, whereas Cr(VI) accelerated also BA degradation. Due to the anionic-type adsorption onto TiO_2 and its acid-catalyzed photocatalytic reduction, the removal of Cr(VI) decreased with increasing pH, while the degradation of BA followed also the same trend. Under the optimum conditions (N-F-TiO_2) = 600 mg L^{-1}, ratio of Cr(VI)/BA = 5, pH = 4, the removal for both Cr and BA followed a pseudo first-order kinetic model. It was found that the selected variables have significant effect both on Cr(VI) removal and BA degradation efficiency. The results revealed the feasibility and the effectiveness of using N-F-codoped TiO_2 as photocatalyst for simultaneous decontamination of Cr(VI) and organic pollutants such as BA due to the appropriate oxidation and reduction ability of the photogenerated h^+_{VB}-e^-_{CB} pairs.

1. Introduction

The increasing level of global industrialization and urbanization has led to the transport and introduction of various contaminants in aquatic environment. The water pollution caused by organic pollutants and heavy metal ions represents an important ecological and health hazard and had gradually gained great scientific interest. Heavy metals enter aquatic environment through the discharge of treated or untreated industrial wastewater and municipal sewage, storm water runoff, acid mine drainage, and other diffuse sources [1]. On the other hand, a wide range of organic micropollutants are derived from a variety of agricultural, municipal, and industrial sources and pathways [2, 3]. Although, the co-existence of organic compounds and metal ions in wastewater is common [4], in conventional methods it is often indispensable to be treated separately, that means complicated process with the requirement of higher cost and more man power [5]. Hence, simultaneous decontamination of heavy metals and organic contaminants constitutes a very interesting and important aspect. In last decades, water pollution had resulted in the development of the so-called advanced oxidation processes (AOPs) as alternative to the conventional water and wastewater treatment methods. These enhanced processes aim to degrade the non biodegradable contaminants of water into harmless species [6]. Among AOPs, heterogeneous photocatalysis employing semiconductor solids has been applied with success for

the oxidation of a variety of organic compounds [7] as well as for the removal/reduction of toxic metals from aqueous solutions [8–10]. Photocatalysis is a well-known and particularly promising method based on the activation of a semiconductor and utilizes the photogenerated positive holes and various oxygen radical species for the oxidation of organic compounds as well as the photogenerated electrons for the reduction of heavy metal ions [11]. Moreover, photoreduction of a metal ion is promoted significantly if it is accompanied by simultaneous oxidation of an organic compound able to act as ligand or as "sacrificial electron donor" [12], because of the enhanced charge separation of photo-induced hole/electron pairs by the simultaneous reduction/oxidation reactions [11].

The application of experimental design methodologies in the development of photocatalytic processes can result in improved remediation efficiency with the lesser number of experiments. Response surface methodology is a powerful and widely used mathematical method suitable for modeling and optimizing chemical reactions and or industrial processes [13].

In the present study, the simultaneous photocatalytic reduction of Cr(VI) and oxidation of benzoic acid (BA) using N-F-codoped TiO_2 under simulated solar irradiation was studied. Cr(VI) and BA were selected as target compounds since they may be present in a great variety of industrial waste effluents and their simultaneous treatment will show both economical and technological profits. Benzoic acid, the simplest aromatic carboxylic acid, is a model compound representative of the aromatic content typically found in various industrial wastewaters. It also constitutes the parent molecule of various phenolic compounds which are usually low biodegradable and high ecotoxic and are commonly found in agro-industrial effluents [14]. BA is used to produce a broad range of organic chemicals [15]. Furthermore, it has a wide usage as preservative in the cosmetic, drug, and food industry because of its antibacterial and antifungal properties at a pH 4 or lower [16]. Among heavy metals, Cr(VI) is one of the most frequent and toxic contaminants in wastewaters arising from various industrial processes such as electroplating, pigment production, leather tanning, textile dying, wood preservation, as well as finishing of metals and plastics [17, 18]. Due to its carcinogenic and mutagenic properties as well as its high mobility, its concentration in drinking water has been regulated in many countries [17]. It is considered to be highly toxic to most of the living organisms when the Cr(VI) concentration level is higher than $0.05\,\text{mg}\,\text{L}^{-1}$ [19]. As a result, the removal of Cr(VI) or its reduction to less harmful and immobile Cr(III) is of great importance. Several studies have reported the simultaneous decontamination of Cr(VI) and organic contaminants such as carboxylic acids, phenols, phthalates, and dyes [11, 20–25]. However, in the above-mentioned researches commercial forms of TiO_2 (anatase, Degussa P25) were used. On the contrary, this study investigates the application of N-F-codoped TiO_2, a photocatalyst with improved photo efficiency and visible light response compared to TiO_2 catalysts [26], for the simultaneous decontamination of organic pollutants and heavy metals. In addition, the assessment of the beneficial role of N-F-doping for the synergistic removal of Cr(VI) and organic pollutants in aqueous substrates has not been performed so far. The main objectives of this research were (a) to assess the simultaneous removal of an organic micropollutant, benzoic acid, and a toxic heavy metal Cr(VI); (b) to investigate the effect of three parameters (initial ratio Cr/Benzoic acid concentration, pH, catalyst concentration) on the total process efficiency; (c) to model and optimize the photocatalytic procedure by means of a central composite design and response surface methodology.

2. Experimental

2.1. Materials and Reagents. Benzoic acid was residue analysis grade, purchased from Sigma-Aldrich (USA), and Cr(VI) in the form of potassium dichromate was purchased from Fluka and used without further purification. N-F-TiO_2 (Ti : N,F molar ratio 1 : 1, named as TNF) was prepared based on a simple sol-gel impregnation method [26]. Titanium n-butoxide [$Ti(OC_4H_9)_4$] was used as inorganic precursor and ammonium fluoride (NH_4F) as the source of N and F dopant atoms. X-ray diffraction analysis showed that the photocatalyst crystal phase is anatase with a crystallite size of ≈ 1.8 Å. A band-gap energy of 2.96 eV was determined using diffuse reflectance UV-Vis spectroscopy, while electron pair resonance revealed the presence of $N_b^{\bullet}$ and Ti^{+3} photoactive centers. The point-of-zero charge (PZC) was determined at pH = 5.7 using the mass titration method [27]. All solvents used (acetonitrile, methanol and LC-grade water) were pesticide residue analysis grade from Merck (Darmstadt, Germany). HVLP 0.45 μm filters were supplied by Millipore (Bedford, USA). Ultrapure water was obtained from a Millipore Waters Milli-Q water purification system.

2.2. Irradiation Procedure. Photocatalytic experiments were carried out in a Suntest XLS+ solar simulator (Atlas, Germany) equipped with a vapor xenon lamp (2.2 kW). The light source was jacked with special glass filters restricting the transmission of wavelengths below 290 nm. The temperature of the samples was maintained at 25°C using a tap water cooling circuit preventing any heating of the suspension. The irradiation intensity was measured by internal radiometer supplied by the manufacturer. Irradiation experiments were performed using a 250 mL Pyrex glass UV-reactor containing 250 mL of aqueous solutions at different pH. The pH of solutions was adjusted by H_2SO_4 or NaOH aqueous solutions. The solutions were mixed with the appropriate amount of catalyst and were magnetically stirred before and during the illumination. The suspensions were kept in the dark for 30 minutes, prior to illumination in order to reach adsorption equilibrium onto semiconductor surface. As the reaction progressed, aliquots of 5 ml were withdrawn from the reactor at specific time intervals for further analysis. In order to remove the N-F-TiO_2 particles the solution samples were filtered through a 0.45 μm filter. Performance of the process was evaluated by analyzing the responses of Cr(VI)

removal and BA degradation percentages after a fixed time of 30 min according to the equation:

$$Y_1(\%) = \left[\frac{(C_0 - C_t)}{C_0}\right] * 100, \quad (1)$$

where C_0 is the initial Cr(VI) or BA concentration and C_t the concentration of Cr(VI) or BA after the photocatalytic treatment.

2.3. Kinetic Studies: Determination of Benzoic Acid and Cr(VI). Benzoic acid concentrations were determined by a Dionex P680 HPLC equipped with a Dionex PDA-100 Photodiode Array Detector using a Discovery C_{18}, (250 mm length × 4.6 mm ID: 5 μm particle size) analytical column from Supelco (Bellefonte, PA, USA). The mobile phase was a mixture of LC-grade water H_2O (70%) at pH 3 (adjusted with formic acid) and acetonitrile (30%) with a flow rate of 1 ml/min. Column temperature was set at 40°C. The detection of BA was realized at 228 nm. The concentration of Cr(VI) was determined by the diphenylcarbazide colorimetric method [11] at a wavelength of 540 nm using a UV-Vis spectrophotometer (Hitachi, U-2000).

2.4. Experimental Design: Data Analysis. A central composite design was employed for the optimization of photocatalytic process in the present study. In order to evaluate the influence of operating parameters on the simultaneous photocatalytic efficiency of BA and Cr(VI), three main factors were chosen: catalyst concentration (mg L^{-1}) (x_1), Cr(VI)/BA ratio (x_2), and pH (x_3). A total number of 17 experiments were determined by the expression: $2^n + 2n + 3 = 2^3$ (8 factor points) +2∗3 (6 axial points) +3 central points, replications) = 17, as shown in Table 1. The three selected experimental parameters were optimized using RSM considering them as independent variables and % Cr(VI) removal and % BA degradation as response variables. The data set obtained from CCD was used for the optimization of the responses and RSM was used to fit the experimental data. A second order model was used to locate the optimum point and can be expressed as follows:

$$Y = \beta_0 + \sum_{i=1}^{k}\beta_i x_i + \sum_{i=1}^{k}\beta_{ii} x_i^2 + \sum_{1\le i\le j}^{k}\beta_{ij} x_i x_j + \varepsilon, \quad (2)$$

where Y is the response variable of degradation efficiency, β_0 is the constant term, β_i represents the coefficients of the linear parameters, x_i represents the variables, β_{ii} represents the coefficients of the quadratic parameters, β_{ij} represents the coefficients of the interaction parameters and ε is the random error [13]. Experimental data were analyzed using Design Expert V. 7.1.5 (Stat-Ease Inc. 2008, Mn, USA). Data were further estimated and evaluated by the analysis of variance (ANOVA). Correlation coefficients (R^2, R^2 *adj.*) were used to evaluate the correlation between the experimental data and the predicted responses and thereby the goodness of the fit for the polynomial models. The statistical significance was also checked by the F value (Fisher variation ratio), probability P value and adequate precision in the same program. The significance of each model term was evaluated based on P value with 95% confidence level ($P > 0.05$). Finally, three-dimensional response surface plots were developed in order to visualize the individual and the interaction effects of the independent variables on degradation efficiency.

Table 1: Central composite design matrix and experimental results for benzoic acid (BA) and Cr(VI) photocatalytic degradation.

Exper. no.	C_{TiO2}-x_1 (mg L^{-1})	Cr/BA ratio-x_2	pH-x_3	(%) removal Cr(VI)	(%) degradation BA
1	200	5	10	32.36	2.5
2	600	15	4	55.22	49.47
3	400	1.59	7	100	17.5
4	400	18.41	7	36.41	32.78
5	600	5	10	54.95	5.1
6	600	5	4	100	36.61
7	400	10	1.95	58.9	47.84
8	400	10	7	45.96	9.49
9	200	5	4	76.16	23.07
10	200	15	10	4.58	6.56
11	400	10	12.05	4.85	2.79
12	200	15	4	24.06	30.34
13	400	10	7	45.57	8.18
14	63.64	10	7	18.85	2.7
15	736.36	10	7	65.82	17.24
16	400	10	7	47.44	8.66
17	600	15	10	32.92	12.08

3. Results and Discussion

3.1. Preliminary Experiments. Preliminary experiments were carried out, before the development of the experimental design, in order to evaluate the possible synergistic effect of the simultaneous photooxidation-photoreduction of the selected pollutants, Cr(VI) and BA. For this reason, experiments were conducted in single and binary systems at pH = 2, catalyst concentration 500 mg L^{-1} and UV intensity 750 W m^{-2}. The initial concentrations used were 0.1 mM Cr(VI) and 0.01 mM BA. Figures 1 and 2 show the reduction of Cr(VI) and oxidation of BA under different conditions, respectively. The adsorbed percentages of Cr(VI) and BA in the binary system were 12.5% and 6%, respectively, while prolonged dark experiments in the presence of N-F-TiO_2 led to neither BA degradation nor metal reduction after 240 min. Direct photolysis in the single systems of Cr(VI) and BA resulted in low removals for both pollutants. Similarly, low removal was observed for both pollutants in the binary system under photolytic treatment, implying no severe interaction between Cr(VI) and BA under direct photolysis. As shown in Figures 1 and 2, in single systems the photocatalytic reduction of Cr(VI) was achieved after 150 min irradiation, whereas the photocatalytic oxidation of BA was much slower and almost complete degradation is

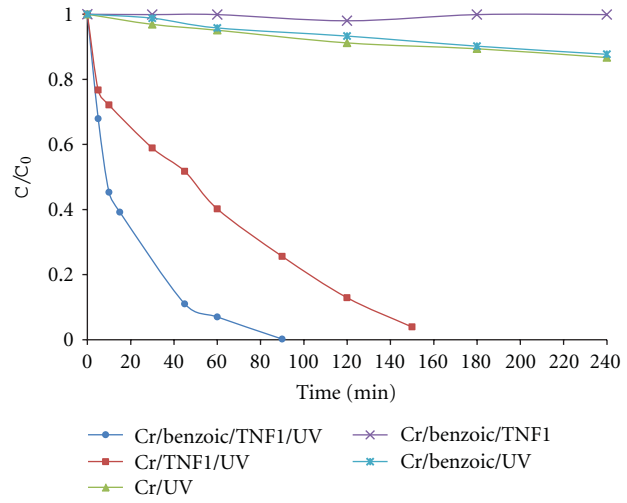

Figure 1: Photocatalytic reduction of Cr(VI) in single and binary systems. ($[Cr(VI)]_0 = 0.1$ mM, $[BA]_0 = 0.01$ mM, pH = 2, N-F-TiO_2 = 500 mg L^{-1}).

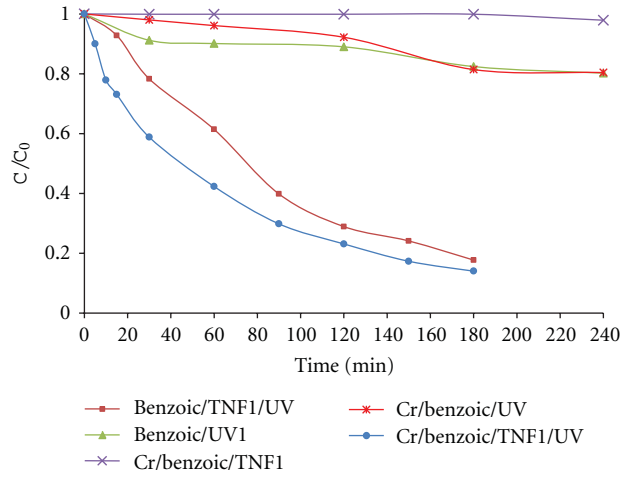

Figure 2: Photocatalytic degradation of benzoic acid in single and binary systems. ($[Cr(VI)]_0 = 0.1$ mM, $[BA]_0 = 0.01$ mM, pH = 2, N-F-TiO_2 = 500 mg L^{-1}).

accomplished after 240 min of irradiation time. On the other hand, the simultaneous photocatalytic treatment of Cr(VI) and BA in the binary system significantly enhanced the reduction/oxidation of substrates each other. In the binary system, the coupled oxidation of the BA consumes photogenerated holes and/or •OH radicals efficiently, blocking the electron-hole recombination and thus, increasing the total efficiency. Moreover, the enhancement of the rates confirmed that Cr(VI) acted as an efficient scavenger of the photogenerated electrons. The results obtained, revealed not only the simultaneous decontamination of two pollutants but also the synergistic effect between the photocatalytic redox reactions .

3.2. RSM Modeling and Optimization for Cr(VI) Photocatalytic Removal. The design matrix and experimental results obtained for the Cr(VI) photocatalytic degradation are depicted in Table 1. The step-wise model fitting was employed in order to find the best model fitted. The quadratic model was selected to describe the relationship of operational parameters and photocatalytic removal based on lack-of-fit analysis and model summary statistics. The quadratic model obtained for the response of % Cr(VI) removal in terms of coded variables can be written as follows (4):

$$\begin{aligned}\%\ \text{Removal Cr (VI)} = {} & +46.32 + 13.54x_1 - 18.57x_2 \\ & - 16.22\ x_3 + 1.63\ x_1x_2 - 0.51\ x_1x_3 \\ & + 5.88\ x_2x_3 - 1.41x_1^2 + 7.73\ x_2^2 \\ & - 5.11x_3^2.\end{aligned} \tag{3}$$

The model adequacy and significance were further checked by ANOVA and the results are shown in Table 2. The ANOVA of the second order quadratic polynomial model showed that the model was highly significant, as the F value for the model was 1841.56 and the corresponding P value was <0.0001. This means that there was only a 0.01% chance for such model F value due to noise. The non significant lack of fit relative to the pure error also confirmed good predictability of the model. The experimental values plotted against the predicted responses for the degradation efficiency of Cr(VI) (Figure 3) showed good correlation $R^2 = 0.9996$ indicating that the model explained the experimental range studied very well. The high model regression coefficient implied that 99.96% of the variations for % Cr(VI) removal were explained by the model. As well, adjusted correlation coefficient of 0.9990 was also very high to advocate for a high significance of the model. The adequacy of the model was also evaluated by the residuals. The normal probability plot of the residuals, shown in Figure 4, revealed that all the points approximate a straight line proving no severe indication of non normality and a good fit of the model. This was also supported by the low value of the coefficient of variation (CV = 1.84%). The significance of each term in the predictive model was evaluated by P values using 5% significance level. Independent variables of the quadratic model, N-F-TiO_2 concentration (x_1), Cr(VI)/BA ratio (x_2), pH (x_3), the second order effect of them, x_1^2, x_2^2, x_3^2 as well as the interaction between Cr(VI)/BA ratio (x_2) and pH (x_3) were highly significant parameters ($P < 0.001$). Moreover, the interaction between N-F-TiO_2 concentration (x_1) and Cr(VI)/BA ratio (x_2) was significant at $P < 0.05$. On the contrary, Cr(VI) removal was not significantly affected by the interaction between N-F-TiO_2 concentration (x_1) and pH (x_3)($P = 0.1416$). The effects of the three independent variables and their interaction on the removal of Cr(VI) were graphically represented by three-dimensional response surface plots by means of response surface methodology. The interaction effect of N-F-TiO_2 concentration and Cr(VI)/BA ratio is shown in Figure 5(a). As can be seen there was an increase in the removal percentage of Cr(VI) with an increase of N-F-TiO_2 concentration and a decrease of Cr(VI)/BA

ratio. The removal percentage increased proportionally by the increase of N-F-TiO_2 dosage due to the increase of adsorption sites on the surface of catalyst as well as the generation of more electrons in the conduction band. An increase in the Cr (VI)/BA ratio by a consequently increase of initial Cr (VI) concentration led to a decreased removal. As initial Cr(VI) concentrations increased, more metal ions were adsorbed on the surface of the photocatalyst. Therefore, the photogenerated e^- required for the removal of Cr(VI) also increased and hence, the available electrons were inadequate for pollutant removal at higher concentrations. Moreover, with the increase in the Cr(VI) concentration, less photons reach the photocatalyst surface (light screening effect), resulting in slower production of the photogenerated pair hole/electron. Consequently, the photocatalytic activity was decreased, since fewer available e^- were available to reduce more metallic ions. Moreover, an increase in pH led to a decrease in the rate of Cr (VI) removal as illustrated in Figure 5(b). This can be attributed to the surface charge properties of the photocatalyst. Since, the point of zero charge of the NF-TiO_2 catalysts has been determined to be 5.7, the N-F-TiO_2 surface is negatively charged at pH > 5.7, whereas is positively charged in more acidic conditions (pH < 5.7). At pH values around 2.5 the predominant species of chromium are the negative charged $HCrO_4^-$ and $Cr_2O_7^{2-}$ ions and at pH values around 6.5 Cr(VI) exists mainly as $HCrO_4^-$ and CrO_4^{2-} [24]. As the pH of the solutions increased, the negatively charged sites of the catalyst increased, thus, the absorption of Cr(VI) anions was prevented due to electrostatic repulsion and consequently their reduction on N-F-TiO_2 surface. The adsorbed percentage of Cr(VI) at pH = 10, Cr(VI)/BA ratio = 5, and [TNF] = 600 mg L^{-1} was found to be 5%. Conversely, as pH decreased, the electrostatic attraction between the positively charged surface and anionic Cr(VI) was enhanced, leading to increased removal. The adsorption percentage (%) of Cr(VI) at pH = 4 and using the same Cr(VI)/BA ratio and catalyst concentration increased to about 21%. An increase in the Cr(VI) photocatalytic reduction with decreasing pH values has been also reported elsewhere [28, 29].

3.3. RSM Modeling and Optimization for Benzoic Acid Photocatalytic Degradation. The experimental design matrix and experimental results obtained for the BA photocatalytic degradation are given in Table 1. Similarly to % Cr(VI) removal, a quadratic model was suggested as the most appropriate to approximate the % photocatalytic degradation of BA. The model can be written in terms of coded variables as follows:

$$\begin{aligned}\%\text{Degr. Benzoic acid} = {} & +8.78 + 4.78x_1 + 4.16x_2 - 13.84x_3 \\ & + 1.06x_1x_2 - 3.07x_1x_3 - 1.14x_2x_3 \\ & + 0.40\,x_1^2 + 5.76\,x_2^2 + 5.82x_3^2 \end{aligned} \quad (4)$$

ANOVA results of the suggested quadratic model (Table 3) and the comparison of actual versus predicted values (Figure 6) indicated that the model could adequately

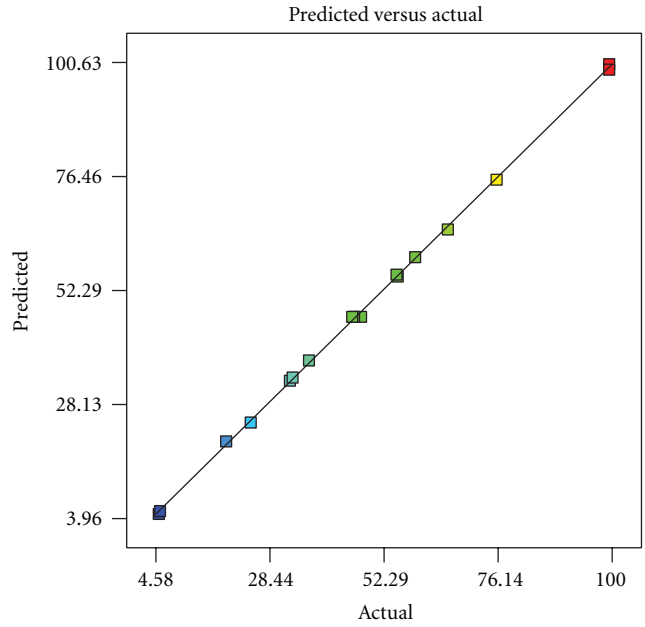

Figure 3: Plot of predicted versus actual values for % Cr(VI) removal.

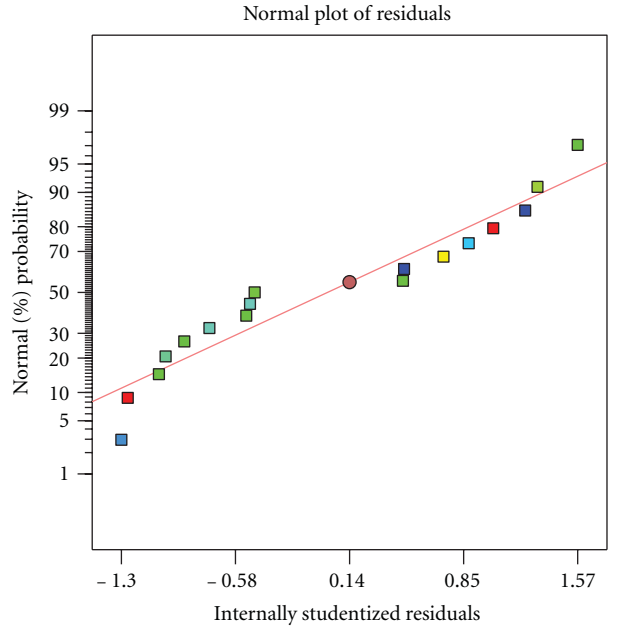

Figure 4: The normal probability (%) plot of the experimental results for % Cr(VI) removal.

be used to describe the % benzoic acid degradation under the experimental range studied. The model F value of 426.95 and P value less than 0.0001 implied the high significance of the model. There was only a 0.01% chance that the "Model F value" could occur due to noise. Moreover, lack of fit was shown to be not significant relative to the pure error, indicating good response to the model. The high model regression coefficient (R^2) of 0.9982 implied that 99.82% of the variability can be revealed by the model and only 0.18%

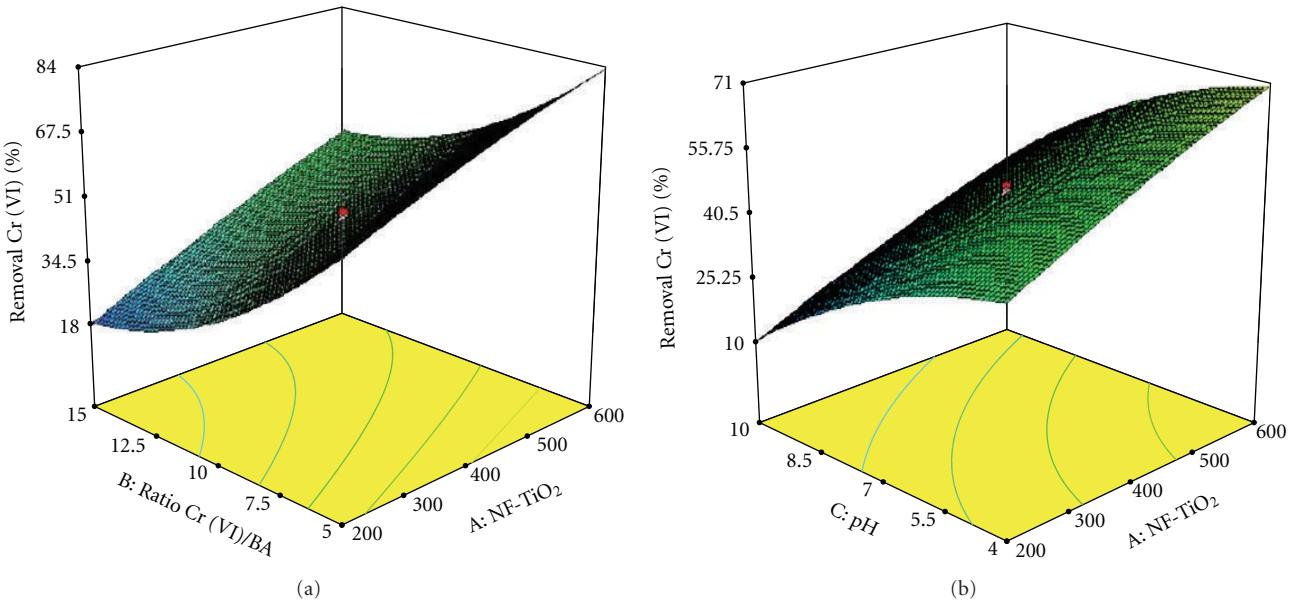

FIGURE 5: 3D response surface plots for % Cr(VI) removal; (a) as a function of N-F-TiO_2 concentration and Cr (VI)/BA ratio; (b) as a function of pH and N-F-TiO_2 concentration.

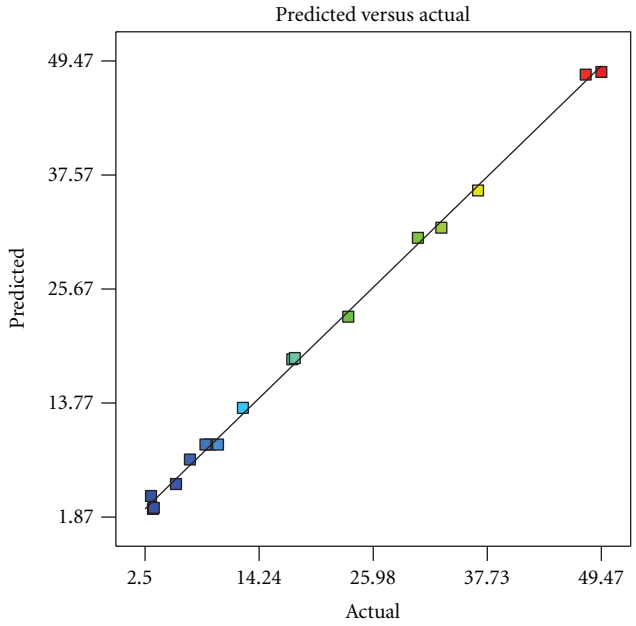

FIGURE 6: Plot of predicted versus actual values for % BA degradation.

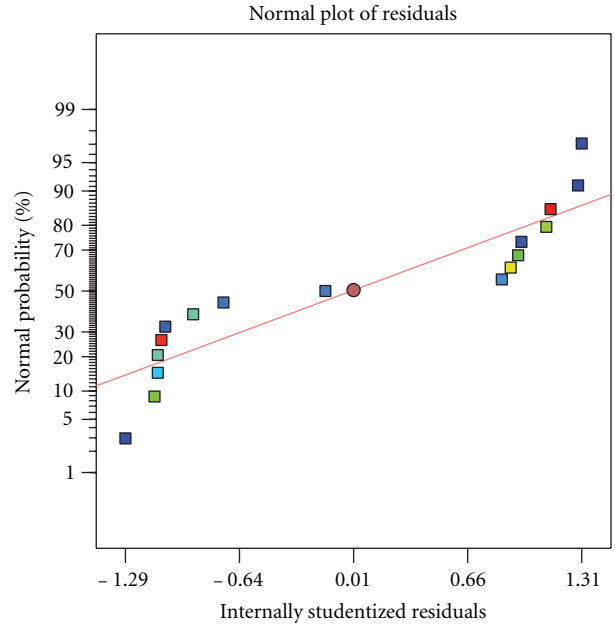

FIGURE 7: The normal prpbability (%) plot of the experimental results for % BA degradation.

of residual variability remained. The R^2 of 0.9982 was in reasonable agreement with adjusted R^2 = 0.9958, indicating also good predictability of the model. A very high degree of precision and a good deal of reliability of the experimental values were indicated by the low value of the coefficient of variation (CV = 5.48%). As can be observed from the residual plot in Figure 7 the data were normally distributed denoting too a good fit of the model. Using 5% significance level, the independent variables of the quadratic model, N-F-TiO_2 concentration (x_1), Cr(VI)/BA ratio (x_2), pH (x_3), the second-order effects of Cr(VI)/BA ratio (x_2^2), and pH (x_3^2) as well as the interaction between ratio N-F-TiO_2 concentration (x_1) and pH (x_3) were highly significant parameters due to $P < 0.001$. Moreover the interactions between N-F-TiO_2 concentration (x_1) and Cr(VI)/BA ratio (x_2) and between Cr(VI)/BA ratio (x_2) and pH (x_3) were significant at $P <$

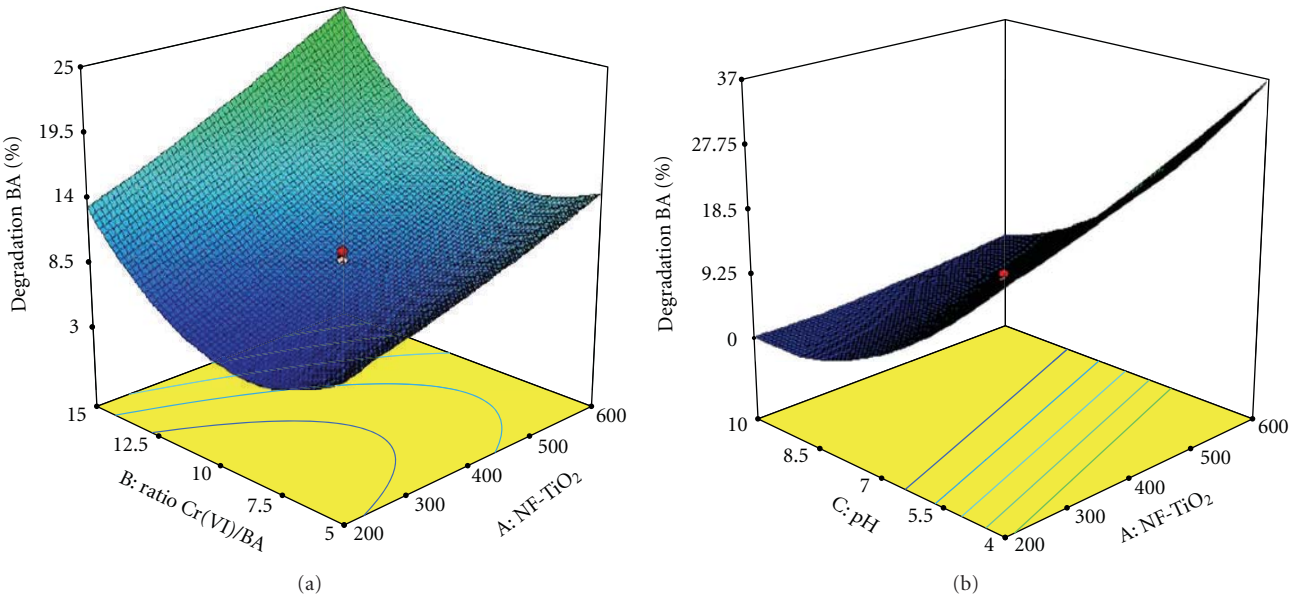

Figure 8: 3D response surface plots for the % BA degradation; (a) as a function of N-F-TiO_2 concentration and Cr(VI)/BA ratio; (b) as a function of pH and N-F-TiO_2 concentration.

Table 2: Analysis of variance (ANOVA) for % removal of Cr(VI).

Source	Sum of squares	df	Mean square	F value	P value Prob > F
Model	12510.88	9	1390.10	1841.56	<0.0001
x_1-TiO_2 mg L^{-1}	2504.00	1	2504.00	3317.23	<0.0001
x_2-Cr/BA ratio	4710.52	1	4710.52	6240.35	<0.0001
x_3-pH	3593.50	1	3593.50	4760.57	<0.0001
x_1 x_2	21.35	1	21.35	28.29	0.0011
x_1 x_3	2.07	1	2.07	2.74	0.1416
x_2 x_3	276.95	1	267.95	366.89	<0.0001
x_1^2	22.49	1	22.49	29.79	0.0009
x_2^2	674.33	1	674.33	893.34	<0.0001
x_3^2	294.43	1	294.43	390.05	<0.0001
Residual	5.28	7	0.75		
Lack of fit	3.34	5	0.67	0.69	0.6829
Pure error	1.95	2	0.97		

Table 3: Analysis of variance (ANOVA) for % degradation of benzoic acid.

Source	Sum of squares	df	Mean square	F value	P value Prob > F
Model	3908.5	9	434.28	426.95	<0.0001
x_1-TiO_2 mg L^{-1}	311.69	1	311.69	306.43	<0.0001
x_2-Cr/BA ratio	236.80	1	236.80	232.80	<0.0001
x_3-pH	2616.02	1	2616.02	2571.86	<0.0001
x_1 x_2	9.05	1	9.05	8.90	0.0204
x_1 x_3	75.34	1	75.34	74.07	<0.0001
x_2 x_3	10.33	1	10.33	10.15	0.0153
x_1^2	1.77	1	1.77	1.74	0.2284
x_2^2	374.00	1	374.00	367.69	<0.0001
x_3^2	382.08	1	382.08	375.63	<0.0001
Residual	7.12	7	1.02		
Lack of fit	6.24	5	1.25	2.84	0.2805
Pure error	0.88	2	0.44		

0.05. On the contrary, the second-order effect of N-F-TiO_2 concentration (x_1^2) was the only insignificant term (P value of 0.2284). Three-dimensional response surfaces computed for % BA degradation are depicted in Figure 8. As shown in Figures 8(a) and 8(b) the degradation percentage increased proportionally to N-F-TiO_2 concentration as expected, confirming the positive influence of the increased number of N-F-TiO_2 active sites/species (mainly holes and $^{\bullet}OH$) on the process kinetics. Several studies have indicated that photocatalytic degradation rate initially increased with catalyst loading and above a certain level of concentration, the reaction rate remains constant or even decreases and becomes independent of the catalyst concentration because of light scattering and screening effects as well as due to the tendency towards agglomeration at high solids concentration [30, 31]. However, this study was based on the use of moderate catalyst concentrations, where this limit was still far away, and thereby the degradation rate increased with NF-TiO_2 concentration within the selected range. From the response surface in Figure 8(b), it was clear that the BA degradation percentage decreased as the pH values increased from acidic to alkaline region. This is related to the ionization state of the surface of catalyst according to the determined PZC (5.7) as well as to that of the parent compound. The pKa of benzoic acid is 4.2 [32] thus, at a pH greater than this value the molecule bears a negative charge. As mentioned above, N-F-TiO_2 surface will be positively charged at pH values

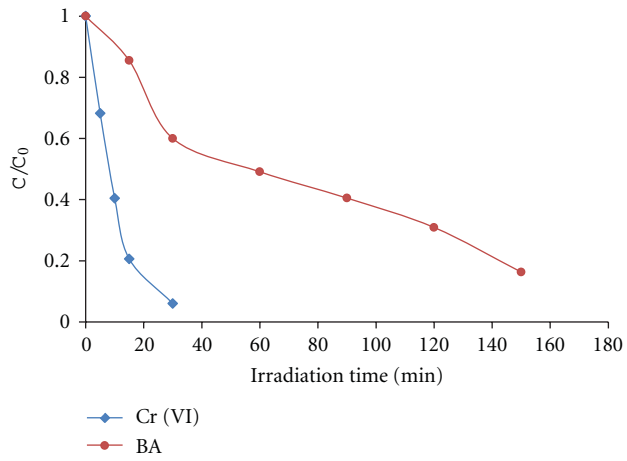

Figure 9: Kinetics of reduction of Cr(VI) and degradation of BA versus irradiation time under optimized conditions ($[\text{N-F TiO}_2]_0$ = 600 mg L^{-1}, Cr(VI)/BA ratio = 5, pH = 4).

Table 4: Photocatalytic kinetic parameters (rate constants, half-lives, correlation coefficients) of Cr(VI) and BA under optimized conditions ($[\text{N-F-TiO}_2]_0$ = 600 mg L^{-1}, Cr/BA ratio = 5, pH = 4).

	k (min^{-1})	$t_{1/2}$ (min)	R^2
Cr(VI)	0.0960	7.219	0.9929
BA	0.0109	63.578	0.9623

lower than 5.7 and negatively charged at higher ones. In consequence, as the pH increased from slightly acidic (5.7–6) to alkaline values, Columbic repulsion between the negative-charged surface of the catalysts and anionic form of BA was observed which led to decreased adsorption and consequently lower degradation. The adsorbed percentage of BA at pH = 10, Cr(VI)/BA ratio = 5, and [TNF] = 600 mg L^{-1} was found to be only 0.5%. An increase in the degradation rate of BA was also observed with an increase in the Cr(VI)/BA ratio (Figure 8(a)). As the Cr(VI) concentration increased, the recombination of the photo-induced hole/electron pairs was strongly inhibited, as the electrons were scavenged by Cr(VI), enhancing the BA degradation. The numerical optimization of the software using desirability approach was employed to find the specific points that maximize the % removal for both pollutants. Based on the models, the optimum conditions for simultaneous removal of Cr(VI) and BA were found as follows: N-F-TiO_2 concentration = 600 mg L^{-1}, Cr(VI)/BA ratio = 5, and pH = 4.

3.4. Model Validation and Confirmation—Evolution of Photocatalytic Reduction of Cr(VI) and Oxidation of Benzoic Acid under Optimized Conditions. To confirm the adequacy of the models for predicting the maximum simultaneous % removal Cr and % degradation of BA, verification experiments were conducted using the optimum conditions. The removal and degradation rates from the validation experiment are depicted in Figure 9. Under optimized conditions pseudo-first order kinetics were recorded for both the photocatalytic reduction of Cr(VI) and degradation of BA. Table 4 lists the values of apparent rate constants, k_{app}, the correlation coefficients and the corresponding half-lives of Cr(VI) and BA. Half of Cr(VI) concentration was consumed within 7.22 min of irradiation under optimal conditions, while BA exhibited a much slower rate than the removal of Cr(VI). Complete Cr (VI) removal was achieved after 30 min of irradiation time. At the same time, the degradation of BA reached about 40%, and prolonged irradiation time was needed before complete degradation was achieved. As reported in the literature, the photocatalytic transformation products of BA using TiO_2 included salicylic acid, p-hydroxybenzoic acid, and 2,3- and/or 2,5-dihydroxybenzoic acid and phenol. The photocatalytic degradation pathway proceeds via $^{\bullet}OH$ attack on the aromatic moiety on several positions to produce hydroxy and dihydroxy derivatives, via decarboxylation (photo-Kolbe) reaction resulting from the direct attack of the carboxylic group by h^+_{VB} and finally ring opening to produce aliphatic acids [15, 32, 33]. The formation of such by-products reacts also with h^+_{VB} /$^{\bullet}OH$ resulting in a more prolonged time for the degradation of parent benzoic acid.

According to previous findings [26] N-F-codoping of TiO_2 enhances the oxidative power of the h^+_{VB} but lessens the reduction ability of e^-_{CB}. This unveils the use of such photocatalytic materials to control the photocatalytic reactions of the redox pair species, e^-_{CB} and h^+_{VB}. Regarding the reduction process, the electrons of the N-F-TiO_2, at states below the CB of TiO_2, have weaker reduction ability, consequently they can reduce preferably strong oxidation agents such as Cr(VI) enhancing the target reduction reaction without the competence of other ineffective reactions for reduction, such as O_2 reduction. As far as the oxidation pathway, the enhancement in the oxidation power of the h^+_{VB} makes the oxidation of organic molecules and especially organic acids and water (for the $^{\bullet}OH$ production) more favourable and consequently enables the reduction reaction to occur more efficiently.

4. Conclusions

The simultaneous photocatalytic reduction of Cr(VI) and oxidation of benzoic acid in the presence of N-F-codoped TiO_2 was investigated focusing on the influence of parameters such as catalyst concentration, Cr(VI)/BA ratio, and pH on the photocatalytic efficiency that was optimized and modeled by response surface methodology (RSM). A considerable enhancement of the photocatalytic efficiency was observed for the binary system than in the single component systems, indicating a promoting synergistic effect. Also, it was noted that the three parameters tested had significant effect on the total efficiency. Under optimized conditions the removal for both Cr(VI) and BA followed pseudo-first order kinetic model. The results provide an efficient treatment method to remove organic and inorganic pollutants simultaneously in complex systems which presents special significance to water pollution control and remediation. Moreover, this study proves that RSM constitutes a powerful tool for optimizing the operational conditions of the simultaneous reduction

of Cr (VI) and oxidation of benzoic acid by photocatalytic processes.

Acknowledgments

This research has been cofinanced by the European Union (European Social Fund, ESF) and Greek national funds through the Operational Program "Education and Lifelong Learning" of the National Strategic Reference Framework (NSRF)—Research Funding Program: Heracleitus II. Investing in knowledge society through the European Social Fund.

References

[1] S. C. Hsu, H. L. Hsieh, C. P. Chen et al., "Tungsten and other heavy metal contamination in aquatic environments receiving wastewater from semiconductor manufacturing," *Journal of Hazardous Materials*, vol. 189, no. 1-2, pp. 193–202, 2011.

[2] J. J. Pignatello, B. G. Katz, and H. Li, "Sources, interactions, and ecological impacts of organic contaminants in water, soil, and sediment: an introduction to the special series," *Journal of Environmental Quality*, vol. 39, no. 4, pp. 1133–1138, 2010.

[3] M. Stuart, D. Lapworth, E. Crane, and A. Hart, "Review of risk from potential emerging contaminants in UK groundwater," *Science of the Total Environment*, vol. 416, pp. 1–21, 2012.

[4] R. Qiu, D. Zhang, Z. Diao et al., "Visible light induced photocatalytic reduction of Cr(VI) over polymer-sensitized TiO_2 and its synergism with phenol oxidation," *Water Research*, vol. 46, no. 7, pp. 2299–2306, 2012.

[5] X. Zhao, Q. Li, X. Zhang, H. Su, K. Lan, and A. Chen, "Simultaneous removal of metal ions and methyl orange by combined selective adsorption and photocatalysis," *Environmental Progress and Sustainable Energy*, vol. 30, no. 4, pp. 567–575, 2011.

[6] A. R. Khataee and M. B. Kasiri, "Artificial neural networks modeling of contaminated water treatment processes by homogeneous and heterogeneous nanocatalysis," *Journal of Molecular Catalysis A*, vol. 331, no. 1-2, pp. 86–100, 2010.

[7] I. K. Konstantinou and T. A. Albanis, "Photocatalytic transformation of pesticides in aqueous titanium dioxide suspensions using artificial and solar light: intermediates and degradation pathways," *Applied Catalysis B*, vol. 42, no. 4, pp. 319–335, 2003.

[8] T. Mishra, J. Hait, N. Aman, R. K. Jana, and S. Chakravarty, "Effect of UV and visible light on photocatalytic reduction of lead and cadmium over titania based binary oxide materials," *Journal of Colloid and Interface Science*, vol. 316, no. 1, pp. 80–84, 2007.

[9] M. I. Litter, "Treatment of chromium, mercury, lead, uranium, and arsenic in water by heterogeneous photocatalysis," *Advances in Chemical Engineering*, vol. 36, pp. 37–67, 2009.

[10] N. Aman, T. Mishra, J. Hait, and R. K. Jana, "Simultaneous photoreductive removal of copper (II) and selenium (IV) under visible light over spherical binary oxide photocatalyst," *Journal of Hazardous Materials*, vol. 186, no. 1, pp. 360–366, 2011.

[11] N. Wang, Y. Xu, L. Zhu, X. Shen, and H. Tang, "Reconsideration to the deactivation of TiO_2 catalyst during simultaneous photocatalytic reduction of Cr(VI) and oxidation of salicylic acid," *Journal of Photochemistry and Photobiology A*, vol. 201, no. 2-3, pp. 121–127, 2009.

[12] P. Banerjee, S. Chakrabarti, S. Maitra, and B. K. Dutta, "Zinc oxide nano-particles—sonochemical synthesis, characterization and application for photo-remediation of heavy metal," *Ultrasonics Sonochemistry*, vol. 19, no. 1, pp. 85–93, 2012.

[13] M. Antonopoulou, V. Papadopoulos, and I. Konstantinou, "Photocatalytic oxidation of treated municipal wastewaters for the removal of phenolic compounds: optimization and modeling using response surface methodology (RSM) and artificial neural networks (ANNs)," *Journal of Chemical Technology & Biotechnology*. In press.

[14] T. Velegraki and D. Mantzavinos, "Conversion of benzoic acid during TiO_2-mediated photocatalytic degradation in water," *Chemical Engineering Journal*, vol. 140, no. 1–3, pp. 15–21, 2008.

[15] A. A. Ajmera, S. B. Sawant, V. G. Pangarkar, and A. A. C. M. Beenackers, "Solar-assisted photocatalytic degradation of benzoic acid using titanium dioxide as a photocatalyst," *Chemical Engineering and Technology*, vol. 25, no. 2, pp. 173–180, 2002.

[16] E. I. Korotkova, O. A. Avramchik, T. M. Angelov, and Y. A. Karbainov, "Investigation of antioxidant activity and lipophilicity parameters of some preservatives," *Electrochimica Acta*, vol. 51, no. 2, pp. 324–332, 2005.

[17] N. Wang, L. Zhu, K. Deng, Y. She, Y. Yu, and H. Tang, "Visible light photocatalytic reduction of Cr(VI) on TiO_2 in situ modified with small molecular weight organic acids," *Applied Catalysis B*, vol. 95, no. 3-4, pp. 400–407, 2010.

[18] V. Prigione, M. Zerlottin, D. Refosco, V. Tigini, A. Anastasi, and G. C. Varese, "Chromium removal from a real tanning effluent by autochthonous and allochthonous fungi," *Bioresource Technology*, vol. 100, no. 11, pp. 2770–2776, 2009.

[19] A. Pandikumar and R. Ramaraj, "Titanium dioxide-gold nanocomposite materials embedded in silicate sol-gel film catalyst for simultaneous photodegradation of hexavalent chromium and methylene blue," *Journal of Hazardous Materials*, vol. 203-204, pp. 244–250, 2012.

[20] B. Sun, E. P. Reddy, and P. G. Smirniotis, "Visible light Cr(VI) reduction and organic chemical oxidation by TiO_2 photocatalysis," *Environmental Science and Technology*, vol. 39, no. 16, pp. 6251–6259, 2005.

[21] X. R. Xu, H. B. Li, and J. D. Gu, "Photocatalytic reduction of hexavalent chromium and degradation of di-N-Butyl phthalate in aqueous TiO_2 suspensions under ultraviolet light irradiation," *Environmental Technology*, vol. 28, no. 9, pp. 1055–1061, 2007.

[22] G. Colón, M. C. Hidalgo, and J. A. Navío, "Photocatalytic deactivation of commercial TiO_2 samples during simultaneous photoreduction of Cr(VI) and photooxidation of salicylic acid," *Journal of Photochemistry and Photobiology A*, vol. 138, no. 1, pp. 79–85, 2001.

[23] S. G. Schrank, H. J. José, and R. F. P. M. Moreira, "Simultaneous photocatalytic Cr(VI) reduction and dye oxidation in a TiO_2 slurry reactor," *Journal of Photochemistry and Photobiology A*, vol. 147, no. 1, pp. 71–76, 2002.

[24] T. Papadam, N. P. Xekoukoulotakis, I. Poulios, and D. Mantzavinos, "Photocatalytic transformation of acid orange 20 and Cr(VI) in aqueous TiO_2 suspensions," *Journal of Photochemistry and Photobiology A*, vol. 186, no. 2-3, pp. 308–315, 2007.

[25] H. Kyung, J. Lee, and W. Choi, "Simultaneous and synergistic conversion of dyes and heavy metal ions in aqueous TiO_2 suspensions under visible-light illumination," *Environmental Science and Technology*, vol. 39, no. 7, pp. 2376–2382, 2005.

[26] Q. Wang, C. Chen, W. Ma, H. Zhu, and J. Zhao, "Pivotal role of fluorine in tuning band structure and visible-light photocatalytic activity of nitrogen-doped TiO_2," *Chemistry—A European Journal*, vol. 15, no. 19, pp. 4765–4769, 2009.

[27] K. Bourikas, J. Vakros, C. Kordulis, and A. Lycourghiotis, "Potentiometric mass titrations: experimental and theoretical establishment of a new technique for determining the point of zero charge (PZC) of metal (hydr)oxides," *Journal of Physical Chemistry B*, vol. 107, no. 35, pp. 9441–9451, 2003.

[28] L. B. Khalil, W. E. Mourad, and M. W. Rophael, "Photocatalytic reduction of environmental pollutant Cr(VI) over some semiconductors under UV/visible light illumination," *Applied Catalysis B*, vol. 17, no. 3, pp. 267–273, 1998.

[29] Y. Ku and I. L. Jung, "Photocatalytic reduction of Cr(VI) in aqueous solutions by UV irradiation with the presence of titanium dioxide," *Water Research*, vol. 35, no. 1, pp. 135–142, 2001.

[30] I. K. Konstantinou and T. A. Albanis, "TiO_2-assisted photocatalytic degradation of azo dyes in aqueous solution: kinetic and mechanistic investigations: a review," *Applied Catalysis B*, vol. 49, no. 1, pp. 1–14, 2004.

[31] V. A. Sakkas, P. Calza, A. D. Vlachou, C. Medana, C. Minero, and T. Albanis, "Photocatalytic transformation of flufenacet over TiO_2 aqueous suspensions: Identification of intermediates and the mechanism involved," *Applied Catalysis B*, vol. 110, pp. 238–250, 2011.

[32] V. G. Gandhi, M. K. Mishra, M. S. Rao, A. Kumar, P. A. Joshi, and D. O. Shah, "Comparative study on nano-crystalline titanium dioxide catalyzed photocatalytic degradation of aromatic carboxylic acids in aqueous medium," *Journal of Industrial and Engineering Chemistry*, vol. 17, no. 2, pp. 331–339, 2011.

[33] A. Assabane, Y. Ait Ichou, H. Tahiri, C. Guillard, and J. M. Herrmann, "Photocatalytic degradation of polycarboxylic benzoic acids in UV-irradiated aqueous suspensions of titania. Identification of intermediates and reaction pathway of the photomineralization of trimellitic acid (1,2,4-benzene tricarboxylic acid)," *Applied Catalysis B*, vol. 24, no. 2, pp. 71–87, 2000.

Hindawi Publishing Corporation
International Journal of Photoenergy
Volume 2012, Article ID 270320, 9 pages
doi:10.1155/2012/270320

Research Article

Energy Effectiveness of Direct UV and UV/H_2O_2 Treatment of Estrogenic Chemicals in Biologically Treated Sewage

Kamilla M. S. Hansen and Henrik R. Andersen

Department of Environmental Engineering, Technical University of Denmark, Building 133, Miljoevej, 2800 Lyngby, Denmark

Correspondence should be addressed to Kamilla M. S. Hansen, kmsh@env.dtu.dk

Received 1 June 2012; Accepted 23 July 2012

Academic Editor: Mika Sillanpää

Continuous exposure of aquatic life to estrogenic chemicals via wastewater treatment plant effluents has in recent years received considerable attention due to the high sensitivity of oviparous animals to disturbances of estrogen-controlled physiology. The removal efficiency by direct UV and the UV/H_2O_2 treatment was investigated in biologically treated sewage for most of the estrogenic compounds reported in wastewater. The investigated compounds included parabens, industrial phenols, sunscreen chemicals, and steroid estrogens. Treatment experiments were performed in a flow through setup. The effect of different concentrations of H_2O_2 and different UV doses was investigated for all compounds in an effluent from a biological wastewater treatment plant. Removal effectiveness increased with H_2O_2 concentration until 60 mg/L. The treatment effectiveness was reported as the electrical energy consumed per unit volume of water treated required for 90% removal of the investigated compound. It was found that the removal of all the compounds was dependent on the UV dose for both treatment methods. The required energy for 90% removal of the compounds was between 28 kWh/m^3 (butylparaben) and 1.2 kWh/m^3 (estrone) for the UV treatment. In comparison, the UV/H_2O_2 treatment required between 8.7 kWh/m^3 for bisphenol A and benzophenone-7 and 1.8 kWh/m^3 for ethinylestradiol.

1. Introduction

The present of estrogenic compounds in the environment and particularly the continuous exposure via wastewater treatment plant (WWTP) effluents have in recent years received considerable attention due to their damaging effects on the aquatic life [1–3]. The estrogenic compounds influence on the endocrine system, resulting in behavioural changes, changes in mating behaviour, and feminization of fish, and have even been linked to reduced sperm productivity in humans [4].

The synthetic steroid estrogen ethinylestradiol (EE2) is often found in low ng/L concentrations in WWTP effluents, and available data suggest that it is an important contributor to the estrogenic activity of WWTP effluents [2, 5–7]. The natural steroid estrogens, 17β-estradiol (E2), and estrone (E1) are also considered important contributors to the estrogenic activity of WWTP effluents. They are less potent than EE2 but are typically found in slightly higher concentrations. Other known contributors to the estrogenic effect are industrial phenols such as nonylphenol (NP), octylphenol (OP), bisphenol A (BPA), and compounds used in personal care products such as parabens and benzophenones. These are typically found in the μg/L concentration range [7–11]. However, these compounds have considerably lower estrogenic activity compared to steroidal estrogens [11, 12].

Degradation of some of these estrogenic compounds by UV photolysis and the advanced oxidation process UV/H_2O_2 in laboratory setups has been reported in the literature [13–17].

Degradation by photolysis and radical oxidation initiated by the UV/H_2O_2 treatment are thus known processes for some estrogens in wastewater. However, the present literature does not give the data needed for estimating the treatment intensity required for treatment of real wastewater since they do not consider realistic flow through conditions, radical scavengers, and the shadow effect seen in real wastewater. Thus, the size of the treatment system and the expected running cost of the treatment if the techniques were applied as a real treatment cannot be found in the literature.

Therefore, this work has used an experimental setup with realistic dimensions from a UV treatment plant intended for disinfection of a wastewater treatment plant effluent by medium pressure UV lamps. With this setup, the removal efficiency by direct UV and the advanced oxidation process UV/H_2O_2 of estrogenic compounds were investigated in tap water and biologically treated sewage. The results of the experiments are reported in units of energy applied for the treatment as recommended by IUPAC [18].

2. Method

2.1. Regents and Materials. All the investigated estrogenic compounds (see Table 1) were purchased from Sigma-Aldrich. Methanol, acetone, and heptane together with 35% hydrogen peroxide, potassium titanium oxide oxalate dihydrate, sodium phosphate monobasic dehydrate, and 85% orthophosphoric acid were obtained from Sigma-Aldrich as well. The chemicals for derivatisation of the steroid estrogens (dithioerythritol, trimethylsilyl imidazole, and N-methyl-N-(trimethylsilyl)-trifluoroacetamide) were purchased from Sigma-Aldrich. All chemicals were of analytical grade except potassium titanium oxide oxalate dihydrate which was of technical grade.

The water used for experiments was wastewater effluent from Usserød Wastewater treatment plant (Hørsholm, Denmark). The water was stored in the dark at 10°C until experiments were performed. The effluent was used for experiment within 3 days after the collection, however once after 12 days as an exception. The water was poured into three 25 L plastic containers and spiked with the mixed solutions so the concentrations of xenoestrogens and steroid estrogens were 1 μg/L and 400 ng/L, respectively. In the experiment with UV/H_2O_2, the hydrogen peroxide (35% solution) was added, so the desired concentration was achieved.

Tap water used in experiments to investigate the matrix effect in comparison with wastewater was from the DTU-Lyngby Campus. This water is not chlorinated, and it has a content of mayor ions similar to the wastewater, but a low concentration of organic matter since it is taken from a deep well (more than 50 years old groundwater).

2.2. Bench-Scale Reactor. The treatments were carried out in a bench-scale, flow-through photoreactor (see Figure 1). The lamp (700 W, Bau47, Scan Research A/S, Herning, Denmark) is located coaxial in the centre of the reactor. The UV lamp was placed inside a quarts sleeve which is pumped with an inert gas to avoid ozone production. The distance from the lamp to the inner side of the reactor is 5.7 cm. A spectrum of the output of the lamp is shown in supporting information of a previous paper [19].

Figure 1 shows a schematically drawing of the experimental setup. The water was pumped from the plastic containers through a flowmeter and into the reactor at the bottom. A valve was used to adjust the flow rate. The samples for analysis were taken from the outlet after one retention time and from the containers (inlet concentration). The blind sample was taken before spiking and addition of hydrogen peroxide. The samples were acidified with phosphate buffer (pH = 3) as preservative except samples for measurement of hydrogen peroxide concentration.

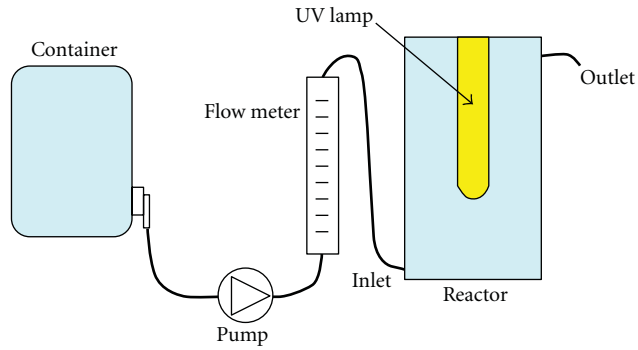

Figure 1: Diagram of the experimental setup.

2.3. Sample Preparation for Chemical Analysis and YES Assay. For each experiment, three samples of 500 mL each were analysed. Surrogate standard was added to every sample before solid-phase extraction (SPE) to compensate for possible losses during sample preparation and analysis. The extractions were performed at commercial packed cartridges (500 mg C18 adsorbent/6 mL cartridge, Supelco), which were conditioned with 2 × 1.5 mL heptane, 1 × 1.5 mL acetone, 2 × 1.5 mL methanol, and 2 × 1.5 mL acidified water (phosphate buffer, pH = 3) before the extraction begins. The water was transmitted to the SPE column by means of vacuum with a flow rate at maximum 5 mL per minute. Afterwards, the column is dried for approximately 1 hour until complete dryness. The samples were eluted with acetone until 5 mL eluent was collected in a test tube. Then the eluent was dried under a stream of nitrogen in a thermostat-controlled heating block to almost completely dryness.

The samples for YES assay, to which no surrogate standard was added, were dissolved in ethanol, while the samples for chemical analysis were further purified as described in the following. One gram of 1% deactivated silica gel (silica gel 60, 0.063–0.200 mm (70–230 mesh ASTM) Merck) was suspended in 3 mL heptane-acetone mixture (65 : 35) and poured into 3 mL glass cartridge. The almost dried samples were resolved in approximately 0.3 mL heptane acetone mixture (65 : 35) and transferred to the top of the silica gel. The test tube was washed with little more of the solvent mixture to minimize the loss of sample. Then glass cartridge containing silica gel and sample was eluted with heptane acetone mixture (65 : 35) until approximately 5 mL eluent was collected. Once again the solvent was evaporated under a stream of nitrogen, but this time to complete dryness. The samples were dissolved in 250 μL heptane acetone mixture and transferred to a GC vial (300 μL, Chromacol) [8, 11, 20].

2.4. Quantification of Xenoestrogens. The analysis of the estrogens was performed by gas chromatography using a

Table 1: The electrical energy per order, EEO, (kWh/m^3) for UV and UV/H_2O_2 treatments of the investigated compounds in treated wastewater from Usserød WWTP. 95% confidence intervals are indicated.

	UV	UV/H_2O_2
Parabens		
Methylparaben (MP)	13.9 ± 0.2	8.1 ± 0.6
Ethylparaben (EP)	15.9 ± 0.7	5.3 ± 0.3
Propylparaben (PP)	19.1 ± 1.1	6.4 ± 0.4
isoButylparaben (isoBP)	14.2 ± 1.6	7.0 ± 0.4
Butylparaben (BP)	28.0 ± 2.9	7.9 ± 0.4
Industrial phenols		
Bisphenol A (BPA)	16.1 ± 1.9	8.7 ± 1.2
isoNonylphenol (isoNP)	11.5 ± 2.6	7.6 ± 1.2
Octylphenol (OP)	8.1 ± 1.6	2.6 ± 0.1
Sunscreen chemicals		
Benzophenone-3 (BP-3)	25.4 ± 1.3	8.5 ± 0.6
Benzophenone-7 (BP-7)	21.1 ± 1.4	8.7 ± 0.5
Octyl methoxycinnamate (OMC)	19.8 ± 2.2	7.1 ± 1.2
Homosalate (HMS)	15.0 ± 1.6	7.7 ± 0.6
3-(4-Methylbenzyliden)camphor (4-MBC)	17.3 ± 2.2	5.0 ± 0.1
Octyl dimethylaminobenzoate (OD-PABA)	4.2 ± 0.7	4.1 ± 0.1
Steroid estrogens		
Estrone (E1)	1.2[a]	N.D.
17β-estradiol (β-E2)	4.9 ± 0.8	2.2 ± 0.2
Ethinylestradiol (EE2)	6.1 ± 0.7	1.8 ± 0.03
Estrogenic potency		
Estradiol equivalent concentration (EEC) according to YES assay	4.9 ± 1.0	N.D.

N.D.: no data. [a]Regression with only two points.

Varian 3800 GC coupled to Varian Saturn 2000 Ion trap (MS-MS). The column used was a Varian, FactorFour capillary column (VF-5 ms, 30 m × 0.25 mm ID DF = 0.25) with a gas flow of 1 mL/min. Seven and half μL sample was injected using Varian 8200 Autosampler in split/splitless injection mode with the Varian 1079 injection gate.

The GC oven temperature was maintained at 100°C for 1 min and then programmed at 20°C/min to 110°C, then at 10°C/min to 250°C, followed by 25°C/min to 285°C, and finally 35°C/min to 320°C, which was held for 7.1 min to ensure that most of other organic compounds also came out. Each compound was quantified based on a characteristic daughter ion of MS-MS spectroscopy, and the other daughter ions were used for confirmation of the identity of the detected chemicals [8, 11, 20].

2.5. Quantification of Steroid Estrogens. After the analysis of parabens, and so forth, the remaining extract of the samples was transferred to 3 mL reactival, and the GC-vials were washed one or two times with acetone to ensure complete transferring of the sample. The samples were dried under nitrogen to complete dryness. Derivatisation mixture was made by mixing 2 mg dithioerythritol (DTE), 2 μL trimethylsilylimidazole (TMSI), and 1000 μL N-methyl-N-(trimethylsilyl)-trifluoroacetamide (MSTFA). To the derivatisation vials, 50 μL of that mixture was added and caped in order to be shaken. The vials were placed in an oven at 60°C for 60 min. Afterwards, the vials were placed at the thermostat-controlled heating block and evaporated to dryness under stream of nitrogen. The samples were dissolved in 250 μL heptane and transferred to GC vials again. The GC oven temperature was maintained at 80°C for 1 min and then programmed at 25°C/min to 230°C, followed by 1°C/min to 248°C, and finally 45°C/min to 320°C, which was held for 3 min to ensure that all interfering compounds were eluted from the column. The method used specific MS/MS parameters and was based on a method evaluation described by Andersen et al. [21].

The range of quantification was for xenoestrogen in general between 0.005 and 1.0 μg/L and typically between 2 and 500 ng/L for the steroid estrogens. The sample preparation and method performance were evaluated in the interlaboratory comparison described by Heath et al. [22].

2.6. YES Assay. The extracts were serially diluted in a growth media for yeast cells. The dilutions were incubated with an estrogen-responsive yeast cell for 72 h. The estrogenic effect was quantified by measuring the development of a red dye which is produced by the yeast cells with an enzyme and is produced proportionally to the estrogenic concentration in the cells. For quantification of the estrogenic effect, a standard curve was made from a stock solution of 17β-estradiol (E2). The method for quantifying the estrogenic potency of the extracts is generally based on the method

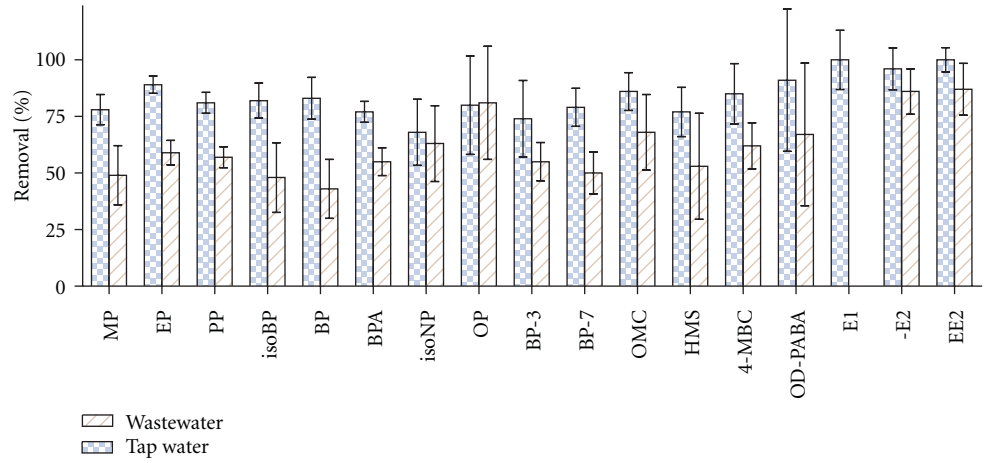

Figure 2: The removal of estrogenic compounds from tap water and wastewater effluent by UV/H_2O_2. The electrical energy dose was 1.8 kWh/m^3, and the initial concentration of hydrogen peroxide was 60 mg/L. The error bars present the 95% confidence interval.

introduced by Routledge and Sumpter [23]. Details of the method variation are described in Hansen et al. [20] and Kusk et al. [11].

2.7. Experiments. Three different types of experiments were performed. First, the effect of concentration of hydrogen peroxide in wastewater on removal of estrogens with an UV dose equivalent to an energy use of 1.8 kWh/m^3 was investigated. Second, the influence of the high concentration of different matrix components was investigated by comparing the removal of estrogens in experiments with either the wastewater effluent or tap water with the optimized hydrogen peroxide dose of 60 mg/L and an UV dose equivalent to an energy use of 1.8 kWh/m^3. Finally, experiments were performed in wastewater with or without addition of 60 mg/L hydrogen peroxide using different UV doses equivalent to an energy use ranging from 1.75 to 10.9 kWh/m^3 or from 2.3 to 16.3 kWh/m^3, respectively.

2.8. Data Treatment. The treatment effectiveness was evaluated based on the electrical energy per order (EEO; unit kWh/m^3), which is defined as the electrical energy consumed per unit volume of water treated required for 90% removal of the investigated compound [18]

$$\log\left(\frac{C}{C_i}\right) = \frac{-1}{\text{EEO}} \cdot \text{EED}, \quad (1)$$

where C_i and C are the initial and the final concentrations, respectively, EED is the electrical energy dose in kWh/m^3, and EEO is the electrical energy per order. The normalised concentration of the investigated chemicals was plotted against the electrical energy dose. Constructed plots were used for determination of the EEO by least square fit according to (1). In some cases, concentration below the limit of quantification was used in the estimation of EEO if a good analytical signal was found with correct ratios between the daughter ions in the mass spectra.

3. Results and Discussion

The UV treatment intensity was characterised by the electric energy consumption. This was done according to recommendation by IUPAC [18]. Since the lamp was completely submerged, all irradiation emitted by the lamp was absorbed by the water, and thus, the electrical energy dose (EED) at each treatment level was calculated as the energy consumption of the lamp divided by the flow rate of the wastewater.

The absorbance of the spiked tap and wastewater was measured on UV-vis spectrophotometer (Cary 50 Bio, Varian), and the spiking of the water did not change the absorbance of the water in the UV and visible range (800–190 nm), even though the water was spiked with 17 different chemicals. The UV dose, each compound was exposed to, is therefore considered as independent of the other compounds.

3.1. The Effect of Water Matrix on the Removal by UV/H_2O_2. A single experiment was done in tap water to compare the efficiency of UV/H_2O_2 treatment in different water matrix. Figure 2 shows the removal of the compound in tap water and wastewater effluent with an initial concentration of hydrogen peroxide of 60 mg/L and UV dose equivalent to an energy use of 1.8 kWh/m^3. The removal of estrogenic chemicals is higher in tap water than in wastewater effluent. This is due to higher concentrations of other organic materials than the spiked compound in the wastewater effluent compared to tap water. These can act as scavengers of $^{\bullet}$OH radicals and result in a shadowing effect, where the compound either blocks the pathway of the light or adsorbs the light.

Furthermore, more of the hydrogen peroxide was activated in the tap water (21%) than in the wastewater (11%), which may be a result of less shadowing effect in the tap water resulting in a larger amount of the light being used for photolysis of hydrogen peroxide. Neamțu and Frimmel [15] found the same tendency when they investigated the removal of BPA.

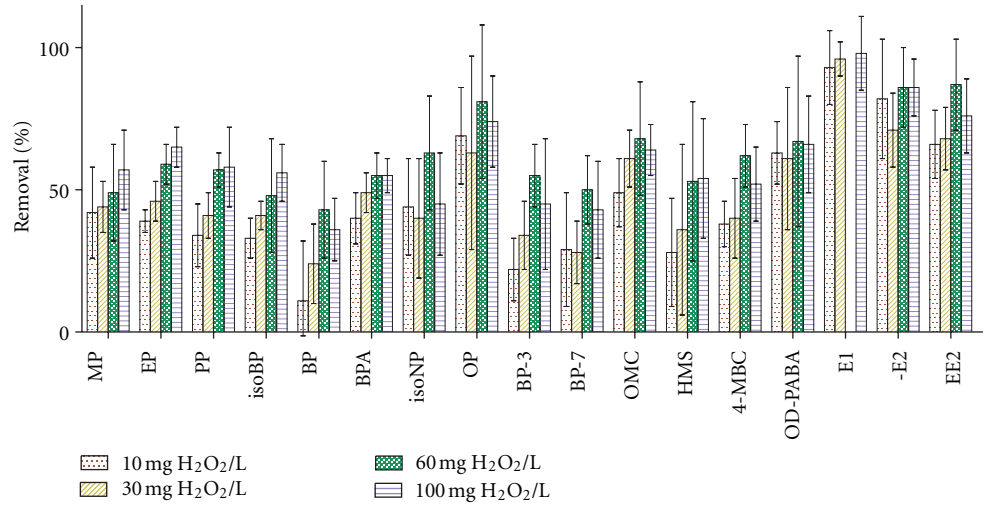

Figure 3: The removal of estrogens in wastewater effluent at varying concentrations of hydrogen peroxide at constant energy dose (1.8 kWh/m^3). The error bars present the 95% confidence interval.

3.2. The Effect of H_2O_2 Concentration on the Removal of Chemicals. The removal of the investigated compounds increased with increasing hydrogen peroxide concentration until 100 mg/L where the removal of most of the compound decreased again (Figure 3). The removal was expected to decrease again at higher concentration due to larger possibility for the hydroxyl radical to react with hydrogen peroxide and form the less reactive $HO_2^{\bullet}$. An inhibition of the degradation of chemicals at high concentration of hydrogen peroxide was found during the study of Neamțu and Frimmel [15] as well.

3.3. Removal. The obtained removal of all investigated compounds is shown in Figures 4 and 5. The more UV irradiation the water was exposed to (higher EED), the higher the removal of the compounds was. When the results from UV and UV/H_2O_2 treatment with an electrical energy dose of 2.3 kWh/m^3 are compared, it is seen that a higher removal was obtained at UV/H_2O_2 treatment than only UV irradiation.

In the case of UV/H_2O_2 treatment, the removal seems more similar than in treatments with UV. With an EED of 2.3 kWh/m^3, the removal was within the range of 51% to 95% (51 to 86 without steroid estrogens), while the range is from 20% to 99% for UV treatment. This may be due to that the mechanism of the removal with $^{\bullet}$OH radicals is nonselective, while the UV treatment depends upon the absorbance and quantum yield, which varies is a discrete property of each compound. The results of estrone (E1) are missing in Figure 4 due to analytical error. The increased removal when hydrogen peroxide was added is consistent with results obtained by Neamțu and Frimmel [15] and Chen et al. [14].

The estrogenic activity of the wastewater effluent treated by UV was measured by YES assay and was found to be 380 ng/L 17β-estradiol equivalents for the spiked wastewater and 15 ng/L 17β-estradiol equivalents for the lowest treatment intensity (2.3 kWh/m^3). Thus, even after the lowest treatment, almost all of the estrogenic activity was removed, and for the following treatments, some estrogenic activity was detected but below the quantification limit.

3.4. Electrical Energy Efficiency. As described in Section 2.8, the normalised concentration of the investigated chemicals was plotted against the electrical energy dose (Figure 6). The values of the EEO for the UV treatment were in the range 1.2–28.0 kWh/m^3 (Table 1). The compounds with lower values of EEO are easier to degrade than the one with higher value. The estrone (E1) was very sensitive towards UV light and has an EEO at 1.2 kWh/m^3. At the lowest treatment level (2.3 kWh/m^3), 99% of estrone was removed, and thus, the regression was made with only two points.

As mentioned, the addition of hydrogen peroxide to the UV treatment resulted in increased removal of the investigated compounds and thus lower energy consumption and lower EEO values (Table 1). Another benefit from addition of hydrogen peroxide was more uniform values of EEO for the investigated compounds. So the compounds with EEO values between 11.5 and 28 kWh/m^3 for UV treatment had a reduction of EEO to approximately 7-8 kWh/m^3 when adding 60 mg/L hydrogen peroxide.

For UV treatment, butylparaben (BP) was the chemical which was most difficult to be removed (EEO = 28.0 kWh/m^3), while for UV/H_2O_2, it was BPA and BP-7 (EEO = 8.7 kWh/m^3). Estrone (E1) would probably be the one that required the smallest amount of energy according to the tendency, but data is missing due to problem with the analysis. The lowest EEO obtained for the UV/H_2O_2 treatment was 1.8 kWh/m^3 (EE2).

The EEO for removal of estrogenic activity was estimated for UV treatment only and was in the same range as the EEOs obtained for 17β-estradiol and ethinyl estradiol. Thus, the measured estrogenic activity is mainly due to the two estrogens E2 and EE2. A previous study with Milli-Q water and approximately 5000-fold higher EE2 concentration removed the estrogenic activity (by YES assay) with the same rate as

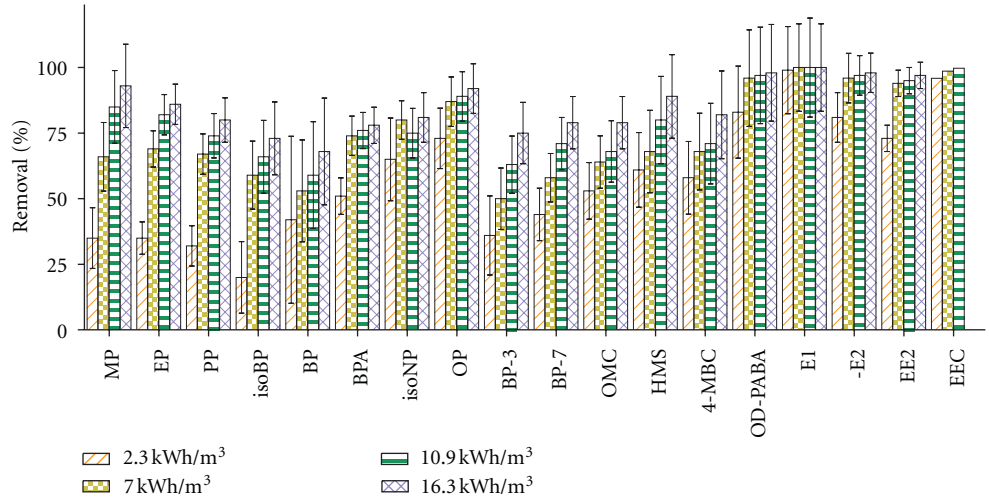

Figure 4: The removal of estrogenic compounds from wastewater effluent by photolysis. The error bars present the 95% confidence interval. The abbreviation can be found in Table 1.

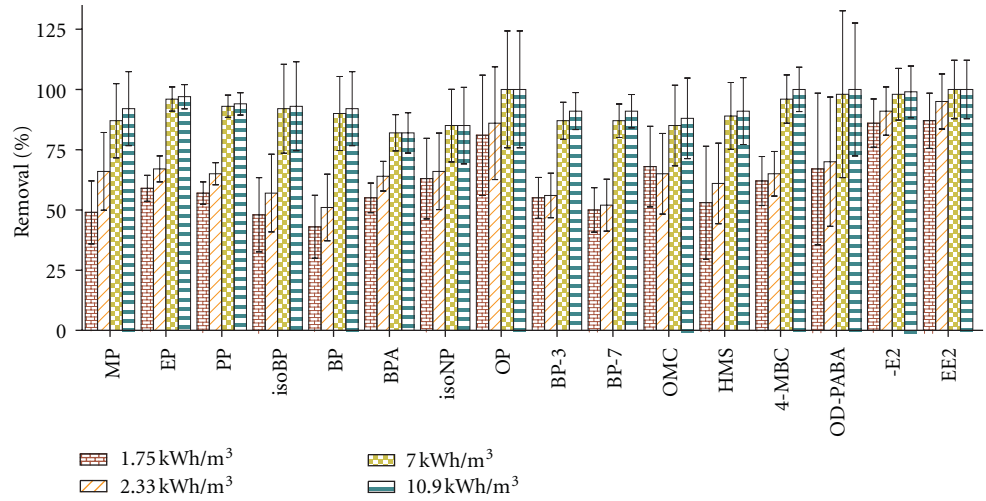

Figure 5: The removal of estrogenic compounds from wastewater effluent by UV/H_2O_2. The initial concentration of hydrogen peroxide was 60 mg/L. The error bars present the 95% confidence interval. The abbreviation can be found in Table 1.

their removal of EE2 by treatment with low-pressure UV and H_2O_2 [16]. Another study [20] was able to remove estrogenic activity by the same rate as the estrogenic compounds by ozonation, which is partially a radical oxidation reaction similar to the UV/H_2O_2 treatment. Consequently, the by-products formed from estrogenic compounds during UV and UV/H_2O_2 treatment do not have estrogenic activity.

3.5. Considerations on Economical Feasibility and Energy Efficiencies. The investigated compounds were all removed by direct UV and UV/H_2O_2. To consider the possibility of these methods to be applied in the wastewater treatment, the energy cost is compared to the current treatment cost.

The Danish Water and Wastewater Association has collected data from a number of treatment plants and calculated the cost of treating 1 m^3 wastewater. The Danish WWTPs can be divided into three groups depending on the size. Large treatment plants treat water from what corresponds to more than 100.000 person equivalent (PE), while medium-sized treatment plants are between 20.000 and 100.000 PE. The small treatment plants treat less than 20.000 PE. The average cost of treating 1 m^3 of wastewater in 2001 was 0.21 € and 0.27 € for large and medium treatment plans, respectively [24]. For small plant, the cost is approximately doubled (0.46 €/m^3). The wastewater treatment plants pay 0.11 €/kWh.

A stream containing numerous contaminants in low concentration requires an energy dose corresponding to the energy needed to remove the most resistant one [25]. For the estrogenic compounds, the most resistant chemical was BP with an EEO value of 28 kWh/m^3 when wastewater was treated with UV irradiation alone. By UV/H_2O_2, BPA and BP-7 required the highest amount of energy to be degraded (EEO = 8.7 kWh/m^3).

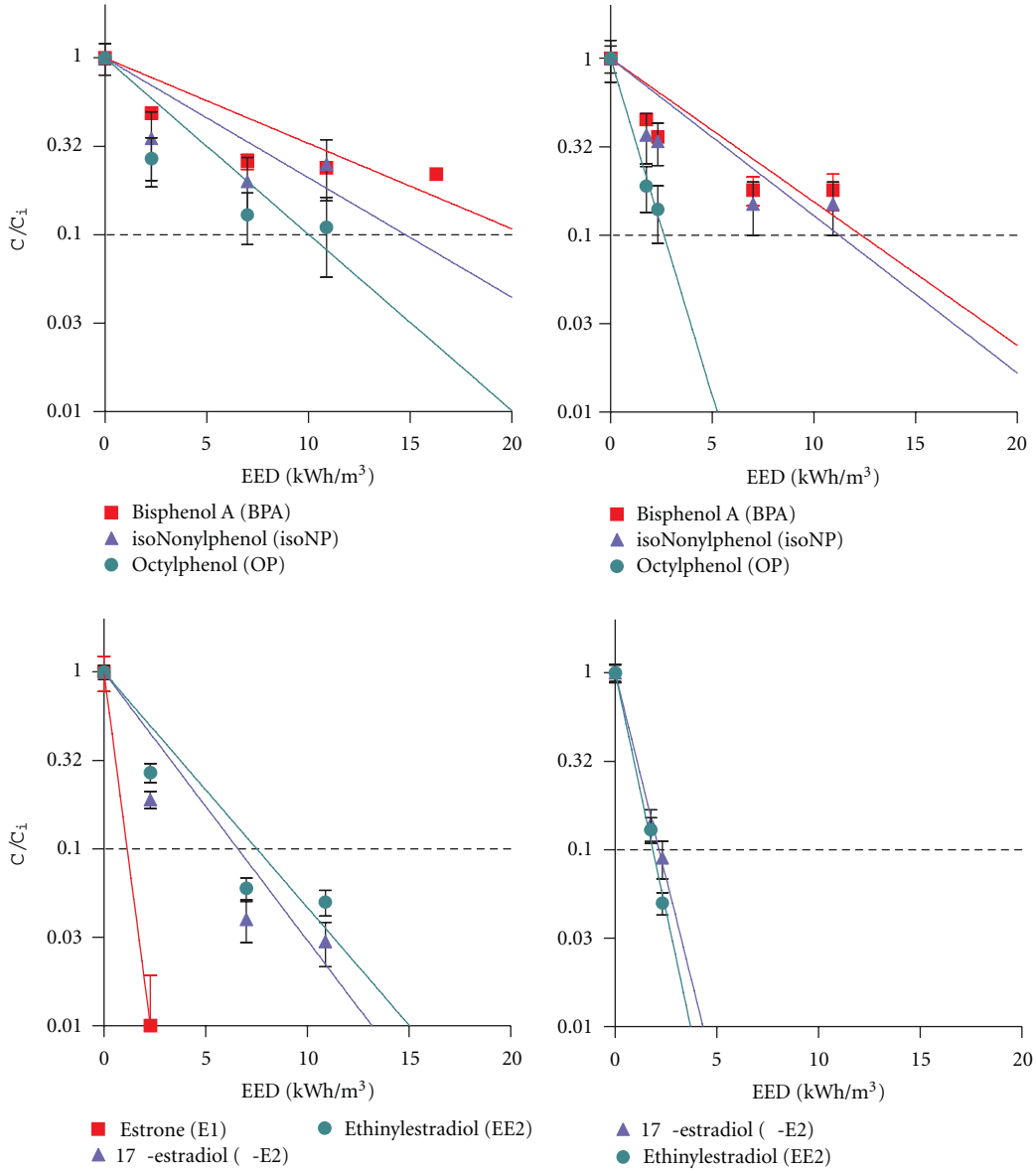

Figure 6: Degradation of selected estrogenic chemicals. Left: direct UV treatment. Right: UV/H_2O_2 treatment with a hydrogen peroxide concentration of 60 mg/L.

Addition of hydrogen peroxide reduced the energy consumption by approximately a factor of three which would be economically advantageous considering the price of electric energy and hydrogen peroxide in Denmark. A treatment with an electrical energy dose of 8.7 kWh/m^3 would remove 90% of the most resistant chemicals, whereas it will require 17.4 kWh/m^3 if the chemicals need to be removed by 99%.

Steroid estrogens are generally considered to be responsible for the majority of estrogenicity in WWTP effluents [6, 7]. Supposing only 90% removal of the steroid estrogens is required in order to achieve an acceptable water quality, a considerable energy reduction would be possible, since the steroid estrogens require less treatment. By the UV/H_2O_2 treatment, the most resistant of the steroid estrogens (E2) requires 2.2 kWh/m^3 to obtain 90% removal. At this level of treatment, the removal of the other compound with EEO in the range of 7-8 kWh/m^3 will be approximately 50% (calculated using (1)).

The cost of a treatment can be found by multiplying the cost of electricity with the value of EEO. Thus, the treatment with high energy consumption would cost 0.93 €/m^3, and if only the steroid estrogens should be removed, the cost of the electrical energy would be 0.24 €/m^3. Beside the cost of electricity, there will also be expenses for hydrogen peroxide and maintenance of equipment.

Comparing with alternative treatment solutions, the current best option for polishing wastewater for estrogenic chemicals is ozonation [20, 26–28]. The EEO for the same estrogenic chemicals, as are the subject of this paper, in treated wastewater from the same source, was described by

Hansen et al. [20]. In that study, the energy required to remove each estrogen by 90% with ozonation, when the energy to produce ozone and the energy required to produce the pure oxygen that is used by the ozone generator was also considered, was 0.14–0.90 kWh/m^3. In the same study, an effluent from another source that had a higher COD and UV-absorbance required energy in the range of 0.22–1.09 kWh/m^3 for removing the estrogens [20].

4. Conclusions

It was found that the water matrix influenced the removal of the investigated compounds. The organic and inorganic substances in wastewater acted as scavenger compound for the $^{\bullet}$OH radicals and blocked the pathway of the UV light. Furthermore, it was found that it is important to optimize the concentration of hydrogen peroxide, since a too low concentration of hydrogen peroxide results in decreased removal of the estrogenic chemicals, while a high hydrogen peroxide concentration may result in a decreasing degradation due to the formation of the less reactive $HO_2^{\bullet}$ radical.

Moreover, it was found that all estrogenic chemicals could be removed by photolysis with varied energy effectiveness and that UV/H_2O_2 reduced the spread between the energy effectiveness of removing the chemicals and lowered the electrical energy dose. Addition of an optimized concentration of hydrogen peroxide reduced the energy consumption by 2-3-fold, which would be economical considering the price of energy and the chemical in Denmark.

In general, it was found that the parabens, the industrial phenols, and the sunscreen chemicals required much higher UV dose than the steroid estrogens. BP was the estrogenic compound that required the highest UV dose to be degraded by direct photolysis, while by UV/H_2O_2, it was BPA and BP-7. Steroid estrogens, which are generally considered to be responsible for the bulk of estrogenicity in WWTP effluents, required the least amount of treatment for removal.

Considering only the energy consumption for the treatment, both UV and UV/H_2O_2 are considerable less effective solutions for removal of estrogenic chemicals in biologically treated wastewater compared to ozonation.

Acknowledgments

The Siemens Foundation, the EU Life Project, APOP, and the Danish Research Council Project, DanEd, are gratefully acknowledged for economic support to this work. Further, technical assistance with analysis by Karina Bomholt Henriksen is recognized. The lamp and photoreactor were a kind gift of Scan Research A/S, Herning, Denmark.

References

[1] C. E. Purdom, P. A. Hardiman, V. J. Bye, N. C. Eno, C. R. Tyler, and J. P. Sumpter, "Estrogenic effects of effluents from sewage treatment works," *Chemistry and Ecology*, vol. 8, no. 4, pp. 275–285, 1994.

[2] E. J. Routledge, D. Sheahan, C. Desbrow, G. C. Brighty, M. Waldock, and J. P. Sumpter, "Identification of estrogenic chemicals in STW effluent. 2. In vivo responses in trout and roach," *Environmental Science & Technology*, vol. 32, no. 11, pp. 1559–1565, 1998.

[3] P. Falås, H. R. Andersen, A. Ledin, and J. L. C. Jansen, "Occurrence and reduction of pharmaceuticals in thewater phase at Swedish wastewater treatment plants," *Water Science and Technology*, vol. 66, no. 4, pp. 783–791, 2012.

[4] H. Segner, K. Caroll, M. Fenske et al., "Identification of endocrine-disrupting effects in aquatic vertebrates and invertebrates: report from the European IDEA project," *Ecotoxicology & Environmental Safety*, vol. 54, no. 3, pp. 302–314, 2003.

[5] C. Desbrow, E. J. Routledge, G. C. Brighty, J. P. Sumpter, and M. Waldock, "Identification of estrogenic chemicals in STW effluent. 1. Chemical fractionation and in vitro biological screening," *Environmental Science & Technology*, vol. 32, no. 11, pp. 1549–1558, 1998.

[6] W. Körner, P. Spengler, U. Bolz, W. Schuller, V. Hanf, and J. W. Metzger, "Substances with estrogenic activity in effluents of sewage treatment plants in southwestern Germany. 2. Biological analysis," *Environmental Toxicology and Chemistry*, vol. 20, no. 10, pp. 2142–2151, 2001.

[7] P. Spengler, J. W. Metzger, and W. Körner, "Substances with estrogenic activity in effluents of sewage treatment plants in southwestern Germany. 1. Chemical analysis," *Environmental Toxicology and Chemistry*, vol. 20, no. 10, pp. 2133–2141, 2001.

[8] H. R. Andersen, M. Lundsbye, H. V. Wedel, E. Eriksson, and A. Ledin, "Estrogenic personal care products in a greywater reuse system," *Water Science and Technology*, vol. 56, no. 12, pp. 45–49, 2007.

[9] E. Eriksson, H. R. Andersen, and A. Ledin, "Substance flow analysis of parabens in Denmark complemented with a survey of presence and frequency in various commodities," *Journal of Hazardous Materials*, vol. 156, no. 1–3, pp. 240–259, 2008.

[10] E. Eriksson, H. R. Andersen, and A. Ledin, "Substance flow analysis and source mapping of chemical UV-filters," *Water, Air, and Soil Pollution*, vol. 8, no. 5-6, pp. 473–484, 2008b.

[11] K. O. Kusk, T. Krüger, M. Long et al., "Endocrine potency of wastewater: contents of endocrine disrupting chemicals and effects measured by in vivo and in vitro assays," *Environmental Toxicology and Chemistry*, vol. 30, no. 2, pp. 413–426, 2011.

[12] J. V. Brian, C. A. Harris, M. Scholze et al., "Accurate prediction of the response of freshwater fish to a mixture of estrogenic chemicals," *Environmental Health Perspectives*, vol. 113, no. 6, pp. 721–728, 2005.

[13] E. J. Rosenfeldt and K. G. Linden, "Degradation of endocrine disrupting chemicals bisphenol A, ethinyl estradiol, and estradiol during UV photolysis and advanced oxidation processes," *Environmental Science & Technology*, vol. 38, no. 20, pp. 5476–5483, 2004.

[14] P. J. Chen, K. G. Linden, D. E. Hinton, S. Kashiwada, E. J. Rosenfeldt, and S. W. Kullman, "Biological assessment of bisphenol A degradation in water following direct photolysis and UV advanced oxidation," *Chemosphere*, vol. 65, no. 7, pp. 1094–1102, 2006.

[15] M. Neamţu and F. H. Frimmel, "Degradation of endocrine disrupting bisphenol A by 254 nm irradiation in different water matrices and effect on yeast cells," *Water Research*, vol. 40, no. 20, pp. 3745–3750, 2006.

[16] Z. Zhang, Y. Feng, Y. Liu, Q. Sun, P. Gao, and N. Ren, "Kinetic degradation model and estrogenicity changes of EE_2 (17α-ethinylestradiol) in aqueous solution by UV and UV/H_2O_2

technology," *Journal of Hazardous Materials*, vol. 181, no. 1–3, pp. 1127–1133, 2010.

[17] D. BŁedzka, D. Gryglik, M. Olak, J. L. Gebicki, and J. S. Miller, "Degradation of n-butylparaben and 4-tert-octylphenol in H_2O_2/UV system," *Radiation Physics and Chemistry*, vol. 79, no. 4, pp. 409–416, 2010.

[18] J. R. Bolton, K. G. Bircher, W. Tumas, and C. A. Tolman, "Figures-of-merit for the technical development and application of advanced oxidation technologies for both electric- and solar-driven systems," *Pure and Applied Chemistry*, vol. 73, no. 4, pp. 627–637, 2001.

[19] T. Kosjek, H. R. Andersen, A. Ledin, E. Heath, and B. Kompare, "Fate of carbamazepine during water treatment," *Environmental Science & Technology*, vol. 43, no. 16, pp. 6256–6261, 2009.

[20] K. M. S. Hansen, H. R. Andersen, and A. Ledin, "Ozonation of estrogenic chemicals in biologically treated sewage," *Water Science and Technology*, vol. 62, no. 3, pp. 649–657, 2010.

[21] H. Andersen, H. Siegrist, B. Halling-Sørensen, and T. A. Ternes, "Fate of estrogens in a municipal sewage treatment plant," *Environmental Science & Technology*, vol. 37, no. 18, pp. 4021–4026, 2003.

[22] E. Heath, T. Kosjek, H. R. Andersen et al., "Inter-laboratory exercise on steroid estrogens in aqueous samples," *Environmental Pollution*, vol. 158, no. 3, pp. 658–662, 2010.

[23] E. J. Routledge and J. P. Sumpter, "Estrogenic activity of surfactants and some of their degradation products assessed using a recombinant yeast screen," *Environmental Toxicology and Chemistry*, vol. 15, no. 3, pp. 241–248, 1996.

[24] Danish Water and Wastewater Association, "Driftsforhold og nøgletal for spildevandsrenseanlæg 2001 (Translate to: Performance parameters and key numbers for wastewater treatment 2001)," A report in Danish, 2012, http://www.danva.dk/.

[25] Calgon Carbon Oxidation Technologies, *The AOT Handbook*, Calgon Carbon Corporation, Pittsburgh, Pa, USA, 2001.

[26] T. A. Ternes, J. Stüber, N. Herrmann et al., "Ozonation: a tool for removal of pharmaceuticals, contrast media and musk fragrances from wastewater?" *Water Research*, vol. 37, no. 8, pp. 1976–1982, 2003.

[27] M. M. Huber, A. Göbel, A. Joss et al., "Oxidation of pharmaceuticals during ozonation of municipal wastewater effluents: a pilot study," *Environmental Science & Technology*, vol. 39, no. 11, pp. 4290–4299, 2005.

[28] A. Joss, H. Siegrist, and T. A. Ternes, "Are we about to upgrade wastewater treatment for removing organic micropollutants?" *Water Science and Technology*, vol. 57, no. 2, pp. 251–255, 2008.

Hindawi Publishing Corporation
International Journal of Photoenergy
Volume 2012, Article ID 681875, 6 pages
doi:10.1155/2012/681875

Research Article

Electrochemical Incineration of Phenolic Compounds from the Hydrocarbon Industry Using Boron-Doped Diamond Electrodes

Alejandro Medel,[1] Erika Bustos,[1] Karen Esquivel,[1,2] Luis A. Godínez,[1] and Yunny Meas[1]

[1] *Centro de Investigación y Desarrollo Tecnológico en Electroquímica, S.C., Parque Tecnológico, Querétaro-Sanfandila, P.O. Box 064-76703, Pedro Escobedo, Querétaro, Mexico*
[2] *Facultad de Ingeniería, Universidad Autónoma de Querétaro, Cerro de las Campanas, C.P. 76000, Santiago de Querétaro, Querétaro, Mexico*

Correspondence should be addressed to Yunny Meas, yunnymeas@cideteq.mx

Received 18 May 2012; Revised 2 August 2012; Accepted 4 August 2012

Academic Editor: Manickavachagam Muruganandham

Electrochemical incineration using boron-doped diamond electrodes was applied to samples obtained from a refinery and compared to the photo-electro-Fenton process in order to selectively eliminate the phenol and phenolic compounds from a complex matrix. Due to the complex chemical composition of the sample, a pretreatment to the sample in order to isolate the phenolic compounds was applied. The effects of the pretreatment and of pH on the degradation of the phenolic compounds were evaluated. The results indicate that the use of a boron-doped diamond electrode in an electrochemical incineration process mineralizes 99.5% of the phenolic sample content. Working in acidic medium (pH = 1), and applying 2 A at 298 K under constant stirring for 2 hours, also results in the incineration of the reaction intermediates reflected by 97% removal of TOC. In contrast, the photo-electro-Fenton process results in 99.9% oxidation of phenolic compounds with only a 25.69% removal of TOC.

1. Introduction

Residual discharges from refineries are complex matrices of varied chemical composition. Among the most dangerous organic contaminants, phenol stands out as a highly toxic compound, which is also biorefractory [1–8]. A typical phenol concentration in industrial discharges from refineries oscillates within a range of 20–200 mg L^{-1} [3, 8, 9], although the actual concentration value can vary depending on the nature of the process [8]. A concentration in the range of 5–25 mg L^{-1} is as toxic for aquatic life as it is for humans [1, 2] and in response to this situation, the maximum permitted limits of phenol residues found in industrial discharges vary between 0.5 and 1.0 mg L^{-1} [2]. In the case of potable drinking water, the European Union (EU), in its 80/778/EC directive, assigned a maximum permitted limit of <0.0005 mg L^{-1} for phenol in all of its forms [1], given that the consumption of water containing these compounds can induce cancer or death [10]. The elevated danger of this contaminant for aquatic life has marked phenol and some phenolic compounds as priority contaminants, in agreement with the criteria of the Environmental Protection Agency (EPA) of the United States [1, 2].

The methods used in the treatment of wastewater for the elimination of phenol are separated into destructive [5, 10, 11] and nondestructive methods [1–4, 6, 12]. Among the destructive methods, biological processes are commonly used; however, no phenol degradation is observed at concentrations above 200 mg L^{-1}, and the microorganisms are completely deactivated at concentrations larger than 3000 mg L^{-1} [1]. Another disadvantage that is observed in some destructive methods is that the successful degradation of phenol results in the generation of subproducts that are harder to degrade [11]. Other processes with destructive character that have been largely studied are the Fenton processes (Fenton, photo-Fenton, electro-Fenton, and photoelectro-Fenton) and the electrochemical oxidation technologies. Considering the last approach, the efficiency of the electrochemical reaction depends highly on the identity of the anode, which can significantly influence the reaction mechanism [8, 13].

It has been demonstrated that electrochemical oxidation with electrodes of high overpotential for oxygen such as Ti/PbO_2, Ti/SnO_2-Sb, and Ti/BDD allows, with high current efficiency, the complete elimination of organic contaminants as well as their intermediate products. On the other hand, the application of the Fenton processes in the treatment of refinery water residues has also been evaluated [8]. Although these processes permit the degradation of the contaminant, the degradation of the intermediates is not particularly feasible [8]. Recently, electrochemical oxidation using boron-doped diamond (BDD) has won widespread acceptance due to the generation of hydroxyl radicals at high potentials, which are promoted in the interfacial zone through the water oxidation process (1). This allows the efficient degradation of the contaminant and of the subproducts of the reaction to CO_2 and H_2O (2), a process known as electrochemical incineration [13–16]

$$H_2O \longrightarrow {}^{\bullet}OH + H^+ + e^- \quad (1)$$

$$R + M({}^{\bullet}OH) \longrightarrow M + mCO_2 + nH_2O + H^+ + e^- \quad (2)$$

Although both technologies show high efficiency in studies with synthetic samples, few studies have been carried out on samples obtained from actual refineries, where the efficiency of the reaction might be reduced due to the complex chemical composition of the effluent. This was made evident by Yavuz and Koparal [7] who evaluated the electrochemical oxidation of phenol in a parallel plate reactor using a ruthenium mixed metal oxide electrode, obtaining phenol removal efficiencies of 99.7% and 94.5% in synthetic and actual samples, respectively. In terms of chemical oxygen demand (COD), values of 88.9% and 70.1% were obtained for synthetic and actual samples, respectively, showing the effects of the chemical composition of actual discharge effluents. In another study, the degradation of phenol with Ti/TiO_2-RuO_2-IrO_2 from refinery samples showed only 74.75% and 48% removal of COD and TOC, respectively, although high quantities of chloride ions were employed [9]. However, these results should not be surprising, considering the composition of the sample and the natural activity of the electrodes. On the other hand, the use of Ti/RuO_2-TiO_2-SnO_2 in the treatment of hydrocarbon industry discharges has recently been evaluated, but the removal efficiency under the evaluated conditions was very low, 20%–47% [17]. Recently a comparative analysis was reported between Ti/BDD and the electro-Fenton approach in actual samples from refineries, indicating that the electro-Fenton process showed a better degradation of phenol in comparison to BDD, although the better degradation of the reaction intermediates (in terms of COD) occurred using BDD [8].

Previous works have shown the complexity that involves the treatment of wastewater from an actual discharge. However, they have also shown that the electrochemical oxidation with BDD seems to be a superior method, ahead of other technologies, given its capacity to incinerate many organic compounds as well as their reaction intermediates. In this work, we evaluate the selective degradation of phenolic compounds in actual samples from a refinery. The objective was to evaluate and compare the efficiency of the degradation of phenolic compounds with boron-doped diamond and with the photoelectro-Fenton process, applying an adequate pretreatment of the sample that allows the selective degradation of these contaminants.

2. Experimental Details

2.1. Characterization and Pretreatment of the Samples Obtained from the Refinery for Selective Degradation of Phenolic Compounds. Four different samples were obtained from a refinery and stored at 4°C before analysis. The determination of pH was performed with a Corning 450 potentiometer that was equipped with a Pinnacle glass electrode.

To avoid any interference that could reflect the presence of other contaminants in the electrochemical degradation of phenolic compounds, 4.5 L of each sample obtained from the refinery were treated with 10% NaOH in order to completely isolate the phenolic compounds from the original matrix. In this process, the selective isolation of phenolic compounds is carried out by the chemical conversion of phenols to phenolates. During this process 2 phases were obtained, one high-density aqueous phase and another with low density. Both samples were then stirred and after dichloromethane extraction, analyzed by GC-MS to identify the main components and to verify the effectiveness of the pretreatment. This analysis was performed using an Agilent 6890 Gas Chromatographer coupled to a 5973 N Mass Spectrometer. A HP-5 MS column (dimensions 30 m × 0.25 mm, 0.25 μm) was used with a stationary phase of 5% phenyl-methyl-siloxane. The carrier gas was helium grade 5 (UAP). The injection of the sample was performed in split mode 5 : 1, with a flow of 0.7 mL min^{-1}. The temperature of the injector was 543K, with an initial oven temperature of 323K (that was maintained for 4 minutes) and a ramp rate of 282K per minute until reaching a stable temperature of 573K for 6 minutes, for a total time of 37.78 minutes. Quantitative analysis of phenolic compounds of the preprocessed samples was performed using the 4-aminoantipyrine method [18]. Using this technique, the detection of phenolic compounds is carried out in their total form.

2.2. Electrochemical Incineration Using Boron-Doped Diamond. After accomplishing the chemical conversion of phenols to phenolates (aqueous phase with high density), three representative samples were taken to a specific pH value for their evaluation in alkaline, neutral, and acid conditions using HCl (Aldrich, analytical grade). These samples were subjected to electrolysis under galvanostatic conditions in a one-compartment electrolytic cell, with a capacity of 100 mL. The anode was boron-doped diamond (6.2 cm^2) and the cathode was Ti (12.5 cm^2). The system was operated at room temperature, with continuous stirring using a magnetic bar. All the experiments were carried out twice in order to confirm reproducibility. The degradation of phenol was monitored using the 4-aminoantipyrine method [18], and the degradation of the intermediates was evaluated through the analysis of total organic carbon (TOC), using a Shimadzu piece of equipment (Model TOC-VCSN). The removal

percentages of TOC and phenol were calculated according to (3), where C_i is the initial ($mg\,L^{-1}$) and C_f is the final concentration ($mg\,L^{-1}$) [19, 20]

$$\%\ \text{removal} = \frac{C_i - C_f}{C_i} \times 100. \quad (3)$$

2.3. Electrolysis with A Photo-Electro-Fenton System. The electrochemical destruction of phenolic compounds with the photoelectro-Fenton system was performed using a carbon fiber $+TiO_2$ anode and a nonmodified carbon fiber as cathode. A current of 0.2 A was imposed to the system for 2 hours, which contained 800 mL of waste water (aqueous phase with high density). The pH was fixed at 3 (adjusted with H_2SO_4). The previously O_2 saturated solution (30 minutes) was radiated with UV ligth ($\lambda = 365$ nm) using a lamp with a power output of $0.71\,\mu w\,cm^{-2}$. In order to promote the generation of the Fenton reagent, 0.05 M $Fe(SO_4)$ was added to the system. The electrolysis was performed at room temperature (20°C), with continuous agitation using a magnetic stirrer [21, 22].

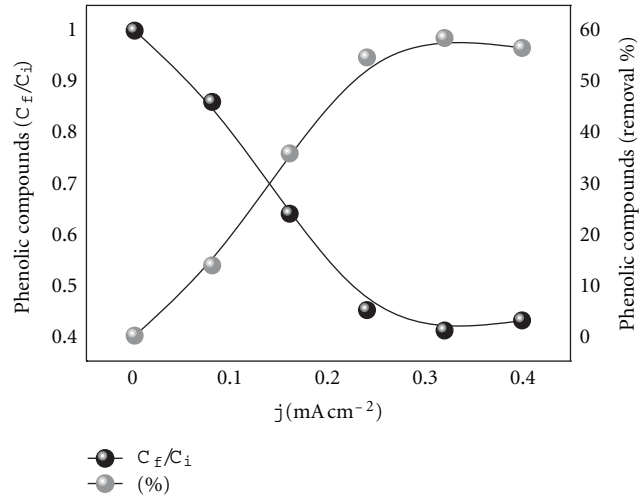

Figure 1: Electro-oxidation of a synthetic solution containing 311 $mg\,L^{-1}$ of phenol in acid solution (pH 1) after the application of different current densities, using BDD and Ti as anode and cathode, respectively. The results are shown as normalized values (left) and percentages of degradation (right).

3. Results and Discussion

3.1. Characterization and Pretreatment of the Samples Obtained from the Refinery for Selective Degradation of Phenolic Compounds. The pH of the samples (without any treatment) was 14. This pH value is related to the nature of the process, given that phenol is commonly used to synthesize chemical products in basic solutions [5]. Therefore, it is expected that the discharge has an alkaline pH. In order to ensure complete conversion of phenolic compounds to sodium phenolates, we proceeded to treat the samples using 10% NaOH. The GC-MS analysis of the pretreated samples showed that in the low-density aqueous phase, the principal components (qualitative analysis) were of aliphatic types (4-methyl-decane, undecane, nonane, tridecane, tetradecane, decane, dodecane, pentacosane, and tricosane). In this analysis, the presence of phenolic compounds was not identified. The absence of phenolic compounds in the low density aqueous phase showed the effectiveness of the pretreatment. This result was verified with the chromatographic analysis of the high-density aqueous phase, where the phenolic compounds (2,4-dimethyl-phenol, 2-methyl-phenol, o-cresol, 3-methyl-phenol, m-cresol, 1-methyl-phenol, p-cresol, 3,5-dimethyl-phenol, 3-ethyl-5-methyl-phenol, 4-benzyl-pyridacine, dibenzothiophene, 4-methyl-phenol, 2,4,6-trimethyl-phenol, 3-metoxy (methyltio)-phenol, 1-methyl-3-phenoxy-benzene) were found. These results were expected considering that the chemical conversion process of phenol to phenolate in strongly alkaline conditions begins at pH 10 and reaches a maximum efficiency at pH 12 [23].

3.2. Electrolysis Using Boron-Doped Diamond. Before performing the degradation experiments, a preliminary analysis using a synthetic solution with a phenol concentration of 311 $mg\,L^{-1}$ was carried out in an alkaline solution, with the goal of identifying the current to be applied. The currents evaluated were 0.5, 1.0, 1.5, 2.0, and 2.5 A, for a 2-hour period, under constant stirring. It was observed that the middle point of the removal was reached at 2 A ($j = 0.32\,A\,cm^{-2}$), as shown in Figure 1. Since in aqueous solution phenols exist as phenolates (phenoxide anions) with the degree of the dissociation increasing with the pH (pH above 12), a pH adjustment to acidic conditions was performed in order to favor the inverse process. Considering that full protonation should take place in the range of pH 2–4 [23] and that the efficiency in the electrochemical oxidation of phenolic compounds and phenol is better in the 0–3 pH range [24, 25], three different values of pH (1, 7 y 14) were evaluated applying the current density selected with the synthetic sample experiments (2 A). The concentrations of phenolic compounds in each sample were 1411, 1976, and 5928 $mg\,L^{-1}$ for the pH values of 1, 7, and 14, respectively. The effect of the pH on the degradation process at 60 minutes is shown in Figure 2. The results show that the best degradation occurred at pH 1, followed by pH 7 and pH 14. The percentages of degradation were 40, 14, and 12%, respectively. After 120 minutes at pH 1, the efficiency of removal was greater than that of pH 7, with an initial concentration of 1411 $mg\,L^{-1}$ and a final concentration of 6.5 $mg\,L^{-1}$, representing a removal percentage of 99.5%, in comparison to 61.9% at pH 7. These results agree with those reported in the literature, where the efficiency of degradation is favored in acidic condition [26]. Under basic conditions on the other hand, the removal of phenolic compounds was not efficient even with an increase in electrolysis time. The influence of pH on the removal of TOC (Figure 3) was also conclusive, showing that at a pH of 1 the removal of TOC proceeded to 97%, with an initial value of 18200 $mg\,L^{-1}$ and a final value of 553 $mg\,L^{-1}$. This behavior was verified before the electrochemical treatment at different pH values, where it was observed that the sample changed its color

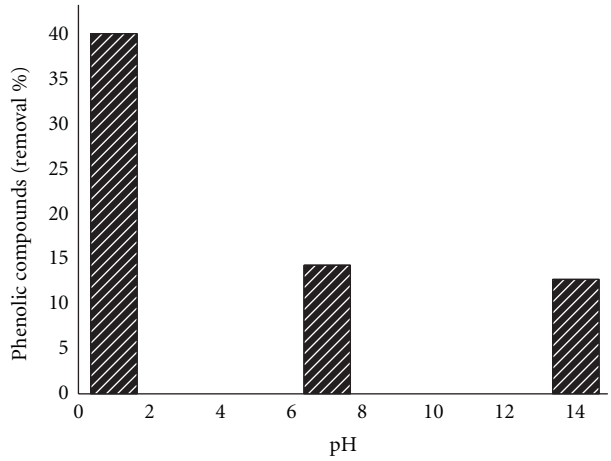

Figure 2: Removal of phenolic compounds in pretreated industrial samples at different pH values (1, 7, and 14), under constant stirring, using BDD and Ti as anode and cathode. 2 A (j = 0.32 A cm^{-2}) for 60 minutes of electrolysis were applied.

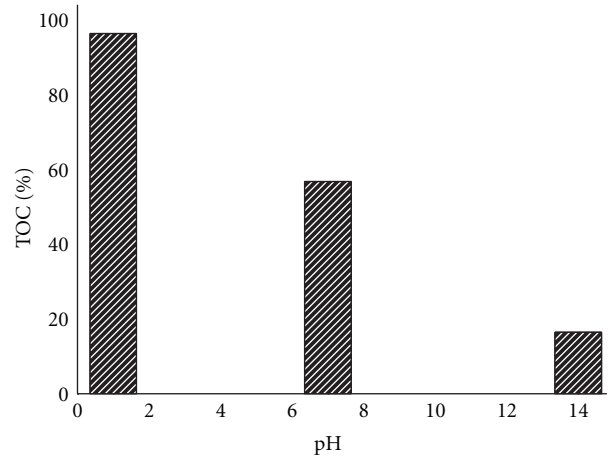

Figure 3: TOC values before and after the electrochemical oxidation process using BDD, at different pH values (1, 7, and 14), applying 2 A (j = 0.32 A cm^{-2}) of current over 2 hours in pretreated industrial samples.

with the progression of the reaction (with agitation at 298K) during 2 hours (Figure 4). While at pH 14, the color of the solution was practically the same, at pH 7 and pH 1, the color in the solution disappeared. Similar results on the effect of the pH were obtained by Wei et al. [27] who evaluated the use of electrochemical technology as pretreatment of heavy oil refinery wastewater. Their results showed a similar effect of the pH, indicating that the better removal occurs under acidic medium, followed by neutral and alkaline conditions. The consistent pH effect observed in this work can be explained by considering that in an acidic environment oxygen evolution is inhibited, thus, improving the oxidation process [27]. The low efficiency of the process under alkaline conditions on the other hand, can be explained by considering that during the electrolysis, the creation of CO_2 allows the formation of carbonates and bicarbonates (4), well known scavengers of hydroxyl radicals [28] as represented by (5) [29]

$$\begin{aligned} CO_2 + NaOH &\longrightarrow NaHCO_3 \\ NaHCO_3 + NaOH &\longrightarrow Na_2CO_3 \end{aligned} \quad (4)$$

$$\begin{aligned} {}^{\bullet}OH + {CO_3}^{2-} &\longrightarrow OH^- + CO_3^{\bullet -} \\ {}^{\bullet}OH + HCO_3^- &\longrightarrow H_2O + CO_3^{\bullet -} \end{aligned} \quad (5)$$

In addition, an alkaline environment can reduce the overpotential for oxygen evolution [30], thus resulting in a low reaction efficiency.

3.3. Electrolysis with A Photoelectro-Fenton System. For the photoelectro-Fenton system, an initial phenolic compounds concentration of 3471 mg L^{-1} became a final concentration of 2.09 mg L^{-1}, demonstrating the effectiveness of the phenol degradation process with a removal of 99.9%. In this case the TOC removal (Figure 5) was not as significant as in the case of the BDD approach, with only 25.7% removal after 120 minutes.

These results are in agreement with literature reports, where it has been demonstrated that the application of a photoelectro-Fenton process in water residues from refineries can produce 98.7% removal of phenol and 75.7% removal of COD, taking into account that the efficiency of the reaction can be improved in the photoelectro-Fenton process [28], which can also have synergistic photolysis effects. The results obtained using BDD were also consistent with the literature, where the removal of phenol has been reported to be 99.53% with a 96.04% removal of COD [8]. The feasibility of the use of the BDD in the treatment of complex wastewater effluents has also been demonstrated by Rocha et al., who obtained high efficiencies from the electrochemical oxidation process [31]. With these results, the electro-oxidation of phenol using boron-doped diamond is proven to be more effective in removing both phenol and TOC, in contrast to the photoelectron-Fenton system, where only a fourth of the total TOC content is removed. This study, therefore, supports BDD as a viable solution for eliminating phenol and other organic compounds from refinery wastewater.

4. Conclusions

The selective degradation of phenolic compounds in samples obtained from the hydrocarbon industry by electrochemical oxidation with BDD was successfully achieved. The degradation of phenolic compounds proceeded with a 97% of removal of TOC by applying a 2 A (j = 0.32 A cm^{-2}) current for 2 hours at 297 K under constant stirring and acidic conditions. In addition, the use of BDD as an anode in the electro-oxidation of phenol in acidic conditions was found to be the best alternative for obtaining the highest removal of intermediates, in contrast to the photoelectro-Fenton system for which, following literature conditions, only 25.7% of TOC was removed. From these results, the use of BDD is

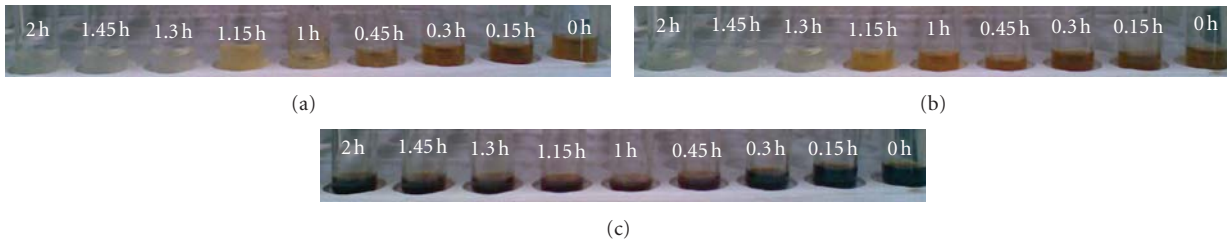

Figure 4: Images of industrial samples treated with BDD applying 2 A ($j = 0.32\,\mathrm{A\,cm^{-2}}$) of current over 2 hours, with constant stirring at pH (a) 1, (b) 7, and (c) 14.

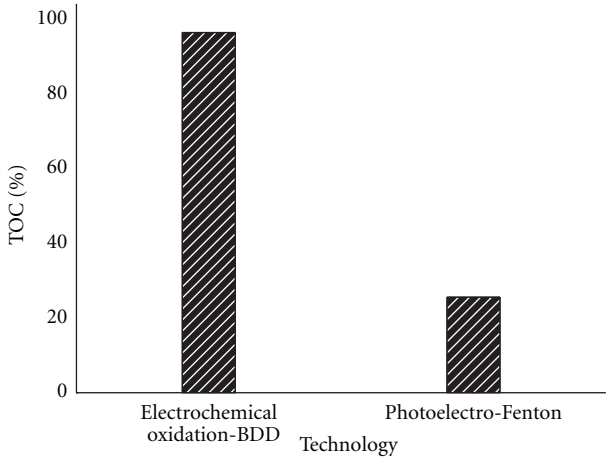

Figure 5: TOC values after 120 minutes of reaction time employing the photo-electron-Fenton process, using carbon fiber modified with TiO_2 in the presence of $120\,\mathrm{mg\,L^{-1}}$ of H_2O_2 and 0.5 mM $Fe(SO_4)_2$ at pH 3, with an application of radiation at 365 nm with a lamp of $0.71\,\mu\mathrm{W\,cm^{-2}}$. The solution was pre-saturated with oxygen.

confirmed as a viable approach for the elimination of recalcitrant organic contaminants in water effluents generated by the refineries.

Acknowledgments

The authors thank the Mexican Council of Science and Technology (CONACyT) for the financing granted for the implementation of this study through the Sector Research Fund for Education-Basic Science-84955 and the Joint Fund of the State Government of Veracruz Llave-96313. A. Medel thanks CONACyT for the fellowship granted.

References

[1] H. Jiang, Y. Fang, Y. Fu, and Q. X. Guo, "Studies on the extraction of phenol in wastewater," *Journal of Hazardous Materials*, vol. 101, no. 2, pp. 179–190, 2003.

[2] Y. Han, X. Quan, S. Chen, H. Zhao, C. Cui, and Y. Zhao, "Electrochemically enhanced adsorption of phenol on activated carbon fibers in basic aqueous solution," *Journal of Colloid and Interface Science*, vol. 299, no. 2, pp. 766–771, 2006.

[3] H. Polat, M. Molva, and M. Polat, "Capacity and mechanism of phenol adsorption on lignite," *International Journal of Mineral Processing*, vol. 79, no. 4, pp. 264–273, 2006.

[4] A. Bódalo, J. L. Gómez, M. Gómez, G. León, A. M. Hidalgo, and M. A. Ruíz, "Phenol removal from water by hybrid processes: study of the membrane process step," *Desalination*, vol. 223, no. 1–3, pp. 323–329, 2008.

[5] H. Ma, X. Zhang, Q. Ma, and B. Wang, "Electrochemical catalytic treatment of phenol wastewater," *Journal of Hazardous Materials*, vol. 165, no. 1–3, pp. 475–480, 2009.

[6] X. Hao, M. Pritzker, and X. Feng, "Use of pervaporation for the separation of phenol from dilute aqueous solutions," *Journal of Membrane Science*, vol. 335, no. 1-2, pp. 96–102, 2009.

[7] Y. Yavuz and A. S. Koparal, "Electrochemical oxidation of phenol in a parallel plate reactor using ruthenium mixed metal oxide electrode," *Journal of Hazardous Materials*, vol. 136, no. 2, pp. 296–302, 2006.

[8] Y. Yavuz, A. S. Koparal, and Ü. B. Öğütveren, "Treatment of petroleum refinery wastewater by electrochemical methods," *Desalination*, vol. 258, no. 1–3, pp. 201–205, 2010.

[9] D. Rajkumar and K. Palanivelu, "Electrochemical treatment of industrial wastewater," *Journal of Hazardous Materials*, vol. 113, no. 1–3, pp. 123–129, 2004.

[10] A. Nuhoglu and B. Yalcin, "Modelling of phenol removal in a batch reactor," *Process Biochemistry*, vol. 40, no. 3-4, pp. 1233–1239, 2005.

[11] Y. Liu, "Simultaneous oxidation of phenol and reduction of Cr(VI) induced by contact glow discharge electrolysis," *Journal of Hazardous Materials*, vol. 168, no. 2-3, pp. 992–996, 2009.

[12] A. V. Radushev, A. V. Plotnikov, and V. N. Tyryshkina, "Regeneration methods of decontamination of phenol-containing waste waters," *Theoretical Foundations of Chemical Engineering*, vol. 42, no. 5, pp. 781–794, 2008.

[13] C. Comninellis, "Electrocatalysis in the electrochemical conversion/combustion of organic pollutants for waste water treatment," *Electrochimica Acta*, vol. 39, no. 11-12, pp. 1857–1862, 1994.

[14] P. A. Michaud, M. Panizza, L. Ouattara, T. Diaco, G. Foti, and C. Comninellis, "Electrochemical oxidation of water on synthetic boron-doped diamond thin film anodes," *Journal of Applied Electrochemistry*, vol. 33, no. 2, pp. 151–154, 2003.

[15] G. Chen, "Electrochemical technologies in wastewater treatment," *Separation and Purification Technology*, vol. 38, no. 1, pp. 11–41, 2004.

[16] B. Marselli, J. Garcia-Gomez, P. A. Michaud, M. A. Rodrigo, and C. Comninellis, "Electrogeneration of hydroxyl radicals on boron-doped diamond electrodes," *Journal of the Electrochemical Society*, vol. 150, no. 3, pp. D79–D83, 2003.

[17] A. M. Z. Ramalho, C. A. Martínez-Huitle, and D. R. D. Silva, "Application of electrochemical technology for removing petroleum hydrocarbons from produced water using a DSA-type anode at different flow rates," *Fuel*, vol. 89, no. 2, pp. 531–534, 2010.

[18] Norma Mexicana NMX-AA-050-SCFI-2001, "Análisis de agua-Determinación de fenoles Totales en aguas naturales, potables, residuales y residuales tratadas".

[19] O. Abdelwahab, N. K. Amin, and E. S. Z. El-Ashtoukhy, "Electrochemical removal of phenol from oil refinery wastewater," *Journal of Hazardous Materials*, vol. 163, no. 2-3, pp. 711–716, 2009.

[20] A. Idris and K. Saed, "Degradation of phenol in wastewater using anolyte produced from electrochemical generation of brine solution," *Global Nest*, vol. 4, pp. 139–144, 2002.

[21] J. M. Peralta-Hernández, Y. Meas-Vong, F. J. Rodríguez, T. W. Chapman, M. I. Maldonado, and L. A. Godínez, "In situ electrochemical and photo-electrochemical generation of the fenton reagent: a potentially important new water treatment technology," *Water Research*, vol. 40, no. 9, pp. 1754–1762, 2006.

[22] J. M. Peralta-Hernández, J. Manríquez, Y. Meas-Vong et al., "Photocatalytic properties of nano-structured TiO_2-carbon films obtained by means of electrophoretic deposition," *Journal of Hazardous Materials*, vol. 147, no. 1-2, pp. 588–593, 2007.

[23] T. Poznyak, R. Tapia, J. Vivero, and I. Chairez, "Effect of pH to the decomposition of aqueous phenols mixture by ozone," *Journal of the Mexican Chemical Society*, vol. 50, pp. 28–35, 2006.

[24] J. L. Nava, F. Núñez, and I. González, "Electrochemical incineration of p-cresol and o-cresol in the filter-press-type FM01-LC electrochemical cell using BDD electrodes in sulfate media at pH 0," *Electrochimica Acta*, vol. 52, no. 9, pp. 3229–3235, 2007.

[25] L. Wei, S. Guo, G. Yan, C. Chen, and X. Jiang, "Electrochemical pretreatment of heavy oil refinery wastewater using a three-dimensional electrode reactor," *Electrochimica Acta*, vol. 55, no. 28, pp. 8615–8620, 2010.

[26] B. Boye, E. Brillas, B. Marselli et al., "Electrochemical incineration of chloromethylphenoxy herbicides in acid medium by anodic oxidation with boron-doped diamond electrode," *Electrochimica Acta*, vol. 51, no. 14, pp. 2872–2880, 2006.

[27] L. Wei, S. Guo, G. Yan, C. Chen, and X. Jiang, "Electrochemical pretreatment of heavy oil refinery wastewater using a three-dimensional electrode reactor," *Electrochimica Acta*, vol. 55, no. 28, pp. 8615–8620, 2010.

[28] A. L. N. Mota, L. F. Albuquerque, L. T. C. Beltrame, O. Chiavone-Filho, A. Machulek, and C. A. O. Nascimento, "Advanced oxidation processes and their application in the petroleum industry: a review," *Brazilian Journal of Petroleum and Gas*, vol. 2, pp. 122–142, 2008.

[29] D. Wu, M. Liu, D. Dong, and X. Zhou, "Effects of some factors during electrochemical degradation of phenol by hydroxyl radicals," *Microchemical Journal*, vol. 85, no. 2, pp. 250–256, 2007.

[30] D. Reyter, D. Bélanger, and L. Roué, "Nitrate removal by a paired electrolysis on copper and Ti/IrO_2 coupled electrodes—Influence of the anode/cathode surface area ratio," *Water Research*, vol. 44, no. 6, pp. 1918–1926, 2010.

[31] J. H. B. Rocha, M. M. S. Gomes, N. S. Fernandes, D. R. Da Silva, and C. A. Martínez-Huitle, "Application of electrochemical oxidation as alternative treatment of produced water generated by Brazilian petrochemical industry," *Fuel*, vol. 96, pp. 80–87, 2012.

Hindawi Publishing Corporation
International Journal of Photoenergy
Volume 2012, Article ID 121239, 8 pages
doi:10.1155/2012/121239

Research Article

Preparation of a Modified PTFE Fibrous Photo-Fenton Catalyst and Its Optimization towards the Degradation of Organic Dye

Zhizhong Ding,[1] Yongchun Dong,[1,2] and Bing Li[1]

[1] *Division of Textile Chemistry & Ecology, School of Textiles, Tianjin Polytechnic University, 399 Binshui Western Road, Xiqing District, Tianjin 300387, China*
[2] *State Key Laboratory Breeding Base of Photocatalysis, Fuzhou University, Fuzhou 350002, China*

Correspondence should be addressed to Yongchun Dong, dyefib@yahoo.com.cn

Received 22 May 2012; Accepted 30 July 2012

Academic Editor: Meenakshisundaram Swaminathan

Polytetrafluoroethylene (PTFE) fiber was grafted with acrylic acid to impart the carboxyl groups onto the fiber surface, which were used to coordinate with both transition metal ions Fe(III) and Cu(II) and a rare metal ion Ce(III) to prepare the metal grafted PTFE fiber complexes as the novel heterogeneous Fenton catalysts for the degradation of the azo dye in water under visible irradiation. Some factors affecting the preparation process, such as nature and concentration of metal ions in the coordination solution, grafting degree of PTFE and reaction temperature were optimized with respect to the content and strength of metal fixation on the fiber and dye degradation efficiency. The results indicated that increasing metal ion concentrations in solution and grafting degree of PTFE fiber as well as higher coordination temperature led to a significant increase in metal content, especially Fe(III) and Cu(II) content of the complexes. Fe(III) ions fixed on the fiber showed the better catalytic performance than Cu(II) and Ce(III) ions fixed when three different complexes with similar metal content being employed, respectively. Moreover, Increasing Fe content or incorporation of Cu(II) ions could significantly improve the catalytic activity of the complexes.

1. Introduction

Dye-containing wastewater from different industrial fields is a principal source of environmental contamination. And these dyes are known to be largely nonbiodegradable and toxic to aquatic plants and animals. In recent years, heterogeneous Fenton process has become a research focus in the treatment of these dyes in water because of its application over a wide pH range and easy separation of the catalyst after the reaction. The modified polyacrylonitrile (PAN) fiber Fe complexes have been regarded as the attractive heterogeneous Fenton catalysts with low cost and high effectiveness [1–5]. However, it was reported that the modifications, especially amidoximation can lead to a significant decrease in the mechanical performance of PAN fiber. Moreover, the tensile strength of the amidoximated PAN fiber was found to be further lower after coordinating with Fe ions in our previous work [2, 6]. This may limit its commercial applications in the future because good mechanical performance is necessary for effective using of the fibers as the catalysts for Fenton system.

Polytetrafluoroethylene (PTFE) fiber has received more and more attention in the past decades because of their outstanding thermal, chemical stability, and mechanical properties even under very harsh conditions [7–9]. In recent years, there have been many reports of using modified PTFE fibers and films containing functional groups for the concentration and separation of metal ions from aqueous media [10–12]. However, little attention has been paid to the heterogeneous Fenton catalyst produced by PTFE modification and metal coordination and its catalytic property for degradation of organic dye. Therefore, our investigations have been directed to the preparation of a fibrous PTFE catalyst with both good catalytic activity and mechanical strength. In this work, the influence of grafting degree of PTFE fiber, nature, and concentration of metal ion in the coordination solution and reaction temperature was optimized with respect to the content and strength of metal

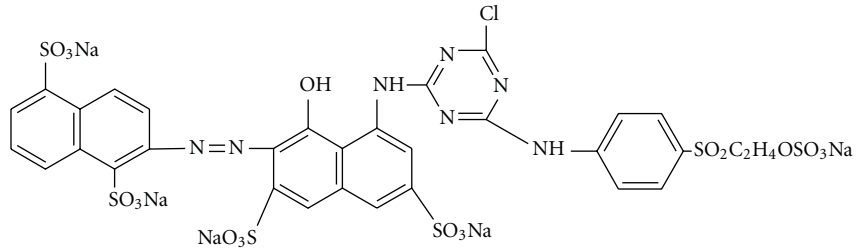

Scheme 1: Chemical structure of RR 195.

fixation on the fiber and decomposition efficiency of organic dye in aqueous solutions.

2. Experimental

2.1. Materials and Reagents. PTFE fibers were commercially available and provided by Fuxin Sengfuli Polymer Materials Co., China. Acrylic acid, hydrogen peroxide (30%, w/w), and ammonium ferrous sulphate were of analytical grade. $FeCl_3 \cdot 7H_2O$, $CuSO_4 \cdot 5H_2O$ and $CeCl_3 \cdot 7H_2O$ were used as the metal ions sources, respectively. Horseradish peroxidase (POD), N,N-diethyl-p-phenylene-deamine (DPD) and Reactive Red 195 (abbr. RR 195) was of laboratory agent grade and used without further purification. RR 195 was a typical azo dye and its molecular structure is presented in Scheme 1. Double distilled and deionized water was used throughout the study.

2.2. Preparation of Metallic Modified PTFE Fiber Complexes

2.2.1. Graft Polymerization of PTFE Fibers. Before modification, PTFE fibers were treated with acetone at room temperature for 30 min, and then dried in a vacuum oven at 50°C for 48 h. 10.0 g of the dried fibers was immersed into the monomer solution containing 100 mL acrylic acid and 200 mL deionized water in a 500 mL flask. 3.0 wt% ammonium ferrous sulphate was also used in the monomer solution to minimize the homopolymerization of acrylic acid during the reaction. The flask containing the monomer solution and fibers was bubbled with nitrogen for 20 min to remove oxygen and sealed. The mixture in the flask was directly subjected to gamma-rays of irradiation from a ^{60}Co source at a dose rate of 0.5 $kGyh^{-1}$ for a given time. After irradiation, the grafted PTFE fibers (denoted as PAA-g-PTFE) were took out and washed with hot water, and acetone repeatedly to remove the residual monomer, homopolymers adhered to the fiber surface. Finally, the obtained grafted fibers were dried in a vacuum oven at 50°C for 24 h and weighed. The grafting degree was obtained using the following formula: $G_f\% = (W_g/W_o - 1) \times 100\%$, where W_o and W_g are the weights of the original and grafted fibers, respectively. It was noticed that the breaking strength of the original PTFE fiber was measured to be 93.35 CN, and little decrease in its breaking strength was observed after the polymerization.

2.2.2. Transition Metal PAA-g-PTFE Complexes. 5.0 g of PAA-g-PTFE was immersed in 150 mL of $FeCl_3$ or $CuSO_4$ aqueous solution, and then the mixture was treated at 50°C and pH 2.0-3.0 for a given time under continuous agitation. The resulting fibrous metal complexes were filtered, washed with deionized water and dried under vacuum at 60°C for 4.0 h to obtain Fe(III-) grafted PTFE fiber complexes (denoted as Fe-PAA-g-PTFE) or Cu(II-) grafted PTFE fiber complexes (denoted as Cu-PAA-g-PTFE). The residual concentrations of Fe(III) or Cu(II) ions in the solutions after coordination were determined by using a WXF120 atomic absorption spectrometry (Beijing Rayleigh Analytical Instrument Corp., China) for calculating the Fe content ($Q_{\text{Fe-PTFE}}$) or Cu content ($Q_{\text{Cu-PTFE}}$) of the complexes.

2.2.3. Rare Metal PAA-g-PTFE Complexes. The complexes were prepared similarly to the transition metal PAA-g-PTFE complexes by using $CeCl_3$ in the coordination solution. And the final complexes were denoted as Ce-PAA-g-PTFE. The Ce content ($Q_{\text{Ce-PTFE}}$) of the complexes was measured and calculated by determining the residual Ce(III) ions in solution after coordination through a Na_2-EDTA-based titrimetric method.

2.2.4. Cu-Fe Bimetallic PAA-g-PTFE Complexes. These complexes were also synthesized similarly to monometallic PAA-g-PTFE complexes by using the mixed coordination solutions containing different concentration of Fe(III) and Cu(II) ions during the coordination processes. Cu-Fe bimetallic PAA-g-PTFE complexes (denoted as Cu-Fe-PAA-g-PTFE) with different molar ratios of Fe(III) to Cu(II) ion (abbr. Cu/Fe molar ratio) were produced by adjusting the concentrations of the metal ions in coordination solution, and in which the concentrations of total metal ions were kept constant at 0.10 mol L^{-1}.

2.3. Catalytic Activity of the Complex towards H_2O_2 Decomposition. The decomposition of H_2O_2 was carried out at the 150 mL Pyrex vessels inside the photoreaction reaction system. A 400 W high pressure mercury lamp (Foshan Osram Illumination Co., China) was used as the illuminating source for photocatalytic reaction. A cutoff filter was used to ensure irradiation only by visible light ($\lambda > 420$ nm) for the high pressure mercury lamp. The intensity of visible light irradiation over the surface of test solution inside photoreaction system was measured to be 9.65 Wcm^{-2} using

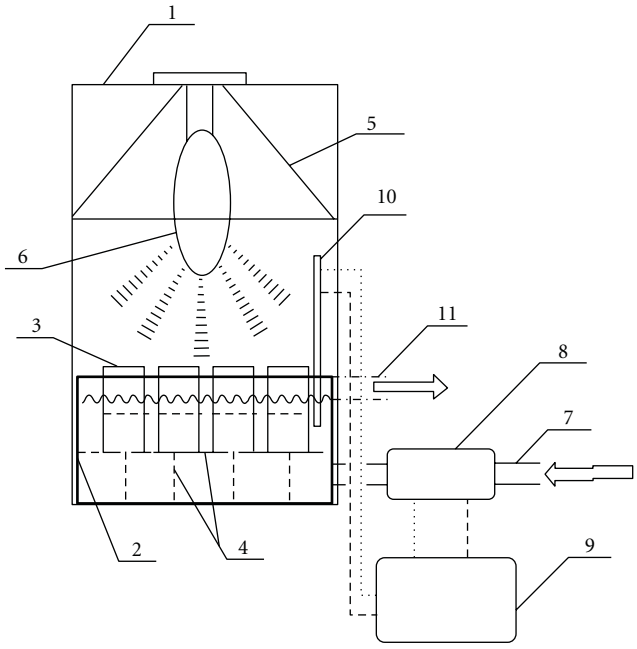

(1) Chamber
(2) Water bath
(3) Glass vessel
(4) Support
(5) Lamp-chimney
(6) Mercury lamp
(7) Water in
(8) Electromagnetic valve
(9) Relay
(10) Thermometer
(11) Water out

Figure 1: The schematic diagram of photoreaction system.

FZ-A radiometer (BNU Light and Electronic Instrumental Co., China), respectively. The diagram of the photoreaction system was presented in Figure 1.

1.0 g of the complex was placed into the vessels containing 100 mL H_2O_2 solution of concentration 10.0 mmol L^{-1} at 25°C. The residual concentration of H_2O_2 in the solution during the reaction was determined though the spectrophotometric DPD method, in which the DPD was oxidized by H_2O_2 based on the POD catalyzed reaction [13]. The analysis of the residual concentration of H_2O_2 was repeated three times for each sample and the results averaged.

2.4. Dye Degradation Procedure. The dye degradation was performed in the photoreaction reaction system mentioned above under visible irradiation. 0.40 g of metal PAA-g-PTFE complex was added into 100 mL of test solution containing 0.04 mmol L^{-1} RR 195 and 6.0 mmol L^{-1} H_2O_2. The reaction temperature was kept at 25 ± 1°C, and the pH of the solution was adjusted with 0.10 mmol L^{-1} HNO_3 and/or NaOH aqueous solution and measured using DHS-25C digital pH meter (Shanghai Jingmi Instrumental Co., China). The degradation of the dye was initialized after the adsorption/desorption equilibrium of the dye on the complex was reached in the dark for 2.0 h. At given irradiation time intervals, 1-2 mL of the test solution was sampled from the reaction vessel and analyzed immediately by recording the UV-vis spectrum

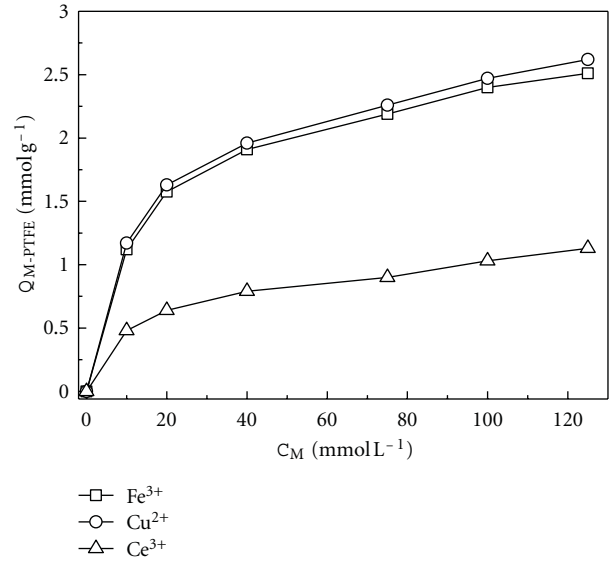

Figure 2: Effect of C_M on $Q_{M\text{-}PTFE}$ of the complexes during the preparation.

of the dye at the λ_{max} (523 nm) with a UV-2401 Shimadzu spectrophotometer. The decoloration percentage of the dye was expressed as $D\% = (1 - C_d/C_{d,0}) \times 100\%$, where $C_{d,0}$ and C_d are the initial and residual concentrations of the dye (mmol L^{-1}), respectively. Moreover, total organic carbon (TOC) was assayed in the dye degradation process by using a Phoenix 8000 TOC analyzer (Tekmar-Dehrmann Inc., USA) and TOC removal percentage of the dye was calculated as follows: TOC removal % = $(1 - TOC_t/TOC_0) \times 100\%$, where TOC_0 and TOC_t are the TOC values (mg L^{-1}) at reaction times 0 and t, respectively.

2.5. Metal Ions Leaching from the Complex. 0.40 g of metal PTFE fiber complex was placed into in 100 mL solution containing 6.0 mmol L^{-1} H_2O_2. The leaching of Fe(III) or/and Cu(II) ions from the complex in solution at room temperature and under visible light irradiation was carried out for 300 min. And the concentrations of Fe(III) or Cu(II) ions in solution at intervals of time were measured using atomic absorption spectrometry method, respectively.

3. Results and Discussion

3.1. Optimization of Coordination Parameters with respect to Metal Contents on PAA-g-PTFE

3.1.1. Metal Ion Concentration in Coordination Solution. In order to investigate the effect of metal ion concentration in coordination solution (C_M) on metal content on PAA-g-PTFE ($Q_{M\text{-}PTFE}$), three metal ions including Fe(III), Cu(II), and Ce(III) ions were selected to react with PAA-g-PTFE with G_f% of 34.53 at 50°C, and results were shown in Figure 2.

It is seen from Figure 2 that all the $Q_{M\text{-}PTFE}$ values significantly increase with increasing C_M, and the increasing tendency gradually declines when C_M being above

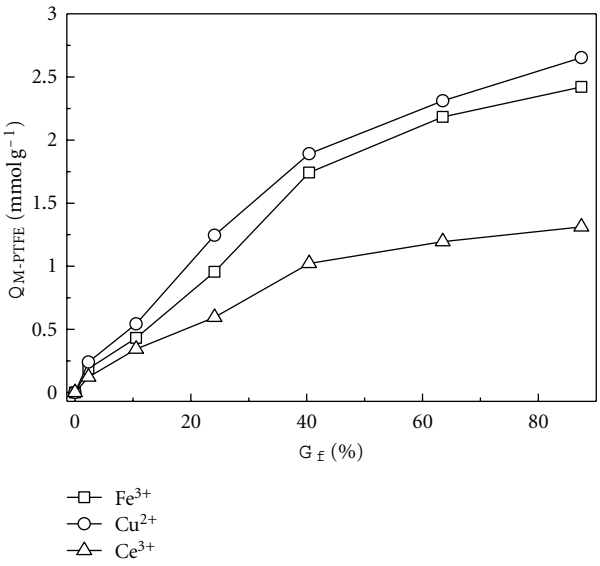

Figure 3: $Q_{M\text{-}PTFE}$ of the complexes as a function of graft degree of PAA-g-PTFE.

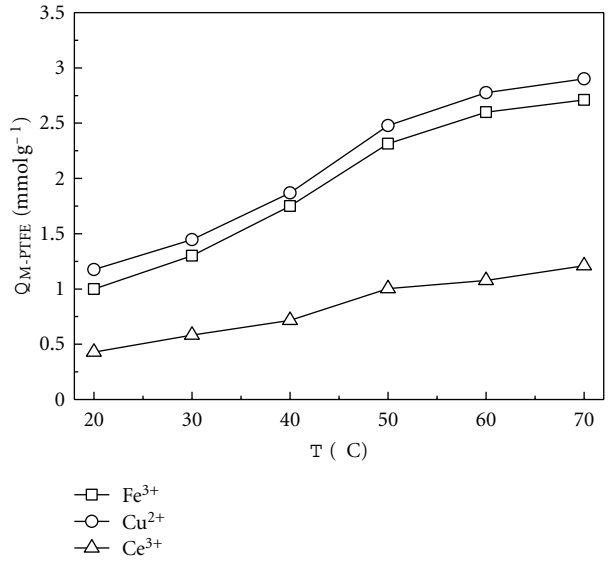

Figure 4: $Q_{M\text{-}PTFE}$ of the complexes at different reaction temperatures.

40.0 mmol L^{-1}, especially for Ce(III) ions. This suggests that higher C_M can enhance the coordination of PAA-g-PTFE with metal ions, particularly two transition metal ions. The previous works [11, 12, 14] have found that the carboxyl groups on PAA-g-PTFE are the main coordinating sites with metal ions. Furthermore, it has been proposed that the oxygen of the carboxyl group has a pair of electrons that can add themselves to a proton or a metal ion to form a complex through a coordinated covalent bond. The metal ions with empty orbitals act as a Lewis acid capable of accepting electron pairs. In contrast, the carboxyl groups that have nonshared electron pairs function as Lewis bases donating their electrons pair [15, 16]. Moreover, transition metal contents ($Q_{Fe\text{-}PTFE}$ and $Q_{Cu\text{-}PTFE}$) on the fiber are much more than Ce content ($Q_{Ce\text{-}PTFE}$) on the fiber, especially at higher metal concentration in solution. This is because the 4f electrons of rare earth metal ion are in the inner orbital of the atomic structure, so that the ligand field has less effect on them and the rare earth metal ions have much lower LFSE values (4.18 kJ moL^{-1}) than d-transition metal ions ($\geq$ 418 kJ moL^{-1}) [5, 17].

3.1.2. Graft Degree of PAA-g-PTFE. To determine the dependence of $Q_{M\text{-}PTFE}$ value on graft degree of PAA-g-PTFE, the complexes were produced by the coordination of PAA-g-PTFE with different G_f% in 0.10 mol L^{-1} metal ion aqueous solution at 50°C, and relationship between G_f% and $Q_{M\text{-}PTFE}$ values was presented in Figure 3.

Figure 3 shows that the $Q_{M\text{-}PTFE}$ value of metal PAA-g-PTFE complexes was greatly enhanced with G_f% of PAA-g-PTFE, particularly when Fe(III) and Cu(II) ion being used. This indicates that increasing G_f% value can benefit the fixation of three metal ions on the surface of PAA-g-PTFE and form the metal PAA-g-PTFE complexes with high $Q_{M\text{-}PTFE}$ because PAA-g-PTFE with high G_f% values has much more carboxyl groups on their surface than those with low G_f% values, thus more easily react with metal ions in solution.

3.1.3. Temperature. PAA-g-PTFE with G_f% of 34.53 was employed to coordinate with three metal ions, respectively, in the solution, for investigating the impact of reaction temperature on $Q_{M\text{-}PTFE}$ value of the resulting metal PAA-g-PTFE complexes, and results were shown in Figure 4.

Figure 4 shows that $Q_{M\text{-}PTFE}$ value of the complexes is increased with elevation of reaction temperature from 20 to 70°C. This obviously demonstrates that it is favorable for the coordination with the temperature rising, which implies that the coordination process is an endothermic process [11]. A possible reason is that higher temperature increases mobility of the polymer chains and the swelling of the fiber in the reaction medium, thus improving the interactions between metal ion and the fiber and resulting in more metal ions fixed on them.

3.2. Comparison of Metal Ions toward H_2O_2 Decomposition. The catalytic activity of three metal PAA-g-PTFE complexes with similar $Q_{M\text{-}PTFE}$ value (approximately 1.30 mmol L^{-1}) was examined with respect to the decomposition of H_2O_2, respectively, and the decay ratios of H_2O_2 as the function of irradiation time were shown in Figure 5.

It is observed from Figure 5 that the decay ratios of H_2O_2 gradually decline with the increasing irradiation time and vary with the nature of metal ions. The decay ratio of H_2O_2 is the lowest for Fe-PAA-g-PTFE, followed by Cu-PAA-g-PTFE, and the highest for Ce-PAA-g-PTFE. This indicates that Fe-PAA-g-PTFE has a stronger catalytic activity than the other complexes at the same conditions. Additionally, from the viewpoint of the toxicity and cost of three metal ions,

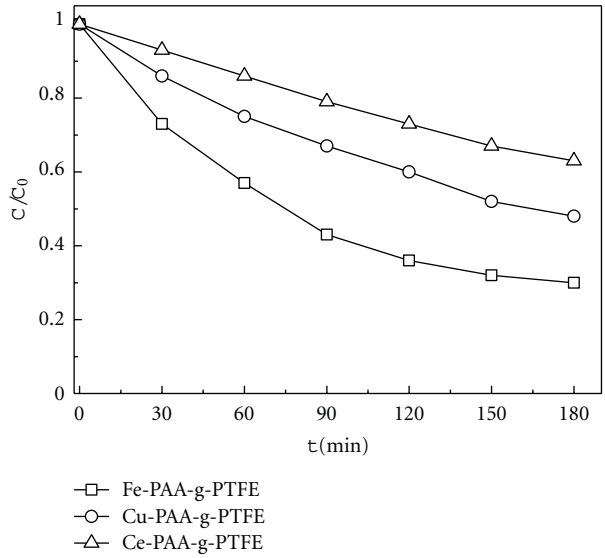

Figure 5: Decomposition of H_2O_2 in the presence of the different catalysts.

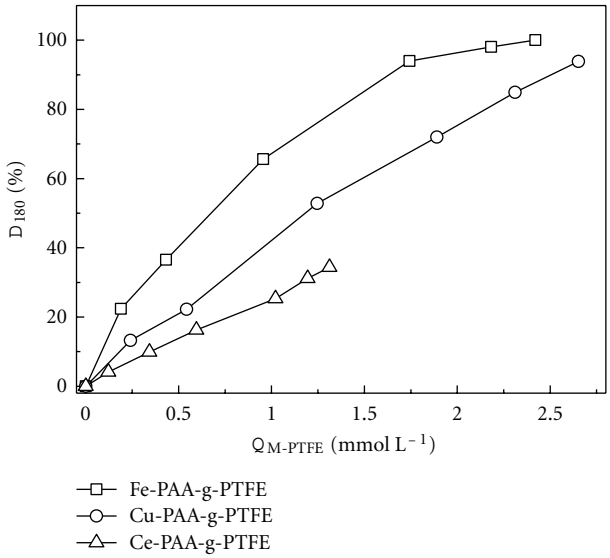

Figure 6: Relationship between $Q_{\text{M-PTFE}}$ and D_{180}%.

Fe(III) ions should been selected to prepare the catalyst for the majority of the future research and practical application.

3.3. Effect of Metal Ion on Dye Degradation. The dye degradations were conducted in the presence of three metal PAA-g-PTFE complexes with different $Q_{\text{M-PTFE}}$ values as the heterogeneous Fenton catalysts, respectively, and the influence of $Q_{\text{M-PTFE}}$ value on decoloration percentage of the dye within 180 min (D_{180}%) was presented in Figure 6.

Figure 6 shows that increasing $Q_{\text{M-PTFE}}$ value can remarkably enhance the dye degradation for all the complexes, particularly Fe-PAA-g-PTFE. Moreover, comparing three metal PAA-g-PTFE complexes with similar $Q_{\text{M-PTFE}}$ values, the highest D_{180}% is achieved when Fe-PAA-g-PTF is used. This means that Fe-PAA-g-PTFE exhibits the strongest catalytic activity for dye degradation, of three complexes. The main reason is that Fe-PAA-g-PTFE leads to the enhanced decomposition of H_2O_2 in solution indicated in Figure 5, thus possibly producing more hydroxyl radicals, which is responsible for the dye degradation. This reaction process is described by (1) and (2). On the other hand, the formed Fe(II) ions on Fe-PAA-g-PTFE may be oxidized to Fe(IV) ions in this work, which are regarded as another reactive intermediate from the photo-Fenton reaction which can decompose dye molecules. A possible formation of Fe(IV) ions was expressed by (3)

$$\text{Fe}^{3+}/\text{PTFE} + \text{H}_2\text{O}_2 \xrightarrow{h\nu} \text{Fe}^{2+}/\text{PTFE} + \text{HO}_2^{\bullet} + \text{H}^{\oplus} \quad (1)$$

$$\text{Fe}^{2+}/\text{PTFE} + \text{H}_2\text{O}_2 \xrightarrow{h\nu} \text{Fe}^{3+}/\text{PTFE} + \text{OH}^{\ominus} + \text{HO}^{\bullet} \quad (2)$$

$$\text{Fe}^{2+}/\text{PTFE} + \text{H}_2\text{O}_2 \xrightarrow{h\nu} \text{Fe}^{4+}/\text{PTFE} \xrightarrow{h\nu} \text{Fe}^{3+}/\text{PTFE} \quad (3)$$

$$\text{Dye} + \text{Fe}^{3+}/\text{PTFE} \xrightarrow{h\nu} \text{Dye}^{*} \cdots \text{Fe}^{3+}/\text{PTFE} \longrightarrow \text{Dye}^{+\bullet} + \text{Fe}^{2+}/\text{PTFE}. \quad (4)$$

Additionally, the photosensitization of the azo dyes can promote a conversion of Fe(III) to Fe(II) ions during photo-assisted Fenton reaction [12]. In this work, it is believed that RR 195 could act as the sensitizer of Fe-PAA-g-PTFE to lead to a charge transfer with the concomitant quenching of the excited dye* and the formation of dye$^+$. This process was suggested by (4).

It is well known the hydroxyl radicals is a powerful oxidant and can ultimately cause mineralization of textile dyes. Consequently, the mineralization of the dye was examined by measuring the TOC values of test solutions during the degradation when three complexes with the similar $Q_{\text{M-PTFE}}$ values were employed, respectively.

Figure 7 shows that TOC removal % of the dye is as a function of irradiation time. It is found that TOC removal % gradually increases with the prolongation of irradiation time. Specifically, TOC removal % for Fe-PAA-g-PTF is much higher than those for the other complexes at the same time. These results demonstrate that three metal PAA-g-PTFE complexes as the photocatalysts can result in a drastic breakdown of dye molecules, and then convert them into water, carbon dioxide, and inorganic compounds. It should also be pointed out that TOC removal % is mainly determined by nature of metal ions, which is well consistent with the impact of nature of metal ions on the degradation mentioned above.

In order to study the catalytic activity of the complexes in a wide pH range, the dye degradation was carried out at different solution pH within 180 min of reaction time. The catalytic activity of the complexes was determined with respect to the dye degradation with the results presented in Figure 8.

Figure 8 shows that the dye degradation can be operated in the presence of the complex over a wide pH 3–9 range, indicating that a significant breakdown of the dye occur, especially at acidic media. Moreover, the catalytic activity

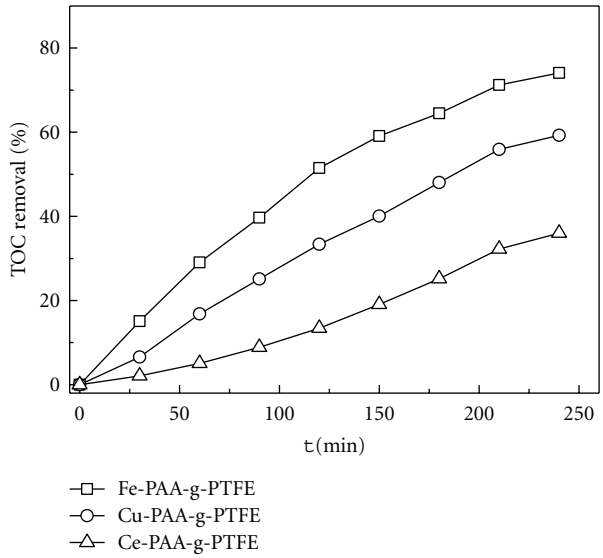

Figure 7: Mineralization of the dye with different catalysts.

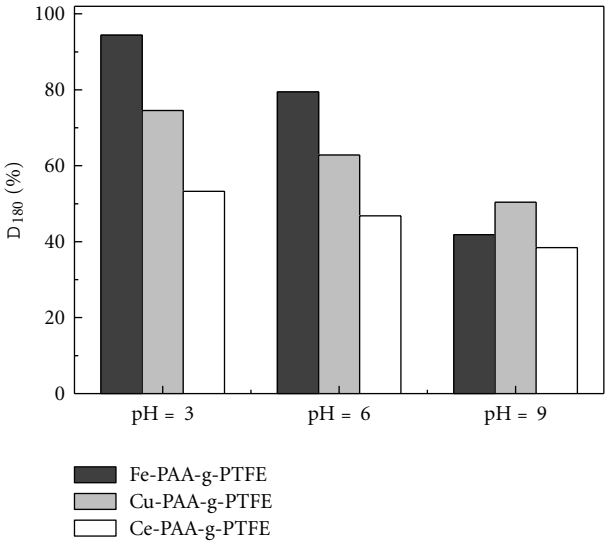

Figure 8: Dye degradation at different pH levels for three catalysts.

of three complexes at acid and neutral medium is ranked in this order: Fe-PAA-g-PTFE > Cu-PAA-g-PTFE > Ce-PAA-g-PTFE. However, higher pH range, especially alkaline pH medium dramatically decreases the catalytic activity of three complexes. It is worth noticing that Cu-PAA-g-PTFE shows a stronger activity than Fe-PAA-g-PTFE at pH 9. This is similar to the performance of Cu/MCM-41 as a highly stable and pH-insensitive heterogeneous photo-Fenton-like Fenton catalyst [18]. Some researches [18, 19] suggested that an advantage of Cu^{2+} ion as a Fenton-like catalyst is its characteristics of a wide-working pH range compared to the conventional Fenton catalyst. Therefore it is believed that Cu-PAA-g-PTFE behaves similarly to Fe-PAA-g-PTFE, and it has a higher catalytic activity over a wide pH range.

3.4. Role of Cu(II) Ion as an Assisted Metal Ion. It has been suggested that the performance of supported Fe catalysts is often improved by adding certain metals. And copper ion has a role as an assistant in photocatalysis [5]. Moreover, it has been presented that the outstanding catalytic activity of bimetal catalysts may be generally ascribed to synergistic effects between copper and iron redox couples. In order to meet the demands for rapid and stable dye degradation in future commercial application, a series of Cu-Fe bimetal PAA-g-PTFE complexes with different Cu/Fe molar ratios were prepared and used in the dye degradation at pH 9 in this work. And Cu/Fe molar ratio of metal PAA-g-PTFE complexes was observed to have a significant impact on the decomposition efficiency of the dye, and the results are given in Table 1.

The data in Table 1 indicate that higher concentration of Cu(II) ions in the solutions increased their Cu/Fe molar ratio. When the molar concentration of Cu(II) ions equals to that of Fe(III) ions in the solution, the Cu/Fe molar ratio of Cu-Fe-PAA-g-PTF is 2.87, much more than 1.0, suggesting that PAA-g-PTF has much higher affinity for Cu(II) ions than Fe(III) ions at the same conditions. More importantly, D_{180}% and TOC removal % of dye degradation in the presence of the bimetal PAA-g-PTFE complexes is much higher than those in the presence of the monometal PAA-g-PTE complexes, and the maximum D_{180}% and TOC removal % was achieved for Cu-Fe-PAA-g-PTFE (ii). These results confirm that catalytic activity of metal PAA-g-PTFE complexes depends highly upon their Cu/Fe molar ratio, and Cu-Fe-PAA-g-PTFE (ii) with a Cu/Fe molar ratio of 2.87 shows the best catalytic activity at alkaline pH medium. This demonstrates the existence of synergetic effect between loaded Fe(III) and Cu(II) ions in the bimetal PAA-g-PTFE complexes, which improved their catalytic activity to a great extent. The main reason may be that the H_2O_2 molecules absorbed on the surface of Cu-Fe-PAA-g-PTFE can reduce Fe(III) to Fe(II) ions through the Fenton-like process under visible light irradiation, and the generated Fe(II) ions are then oxidized by H_2O_2 to complete the Fe(III)/Fe(II) ions cycle and produce hydroxyl radicals. Meanwhile, the formed Fe(II) ions can also react with the loaded Cu(II) ions to form the Cu(I) and Fe(III) ions (5) to accelerate the transformation of Fe(III)/Fe(II) ions and Cu(II)/Cu(I) ions in Cu-Fe-PAA-g-PTFE, thus giving rise to additional hydroxyl radicals during the degradation:

$$\mathrm{Fe^{3+}/PTFE + Cu^{+}/PTFE \rightleftharpoons Fe^{2+}/PTFE + Cu^{2+}/PTFE.} \quad (5)$$

3.5. Metal Ions Leaching from the Catalyst. One problem with the heterogeneous photocatalysts is metal leaching from the catalyst that causes secondary contamination to wastewater in pilot-scale application. The leaching concentrations of metal ions from metal PAA-g-PTFE complexes in solution were measured. The results indicated that metal ions were continuously leached out from the complexes after the reaction started, and the final measured concentrations of both metal ions in the solution within 300 min at different pH levels were shown in Tables 2 and 3.

Table 1: Effect of Cu/Fe molar ratio of the catalysts on dye decomposition.

Samples	C_M (mol L^{-1})		$Q_{M\text{-}PTFE}$ (mmol L^{-1})			Cu/Fe	D_{180}%	TOC Removal %
	Fe(III)	Cu(II)	Fe(III)	Cu(II)	Total			
Fe-PAA-g-PTFE	0.100	0.000	1.89	0.00	1.89	0	47.3	37.3
Cu-Fe-PAA-g-PTFE (i)	0.075	0.025	1.13	0.75	1.88	0.66	61.2	54.6
Cu-Fe-PAA-g-PTFE (ii)	0.050	0.050	0.54	1.55	2.09	2.87	84.6	72.7
Cu-Fe-PAA-g-PTFE (iii)	0.025	0.075	0.31	1.75	2.06	5.65	78.4	56.7
Cu-PAA-g-PTFE	0.000	0.100	0.00	1.98	1.98	/	51.9	45.1

Table 2: Leaching of Fe ions from Fe-PAA-g-PTFE with different Q_{Fe} values.

Fe-PAA-g-PTFE	Fe(III) ions concentration in solution (mg L^{-1})		
	pH = 3	pH = 7	pH = 9
Q_{Fe} = 0.432 mmol L^{-1}	0.49	0.37	0.07
Q_{Fe} = 0.955 mmol L^{-1}	0.72	0.57	0.15
Q_{Fe} = 1.743 mmol L^{-1}	0.95	0.73	0.22
Q_{Fe} = 2.183 mmol L^{-1}	1.22	0.94	0.43
Q_{Fe} = 2.421 mmol L^{-1}	1.53	1.23	0.57

Table 3: Impact of Cu/Fe molar ratio on leaching of metal ions from Cu-Fe bimetallic PTFE fiber complexes.

Samples	Metal ions concentration in solution (mg L^{-1})					
	pH = 3		pH = 7		pH = 9	
	Fe(III)	Cu(II)	Fe(III)	Cu(II)	Fe(III)	Cu(II)
Fe-PAA-g-PTFE	0.93	0.00	0.82	0.00	0.29	0.00
Cu-Fe-PAA-g-PTFE (i)	0.63	0.35	0.53	0.29	0.19	0.12
Cu-Fe-PAA-g-PTFE (ii)	0.21	0.76	0.13	0.49	0.06	0.24
Cu-Fe-PAA-g-PTFE (iii)	0.17	0.92	0.10	0.45	0.08	0.19
Cu-PAA-g-PTFE	0.00	1.25	0.00	0.89	0.00	0.31

It can be noticed from Table 2 that increasing Q_{Fe} value is accompanied by increasing Fe ion concentration in solution at three investigated pH levels. This means that Fe-PAA-g-PTFE with higher Q_{Fe} value can leach more Fe(III) ions than that with lower Q_{Fe} value. It is obvious from the results shown in Table 3 that Fe(III) and Cu(II) ion concentrations in solution are much affected by Cu/Fe molar ratio of the complexes. On the other hand, higher pH level caused a gradual decrease in leached Fe(III) or Cu(II) ion concentration in solution, revealing that metal ions leaching from the complexes is dependent on the solution pH. Moreover, it should be pointed out that the final leached concentration of Fe(III) or Cu(II) ions is lower than 1.0 mg L^{-1} for both complexes, especially at pH 7 and 9. This result implies that both metal ions were attached on the surface of the modified PTFE via the hydroxyl group. Thus, these complexes can be regarded as the effective and stable heterogeneous photocatalysts for the dye degradation over a broad pH range due to a minimal threshold concentration of 3–15 mg L^{-1} Fe which allows the homogeneous Fenton reaction to proceed within a reasonable period of time. Additionally, it is well known that Cu ion is hazardous to both marine animals and humans. The discharge standard was suggested by the Environmental Protection Agency is 1.0 mg L^{-1} [18], which is higher than the final leached concentration of Cu(II) ions for Cu-Fe bimetallic PTFE fiber complexes except Cu-Fe-PAA-g-PTFE (iii) and Cu-PAA-g-PTFE.

4. Conclusions

The novel heterogeneous photo-Fenton catalysts were produced by a modification of PTFE fibers through graft polymerization of acrylic acid to introduce the carboxyl groups onto the fiber surface, which were used to coordinate with transition metal ions (Fe(III) and Cu(II)) or rare metal ion (Ce(III)). Increasing metal ion concentrations in solution and grafting degree of PTFE fiber as well as higher coordination temperature could lead to a significant increase in metal content, especially Fe(III) and Cu(II) content of the catalysts. Moreover, Fe(III) and Cu(II) ions reacted with the modified PTFE fibers more easily than Ce(III) ion at the same conditions to form the complexes with higher metal content. Fe(III) ions fixed on the fiber showed a much powerful catalytic performance for the decomposition of H_2O_2 and the oxidative degradation of the dye than Cu(II) and Ce(III) ions fixed when three different complexes with similar metal content being employed as the catalysts, respectively. Also, taking into the toxicity of Cu (II) and Ce(III) ions and the cheapness of iron salt, thus, Fe(III) modified PTFE fiber complex was proposed to act as an effective catalyst for the dye degradation under visible irradiation. And increasing Fe content could remarkably improve the catalytic activity of the complex. Comparing with the three monometallic complexes, Cu-Fe bimetallic modified PTFE fiber complexes exhibited the excellent catalytic activity because of the existence of synergetic effect between Fe(III) and Cu(II) ions. Their catalytic activity depended highly on Cu/Fe molar ratio. 2.87 is the optimum Cu/Fe molar ratio to obtain the best catalytic activity for the bimetallic complexes. However, increasing the amount of Fe(III) or/and Cu(II) ions fixed on the fibers resulted in the relatively higher concentrations of both ions leaching from them, especially at low pH ranges. To sum up, the highest dye degradation efficiency and the accepted concentrations of metal ions leaching from the complexes were found when it was prepared with a mixture

of 0.05 mol L^{-1} Fe(III) and 0.05 mol L^{-1} Cu(II) ions at 50°C by poly acrylic acid grafted PTFE fiber as the supported material using a simple exhausting method.

Acknowledgments

The authors thank the Tianjin Municipal Science and Technology Committee for a Research Program of Application Foundation and Advanced Technology (11JCZDJ24600). This research was also supported in part by a Grant from the Natural Science Foundation of China (20773093).

References

[1] V. V. Ishtchenko, K. D. Huddersman, and R. F. Vitkovskaya, "Part 1. Production of a modified PAN fibrous catalyst and its optimisation towards the decomposition of hydrogen peroxide," *Applied Catalysis A*, vol. 242, no. 1, pp. 123–137, 2003.

[2] V. V. Ishtchenko, R. F. Vitkovskaya, and K. D. Huddersman, "Investigation of the mechanical and physico-chemical properties of a modified PAN fibrous catalyst," *Applied Catalysis A*, vol. 242, no. 2, pp. 221–231, 2003.

[3] R. F. Vitkovskaya, I. G. Rumynskaya, E. P. Romanova, and L. Y. Tereshchenko, "Fibre catalyst from modified polyacrylonitrile fibres," *Fibre Chemistry*, vol. 35, no. 3, pp. 202–207, 2003.

[4] Z. Han, Y. Dong, and S. Dong, "Copper-iron bimetal modified PAN fiber complexes as novel heterogeneous Fenton catalysts for degradation of organic dye under visible light irradiation," *Journal of Hazardous Materials*, vol. 189, no. 1-2, pp. 241–248, 2011.

[5] Y. Dong, Z. Han, S. Dong, J. Wu, and Z. Ding, "Enhanced catalytic activity of Fe bimetallic modified PAN fiber complexes prepared with different assisted metal ions for degradation of organic dye," *Catalysis Today*, vol. 175, no. 1, pp. 299–309, 2011.

[6] Z. Han, Y. Dong, and S. Dong, "Comparative study on the mechanical and thermal properties of two different modified PAN fibers and their Fe complexes," *Materials and Design*, vol. 31, no. 6, pp. 2784–2789, 2010.

[7] S. Parra, I. Guasaquillo, O. Enea et al., "Abatement of an azo dye on structured C-Nafion/Fe-ion surfaces by photo-Fenton reactions leading to carboxylate intermediates with a remarkable biodegradability increase of the treated solution," *The Journal of Physical Chemistry B*, vol. 107, no. 29, pp. 7026–7035, 2003.

[8] S. Wu, E. T. Kang, K. G. Neoh, H. S. Han, and K. L. Tan, "Surface modification of poly(tetrafluoroethylene) films by graft copolymerization for adhesion improvement with evaporated copper," *Macromolecules*, vol. 32, no. 1, pp. 186–193, 1999.

[9] M. C. Zhang, E. T. Kang, and K. G. Neoh, "Consecutive graft copolymerization of glycidyl methacrylate and aniline on poly(tetrafluoroethylene) films," *Langmuir*, vol. 16, no. 24, pp. 9666–9672, 2000.

[10] Q. Zhang, S. Zhang, S. Chen, P. Li, T. Qin, and S. Yuan, "Preparation and characterization of a strong basic anion exchanger by radiation-induced grafting of styrene onto poly(tetrafluoroethylene) fiber," *Journal of Colloid and Interface Science*, vol. 322, no. 2, pp. 421–428, 2008.

[11] C. Xiong and C. Yao, "Preparation and application of acrylic acid grafted polytetrafluoroethylene fiber as a weak acid cation exchanger for adsorption of Er(III)," *Journal of Hazardous Materials*, vol. 170, no. 2-3, pp. 1125–1132, 2009.

[12] J. F. Wei, Z. P. Wang, J. Zhang, Y. Y. Wu, Z. P. Zhang, and C. H. Xiong, "The preparation and the application of grafted polytetrafluoroethylene fiber as a cation exchanger for adsorption of heavy metals," *Reactive and Functional Polymers*, vol. 65, no. 1-2, pp. 127–134, 2005.

[13] M. Cheng, W. Song, W. Ma et al., "Catalytic activity of iron species in layered clays for photodegradation of organic dyes under visible irradiation," *Applied Catalysis B*, vol. 77, no. 3-4, pp. 355–363, 2008.

[14] N. M. El-Sawy and F. Al Sagheer, "Radiation-induced graft polymerization of acrylic acid onto poly(tetrafluoroethylene-perfluorovinyl ether) copolymer films: complexation with some transition metals and biological activity," *European Polymer Journal*, vol. 37, no. 1, pp. 161–166, 2001.

[15] I. A. Şengil and M. Özacar, "Biosorption of Cu(II) from aqueous solutions by mimosa tannin gel," *Journal of Hazardous Materials*, vol. 157, no. 2-3, pp. 277–285, 2008.

[16] C. Xiong, C. Yao, and X. Wu, "Adsorption of rhenium(VII) on 4-amino-1,2,4-triazole resin," *Hydrometallurgy*, vol. 90, no. 2–4, pp. 221–226, 2008.

[17] G. Henrici-Olive and S. Olive, *Coordination and Catalysis*, Chemie, Weinheim, Germany, 1977.

[18] F. L. Y. Lam, A. C. K. Yip, and X. Hu, "Copper/MCM-41 as a highly stable and pH-insensitive heterogeneous photo-Fenton-like catalytic material for the abatement of organic wastewater," *Industrial and Engineering Chemistry Research*, vol. 46, no. 10, pp. 3328–3333, 2007.

[19] M. Neamtu, A. Yediler, I. Siminiceanu, and A. Kettrup, "Oxidation of commercial reactive azo dye aqueous solutions by the photo-Fenton and Fenton-like processes," *Journal of Photochemistry and Photobiology A*, vol. 161, no. 1, pp. 87–93, 2003.

Hindawi Publishing Corporation
International Journal of Photoenergy
Volume 2012, Article ID 694721, 8 pages
doi:10.1155/2012/694721

Research Article

Potential of Ceria-Based Catalysts for the Oxidation of Landfill Leachate by Heterogeneous Fenton Process

E. Aneggi,[1] V. Cabbai,[1] A. Trovarelli,[2] and D. Goi[3]

[1] *Department of Chemistry, Physics and Environment, University of Udine, Via del Cotonificio, 108-331100 Udine, Italy*
[2] *Catalysis Group, Department of Chemistry, Physics and Environment, University of Udine, Via del Cotonificio, 108-331100 Udine, Italy*
[3] *Civil Environmental Group, Department of Chemistry, Physics and Environment, University of Udine, Via del Cotonificio, 108-331100 Udine, Italy*

Correspondence should be addressed to D. Goi, goi@uniud.it

Received 26 May 2012; Accepted 22 July 2012

Academic Editor: Meenakshisundaram Swaminathan

In this study, ceria and ceria-zirconia solid solutions were tested as catalyst for the treatment of landfill leachate with a Fenton-like process. The catalysts considered in this work were pure ceria and ceria-zirconia solid solutions as well as iron-doped samples. All the catalysts were extensively characterized and applied in batch Fenton-like reactions by a close batch system, the COD (chemical oxygen demand) and TOC (total organic carbon) parameters were carried out before and after the treatments in order to assay oxidative abatement. Results show a measurable improvement of the TOC and COD abatement using ceria-based catalysts in Fenton-like process and the best result was achieved for iron-doped ceria-zirconia solid solution. Our outcomes point out that heterogeneous Fenton technique could be effectively used for the treatment of landfill leachate and it is worth to be the object of further investigations.

1. Introduction

Landfill leachate is a liquid waste of primary environmental concern because of the quantity and quality of the harmful pollutants contained in it. There are a large number of various types of organic and inorganic substances, depending on the age and type of solid wastes located in the landfill. Leachate from sanitary landfills can be an important source of ground water contamination and for this reason it is collected from the bottom of the landfill to be treated; further, this highly contaminated liquid waste accumulates a great diversity of harmful pollutants. Some of them are particularly refractory and for this reason traditional wastewater treatment plants are not efficient in their abatement. Inorganic and organic content of leachate is characteristically related to environmental risk because of scarce biodegradation, severe bioaccumulation, and potential health damages [1, 2]. It is well known that conventional biological liquid waste treatments alone are unable to achieved complete removal of the leachate pollution over the life of the landfill. In truth conventional biological processes are time consuming and low-efficiency methods to treat directly leachate, consequently physicochemical processes are frequently utilized to pretreat this liquid waste in order to reduce organic refractory before biological action in treatment plants units [3].

The most employed and studied methods in landfill leachate pretreatment are chemical or electrochemical coagulation [4], precipitation [5], and oxidation [6, 7]. Among these, a particular attention is given to oxidation techniques and especially to advanced oxidation processes (AOPs).

AOPs are methods able to convert nonbiodegradable organic pollutants into nontoxic biodegradable forms [8, 9], by the production of highly oxidizing hydroxyl radical species that promptly oxidize organic pollutants by a broad range of actions.

As a matter of fact oxidation by hydroxyl radicals species can be activated starting from H_2O_2 by intervention of transition metal salts (e.g., iron salts) [10], from ozone [11] or UV-light [12], leading to a more effective method to

decompose certain refractory contaminants of leachate. In particular, Fenton oxidation is a well-known AOP used as pretreatment of leachate worldwide [10].

The Fenton's reagent works at mild temperature and pressure generating hydroxyl radicals following the generally accepted structure of reactions:

$$\begin{aligned} Fe^{2+} + H_2O_2 &\longrightarrow Fe^{3+} + OH^{\bullet} + OH^{-} \\ RH + OH^{\bullet} &\longrightarrow H_2O + R^{\bullet} \\ R^{\bullet} + Fe^{3+}\text{-oxidation} &\longrightarrow R^{+} + Fe^{2+} \end{aligned} \quad (1)$$

This reaction is followed by other very complex oxidation reactions in which a lot of radical forms are generated and take part in the overall Fenton oxidation. The H_2O_2 can act both as a scavenger or initiator, all organics in liquid waste can participate in radical generation [10] and the ferric iron catalyzes and decomposes H_2O_2 to additional radical forms contributing to the oxidation [13]. Moreover, the reaction of ferrous iron forms ferric hydroxo complexes which can contribute to the coagulation capacity of the Fenton reagent [14]. The reactions including hydrogen peroxide and ferric ions or other transition metal ions are also reported as Fenton-like reactions [15, 16]; moreover, some new wet peroxidations, in which various catalysts are added with hydrogen peroxide to remove organic compounds by low temperature reactions, are presented as heterogeneous Fenton-like systems [17–19].

The Fenton process is one of the most interesting AOPs when it is used to treat or pretreat heavily contaminated liquid wastes, and a lot of full-scale applications are installed over the world. The main advantage is to reach treatment of liquid wastes at mild conditions of temperature and pressure, but the most important drawback is the production of a sludge which needs to be treated as well. It is also a recognized concept that Fenton process, at reasonable reagents concentration, cannot lead to the complete mineralization of all organic compounds and often only partial oxidation occurs even in assisted oxidations [20].

Leachate treatment by classic Fenton process was often studied to assay potential increase of the biodegradability or reduction of toxicity or color removal [21–23]. Recently, photo-Fenton [24] and electro-Fenton [25] processes have been investigated for landfill leachate treatment and several studies have been dedicated to heterogeneous Fenton treatment of phenolic [19, 26, 27] or industrial wastewater [28–31]. Heterogeneous process could be a promising alternative due to the more important drawback of classic Fenton, the large amount of iron required for the reaction that dramatically exceeds the legally quantity permitted for effluent discharge (<2 mg/L) and consequently requires a final waste management. At present, at the best of our knowledge, only one experience is reported about leachate treatment by heterogeneous catalytic Fenton-like systems [32], which can potentially be a promising way to activate radicals oxidizing species with minor sludge production. The experience reported in this paper tries to give a contribution to this theme.

The use of ceria-based materials in catalytic science is well established [33, 34]. Ceria is presently used in a large number of industrial processes and it accounts for a large part of the rare earth oxide market. Undoubtedly, its major commercial application is in the treatment of emissions from internal combustion engines where ceria-based materials have been used in the past 30 years [35]. Its more important action in three-way catalysts (TWCs) is to take up and release oxygen following variations in the stoichiometric composition of the feedstream; however, several other processes also benefit from the use of cerium and its derivates. Organosoluble compounds of cerium are used as fuel additives for diesel engines and industrial boilers to reduce carbon deposits after combustion. Cerium oxide is used also as a catalytically active component to oxidize the liquid portion of particulate present in diesel engine exhaust. CeO_2 is also used as an additive or a promoter in commercial applications such as fluid catalytic cracking, ammoxidation and dehydrogenation processes [33–37]. Moreover, in the last years several ceria-based catalysts were investigated for CWAO (catalytic wet air oxidation) [38–40] and CWOP (catalytic wet peroxide oxidation) [41–44] techniques. The main purpose of this work is to investigate doped ceria materials in the treatment of landfill leachate by a heterogeneous Fenton process.

2. Materials and Methods

2.1. Characterization and Sampling of Landfill Leachate. The leachate used in this study was drawn from an aged landfill near the city of Udine (northeast Italy); the landfill is not equipped with a recirculation system and it produces a stable leachate with high concentrations of COD and low BOD/COD ratio with a brown-green color. All the measures are carried out following the Standard Methods for the Examination of Water and Wastewater [45], COD was determined by colorimetric method utilizing a Hach Lange-DR 5000 spectrophotometer and quenching measurable residual H_2O_2 to prevent interference by addition of $MnO_{2(s)}$. Residual H_2O_2 was checked and determined to be zero by using test strips (Peroxide test sticks Quantofix, Sigma Aldrich). The TOC analyses were performed by a TOC-VCPN, Shimadzu analyzer.

2.2. Preparation and Characterization of the Catalysts. The catalysts, ceria (CeO_2, CZ100), ceria-zirconia solid solutions ($Ce_{0.44}Zr_{0.56}O_2$, CZ44) and Fe-doped materials ($Ce_{0.85}Fe_{0.15}O_{1.925}$, CF and $Ce_{0.45}Zr_{0.40}Fe_{0.15}O_{1.925}$, CZF) were prepared by coprecipitation starting from nitrates. Precipitates were dried at 393 K and calcined at 773 K for 2 h. Fe-doped materials were also calcined at higher temperature (1073 K) to investigate the behavior of iron-phase in the system.Textural characteristics of all samples were measured according to the BET method by nitrogen adsorption at 77 K, using a Tristar 3000 gas adsorption analyzer (Micromeritics).

Structural features of the catalysts were characterized by X-ray diffraction (XRD). XRD patterns were recorded on a Philips X'Pert diffractometer operated at 40 kV and 40 mA using nickel-filtered Cu-K_α radiation. Spectra were collected using a step size of 0.02° and a counting time of 40 s per angular abscissa in the range 20°–145°. The Philips X'Pert

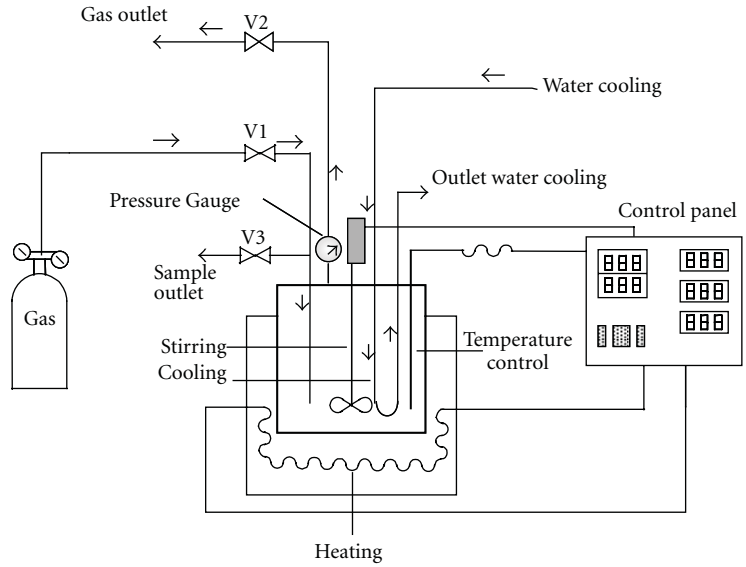

Figure 1: Schematic representation of the batch oxidation reactor used for tests.

HighScore software was used for phase identification. The mean crystalline size was estimated from the full width at the half maximum (FWHM) of the X-ray diffraction peak using the Scherrer equation [46] with a correction for instrument line broadening. Rietveld refinement [47] of XRD pattern was performed by means of GSAS-EXPGUI program [48, 49]. The accuracy of these values was estimated by checking their agreement against the values of the lattice constant, assumed to comply with the Vegard's law [50].

In order to evaluate the oxygen/storage capacity (OSC) of samples TGA, experiments in Ar/H_2 (5%) flow (total flow 100 mL/min) were carried out. Each sample was treated in N_2 atmosphere for 1 h at 553 K. Then, it was heated at a constant rate (10 K/min) till 673 K and kept at this temperature for 15 minutes, to eliminate the absorbed water. Finally, Ar/H_2 mixture was introduced while keeping the temperature at 673 K for 30 minutes. The observed weight loss is due to oxygen removal by H_2 to form water, and it can be associated to total oxygen storage capacity at that temperature [51, 52].

Table 1: Characterization of the landfill leachate used in this study.

Parameter	Unit of measurement	Values
pH	—	9
BOD_5	mg O_2/L	60
COD	mg O_2/L	2500
BOD_5/COD	—	0.024
TN	mg N/L	1860
TOC	mg C/L	575
AOS	—	−2.52
ΔOD	mg O_2/L	0.38
Ammonia	mg NH_4^+/L	2150
Chloride	mg Cl^-/L	—
Color	PtCo unit	3600
Total iron	mg Fe/L	1.2
Nitrate	mg NO_3/L	—
Orthophosphate	mg PO_4^{3-}/L	60
Sulfate	mg SO_4^{2-}/L	—

2.3. Catalytic Activity

2.3.1. Heterogeneous Fenton. A pressure vessel (Parr Instruments) equipped with a glass batch reactor with continuous stirring (400 rpm) (Figure 1) was used to carry out Fenton-like oxidative reactions. The experiments were conducted for 120 minutes at 343 K stirring 100 mL of leachate with 10 mg of catalysts and 5 mL of H_2O_2 (3%). At the end of the reaction (2 hours), samples were taken out and analyzed. Each experiment was repeated three times to obtain the reproducibility (error bars are included in figures).

3. Results and Discussion

3.1. Textural and Structural Characterization. The leachate selected to test oxidative Fenton-like process was characterized by a small concentration of iron in the raw mixture, a high pH value, a slight high value of COD and TOC if compared to average values of other old landfill leachate [53]. The main properties are described in Table 1.

Textural and structural characterization of all catalysts is reported in Table 2. Materials have surface area in the range 55–135 m^2/g. Ceria-zirconia solid solutions (CZ44 and CZF) show higher surface area with respect to ceria-based samples (CZ100 and CF) due to the stabilization effect of zirconia.

The introduction of ZrO_2 significantly enhances textural properties, indeed, sintering in ceria-zirconia is less important in accordance with its better thermal resistance [54].

Doping ceria has a significant positive effect on the catalytic, oxygen storage/redox and thermal properties of catalysts. The introduction of Zr^{4+} induces a structural modification and this factor plays a key role in the redox

Table 2: Characteristics of catalysts used in this study and crystallographic parameters of modified ceria samples as obtained from Rietveld refinement and Vegard's law.

Sample	Composition	BET surface area (m^2/g)	Crystallite size (nm)[a]	Phase	Cell parameter	
					$a = b = c$ (Å)	From Vegard's law
CZ100	CeO_2	53	7	Cubic	5.411 (1)	5.411
CZ44	$Ce_{0.44}Zr_{0.56}O_2$	90	4.7	Cubic	5.281 (1)	5.285
CF	$Ce_{0.85}Fe_{0.15}O_{1.925}$	77	7.5	Cubic	5.396 (1)	5.263
CF (1073 K)	$Ce_{0.85}Fe_{0.15}O_{1.925}$	22	31.1	Cubic	5.408 (1)	5.263
CZF	$Ce_{0.45}Zr_{0.40}Fe_{0.15}O_{1.925}$	132	3.5	Cubic	5.295 (1)	5.163
CZF (1073 K)	$Ce_{0.45}Zr_{0.40}Fe_{0.15}O_{1.925}$	22	8.9	Cubic	5.292 (1)	5.163

[a]Calculated with Scherrer formula from X-ray diffraction patterns.

behaviour of ceria-zirconia solid solutions. The substitution of Ce^{4+} with Zr^{4+} produces a contraction of the cell volume and induces stress in the structure and consequently structural defects that increase the oxygen mobility. It is important to point out that the oxygen mobility is increased if no modification in the structure of solid solution is observed. From these considerations, we noted that better performances are achieved for solid solutions with cubic symmetry and with a high level of Zr^{4+}. Alternatively, a higher amount of ZrO_2 decreases the number of redox sites and consequently the activity of the system. There is an inverse relationship between the two effects; in order to obtain an active system it is important to balance the amount of structural defects and the amount of ceria. Literature data suggest that better results are obtained for compositions between CZ50 and CZ90 [55–58].

The structural features of all samples were analyzed by XRD.

In CeO_2-ZrO_2 system, several phases could be formed, depending on preparation conditions and concentration of single-oxide constituents [59]. In general, for a CeO_2 content <20 mol% a single-phase monoclinic cell is observed, while in CeO_2-rich compositions (CeO_2 > 70 mol%) solid solutions of cubic symmetry are formed. At intermediate levels, regions of tetragonal (t, t′, and t″ phases) and cubic symmetry coexist in the phase diagram, their formation depending on the preparation method used. In our case, the Rietveld analysis of the diffraction profile of the materials has been carried out by opening the fitting to cubic, tetragonal and a mixture of the two.

As shown in Table 2, XRD measurements suggest that for binary ceria-zirconia samples with cerium content greater than 40 mol% the formation of a cubic fluorite lattice is favored, in accordance with the literature [60]. Thus, our ceria and ceria-zirconia solid solution crystallize in a cubic fluorite structure of *Fm*3*m* symmetry. In CZ44, no peak splitting that would indicate the presence of two phases could be detected, and therefore, the diffraction patterns demonstrate the formation of a single solid solution-like ceria-zirconia phase. This cannot exclude the presence of different arrangements of oxygen sublattice or the presence of a multiphase system at a nanoscale level, not detected by XRD. In fresh samples doped with Fe, XRD features allow to detect only the CeO_2 or $Ce_{0.44}Zr_{0.56}O_2$ cubic phase *Fm*3*m,* while Fe_2O_3 or other iron oxide phases are not visible (Figure 2(a)). XRD peaks are broad and the values of crystallite size obtained according to Scherrer equation are about 7.5 nm for sample CF and 3.5 nm for sample CZF. In order to understand better the structural properties of Fe-doped system, CF and CZF catalysts were calcined at higher temperatures (1023 K).

After calcination, in the XRD profile of CF, peaks assigned to rhombohedral Fe_2O_3 (hematite) with *R-3c* symmetry are visible (Figure 2(b)).

The lack of peak due to iron oxide in fresh CF samples could indicate the formation of solid solution between Ce and Fe. However, a comparison between lattice parameters retrieved from Rietveld refinement and from Vegard law (values of cell parameter expected if all the iron contained were dissolved in the lattice) indicates that only a small percentage of iron is dissolved in ceria (Table 2).

After aging, the increase of cell parameter indicates a segregation of the iron eventually dissolved in the lattice with formation of weak signal due to crystalline Fe_2O_3. It is known that lower valence ions such as Fe^{3+} are extremely difficult to dissolve into the ceria lattice, especially when treating at high temperature [61]. Mutual dissolution of Ce and Fe into Fe_2O_3 and CeO_2 has been reported to exist in Fe-rich Ce/Fe mixed oxides prepared by coprecipitation [62].

For CZF, the value of cell parameter retrieved by Rietveld refinement is not in agreement with that computed from Vegard's law: the adding of a cation (Fe^{3+}) with ionic radius smaller than Ce^{4+} and Zr^{4+} should produce a decrease in cell volume in the case of a solid solution. Conversely, we observe a value higher than expected indicating that Fe_2O_3 is probably deposited on the surface. Moreover, iron could be present as interstitial and/or extralattice or amorphous interparticle iron. As in the case of pure ceria, we cannot exclude that a small fraction of Fe is dissolved within ceria-zirconia framework.

3.2. Catalytic Activity. We investigated the heterogeneous process on different ceria-based catalysts performing reactions at 343 K for 2 hours, without any pH correction of the leachate (pH 9). Preliminary tests were carried out in order to verify the activity of catalyst and/or H_2O_2. In absence of catalyst and H_2O_2 (Figure 3), the abatement of COD and TOC, due only to the thermal treatment at 343 K, is small, respectively 1% and 14%.

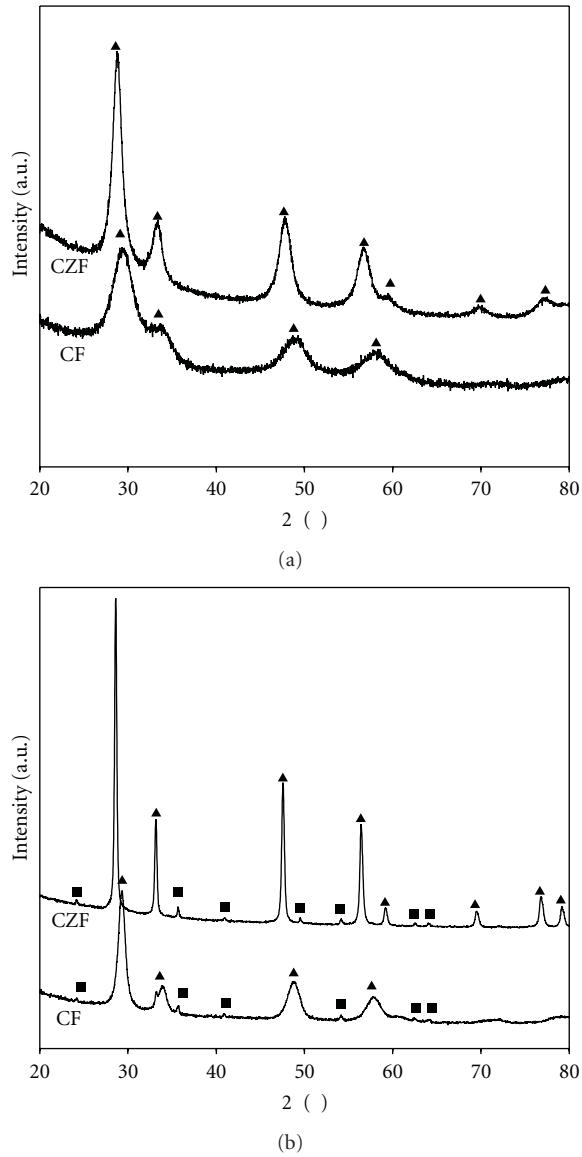

Figure 2: XRD profile for fresh (a) and aged (b) iron-doped samples (▲: CeO_2 and $CeZrO_2$; ■: Fe_2O_3).

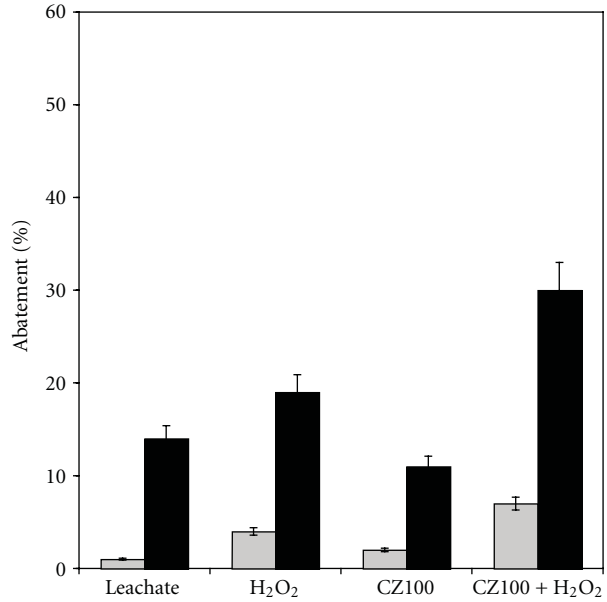

Figure 3: COD (light grey) and TOC (black) abatement for reaction with and without catalyst and H_2O_2 (reaction conditions: 10 mg of catalyst, 5 mL of H_2O_2, pH = 9, T = 343 K).

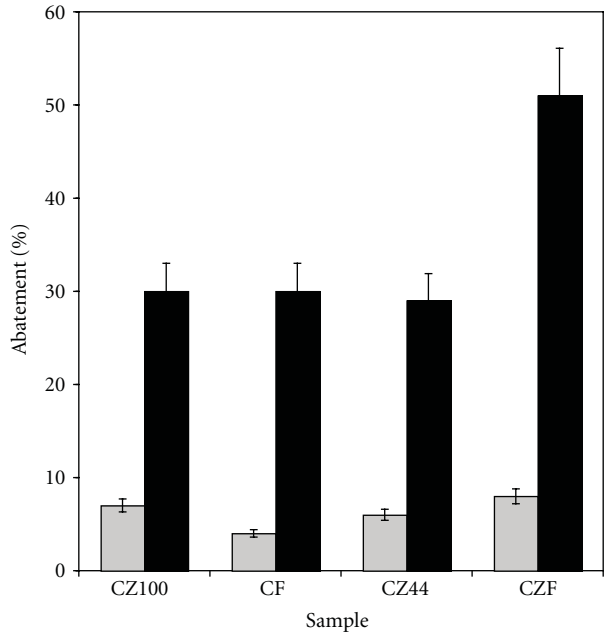

Figure 4: COD (light grey) and TOC (black) abatement for different catalysts (reaction conditions: 10 mg of catalyst, 5 mL of H_2O_2, pH = 9, T = 343 K).

As shown in the plot, the advantage of the addition, for the abatement of COD and TOC, of bare ceria is negligible. In absence of the catalyst, but with 5 mL of H_2O_2 (3%), a small improvement in the activity was observed due to the oxidation capacity of the hydrogen peroxide alone. This activity could be explained considering that the small amount of iron presented in the leachate (Table 1) can interact with H_2O_2 (Fe/H_2O_2 ratio was 1 : 687) catalyzing the formation of $^{\bullet}$OH radicals as in the homogeneous Fenton. When pure ceria and hydrogen peroxide were used in combination, the catalytic activity was further improved reaching an abatement of COD and TOC of 7% and 30%, respectively, confirming the positive synergic action of the two agents in the heterogeneous Fenton-like process. From these preliminary tests, we can conclude that ceria alone is not active and a synergic action between catalyst and hydrogen peroxide is necessary to obtain higher performance.

After blank tests, the activity of the four ceria-based catalysts (CZ100, CZ44, CF, and CZF) was investigated and the results are shown in Figure 4.

Ceria and ceria-zirconia solid solutions show very similar results. The catalytic activity of ceria-based systems could

be attributed to the capacity of cerium oxide to decompose H_2O_2, as reported in a previous study in which the decomposition of hydrogen peroxide, with formation of radical species, in an aqueous suspension of CeO_2 was investigated [63]. The mechanism for H_2O_2 decomposition in the presence of water-oxide interfaces is still not completely elucidated, but it was suggested that it occurs on the surface with OH or HO_2 radicals production.

The catalytic activity of cerium oxide is correlated with its oxygen storage capacity. One of the most important roles of CeO_2 in catalytic redox reactions is to provide surface active sites [64] and to act as an oxygen storage/transport medium by its redox cycle between Ce^{4+} and Ce^{3+}. That is, the presence of surface active oxygens from one side and the oxygen storage capacity from the other are among the most important factors to be considered. These, in turn, are strongly influenced by surface area and surface/bulk composition.

As pointed out previously, doping ceria with Zr^{4+} increase, the oxygen mobility, but a higher amount of ZrO_2 decreases the number of redox sites and consequently the activity of the system. In order to explain the activity of the two systems, we need to take into account the right combination of surface area and composition.

For this reason, it is important to correlate overall activity with total available surface active oxygens, TSAO (which are linearly dependent on the amount of ceria) and total oxygen storage capacity, OSC (which generally shows a volcano-type relation with composition). The number of *total surface oxygens* (TSO) has been estimated according to Madier et al. [65] starting from the structure and the molar composition of the oxide considering the exposure of (100), (110), and (111) surfaces and assuming that Zr atoms do not participate in the redox process. The number of *total surface available oxygens* (TSAO) represents a fraction of total surface oxygens considering that only one atom out of four is involved in the Ce^{4+}-Ce^{3+} redox process [65–67]. OSC data collected according to the method described in the experimental. Results are reported in Table 3.

Even though CZ100 has a lower surface area, pure ceria and CZ44 show almost the same value of TSAO (225 μmol O/g and 182 μmol O/g, resp.). A more pronounced difference was found in OSC (1669 μg O_2/g and 3721 μg O_2/g for CZ100 and CZ44, resp.) that takes into account surface and bulk oxygens. In both catalysts, the surface area is quite high, consequently the abstraction of oxygen involves mainly surface sites, with little or no participation of the bulk in the reaction. Therefore, the more important factor is the availability of surface oxygen. In our materials (CZ100 and CZ44), the availability of surface oxygen is almost the same; therefore the two systems, CZ100 and CZ44, exhibit a very similar catalytic activity in the treatment of landfill leachate.

For CZF, the simultaneously presence of iron and zirconia significantly increased the abatement of TOC (51%) but has no significant effect on COD.

CF sample is characterized by the formation of cubic ceria-like solid solution where Fe cations are dissolved within ceria structure. In this case, the interaction takes place through the sharing of oxygen anion defined by the Fe–O–Ce bonds formed in the Fe-doped CeO_2 lattice [62].

Table 3: TSAO and OSC for CZ100 and CZ44.

Sample	TSAO (μmol O/g)	OSC (μg O_2/g)
CZ100	225	1669
CZ44	182	3721

In CZF sample, the lack of these interactions due to the lower amount of ceria and consequently to the lower amount of Ce-Fe-O entities formed in the system, can explain the different behavior of this catalyst. Indeed, in this case, a higher amount of Fe (due to weaker interaction with Ce and to the amorphous Fe_2O_3 phase on the surface) is available for the reaction with the leachate.

Our research pointed out the good activity of ceria-based heterogeneous treatment and we can conclude that ceria based catalyst is a very promising class of materials for this kind of application.

Further studies will be dedicated to a better understanding of the mechanism of reaction of ceria-based catalyst and to the optimization of the reaction conditions and catalytic stability.

4. Conclusions

Our study shows that the heterogeneous Fenton process could be successfully used in the treatment of landfill leachate substituting homogeneous treatment. Promising results were obtained in leachate oxidation by a heterogeneous Fenton-like process over ceria-based catalysts with an abatement of TOC higher than 50%.

This is just a first investigation into the potentiality of heterogeneous reaction, but the results appear encouraging. In heterogeneous reactions, several variables are involved and need to be completely understood for a good optimization of the catalyst. Further studies will be dedicated to a better understanding of the mechanism of reaction of ceria-based catalysts and the role of iron and zirconia in the reactions and leaching. Moreover, we need to optimize the reaction conditions, such as pH, temperature, and catalyst/peroxide ratio. Additional investigations should be performed in order to deeply explore a promising technique such as heterogeneous Fenton. At the moment, several aspects need to be investigated in more detail, but the results open a new field of research and point out a very interesting class of catalyst that could be used for landfill leachate treatment and worthy to be the subject of further investigations.

Acknowledgments

The authors thank financial support from AMGA Spa, Udine and Passavant Impianti Spa, Milan. They are also grateful to Dott. Stefano Turco and Mr. Aldo Bertoni for laboratory help.

References

[1] L. H. Keith and W. A. Teliard, "Priority pollutants: a perspective view," *Environmental Science & Technology*, vol. 13, pp. 416–423, 1979.

[2] K. Knox and P. H. Jones, "Complexation characteristics of sanitary landfill leachates," *Water Research*, vol. 13, no. 9, pp. 839–846, 1979.

[3] M. Hagman, E. Heander, and J. L. C. Jansen, "Advanced oxidation of refractory organics in leachate—potential methods and evaluation of biodegradability of the remaining substrate," *Environmental Technology*, vol. 29, no. 9, pp. 941–946, 2008.

[4] C. Papastavrou, D. Mantzavinos, and E. Diamadopoulos, "A comparative treatment of stabilized landfill leachate: coagulation and activated carbon adsorption vs. electrochemical oxidation," *Environmental Technology*, vol. 30, no. 14, pp. 1547–1553, 2009.

[5] N. Meunier, P. Drogui, C. Montané, R. Hausler, G. Mercier, and J. F. Blais, "Comparison between electrocoagulation and chemical precipitation for metals removal from acidic soil leachate," *Journal of Hazardous Materials*, vol. 137, no. 1, pp. 581–590, 2006.

[6] F. J. Rivas, F. Beltrán, F. Carvalho, B. Acedo, and O. Gimeno, "Stabilized leachates: sequential coagulation-flocculation plus chemical oxidation process," *Journal of Hazardous Materials*, vol. 116, no. 1-2, pp. 95–102, 2004.

[7] M. J. K. Bashir, M. H. Isa, S. R. M. Kutty et al., "Landfill leachate treatment by electrochemical oxidation," *Waste Management*, vol. 29, no. 9, pp. 2534–2541, 2009.

[8] E. Khan, R. W. Babcock, T. M. Hsu, and H. Lin, "Mineralization and biodegradability enhancement of low level p-nitrophenol in water using Fenton's reagent," *Journal of Environmental Engineering*, vol. 131, no. 2, pp. 327–331, 2005.

[9] E. C. Catalkaya and F. Kargi, "Advanced oxidation of diuron by photo-fenton treatment as a function of operating parameters," *Journal of Environmental Engineering*, vol. 134, no. 12, pp. 1006–1013, 2008.

[10] E. Neyens and J. Baeyens, "A review of classic Fenton's peroxidation as an advanced oxidation technique," *Journal of Hazardous Materials*, vol. 98, no. 1–3, pp. 33–50, 2003.

[11] P. Westerhoff, G. Aiken, G. Amy, and J. Debroux, "Relationships between the structure of natural organic matter and its reactivity towards molecular ozone and hydroxyl radicals," *Water Research*, vol. 33, no. 10, pp. 2265–2276, 1999.

[12] S. Zhao, H. Ma, M. Wang et al., "Role of primary reaction initiated by 254 nm UV light in the degradation of p-nitrophenol attacked by hydroxyl radicals," *Photochemical and Photobiological Sciences*, vol. 9, no. 5, pp. 710–715, 2010.

[13] J. De Laat and H. Gallard, "Catalytic decomposition of hydrogen peroxide by Fe(III) in homogeneous aqueous solution: mechanism and kinetic modeling," *Environmental Science and Technology*, vol. 33, no. 16, pp. 2726–2732, 1999.

[14] S. H. Lin and C. C. Lo, "Fenton process for treatment of desizing wastewater," *Water Research*, vol. 31, no. 8, pp. 2050–2056, 1997.

[15] S. Parsons, *Advanced Oxidation Processes for Water and Wastewater Treatment*, IWA publishing, Alliance House, London, UK, 2004.

[16] C. Jiang, S. Pang, F. Ouyang, J. Ma, and J. Jiang, "A new insight into Fenton and Fenton-like processes for water treatment," *Journal of Hazardous Materials*, vol. 174, no. 1–3, pp. 813–817, 2010.

[17] M. D. Gurol and S. Lin, "Continuous catalytic oxidation processes," US PATENT 5755977, 1998.

[18] S. Sabhi and J. Kiwi, "Degradation of 2,4-dichlorophenol by immobilized iron catalysts," *Water Research*, vol. 35, no. 8, pp. 1994–2002, 2001.

[19] Y. F. Han, N. Phonthammachai, K. Ramesh, Z. Zhong, and T. I. M. White, "Removing organic compounds from aqueous medium via wet peroxidation by gold catalysts," *Environmental Science and Technology*, vol. 42, no. 3, pp. 908–912, 2008.

[20] P. L. Huston and J. J. Pignatello, "Degradation of selected pesticide active ingredients and commercial formulations in water by the photo-assisted Fenton reaction," *Water Research*, vol. 33, no. 5, pp. 1238–1246, 1999.

[21] Y. Deng and J. D. Englehardt, "Treatment of landfill leachate by the Fenton process," *Water Research*, vol. 40, no. 20, pp. 3683–3694, 2006.

[22] A. Goi, Y. Veressinina, and M. Trapido, "Fenton process for landfill leachate treatment: evaluation of biodegradability and toxicity," *Journal of Environmental Engineering*, vol. 136, no. 1, pp. 46–53, 2010.

[23] T. Yilmaz, A. Aygün, A. Berktay, and B. Nas, "Removal of COD and colour from young municipal landfill leachate by Fenton process," *Environmental Technology*, vol. 31, no. 14, pp. 1635–1640, 2010.

[24] E. M. R. Rocha, V. J. P. Vilar, A. Fonseca, I. Saraiva, and R. A. R. Boaventura, "Landfill leachate treatment by solar-driven AOPs," *Solar Energy*, vol. 85, no. 1, pp. 46–56, 2011.

[25] S. Mohajeri, H. A. Aziz, M. H. Isa, M. A. Zahed, and M. N. Adlan, "Statistical optimization of process parameters for landfill leachate treatment using electro-Fenton technique," *Journal of Hazardous Materials*, vol. 176, no. 1–3, pp. 749–758, 2010.

[26] S. Navalon, R. Martin, M. Alvaro, and H. Garcia, "Gold on diamond nanoparticles as a highly efficient fenton catalyst," *Angewandte Chemie—International Edition*, vol. 49, no. 45, pp. 8403–8407, 2010.

[27] R. Martín, S. Navalon, M. Alvaro, and H. Garcia, "Optimized water treatment by combining catalytic Fenton reaction using diamond supported gold and biological degradation," *Applied Catalysis B*, vol. 103, no. 1-2, pp. 246–252, 2011.

[28] A. G. Chakinala, P. R. Gogate, A. E. Burgess, and D. H. Bremner, "Industrial wastewater treatment using hydrodynamic cavitation and heterogeneous advanced Fenton processing," *Chemical Engineering Journal*, vol. 152, no. 2-3, pp. 498–502, 2009.

[29] I. Oller, S. Malato, and J. A. Sánchez-Pérez, "Combination of Advanced Oxidation Processes and biological treatments for wastewater decontamination-A review," *Science of the Total Environment*, vol. 409, pp. 4141–4166, 2010.

[30] T. D. Nguyen, N. H. Phan, M. H. Do, and K. T. Ngo, "Magnetic Fe_2MO_4 (M:Fe, Mn) activated carbons: fabrication, characterization and heterogeneous Fenton oxidation of methyl orange," *Journal of Hazardous Materials*, vol. 185, no. 2-3, pp. 653–661, 2011.

[31] N. Panda, H. Sahoo, and S. Mohapatra, "Decolourization of Methyl Orange using Fenton-like mesoporous Fe_2O_3-SiO_2 composite," *Journal of Hazardous Materials*, vol. 185, no. 1, pp. 359–365, 2011.

[32] L. A. Galeano, M. Á. Vicente, and A. Gil, "Treatment of municipal leachate of landfill by fenton-like heterogeneous catalytic wet peroxide oxidation using an Al/Fe-pillared montmorillonite as active catalyst," *Chemical Engineering Journal*, vol. 178, pp. 146–153, 2011.

[33] S. Bernal, J. Kaspar, and A. Trovarelli, "Recent progress in catalysis by ceria and related compounds—preface," *Catal Today*, vol. 50, pp. 173–173, 1999.

[34] A. Trovarelli, *Catalysis by Ceria and Related Materials*, Imperial College Press, London, UK, 2002.

[35] A. Trovarelli, C. De Leitenburg, M. Boaro, and G. Dolcetti, "The utilization of ceria in industrial catalysis," *Catalysis Today*, vol. 50, no. 2, pp. 353–367, 1999.

[36] A. Trovarelli, C. De Leitenburg, and G. Dolcetti, "Design better cerium-based oxidation catalysts," *Chemtech*, vol. 27, no. 6, pp. 32–37, 1997.

[37] L. Vivier and D. Duprez, "Ceria-based solid catalysts for organic chemistry," *ChemSusChem*, vol. 3, no. 6, pp. 654–678, 2010.

[38] N. D. Tran, M. Besson, C. Descorme, K. Fajerwerg, and C. Louis, "Influence of the pretreatment conditions on the performances of CeO_2-supported gold catalysts in the catalytic wet air oxidation of carboxylic acids," *Catalysis Communications*, vol. 16, no. 1, pp. 98–102, 2011.

[39] S. Yang, W. Zhu, Z. Jiang, Z. Chen, and J. Wang, "nfluence of the structure of TiO_2, CeO_2, and CeO_2-TiO_2 supports on the activity of Ru catalysts in the catalytic wet air oxidation of acetic acid," *Rare Metals*, vol. 30, pp. 488–495, 2011.

[40] J. J. Delgado, X. Chen, J. A. Pérez-Omil, J. M. Rodríguez-Izquierdo, and M. A. Cauqui, "The effect of reaction conditions on the apparent deactivation of Ce-Zr mixed oxides for the catalytic wet oxidation of phenol," *Catalysis Today*, vol. 180, pp. 25–33, 2011.

[41] Y. Liu and D. Sun, "Effect of CeO_2 doping on catalytic activity of Fe_2O_3/γ-Al_2O_3 catalyst for catalytic wet peroxide oxidation of azo dyes," *Journal of Hazardous Materials*, vol. 143, no. 1-2, pp. 448–454, 2007.

[42] R. C. Martins, N. Amaral-Silva, and R. M. Quinta-Ferreira, "Ceria based solid catalysts for Fenton's depuration of phenolic wastewaters, biodegradability enhancement and toxicity removal," *Applied Catalysis B*, vol. 99, no. 1-2, pp. 135–144, 2010.

[43] S. Silva Martínez, J. Vergara Sánchez, J. R. Moreno Estrada, and R. Flores Velásquez, "FeIII supported on ceria as effective catalyst for the heterogeneous photo-oxidation of basic orange 2 in aqueous solution with sunlight," *Solar Energy Materials and Solar Cells*, vol. 95, no. 8, pp. 2010–2017, 2011.

[44] P. A. Deshpande, D. Jain, and G. Madras, "Kinetics and mechanism for dye degradation with ionic Pd-substituted ceria," *Applied Catalysis A*, vol. 395, no. 1-2, pp. 39–48, 2011.

[45] APHA, AWWA, and WEF, *Standard Methods for the Examination of Water and Wastewater*, American Public Health Association, American Water Works Association, Water Environment Federation, Washington, DC, USA, 20th edition, 1999.

[46] R. Jenkins and R. Snyder, *To X-Ray Powder Diffractometry*, Wiley, New York, NY, USA, 1996.

[47] R. A. Young, *The Rietveld Method IUCr*, Oxford University Press, New York, NY, USA, 1993.

[48] A. C. Larson and R. B. V. Dreele, *General Structure Analysis System 'GSAS'*, Los Alamos National Laboratory, 2000.

[49] B. H. Toby, "EXPGUI, a graphical user interface for GSAS," *Journal of Applied Crystallography*, vol. 34, no. 2, pp. 210–213, 2001.

[50] D. J. Kim, "Lattice-parameters, ionic conductivities, and solubility limits in fluorite-structure MO2 Oxide [M = Hf4+, Zr4+, Ce4+, Th4+, U4+] Solid Solutions ," *Journal of the American Ceramic Society*, vol. 72, no. 8, pp. 1415–1421, 1989.

[51] E. Aneggi, M. Boaro, C. De Leitenburg, G. Dolcetti, and A. Trovarelli, "Insights into the redox properties of ceria-based oxides and their implications in catalysis," *Journal of Alloys and Compounds*, vol. 408-412, pp. 1096–1102, 2006.

[52] E. Mamontov, R. Brezny, M. Koranne, and T. Egami, "Nanoscale heterogeneities and oxygen storage capacity of Ce 0.5Zr0.5O2," *Journal of Physical Chemistry B*, vol. 107, no. 47, pp. 13007–13014, 2003.

[53] R. Q. Syed and W. Chiang, *Sanitary Landfill Leachate, Generation, Control and Treatment*, Technomic, Basel, Switzerland, 1994.

[54] J. Kaspar and P. Fornasiero, "Structural properties and thermal stability of ceria-zirconia and related materials," in *Catalysis by Ceria and Related Materials*, A. Trovarelli, Ed., Imperial College Press, London, UK, 2002.

[55] A. Trovarelli, F. Zamar, J. Llorca, C. De Leitenburg, G. Dolcetti, and J. T. Kiss, "Nanophase fluorite-structured CeO_2-ZrO_2 catalysts prepared by high-energy mechanical milling: analysis of low-temperature redox activity and oxygen storage capacity," *Journal of Catalysis*, vol. 169, no. 2, pp. 490–502, 1997.

[56] S. Rossignol, F. Gérard, and D. Duprez, "Effect of the preparation method on the properties of zirconia-ceria materials," *Journal of Materials Chemistry*, vol. 9, no. 7, pp. 1615–1620, 1999.

[57] H. Vidal, J. Kašpar, M. Pijolat et al., "Redox behavior of CeO_2-ZrO_2 mixed oxides. I. Influence of redox treatments on high surface area catalysts," *Applied Catalysis B*, vol. 27, no. 1, pp. 49–63, 2000.

[58] H. Vidal, J. Kašpar, M. Pijolat et al., "Redox ehaviour of CeO_2-ZrO_2 mixed oxides II. Influence of redox treatments on low surface area catalysts," *Applied Catalysis B*, vol. 30, no. 1-2, pp. 75–85, 2001.

[59] J. Kaspar, P. Fornasiero, G. Balducci, R. Di Monte, N. Hickey, and V. Sergo, "Effect of ZrO_2 content on textural and structural properties of CeO_2-ZrO_2 solid solutions made by citrate complexation route," *Inorganica Chimica Acta*, vol. 349, pp. 217–226, 2003.

[60] P. Fornasiero, G. Balducci, R. Di Monte et al., "Modification of the redox behaviour of CeO_2 induced by structural doping with ZrO_2," *Journal of Catalysis*, vol. 164, no. 1, pp. 173–183, 1996.

[61] Z. Tianshu, P. Hing, H. Huang, and J. Kilner, "Sintering and densification behavior of Mn-doped CeO_2," *Materials Science and Engineering B*, vol. 83, no. 1–3, pp. 235–241, 2001.

[62] F. J. Pérez-Alonso, M. L. Granados, M. Ojeda et al., "Chemical structures of coprecipitated Fe-Ce mixed oxides," *Chemistry of Materials*, vol. 17, no. 9, pp. 2329–2339, 2005.

[63] A. Hiroki and J. A. LaVerne, "Decomposition of hydrogen peroxide at water-ceramic oxide interfaces," *Journal of Physical Chemistry B*, vol. 109, no. 8, pp. 3364–3370, 2005.

[64] A. Trovarelli, "Catalytic properties of ceria and CeO_2-Containing materials," *Catalysis Reviews*, vol. 38, no. 4, pp. 439–520, 1996.

[65] Y. Madier, C. Descorme, A. M. Le Govic, and D. Duprez, "Oxygen mobility in CeO_2 and $CexZr_{(1-x)}O_2$ compounds: study by CO transient oxidation and $^{18}O/^{16}O$ isotopic exchange," *Journal of Physical Chemistry B*, vol. 103, no. 50, pp. 10999–11006, 1999.

[66] M. Boaro, C. De Leitenburg, G. Dolcetti, and A. Trovarelli, "The dynamics of oxygen storage in ceria-zirconia model catalysts measured by CO oxidation under stationary and cycling feedstream compositions," *Journal of Catalysis*, vol. 193, no. 2, pp. 338–347, 2000.

[67] C. E. Hori, H. Permana, K. Y. S. Ng et al., "Thermal stability of oxygen storage properties in a mixed CeO_2-ZrO_2 system," *Applied Catalysis B*, vol. 16, no. 2, pp. 105–117, 1998.

Hindawi Publishing Corporation
International Journal of Photoenergy
Volume 2012, Article ID 914757, 7 pages
doi:10.1155/2012/914757

Research Article

Investigation on the Adsorption and Photooxidation of Glycerol at TiO_2 Nanotubular Arrays

Simonetta Palmas,[1] Anna Da Pozzo,[1] Michele Mascia,[1] Annalisa Vacca,[1] and Roberto Matarrese[2]

[1] *Dipartimento di Ingegneria Meccanica, Chimica e Materiali, Università degli Studi di Cagliari, Piazza d'Armi, 09123 Cagliari, Italy*
[2] *Dipartimento di Energia, Politecnico di Milano, Piazza L. Da Vinci 32, 20133 Milano, Italy*

Correspondence should be addressed to Simonetta Palmas, simonetta.palmas@dimcm.unica.it

Received 1 June 2012; Accepted 18 July 2012

Academic Editor: Manickavachagam Muruganandham

A study is presented on the adsorption of glycerol at TiO_2 as well as on its oxidative process during the contemporary water Photoelectro-splitting for hydrogen production. A deepening in the understanding on the working mechanism of the TiO_2 nanotubular photoanodes and on the interactions between glycerol and these structures has been gained through photocurrent tests, voltammetric scans, and EIS analysis. A range of wavelength of the incident radiation is investigated from 340 to 400 nm at which the effect of glycerol on the photocurrent is measured. Quantitative analysis of the EIS results is performed by the equivalent circuit approach.

1. Introduction

The growing attention on innovative processes using glycerol as starting material for the obtainment of more valuable products such as other chemicals or energy is due to the great increase of its market availability as byproduct in the biodiesel production [1]. Since the international legislation is addressed to a greater production of bio- or renewable fuels to be used for transportation, the crude glycerol production from the biodiesel industry is increasing exponentially. Consequently, the commercial price of glycerol is greatly lowered and several perspectives of research for its use are of big interest [2–5]. To face this issue, following the principles of sustainable chemistry means to pay attention to avoid the use and the generation of harmful substances, to reduce the energy consumption, and to use renewable resources such as solar energy.

In this context, a very interesting way to use this chemical is in the photo-electrocatalytic hydrogen production, conceiving a system which can couple, under a suitable combination between irradiation and external potential bias, the cathodic hydrogen production and the oxidation of glycerol, used as sacrificial reagent at the photoanode. Actually, among the possible ways to increase the efficiency of a photoelectrochemical cell, the presence of a sacrificial agent into the solution must be considered as effective to prevent the electron-hole recombination process.

For photocatalytic hydrogen generation, compounds such as alcohols, EDTA, or ions such as I^-, IO_3^- CN^-, and Fe^{3+}, but also many other organic pollutants, such as oxalic acid, formic acid, and formaldehyde, can be used as sacrificial reagents ([6–8] and references therein).

As above reported, due to its wide market availability, glycerol has been proposed in the present paper as sacrificial agent; moreover, a further enhancement of the process could consider the possibility to make the oxidation of glycerol selective in order to address the process to obtain its more valuable oxidation byproducts such as dihydroxyacetone, glyceric acid, or glyceraldehyde.

In the field of photo-electrocatalytic hydrogen production, the use of photoanodes based on nanotubular TiO_2 has been assessed by several studies that highlighted their optimal properties in terms of corrosion resistance, reactivity, photoactivity, low cost, and availability [9, 10]. In our laboratory, several studies have been carried out [11] that showed and proved the feasibility of using glycerol as hole scavenger

in the process. A recent study [12] also proposed some possible mechanisms of adsorption of glycerol on nanostructured titania, evidencing the importance of the defectivity of the oxide for its photoactivity and for its capacity to adsorb glycerol molecules. Glycerol resulted strongly adsorbable on the oxygen vacancies of TiO_2 greatly influencing the behaviour of the structures during photocatalysis. The present work wants to give a contribution to the research in this field, widening the range of investigated wavelength of the incident radiation, in view of a possible optimization of the process and its addressing to practical applications. Actually, it must be considered that most of the investigations carried out so far in our laboratory, as well as most of the works present in the literature concerning nanostructured titania, were focused on the photo-activity of the samples in the UV range, where the TiO_2 has its maximum performance.

For the purposes of possible practical applications that can exploit a larger percentage of the solar spectrum, it is useful to widen the field of investigation to different wavelengths of incident radiation. The present study investigates in particular a wavelength range from 340 to 400 nm to evaluate the effect of glycerol in this wider spectrum of conditions.

2. Experimental

2.1. Preparation of the Electrode. The electrodes were prepared starting from Ti foils (0.25 mm thick, 99.7% metal basis, Aldrich) and following the same procedure adopted and described elsewhere [13]. After a preliminary degreasing treatment, the Ti foil was electrochemically oxidised at 20 V in 0.4 M NH_4NO_3 + 0.25 M NaF for three hours. Then, it was annealed 3 h at 400°C, in air.

2.2. The Electrochemical Cell. A three-electrode cell was used for the electrochemical runs, in which the TiO_2 sample was the working electrode; for all the experiments, its surface was shielded so that a nominal area of 1 cm^2 was exposed to the electrolyte. A platinum grid and a saturated calomel electrode (SCE) constituted the counter and the reference electrodes, respectively; all the values of potential in the text are referred to SCE.

2.3. Experimental Runs. All the tests were performed in KOH 0.1 M solution with or without the presence of glycerol 0.1 M. Electrochemical impedance spectroscopy (EIS) measurements were performed at different bias potentials in a frequency range from 100 kHz to 0.1 Hz. A frequency response analyzer (FRA, Model 7200 AMEL) coupled with a potentiostat (AMEL 7050) have been employed for these experiments. EIS data were quantitatively interpreted by the equivalent circuit approach. Zassist and ZSimpWin software packages were used to perform impedance experiments and data manipulation, respectively.

Polarisation curves were obtained in the dark or under irradiation by imposing a potential ramp from the open circuit voltage (OCV) to about 1 V with a scan rate of 5 mV s^{-1}. Photocurrents were calculated by subtracting the values obtained in the dark from those measured under radiation.

The light source was a 300-W Xe lamp (Lot Oriel) the behaviour of the sample was studied using four filters with centre wavelength at 340, 365, 380, and 400 nm. The average light intensity striking on the surface of the electrode ranged from 1.5 to 11 mWcm^{-2} depending on the filter. To compare results, photocurrents (I) have been normalized with respect to the incident light power (P).

Voltammetric scans were performed starting from the OCV towards the negative potential down to −1.5 V, with a scan rate of 200 mV s^{-1}.

The effect of the adsorption of glycerol was particularly investigated by performing different scans after that sample was maintained in contact with 0.1 M glycerol solution for increasing intervals of time. The effect of desorption was investigated maintaining the sample in KOH 0.1 M solution.

For all the runs, chemicals were of reagent grade (supplied by Aldrich) and they were used as received.

3. Results and Discussion

In order to use glycerol as a sacrificial agent in the process of hydrogen production by solar energy, a deep understanding on the working mechanism of the electrodes and on the interactions between glycerol and nanotubular TiO_2 has to be gained. For some years, our work has been aimed to this end; we found out that photo-catalytic response of TiO_2 nanotubular arrays depends on a wide number of factors related to the specific conditions of synthesis and to the morphological and electronic properties of the samples [11–14]. Moreover, we also investigated the opportunity to enhance the photo-electrochemical yield through the use of glycerol as hole scavenger [11, 12]. Depending on the electrodes, different percentage increases in the current yield were obtained: in some cases the addition of glycerol showed to be of scarce effect [11]; in other cases, we obtained increases of more than the 100% [12]. In the present work the study has been focused to the behaviour of those samples that gave the best performance, by investigating in detail the responses in photocurrent tests in an extended range of wavelength. The results from these experiments, along with those derived from voltammetric and EIS analysis are presented in the following.

Figure 1 reports the results of the photo-electrochemical tests performed at different wavelengths, in solutions without and with the presence of glycerol as hole scavenger. Results obtained at 365 nm are in agreement with those obtained for a sample synthesized under the same operative conditions [12]. In all the cases, curves always show an initial increasing trend of photocurrent with the applied potential and a second part less dependent on it. Moreover, potential value being the same, photocurrents decrease with the wavelength according to the absorption coefficient of the TiO_2.

To evaluate quantitatively the enhancement of photocurrent after the addition of glycerol, the ratio **j** between the photocurrent responses in presence (I_G) and in absence of glycerol (I_{KOH}) has been compared at two significant potential values: the first (E_1) where photocurrents are highly potential dependent was fixed as 0.05 V higher than the current onset, and the second (E_2) in the range where

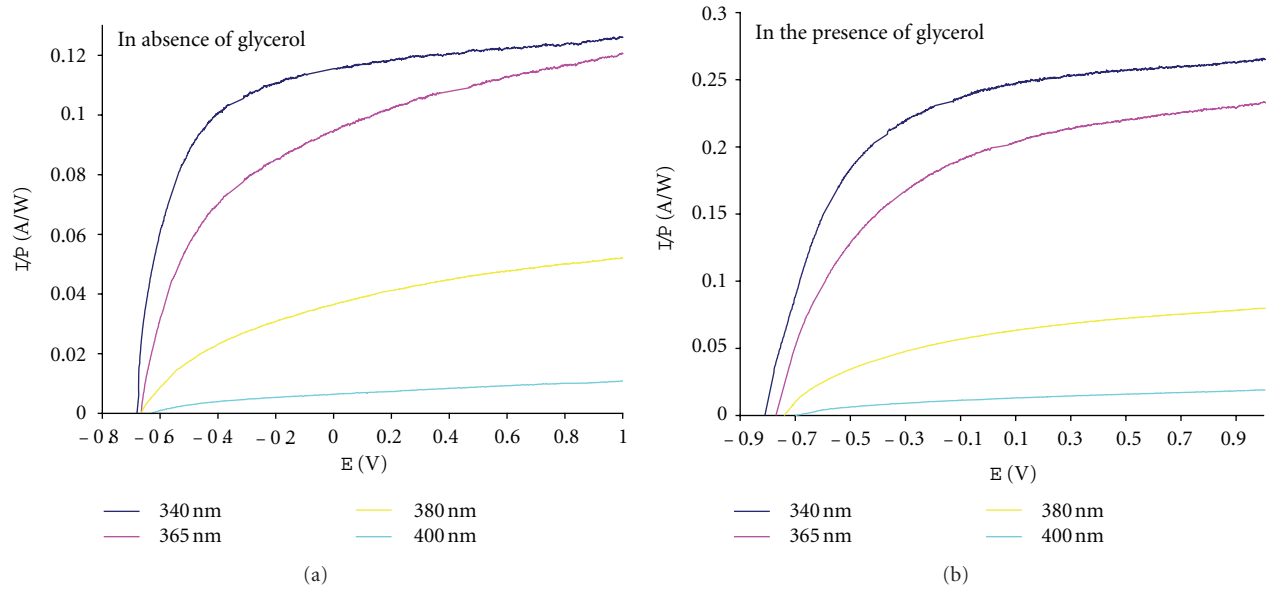

Figure 1: Trend of photocurrents (normalized to incident power light) versus potential, at different wavelengths, in absence and in presence of glycerol.

currents have reached their steady state values was fixed at 1 V from the current onset. Data are reported in Table 1. As it can be seen, a positive effect of glycerol, indicated by the **j** values greater than unit, is achieved at all the wavelengths: higher **j** values are measured, in the range of 2–4, near the on set potential, confirming the positive effect of glycerol in reducing the high rate of recombination of photogenerated charges occurring at this potential. The effect of glycerol is less evident in the presence of a higher external applied potential: values of **j** go down around the value of 2 so highlighting how the applied potential also contributed to the lowering of the charge recombination process.

If the trend of **j** with the wavelength is considered, it is possible to note that while at the higher potential (E_2), the ratio **j** remains more or less stable around 2 at all the considered wavelengths, and at the lower potential (E_1), the best performances are obtained in the range of visible light. This is a very remarkable result especially if we consider how the applied potential affects the energetic yield of an electrically driven photoprocess [15]:

$$\varepsilon = \frac{I\left(E_{\text{rev}}{}^{0} - \left|E_{\text{app}}\right|\right)}{P}, \tag{1}$$

in which $E_{\text{rev}}{}^{0} = 1.23\,\text{V}$ is the standard reversible potential for water splitting, and P is the light power.

As it can be observed, the yield takes into account the net power output obtained in the process, being E_{appl} the difference between the bias potential and the OCV under the irradiated power light. From this equation it is evident that the possibility to work at lower potential has to be preferred in this kind of processes.

In the present case, the results obtained indicate that the presence of glycerol particularly favours conditions of lower applied potential and higher wavelength that are the best conditions to carry out the considered process in an ecofriendly way.

To better understand the working mechanism of the electrode and the interactions occurring between glycerol and nanotubular TiO_2, EIS measurements were carried out at the irradiated sample; also in this case, two different ranges of potential were investigated, near to the OCV and at higher values where the saturation current was achieved.

Figure 2 reports the spectra, in terms of Bode and Nyquist plots, obtained in absence and in presence of glycerol, at the potential of 0.5 V.

No significant differences are evident in Bode phase angle diagrams. As the Bode modulus versus frequency plot is considered, at the higher frequencies, where as it is known the solution resistance (R_S) dominates the impedance, values overlapped, confirming the almost equal resistance of the solution, whose conductivity is given mainly by the supporting electrolyte. As the frequency decreases, the curves still remain overlapped; only at values lower than about 1 Hz, a slight separation of the modulus appeared, whose meaning can be better seen on the Nyquist plot, where, at the lower frequencies, the semicircle related to charge transfer occurring at the interface electrode-electrolyte appears. According to the higher photocurrents obtained in presence of glycerol, the semicircle related to the reaction happening at the electrode-electrolyte interfaces shows a smaller diameter when glycerol is present, indicating a more easy charge transfer with the solution.

Other important information can be gathered from the EIS performed at the potential near the OCV, (Figure 3); under this potential the extent of the occurring reactions is very low, and more interesting information can be obtained on the capacitive behaviour of the sample.

Referring to Bode diagram of modulus, also at this potential, the values overlapped at the higher frequencies, but

Table 1: I_G/I_{KOH} values obtained at the different wavelengths and at two different potentials.

$j = I_G/I_{KOH}$		Wavelength (nm)			
		340	365	380	400
Potential (V)	E_1	*2.4*	*3.1*	*3*	*4*
	E_2	*2.1*	*2.1*	*1.8*	*1.9*

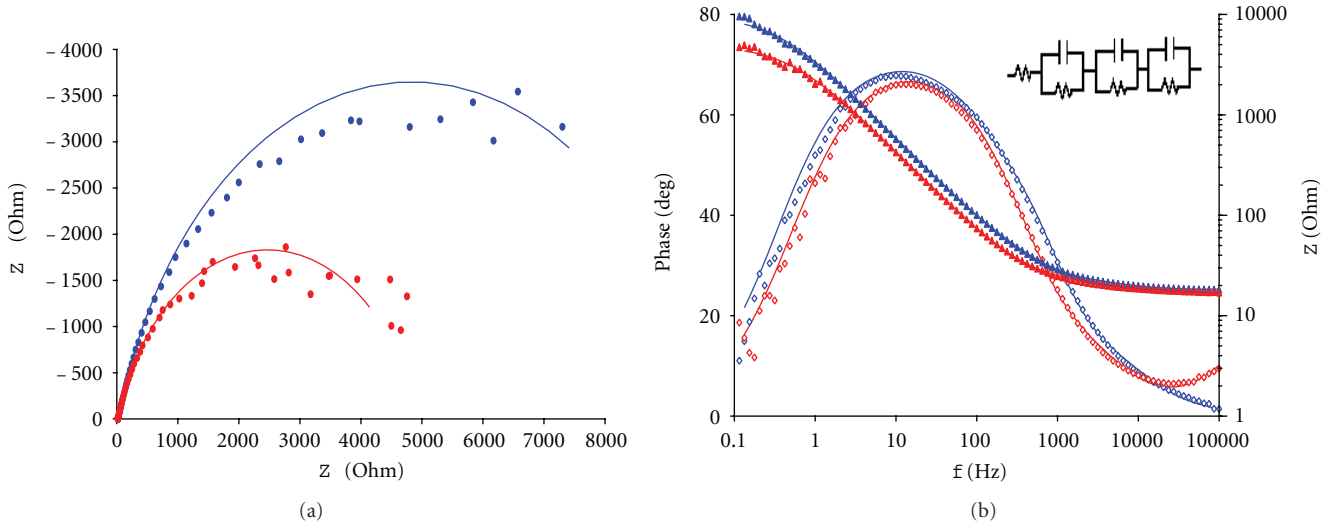

Figure 2: EIS results under irradiation: (a) Nyquist plots; (b) phase angle (empty symbols) and modulus (solid symbols) Bode plots; $E = 0.5$ V, $\lambda = 365$ nm. Blue symbols: in absence of glycerol. Red symbols: in presence of glycerol. Solid lines refer to the model fit.

in this case, curves are differentiated starting from about 80 Hz, being values obtained in presence of glycerol lower. In particular, a wide range of the curves with linear trend can be identified with negative slope equal to unit; according to the theory, an indication of the value of the double layer capacitance ($1/C_{dl}$) can be obtained from the intersection of the straight line with the y-axis. As expected, the increased C_{dl} in presence of glycerol suggests a significant adsorption of glycerol at the electrode surface.

The presence of adsorbed glycerol can be confirmed also by the analysis of Nyquist plot at the intermediated frequencies, as visible in Figure 3, where a suitable magnification of the plot has been presented. In this range of frequencies, a linear trend of the data is detected, whose unit slop indicated that diffusion processes of the reactive species inside the tubes may be relevant, both in absence and in presence of glycerol.

Data were quantitatively interpreted by means of the equivalent circuit approach in which the behaviour of the experimental system was compared with the one of a suitable electrical circuit (equivalent circuit) submitted to the same input potential signal. A fitting procedure between the response of the experimental system and that of the equivalent circuit allowed to evaluate the circuital elements to which a physical meaning can be attributed.

In the present case, an equivalent circuit with three-time constants was able to interpret the data obtained under irradiation in the two ranges of potentials, respectively, at OCV ($R_S(R_1C_1)(R_2C_2)W$) and under saturation current regime ($R_S(R_1C_1)(R_2C_2)(R_3C_3)$).

It must be observed that both the circuits include the resistance R_S which takes into account the solution resistance which was found in all cases very low due to the high conductivity of the solution. The other elements are used to represent the response of the electrode film and the electrode/solution interphase. Tables 2 and 3 resume the values of the circuital parameters calculated by the fit of experimental data.

For the circuits interpreting the system at OCV, the presence of an element with high time constant (R_2C_2), along with the Warburg element may describe a slow process of diffusion and adsorption. Actually, the presence of the W element highlights the relevance of diffusion effects; the following relationship can be written for the impedance of the W element:

$$Z_W = \frac{1}{\sqrt{2\omega}Y_0} - j\frac{1}{\sqrt{2\omega}Y_0}, \tag{2}$$

in which the Warburg coefficient Y_0 depends on typical properties of the system, such as diffusivity and concentration of the active specie, electrode area involved, and temperature.

In order to describe data at higher potential, in addition to the R_fC_f, other two elements are needed. In this case, a constant phase element (CPE) was needed to represent the nonideal behavior of the capacitor. Actually, impedance of a CPE may be expressed as

$$\left(Z_{CPE} = \frac{1}{Q(j\omega)^n}\right), \tag{3}$$

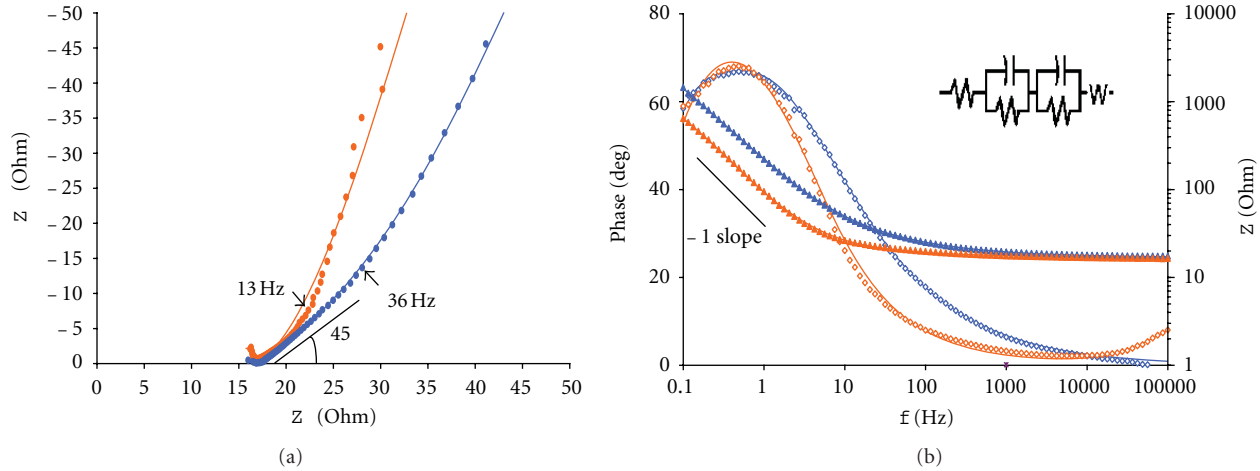

Figure 3: EIS results under irradiation: (a) Nyquist plots; (b) phase angle (empty symbols) and modulus (solid symbols) Bode plots; E = OCV, λ = 365 nm. Blu symbols: in absence of glycerol. Orange symbols: in presence of glycerol. Solid lines refer to the model fit.

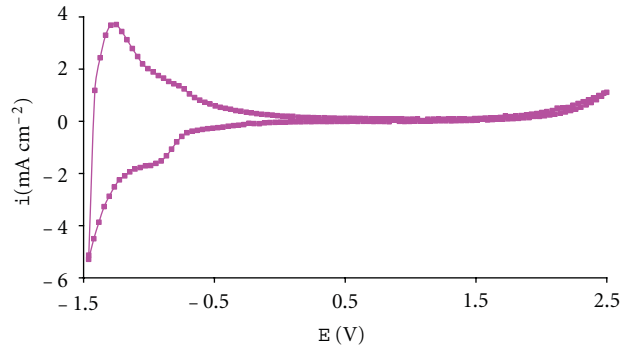

Figure 4: Example of cyclic voltammetry carried out at 0.1 M glycerol solution at TiO_2 electrode.

being $n = 1$ for a perfect capacitor. Its time constant ($\tau_3 = (RQ)^{1/n}$) in the order of seconds, along with that of the R_2C_2 (τ_2 in the order of μs) indicate fast processes occurring at the electrode at this potential value. Accordingly, a lower diameter is recorded in the loops of the Nyquist plots compared to that recorded at the OCV and higher currents are measured.

To deeply investigate adsorption process, voltammetric scans were carried out in KOH solutions containing glycerol in the range of negative potentials from the OCV to about −1.5 V. An example of these results is shown in Figure 4. Previous studies [12] showed that the height of the cathodic peak observed at about −1 V may indicate the extent of the adsorption of glycerol on the surface of TiO_2. In this case, CV runs were performed after the sample was contacted for increasing times by glycerol solution. CV runs were then repeated after desorption in KOH solvent.

In Table 4, the height of the cathodic peak is reported as a function of the adsorption and desorption times. Data suggest a slow adsorption process occurring on the superficial state of TiO_2 nanotubes, and a quite reversible, even slower desorption process.

Also in this case, a series of EIS measurements have been carried out, with and without glycerol in the dark, in order to study the behaviour of the sample as a function of the adsorption time, and the results interpreted by suitable equivalent circuits.

Figure 5 shows the Nyquist plots obtained at the sample maintained in contact with glycerol alkaline solution for increasing intervals of time. In the same figure, Nyquist plot obtained in a KOH solution is reported as comparison. Also in this case, a suitable magnification of the diagram has been chosen to highlight the range of major changes caused by the absorption process.

As well visible in Figure 5, only after 20 h, glycerol adsorption noticeably modifies the first semicircle of the plot. At the higher frequencies (data not reported), the trend of impedance values is not particularly meaningful showing, as expected, a simply resistive behaviour, since reactions do not occur in the system without illumination and near the open circuit potential.

As shown in Figure 5(b), the data obtained after 20 and 40 hours of desorption tend to merge with those obtained before the glycerol adsorption; the adsorption process is reversible but the desorption process results to be quite slow.

A quantitative analysis of the kinetics of adsorption is reported in Table 5, where the circuital parameters are compared. In particular, as already outlined in the previous figures, the sample resistance R_f increases with the adsorption of glycerol and then it decreases after desorption. The fact that the adsorption of glycerol leads to the increase in the material resistance supports the hypothesis [12], that it is preferentially adsorbed on the superficial states responsible of the conductibility of the electrode.

Also in this case, the high value of the time constant $\tau 2$ as well as the presence of a Warburg element indicate that, in these conditions, the adsorption represents the rate determining step of the whole process. However, as the specific values of Y_0 are compared, their variation is quite difficult to be interpreted; in fact, as already pointed out, although the coefficient Y_0 could be related to the diffusion coefficient of

Table 2: Circuit parameters obtained by fitting the experimental impedance results with the selected equivalent circuit. Data obtained under irradiation ($\lambda = 365$ nm) in the presence and in absence of glycerol, $E =$ OCV.

	$E =$ OCV					
	C_f (μF cm^{-2})	R_f (Ω cm^2)	C_2 (μF cm^{-2})	R_2 (Ω cm^2)	τ_2 (s)	Y_0 (μS s$^{0.5}$ cm^{-2})
KOH	10	17.2	1200	2544	3.04	4700
G	0.23	16.66	2460	1041	2.55	14500

Table 3: Circuit parameters obtained by fitting the experimental impedance results with the selected equivalent circuit. Data obtained under irradiation ($\lambda = 365$ nm) in the presence and in absence of glycerol, $E = 0.5$ V.

	$E = 0.5$ V								
	C_f (μF cm^{-2})	R_f (Ω cm^2)	C_2 (μF cm^{-2})	R_2 (Ω cm^2)	τ_2 (s)	Q_3 (μS s^n cm^{-2})	n_3	R_3 (Ω cm^2)	τ_3 (s)
KOH	82.5	24.93	10.1	2.40	24	55.8	0.83	9619	0.47
G	0.13	17.63	22.1	2.45	54	78.8	0.82	4903	0.31

Table 4: Heights of the cathodic peak observed at -1 V as a function of the adsorption (t_{ads}) and desorption (t_{des}) times.

	KOH 0.1 M	KOH 0.1 M + glycerol 0.1 M			KOH 0.1 M	
		$t_{ads} = 0$	$t_{ads} = 4$ h	$t_{ads} = 20$ h	$t_{des} = 20$ h	$t_{des} = 40$ h
Height of the cathodic peak (V)	-1.8	-3	-3.5	-4	-3	-2

Table 5: Circuit parameters obtained by fitting the experimental impedance results with the selected equivalent circuit. Data obtained in the dark at the OCV potential, as a function of the adsorption (t_{ads}) and desorption (t_{des}) times.

	C_f (μF cm^{-2})	R_f (Ω cm^2)	C_2 (μF cm^{-2})	R_2 (Ω cm^2)	τ_2 (s)	Y_0 (mS s$^{0.5}$ cm^{-2})
KOH	0.031	11.83	940	6939	6.5	8.8
$t_{ads} = 0$	0.026	12.15	939	7349	6.90	6.5
$t_{ads} = 4$ h	0.19	12.5	1200	10600	12.74	14.6
$t_{ads} = 20$ h	0.021	16.11	900	4956	4.46	4.95
$t_{des} = 40$ h	0.02	12.36	206	13100	2.70	3.01

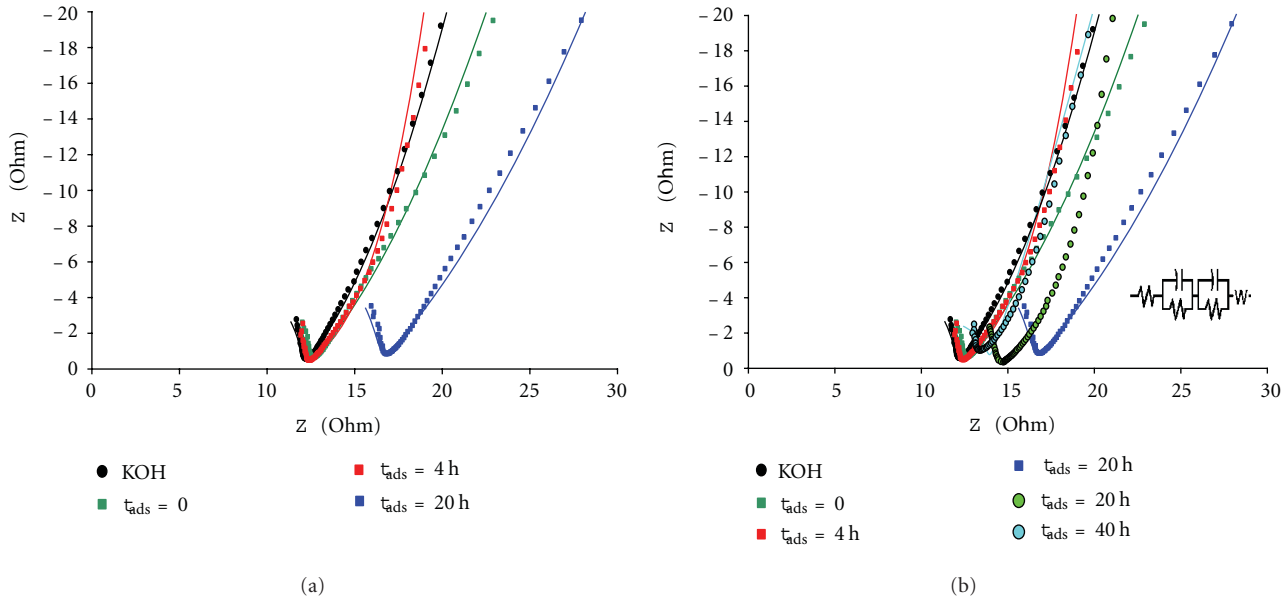

Figure 5: (a) Effect of G adsorption on the Nyquist plots; each curve is obtained after the sample was maintained in contact with (G) = 0.1 M alkaline solution for increasing intervals of time t. Black symbols refer to test performed in the solvent without G. (b) Effect of G desorption. Solid lines refer to the model fit.

the species, other factors are included in its formula, such as the area or concentration of the active species, which, in a complex structure like this, are not easy to be identified.

4. Conclusions

This work deepened the study carried out in our laboratory on photo catalytic hydrogen production enhanced by the presence of glycerol as sacrificial agent. Results have been presented in order to better understand the working mechanism of the electrodes and the interactions occurring between glycerol and nanotubular TiO_2. Results obtained highlighted that adsorption process has to be considered and correlated to the morphology and the defectivity of the sample. On the one hand greater defectivity increases the adsorption capacity of the electrode, which is necessary to ensure increased efficiencies of photocurrent, but on the other hand an excessive reduction in conductivity must be prevented in order not to affect the sample performance. Further studies are still on the way on different electrodes in order to optimise morphology and defectivity of the sample to be destined to the specific process.

References

[1] M. Pagliaro, R. Ciriminna, H. Kimura, M. Rossi, and C. Della Pina, "From glycerol to value-added products," *Angewandte Chemie International*, vol. 46, no. 24, pp. 4434–4440, 2007.

[2] M. G. Alvarez, A. M. Segarra, S. Contreras, J. E. Sueiras, F. Medina, and F. Figueras, "Enhanced use of renewable resources: transesterification of glycerol catalyzed by hydrotalcite-like compounds," *Chemical Engineering Journal*, vol. 161, no. 3, pp. 340–345, 2010.

[3] R. Rudie, "Corgill Dow sows seeds of future fibers; will build $300 million PLA polymer plant," *International Fiber Journal*, vol. 15, no. 1, pp. 8–12, 2000.

[4] M. A. Dasari, P. P. Kiatsimkul, W. R. Sutterlin, and G. J. Suppes, "Low-pressure hydrogenolysis of glycerol to propylene glycol," *Applied Catalysis A*, vol. 281, no. 1-2, pp. 225–231, 2005.

[5] V. Augugliaro, H. A. H. El Nazer, V. Loddo et al., "Partial photocatalytic oxidation of glycerol in TiO*2* water suspensions," *Catalysis Today*, vol. 151, no. 1-2, pp. 21–28, 2010.

[6] H. Wu and Z. Zhang, "Photoelectrochemical water splitting and simultaneous photoelectrocatalytic degradation of organic pollutant on highly smooth and ordered TiO_2 nanotube arrays," *Journal of Solid State Chemistry*, vol. 184, no. 12, pp. 3202–3207, 2011.

[7] M. Canterino, I. Di Somma, R. Marotta, R. Andreozzi, and V. Caprio, "Energy recovery in wastewater decontamination: simultaneous photocatalytic oxidation of an organic substrate and electricity generation," *Water Research*, vol. 43, no. 10, pp. 2710–2716, 2009.

[8] A. Galińska and J. Walendziewski, "Photocatalytic water splitting over Pt-TiO_2 in the presence of sacrificial reagents," *Energy and Fuels*, vol. 19, no. 3, pp. 1143–1147, 2005.

[9] S. Rani, S. C. Roy, M. Paulose et al., "Synthesis and applications of electrochemically self-assembled titania nanotube arrays," *Physical Chemistry Chemical Physics*, vol. 12, no. 12, pp. 2780–2800, 2010.

[10] P. Roy, S. Berger, and P. Schmuki, "TiO_2 nanotubes: synthesis and applications," *Angewandte Chemie International*, vol. 50, no. 13, pp. 2904–2939, 2011.

[11] S. Palmas, A. M. Polcaro, J. R. Ruiz, A. Da Pozzo, M. Mascia, and A. Vacca, "TiO_2 photoanodes for electrically enhanced water splitting," *International Journal of Hydrogen Energy*, vol. 35, no. 13, pp. 6561–6570, 2010.

[12] S. Palmas, A. Da Pozzo, M. Mascia, A. Vacca, P. C. Ricci, and R. Matarrese, "On the redox behaviour of glycerol at TiO_2 electrodes," *Journal of Solid State Electrochemistry*, vol. 16, pp. 2493–2502, 2012.

[13] S. Palmas, A. Da Pozzo, M. Mascia et al., "Effect of the preparation conditions on the performance of TiO_2 nanotube arrays obtained by electrochemical oxidation," *International Journal of Hydrogen Energy*, vol. 36, no. 15, pp. 8894–8901, 2011.

[14] S. Palmas, A. Da Pozzo, F. Delogu, M. Mascia, A. Vacca, and G. Guisbiers, "Characterization of TiO_2 nanotubes obtained by electrochemical anodization in organic electrolytes," *Journal of Power Sources*, vol. 204, pp. 265–272, 2012.

[15] O. K. Varghese and C. A. Grimes, "Appropriate strategies for determining the photoconversion efficiency of water photoelectrolysis cells: a review with examples using titania nanotube array photoanodes," *Solar Energy Materials and Solar Cells*, vol. 92, no. 4, pp. 374–384, 2008.

Hindawi Publishing Corporation
International Journal of Photoenergy
Volume 2012, Article ID 430638, 8 pages
doi:10.1155/2012/430638

Research Article

Photocatalytic Degradation of Aniline Using TiO_2 Nanoparticles in a Vertical Circulating Photocatalytic Reactor

F. Shahrezaei,[1] Y. Mansouri,[2,3] A. A. L. Zinatizadeh,[4] and A. Akhbari[4]

[1] *Academic Center for Education, Culture, and Research (ACECR), Kermanshah 67145-1317, Iran*
[2] *Environmental Epidemiological Research Center, Kermanshah University of Medical Science, Kermanshah 67146-73159, Iran*
[3] *Department of Analytical Chemistry, Faculty of Chemistry, Razi University, Kermanshah 67149-67346, Iran*
[4] *Water and Wastewater Research Center (WWRC), Department of Applied Chemistry, Faculty of Chemistry, Razi University, Kermanshah 67149-67346, Iran*

Correspondence should be addressed to Y. Mansouri, yadollamansouri@yahoo.com
and A. A. L. Zinatizadeh, aliazinatiz@yahoo.com

Received 16 April 2012; Accepted 29 June 2012

Academic Editor: Mika Sillanpää

Photocatalytic degradation of aniline in the presence of titanium dioxide (TiO_2) and ultraviolet (UV) illumination was performed in a vertical circulating photocatalytic reactor. The effects of catalyst concentration (0–80 mg/L), initial pH (2–12), temperature (293–323 K), and irradiation time (0–120 min) on aniline photodegradation were investigated in order to obtain the optimum operational conditions. The results reveal that the aniline degradation efficiency can be effectively improved by increasing pH from 2 to 12 and temperature from 313 to 323 K. Besides, the effect of temperature on aniline photo degradation was found to be unremarkable in the range of 293–313 K. The optimum catalyst concentration was about 60 mg/L. The Langmuir Hinshelwood kinetic model could successfully elucidate the effects of the catalyst concentration, pH, and temperature on the rate of heterogeneous photooxidation of aniline. The data obtained by applying the Langmuir Hinshelwood treatment are consistent with the available kinetic parameters. The activated energy for the photocatalytic degradation of aniline is 20.337 kj/mol. The possibility of the reactor use in the treatment of a real petroleum refinery wastewater was also investigated. The results of the experiments indicated that it can therefore be potentially applied for the treatment of wastewater contaminated by different organic pollutants.

1. Introduction

Aniline is one of the most toxic pollutants; it is released into the environment after its use in the manufacturing of dyes, rubber, polymers, herbicides, pesticides, fungicides, and pharmaceuticals [1]. Aniline is also found in the effluents of petroleum refinery plants. Because of its toxic and recalcitrant nature and the wide application of aniline containing chemicals, aniline is considered to be an increasing threat to both the environment and human health. Therefore, aniline has aroused great attention and is classified as a persistent organic pollutant by the European Economic Community and US Environmental Protection Agency [2]. So there is an urgent need to develop efficient and economical methods to remove this pollutant from wastewater.

Several solutions are proposed in this regard, including adsorption [3], chemical oxidation [4, 5], biological [6], and catalytic wet air oxidation (CWAO) [7]. Unfortunately, the main drawback of these techniques relates to the disposal of the spent contaminated activated sludges, the control of the appropriate reaction conditions, low efficiencies and reaction rates, and operation only within a narrow pH range [8, 9].

During the past decade, great interest has been focused on a promising technology based on the oxidation of the hazardous and refractory organic compounds, by the use of advanced oxidation processes (AOPs) [10]. Various combinations of hydrogen peroxide, ozone, and ultraviolet light are used to generate hydroxyl radicals ($HO^{\bullet}$) in the AOPs. Hydroxyl radicals are the principal agents responsible for the oxidation of numerous aqueous organic contaminants and are quite energy intensive. One emerging technology, however, utilizes illuminated semiconductors and is commonly referred to as the heterogeneous photocatalysis.

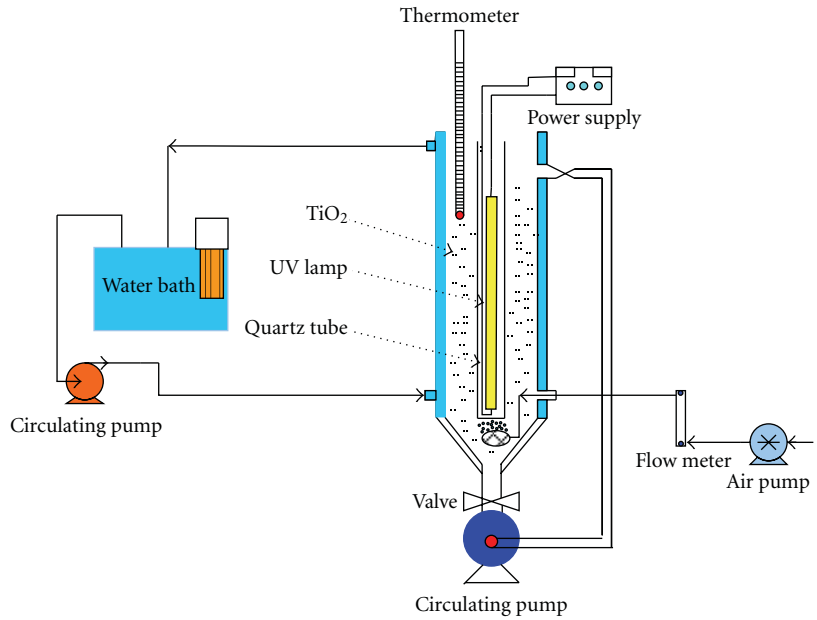

Figure 1: Experimental setup of photoreactor.

The heterogeneous photocatalysis oxidation (HPO) process employing TiO_2 and UV light has emerged as a promising new route for the degradation of persistent organic pollutants, and produces more biologically degradable and less toxic substances [11, 12]. This process is highly dependent on the insitu generation of hydroxyl radicals under ambient conditions which are capable of converting a wide spectrum of toxic organic compounds including the nonbiodegradable ones into relatively innocuous end products such as CO_2 and H_2O.

In spite of the considerable success of TiO_2/UV for the treatment of various types of wastewater, its application as a possible technique for the degradation of aniline is rather scarce in the literature. The main objective of the present study, therefore, is to evaluate the reduction of aniline in aqueous solutions using UV/TiO_2 at different operating conditions.

Furthermore, most of the studies on aniline decomposition by AOPs up to date have not provided in depth on the degradation kinetics which are also important scientific information; hence, this study also investigated into more details on kinetics of aniline degradation by UV/TiO_2 in order to develop the rate equations which can provide fundamental knowledge for future use. Also, the removal efficiency was studied using real petroleum refinery wastewater to explore the applicability of the technique in industry.

2. Experimental

2.1. Chemicals. The chosen catalyst of titanium dioxide was mainly anatase (80% anatase and 20% rutile, Degussa P 25) with a particle size of 30 nm and a surface area of 50 m^2/g (purchased from Plasmachem Co.). This catalyst is the best one which gives an optimal efficiency of catalysis, furthermore, good interparticle contacts are formed between anatase and rutile particles in water [13]. Sulfuric acid and sodium hydroxide solutions were used to adjust the pH of samples [14].

2.2. Analytical Methods. The aniline concentrations in feed and permeate solutions were determined spectrophotometrically at 280 nm, after dilution with 1 M NaOH, using a UV spectrophotometer (DR 5000, Hach, Jenway, USA). TOC was determined with a Shimadzu TOC-5000 total organic carbon analyzer. The identification of the compounds in the real wastewater before and after the degradation was performed by means of the GC/MS system.

GC/MS analysis of the organic compounds was performed using an HP-6890 GC system coupled with a 5973 network mass selective detector and equipped with an HP5-MS capillary fused silica column (60 m, 0.25 mm I.D.; 0.25 mL film thickness). Real wastewater (1 μL) in hexane (HPLC grade) was injected and analyzed with the column held initially at 40°C for 1 min and then increased to 250°C with a 3°C/min heating ramp and subsequently kept at 250°C for 20 min. Other operating conditions were as follows: carrier gas, He (99.999%); with a flow rate of 1 mL/min; injector temperature, 250°C; split ratio, 1 : 50. Mass spectra were taken at 70 eV. The pH meter model HANNA-pH 211 was used to measure the pH. Turbidity was measured by a turbidimeter model 2100 P (Hach Co.).

2.3. Photoreactor Configuration. Figure 1 shows the experimental setup of the photoreactor used for the degradation of aniline. Experiments were carried out in a vertical reactor with the capacity of about 1200 mL and a conic shape in the lower part of its body. The UV lamp 22 cm body length and 16 cm arc length) was a mercury 400 W (200–550 nm) lamp. The UV lamp was positioned inside a quartz tube and totally immersed in the reactor. Therefore, the maximum

Table 1: Experimental design for photocatalytic degradation of aniline.

Factors	Values	Other conditions
Initial pH	2	—
	4	Initial concentration of aniline: 50 mg/L TiO_2 concentration: 60 mg/L Temperature: 293 K
	6	
	8	
	10	—
	12	
TiO_2 concentration (mg/L)	20	Initial concentration of aniline: 50 mg/L Initial pH: 6 Temperature: 293 K
	40	
	60	
	80	—
Temperature (K)	293	—
	303	Initial concentration of aniline: 50 mg/L Initial pH: 6 TiO_2 concentration: 60 mg/L
	313	
	323	

light utilization was achieved. A pump was located below the reactor and provided an adjustable circulating stream, feeding from top of the reactor and discharging from the bottom just below the lamp for the well mixing and fluidizing of nanoparticles of catalyst along the quartz tube. It was not expected that a single pass of polluted water through a short reactor would give adequate degradation. If particles in the water surrounding a lamp are well mixed then each particle on average achieves equal exposure for regulating the temperature; the reactor vessel was equipped with a water-flow jacket, using an external circulating flow of a water bath. Air flow was supplied to the reactor at a constant flow rate (3 L/min) using a lab scale air compressor.

2.4. Experimental Design. Based on the literature, four operational and process factors, namely, pH (2–12), catalyst concentration (0–80 mg/L), temperature (293–323 K), and reaction time (30–120 min) were introduced with the most significant impact on the photocatalytic degradation of pollutants using TiO_2 nanoparticles and UV illumination which were considered as the system variables, and aniline removal efficiency was calculated as the process response [15]. The experimental design is listed in Table 1.

2.5. Photoreactor Operation. In the first stage, to run the experiments, 1200 mL of a sample, containing a known level of aniline (50 mg/L) and with the appropriate amount of added catalyst, was transferred to the reactor. The solution was then exposed to continuous aerating and circulating. After adjustment of temperature and pH, the UV irradiation was begun. In the second stage, the photoreactor was operated under the experiments' conditions (Table 1) to compare the effects of various factors on aniline photodegradation efficiency.

2.6. Photodegradation Kinetic Parameters. The mechanism of aniline degradation catalyzed by TiO_2 is proposed to consist of the following three steps: (1) adsorption of organic pollutant on the surface of TiO_2 (2) surface photodegradation of organic pollutant, and (3) desorption of final products from the surface of TiO_2. The photodegradation of organic pollutants is the rate-predominant step which involves the excitation of the titanium dioxide by a UV light wavelength of $\lambda \leq 400$ nm, electron-hole pairs (e^-_{cb}, h^+_{vb}) are generated, and the hydroxyl radicals are generated by the hole which can degrade organic pollutants present in the wastewater. Oxygen, provided from the air (when the system is stirred and aerated), dissolved in the solution scavenges the electron generated, preventing the recombination of electrons and holes. UV illumination of TiO_2 yields conduction band electrons and valence band holes, which interact with surface adsorbed molecular oxygen to yield superoxide radical anions, O_2, and with water and hydroxyl to produce the highly reactive $HO^\bullet$ radicals, respectively. The latter radical species are well known to oxidize a large number of organic substrates [16–18]. Acknowledging the above-mentioned reaction steps for photocatalysis, the elementary reaction equations are expressed as the following equations:

$$TiO_2 + h\nu \longrightarrow e^-_{cb} + h^+_{vb} \quad (1)$$

$$e^-_{cb} + O_2(\text{ads}) \longrightarrow O_2^{-\bullet} \quad (2)$$

$$h^+_{vb} + OH^- \longrightarrow OH^\bullet \quad (3)$$

$$h^+_{vb} + H_2O \longrightarrow OH^\bullet + H^+ \quad (4)$$

$$OH^\bullet + \text{aniline} \longrightarrow \text{oxidative intermediates} \longrightarrow CO_2 + H_2O. \quad (5)$$

In general, the kinetics of photocatalytic reactions of organic water impurities, including aniline, phenol and its derivatives, follows the Langmuir-Hinshelwood (L-H) which is considered to follow pseudo first- order decay kinetics [19];

$$r = -\frac{dC}{dt} = \frac{kK_{\text{ad}}C}{1 + K_{\text{ad}}C}, \quad (6)$$

where r is the reaction rate, k is the aniline degradation rate constant, K_{ad} is the adsorption equilibrium constant, and C is the concentration of substrate remaining in the solution at time (t). In this study, aniline concentration C was less than 1×10^{-3} mol/L, which made $KC \ll 1$; hence, (6) can be transformed to (7) as follows [20]:

$$r = -\frac{dC}{dt} = kK_{ad}\, C. \tag{7}$$

A linear form of (7) is

$$\ln\left(\frac{C_0}{C}\right) = kK_{ad}\, C = K_{ap}t, \tag{8}$$

where K_{ap} is the apparent reaction rate constant, which can be calculated from the slope of the in plot, and C_0 is the initial substrate concentration. The effects of various reaction parameters on the photocatalytic performance of TiO_2 were expressed in terms of K_{ap}.

3. Results and Discussion

3.1. Influence of Catalyst Concentration. The effect of photocatalyst (TiO_2) concentration on the degradation of aniline in the photoreactor was investigated. The experiments were conducted at various amounts of TiO_2 concentration of 0 (only UV), 20, 40, 60, and 80 mg/L while initial aniline concentration, pH, and temperature of bulk liquid used were 50 mg/L, 6, and 293 K, respectively. The effect of the amount of TiO_2 on the removal of aniline was significant as shown in Figure 2, confirming the positive influence of the increased number of TiO_2 active sites on the process kinetics. It could be seen from Figure 2 that photocatalytic degradation efficiency has increased up to 60 mg/L and then declined with increasing catalyst loading. The changes of K_{ap} versus catalyst concentration are illustrated in Figure 3 and Table 2. The values of K_{ap} increased with increasing catalyst concentration up to 60 mg/L. Then, the apparent degradation rate constant K_{ap} decreased slightly, when catalyst concentration was higher than 60 mg/L.

The maximum values of the aniline removal efficiency and K_{ap} were obtained to be 62% and 0.265 (h^{-1}) at irradiation time and catalyst concentration, respectively, 2 h and 60 mg/L, whereas the minimum values of the responses were obtained under UV light power at 400 W without the use of TiO_2 nanoparticles. The removal efficiency and K_{ap} of the photodegradation of aniline under UV light were only 19% and 0.061 h^{-1}, respectively. Thus, it is necessary to apply the photocatalyst into the system to enhance the rate of reaction.

The increase of aniline removal efficiency and K_{ap} with increasing in catalyst concentration seems to be the results of an increase in the total surface area of TiO_2, namely, an increase of the active sites and an increase in the hydroxyl radicals generation. However, when enough TiO_2 is present in the reactor for adsorbing aniline molecules, the extra higher quantities of TiO_2 nanoparticles would not have more positive effect on the aniline degradation efficiency. On the contrary, when TiO_2 was overdosed, the number of active sites on the TiO_2 particle surface, which was available for the photocatalytic reaction, might approach constant or even decrease slightly because of the decrease of light penetration and the increase of UV light scattering. Therefore, there is an optimum TiO_2 dosage for aniline removal, in this case, the optimal TiO_2 dosage for aniline photodegradation was about 60 mg/L. Similar phenomena have already been reported in other TiO_2 suspension photocatalytic systems. For example, the optimum TiO_2 dosage for the photocatalytic degradation

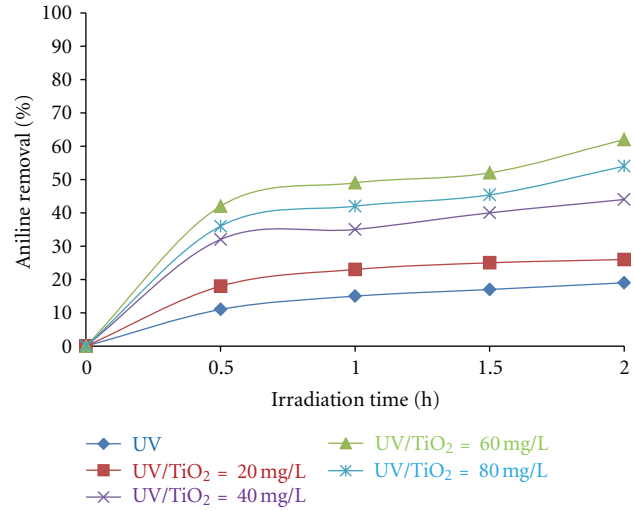

Figure 2: Effect of catalyst concentration on aniline removal (initial pH: 6, temperature (T): 293 K).

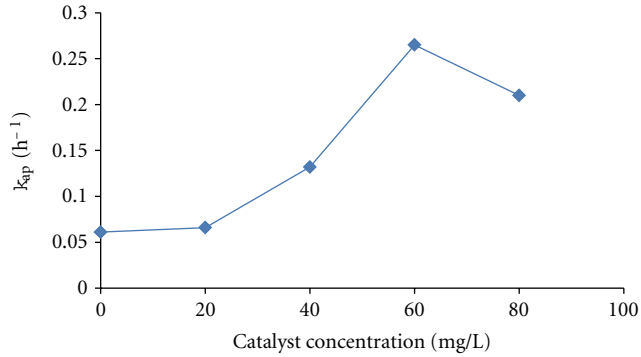

Figure 3: Changes of the apparent aniline photocatalytic reaction constant K_{ap} at different catalyst concentration (initial pH: 6, temperature (T): 293 K, and irradiation time: 2h).

Table 2: Effect of catalyst concentration on photocatalytic degradation of aniline under UV illumination in HCBR (experimental conditions: initial aniline: 50 mg/L; initial pH: 6, temperature: 293 K).

Catalyst concentration (mg/L)	Equation	K_{ap}	R^2
0 (only UV)	$0.061x + 0.178$	0.061	0.97
20	$0.066x + 0.178$	0.066	0.897
40	$0.132x + 0.311$	0.132	0.988
60	$0.265x + 0.397$	0.265	0.939
80	$0.210x + 0.330$	0.21	0.957

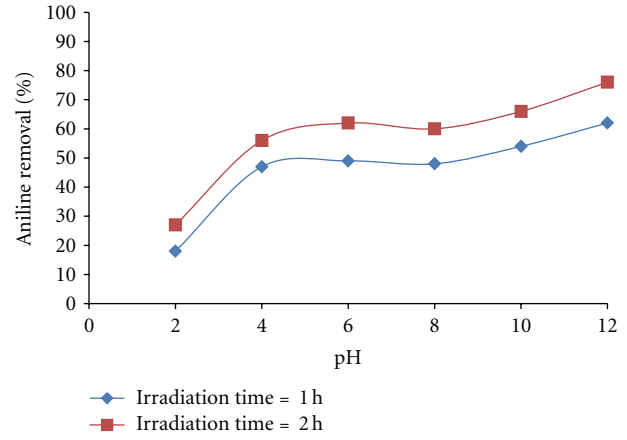

Figure 4: Effect of pH on aniline removal at two typical irradiation times (1 h and 2 h); (catalyst concentration: 60 mg/L and T = 293 K.)

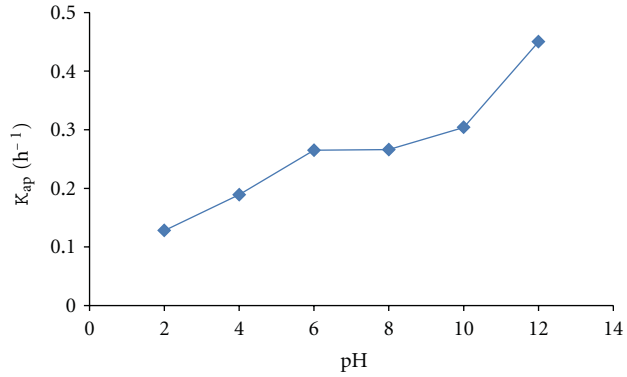

Figure 5: Changes of the apparent aniline photocatalytic reaction constant K_{ap} at different pH (catalyst concentration: 60 mg/L, temperature (T): 293 K, and irradiation time: 2h).

of fungicide carbendazim is about 70 mg/L [21]. This is due to the increase of internal mass transfer resistance and light shielding effect, which can further result in the decrease of overall reaction rate at very high TiO_2 dosage [22].

3.2. Effect of pH. Changing electrolyte pH can vary the surface charge at the TiO_2 surface and also shifts the potential of some redox reaction, thus, it affects the adsorption of organic solutes, consequently, its reactivity and some reaction rate. The effect of pH on aniline degradation rate was investigated in the range of 2–12 at aniline concentration 50 mg/L and TiO_2 concentration of 60 mg/L. The comparison of aniline removal rate at different pH values at two different times of 60 and 120 min is shown in Figure 4. The changes of K_{ap} versus pH were illustrated in Figure 5.

From Figure 4, it is observed that as the pH increases from acidic to alkaline the rate of aniline removal efficiency increases and is maximum at pH 12. In case of initial pH values 2, 4, 6, 8, 10, and 12.0, the percentage removal of aniline, was 27, 56, 62, 60, 66, and 76, and K_{ap} was 0.128, 0.189, 0.265, 0.266, 0.304, and 0.45, respectively, as shown in Figures 4 and 5 and Table 3. The increasing aniline removal

Table 3: Effect of pH on photocatalytic degradation of aniline under UV illumination in HCBR (experimental conditions: initial aniline: 50 mg/L; catalyst concentration: 60 mg/L; temperature: 293 K).

pH	Equation	K_{ap}	R^2
2	$0.128x + 0.058$	0.128	0.991
4	$0.189x + 0.451$	0.189	0.989
6	$0.265x + 0.397$	0.265	0.94
8	$0.266x + 0.304$	0.266	0.91
10	$0.304x + 0.502$	0.304	0.951
12	$0.450x + 0.504$	0.450	0.991

efficiency and K_{ap} with increasing pH can be attributed to the increase in the number of OH^- ions at the surface of TiO_2, since OH^- can be formed by trapping photo-produced holes. Also, the dissociation of aniline probably changes its reactivity. Similarly, the decrease at the lowest pH can be explained by the lack of OH^- ions. Richard et al. [23] found that OH^- was the sole oxidant under the condition of pH 11 and its role was larger in this case than in neutral and acid medium. So K_{ap} increases rapidly with the increasing of pH when greater than 10. In general, the results indicate that the efficiency of the process is not much affected over a wide range of pH, which is quite satisfactory in view of applications.

3.3. Effect of Temperature. In general, the activated energy of photocatalytic reaction is slightly affected by the temperature, but consecutive redox reaction may be largely influenced by temperature which affects both collision frequency of molecules and adsorption equilibria [15]. So the overall effect on the photocatalytic performance will depend on the relative importance of these phenomena. The effect of temperature on the aniline photodegradation in aqueous solution with the presence of TiO_2 and UV was investigated in the range of 293–323 K. The results are demonstrated in Figure 6. As seen in the figure, increase in temperature from 293 to 323 K has reduced the required time for the aniline removal. For the removal of around 60%, for instance, the required time has been decreased from more than 120 min to about 30 min. As noted in Figure 6, the maximum aniline removal was determined to be 82% at irradiation and temperature of 2 h and 323 K, respectively.

The reason of this observation is thought to be the fact that temperature is an important factor affecting the adsorption and photocatalysis. In the case of photocatalytic process, the photocatalytic degradation rate increases with increasing temperature. However, the results indicate that the reaction rate plays a more important role than adsorption rate in the degradation process of aniline. In other words, higher temperature provides higher TiO_2 electron transfers in valance bond to higher energy levels and hence facilitating the electron-hole production that could be utilized in initiating oxidation and reduction reactions, respectively [24]. The species photon-generated holes (h^+_{vb}), and electrons (e_{cb}), and hydroxyl radicals ($OH^\bullet$) can thus degrade organic pollutant to intermediates, and then the intermediates are further degraded to CO_2 and H_2O.

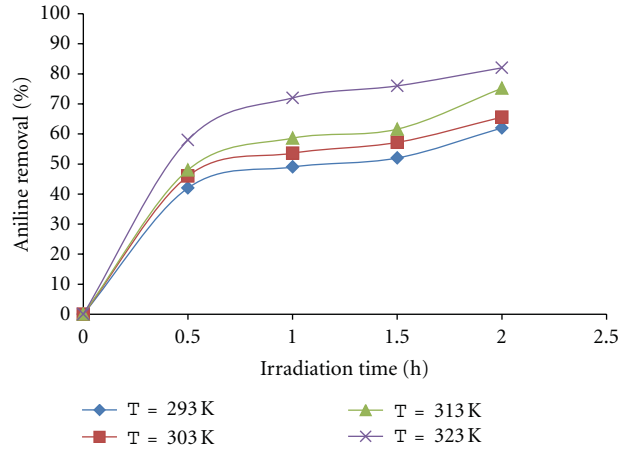

Figure 6: Effect of temperature on aniline removal (initial pH: 6, catalyst concentration: 60 mg/L).

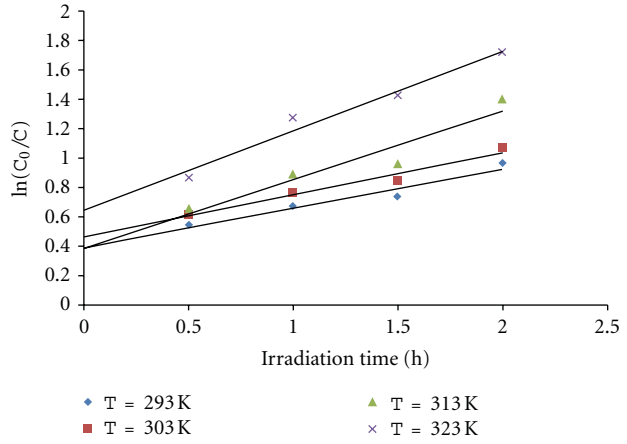

Figure 7: Linear fit of reactions at different temperature (initial pH: 6, catalyst concentration: 60 mg/L).

In order to obtain activation energy (E) for photocatalytic degradation of aniline, the rate data were modeled by first-order kinetics as in the following equation:

$$\frac{dC}{dt} = -kC, \tag{9}$$

where t is reaction time, C is concentration of aniline, and k is the rate constant which has the following temperature dependency:

$$k = A \exp\left(\frac{-E}{RT}\right), \tag{10}$$

where A is the preexponential factor, E is the activation energy, R is the universal gas constant, and T is the temperature in Kelvin. Integrating (9) gives

$$\ln\left(\frac{C_0}{C}\right) = k \cdot t. \tag{11}$$

Figure 7 shows the correlation between the $\ln(C_0/C)$ and the reaction time (t) in the photoreactor drawn based on (11) under conditions (pH of 6, catalyst concentration of 60 mg/L) at four different temperatures (293, 303, 313, and 323).

Table 4: Effect of temperature on photocatalytic degradation of aniline under UV illumination in HCBR (experimental conditions: initial aniline: 50 mg/L; catalyst concentration: 60 mg/L; pH: 6).

Temperature (K)	Equation	K_{ap}	R^2
293	$0.266x + 0.397$	0.266	0.969
303	$0.286x + 0.466$	0.286	0.984
313	$0.459x + 0.397$	0.459	0.956
323	$0.539x + 0.646$	0.539	0.985

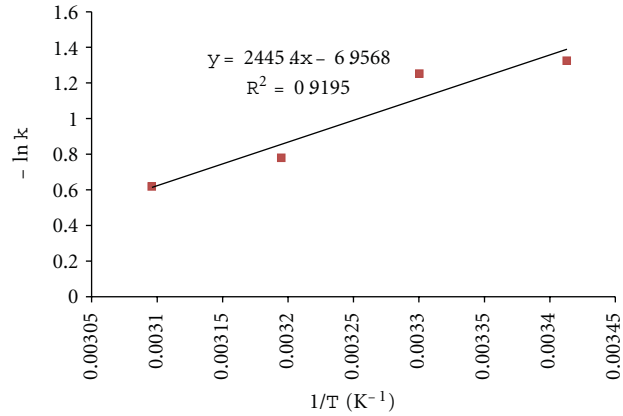

Figure 8: Effect of temperature on rate constants.

The data fitted well with an $R^2 > 0.96$. The high values of the determination coefficients (R^2) clearly indicate that first-order kinetics can be applied with a good degree of precision. The values of kinetic constant (k) were calculated to be in the range of 0.266–0.539 (h^{-1}) (Figure 7 and Table 4). As expected, the rate constant k increases with increasing temperature, and k is very sensitive to the change of temperature. To calculate the activated energy E and constant A, (10) was transformed into a logarithmic form, which was plotted in Figure 8. From the slope and intercept of the best-fit line, the following values were found, A = 1048.1 and E = 20.337 kJ/mol.

Finally, the reaction kinetic equation of photocatalytic degradation of aniline is

$$-\frac{dC}{dt} = 1048.1 \exp\left(\frac{20327}{RT}\right)\text{COD}. \tag{12}$$

This indicates that the reaction has high activation energy.

3.4. Investigation on Mineralization of Aniline. Total organic carbon (TOC) is the amount of carbon bound in an organic compound and is often used as a nonspecific indicator of water quality. Using this criterion, the mineralization of aniline was investigated under the process of photocatalytic degradation under optimum operating conditions. For the initial concentration of 50 mg/L of aniline and under the optimum conditions, the TOC values were

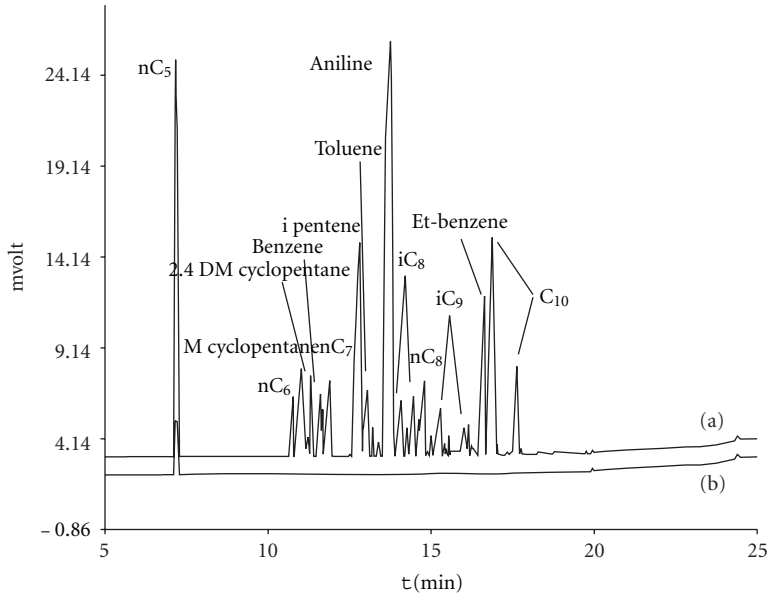

Figure 9: Comparison of chromatograms for degradation of aniline and other compounds in real petroleum refinery wastewater (catalyst concentration: 100 mg/L, initial PH: 7, temperature (T): 293 K, and irradiation time: 2h).

measured at different times and the appropriate conversion was calculated. Using the photocatalysis process and after 120 min, TOC decreased from 39 mg/L to about 12.4 mg/L, equivalent of about 68.2% efficiency. The results indicate an effective mineralization of aniline a short time (about 60 min).

3.5. Treatment of Petroleum Refinery Wastewater containing Aniline in the Vertical Circulating Photocatalytic Reactor. In order to investigate the performance of this circulating photocatalytic reactor in the removal of aniline from real wastewater, a laboratory test was performed using the pretreated petroleum refinery wastewater sample (after electrochemical methods). The sample was collected from the point that the wastewater is just leaving the dissolved air flotation (DAF) and just into the biological treatment unit in the Kermanshah refinery plant. Total chemical oxygen demand (TCOD), measured at this point, was about 220 mg/L. Other specifications were, pH: 7.1, turbidity: 85 NTU, and total dissolved solids (TDS): 560 mg/L. In the line with this, the reactor was operated under conditions (pH of 7.1 (natural), catalyst concentration of 100 mg/L, and irradiation time of 120 min) at temperatures of 293 K. In order to identify the present organic compounds in the samples and to compare the efficiency of degradation for different compounds, 10 mL samples of wastewater were taken before and after the degradation. The catalyst particles were separated and analyzed by means of the GC/MS. In Figure 9, (a) and (b) present the chromatograms of the analyzing wastewater before and after the degradation under optimum conditions. The major peaks have been labeled by name according to the GC/MS identification. Comparison of two chromatograms in the figure proved that all pollutants were degraded at relatively high efficiencies. The maximum TCOD removal efficiency was found to be more than 85%.

4. Conclusions

The influences of catalyst concentration, initial pH, temperature, and irradiation time on the degradation rate of aniline were investigated in a vertical circulating photocatalytic reactor. The variation of pH has a pronounced effect on degradation rate; alkaline condition promotes the rate considerably because of change of surface charge, whereas acidic environment casts a negative effect on degradation. Besides, the catalyst concentration also influences the degradation rate, and the rate constant reaches the peak when the TiO_2 concentration is 60 mg/L and then decreases when increasing to 80 mg/L. The temperature (in the range of 293–313 K) did not show a strong effect on the process, as only a small difference is observed in the results obtained with different temperature (293, 303, and 313 K). However, the results reveal that the aniline degradation efficiency can be effectively improved by increasing pH from 2 to 12 or increasing the temperature from 313 to 323 K. Conclusively, an optimum condition for vertical circulating photocatalytic reactor operation with initial aniline concentration of 50 mg/L was achieved as follows: initial pH at 12, catalyst concentration at 60 mg/L, and temperature at 323 K. The activation energy for the photocatalytic degradation of anilines is 20.337 kJ/mol and Langmuir Hinshelwood can be used to describe the photodegradation reaction. The possibility of vertical circulating photocatalytic reactor in the treatment of petroleum refinery wastewater was also investigated. The results of the experiments indicated that it can therefore be potentially applied for the treatment of wastewater contaminated by different organic pollutants.

Acknowledgments

The financial supports provided by Kermanshah Oil Refinery Company (KORC) is greatly acknowledged. The authors acknowledge the laboratory equipments provided by Academic Center for Education, Culture, and Research (ACECR), Razi University, Kermanshah, that have resulted in this paper.

References

[1] USEPA, United States Environmental Protection Agency, OPPT Chemical Fact Sheets, Aniline Fact Sheet, Support Document (CAS No. 62-53-3) December 1994.

[2] J. Li and Z. Jin, "Effect of hypersaline aniline-containing pharmaceutical wastewater on the structure of activated sludge-derived bacterial community," *Journal of Hazardous Materials*, vol. 172, no. 1, pp. 432–438, 2009.

[3] J. O'Brien, T. F. O'Dwyer, and T. Curtin, "A novel process for the removal of aniline from wastewaters," *Journal of Hazardous Materials*, vol. 159, no. 2-3, pp. 476–482, 2008.

[4] S. V. Kotelevtsev, O. O. P. Hanninen, P. A. Lindström-Seppa et al., "Mutagenicity of bleached and unbleached effluents from Baikalsk pulp and paper mill at Lake Baikal, Russia," *Aquatic Ecosystem Health & Management*, vol. 3, no. 1, pp. 95–104, 2000.

[5] J. Sarasa, S. Cortés, P. Ormad, R. Gracia, and J. L. Ovelleiro, "Study of the aromatic by-products formed from ozonation of anilines in aqueous solution," *Water Research*, vol. 36, no. 12, pp. 3035–3044, 2002.

[6] N. Goonewardena, M. Nasu, A. Okuda, K. Tani, Y. Takubo, and M. Kondo, "Biodegradation of aniline and abundance of potential degraders in river waters.," *Biomedical and Environmental Sciences*, vol. 5, no. 1, pp. 25–32, 1992.

[7] G. Ersoäz and S. Atalay, "Kinetic modeling of the removal of aniline by low-pressure catalytic wet air oxidation over a nanostructured Co_3O_4/CeO_2 catalyst," *Industrial and Engineering Chemistry Research*, vol. 50, no. 1, pp. 310–315, 2011.

[8] N. A. Laoufi, D. Tassalit, and F. Bentahar, "The degradation of phenol in water solution by TiO_2 photocatalyst in a helical reactor," *Global Nest Journal*, vol. 10, pp. 404–418, 2008.

[9] M. S. Kuyukina, I. B. Ivshina, M. K. Serebrennikova et al., "Petroleum-contaminated water treatment in a fluidized-bed bioreactor with immobilized *Rhodococcus* cells," *International Biodeterioration and Biodegradation*, vol. 63, no. 4, pp. 427–432, 2009.

[10] N. Azbar, T. Yonar, and K. Kestioglu, "Comparison of various advanced oxidation processes and chemical treatment methods for COD and color removal from a polyester and acetate fiber dyeing effluent," *Chemosphere*, vol. 55, no. 1, pp. 35–43, 2004.

[11] I. Oller, W. Gernjak, M. I. Maldonado, L. A. Pérez-Estrada, J. A. Sánchez-Pérez, and S. Malato, "Solar photocatalytic degradation of some hazardous water-soluble pesticides at pilot-plant scale," *Journal of Hazardous Materials*, vol. 138, no. 3, pp. 507–517, 2006.

[12] A. García-Ripoll, A. M. Amat, A. Arques et al., "Increased biodegradability of UltracidTM in aqueous solutions with solar TiO_2 photocatalysis," *Chemosphere*, vol. 68, no. 2, pp. 293–300, 2007.

[13] T. Ohno, K. Sarukawa, K. Tokieda, and M. Matsumura, "Morphology of a TiO_2 photocatalyst (Degussa, P-25) consisting of anatase and rutile crystalline phases," *Journal of Catalysis*, vol. 203, no. 1, pp. 82–86, 2001.

[14] APHA, *Standard Methods for the Examination of Water and Wastewater*, American Public Health Association, Washington, DC, USA, 19th edition, 1999.

[15] L. Wenhua, L. Hong, C. Sao'an, Z. Jianqing, and C. Chunan, "Kinetics of photocatalytic degradation of aniline in water over TiO_2 supported on porous nickel," *Journal of Photochemistry and Photobiology A*, vol. 131, no. 1–3, pp. 125–132, 2000.

[16] R. Wang, D. Ren, S. Xia, Y. Zhang, and J. Zhao, "Photocatalytic degradation of Bisphenol A (BPA) using immobilized TiO_2 and UV illumination in a horizontal circulating bed photocatalytic reactor (HCBPR)," *Journal of Hazardous Materials*, vol. 169, no. 1–3, pp. 926–932, 2009.

[17] S. Horikoshi, N. Watanabe, M. Mukae, H. Hidaka, and N. Serpone, "Mechanistic examination of the titania photocatalyzed oxidation of ethanolamines," *New Journal of Chemistry*, vol. 25, no. 8, pp. 999–1005, 2001.

[18] A. Emeline, A. Salinaro, V. K. Ryabchuk, and N. Serpone, "Photo-induced processes in heterogeneous nanosystems. From photoexcitation to interfacial chemical transformations," *International Journal of Photoenergy*, vol. 3, no. 1, pp. 1–16, 2001.

[19] L. Sánchez, J. Peral, and X. Domènech, "Photocatalyzed destruction of aniline in UV-illuminated aqueous TiO_2 suspensions," *Electrochimica Acta*, vol. 42, no. 12, pp. 1877–1882, 1997.

[20] J. M. Herrmann, "Heterogeneous photocatalysis: fundamentals and applications to the removal of various types of aqueous pollutants," *Catalysis Today*, vol. 53, no. 1, pp. 115–129, 1999.

[21] J. Saien and S. Khezrianjoo, "Degradation of the fungicide carbendazim in aqueous solutions with UV/TiO_2 process: optimization, kinetics and toxicity studies," *Journal of Hazardous Materials*, vol. 157, no. 2-3, pp. 269–276, 2008.

[22] K. Mehrotra, G. S. Yablonsky, and A. K. Ray, "Macro kinetic studies for photocatalytic degradation of benzoic acid in immobilized systems," *Chemosphere*, vol. 60, no. 10, pp. 1427–1436, 2005.

[23] C. Richard, P. Boule, and J. M. Aubry, "Oxidizing species involved in photocatalytic transformations on zinc oxide," *Journal of Photochemistry and Photobiology A*, vol. 60, no. 2, pp. 235–243, 1991.

[24] J. Saien and H. Nejati, "Enhanced photocatalytic degradation of pollutants in petroleum refinery wastewater under mild conditions," *Journal of Hazardous Materials*, vol. 148, no. 1-2, pp. 491–495, 2007.

Hindawi Publishing Corporation
International Journal of Photoenergy
Volume 2012, Article ID 381971, 7 pages
doi:10.1155/2012/381971

Research Article

Photoreduction of Cr(VI) Ions in Aqueous Solutions by UV/TiO_2 Photocatalytic Processes

Chih Ming Ma,[1] Yung Shuen Shen,[2] and Po Hsiang Lin[3]

[1] *Department of Cosmetic Application and Management, St. Mary's Medicine Nursing and Management College, Yi-Lan 266, Taiwan*
[2] *Holistic Education Center, Mackay Medical College, Taipei 252, Taiwan*
[3] *Department of Environmental Engineering, Da-Yeh University, Changhwa 512, Taiwan*

Correspondence should be addressed to Chih Ming Ma, cmma@smc.edu.tw

Received 1 June 2012; Revised 19 July 2012; Accepted 31 July 2012

Academic Editor: Meenakshisundaram Swaminathan

This study discussed the photoreduction of Cr(VI) ions in aqueous solutions by UV/TiO_2 photocatalytic processes under various operational factors. Experimental results showed that the removal rate of Cr(VI) increased with decreasing solution pH values and with increasing dosages of organic compounds, indicating that the recombination rate of electrons and h^+ can be retarded in the reaction systems by the addition of the scavenger, thus raising the reaction rate of Cr(VI). The relationship of the chemical reaction rate of Cr(VI), TiO_2 dosage, and changes of Cr(VI) concentration was expressed by the pseudo-first-order kinetic equation. Comparing the experimental results of two different doping metals in modified TiO_2 photoreduction systems, the removal rate of Cr(VI) by the Ag/TiO_2 process is larger, possibly because the electron transferring ability of Ag is superior to that of Cu. However, the photoreduction rates of Cr(VI) by modified UV/TiO_2 processes are worse than those by a nonmodified commercial UV/TiO_2 process.

1. Introduction

Chromium is a common toxic pollutant present in industrial effluents [1, 2]. Conventional methods used in the removal of Cr(VI) ions from wastewater include reducing following hydroxide precipitation, ion exchange, adsorption, electrochemical precipitation, foam separation, membrane separation, solvent extraction, and bacterial reduction [2–4]. In recent years, different semiconductors have been intensively studied as the photocatalysts for photoreduction reactions, as electron-hole pairs can be generated by the photoexcitation of the photoreduction process to remove and recycle heavy metals and to reduce heavy metal pollutants in aqueous solution [5–8]. The photocatalysts which are often used include TiO_2, CdS, and ZnO. TiO_2 has been extensively studied in regard to its application as the physical sunblock in sunscreens or other cosmetic products and in environmental remediation processes because of its high degree of photocatalytic activity, chemical stability, and nontoxicity [5–10].

In the reaction process of UV/TiO_2, an electron-hole pair is generated after TiO_2 has been exposed to ultraviolet light (UV) with a wavelength (λ = 365 nm) in the near visible spectrum. The electrons then reduce the heavy metals; this is the reduction path. The hole generates the free radical through a series of reactions, and then organic matters are oxidized into carbon dioxide; this is the oxidation path. However, a shortcoming of this process is that the electron-hole pair may be bound again, thus decreasing the efficiency of the photoreduction. Hence, the addition of an organic hole scavenger enhances the photoreduction effect. Generally, organic holes scavengers comprise organic compounds such as methanol, ethanol, formic acid, and acetic acid [11].

Chromium is widely used in several industrial processes such as metal plating and paint making. Due to its acute toxicity and high mobility in water, Cr(VI) is in the list of priority pollutants of most countries [6]. On the other hand, Cr(III) is readily precipitated or adsorption onto solid phase. Cr(VI) has a toxicity one hundred times higher than that of Cr(III). Advanced oxidation processes have demonstrated their usefulness in cleaning of industrial wastewater [12–14]. After the photoreduction of Cr(VI), it can be separated from the suspension by several procedures. From the environmental point of view knowledge of chromium, photoreduction mechanism is essential not only for tracing Cr(VI) fate in

environment, but also for understanding its role in remediation of pollution by organic compounds [9].

The aim of this study was to use commercial TiO_2 and an organic hole scavenger together. Previous work has seldom probed into the doping metals (Ag and Cu) used in the TiO_2 photoreduction system; therefore, this study examined the impact of different calcination temperatures on the activity of modified photocatalysts with $Ag(NO_3)$- and $CuCl_2$-doped commercial TiO_2. Further, the Cr(VI) removal under various operational factors, such as solution pH values, TiO_2 dosages, types, and dosages of organic compound, was explored, and a possible reaction kinetic equation has been proposed to simulate the kinetic behaviors of various species in the reaction.

2. Materials and Method

The materials of this experiment comprised laboratory methanol, ethanol, and isopropanol with different concentrations (0.29 mM, 0.74 mM, 1.47 mM, 2.94 mM, and 5.88 mM) to observe the dosage effect of organic hole scavengers, potassium dichromate (Katayama Chemical) to prepare 20 mg L^{-1} of aqueous solution, and the photocatalyst using Degussa P-25 (Union Chemical Ind.).

2.1. Wastewater Preparation. 0.1130 g potassium dichromate was weighed and then combined with 2 L RO water to prepare the aqueous solution with a Cr(VI) concentration of 20 mg L^{-1}.

2.2. Photocatalyst Modification. Via the incipient wetness method, Cu and Ag were calcined in a modified TiO_2 process. First, the critical moisture content of TiO_2 was measured by solvent, the fixed amount of metal precursor was dissolved in the deionized water with the critical moisture content, TiO_2 was slowly added to the metal-containing aqueous solution and well stirred, TiO_2 was calcined in a high-temperature furnace, and then the grains pulverized into powder once it had cooled to room temperature. The crystallization level morphology and the specific BET surface area of the photocatalyst were determined by a Siemens D-8 X-ray diffractometer (XRD) and a Micromeritics ASAP 2000 analyzer, respectively. Field emission scanning electron microscopy (FESEM, JEOL, JSM-6500F) was operated at 15 kV and used to measure the surface morphology of the prepared samples.

At the same Cr(VI) concentration, the samples were analyzed every half hour under different pH values, organic hole scavengers, dosages of organic hole scavenger, and dosages of photocatalyst over the four-hour reaction period. The optimum operational conditions thus attained were the optimum reaction conditions of modified TiO_2. With different doping amounts of metal and at different calcination temperatures under the optimum operational conditions obtained, an analysis of the variations of Cr(VI) concentration was made every half hour. The samples were filtered and analyzed by an HITACHI U-2000 Spectrophotometer.

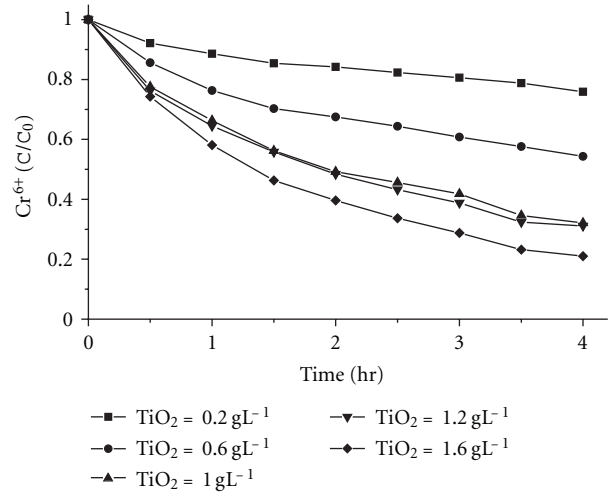

Figure 1: Effect of the TiO_2 dosage on the photocatalytic reduction.

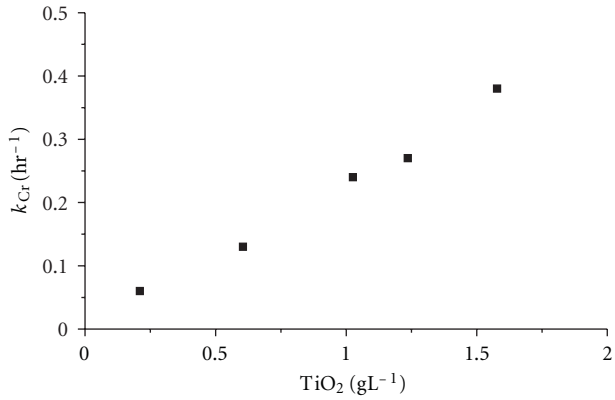

Figure 2: Relationship of the rate constant on the photocatalytic reduction.

3. Results and Discussion

This study utilized the UV/TiO_2 process to treat Cr(VI) pollutants in aqueous solution. In this section, the experimental results of the photoreduction of Cr(VI) by a nonmodified TiO_2 system and modified TiO_2 are explained and discussed. In the experiment, the variations of Cr(VI) concentration over time were as shown in Figure 1; the removal rate of Cr(VI) was 24.1% when the TiO_2 dosage was 0.2 g L^{-1}, and 80% when the TiO_2 dosage was 1.6 g L^{-1}. Therefore, as the TiO_2 dosage increased, the removal rate increased.

In a simulation of the Cr(VI) removal rate using the pseudo-first-order kinetic equation, the relationship of the removal rate and time was obtained, as shown in Figure 2. The photoreduction reaction rate sped up as the TiO_2 dosage increased, indicating that the increase of TiO_2 dosage facilitated the photocatalytic reaction. Similar results were obtained in the presence of other studies [11, 15, 16]. Therefore, it was estimated that before the optical screening appeared, and the TiO_2 dosage had a linear relationship with the pseudo-first-order removal rate.

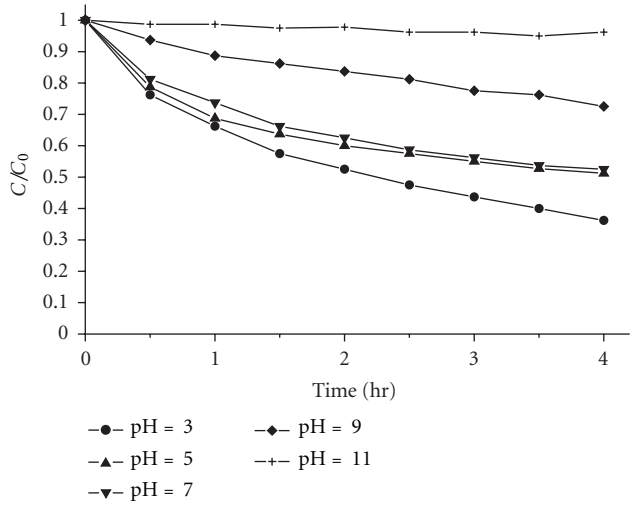

Figure 3: Effect of the pH on the photocatalytic reduction.

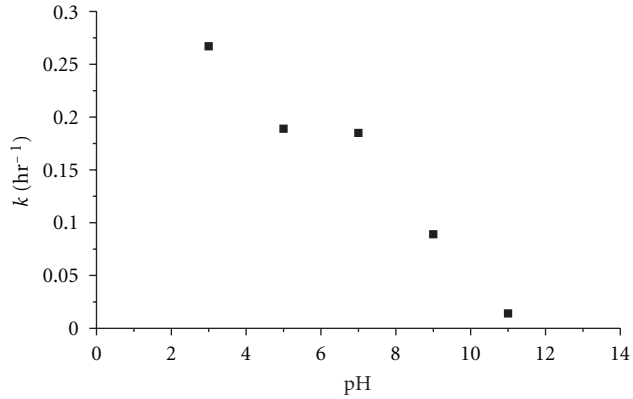

Figure 4: Relationship of the rate constant under different pH.

In order to clarify the relationship of the pseudo-first-order Cr(VI) removal rate, TiO_2 dosage, and changes of Cr(VI) concentration, it was assumed that three factors were present in the pseudo-first-order reaction kinetic equation as follows:

$$-r_a = \frac{d[C]}{dt} = k[C][\mathrm{TiO_2}]^n = k_{\mathrm{Cr}}[C], \tag{1}$$

where k_{Cr} is $k[\mathrm{TiO_2}]^n$, k is Cr(VI) reduction rate, k_{Cr} is pseudo-first-order rate, $[C]$ is variations of Cr(VI) concentration over time, and $[\mathrm{TiO_2}]$ is TiO_2 dosage.

With the logarithm of the equation above, we then have

$$\ln k_{\mathrm{Cr}} = \ln k + n \ln[\mathrm{TiO_2}], \tag{2}$$

by plotting $\ln k_{\mathrm{Cr}}$ and $\ln[\mathrm{TiO_2}]$, intercepting to get $\ln k = -1.4058$ and $k = 0.2344$; then from the slope we have $n = 0.87$. Thus, for the relationship of the pseudo-first-order

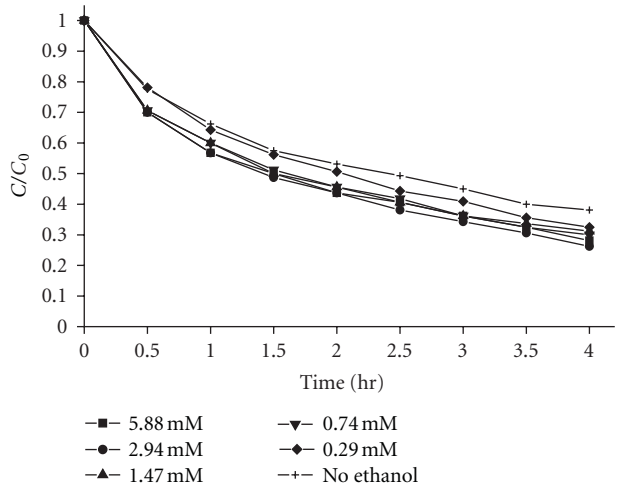

Figure 5: Effect of initial concentration on the photocatalytic reduction.

removal rate, TiO_2 dosage and variations of Cr(VI) concentration over time, the following equation was derived from the three equations above:

$$-r_a = \frac{d\left[\mathrm{Cr^{6+}}\right]}{dt} = 0.2344\left[\mathrm{Cr^{6+}}\right][\mathrm{TiO_2}]^{0.87} \quad (R^2 = 0.9887). \tag{3}$$

The Cr(VI) reduction rate was in an 0.87th power relation with the TiO_2 dosage. The initial Cr(VI) concentration was fixed at 20 mg L^{-1} for treatment of Cr(VI) in aqueous solution by UV/TiO_2. The changes of Cr(VI) over time under different values are shown in Figure 3, from which we could know that with the increase of pH value, the Cr(VI) removal rate gradually declined. At pH = 3, the removal rate was 63.5%, but, at pH = 11, the removal rate was just 5.1%.

As for the experimental results, the Cr(VI) removal rate was simulated by the pseudo-first-order kinetic equation to determine the removal rate and time, as shown in Figure 4. Similar results were obtained in the presence of other studies [11, 15, 16], who discussed the influence of different pH values of photocatalyst on the removal rate of Cr(VI) by photoreduction processes. As pointed out by Chen and Cao (2005) [16], as pH value increased, the reduction rate of dichromate ions gradually decreased because the increase of pH value reduced the adsorption of dichromate ions on the surface of the photocatalyst; also, at high pH value, $Cr(OH)_3$ covered the surface active position of TiO_2 so that the trivalent chromium deposits on TiO_2 depressed the photocatalytic activity. Consequently, for the photoreduction of Cr(VI) in aqueous solution by UV/TiO_2 process, a low pH value had the best reduction efficiency. The variations of Cr(VI) concentration over time in the experiment to discover the dosing effect of organic hole scavengers are shown in Figure 5. The Cr(VI) removal rate was the best, as high as 74% for a dosage of 2.94 mM, in the ethanol system.

Ethanol was used as the hole scavenger and at the optimum dosage of 2.94 mM, under different pH values and

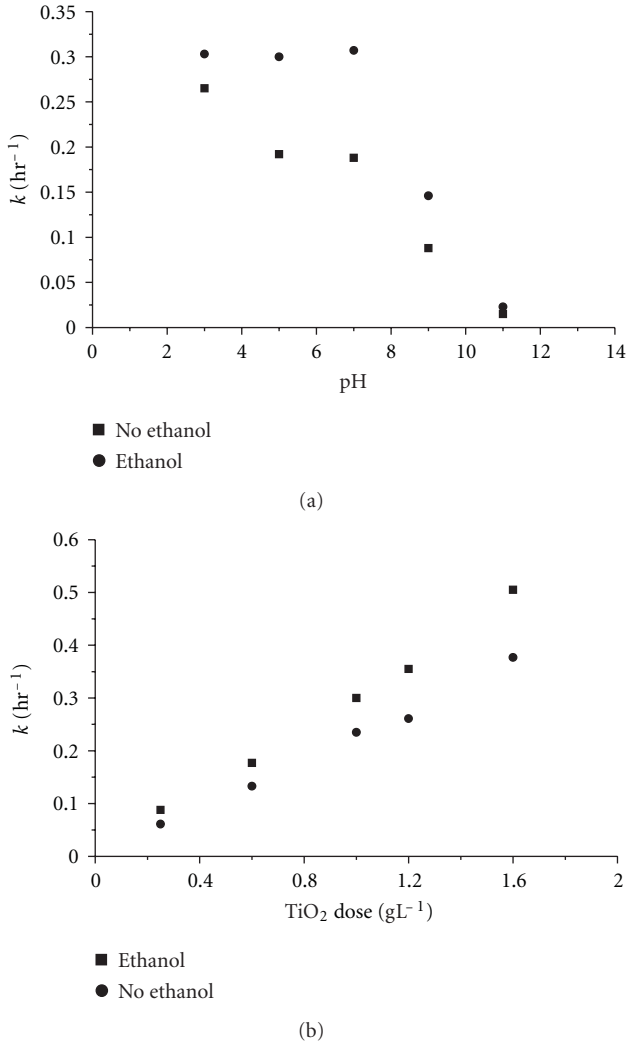

Figure 6: Relationship of the rate constant under different pH values and different TiO_2 dose.

different TiO_2 dose, and the influence of adding ethanol as the hole scavenger on the Cr(VI) removal rate was determined. The results are presented in Figure 6.

Adding ethanol facilitated the photoreduction of Cr(VI), but, at high pH values, the addition of ethanol did not achieve this result; when TiO_2 was added, ethanol promoted the Cr(VI) removal rate. Plotting $\ln[TiO_2]$ and $\ln k$ after adding ethanol and using the pseudo-first-order removal rate, the relationship of TiO_2 dosage and variations of Cr(VI) concentration could be determined as follows:

$$-r_E = \frac{d[Cr^{6+}]}{dt} = 0.3132[Cr^{6+}][TiO_2]^{0.81} \quad (R^2 = 0.9789). \tag{4}$$

When ethanol was added as the hole scavenger, the pseudo-first-order Cr(VI) removal rate was higher than before the addition.

The Cr(VI) removal rate was examined under nonreduced and reduced modified TiO_2 systems at the fixed pH = 3, with a 2.94 mM dose of ethanol as the organic hole scavenger; the Cr(VI) removal reaction behaviors under various operational factors were solved by the pseudo-first-order reaction kinetic equation.

Table 1: The rate constant of reduction and nonreduction on the Cr(VI) concentration after the doping of metallic ions.

	Reduced			Nonreduced		
	0.5%	2.0%	5.0%	0.5%	2.0%	5.0%
Cu	0.110	0.101	0.129	0.111	0.097	0.104
Ag	0.131	0.129	0.156	0.107	0.123	0.136

Table 2: Surface area of P-25 TiO_2, 5% Ag/TiO_2 and 5% Cu/TiO_2.

Material	Metals added (wt%)	Surface area ($m^2\,g^{-1}$)
TiO_2 (P-25)	—	53.61
Ag/TiO_2	0.5	57.82
	2.0	57.68
	5.0	59.38
Cu/TiO_2	0.5	57.03
	2.0	58.42
	5.0	58.79

This section discusses the effects of reduction and nonreduction on the Cr(VI) concentration after the doping of metallic ions. The experimental results were as shown in Table 1. The Cr(VI) removal rate of reduced 5 wt% Cu/TiO_2 was $0.1298\,hr^{-1}$, which was 1.24 times that of the nonreduced. In the Ag-doped system, the Cr(VI) removal rates of the triple doping after reduction were higher than those of the nonreduced. The Cr(VI) removal rate of reduced 5 wt% Ag/TiO_2 was $0.156\,hr^{-1}$, 1.14 times higher than that of nonreduced 5 wt% Ag/TiO_2. Furthermore, the surface area of Ag/TiO_2 and Cu/TiO_2 from the BET surface area measurements was only slightly increased, as shown in Table 2. Figure 7 presents the surface structure and morphology of 5% Ag/TiO_2 before and after photocatalysis. It was clearly observed from SEM images that surface of catalyst was no difference between them.

For the experiment results of the two kinds of modified TiO_2, the removal rate simulated by the pseudo-first-order kinetic equation and the doped percent were plotted, as shown in Figure 8, to explore the relationship of two kinds of modified TiO_2 under the condition of reduced or nonreduced. As the figure clearly shows, reduced or not, the Cr(VI) removal rate of $Ag(NO)_3$-modified TiO_2 was higher than that of $CuCl_2$-modified TiO_2. These results were consistent with other studies [17, 18] discussion on the modified TiO_2 and TiO_2 reduction reaction. Ag had a higher electron capture, and Ag ions doped on TiO_2 played the role of an electron storage system to improve photocatalytic activity so as to quickly transfer electrons.

The Cr(VI) removal rates in the two systems with the initial Cr(VI) concentration of $20.0\,mg\,L^{-1}$, pH = 3, $[M/TiO_2] = 1.0\,g\,L^{-1}$, and ethanol concentration of 2.94 mM are shown in Figure 9. The modified photocatalyst had a lower Cr(VI) removal rate than that of the nonmodified photocatalyst, with 5 wt% Ag/TiO_2 having the best Cr(VI)

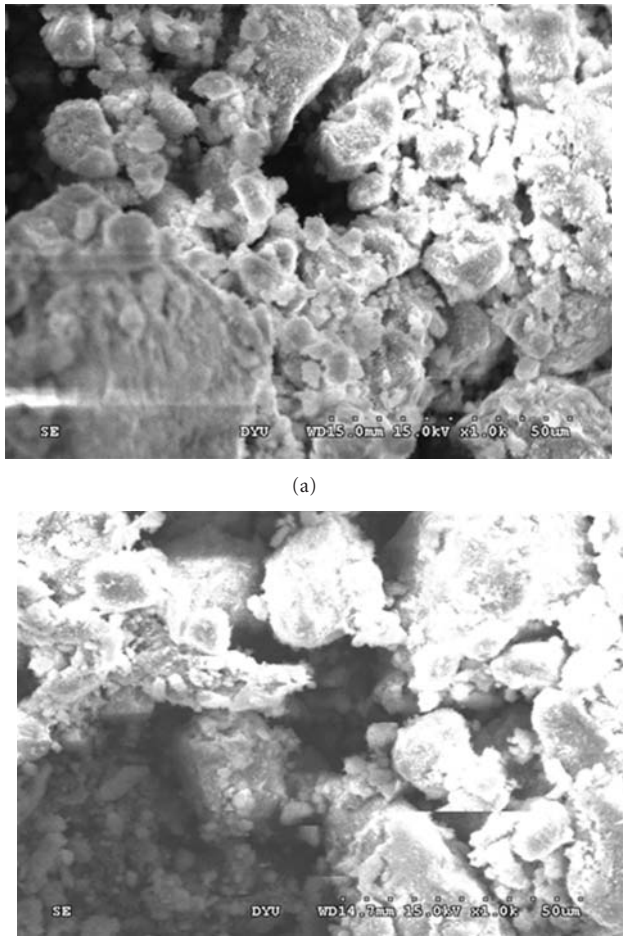

Figure 7: SEM images of 5% Ag/TiO_2 (a) before photoreduction and (b) after photoreduction.

reduction rate of the modified photocatalysts, but a removal rate of less than 50%; the Cr(VI) removal rate of the nonmodified photocatalyst reached 64%. The experimental results were consistent with the results of the modified TiO_2 prepared by the other study [14, 15], and the Cr(VI) reduction rate after being modified was lower than that of the nonmodified.

The reduction of Cr(VI) by electrons in aqueous solution basically follows the following reactions:

$$Cr^{6+} + 3e^- \longrightarrow Cr^{3+}. \quad (5)$$

Liu et al. [18] reported that Cr(VI) photocatalytic reduction by directly capturing photogenerated electrons is possible, but is mainly realized indirectly by getting electrons from surface Ti^{3+} of TiO_2 photocatalyst. The reactions were as follows [18]:

$$Cr^{6+}_{\text{suspension}} \longrightarrow Cr^{6+}_{\text{adsorbed}}, \quad (6)$$

$$TiO_2 \longrightarrow e^- + h^+, \quad (7)$$

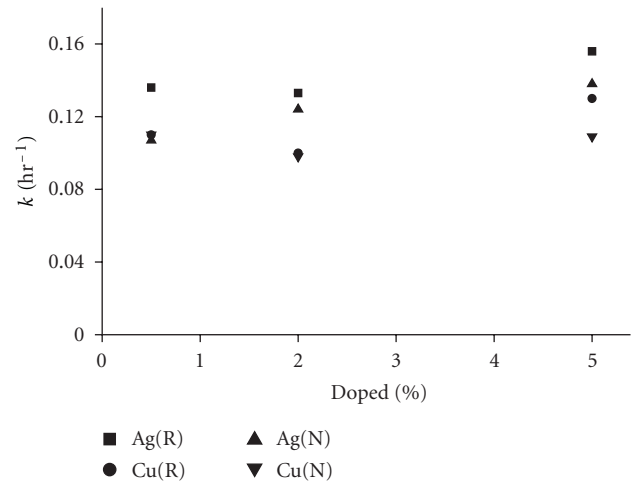

Figure 8: Relationship of the rate constant on the photocatalytic reduction by modified TiO_2.

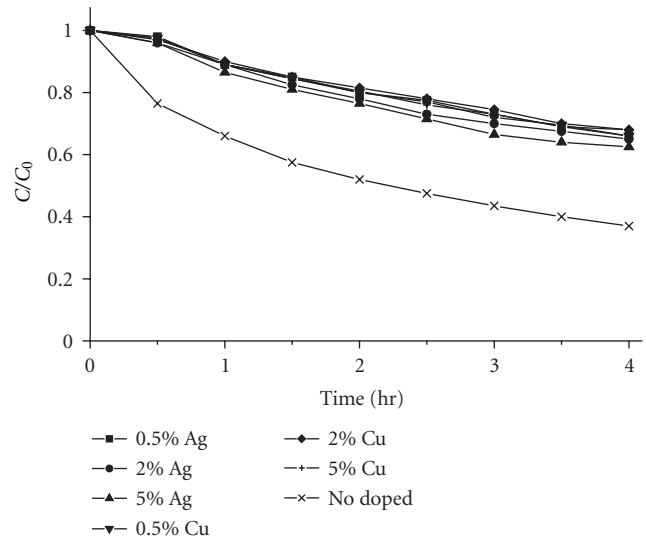

Figure 9: Relationship of the Cr(VI) removal rates on the photocatalytic reduction by modified TiO_2.

$$Ti^{4+} + e^- \longrightarrow Ti^{3+}, \quad (8)$$

$$Ti^{3+} + Cr^{6+}_{\text{adsorbed}} \longrightarrow Cr^{3+}_{\text{adsorbed}} + Ti^{4+}, \quad (9)$$

$$Cr^{6+}_{\text{adsorbed}} + 3e^- \longrightarrow Cr^{3+}_{\text{adsorbed}}. \quad (10)$$

During the photoreduction of Cr(VI) ions in aqueous solutions by UV/TiO_2 photocatalytic processes, the TiO_2 surface changed from the original white to light yellow after adsorption, and light green after the reaction. This meant that, after photoreduction, Cr(VI) deposited on the TiO_2 surface in the form of Cr(III). Comparing with the experimental results reported by previous researcher [11], chromium on the surface of TiO_2 particles was identified to be Cr(III), while no indication of the presence of Cr(VI) was observed.

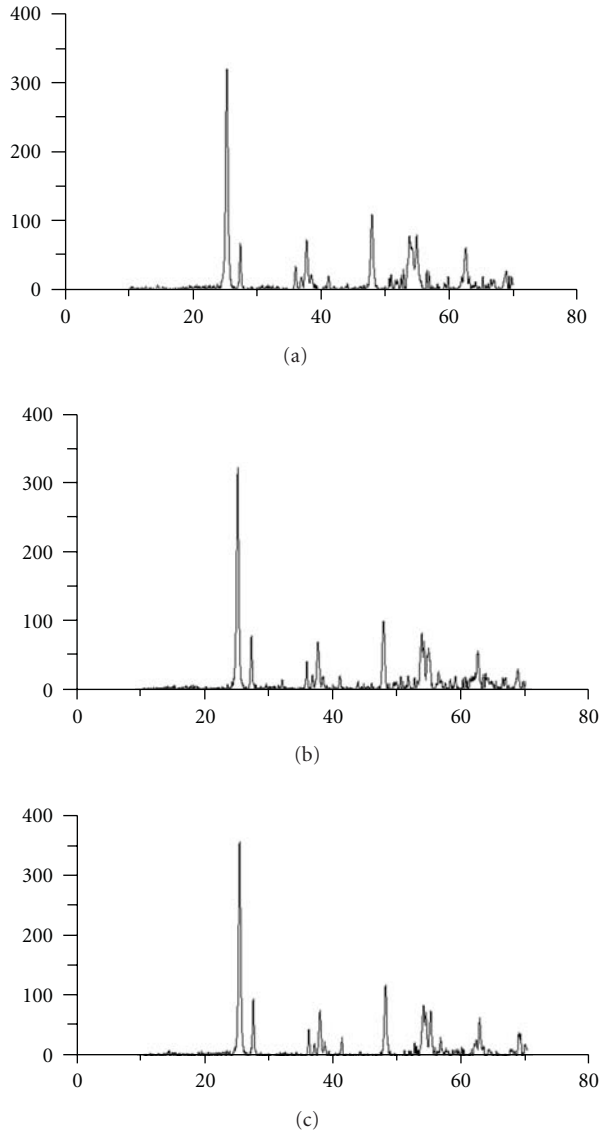

Figure 10: X-ray diffraction patterns of catalysts: (a) TiO_2 (P25), (b) 5% Ag/TiO_2, and (c) 5% Cu/TiO_2.

The impact of Cr(III) deposition on TiO_2 surface properties and structure after photoreduction was determined by XRD. The results are presented in Figure 10. For the XRD measurement, the crystal type analysis of doped 5% nonreduced Cu- and 5% nonreduced Ag-modified TiO_2 after reaction was made. The wave peaks appeared at the same angle, so it was concluded that Cr(III) deposition after reaction had no influence on the crystal type of TiO_2.

4. Conclusions

The photoreduction reaction rate of Cr(VI) by UV/TiO_2 photocatalytic process increased with the increasing TiO_2 dosage in the solution; from the pseudo-first-order model and Cr(VI) removal experiments, it was found that the relationship of the pseudo-first-order Cr(VI) removal rate, TiO_2 dosage, and variations of Cr(VI) concentration was

$$-r_a = \frac{d[\mathrm{Cr}^{6+}]}{dt} = 0.2344[\mathrm{Cr}^{6+}][\mathrm{TiO_2}]^{0.87}. \quad (11)$$

The Cr(VI) reduction rate was in a 0.87th power relation with the TiO_2 dosage. When ethanol was added as the organic hole scavenger, the relationship of the pseudo-first-order Cr(VI) removal rate, TiO_2 dosage, and variations of Cr(VI) concentration was

$$-r_E = \frac{d[\mathrm{Cr}^{6+}]}{dt} = 0.3132[\mathrm{Cr}^{6+}][\mathrm{TiO_2}]^{0.81}. \quad (12)$$

The added ethanol facilitated the Cr(VI) reduction rate and resulted in a better reduction effect than when ethanol was not added. The photoreduction reaction rate of Cr(VI) by the UV/TiO_2 photocatalytic process decreased with the increasing pH values of the solution. We found from the Cr(VI) removal experiment that as pH value increased, the reduction rate of dichromate ions gradually decreased because the increase in pH value reduced the adsorption of dichromate ions on the surface of the photocatalyst; also, at high pH value, $Cr(OH)_3$ covered the surface active position of TiO_2 so that the trivalent chromium deposited on TiO_2 depressed the photocatalytic activity.

With the solutions at pH = 3, methanol, ethanol, and isopropanol were added as organic hole scavengers. Methanol and ethanol had the largest Cr(VI) removal rates of 0.3029 and 0.3066 hr^{-1}, respectively, at a concentration of 2.94 mM. With the increasing isopropanol concentration, the Cr(VI) removal rate gradually rose and reached 0.2848 hr^{-1} at 5.88 mM. In the photocatalytic reduction experiment of Cr(VI) by $CuCl_2$ and $Ag(NO_3)$-doped TiO_2, the $Ag(NO_3)$-doped TiO_2 process had the better removal rate of Cr(VI), with the optimum removal rate of 38.1%, which was 1.04 times the 36.6% removal rate of the $CuCl_2$-doped TiO_2 process. However, the removal rates of modified TiO_2 were lower than those of nonmodified TiO_2.

Acknowledgments

Financial support from the National Science Council, through Grant NSC-100-2622-E-562-002-CC3, is gratefully acknowledged.

References

[1] E. Vaiopoulou and P. Gikas, "Effects of chromium on activated sludge and on the performance of wastewater treatment plants: a review," *Water Research*, vol. 46, no. 3, pp. 549–570, 2012.

[2] M. Owlad, M. K. Aroua, W. A. W. Daud, and S. Baroutian, "Removal of hexavalent chromium-contaminated water and wastewater: a review," *Water, Air, and Soil Pollution*, vol. 200, no. 1–4, pp. 59–77, 2009.

[3] P. Religa, A. Kowalik, and P. Gierycz, "Application of nanofiltration for chromium concentration in the tannery wastewater," *Journal of Hazardous Materials*, vol. 186, no. 1, pp. 288–292, 2011.

[4] L. Altaş, "Effects of chromium (VI) on the activities of ureolytic mixed culture," *Journal of Chemical Technology and Biotechnology*, vol. 84, no. 2, pp. 229–235, 2009.

[5] M. V. Dozzi, A. Saccomanni, and E. Selli, "Cr(VI) photocatalytic reduction: effects of simultaneous organics oxidation and of gold nanoparticles photodeposition on TiO_2," *Journal of Hazardous Materials*, vol. 211-212, pp. 188–195, 2012.

[6] G. Cappelletti, C. L. Bianchi, and S. Ardizzone, "Nano-titania assisted photoreduction of Cr(VI). The role of the different TiO_2 polymorphs," *Applied Catalysis B*, vol. 78, no. 3-4, pp. 193–201, 2008.

[7] S. G. Schrank, H. J. José, and R. F. P. M. Moreira, "Simultaneous photocatalytic Cr(VI) reduction and dye oxidation in a TiO_2 slurry reactor," *Journal of Photochemistry and Photobiology A*, vol. 147, no. 1, pp. 71–76, 2002.

[8] H. Lahmar, M. Kebir, N. Nasrallah, and M. Trari, "Photocatalytic reduction of Cr(VI) on the new hetero-system $CuCr_2O_4$/ZnO," *Journal of Molecular Catalysis A*, vol. 353-354, pp. 74–79, 2012.

[9] P. Mytych, A. Karocki, and Z. Stasicka, "Mechanism of photochemical reduction of chromium(VI) by alcohols and its environmental aspects," *Journal of Photochemistry and Photobiology A*, vol. 160, no. 3, pp. 163–170, 2003.

[10] A. Idris, N. Hassan, R. Rashid, and A. F. Ngomsik, "Kinetic and regeneration studies of photocatalytic magnetic separable beads for chromium (VI) reduction under sunlight," *Journal of Hazardous Materials*, vol. 186, no. 1, pp. 629–635, 2011.

[11] Y. Ku and I. L. Jung, "Photocatalytic reduction of Cr(VI) in aqueous solutions by UV irradiation with the presence of titanium dioxide," *Water Research*, vol. 35, no. 1, pp. 135–142, 2001.

[12] R. Velmurugan, K. Selvam, B. Krishnakumar, and M. Swaminathan, "An efficient reusable and antiphotocorrosive nano ZnO for the mineralization of Reactive Orange 4 under UV-A light," *Separation and Purification Technology*, vol. 80, no. 1, pp. 119–124, 2011.

[13] C. M. Ma, G. B. Hong, H. W. Chen, N. T. Hang, and Y. S. Shen, ". Photooxidation contribution study on the decomposition of azo dyes in aqueous solutions by VUV-based AOPs," *International Journal of Photoenergy*, vol. 2011, Article ID 156456, 8 pages, 2011.

[14] R. Amadelli, L. Samiolo, A. Maldotti, A. Molinari, and D. Gazzoli, "Selective photooxidation and photoreduction processes at TiO_2 surface-modified by grafted vanadyl," *International Journal of Photoenergy*, vol. 2011, Article ID 259453, 10 pages, 2011.

[15] T. Aarthi and G. Madras, "Photocatalytic reduction of metals in presence of combustion synthesized nano-TiO_2," *Catalysis Communications*, vol. 9, no. 5, pp. 630–634, 2008.

[16] S. F. Chen and G. Y. Cao, "Study on the photocatalytic reduction of dichromate and photocatalytic oxidation of dichlorvos," *Chemosphere*, vol. 60, no. 9, pp. 1308–1315, 2005.

[17] G. Guan, T. Kida, and A. Yoshida, "Reduction of carbon dioxide with water under concentrated sunlight using photocatalyst combined with Fe-based catalyst," *Applied Catalysis B*, vol. 41, no. 4, pp. 387–396, 2003.

[18] S. X. Liu, Z. P. Qu, X. W. Han, and C. L. Sun, "A mechanism for enhanced photocatalytic activity of silver-loaded titanium dioxide," *Catalysis Today*, vol. 93, no. 5, pp. 877–884, 2004.

Hindawi Publishing Corporation
International Journal of Photoenergy
Volume 2012, Article ID 578916, 7 pages
doi:10.1155/2012/578916

Research Article

Photocatalytic Treatment of Shower Water Using a Pilot Scale Reactor

Yash Boyjoo, Ming Ang, and Vishnu Pareek

Department of Chemical Engineering, Curtin University, Perth, WA 6102, Australia

Correspondence should be addressed to Vishnu Pareek, v.pareek@curtin.edu.au

Received 27 April 2012; Revised 13 June 2012; Accepted 14 June 2012

Academic Editor: Mika Sillanpää

Treatment of shower water deserves special consideration for reuse not only because of its low pollutant loading but also because it is produced in large quantities. In this study, a pilot scale study of photocatalytic degradation of impurities in real shower water was performed in a 31 L volume reactor using titanium dioxide as the photocatalyst. The reactor was operated in a continuous slurry recirculation mode. Several operational parameters were studied including the slurry initial pH, catalyst concentration, air flow rate, and slurry recirculation rate. Up to 57% of total organic carbon (TOC) elimination was obtained after 6 hours of treatment (for 3.0 slurry initial pH, 0.07 gL^{-1} catalyst concentration, 1.8 $Lmin^{-1}$ air flow rate, and 4.4 $Lmin^{-1}$ slurry recirculation rate). This study showed that photocatalysis could be successfully transposed from bench scale to pilot scale. Furthermore, the ease of operation and the potential to use solar energy make photocatalysis an attractive prospect with respect to treatment of grey water.

1. Introduction

Fresh water is getting scarcer. The number of people living in water-stressed or water-scarce countries is estimated to increase from half a billion now to three billion in 2025 [1]. Water reuse has been dubbed as the greatest challenge of the 21st century [2], and, as such, great emphasis is being put into the development of new technologies for the treatment of wastewater for reuse.

Since the discovery, in 1977, that titanium dioxide (TiO_2) could decompose cyanide in water [3], the field of photocatalysis has been receiving increasing interest. Photocatalysis is an advanced oxidation process (AOP) that uses a catalyst (often TiO_2), UV light, and an electron acceptor (O_2, O_3, H_2O_2) to completely decompose organic pollutants found in liquids or gases. The basis of the process is the use of low energy UV-A photons (for which the energy is greater or equal to the band gap energy of the catalyst) to excite the semiconductor catalyst into charge separation and generate electron-hole pairs. The electrons and holes, on separation, assist in the production of the very reactive hydroxyl radical in the aqueous phase which can destroy many toxic organic pollutants. This technology however works best at low pollutant concentrations (mgL^{-1} or $mmolL^{-1}$) and when the catalyst is finely dispersed within the medium. The overall process can be described by the following reaction equation:

$$\text{organic pollutants} + O_2 \xrightarrow{\text{semiconductor + UVA light}} CO_2 + H_2O + \text{mineral acid.} \quad (1)$$

Shower water is part of grey water and is produced by every household at a substantial amount (15–55 L day^{-1}) with a pollutant loading up to 100 mgL^{-1} [4]. Existing technologies for the treatment of grey water include membrane filtration, coagulation, ion exchange, and membrane bioreactors [5, 6]. However these techniques are either costly or merely transfer the pollutants from one medium to another. As a result, shower water is a good candidate for photocatalytic treatment. The treated water could be reused where potable water is not required. Such applications include toilet flushing, landscape irrigation, and car washing.

Countless researches have been made on the photocatalytic treatment of single or a few organic components in water [7–9]. Real wastewaters on the other hand have a

Table 1: Shower water characterization.

TOC (mgL^{-1})	24.62 ± 0.44
pH	7.37 ± 0.14
Main constituents (as per the products' ingredients list)	Anionic surfactants (sodium laureth sulphate, sodium cocoamphoacetate, sodium lauryl sulphate, ammonium laureth sulphate), cationic surfactants (cocamide MEA), nonionic surfactants (lauryl glucoside, cetyl alcohol), fragrance, antimicrobial agents.

multitude of pollutants and take longer to treat (typically a few hours) [10–14].

The photooxidation of surfactants, the main components of shower water, was extensively studied by Hidaka and coworkers [15–19]. They found that photodegradation decreases in the following order: anionic > nonionic > cationic surfactants, and postulated that photocatalysis was mainly a surface reaction due to the short lifetime of hydroxyl radicals. Sanchez et al. [20] successfully obtained 65% dissolved organic carbon (DOC) removal with hotel grey water at 29 mgL^{-1} initial DOC concentration while Zhu et al. found [21] that photocatalysis can effectively remove carbonaceous and nitrogenous biochemical oxygen demand from synthetic grey waters. Photocatalysis has also been reported to be efficient in the disinfection of E-coli [22], a microorganism bound to be present in wastewater that had had contact with humans. The vast majority of photocatalytic research has been performed at bench scale. If it is desired to commercialise this technique, pilot scale experiments are required so as to obtain a better understanding of the operational and hydrodynamic factors involved with higher throughputs.

The objective of this research was to study pollutant degradation in shower water in a pilot scale photocatalytic reactor (31 L volume) operating in a recirculation mode. The effect of several parameters such as the initial slurry pH, air flow rate, slurry recirculation rate, and catalyst dosage was studied. All experiments were carried out for a period of 6 hours, which was deemed a reasonable treatment time.

2. Experimental

2.1. Shower Water Characterisation. Shower water was collected daily from the researcher's home and stocked in the laboratory prior to the experiments. The same cleaning products were used each time (shampoo, face wash, and body soap) to maintain consistency. The characteristics of the collected shower water are presented in Table 1.

The TOC level of the shower water suggests that it is a low strength grey water. The main constituents of liquid soaps and shampoos are surfactants which can add up to 80% by weight of chemicals content [23]. Some other constituents that may be present in trace amounts in the shower water include sebum, microorganisms, and dyes.

2.2. Reagents and Analytical Methods. Aeroxide P25 titanium dioxide was purchased from Sigma Aldrich and was used as received. The catalyst had the following properties: 21 nm particle size, $50 \pm 15\,m^2\,g^{-1}$ BET specific surface area, >99.5% TiO_2 content [24], and a band gap energy of 3.2 eV, corresponding to photons with wavelengths less or equal to 385 nm [25]. A 6 M hydrochloric acid was used to modify the slurry pH prior to reaction. Compressed air was used as feed gas to the reactor and for UV lamp cooling. Tap water was used to dilute the shower water (if required). Slurry pH was measured with a TPS digital pH meter, which was calibrated periodically. Samples collected were filtered with 0.45 microns syringe filters and analysed for total organic carbon (TOC) on a Shimadzu TOC-$V_{CPH/CPN}$ analyser (Shimadzu Corporation, Japan).

2.3. Reactor Setup. Figure 1 shows the reactor setup used in this study. The reactor volume was 31 L (30 cm diameter) and was operated in recirculation mode. Ambient air was supplied by a compressor via a 10 cm distributor centred at the bottom of the reactor. Part of the compressed air was also used as coolant for the UV lamp. The UV mercury lamp, purchased from Primarc Ltd. (PM 3426, 800 W, 20 cm length medium pressure mercury lamp), was fitted into a quartz tube and suspended in the middle of the reactor. A digital thermocouple provided the temperature within the reactor. The temperature was maintained between 26 and 28°C by varying the rate of cooling water which ran through a coiled heat exchanger located around walls at the bottom of the reactor. An Iwaki magnetic pump was used for slurry circulation. Slurry flow rate was varied using valve V2 while air flow rate was varied via valve V5.

2.4. Procedure. Shower water was diluted with tap water (if required) and mixed with the titanium dioxide powder in a 60 L tank. The pH was adjusted, and the slurry was allowed to mix for 30 minutes to allow for dark adsorption of pollutants onto the catalyst surface. Compressed air as well as cooling water was started, and the slurry was transferred to the reactor via the Iwaki magnetic pump. Once the reactor was filled, valve V1 was closed, valve V3 was opened to allow the reactor to operate in recirculation mode, and, finally, the lamp was switched on. Samples were taken in 20 mL aliquots via sample valve V6 and were filtered prior to analysis.

3. Results and Discussion

Since the shower water consisted of a myriad of organic components, a realistic way of reporting the pollutant concentration was by measuring the total organic carbon (TOC in mgL^{-1}) of the samples. The average reaction rate for TOC elimination was calculated using the following equation:

$$-R_{TOC} = \frac{TOC_{initial} - TOC_{final}}{\tau}, \quad (2)$$

where $-R_{TOC}$ is the average rate of degradation of TOC ($molL^{-1}min^{-1}$), $TOC_{initial}$ and TOC_{final} are the initial and

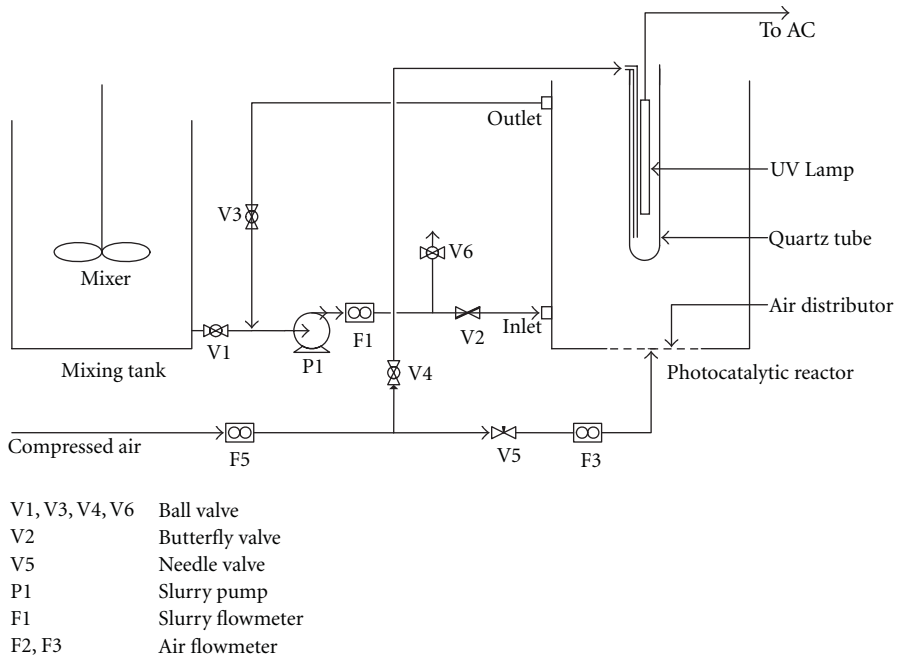

Figure 1: Experimental setup for photocatalysis experiments. Shower water was mixed for 30 minutes with catalyst and acid in mixing tank initially before mixture was sent to the photocatalytic reactor via pump P1. Reactor was operated in recirculation mode.

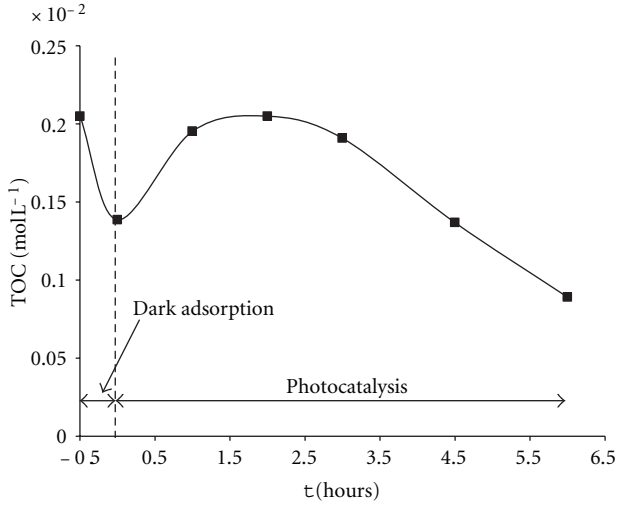

Figure 2: Temporal course for shower water photocatalysis at optimum conditions (TOC initial concentration = $24.62 \pm 0.44\,\text{mgL}^{-1}$, average reaction temperature = 27°C, initial slurry pH = 3.00, $0.07\,\text{gL}^{-1}$ catalyst loading, $1.8\,\text{Lmin}^{-1}$ air flow rate and $4.4\,\text{Lmin}^{-1}$ slurry flow rate).

final TOC concentration (molL^{-1}), and τ is the real contact time (minutes) in the reactor which is 360 minutes.

3.1. Photocatalysis of Shower Water. The temporal course at optimum conditions for the photocatalysis of shower water in terms of TOC reduction is illustrated in Figure 2. Part of the TOC was adsorbed onto the catalyst surface during the dark adsorption stage. Upon irradiation, the TOC concentration increased to a maximum within the first two hours of reaction that corresponded to the initial TOC concentration prior to dark adsorption. This phenomenon had been observed previously [17, 26, 27] for the photocatalytic oxidation of anionic surfactants at low initial concentrations. The initial increase in TOC can be attributed to the formation of intermediates on the catalyst surface followed by photodesorption of the intermediates back into the liquid medium. Several types of intermediates are formed via the photooxidation of long chained hydrocarbons. Zhang et al. [27] reported the formation of aldehyde and peroxide intermediates during the photooxidation of surfactants.

A reduction in the TOC concentration was then observed after 2 hours due to the onset of oxidation of organic pollutants. This reduction was only moderate from $t = 2\,\text{h}$ to $t = 3\,\text{h}$ probably due to a large quantity of long chained organics/intermediates still remaining in the solution. However, as the photoreaction proceeded, the long chained organics/intermediates cleaved into smaller chained intermediates for which mineralisation to carbon dioxide, water, and mineral acids took place at a faster rate, as observed after $t = 3\,\text{h}$. A maximum of 57% TOC degradation was obtained within 6 hours of treatment at optimum conditions.

3.2. Effect of Slurry Initial pH. The initial pH of the slurry is an important parameter that needs to be considered as it influences the surface charge properties of the catalyst particles [9], hence the adsorption of charged pollutants. Figure 3 shows the effect of the slurry initial pH on the average rate of TOC degradation. There was a gradual increase in the average reaction rate as the pH was decreased from 7.4 (natural pH) to 5.0. The increase in reaction rate

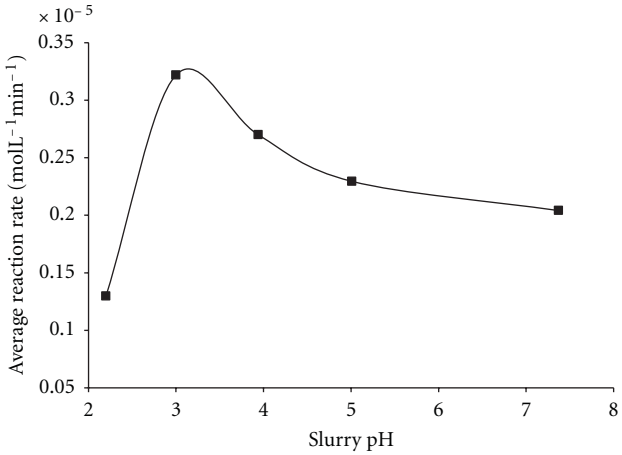

Figure 3: Effect of slurry initial pH on average reaction rate (TOC initial concentration = 24.62 ± 0.44 mgL^{-1}, average reaction temperature = 27°C, 0.07 gL^{-1} catalyst loading, 1.8 Lmin^{-1} air flow rate and 4.4 Lmin^{-1} slurry flow rate).

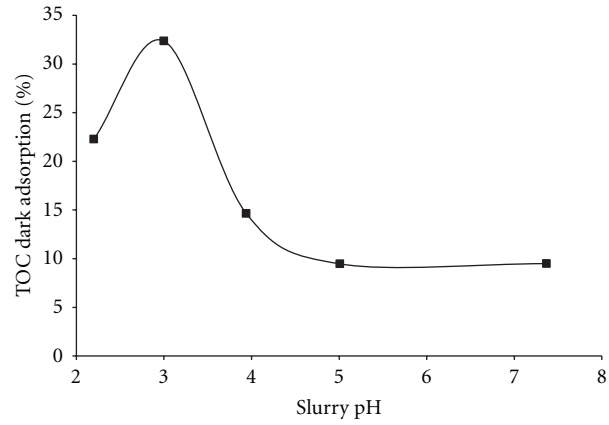

Figure 4: Effect of slurry initial pH on amount of TOC adsorbed in the dark.

became steeper as the pH was further lowered and reached a maximum at pH = 3.0. Further lowering of the pH to 2.2 led to a sharp decrease in the reaction rate.

Titanium dioxide is amphoteric by nature which means that past a certain pH, it can be either positively or negatively charged. That pH, which is called the point of zero charge (ZPC), occurs at a value of 6.5 for Aeroxide P25 titanium dioxide [28]. Hence when pH < ZPC, the TiO_2 is positively charged while at pH > ZPC, it is negatively charged as shown as follows:

$$\text{when pH} < \text{ZPC: TiOH} + \text{H}^+ \longleftrightarrow \text{TiOH}_2^+, \quad (3)$$

$$\text{when pH} > \text{ZPC: TiOH} + \text{OH}^- \longleftrightarrow \text{TiO}^- + \text{H}_2\text{O}. \quad (4)$$

This implies that at lower pH, the positively charged TiO_2 surface can easily attract the negatively charged species from the solution, hence facilitating their photooxidation. The main components of the shower water used were anionic surfactants as presented in Table 1. As the pH of the slurry was decreased, the positive surface charge of the TiO_2 increased, attracting more and more anionic groups to its surface. This is further evident with the change in the dark adsorption with slurry pH in Figure 4, which shows that pollutant species during the dark adsorption remained constant between pH of 7.4 and 5.0 but then increased sharply to reach a maximum of 32.4% adsorption at pH 3.0. Another research involving anionic surfactants has also shown preferential photooxidation at low pH [29, 30].

Being radical scavengers, carbonate anions present in the wastewater can inhibit photooxidation [31]. However an acidic medium can remove these unwanted anions as per the following equations:

$$\text{HCO}_3^- + \text{H}^+ \longrightarrow \text{H}_2\text{O} + \text{CO}_2, \quad (5)$$

$$\text{CO}_3^{2-} + 2\text{H}^+ \longrightarrow \text{H}_2\text{O} + \text{CO}_2. \quad (6)$$

Nonetheless, Figure 3 shows that a further reduction of pH to 2.2 was in fact detrimental to the degradation of TOC. This was attributed to high levels of Cl^- ions in the solution. Cl^- ions are scavengers of hydroxyl radicals as well as holes [32] and can therefore greatly reduce the photooxidation process. As the pH was decreased from 3.0 to 2.2, the concentration of Cl^- increased exponentially from 1×10^{-3} M to 6.3×10^{-3} M, hence explaining the rapid decrease in the TOC removal rate. The optimum pH of 3.0 was maintained throughout subsequent experiments.

3.3. Effect of Catalyst Dosage. Most wastewater photocatalytic treatment studies report an optimum catalyst concentration. Beyond that optimum, the rate of reaction either remains unchanged or decreases. Figure 5 shows the effect of catalyst loading on the average reaction rate with the range of catalyst loading investigated between 0.03 and 0.15 gL^{-1}. It is clear that the optimum catalyst concentration was about 0.07 gL^{-1}.

Reported optimum catalyst loadings for wastewater treatment are usually within a range of 0.1–1 gL^{-1} [7, 8, 33]; however some studies have also reported lower optimum loadings (0.05 gL^{-1}) [34]. However, in all cases, the optimum value strongly depends on the reactor design, pollutant type, and concentration [35].

In the current study, a relatively low value of optimum catalyst loading could be attributed to low concentrations of shower water as well as the large reactor diameter. Lower catalyst loadings provided sufficient sites for photoreaction and allowed a maximum possible illumination of the reaction space. Beyond those loadings, the decrease in average reaction rate was probably due to the backscattering of light by the catalyst particles, entailing a shielding effect on the remaining reaction space. Simulation studies are currently being carried out to verify these hypotheses.

The effect of catalyst concentration, W_{cat} (g_{cat}L^{-1}), on the average reaction rate, $-R_{\text{TOC}}$ (molL^{-1} min^{-1}), could be described as:

$$-R_{\text{TOC}} = A + \frac{B}{(W_{\text{cat}} - C)^2 + D}, \quad (7)$$

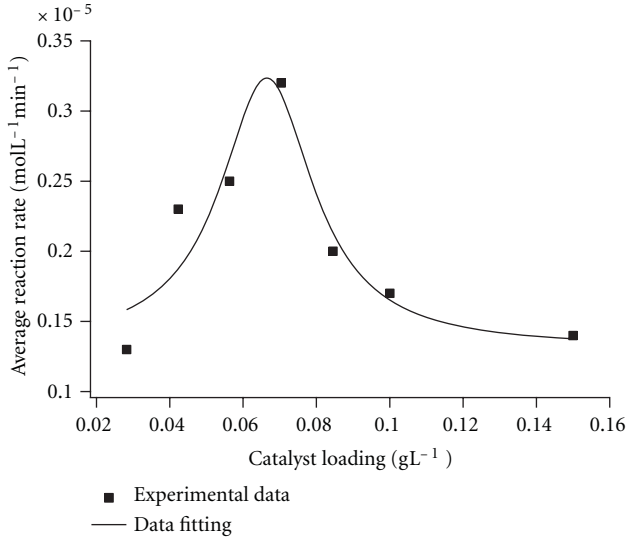

Figure 5: Effect of catalyst loading on average reaction rate (TOC initial concentration = 24.62 ± 0.44 mgL^{-1}, average reaction temperature = 27°C, initial slurry pH = 3.00, 1.8 Lmin^{-1} air flow rate and 4.4 Lmin^{-1} slurry flow rate).

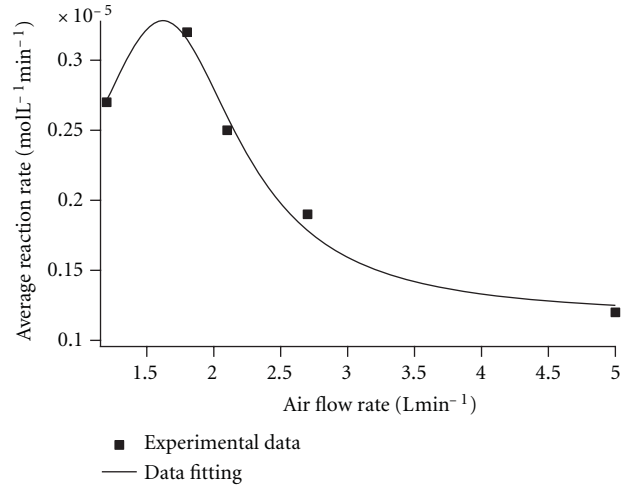

Figure 6: Effect of air flow rate on average reaction rate (TOC initial concentration = 24.62 ± 0.44 mgL^{-1}, average reaction temperature = 27°C, initial slurry pH = 3.00, 0.07 gL^{-1} catalyst loading and 4.4 Lmin^{-1} slurry flow rate).

where the values for A, B, C, and D are 1.31×10^{-6} molL^{-1} min^{-1}, 4.66×10^{-10} $g_{cat}{}^2$molL^{-3} min^{-1}, 6.64×10^{-2} g_{cat}L^{-1}, and 2.42×10^{-4} $g_{cat}{}^2$L^{-2}, respectively.

3.4. Effect of Air Flow Rate. Upon irradiation, the catalyst particles generate positive holes and electrons. The photooxidation process requires an oxidising agent to remove electrons from the catalyst surface and prevent them from recombining with positive holes which are responsible for the creation of hydroxyl radicals. In this study, the oxidant was oxygen in the air.

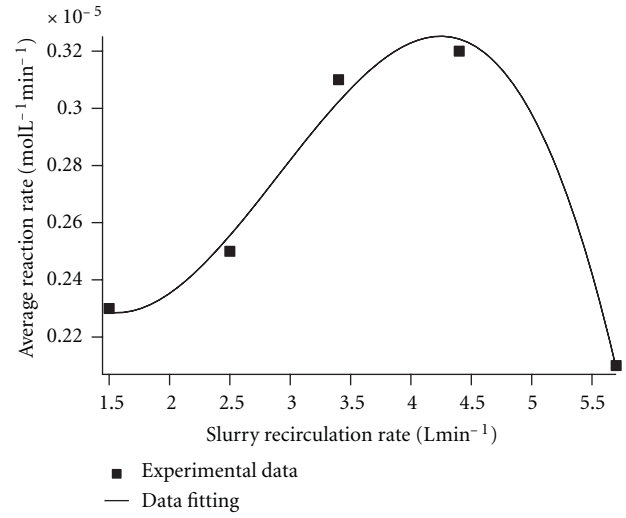

Figure 7: Effect of slurry recirculation rate on average reaction rate (TOC initial concentration = 24.62 ± 0.44 mgL^{-1}, average reaction temperature = 27°C, initial slurry pH = 3.00, 0.07 gL^{-1} catalyst loading and 1.8 Lmin^{-1} air flow rate).

The range of air flow rate investigated was between 1.5 and 5.0 Lmin^{-1} as depicted in Figure 6. The average TOC degradation rate was found to increase until an optimum was reached at 1.8 Lmin^{-1} air flow rate after which a steep decrease in the reaction rate was observed. Visual observations showed that fine bubbles were formed at the lower air flow rates. However, beyond the optimum air flow rate, larger bubbles of widespread sizes were observed. Larger bubbles meant reduced surface area for mass transfer of oxygen from the gas to liquid phase, hence the reduction in the average reaction rate. Agustina et al. [36] made a similar observation in their study of winery wastewater treatment with the same reactor. On the other hand, at low air flow rates in the vicinity of 1.5 Lmin^{-1}, air bubbles had a tendency to penetrate the slurry outlet, leading to irregular liquid pumping, hence a reduced average reaction rate.

The effect of air flow rate, Q_{Air} (Lmin^{-1}), on the average reaction rate, $-R_{TOC}$ (molL^{-1} min^{-1}), could be described as

$$-R_{TOC} = A + \frac{B}{(Q_{Air} - C)^2 + D}, \tag{8}$$

where the values for A, B, C, and D are 7.06×10^{-5} molL^{-1} min^{-1}, 5.93×10^{-5} molLmin^{-3}, 1.62 Lmin^{-1}, and 0.47 L^2 min^{-2}, respectively.

3.5. Effect of Slurry Recirculation Rate. The recirculation rate of the slurry was varied to study the effect of the residence time. The circulation rate was varied between 1.5 and 5.7 Lmin^{-1}, and its effect on the average reaction rate is presented in Figure 7. Maximum degradation was obtained at a recirculation rate of 4.4 Lmin^{-1}. At higher recirculation rate, the slurry inlet momentum was high enough that air bubbles had the tendency to be pushed towards the slurry outlet. Introducing air bubbles into the pipelines made pumping irregular and therefore reduced the average

Table 2: Breakdown of electrical cost for 1 run of photocatalytic shower water treatment at optimum conditions.

Equipment	Power rating (kW)	Power usage (%)	Usage (h)	Energy usage (kWh)	Cost @ 0.35 US$kWh^{-1} (US$m^{-3})
Pump	0.135	70	6	0.57	6.5
UV lamp	0.8	80	6	3.84	42.9
Total				4.41	49.4

reaction rate. Pareek et al. [37] found maximum degradation at a recirculation rate of 0.2 Lmin^{-1} in an 18 L volume reactor for the photodegradation of Bayer liquor. However in their study, catalyst suspension was assisted by fine air bubbles homogeneously distributed within the reactor. In this study, air bubbles were supplied from a 10 cm distributor centred at the bottom of the reactor. These bubbles were not dispersed throughout the reactor space, and, as a result, a relatively high volumetric flow rate was necessary to suspend the catalyst particles.

The effect of slurry recirculation rate, Q_{Slurry} (Lmin^{-1}), on the average reaction rate, $-R_{\text{TOC}}$ (molL^{-1} min^{-1}), could be described as

$$-R_{\text{TOC}} = k_0 + k_1 Q_{\text{Slurry}} + k_2 {Q_{\text{Slurry}}}^2 + k_3 {Q_{\text{Slurry}}}^3. \quad (9)$$

The values of k_0, k_1, k_2, and k_3 are 3.66×10^{-6} molL^{-1} min^{-1}, -2.00×10^{-6} molL^{-2}, 8.75×10^{-7} molminL^{-3}, and -1.00×10^{-7} molmin^{2}L^{-4}, respectively.

3.6. Electricity Cost Analysis. Based on the current electricity cost in Perth, Australia (0.35 US$kWh^{-1}), a cost analysis was performed as detailed in Table 2.

Therefore for a 31 L throughput, the treatment cost for shower water amounted to 49.4 US$m^{-3}. This value was close to the price range obtained by Pareek et al. [37] (60–270 US$m^{-3}) for the photocatalytic treatment of industrial Bayer liquor but is much larger than the reported 3.75 Euros·m^{-3} for the photocatalytic treatment of herbicides [38] most probably due to the size (bench scale) of the latter research. However, it is possible to operate the reactor with solar light; it is envisaged that operational cost of a large-scale photoreactor for shower water purification will be much less.

4. Conclusions

A pilot scale study for the photocatalytic degradation of real shower water showed that photocatalysis can be an efficient treatment process. At optimum conditions (3.0 slurry initial pH, 0.07 gL^{-1} catalyst concentration, 4.4 Lmin^{-1} slurry recirculation rate, and 1.8 Lmin^{-1} air supply), a 57% of TOC degradation was obtained after 6-hour treatment time, although higher TOC degradation is expected if the treatment time is increased. This study showed that photocatalysis could be successfully transposed from bench scale to pilot scale. Furthermore, the ease of operation of the process makes photocatalysis an attractive prospect in terms of grey water treatment.

References

[1] A. Stikker, "Water today and tomorrow: prospects for overcoming scarcity," *Futures*, vol. 30, no. 1, pp. 43–62, 1998.

[2] T. Asano, "Water from (waste)water—the dependable water resource," *Water Science and Technology*, vol. 45, no. 8, pp. 24–33, 2002.

[3] A. Fujishima and X. Zhang, "Titanium dioxide photocatalysis: present situation and future approaches," *Comptes Rendus Chimie*, vol. 9, no. 5-6, pp. 750–760, 2006.

[4] E. Eriksson, K. Auffarth, M. Henze, and A. Ledin, "Characteristics of grey wastewater," *Urban Water*, vol. 4, no. 1, pp. 85–104, 2002.

[5] F. Li, K. Wichmann, and R. Otterpohl, "Review of the technological approaches for grey water treatment and reuses," *Science of the Total Environment*, vol. 407, no. 11, pp. 3439–3449, 2009.

[6] B. Jefferson, A. Laine, S. Parsons, T. Stephenson, and S. Judd, "Technologies for domestic wastewater recycling," *Urban Water*, vol. 1, no. 4, pp. 285–292, 2000.

[7] V. Belgiorno, L. Rizzo, D. Fatta et al., "Review on endocrine disrupting-emerging compounds in urban wastewater: occurrence and removal by photocatalysis and ultrasonic irradiation for wastewater reuse," *Desalination*, vol. 215, no. 1–3, pp. 166–176, 2007.

[8] M. Pera-Titus, V. García-Molina, M. A. Baños, J. Giménez, and S. Esplugas, "Degradation of chlorophenols by means of advanced oxidation processes: a general review," *Applied Catalysis B*, vol. 47, no. 4, pp. 219–256, 2004.

[9] U. I. Gaya and A. H. Abdullah, "Heterogeneous photocatalytic degradation of organic contaminants over titanium dioxide: a review of fundamentals, progress and problems," *Journal of Photochemistry and Photobiology C*, vol. 9, no. 1, pp. 1–12, 2008.

[10] I. A. Balcioglu and I. Arslan, "Application of photocatalytic oxidation treatment to pretreated and raw effluents from the Kraft bleaching process and textile industry," *Environmental Pollution*, vol. 103, no. 2-3, pp. 261–268, 1998.

[11] A. C. Rodrigues, M. Boroski, N. S. Shimada, J. C. Garcia, J. Nozaki, and N. Hioka, "Treatment of paper pulp and paper mill wastewater by coagulation-flocculation followed by heterogeneous photocatalysis," *Journal of Photochemistry and Photobiology A*, vol. 194, no. 1, pp. 1–10, 2008.

[12] P. A. Pekakis, N. P. Xekoukoulotakis, and D. Mantzavinos, "Treatment of textile dyehouse wastewater by TiO_2 photocatalysis," *Water Research*, vol. 40, no. 6, pp. 1276–1286, 2006.

[13] H. El Hajjouji, F. Barje, E. Pinelli et al., "Photochemical UV/TiO_2 treatment of olive mill wastewater (OMW)," *Bioresource Technology*, vol. 99, no. 15, pp. 7264–7269, 2008.

[14] C. Fotiadis, N. P. Xekoukoulotakis, and D. Mantzavinos, "Photocatalytic treatment of wastewater from cottonseed processing: effect of operating conditions, aerobic biodegradability and ecotoxicity," *Catalysis Today*, vol. 124, no. 3-4, pp. 247–253, 2007.

[15] H. Hidaka, H. Kubota, M. Graätzel, E. Pelizzetti, and N. Serpone, "Photodegradation of surfactants II: degradation of sodium dodecylbenzene sulphonate catalysed by titanium dioxide particles," *Journal of Photochemistry*, vol. 35, no. 2, pp. 219–230, 1986.

[16] H. Hidaka, K. Ihara, Y. Fujita, S. Yamada, E. Pelizzetti, and N. Serpone, "Photodegradation of surfactants IV: photodegradation of non-ionic surfactants in aqueous titanium dioxide suspensions," *Journal of Photochemistry and Photobiology A*, vol. 42, no. 2-3, pp. 375–381, 1988.

[17] H. Hidaka, T. Oyama, T. Horiuchi, T. Koike, and N. Serpone, "Photo-induced oxidative synergistic degradation of mixed anionic/cationic surfactant systems in aqueous dispersions. A detailed study of the DBS/HTAB system," *Applied Catalysis B*, vol. 99, no. 3-4, pp. 485–489, 2010.

[18] H. Hidaka and J. Zhao, "Photodegradation of surfactants catalyzed by a TiO_2 semiconductor," *Colloids and Surfaces*, vol. 67, pp. 165–182, 1992.

[19] J. Zhao, H. Oota, H. Hidaka, E. Pelizzetti, and N. Serpone, "Photodegradation of surfactants X. Comparison of the photo-oxidation of the aromatic moieties in sodium dodecylbenzene sulphonate and in sodium phenyldodecyl sulphonate at TiO_2H_2O interfaces," *Journal of Photochemistry and Photobiology A*, vol. 69, no. 2, pp. 251–256, 1992.

[20] M. Sanchez, M. J. Rivero, and I. Ortiz, "Photocatalytic oxidation of grey water over titanium dioxide suspensions," *Desalination*, vol. 262, no. 1–3, pp. 141–146, 2010.

[21] X. Zhu, M. A. Nanny, and E. C. Butler, "Photocatalytic oxidation of aqueous ammonia in model gray waters," *Water Research*, vol. 42, no. 10-11, pp. 2736–2744, 2008.

[22] R. van Grieken, J. Marugán, C. Sordo, and C. Pablos, "Comparison of the photocatalytic disinfection of E. coli suspensions in slurry, wall and fixed-bed reactors," *Catalysis Today*, vol. 144, no. 1-2, pp. 48–54, 2009.

[23] K. Y. Lai, *Liquid Detergents*, Taylor & Francis, 2005.

[24] Inorganic materials for catalyst innovation, "AEROSIL, AEROXIDE and SIPERNAT metal oxides and silica based materials industry information 2242," Evonik Industries, 2011.

[25] M. I. Cabrera, O. M. Alfano, and A. E. Cassano, "Absorption and scattering coefficients of titanium dioxide participate suspensions in water," *Journal of Physical Chemistry*, vol. 100, no. 51, pp. 20043–20050, 1996.

[26] Y. Y. Eng, V. K. Sharma, and A. K. Ray, "Photocatalytic degradation of nonionic surfactant, Brij 35 in aqueous TiO_2 suspensions," *Chemosphere*, vol. 79, no. 2, pp. 205–209, 2010.

[27] R. Zhang, L. Gao, and Q. Zhang, "Photodegradation of surfactants on the nanosized TiO_2 prepared by hydrolysis of the alkoxide titanium," *Chemosphere*, vol. 54, no. 3, pp. 405–411, 2004.

[28] J. R. Regalbuto, *Catalyst Preparation: Science and Engineering*, CRC Press/Taylor & Francis, 2007.

[29] T. Oyama, A. Aoshima, S. Horikoshi, H. Hidaka, J. Zhao, and N. Serpone, "Solar photocatalysis, photodegradation of a commercial detergent in aqueous TiO_2 dispersions under sunlight irradiation," *Solar Energy*, vol. 77, no. 5, pp. 525–532, 2004.

[30] M. Sanchez, M. J. Rivero, and I. Ortiz, "Kinetics of dodecylbenzenesulphonate mineralisation by TiO_2 photocatalysis," *Applied Catalysis B*, vol. 101, no. 3-4, pp. 515–521, 2011.

[31] R. Andreozzi, V. Caprio, A. Insola, and R. Marotta, "Advanced oxidation processes (AOP) for water purification and recovery," *Catalysis Today*, vol. 53, no. 1, pp. 51–59, 1999.

[32] M. N. Chong, B. Jin, C. W. K. Chow, and C. Saint, "Recent developments in photocatalytic water treatment technology: a review," *Water Research*, vol. 44, no. 10, pp. 2997–3027, 2010.

[33] J. Lea and A. A. Adesina, "The photo-oxidative degradation of sodium dodecyl sulphate in aerated aqueous TiO_2 suspension," *Journal of Photochemistry and Photobiology A*, vol. 118, no. 2, pp. 111–122, 1998.

[34] A. E. H. Machado, J. A. de Miranda, R. F. de Freitas et al., "Destruction of the organic matter present in effluent from a cellulose and paper industry using photocatalysis," *Journal of Photochemistry and Photobiology A*, vol. 155, no. 1–3, pp. 231–241, 2003.

[35] P. R. Gogate and A. B. Pandit, "A review of imperative technologies for wastewater treatment I: oxidation technologies at ambient conditions," *Advances in Environmental Research*, vol. 8, no. 3-4, pp. 501–551, 2004.

[36] T. E. Agustina, H. M. Ang, and V. K. Pareek, "Treatment of winery wastewater using a photocatalytic/photolytic reactor," *Chemical Engineering Journal*, vol. 135, no. 1-2, pp. 151–156, 2008.

[37] V. K. Pareek, M. P. Brungs, and A. A. Adesina, "Continuous process for photodegradation of industrial bayer liquor," *Industrial and Engineering Chemistry Research*, vol. 40, no. 23, pp. 5120–5125, 2001.

[38] G. Li Puma, B. Toepfer, and A. Gora, "Photocatalytic oxidation of multicomponent systems of herbicides: scale-up of laboratory kinetics rate data to plant scale," *Catalysis Today*, vol. 124, no. 3-4, pp. 124–132, 2007.

Hindawi Publishing Corporation
International Journal of Photoenergy
Volume 2012, Article ID 303961, 9 pages
doi:10.1155/2012/303961

Research Article

A New Photocatalytic System Using Steel Mesh and Cold Cathode Fluorescent Light for the Decolorization of Azo Dye Orange G

Ming-Chin Chang,[1] Chin-Pao Huang,[2] Hung-Yee Shu,[1] and Yung-Chen Chang[1]

[1] *Institute of Environmental Engineering, Hungkuang University, 34 Chung-Chie Road, Shalu, Taichung 433, Taiwan*
[2] *Department of Civil and Environmental Engineering, University of Delaware, Newark, DE 19716, USA*

Correspondence should be addressed to Hung-Yee Shu, hyshu@sunrise.hk.edu.tw

Received 1 June 2012; Accepted 23 June 2012

Academic Editor: Mika Sillanpää

High color and organic composition, the effluents from the textile dyeing and finishing industry, can be treated by photocatalytic oxidation with UV/TiO_2. The objective of this study was to prepare a new photocatalytic system by coating nanosized TiO_2 particles on steel mesh support and using cold cathode fluorescent light (CCFL) irradiation at 365 nm in a closed reactor for the oxidation of azo dye C.I. Orange G (OG). Various factors such as reaction time, coating temperature, TiO_2 dosage, pH, initial dye concentration, and service duration were studied. Results showed efficient color removal of the OG azo dye by the photocatalytic system with TiO_2-coated temperature at 150°C. The optimal TiO_2 dosage for color removal was 60 g m^{-2}. An acidic pH of 2.0 was sufficient for photocatalytic oxidation whereas basic condition was not. The rate of color removal decreased with increase in the initial dye concentration. The TiO_2-coated steel mesh can be used repeatedly over 10 times without losing the photocatalytic efficiency. Results of FTIR and IC indicated the breakage of N=N bonds, with sulfate as the major and nitrite and nitrate as the minor products, which implied degradation of dye molecules.

1. Introduction

Most dyestuffs from the effluent of textile dyeing and finishing industry are organic compounds with high color intensity, recalcitrant to conventional biological wastewater treatment, and thus of major environmental concerns [1–4]. Furthermore, chemical coagulation integrated with activated sludge process was not able to meet the increasingly stringent criteria of color in dye wastewater treatment in Taiwan [5]. There is great demand of technology to decolorize the highly colored dye wastewater more effectively. Azo dyes with nitrogen double bond N=N are the largest class of commercial dyestuffs used in the textile industries. There were reports of successful color removal with final mineralization from azo dye wastewater using advanced oxidation processes (AOPs) such as UV/H_2O_2 [6–9], UV/O_3 [10, 11], or Fenton reaction [12, 13]. Additionally, it has been reported that photocatalytic processes such as UV-TiO_2 system can also be effective in treating dye wastewaters [14–18] except that when applied in suspension further separation of TiO_2 particles is necessary. Therefore, fixing the TiO_2 particles onto supported materials such as silica gel and plates can avoid the particle separation step and enables the easy operation of heterogeneous TiO_2 photocatalysis [19–23]. The objective of this study was to study the degradation of azo dye C.I. Orange G (OG) using a batch photocatalytic reactor in which the photocatalytic TiO_2 particles were coated on steel mesh and cold cathode fluorescent lamp (CCFL) was used (wavelength of 365 nm) as the source of irradiation. The CCFL lamp has thin and simple structure, is less temperature sensitive, and is easy to configure as well as it is brighter than the traditional mercury arc mercury lamp. It is more durable than other light sources. CCFL light is time-saving and less cost which is used broadly in computer products and applications such as liquid crystal display (LCD) backlight displays, PC case lights, and scanners, photocopy machines, industry machines such as appliance lighting, automotive fittings such as dashboard backlights, decoration light, advertisement such as signage board, exit light, and light box, and decoration such as indoors light and

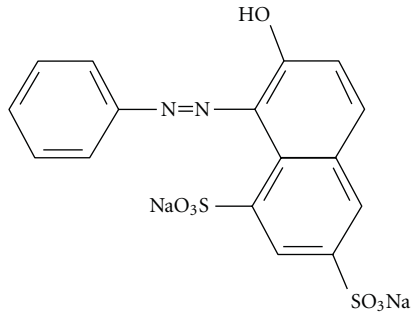

Figure 1: The chemical structure of monoazo dye Orange G. ($C_{16}H_{10}N_2Na_2O_7S_2$).

outdoors light. Factors such as coating temperature, TiO_2 dosage, pH, initial dye concentration, and reaction time that may affect the degree of the dye degradation were studied. Changes in color intensity, pH, and ORP were monitored in addition to the analysis of reaction products by FTIR and IC.

2. Materials and Methods

2.1. Materials and Apparatus. The monoazo dye, C.I. Orange G (OG, $C_{16}H_{10}N_2Na_2O_7S_2$, 60%) with a molecular weight of 452.38 and a characteristic wavelength (λ_{max}) of 479 nm was purchased from Sigma-Aldrich, Inc., and used as received without further purification. Figure 1 shows the chemical structure of OG. The commercial nanosized titanium dioxide (TiO_2), Degussa P-25, with a specific surface area of 48.68 $m^2\,g^{-1}$ from Aldrich was used as the catalyst. The steel mesh (mesh size number 140, 0.106 mm) was purchased from a local hardware store and trimmed into pieces with a gross area of 252 cm^2 (36 × 7 cm). Initially, the steel mesh was trimmed, washed with distilled water, dried at room temperature (25°C), weighed, and then stored in desiccator for further use. A given amount of Degussa P-25 TiO_2 nanoparticle (e.g., 7.5–50.0 g) was mixed with 250 mL of distilled water to make suspension at concentrations of 30–200 $g\,L^{-1}$. The pretreated steel mesh piece was dipped in the TiO_2 suspension then dried under certain temperature for one hour. The steel mesh piece was then washed with distilled water to remove any loose TiO_2 particles from the surface. The dipping, washing, and drying steps were repeated three times to reach a certain weight of TiO_2 on the steel mesh surface. Table 1 shows the amount of TiO_2 coated on the steel mesh surface (gross area of 252 cm^2) in the range of 0.3025–1.6855 g which yielded specific surface TiO_2 concentration in the range of 12–67 $g\,m^{-2}$. Based on images obtained with Field Emission Scanning Electron Microscope (FESEM), model JEOL 6330CF, of the TiO_2-coated steel mesh, it is seen that TiO_2 particles were uniformly coated on the steel mesh surface as shown in Figure 2. The crystallinity of TiO_2 particles was characterized by XRD (Thin-Film X-ray Diffractometer, X-RAY/TF) which yielded an anatase to rutile ratio of 7 : 3 as expected. Table 2 shows the BET surface area and porosity of TiO_2-coated steel mesh as a function of drying temperature using Micromeritics Gemini V. The

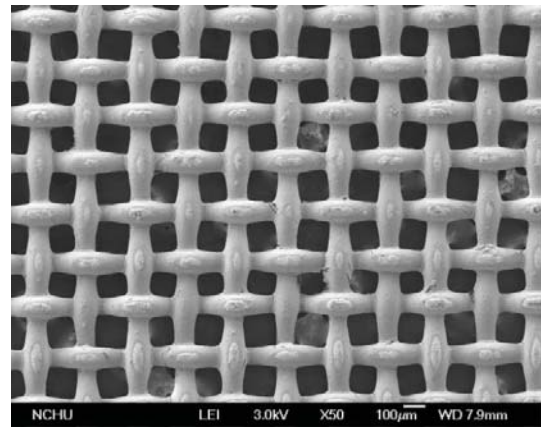

(a)

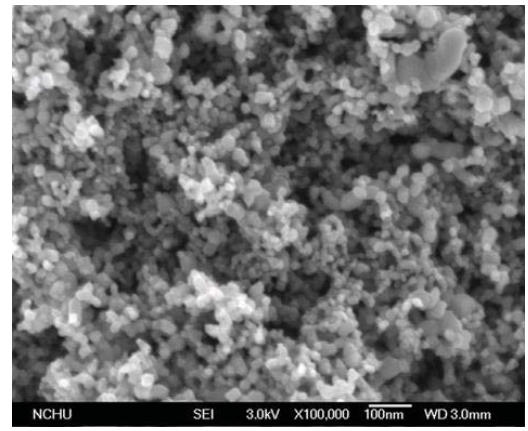

(b)

Figure 2: The morphology of TiO_2 powder coated on steel mesh at 150°C was identified by a JEOL 6330CF Field Emission Scanning Electron Microscope (FESEM). (a) 50 times enlargement and (b) 100,000 times enlargement.

photocatalytic reactor was a closed rectangular black tank (length × width × height equal to 360 × 70 × 78 mm) made of acrylic resin with a removable upper cover underneath of which was six cold cathode fluorescent lamps (CCFL) each of which has a diameter of 0.25 cm, length of 30 cm, light intensity of 4 W, and irradiation wavelength of 365 nm. The dye solution, 200 mL, was introduced to the photocatalytic reactor at which bottom was placed the TiO_2-coated steel mesh with total gross surface area 252 cm^2 (power per unit area of one lamp of 0.35 $mW\,cm^{-2}$); the depth of the dye solution was 0.794 cm neglecting the thickness of the steel mesh. The CCFL lamps were located 6.0 cm above the surface of the dye solution which yielded a total light energy of 2.1 $mW\,cm^{-2}$ measured at the surface of the solution.

2.2. Photocatalytic Procedure. OG azo dye solution at various concentrations was prepared with deionized water. The experimental variables studied included reaction time, TiO_2 dosage, initial dye concentration, and application duration of TiO_2. At a predetermined reaction time, an aliquot of the solution was withdrawn and analyzed for residual

Table 1: The TiO_2-coated weight on the steel meshes.

TiO_2 weight (g) (W_1)	TiO_2 solution concentration (g L^{-1}) (W_1/V)	TiO_2 weight on the coated steel meshes (g) (W_2)	TiO_2 weight per unit area (g m^{-2}) (W_2/A)
7.5	30	0.3025	12
12.5	50	0.5098	20
25.0	100	1.0149	40
37.5	150	1.5054	60
50.0	200	1.6855	67

V: the TiO_2 solution of 250 mL, A: the steel net area of 252 cm^2.

Table 2: The specific surface area and porosity of TiO_2 by various drying temperature for samples with TiO_2 load of 60 g m^{-2}.

Drying temperature °C	Specific surface area m^2 g^{-1}	Porosity Å
100	39.41	9.4077
150	43.35	8.8541
200	49.76	8.4902
250	61.42	9.1983
300	55.35	8.3969

dye concentration, TOC, and color. Dye concentration was determined by measuring the absorbance at wavelength of 479 nm using Hitachi U-2000 spectrophotometer. TOC was obtained with a Total Organic Carbon Analyzer from O.I. Analytical Aurora, model 1030. Color intensity was determined based on the American Dye Manufacturers Institute (ADMI) standard color measurement by applying the Adams-Nickerson color difference formula following method 2120E of the Standard Methods. The pH and redox potential (ORP) were monitored by a Eutech PH5500 dual channel pH/ion meter with specific probes. Besides, the degradation products were identified using Perkin Elmer FT-IR spectrophotometer model Spectrum One. Ions such as sulfate, nitrate, and nitrite were identified with ion chromatography (IC), Dionex ICS-1000.

3. Results and Discussion

3.1. Effect of Combining CCFL UV 365 Irradiation and TiO_2 Catalyst. The color removal was first compared for various systems, that is, CCFL/TiO_2, CCFL alone, and TiO_2 alone at the initial OG concentration of 50 mg L^{-1}, TiO_2 dosage of 60 g m^{-2} and 6 CCFL lamps with total light intensity of 24 W at wavelength of 365 nm in 120 min of reaction in the closed reactor. Figure 3 shows results of color removal by various systems. Results indicated that the system of CCFL alone, and TiO_2 alone could not remove color at any significant level. The CCFL/TiO_2 system removed color and TOC effectively with almost 100 and 95% removal, respectively, in 2 h. It was also observed that the pH remained relatively constant from 5.5 to 5.0 with time. This was expected as TiO_2 is a known photocatalyst that upon radiation with light which wavelength is shorter than that of its bandgap can generate hydroxyl radicals, strong oxidation agents that can oxidize a wide group of organic compounds nonspecifically [14–18].

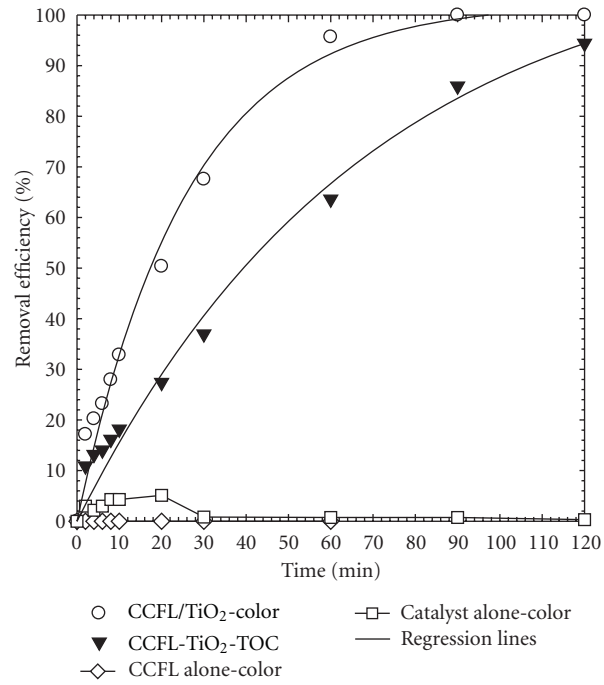

Figure 3: Effect of combining CCFL UV 365 irradiation and TiO_2 catalyst. The conditions were initial dye concentration of 50 mg L^{-1}, TiO_2 coated amounts of 60 g m^{-2}, light intensity of 2.1 mW cm^{-2}, and reaction time during 120 min.

3.2. Effect of Coating Temperature. The effect of TiO_2-coating temperature on color removal was studied at the initial OG concentration of 50 mg L^{-1}, TiO_2 load dosage of 40 g m^{-2} and 6 CCFL lamps in 120 min in the closed reactor. Figure 4 shows insignificant color removal in the range of 100–300°C. It was noted that pH remained unchanged at around 5 to 6. The reaction kinetics of UV/TiO_2 photocatalytical system was proved to follow the Langmuir-Hinshelwood (L-H) reaction kinetics [24–27]. And in most of the designed reaction conditions, the L-H kinetic model of the UV/TiO_2 system can be further simplified into pseudo-first-order reaction kinetics. Therefore, the color removal of this study was treated using pseudo first-order reaction as follows:

$$C_{\text{dye}} = C_{\text{dye0}} \times e^{-kt}, \quad (1)$$

where k denotes the observed first-order reaction rate constant (min^{-1}), t is the reaction time (min), $C_{\text{dye,0}}$ designates

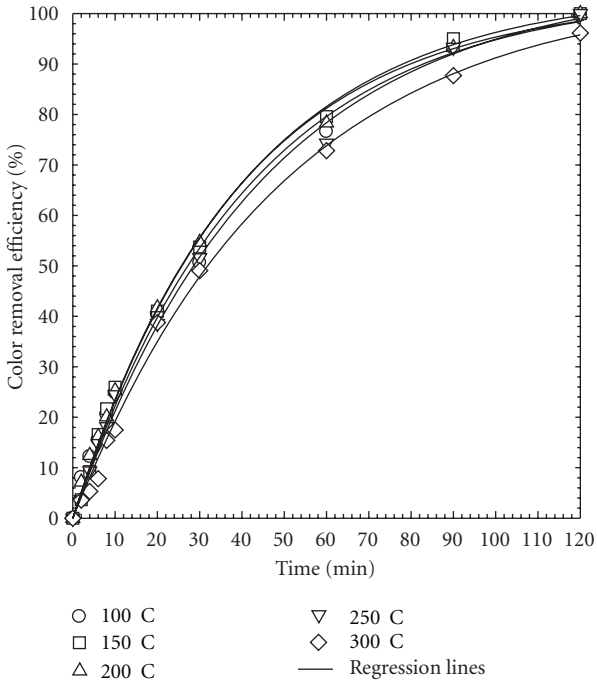

Figure 4: Effect of drying temperature. The conditions were initial dye concentration of 50 mg L^{-1}, TiO_2-coated amounts of 40 g m^{-2}, light intensity of 2.1 mW cm^{-2}, and reaction time during 120 min.

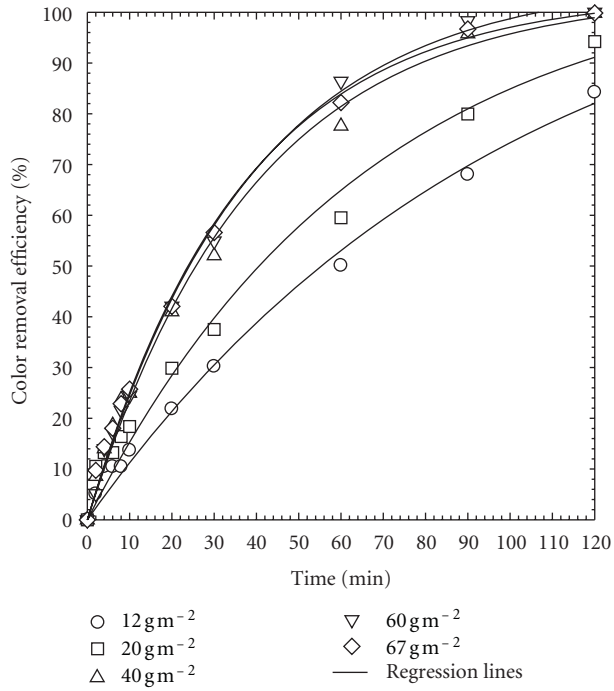

Figure 5: Effect of surface loading of TiO_2. The conditions were initial dye concentration of 50 mg L^{-1}, light intensity of 2.1 mW cm^{-2}, and reaction time during 120 min.

the initial concentration (mg L^{-1}) of OG and $C_{dye,t}$ is the concentration (mg L^{-1}) of OG at time t. The curve fitting of experimental results by (1) were shown in the figures as solid lines to present well-fit of kinetic model to the experimental data. The calculated rate constants (from curve fitting) were 2.36, 2.62, 2.52, 2.27, and 2.23 10^{-2} min^{-1} at 100, 150, 200, 250, and 300°C, respectively, as shown in Table 3(a). The best rate occurred at a coating temperature of 150°C. Note that this temperature was chosen further as the working condition.

3.3. Effect of TiO_2 Load Dosage. Figure 5 shows the removal of color as a function of surface dosage of TiO_2. Results indicated that the color removal increased from 80 to 100% in 120 min when the surface loading of TiO_2 particles increased from 12 to 60 g m^{-2}. The color removal then decreased from 100 to 90% when the surface loading of TiO_2 increased from 60 to 67 g m^{-2}. An optimal TiO_2 loading for color removal occurred at 60 g m^{-2}. The rate constants followed similar trend as percent color removal; the observed rate constants were 1.10, 1.41, 2.41, 3.23, and 2.80 (10^{-2} min^{-1}) at surface TiO_2 loading dosage of 12, 20, 40, 60, and 67 g m^{-2}, respectively, as shown in Table 3(b). Note that the maximum rate constant also occurred at TiO_2 loading of 60 g m^{-2}.

3.4. Effect of pH. The effect of pH on the degradation of azo dye was conducted by adjusting the initial pH value of 5.3 to the range of 2 to 11 using HCl and/or NaOH with initial OG dye concentration of 50 mg L^{-1} and 60 g m^{-2} of TiO_2 dosage. Figure 6 shows the change of dye concentration as a function of time at various pH values. Results indicated that the color removal increased rapidly at acidic pH of 2 and 3 then became slow as the pH increased. This could be attributed to loss of hydroxyl radicals as pH increased. The effect of pH on the photodegradation of acid dye can be better described by the interaction between the dye compound and the photocatalyst. Better contact between the dye chemical and TiO_2 is necessary for the degradation reaction. As pH increases, the surface of TiO_2 becomes negatively charged. (note: the pH_{zpc} of TiO_2 is 5.5). Negatively charged TiO_2 surface discourages the adsorption of the anion acid dye. The rate constants followed similar trend to that of color removal. The rate constants at pH 2 and 3 were 13.28 and 16.6 (10^{-2} min^{-1}), respectively, which were greater than 2.69 (10^{-2} min^{-1}) at pH 4 as shown in Table 3(c). At original pH 5.3, the degradation of OG dye was sufficient fast and reached 100% removal during 120 min reaction time. Furthermore, the effluent from acid dye bath dyeing processing (OG dye was applied) usually presents acidic pH at about 3-4. Thus, it is not suggested that the wastewater treatment plan adjust pH to 2-3 for better treatment efficiency. But it is encouraged to use the advantage of acid dye bath at acidic pH to elevate the reaction rate and removal efficiency.

3.5. Effect of Dye Initial Concentration. To present the validity of L-H model on our CCFL/TiO_2 system, the effect of initial dye concentrations on the photodegradation of azo OG dye was studied at initial concentrations of 12.5–75 mg L^{-1}, TiO_2 dosage of 60 g m^{-2} and 6 CCFL lamps for a period of

Table 3: The first-order reaction rate constant k (10^2 min^{-1}).

(a) Effect of coating temperature		(b) Effect of TiO_2 load dosage		(c) Effect of initial concentration		(d) Effect of initial pH		(e) Duration test	
Temperature, °C	k	Load dosage, g m^{-2}	k	Concentration, mg L^{-1}	k	pH	k	Cycle	k
100	2.36	12	1.10	12.5	12.54	2	13.28	1	3.46
150	2.62	20	1.41	18.8	9.67	3	16.60	2	2.41
200	2.52	40	2.41	25	7.71	4	2.64	3	2.14
250	2.27	60	3.23	50	2.83	5.3	2.69	4	2.06
300	2.23	67	2.80	75	2.0	9	2.67	5	1.62
						11	1.53	6	1.80
								7	1.71
								8	1.73
								9	1.66
								10	1.55

Time for (a) and (b) at 60 min; (c) at 20 min.
Time for (d) at 20 min; (e) at 30 min.

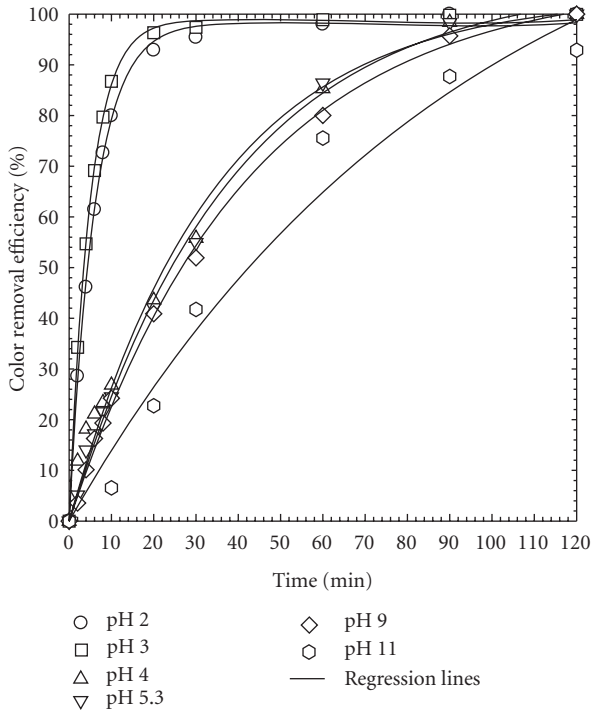

Figure 6: Effect of initial pH. The conditions were TiO_2-coated amounts of 60 g m^{-2}, light intensity of 2.1 mW cm^{-2}, and reaction time during 120 min.

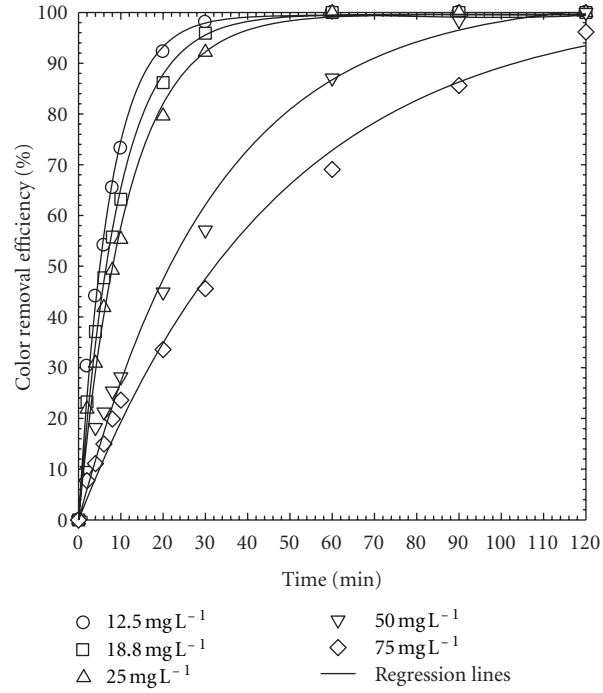

Figure 7: Effect of initial concentration. The conditions were TiO_2-coated amounts of 60 g m^{-2}, light intensity of 2.1 mW cm^{-2}, and reaction time during 0∼120 min.

120 min in the closed reactor. Figure 7 shows results of dye photodegradation as a function of reaction time at various initial dye concentrations. Results indicated that the rate of dye removal decreased from 12.54 to 2.0 (10^{-2} min^{-1}) when the initial dye concentration was increased from 12.5 to 75 mg L^{-1} as shown in Table 3(d). The rate constant then remained constant and independent of the dye concentration as the initial dye concentration increased to greater than 50 mg L^{-1}. This is typical Langmuir-Hinshelwood (L-H) reaction kinetics which is generally capable for modeling UV/TiO_2 photocatalytic oxidation process [24–27]. According to the L-H reaction kinetics, the rate of dye degradation can be described by the following equation:

$$r = \frac{dC}{dt} = \frac{kK_AC}{1 + K_AC}, \tag{2}$$

where r is the degradation rate of dye (mg L^{-1} min^{-1}), k, K_A, and C are the rate constant (mg L^{-1} min^{-1}), equilibrium adsorption constant (L mg^{-1}), and residual dye concentration (mg L^{-1}), respectively. According to the above equation, at high dye concentration, that is, $1 \ll KC$, the rate equation is

$$r = k. \tag{3}$$

Likewise, at low dye concentration, that is, $1 \gg KC$, (2) becomes

$$r = kK_AC. \tag{4}$$

That is, as the initial concentration increases, the reaction no longer follows the first order expression; rather it becomes independent of the dye concentration as shows in (3). By rearranging (2), one has

$$\frac{1}{r_0} = \frac{1}{kK_A} \times \frac{1}{C_0} + \frac{1}{k}, \tag{5}$$

where r_0 and C_0 are the initial rate (mg L^{-1} min^{-1}) and initial dye concentration (mg L^{-1}), respectively. A plot of the reciprocals of initial rate and initial concentration yields the rate constant, k, and the adsorption constant, K (Figure 8). The initial rate r_0 was calculated by the first 2 min of Figure 7 with TiO_2 loading dosage at 12 and 60 g m^{-2}, respectively (Table 4). From the slope ($1/kK_A$) and the intercept ($1/k$) of Figure 8, the calculated k and K_A were 2.08 mg L^{-1} min^{-1} and 0.1257 L mg^{-1} for TiO_2 loading dosage at 12 g m^{-2} and 4.41 mg L^{-1} min^{-1} and 0.0346 L mg^{-1} at 60 g m^{-2}, respectively. The rate constants (k) obtained in this work of 2.08 and 4.41 mg L^{-1} min^{-1} were higher than that of previous works [24–27] such as 1.66, 1.67, 0.95, and 0.17 mg L^{-1} min^{-1} for various dyes direct red 16, remazol black 5, procion red MX-5B, and indigo carmine, respectively. Similarly, the equilibrium adsorption constants (K_A) of 0.1257 and 0.0346 L mg^{-1} from this wok were in the range of previous studies, such as 0.0093, 0.072, 0.071, and 0.78 L mg^{-1} for various dyes as above. The results indicate that the photocatalytic degradation of Orange G by CCFL/TiO_2 process followed the Langmuir-Hinshelwood kinetic model.

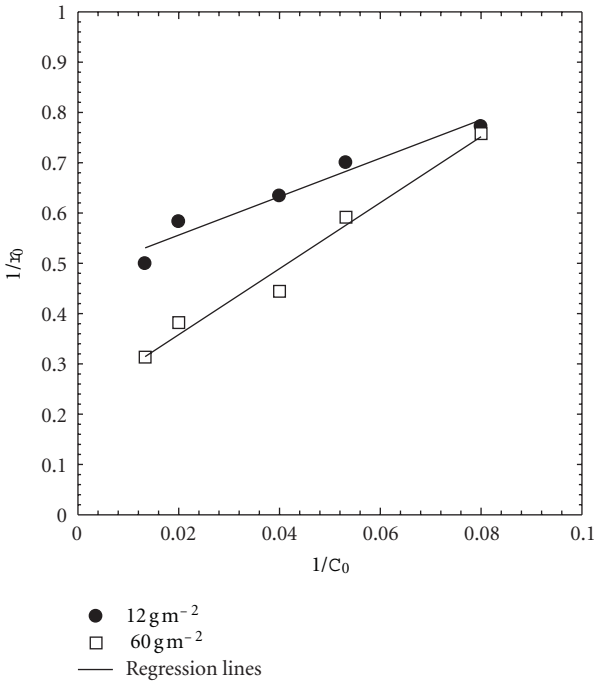

Figure 8: Langmuir-Hinshelwood kinetic model (comparison of two different TiO_2 loading dosage of 12 and 60 g m^{-2} with light intensity of 2.1 mW cm^{-2}).

Table 4: The effect of dye concentration on initial rate r_0 (mg L^{-1} min^{-1}) with TiO_2 loading dosage at 12 and 60 g m^{-2}.

OG concentration, C_0 (mg L^{-1})	12.5	18.8	25	50	75
r_0-12 g m^{-2}	1.30	1.43	1.58	1.72	2.00
r_0-60 g m^{-2}	1.32	1.69	2.25	2.62	3.19

3.6. The Product Analysis by FTIR and IC. The change of functional groups of azo dye after photocatalytic treatment was surveyed. The initial dye concentration was 50 mg L^{-1} and was treated with a TiO_2 dosage of 60 g m^{-2} and reaction time of 120 min. The scan spectra for the functional groups is SO_3Na of 1150~1250 cm^{-1}, N=N of 1400~1500 cm^{-1}, C=O of 1690~1760 cm^{-1}, C–H, and N–H of 3300~3500 cm^{-1}. The residual color was 0 and the residual TOC was 2.13 mg L^{-1}. After the photocatalytic oxidation, a new double-bond C=O at 1637 cm^{-1} was produced. Meanwhile the N=N from dye at 1426, 1463, and 1496 cm^{-1} disappeared due to attack by the hydroxyl radicals that cleaved the double-bond N=N. Accordingly, the dye molecule was degraded and decolorized. The ions such as sulfate, chloride, nitrite, and nitrate were determined. Figure 9 shows that the major ion concentration of sulfate significantly increased to 11 mg L^{-1} over time. The nitrate ion concentration was about 0.4 to 0.5 mg L^{-1} and nitrite concentration was low at 0.1 mg L^{-1}. The chloride ion produced due to the impurity of OG dye was low as 1.5 mg L^{-1}.

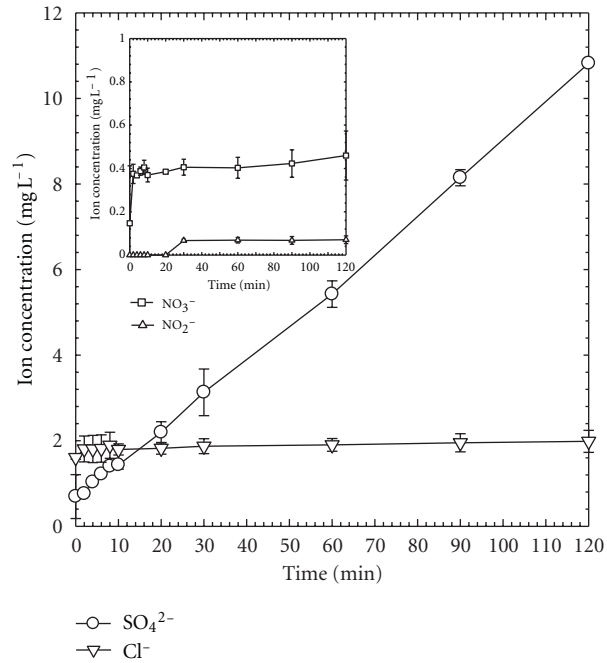

Figure 9: The product analysis by IC. The conditions were initial dye concentration of 50 mg L^{-1}, TiO_2-coated amounts of 60 g m^{-2}, and light intensity of 2.1 mW cm^{-2} at 120 min.

3.7. Application Duration. The TiO_2-coated steel mesh was used repeatedly to treat the OG solution. Figure 10 shows the system performance over 10 cycles. Results indicated that although the rate of OG degradation decreased as the reuse cycle of catalyst increased, the total amount of dye removal remained relatively unchanged at 100% in the treatment time range of 100–120 min, however. In the meantime, there was nearly no loss of TiO_2 in each operation even after 10 cycles. The observed rate constants declined with more reuse cycles as shown in Table 3(e), however. This can be attributed to potential surface poisoning of the photocatalyst, TiO_2 due to adsorption of reaction products. Further investigation is in progress to assess the reactivity of the TiO_2 during the course of photocatalytic reactions.

4. Conclusions

TiO_2 supported on steel mesh and illuminated with cold cathode fluorescent light (CCFL) was effective in removal color and dye from the OG azo dye solution. Coating TiO_2 at 150°C yielded the fastest color removal rate. An optimal TiO_2 surface loading or dosage of 60 g m^{-2} exhibited the highest color removal as well as the fastest rate; increase in surface TiO_2 loading had no benefit in increasing the color removal, however. An acidic pH of 2-3 had the best photocatalytic oxidation rate; the rate of color removal decreased when pH was increased to greater than 4. The rate of color removal decreased with initial dye concentration as was expected by the Langmuir-Hinshelwood kinetics. Based on FTIR analysis, there was decrease of N=N bonding which indicated chemical transformation of the dye OG

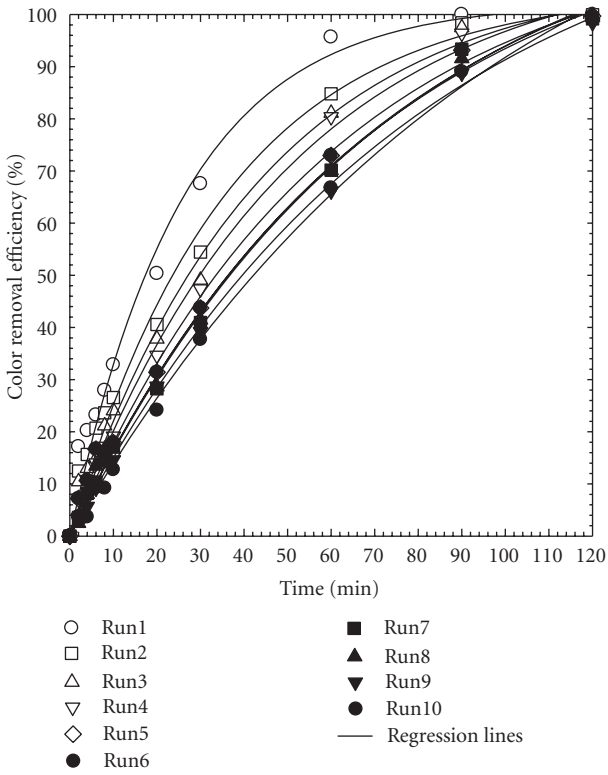

Figure 10: Duration test on color removal. The conditions were initial dye concentration of 50 mg L^{-1}, TiO_2-coated amounts of 60 g m^{-2}, light intensity of 2.1 mW cm^{-2}, and reaction time during 120 min.

compound. Results of analyzing the inorganic byproducts revealed that sulfate production was predominant; nitrite and nitrate were produced at minor quantities. The TiO_2-coated steel mesh can be repeatedly used over 10 cycles without significant loss of catalyst mass; the percent dye removal remained close to 100% in 10 cycles except slight decrease in reaction rate constants apparently due to possible surface poisoning. In general, the new photocatalytic system showed great potential in ease of implementation and cost for the treatment of dye industrial wastewater for color removal.

Acknowledgments

The authors appreciate the partial research funding granted by the Taiwan National Science Foundation (NSC 97-2918-I-241-001 and NSC 96-2221-E-241-005-MY2) as well as the analysis by NSC instrumental center of National Chung Hsing University and National Tsing Hua University.

References

[1] M. A. Brown and S. C. DeVito, "Predicting azo dye toxicity," *Critical Reviews in Environmental Science and Technology*, vol. 23, no. 3, pp. 249–324, 1993.

[2] H. Y. Shu, C. R. Huang, and M. C. Chang, "Decolorization of mono-azo dyes in wastewater by advanced oxidation process: a case study of acid red 1 and acid yellow 23," *Chemosphere*, vol. 29, no. 12, pp. 2597–2607, 1994.

[3] B. Manu and S. Chaudhari, "Decolorization of indigo and azo dyes in semicontinuous reactors with long hydraulic retention time," *Process Biochemistry*, vol. 38, no. 8, pp. 1213–1221, 2003.

[4] J. Ge and J. Qu, "Ultrasonic irradiation enhanced degradation of azo dye on MnO_2," *Applied Catalysis B*, vol. 47, no. 2, pp. 133–140, 2009.

[5] C. M. Kao, M. S. Chou, W. L. Fang, B. W. Liu, and B. R. Huang, "Regulating colored textile wastewater by 3/31 wavelength admi methods in Taiwan," *Chemosphere*, vol. 44, no. 5, pp. 1055–1063, 2001.

[6] H. Y. Shu, M. C. Chang, and H. J. Fan, "Decolorization of azo dye acid black 1 by the UV/H_2O_2 process and optimization of operating parameters," *Journal of Hazardous Materials*, vol. 113, no. 1-3, pp. 201–208, 2004.

[7] H. Y. Shu, M. C. Chang, and H. J. Fan, "Effects of gap size and UV dosage on decolorization of C.I. Acid Blue 113 wastewater in the UV/H_2O_2 process," *Journal of Hazardous Materials*, vol. 118, no. 1–3, pp. 205–211, 2005.

[8] H. Y. Shu, M. C. Chang, and W. P. Hsieh, "Remedy of dye manufacturing process effluent by UV/H_2O_2 process," *Journal of Hazardous Materials*, vol. 128, no. 1, pp. 60–66, 2006.

[9] E. Rodríguez, R. Peche, J. M. Merino, and L. M. Camarero, "Decoloring of aqueous solutions of indigocarmine dye in an acid medium by H_2O_2/UV advanced oxidation," *Environmental Engineering Science*, vol. 24, no. 3, pp. 363–371, 2007.

[10] H. Y. Shu and M. C. Chang, "Decolorization effects of six azo dyes by O_3, UV/O_3 and UV/H_2O_2 processes," *Dyes and Pigments*, vol. 65, no. 1, pp. 25–31, 2005.

[11] C. H. Wu and H. Y. Ng, "Degradation of C.I. Reactive Red 2 (RR2) using ozone-based systems: comparisons of decolorization efficiency and power consumption," *Journal of Hazardous Materials*, vol. 152, no. 1, pp. 120–127, 2008.

[12] T. H. Kim, C. Park, J. Yang, and S. Kim, "Comparison of disperse and reactive dye removals by chemical coagulation and Fenton oxidation," *Journal of Hazardous Materials*, vol. 112, no. 1-2, pp. 95–103, 2004.

[13] F. Ay, E. C. Catalkaya, and F. Kargi, "Advanced oxidation of direct red (DR 28) by fenton treatment," *Environmental Engineering Science*, vol. 25, no. 10, pp. 1455–1462, 2008.

[14] A. T. Toor, A. Verma, C. K. Jotshi, P. K. Bajpai, and V. Singh, "Photocatalytic degradation of Direct Yellow 12 dye using UV/TiO_2 in a shallow pond slurry reactor," *Dyes and Pigments*, vol. 68, no. 1, pp. 53–60, 2006.

[15] M. Muruganandham and M. Swaminathan, "Photocatalytic decolourisation and degradation of Reactive Orange 4 by TiO_2-UV process," *Dyes and Pigments*, vol. 68, no. 2-3, pp. 133–142, 2006.

[16] X. Yin, F. Xin, F. Zhang, S. Wang, and G. Zhang, "Kinetic study on photocatalytic degradation of 4BS Azo dye over TiO_2 in slurry," *Environmental Engineering Science*, vol. 23, no. 6, pp. 1000–1008, 2006.

[17] A. Akyol and M. Bayramoglu, "The degradation of an azo dye in a batch slurry photocatalytic reactor," *Chemical Engineering and Processing*, vol. 47, no. 12, pp. 2150–2156, 2008.

[18] R. B. M. Bergamini, E. B. Azevedo, and L. R. R. D. Araújo, "Heterogeneous photocatalytic degradation of reactive dyes in aqueous TiO_2 suspensions: decolorization kinetics," *Chemical Engineering Journal*, vol. 149, no. 1–3, pp. 215–220, 2009.

[19] G. Mascolo, R. Comparelli, M. L. Curri, G. Lovecchio, A. Lopez, and A. Agostiano, "Photocatalytic degradation of methyl red by TiO_2: comparison of the efficiency of immobilized nanoparticles versus conventional suspended catalyst,"

Journal of Hazardous Materials, vol. 142, no. 1-2, pp. 130–137, 2007.

[20] B. Mounir, M. N. Pons, O. Zahraa, A. Yaacoubi, and A. Benhammou, "Discoloration of a red cationic dye by supported TiO_2 photocatalysis," *Journal of Hazardous Materials*, vol. 148, no. 3, pp. 513–520, 2007.

[21] M. Nikazar, K. Gholivand, and K. Mahanpoor, "Photocatalytic degradation of azo dye Acid Red 114 in water with TiO_2 supported on clinoptilolite as a catalyst," *Desalination*, vol. 219, no. 1–3, pp. 293–300, 2008.

[22] A. R. Khataee, M. N. Pons, and O. Zahraa, "Photocatalytic degradation of three azo dyes using immobilized TiO_2 nanoparticles on glass plates activated by UV light irradiation: influence of dye molecular structure," *Journal of Hazardous Materials*, vol. 168, no. 1, pp. 451–457, 2009.

[23] X. Wang, Y. Liu, Z. Hu, Y. Chen, W. Liu, and G. Zhao, "Degradation of methyl orange by composite photocatalysts nano-TiO_2 immobilized on activated carbons of different porosities," *Journal of Hazardous Materials*, vol. 169, no. 1–3, pp. 1061–1067, 2009.

[24] T. Aarthi, P. Narahari, and G. Madras, "Photocatalytic degradation of Azure and Sudan dyes using nano TiO_2," *Journal of Hazardous Materials*, vol. 149, no. 3, pp. 725–734, 2007.

[25] K. Sahel, N. Perol, H. Chermette, C. Bordes, Z. Derriche, and C. Guillard, "Photocatalytic decolorization of Remazol Black 5 (RB5) and Procion Red MX-5B-Isotherm of adsorption, kinetic of decolorization and mineralization," *Applied Catalysis B*, vol. 77, no. 1-2, pp. 100–109, 2007.

[26] N. Barka, A. Assabbane, A. Nounah, and Y. A. Ichou, "Photocatalytic degradation of indigo carmine in aqueous solution by TiO_2-coated non-woven fibres," *Journal of Hazardous Materials*, vol. 152, no. 3, pp. 1054–1059, 2008.

[27] J. Saien, M. Asgari, A. R. Soleymani, and N. Taghavinia, "Photocatalytic decomposition of direct red 16 and kinetics analysis in a conic body packed bed reactor with nanostructure titania coated Raschig rings," *Chemical Engineering Journal*, vol. 151, no. 1–3, pp. 295–301, 2009.

Hindawi Publishing Corporation
International Journal of Photoenergy
Volume 2012, Article ID 640487, 7 pages
doi:10.1155/2012/640487

Research Article

Synthesis and Bactericidal Ability of TiO_2 and Ag-TiO_2 Prepared by Coprecipitation Method

Robert Liu,[1] H. S. Wu,[1] Ruth Yeh,[1] C. Y. Lee,[1] and Yungtse Hung[2]

[1] *Department of Chemical and Materials Engineering, Minghsin University of Science and Technology, Hsinchu 30401, Taiwan*
[2] *Department of Civil and Environmental Engineering, Cleveland State University, Cleveland, OH 44115-2214, USA*

Correspondence should be addressed to Ruth Yeh, yehyl@must.edu.tw

Received 23 March 2012; Accepted 5 May 2012

Academic Editor: Meenakshisundaram Swaminathan

Preparation of photocatalysts of TiO_2 and Ag-TiO_2 was carried out by coprecipitation method. The prepared photocatalysts were characterized by X-ray diffraction (XRD), SEM, EDX, and XRF analysis. The disinfection of *E. coli*, a model indicator organism for the safe water supply, was investigated by using TiO_2 and Ag-TiO_2 under different light sources. The treatment efficacy for the inactivation of *E. coli* would be UV/Ag-TiO_2; visible/Ag-TiO_2; dark/Ag-TiO_2; UV (all 100%) > UV/TiO_2 (99%) > visible/TiO_2 (96%) > dark/TiO_2 (87%) > visible (23%) > dark (19%). The order of disinfection efficiency by their corresponding kinetic initial apparent rate constants, k_{app}, (min^{-1}) would be UV/Ag-TiO_2; visible/Ag-TiO_2 (both 6.67) > UV (6.6) > dark/Ag-TiO_2 (6.56) > UV/TiO_2 (1.62) > visible/TiO_2 (1.08) > dark/TiO_2 (0.7) > visible (0.28) > dark (0.03). The application of TiO_2 doped with silver strongly improved the ability of disinfection treatment. The study of mineralization of *E. coli* by measurement of TOC (total organic carbon) removal percentage showed that the visible light may effectively be applied for the disinfection unit of water and wastewater treatment system by using photocatalysts of Ag-TiO_2.

1. Introduction

Increasing demand and shortage of satisfactory clean water supplies due to the rapid development of industrialization, population growth, and serious droughts have become a global issue [1–3]. It is estimated that around 1.2 billion people lack access to safe drinking water, 2.6 billion have little or no sanitation, and millions of people died of severe waterborne diseases annually [3, 4]. Therefore, the quality of drinking water is becoming more and more of a concern worldwide. For suppressing the worsening of clean water shortage, disinfection development of advanced water treatment technologies with low cost and high efficiency to treat wastewater is also desirable. Pathogens are disease-causing organisms that grow and multiply within the host and excreted in human feces. Pathogens associated with water include bacteria, viruses, protozoa, and helminthes [5]. The microbiological standards for water and wastewater treatment system in their final disinfection treatment unit use coliform bacteria (typically *Escherichia coli* or *E. coli*) as indicator organisms whose presence suggestes that water is fecal contaminated. The final disinfection step to kill any remaining pathogenic organisms for water and wastewater treatment system includes some commonly used technologies, such as chlorination, ozonation, and UV irradiation. Chlorination has been the most commonly and widely used disinfection process. The disinfected byproducts generated from chlorination are mutagenic and carcinogenic to human health [5–7], while ozonation, or UV radiation may be too costly and can only be used as primary disinfectant because they cannot ensure a detectable residual [1, 8].

Heterogeneous photocatalysis has recently emerged as an alternative technology of advanced oxidation processes (AOP) for bacteria inactivation [9–16] and organic pollutants oxidation [17–29]. Out of the various semiconductor photocatalysts used, TiO_2 has been found to be the most suitable because of its nontoxic, insoluble, inexpensive, stable, ant its high production of oxidative hydroxyl radicals ($^{\bullet}OH$). But the rapid recombination of electron-hole pair limits the efficiency of TiO_2. It is experimentally found that Ag particles in Ag doped TiO_2 increase the bactericidal efficiency of TiO_2 by acting as electron traps [1, 30–34].

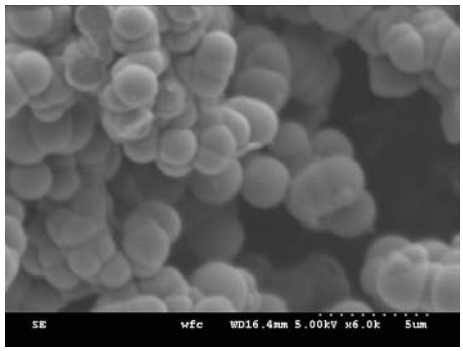

Figure 1: SEM micrograph of Ag-TiO_2 sintering at 550°C (×6.0k).

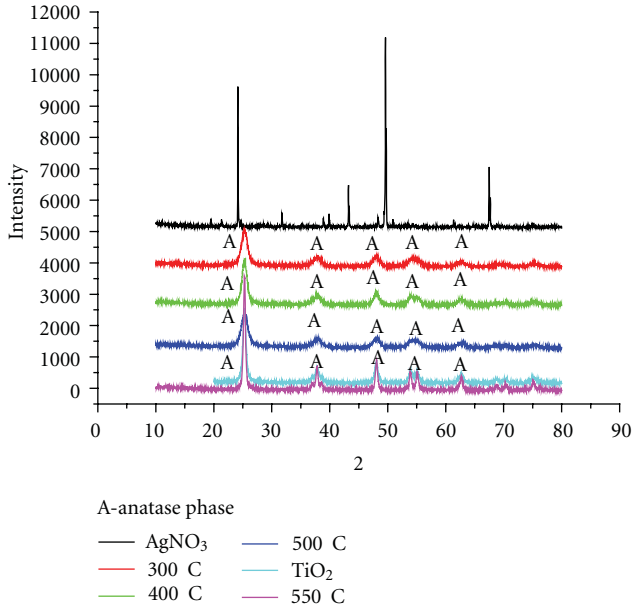

Figure 2: XRD pattern of prepared TiO_2 and Ag-TiO_2 with different sintering temperature.

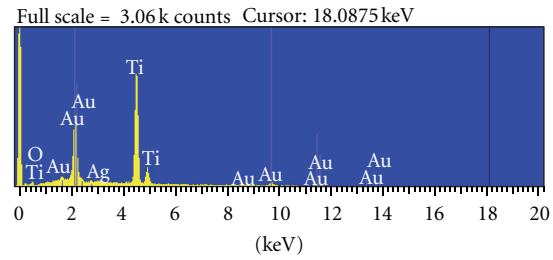

Figure 3: EDX of Ag-TiO_2 sintering at 550°C.

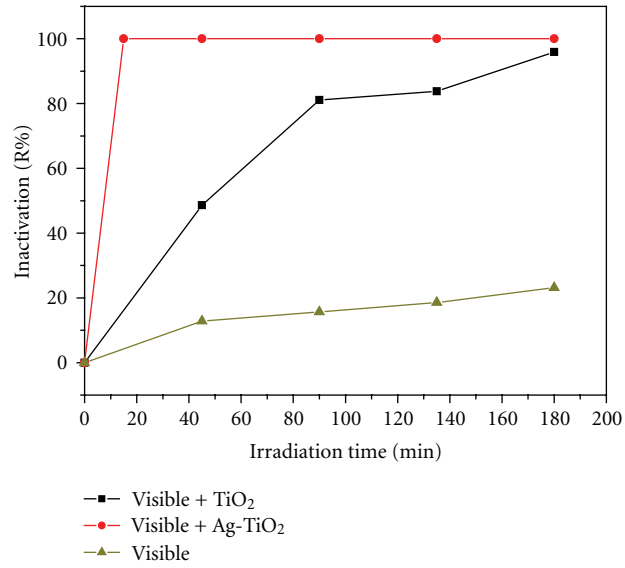

Figure 4: R percentage versus irradiation time of visible light (dosage = 0.01 g/10 mL).

The aim of this work was the preparation of TiO_2 and Ag doped TiO_2 (Ag-TiO_2) by the simple coprecipitation method. The prepared photocatalysts were characterized by X-ray diffraction (XRD), SEM, EDX, and XRF analysis. The photocatalytic inactivation and disinfection of *E. coli*, one the most common gram-negative model bacteria, using prepared TiO_2 and Ag-TiO_2 under irradiation of different light sources were studied and compared. The mineralization of *E. coli* by the study of TOC (total organic carbon) removal percentage was also investigated by different light sources.

2. Experimental

2.1. Materials. All chemicals used such as $Ti(SO)_2$, urea, or silver nitrate were of reagent grade (SHOWA Chemical Co., LTD., Japan or Ruenn-Jye Tech. Corp., Taiwan). The photocatalytic antibacterial activities of the samples were evaluated using *E. coli* as an indicator bacterium. *E. coli* (BCRC10316) was obtained from FIRDI, Taiwan. Nutrient broth (NB, Pronadisa, Lab conda S.A.) and agar (American bacteriological agar; Pronadisa, Lab conda S.A.) were used for the liquid culture medium and solid culture medium of bacteria, respectively.

2.2. Preparation of TiO_2 and Ag-TiO_2. For the preparation of Ag-TiO_2 powder, 75 g of urea was first dissolved into 400 mL DI-water. Then add 46 mL of $Ti(SO_4)_2$ and 0.169 g of $AgNO_3$ into the bottle on the oil bath and uniformly mixed. Reactions were carried out for 24 h at 80°C by continuously magnetic stirring and heating. After cooling to room temperature, the separation of solid and solution was obtained by centrifugal filtration. The solids were washed by DI-water until pH of the washing water reached neutral. The solids were filtered again and removed to the oven for drying at 70°C and 24 h. By grinding, the powder was then calcined at 550°C for 4 h. The Ag-TiO_2 was obtained with Ag : Ti = 1 : 99 (molar ratio). To prepare TiO_2, the same procedure was repeated without the addition of silver nitrate.

2.3. Characterization of Prepared Photocatalysts. Structure characterization of as prepared photocatalysts was performed by means of XRD (XRD-6000, Shimadzu, Japan)

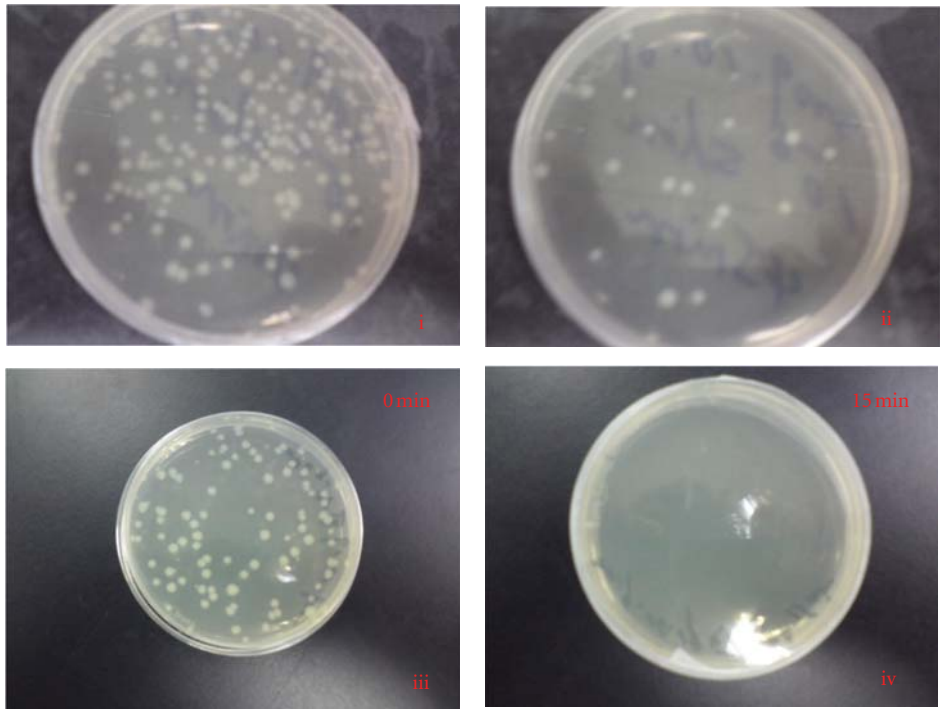

Figure 5: Inactivation effect of *E. coli* by visible light irradiation using TiO_2 (i) (0 min.) and (ii) (15 min.) and Ag-TiO_2 (iii) and (iv) as photocatalysts.

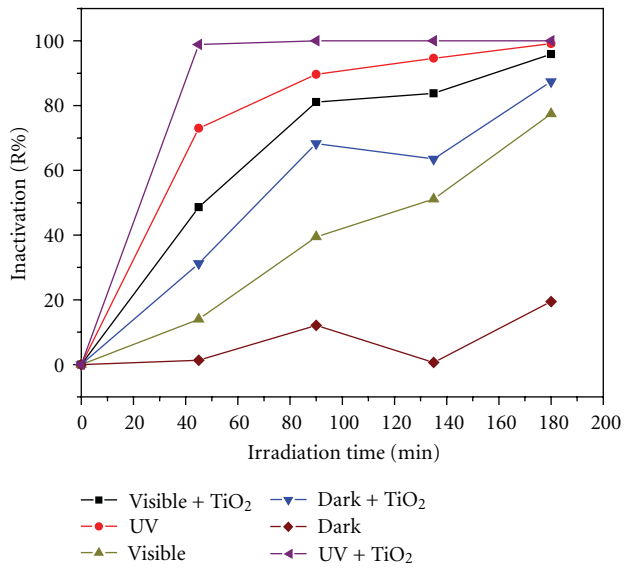

Figure 6: *R* percentage versus irradiation time of different light sources using TiO_2 as photocatalysts.

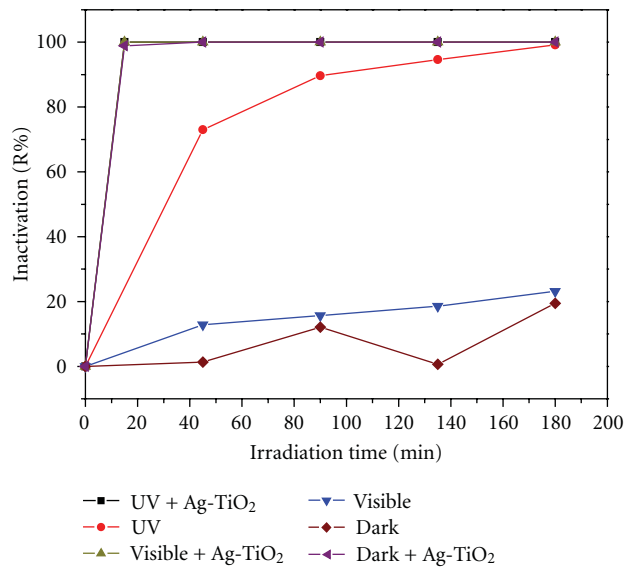

Figure 7: *R* percentage versus irradiation time of different light sources using Ag-TiO_2 as photocatalysts.

with Cu Kα radiation. Morphology of Ag-TiO_2 was investigated by SEM (Scanning electron microscope, S-3000N, Hitachi, Japan). EDX (Energy dispersive X-ray spectroscopy) used indicates the presence of silver. The chemical compositions of the particles were analyzed by XRF (X-ray fluorescence, XEPOS/XEP01, Spectro Co., Germany).

2.4. Inactivation of E. coli. The antibacterial properties of *E. coli* by using photocatalysts were studied under the following process. (1) Preparation of liquid growth medium of nutrient broth (NB): add 0.8 g of NB and 100 mL Di-water into 250 mL of flask and sterilized under autoclave for 20 minutes. (2) Preparation of solid medium: mix 0.8 g NB, 1.5 g agar, and 100 mL DI-water and sterilized under autoclave at 121°C for 20 minutes and then cool until 50°C. Pour the contents into petri dishes to form solid medium. (3) Add *E. coli* from FIRDI onto petri dishes and incubated at 37°C for 2 days. (4) Remove *E. coli* from the surface of solid medium from

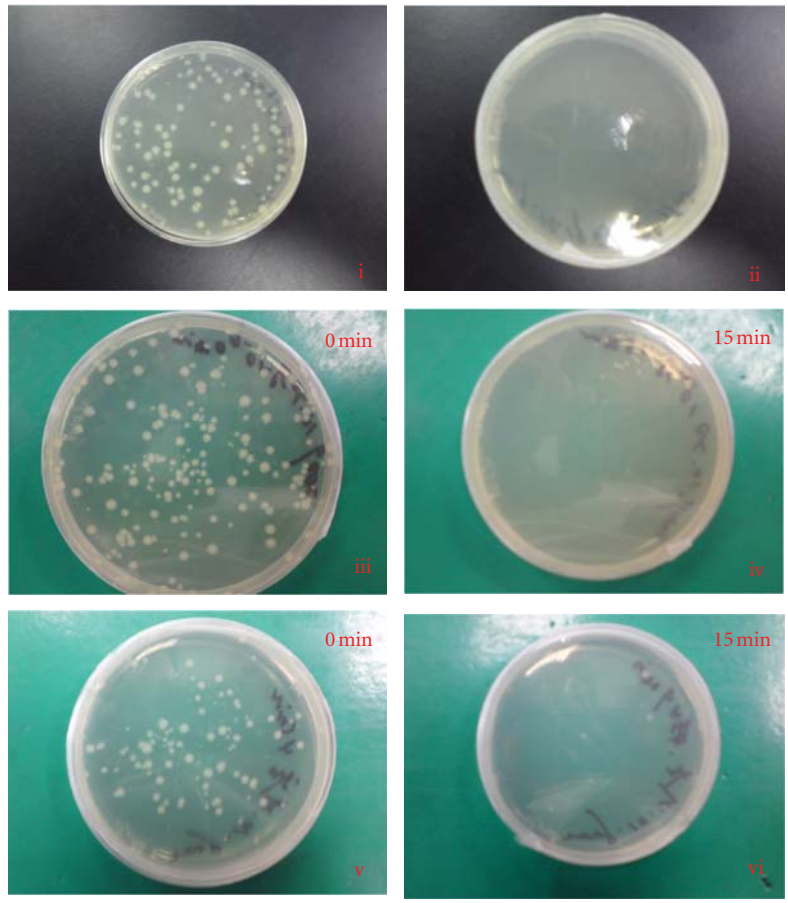

Figure 8: Inactivation effect of *E. coli* by irradiation of different light sources (UV (i) (0 min.) and (ii) (15 min.) and visible (iii) and (iv) and dark (v) and (vi)) using Ag-TiO_2 as photocatalysts.

(3) when cooled and inoculate onto (1) by the same cultural procedure as (3). (5) Dilution of *E. coli* from (4): add 1 mL of inoculated *E. coli* from liquid culture medium of NB and into a clean test tube containing 9 mL of sterilized water. Add 0.01 g of Ag-TiO_2 into the prepared test tube. The test tube was incubated for 24 h at 37°C, and the numbers of viable cells of bacterial colonies (CFU/mL, colonies forming units per milliliter) were visually identified and counted. Repeat the serial dilution by 10^1, 10^2, 10^3, 10^4, 10^5, and 10^6. The best dilution for the *E. coli* bactericidal effect by photocatalysts would be 10^6 for all the following inactivation experiments. (6) The inactivation of *E. coli* bacteria: the bactericidal studies by the photocatalysts were carried out under the irradiation of visible light (Philips, Poland, 9 watts), UV light (UV-C, Philips, Poland, 9 watts), and no light. The distance between the light and the top of test tube remains 30 cm and fully covered and protected on the outside. Then lay the setup into the laminar flow cabinet and investigate the inactivation experiments. The similar procedure was applied as (5) by using the dosages of 0.01 g/10 mL of TiO_2 or Ag-TiO_2. The dilution chosen would be 10^6, and sampling time for each experiment would be 0, 15, 45, 90, 135, and 180 minutes. Samples were all plated in triplicate, and the counts on the three plates were averaged. Control experiments were also conducted in the absence of the photocatalysts.

The inactivation efficiency $R(\%)$ of *E. coli* as model bacteria by the prepared photocatalysts of TiO_2 and Ag-TiO_2 were calculated by the following equation:

$$R(\%) = \frac{(C_0 - C)}{C_0} \times 100\%, \quad (1)$$

where $R(\%)$ is the inactivation efficiency or viable cells inactivated or removed percentages. C_0 is initial CFU/mL, and C is final CFU/mL.

3. Results and Discussion

3.1. Catalyst Characterization. Ag-TiO_2 after 550°C sintering was characterized by the SEM. The micrographs taken at 6000-times magnification are shown in Figure 1. It is found that the dope of silver is not very obvious and the aggregation of tiny TiO_2 particles occurred. The average particle size was found to be about 2.5 μm from the figure. The XRD patterns of TiO_2 and Ag-TiO_2 as shown in Figure 2 almost coincide and thus suggest that the silver is well dispersed on the TiO_2 surface. Anatase type structure is obtained for both prepared TiO_2 and Ag-TiO_2. Figure 2 also shows the XRD patterns of Ag-TiO_2 annealed at different temperatures and all exhibited anatase without rutile. With

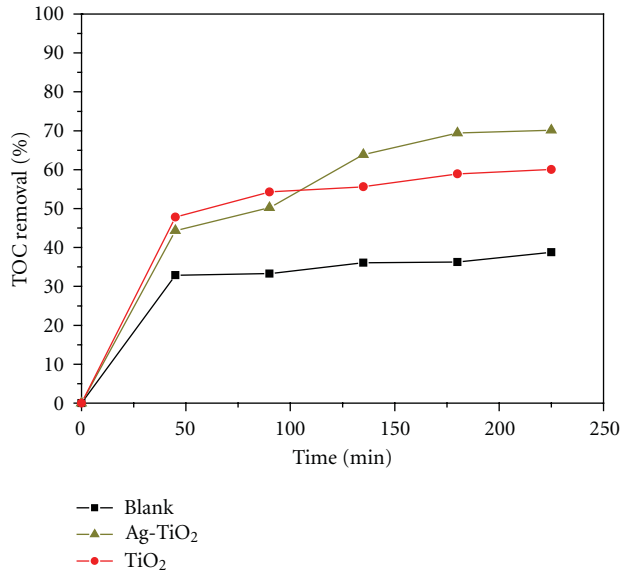

Figure 9: TOC removal percentage of *E. coli* versus visible light irradiation by using TiO_2 and Ag-TiO_2 as photocatalysts.

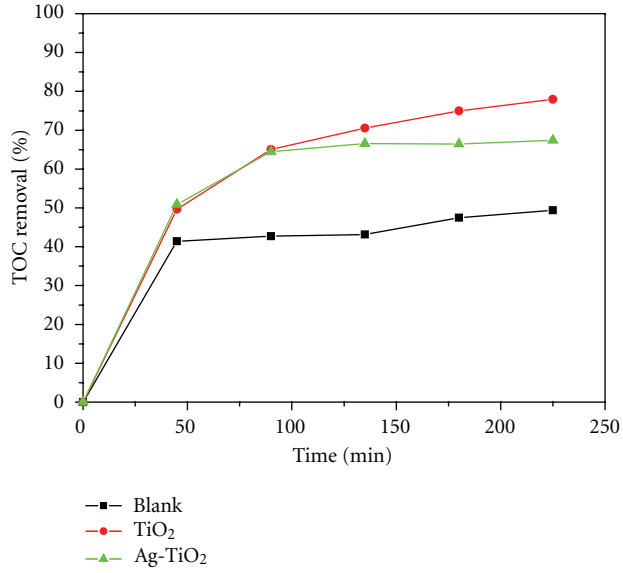

Figure 10: TOC removal percentage of *E. coli* versus UV light irradiation by using TiO_2 and Ag-TiO_2 as photocatalysts.

increasing temperature of calcination, the intensities of the TiO_2 peaks are increased. Therefore, the photocatalysts of Ag-TiO_2 used for the inactivation of *E. coli* will be prepared by 550°C sintering. From Figure 2, there is only TiO_2 in the anatase form and no peaks of Ag were observed. It can be explained that the amount of Ag is too little to be appeared on the patterns. Figure 3 is the EDX diagram of Ag-TiO_2 which indicates the presence of silver on the prepared photocatalysts.

The compositions of the prepared Ag-TiO_2 were determined by the analysis of XRF. The result was shown in Table 1. It indicates that silver exists and composition was

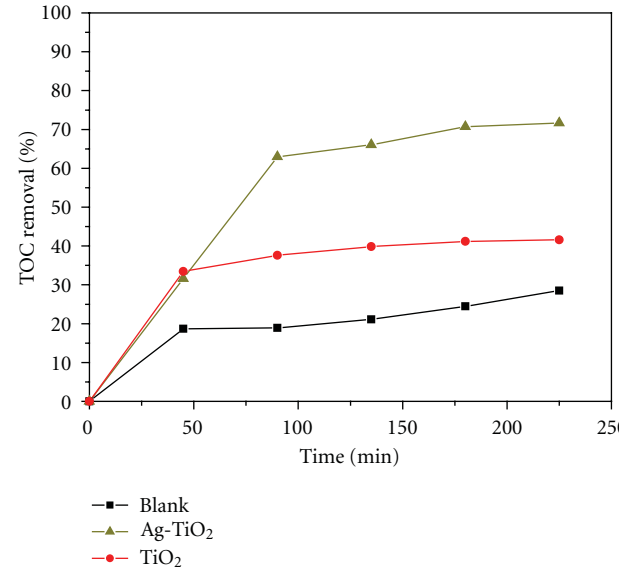

Figure 11: TOC removal percentage of *E. coli* versus adsorption time under dark by using TiO_2 and Ag-TiO_2 as photocatalysts.

very close to the predetermined value, that is, Ag : Ti = 1 : 99 (molar).

3.2. Inactivation of *E. coli*

3.2.1. Comparison between TiO_2 and Ag-TiO_2 under Visible Light. Figures 4 and 5 show the inactivation of *E. coli* under the irradiation of visible light by using photocatalysts of TiO_2 or Ag-TiO_2. It is quite clear that Ag doped TiO_2 improves very obviously the antibacterial activities of *E. coli* on both inactivation efficiency (R%) and rate of reaction. It takes about 15 minutes to reach 99% inactivation for Ag-TiO_2 and 180 minutes of 90% for TiO_2.

According to the kinetic Langmuir-Hinshelwood model [21]:

$$r = -\frac{dC}{dt} = \frac{(k_r K C)}{(1 + K C)}. \tag{2}$$

During the initial stage of reaction, concentration of *E. coli* is high, the reaction becomes zero order, that is,

$$r = -\frac{dC}{dt} = k_r. \tag{3}$$

Therefore,

$$(C - C_0) = -k_r t \quad \text{or} \quad R\% = \frac{(C_0 - C)}{C_0} = \frac{k_r}{C_0}\ t = k_{\text{app}} t, \tag{4}$$

where r is the rate of *E. coli* inactivation, C_0 is the initial concentration of *E. coli*, C is the concentration of *E. coli* during the initial stage of reaction (straight-line region) at time t, k_r is the reaction rate constant, k is the adsorption coefficient of *E. coli* onto particle, and k_{app} is the apparent rate constants (min^{-1}).

Table 1: XRF of prepared Ag-TiO_2.

Components	Conc.: mol%	STD-DEV	Intens.: cps/μA
Ti (titanium)	97.83	0.08	138.140
V (vanadium)	1.2	0.07	2.533
Ag (silver)	0.81	0.03	3.575
Fe (iron)	0.16	0.03	0.248

Table 2: Values of R (%) and k_{app} by using different light sources and different photocatalysts of TiO_2 and Ag-TiO_2 or light only.

TiO_2	R (%)	k_{app} (min^{-1})	Ag-TiO_2	R (%)	k_{app} (min^{-1})
Dark	19%	0.03	Dark	19.46%	0.03
Visible	23%	0.28	Visible	23.14%	0.28
Dark + TiO_2	87%	0.7	UV	100%	1.67
Visible + TiO_2	96%	1.08	Dark + Ag-TiO_2	100%	6.56
UV	99%	1.56	Visible + Ag-TiO_2	100%	6.67
UV+TiO_2	100%	2.22	UV + Ag-TiO_2	100%	6.67

By the linear transform of $R\% = k_{app}t$ for the initial stage of bactericidal reaction, the initial apparent rate constant was obtained from Figure 4. Therefore, k_{app} would be 6.67 for visible/Ag-TiO_2 1.08 for visible/TiO_2, and only 0.25 for visible light system.

3.2.2. Comparison between TiO_2 and Ag-TiO_2 under Di erent Light Sources. Figure 6 shows the inactivation efficiency against irradiation time by using TiO_2 photocatalysts under different light sources. It appears that UV light plays the major role for the activation of TiO_2. Also, UV light is commonly used for disinfection unit of water and wastewater treatment. Therefore, UV-TiO_2 and UV is better than other system.

Figures 7 and 8 show the treatment of *E. coli* by using Ag-TiO_2 photocatalysts with different light sources. It happened that the application of Ag shows superior capabilities of *E. coli* inactivation no matter what kind of light sources used or just under dark. The reason for better dark treatment may be due to the adsorption effect of the photocatalyst [19, 20]. Table 2 summarized the values of R% and k_{app} by different light sources and different photocatalysts of TiO_2 and Ag-TiO_2 applied in the inactivation of *E. coli* experiments with results shown as in Figures 6 and 7.

3.2.3. Mineralization of E. coli. In order to study the mineralization of *E. coli*, TOC measurement was used. The results were shown in Figures 9, 10, and 11 for irradiation of visible light, UV light, and dark, respectively. It is interesting to note that Figure 11 in the dark and the adsorption of Ag-TiO_2 is very pronouncing compared with others. From Figures 9 and 10, mineralization of *E. coli* by Ag-TiO_2 indicated that enhanced degradation effect under visible light occurred when compared to that of UV irradiation. It may be due to both vital adsorption and electron charge separation mechanisms [20, 22]. While under UV light, Ag deposits act majorly as electron traps, it leads to less enhancement in the mineralization of Ag-TiO_2 system. The results were coincided with the reference of Rupa et al. [20].

4. Conclusions

(1) Photocatalysts of TiO_2 and Ag-TiO_2 were successfully prepared by coprecipitation method annealed at 550°C;

(2) the composition of Ag-TiO_2 prepared is about Ag : Ti = 1 : 99 (molar), and particle size is 0.25 μm;

(3) silver-deposited TiO_2 photocatalysts enhanced the inactivation of *E. coli* by visible irradiation when compared to that by using TiO_2. The similar 100% of high antibactericidal efficiencies and six times of rate of reaction compared to the usage of TiO_2 were obtained for either using visible light or UV light or even no light irradiation by the application of Ag-TiO_2;

(4) the study of mineralization of *E. coli* shows that better results of TOC removal percentage obtained for visible light application than the irradiation of UV light;

(5) the visible light may effectively be applied for the disinfection unit of water and wastewater treatment system by using photocatalysts of Ag-TiO_2.

References

[1] D. M. A. Alrousan, P. S. M. Dunlop, T. A. Mcmurray, and J. A. Byrne, "Photocatalytic inactivation of *E. coli* in surface water using immobilised nanoparticle TiO_2 films," *Water Research*, vol. 43, no. 1, pp. 47–54, 2009.

[2] G. M. Masters and W. P. Ela, *Introduction to Environmental Engineering and Science*, Prentice Hall, New Jersey, NJ, USA, 3rd edition, 2008.

[3] M. N. Chong, B. Jin, C. W. K. Chow, and C. Saint, "Recent developments in photocatalytic water treatment technology: a review," *Water Research*, vol. 44, no. 10, pp. 2997–3027, 2010.

[4] S. Malato, P. F. Ibáñez, M. I. Maldonado, J. Blanco, and W. Gernjak, "Decontamination and disinfection of water by solar photocatalysis: recent overview and trends," *Catalysis Today*, vol. 147, no. 1, pp. 1–59, 2009.

[5] J. Coleman, C. P. Marquis, J. A. Scott, S. S. Chin, and R. Amal, "Bactericidal effects of titanium dioxide-based photocatalysts," *Chemical Engineering Journal*, vol. 113, no. 1, pp. 55–63, 2005.

[6] J. Lu, T. Zhang, J. Ma, and Z. Chen, "Evaluation of disinfection by-products formation during chlorination and chloramination of dissolved natural organic matter fractions isolated from a filtered river water," *Journal of Hazardous Materials*, vol. 162, no. 1, pp. 140–145, 2009.

[7] H. Yang and H. Cheng, "Controlling nitrite level in drinking water by chlorination and chloramination," *Separation and Purification Technology*, vol. 56, no. 3, pp. 392–396, 2007.

[8] L. Rizzo, "Inactivation and injury of total coliform bacteria after primary disinfection of drinking water by TiO_2 photocatalysis," *Journal of Hazardous Materials*, vol. 165, no. 1–3, pp. 48–51, 2009.

[9] D. Gumy, A. G. Rincon, R. Hajdu, and C. Pulgarin, "Solar photocatalysis for detoxification and disinfection of water: different types of suspended and fixed TiO_2 catalysts study," *Solar Energy*, vol. 80, no. 10, pp. 1376–1381, 2006.

[10] Z. Huang, P. C. Maness, D. M. Blake, E. J. Wolfrum, S. L. Smolinski, and W. A. Jacoby, "Bactericidal mode of titanium dioxide photocatalysis," *Journal of Photochemistry and Photobiology A*, vol. 130, no. 2-3, pp. 163–170, 2000.

[11] P. S. M. Dunlop, J. A. Byrne, N. Manga, and B. R. Eggins, "The photocatalytic removal of bacterial pollutants from drinking water," *Journal of Photochemistry and Photobiology A*, vol. 148, no. 1–3, pp. 355–363, 2002.

[12] Y. Kikuchi, K. Sunada, T. Iyoda, K. Hashimoto, and A. Fujishima, "Photocatalytic bactericidal effect of TiO_2 thin films: dynamic view of the active oxygen species responsible for the effect," *Journal of Photochemistry and Photobiology A*, vol. 106, no. 1–3, pp. 51–56, 1997.

[13] K. Sunada, T. Watanabe, and K. Hashimoto, "Studies on photokilling of bacteria on TiO_2 thin film," *Journal of Photochemistry and Photobiology A*, vol. 156, no. 1–3, pp. 227–233, 2003.

[14] S. Gelover, L. A. Gómez, K. Reyes, and M. T. Leal, "A practical demonstration of water disinfection using TiO_2 films and sunlight," *Water Research*, vol. 40, no. 17, pp. 3274–3280, 2006.

[15] A. G. Rincón and C. Pulgarin, "Effect of pH, inorganic ions, organic matter and H_2O_2 on *E. coli* K12 photocatalytic inactivation by TiO_2: implications in solar water disinfection," *Applied Catalysis B*, vol. 51, no. 4, pp. 283–302, 2004.

[16] J. A. Ibáñez, M. I. Litter, and R. A. Pizarro, "Photocatalytic bactericidal effect of TiO_2 on Enterobacter cloacae. Comparative study with other Gram (−) bacteria," *Journal of Photochemistry and Photobiology A*, vol. 157, no. 1, pp. 81–85, 2003.

[17] N. Sobana, K. Selvam, and M. Swaminathan, "Optimization of photocatalytic degradation conditions of direct red 23 using nano-Ag doped TiO_2," *Separation and Purification Technology*, vol. 62, no. 3, pp. 648–653, 2008.

[18] N. Sobana, M. Muruganadham, and M. Swaminathan, "Nano-Ag particles doped TiO_2 for efficient photodegradation of direct azo dyes," *Journal of Molecular Catalysis A*, vol. 258, no. 1-2, pp. 124–132, 2006.

[19] M. K. Seery, R. George, P. Floris, and S. C. Pillai, "Silver doped titanium dioxide nanomaterials for enhanced visible light photocatalysis," *Journal of Photochemistry and Photobiology A*, vol. 189, no. 2-3, pp. 258–263, 2007.

[20] A. V. Rupa, D. Manikandan, D. Divakar, and T. Sivakumar, "Effect of deposition of Ag on TiO_2 nanoparticles on the photodegradation of reactive Yellow-17," *Journal of Hazardous Materials*, vol. 147, no. 3, pp. 906–913, 2007.

[21] A. K. Gupta, A. Pal, and C. Sahoo, "Photocatalytic degradation of a mixture of crystal violet and methyl red dye in aqueous suspensions using Ag^+ doped TiO_2," *Dyes and Pigments*, vol. 69, no. 3, pp. 224–232, 2006.

[22] L. Ren, Y. P. Zeng, and D. Jiang, "Preparation, characterization and photocatalytic activities of Ag-deposited porous TiO_2 sheets," *Catalysis Communications*, vol. 10, no. 5, pp. 645–649, 2009.

[23] Y. Liu, C. Y. Liu, Q. H. Rong, and Z. Zhang, "Characteristics of the silver-doped TiO_2 nanoparticles," *Applied Surface Science*, vol. 220, no. 1–4, pp. 7–11, 2003.

[24] V. Vamathevan, R. Amal, D. Beydoun, G. Low, and S. McEvoy, "Photocatalytic oxidation of organics in water using pure and silver-modified titanium dioxide particles," *Journal of Photochemistry and Photobiology A*, vol. 148, no. 1–3, pp. 233–245, 2002.

[25] S. Rengaraj and X. Z. Li, "Enhanced photocatalytic activity of TiO_2 by doping with Ag for degradation of 2,4,6-trichlorophenol in aqueous suspension," *Journal of Molecular Catalysis A*, vol. 243, no. 1, pp. 60–67, 2006.

[26] J. M. Herrmann, H. Tahiri, Y. Ait-Ichou, G. Lassaletta, A. R. González-Elipe, and A. Fernandez, "Characterization and photocatalytic activity in aqueous medium of TiO_2 and Ag-TiO_2 coatings on quartz," *Applied Catalysis B*, vol. 13, no. 3-4, pp. 219–228, 1997.

[27] M. Bideau, B. Claudel, C. Dubien, L. Faure, and H. Kazouan, "On the "immobilization" of titanium dioxide in the photocatalytic oxidation of spent waters," *Journal of Photochemistry and Photobiology A*, vol. 91, no. 2, pp. 137–144, 1995.

[28] A. R. Malagutti, H. A. J. L. Mourão, J. R. Garbin, and C. Ribeiro, "Deposition of TiO_2 and Ag:TiO_2 thin films by the polymeric precursor method and their application in the photodegradation of textile dyes," *Applied Catalysis B*, vol. 90, no. 1-2, pp. 205–212, 2009.

[29] M. S. Lee, S. S. Hong, and M. Mohseni, "Synthesis of photocatalytic nanosized TiO_2-Ag particles with sol-gel method using reduction agent," *Journal of Molecular Catalysis A*, vol. 242, no. 1-2, pp. 135–140, 2005.

[30] J. Ma, Z. Xiong, T. D. Waite, W. J. Ng, and X. S. Zhao, "Enhanced inactivation of bacteria with silver-modified mesoporous TiO_2 under weak ultraviolet irradiation," *Microporous and Mesoporous Materials*, vol. 144, no. 1–3, pp. 97–104, 2011.

[31] L. Mai, D. Wang, S. Zhang, Y. J. Xie, C. M. Huang, and Z. Zhang, "Synthesis and bactericidal ability of Ag/TiO_2 composite films deposited on titanium plate," *Applied Surface Science*, vol. 257, no. 3, pp. 974–978, 2010.

[32] M. V. Liga, E. L. Bryant, V. L. Colvin, and Q. Li, "Virus inactivation by silver doped titanium dioxide nanoparticles for drinking water treatment," *Water Research*, vol. 45, no. 2, pp. 535–544, 2011.

[33] W. Su, S. S. Wei, S. Q. Hu, and J. X. Tang, "Preparation of TiO_2/Ag colloids with ultraviolet resistance and antibacterial property using short chain polyethylene glycol," *Journal of Hazardous Materials*, vol. 172, no. 2-3, pp. 716–720, 2009.

[34] D. Wu, H. You, D. Jin, and X. Li, "Enhanced inactivation of Escherichia coli with Ag-coated TiO_2 thin film under UV-C irradiation," *Journal of Photochemistry and Photobiology A*, vol. 217, no. 1, pp. 177–183, 2011.

Hindawi Publishing Corporation
International Journal of Photoenergy
Volume 2012, Article ID 103672, 8 pages
doi:10.1155/2012/103672

Research Article

Enhancement of Photocatalytic Activity of ZnO/SiO_2 by Nanosized Pt for Photocatalytic Degradation of Phenol in Wastewater

R. M. Mohamed[1,2] and M. A. Barakat[3,4]

[1] *Chemistry Department, Faculty of Science, King Abdulaziz University, P.O. Box. 80203, Jeddah 21589, Saudi Arabia*
[2] *Nanostructured Materials and Nanotechnology Division, Advanced Materials Department, Central Metallurgical Research & Development Institute (CMRDI), P.O. Box 87 Helwan, Cairo 11421, Egypt*
[3] *Department of Environmental Sciences, Faculty of Meteorology, Environment, and Arid Land Agriculture, King Abdulaziz University, Jeddah 21589, Saudi Arabia*
[4] *Minerals Technology Department, Central Metallurgical Research & Development Institute (CMRDI), Cairo 11421, Egypt*

Correspondence should be addressed to M. A. Barakat, mabarakat@gmail.com

Received 20 March 2012; Revised 24 May 2012; Accepted 2 June 2012

Academic Editor: Manickavachagam Muruganandham

ZnO-SiO_2 nanoparticles were synthesized by a sol-gel technique from $Zn(NO_3)_2 \cdot 6H_2O$ and tetraethyl orthosilicate (TEOS). The synthesized samples were further modified by nanosized Pt from H_2PtCl_6 solution through photoassisted deposition (PAD) and impregnation (Img) routes. The obtained samples were characterized by a series of techniques including X-ray diffraction (XRD), UV-Vis diffuse reflectance spectroscopy, N_2 adsorption, extended X-ray absorption fine structure (EXAFS), and transmission electron microscopy (TEM). The photocatalytic activity of the Pt-ZnO/SiO_2 was evaluated by photocatalytic degradation of phenol in synthetic wastewater under UV-irradiation. Results obtained revealed that the surface area and the photocatalytic activity of the prepared samples were increased in the order ZnO/SiO_2 < PAD: Pt-ZnO/SiO_2 < img: Pt-ZnO/SiO_2. The surface area decreased from 480 to 460 and 450 m^2/g, while the efficiency of the phenol degradation increased from 80 to 85 and 100%, with the ZnO/SiO_2, Img: Pt-ZnO-SiO_2, and PAD: Pt-ZnO-SiO_2 samples, respectively.

1. Introduction

Zinc oxide (ZnO) is an n-type semiconductor with a wide direct bandgap of 3.37 eV. Recently, much effort has been devoted to study ZnO as a promising photocatalyst for photocatalytic degradation of water pollutants, owing to its high activity, low cost, and environmentally friendly feature [1–4]. ZnO microcrystal showed also good photocatalytic activity for dye wastewater treatment [5].

However, a major drawback of ZnO is the large bandgap of 3.37 eV; so, wavelengths below 400 nm are necessary for excitation. Another disadvantage of ZnO is that charge carrier recombination of photogenerated electron/hole pairs occurs within nanoseconds and the photocatalytic activity is low [6–9]. Therefore, it is necessary to improve its visible-light activities by extending its absorption threshold from the UV light region to the visible light region and also reduce the recombination of photogenerated electron/hole. Different works were performed recently to improve the activity of ZnO catalyst. Development of core/shell-structured materials on a nanometer scale has been receiving extensive attention [10, 11]. The shell can alter the charge, functionality, and reactivity of surface or improve the stability and dispersive ability of the core material. Furthermore, catalytic, optical, or magnetic functions can be imparted to the core particles by the shell material. In general, the synthesis of core/shell-structured material has the goal of obtaining a new composite material having synergetic or complementary behaviors between the core and shell materials. Many studies on the synthesis of composites such as NiO [12], V_2O_5 [13], TiO_2 [14], Fe_2O_3 [15], Pt [16], and Ag [17, 18] coated with SiO_2 shells have been reported. SiO_2 is one of the most

studied shell candidates due to its relative ease in preparation, good environmental stability, and compatibility with other materials, which motivated us to prepare the core/shell-structured composite of ZnO and SiO_2 and expected to achieve novel properties resulting from the synergic interaction of these two chemical components. One of the most promising methods to increase the photocatalytic efficiency is surface modification of ZnO, this can be achieved by metal doping into the ZnO catalyst. Dopant can act as a sink to collect photogenerated electrons from the conduction band of the semiconductor. Thus, it hinders the recombination of photogenerated electrons and holes through increasing the charge separation [19–22]. The surface modification of ZnO nanoparticles by preparing charge-transfer catalysts with mixing multicomponent oxides can enhance the surface chemical and physical properties and be considered as the key for the successful photocatalytic applications of such nanoparticles. Several metal ions such as Fe [23] and Ag [24, 25] have been used as dopants for ZnO to improve its photocatalytic activity. Photocatalytic degradation of phenolic compounds with semiconducting oxides holds promise for the purification and treatment of both drinking and industrial wastewater [26–28]. The presence of such organic pollutants in aquatic environments has caused several environmental pollution problems.

In the present work, Pt/ZnO-SiO_2 nanoparticles with large specific surface areas had been synthesized by the application of a photoassisted deposition (PAD) and impregnation (Img) methods, and the properties of the nanoparticles were characterized by XRD, TEM, EXAFS, UV-Vis/DRS, and BET analysis. The photocatalytic activity of the synthesized nanoparticles was evaluated by the photodegradation of phenol (as a model for pollutants in wastewater) under UV irradiation.

2. Experimental Methods

2.1. Chemicals. $Zn(NO_3)_2 \cdot 6H_2O$, H_2PtCl_6, and tetraethyl orthosilicate (TEOS) were purchased from Aldrich and selected as the precursors of zinc, platinum, and silica, respectively. Standard grade phenol was purchased from Merck with 99.5% purity. 1 M NaOH and 1 M HCl solutions were used for pH adjustment. All chemicals used in this work were of reagent-grade quality. The water used was deionized water.

2.2. Preparation of ZnO/SiO_2. ZnO/SiO_2 nanoparticles were synthesized via a sol-gel technique and calcination. In a typical procedure, 20 mL TEOS was mixed with ethyl alcohol (C_2H_5OH), ultrapure water (H_2O), and nitric acid (HNO_3) under vigorous stirring for 1 hr. The overall molar ratio of TEOS : C_2H_5OH : H_2O : HNO_3 was 1: 4 : 8 : 0.02. Subsequently, after 60 min, an aqueous solution of $Zn(NO_3)_2 \cdot 6H_2O$ was added in to the above solution under vigorous stirring for 60 min. The reaction was performed at room temperature. The prepared samples were aged for 24 h. Finally, the samples were evaporated and dried at 80°C, followed by calcination at 550°C for 3 h in air.

2.3. Preparation of Pt Loaded on ZnO/SiO_2 Using PAD Method. Pt metal (3 wt%) was deposited on ZnO-SiO_2 from aqueous solution of H_2PtCl_6 under UV-light irradiation. The samples were dried at 100°C and reduced by H_2 (20 mL/min) at 350°C for 4 h.

2.4. Preparation of Pt Loaded on ZnO/SiO_2 Using Img Method. In a typical impregnation (Img) method, the 3 wt% of Pt metal was deposited by a simple impregnation of ZnO-SiO_2 in the absence of light with aqueous solution of H_2PtCl_6. The samples were dried at 100°C and reduced by H_2 (20 mL/min) at 350°C for 4 h.

2.5. Characterization Techniques. To determine the crystallite sizes and identities of the Pt loaded on ZnO/SiO_2 nanocomposite photocatalyst, X-ray diffraction (XRD) analysis was carried out at room temperature using Rigaku X-ray diffractometer with Cu Kα radiation over a 2θ collection range of 10–80°. The shape of the samples was tested using Hitachi H-9500 transmission electron microscope (TEM), the prepared samples were prepared by suspending the prepared samples in ethanol, followed by ultrasonication for 30 min, then a small amount of this solution onto a carbon-coated copper grid and drying for TEM. Specific surface area was calculated from measurements of N_2-adsorption using Nova 2000 series chromatech apparatus at 77 K. Prior to the measurements, all samples were treated under vacuum at 200°C for 2 h. The band gap of the samples was identified by UV-visible diffuse reflectance spectra (UV-Vis-DRS) in air at room temperature in the wavelength range of 200–800 nm using Shimadzu UV-2450 spectrophotometer. The extended X-ray absorption fine structure (EXAFS) is performed at BL-7C facility [29] of the Photon Factory at the National Laboratory for High Energy Physics, Tsukuba, Tokyo, Japan. A Si (1 1 1) double-crystal was used to monochromatize the X-rays from the 2.5 GeV electron storage ring. The K-edge EXAFS spectra of Fe were measured in the fluorescence mode at 25°C. The Fourier transformation was performed on K^3-weighted EXAFS oscillations in effective range from 0–5 Å.

2.6. Photocatalytic Activity Measurements. Photodegradation experiments were performed with a photocatalytic reactor system at 25°C. This bench-scale system consisted of a cylindrical Pyrex-glass cell with 1 L. A 150-Watts mercury lamp was placed in a 5 cm diameter quartz tube with one end tightly sealed by a Teflon stopper. The photoreactor was filled with 1 L of 100 mg/L aqueous phenol solution with 1 g/L of each of the three prepared nanoparticles samples. The whole reactor was cooled with a water-cooled jacket on its outside to the temperature. Compressed air was purged into the solution by bubbling compressed air from the bottom to maintain an aerobic condition [30]. Magnetic stirrer was also used to keep the solution chemically uniform. The pH of the solutions was adjusted and kept constant at 7 during the experiments by adding NaOH (1 M) and HCl (1 M) using an Orion Model 801 A pH meter. The experiments were carried out for 60 minutes. The liquid samples were filtered for analysis through 0.2 μm syringe

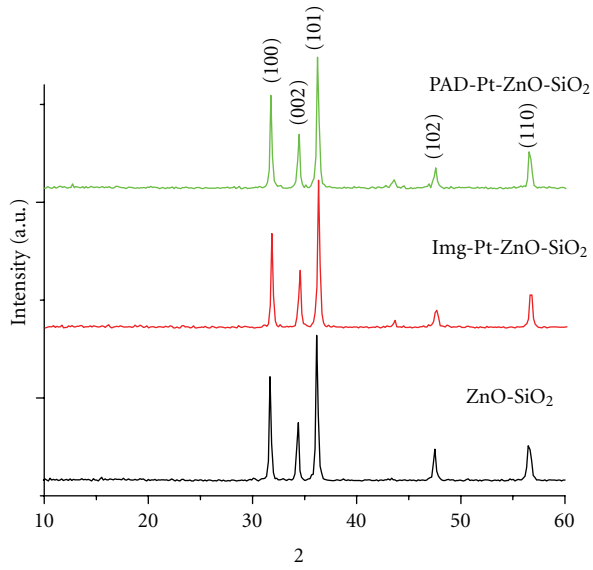

Figure 1: XRD patterns of the (ZnO-SiO_2, Img: Pt-ZnO-SiO_2 and PAD: Pt-ZnO-SiO_2).

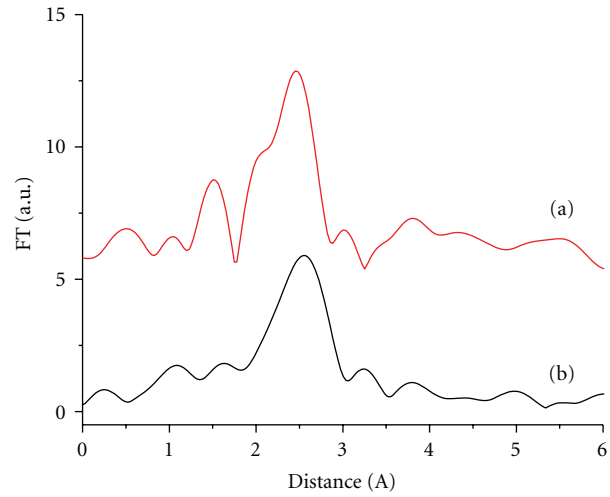

Figure 2: Fourier transforms of the Pt L_{III}-edge EXAFS spectra for Img: Pt-ZnO-SiO_2 (a) and PAD: Pt-ZnO-SiO_2 (b).

filters. The residual phenol was analyzed by the reaction with 4-aminoantipyrine [31]. Diluted sample of phenol was treated with 2 mL of 4 N NH_4OH, 1 mL of 1.5% 4-aminoantipyrine, and 1 mL of 4% K_3 [Fe $(CN)_6$] and quantitatively diluted to 100 mL with H_2O. After 5 min, the reaction was determined colorimetrically at 510 nm. The photodegradation efficiency of phenol has been calculated applying the following equation:

$$\%\ \text{Photodegradation efficiency} = \frac{C_0 - C}{C_0} \times 100, \quad (1)$$

where C_0 is the initial phenol concentration; C is the retained phenol in solution.

3. Results and Discussions

3.1. Phase Analysis. The XRD patterns of the ZnO-SiO_2 and Pt-doped ZnO-SiO_2 nanoparticles prepared by (Img) and (PAD) routes are shown in Figure 1. It can be seen that the diffraction patterns of ZnO-SiO_2 sample and all Pt-doped ZnO-SiO_2 are mainly composed of ZnO phase which still exists after applying both mentioned preparation methods. While in the Pt-doped samples, no diffraction peaks of Pt were observed, this is probably attributed to the low Pt-doping content (ca. 3 wt%). Moreover, it is obvious that Pt is well dispersed over the ZnO-SiO_2 surface.

3.2. Nanostructure Characterization. Figure 2 displays the Fourier transforms of Pt L_{III}-edge EXAFS spectra of the Pt-loaded catalysts. It can be noticed that the presence of the peak assigned to the Pt–Pt bond of Pt metal at around 2.5 Å is an indication of the formation of nanosized Pt metal [32]. In addition, the intensity of the Pt–Pt peak of the PAD: Pt-ZnO-SiO_2 catalyst is smaller than that prepared by impregnation route. Therefore, Pt metal particles formed on (PAD: Pt-ZnO-SiO_2) showed smaller particle size than (Img: Pt-ZnO-SiO_2). The grain sizes of PAD: Pt-ZnO-SiO_2 and Img: Pt-ZnO-SiO_2 nanocomposite photocatalysts were displayed in TEM images as shown in Figure 3. The particle size distribution obtained from the analysis of TEM images is shown in Figure 4. The result reveal that the nano-sized Pt metal with a mean diameter (d) of ca. 3 nm having a narrow size distribution was found on the PAD: Pt-ZnO-SiO_2 catalyst, whereas the aggregated Pt metal within various sizes is observed on Img: Pt-ZnO-SiO_2 catalyst (d = 15 nm) which is in agreement with the results of EXAFS measurement. These findings suggest that the size of Pt metal particles depends on the preparation method. Also, TEM micrographs showed the homogenous distribution of Pt over ZnO-SiO_2 matrix which was prepared by PAD method.

3.3. Surface Area Analysis. Specific surface area (S_{BET}) of ZnO/SiO_2, PAD: Pt-ZnO-SiO_2, and Img: Pt-ZnO-SiO_2 powder samples were determined. The S_{BET} values were 480, 460, and 450 m^2/g for the ZnO-SiO_2, PAD: Pt-ZnO-SiO_2, and Img: Pt-ZnO-SiO_2, respectively. The parameters of surface area and the data calculated from the t-plot are collected in Table 1. Furthermore, the total pore volume of Pt-ZnO-SiO_2 is higher than that of ZnO-SiO_2. The values of S_{BET} and S_t are generally close in most samples indicating the presence of mesopores. The values of S_{micro} are high compared to that of S_{meso} implying that the main surface is mesoporous solid. The surface texture data are correlated with the catalytic activity as will be mentioned later on. The N_2 adsorption-desorption isotherm of the prepared samples is shown in Figure 5. It is clear that the isotherm shows a typical type IV sorption behavior, which confirms the presence of mesoporous form.

3.4. Band-Gap Analysis (UV-Vis-DRS). Study of the UV-visible radiation absorption is an important tool for evaluating the changes in the absorbance spectra of the prepared semiconductor materials. This is expressed by the band-gap

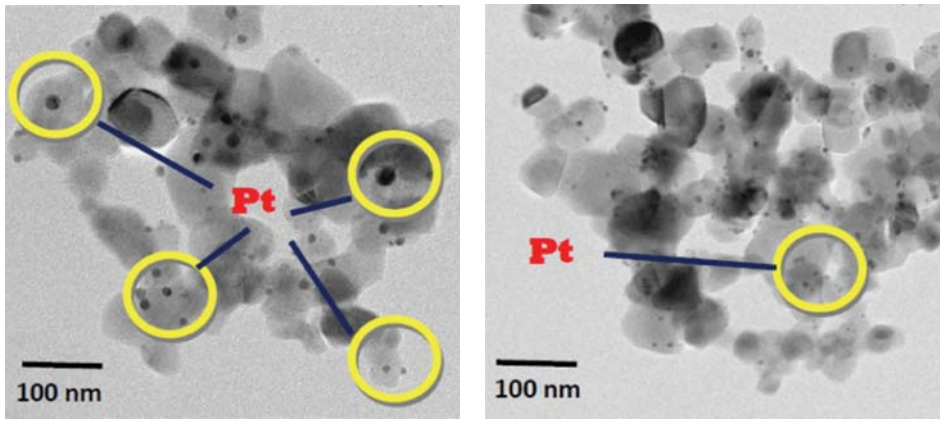

(a) (b)

Figure 3: The TEM images of the Img: Pt-ZnO-SiO_2 (a) and PAD: Pt-ZnO-SiO_2 (b) catalysts.

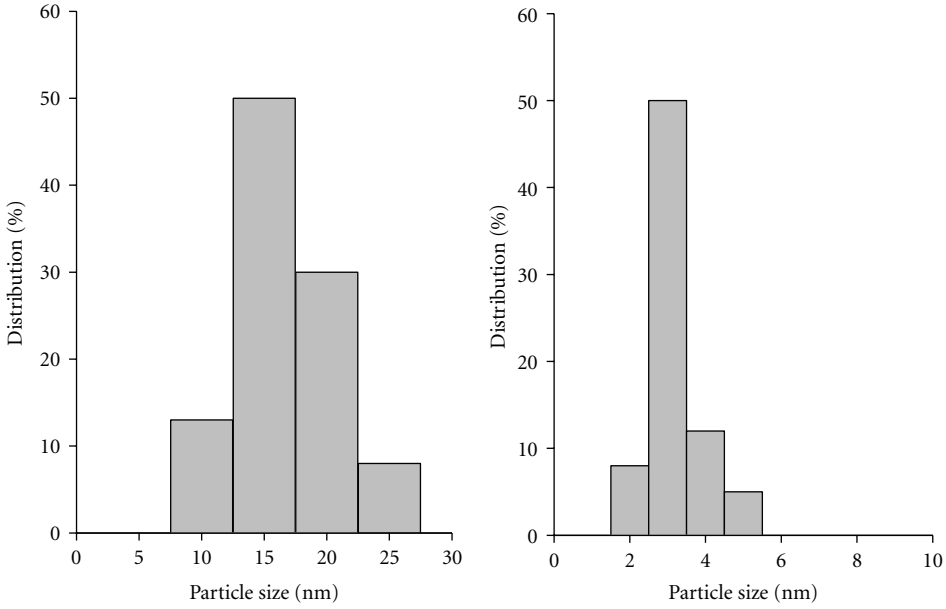

(a) (b)

Figure 4: Size distribution diagrams of Pt metal obtained from the TEM images of the Img: Pt-ZnO-SiO_2 (a) and PAD: Pt-ZnO-SiO_2 (b) catalysts.

(E_g) measurement which can be altered by different parameters. For instance, E_g value for pure ZnO phase is usually reported 3.37 [7]; however, these values are influenced by the synthesis method, and also affected by the existence of impurities doping the crystalline network and also the average crystal size of the semiconductor. In a previous study, different methods for calculating the E_g from the UV-Vis reflectance spectra were used. For example, some authors calculated the E_g values by a direct extrapolation of the $F(R)$ spectrum, whereas others reported the wavelength corresponding to the maximum absorption [33]. As a consequence, quite different E_g values for ZnO samples are found in the literature. For instance, threshold wavelength values of 240 nm [34], 290 nm [35], and 360 nm [36] correspond to bandgaps 5.15, 4.28, and 3.45, respectively. Figure 6 gives UV-Vis-DRS of (ZnO-SiO_2, Img: Pt-ZnO-SiO_2, and PAD: Pt-ZnO-SiO_2). The results showed an increase in the absorbance in the visible light region with the Pt doping. The values of E_g for the synthesized semiconductors can be derived from the spectra by plotting $(F(R) \cdot \mathrm{h}\ )^{1/2}$ against h [37, 38] as shown in Figure 7 and tabulated as shown in Table 2. The results revealed that the calculated values of E_g for (ZnO-SiO_2, Img: Pt-ZnO-SiO_2, and PAD: Pt-ZnO-SiO_2) were 3.4, 3.25, and 3.05 eV, respectively. This indicates shifting the spectra of the PAD: Pt-ZnO-SiO_2 sample to the visible light area.

3.5. Evaluation of Photocatalytic Activity. The photocatalytic activity of the synthesized nanoparticles samples was evaluated by degradation of phenol in solution under UV light. Figure 8 displays the photocatalytic degradation of

Table 1: Texture parameters of ZnO-SiO_2, Img: Pt-ZnO-SiO_2, and PAD: Pt-ZnO-SiO_2.

Sample	S_{BET} (m^2/g)	S_t (m^2/g)	S_{micro} (cm^2/g)	S_{ext} (cm^2/g)	V_p (cm^3/g)	V_{micro} (cm^3/g)	V_{meso} (cm^3/g)	r (Å)
ZnO-SiO_2	480	485	380	100	0.866	0.069	0.803	38.00
Img: Pt-ZnO-SiO_2	450	455	500	365	0.726	0.022	0.704	36.00
PAD: Pt-ZnO-SiO_2	460	465	650	385	0.668	0.066	0.602	34.00

Note: (S_{BET}) BET-Surface area, (S_t) surface area derived from V_{l-t} plots, (S_{mic}) surface area of micropores, (S_{ext}) external surface area, (V_p) total pore volume, (V_{mic}) pore volume of micropores, (V_{mes}) pore volume of mesopores, and (r^-) mean pore radius.

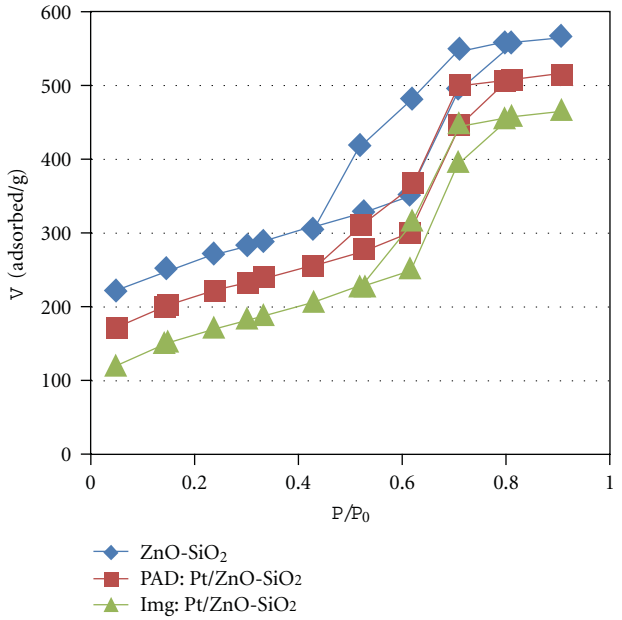

Figure 5: N_2 sorption isotherms of ZnO-SiO_2, PAD-Pt/ZnO-SiO_2, and Img-Pt/ZnO-SiO_2.

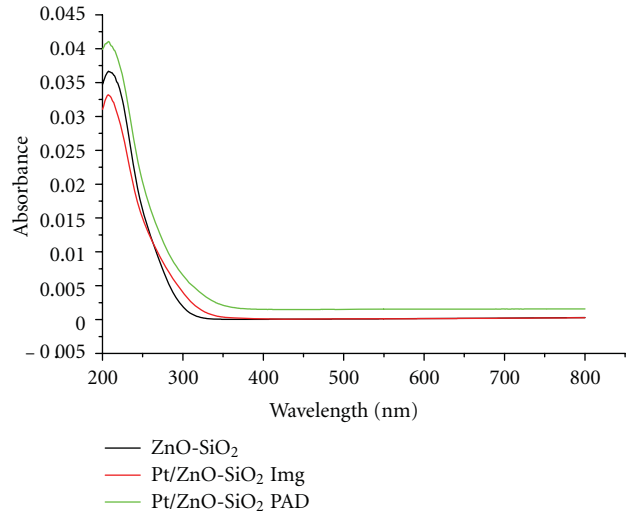

Figure 6: Diffuse reflectance UV-Vis absorption spectra of ZnO-SiO_2, Img: Pt-ZnO-SiO_2, and PAD: Pt-ZnO-SiO_2.

Table 2: The calculated band gap energy of ZnO-SiO_2, Img: Pt-ZnO-SiO_2, and PAD: Pt-ZnO-SiO_2.

Sample	Band gap energy (eV)
ZnO-SiO_2	3.40
Img: Pt-ZnO-SiO_2	3.25
PAD: Pt-ZnO-SiO_2	3.05

100 mg/L phenol pertaining to (ZnO-SiO_2, Img: Pt-ZnO-SiO_2, and PAD: Pt-ZnO-SiO_2) at solution pH 7 for different time intervals. It can be seen that the rate of phenol photodegradation increased gradually with time reaching maximum efficiency values of 80, 85, and 99.9% after 1 h with parent ZnO-SiO_2, Img: Pt-ZnO-SiO_2, and PAD: Pt-ZnO-SiO_2 samples, respectively. Considering that the pure Pt oxides have no photocatalytic oxidation properties, such change in the photodegradation activity may be explained in terms of the differences in interaction between Pt and ZnO-SiO_2 that led to several modifications in physical properties such as bandgap, particle size, and surface texture. Also, one could observe that the catalytic activity of ZnO-SiO_2 generally increased with the addition of Pt promoters. Figure 9 shows the good correlation between the physical properties of the synthesized samples, such as bandgap, surface area, and pore volume, with their catalytic activity. It was obvious that the photodegradation activity was gradually increased with the decrease of bandgap and the increase of the surface area and pore volume. The maximum photocatalytic degradation of phenol was achieved in the case of PAD: Pt-ZnO-SiO_2 in which the surface area and pore volume were maximum with lower bandgap value. It is believed that the lack of electron scavengers (surface Zn^{2+}) and hole traps (surface hydroxyl groups) is responsible for the rapid recombination rate of e^-/h^+, which leads to lower photocatalytic activity with the parent ZnO-SiO_2 sample [6–9]. The photocatalytic activities of the Pt-doped ZnO-SiO_2 nanoparticles increased due to that Pt plays two important roles; noble metal incorporation into TiO_2 dielectric provides an absorption feature due to the surface plasmon resonance (SPR) occurring over the visible range of the spectrum. In particular, Ag, Pt, and Au metals are the most popular materials due to the strong SPR character [39, 40]. On the other hand, the superior driven photocatalytic efficiency of the Pt/TiO_2 nanocomposite photocatalyst can be ascribed to the high efficiency of charge-pair separation due to the presence of deposited Pt serving as electron sinks to retard the rapid e^--h^+ couple recombination, the good photoabsorption capacity in the visible light region, and the higher concentration of surface hydroxyl groups, which are able to effectively scavenge photogenerated valence band holes [41].

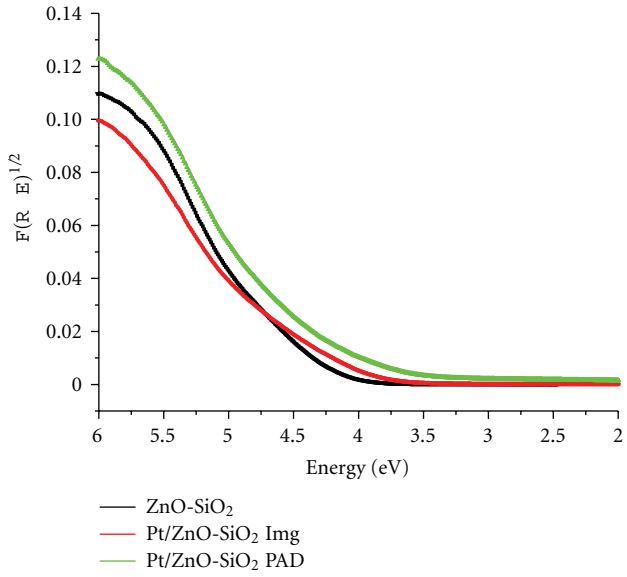

Figure 7: Bandgap calculated from the DR-UV-Vis spectra of ZnO-SiO_2, Img: Pt-ZnO-SiO_2, and PAD: Pt-ZnO-SiO_2.

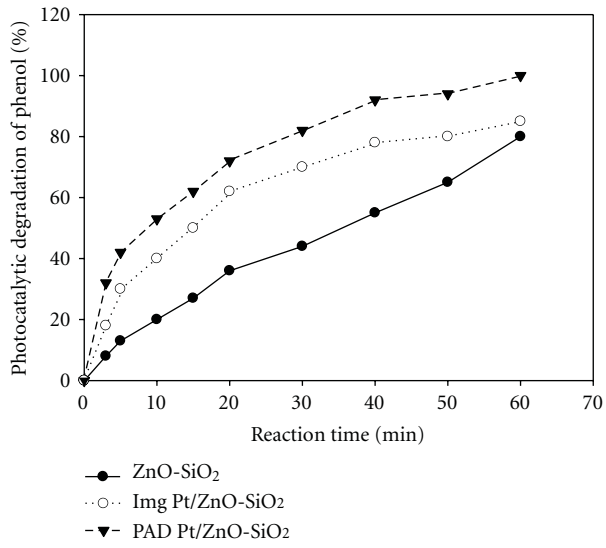

Figure 8: Photocatalytic degradation of phenol (%) for ZnO-SiO_2, Img: Pt-ZnO-SiO_2, and PAD: Pt-ZnO-SiO_2. (a) PAD: Pt-ZnO-SiO_2, (b) Img: Pt-ZnO-SiO_2, and (c) ZnO-SiO_2.

Accordingly, the highest activity was more clear in the PAD: Pt-ZnO-SiO_2 sample in which the Pt diffuses in the lattice of the semiconductor. Thus, it lowered both the bandgap (as confirmed from the UV-Vis-DRS spectra analysis) and particle size (as confirmed from the TEM analysis). This resulted in increase in the surface area and pore volume, and consequently showed the best photoactivity with phenol degradation.

4. Conclusions

Pt doping, through photoassisted deposition (PAD) and impregnation (Img) routes, can greatly enhance the performance of ZnO-SiO_2 as a photocatalyst. The nano-sized

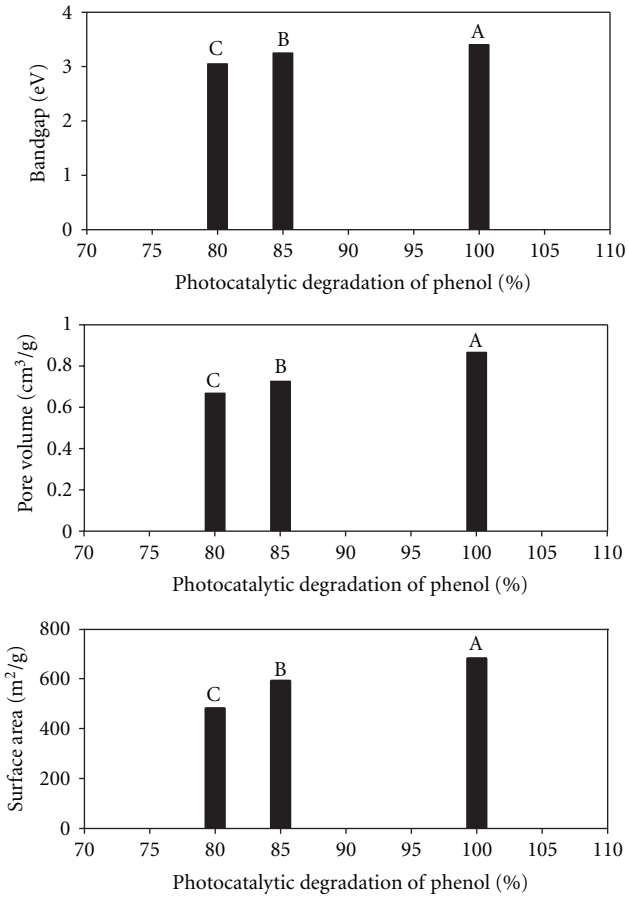

Figure 9: Effect of physical parameters of the materials on their photocatalytic activity.

Pt metal with a mean diameter (d) of ca. 3 nm having a narrow size distribution was found on the PAD: Pt-ZnO-SiO_2 catalyst, whereas the aggregated Pt metal with various sizes is observed on Img: Pt-ZnO-SiO_2 catalyst (d = 15 nm). The surface area of the synthesized samples was decreased from 480 to 460 and 450 m^2/g with ZnO-SiO_2, PAD: Pt-ZnO-SiO_2, and Img: Pt-ZnO-SiO_2, respectively. The UV-Vis-DRS spectra analysis confirmed the lowest bandgab of PAD: Pt-ZnO-SiO_2 with a value of 3.05, comparing to 3.25 and 3.4 with Img: Pt-ZnO-SiO_2 and ZnO-SiO_2, respectively. The photocatalytic degradation of phenol in synthetic wastewater solution was found to be much more effective in the PAD: Pt-ZnO-SiO_2. The degradation efficiency increased from 80 to 85 and 99.9%, with the ZnO/SiO_2, Img: Pt-ZnO-SiO_2, and PAD: Pt-ZnO-SiO_2 samples, respectively. The smallest particle size and lowest bandgab of the PAD: Pt-ZnO-SiO_2 sample resulted in a high increase in the surface area and pore volume and consequently showed the best photoactivity with phenol degradation.

Acknowledgments

This paper was funded by the Deanship of Scientific Research (DSR), King Abdulaziz University (KAU), Jeddah, under Grant no. (265/155/1431). The authors, therefore,

acknowledge with thanks DSR and KAU for technical and financial support.

References

[1] C. Hariharan, "Photocatalytic degradation of organic contaminants in water by ZnO nanoparticles: revisited," *Applied Catalysis A*, vol. 304, no. 1-2, pp. 55–61, 2006.

[2] M. Mrowetz and E. Selli, "Photocatalytic degradation of formic and benzoic acids and hydrogen peroxide evolution in TiO_2 and ZnO water suspensions," *Journal of Photochemistry and Photobiology A*, vol. 180, no. 1-2, pp. 15–22, 2006.

[3] T. Pauporté and J. Rathouský, "Electrodeposited mesoporous ZnO thin films as efficient photocatalysts for the degradation of dye pollutants," *Journal of Physical Chemistry C*, vol. 111, no. 21, pp. 7639–7644, 2007.

[4] J. Yu and X. Yu, "Hydrothermal synthesis and photocatalytic activity of zinc oxide hollow spheres," *Environmental Science and Technology*, vol. 42, no. 13, pp. 4902–4907, 2008.

[5] J. H. Sun, S. Y. Dong, Y. K. Wang, and S. P. Sun, "Preparation and photocatalytic property of a novel dumbbell-shaped ZnO microcrystal photocatalyst," *Journal of Hazardous Materials*, vol. 172, no. 2-3, pp. 1520–1526, 2009.

[6] M. Zhou, J. Yu, and B. Cheng, *Journal of Hazardous Materials*, vol. 137, 2006.

[7] C. F. Klingshirn, "ZnO: material, physics and applications," *ChemPhysChem*, vol. 8, no. 6, pp. 782–803, 2007.

[8] A. Singhal, S. N. Achary, A. K. Tyagi, P. K. Manna, and S. M. Yusuf, "Colloidal Fe-doped ZnO nanocrystals: facile low temperature synthesis, characterization and properties," *Materials Science and Engineering B*, vol. 153, no. 1–3, pp. 47–52, 2008.

[9] C. R. Estrellan, C. Salim, and H. Hinode, "Photocatalytic activity of sol-gel derived TiO_2 co-doped with iron and niobium," *Reaction Kinetics and Catalysis Letters*, vol. 98, no. 1, pp. 187–192, 2009.

[10] J. J. Schneider, "Magnetic core/shell and quantum-confined semiconductor nanoparticles via chimie douce organometallic synthesis," *Advanced Materials*, vol. 13, no. 7, pp. 529–533, 2001.

[11] H. B. Lee, Y. M. Yoo, and Y. H. Han, "Characteristic optical properties and synthesis of gold-silica core-shell colloids," *Scripta Materialia*, vol. 55, no. 12, pp. 1127–1129, 2006.

[12] R. M. Mohamed and E. S. Aazam, "Photocatalytic oxidation of carbon monoxide over NiO/SnO_2 nanocomposites under UV irradiation," *Journal of Nanotechnology*, vol. 2012, Article ID 794874, 9 pages, 2012.

[13] A. A. Ismail, I. A. Ibrahim, and R. M. Mohamed, "Sol-gel synthesis of vanadia-silica for photocatalytic degradation of cyanide," *Applied Catalysis B*, vol. 45, no. 2, pp. 161–166, 2003.

[14] J. Zhang, Z. Liu, B. Han et al., "Preparation of silica and TiO_2-SiO_2 core-shell nanoparticles in water-in-oil microemulsion using compressed CO_2 as reactant and antisolvent," *Journal of Supercritical Fluids*, vol. 36, no. 3, pp. 194–201, 2006.

[15] V. Maurice, T. Georgelin, J. M. Siaugue, and V. Cabuil, "Synthesis and characterization of functionalized core-shell γFe_2O_3-SiO_2 nanoparticles," *Journal of Magnetism and Magnetic Materials*, vol. 321, no. 10, pp. 1408–1413, 2009.

[16] R. M. Mohamed, "Characterization and catalytic properties of nano-sized Pt metal catalyst on TiO_2-SiO_2 synthesized by photo-assisted deposition and impregnation methods," *Journal of Materials Processing Technology*, vol. 209, no. 1, pp. 577–583, 2009.

[17] K. S. Chou and C. C. Chen, "Fabrication and characterization of silver core and porous silica shell nanocomposite particles," *Microporous and Mesoporous Materials*, vol. 98, no. 1–3, pp. 208–213, 2007.

[18] R. M. Mohamed and I. A. Mkhalid, "Characterization and catalytic properties of nano-sized Ag metal catalyst on TiO_2-SiO_2 synthesized by photo-assisted deposition and impregnation methods," *Journal of Alloys and Compounds*, vol. 501, no. 2, pp. 301–306, 2010.

[19] M. J. Height, S. E. Pratsinis, O. Mekasuwandumrong, and P. Praserthdam, "Ag-ZnO catalysts for UV-photodegradation of methylene blue," *Applied Catalysis B*, vol. 63, no. 3-4, pp. 305–312, 2006.

[20] T.-Y. Han, C.-F. Wu, and C.-T. Hsieh, "Hydrothermal synthesis and visible light photocatalysis of metal-doped titania nanoparticles," *Journal of Vacuum Science and Technology B*, vol. 25, no. 2, article 430, 6 pages, 2007.

[21] R. Ullah and J. Dutta, "Photocatalytic degradation of organic dyes with manganese-doped ZnO nanoparticles," *Journal of Hazardous Materials*, vol. 156, no. 1–3, pp. 194–200, 2008.

[22] R. Slama, F. Ghribi, A. Houas, C. Barthou, and L. El Mir, *International Journal of Nanoelectronics and Materials*, vol. 3, p. 133, 2010.

[23] R. M. Mohamed, M. A. Al-Rayyani, E. S. Baeissa, and I. A. Mkhalid, "Nano-sized Fe-metal catalyst on ZnO-SiO_2: (photo-assisted deposition and impregnation) Synthesis routes and nanostructure characterization," *Journal of Alloys and Compounds*, vol. 509, no. 24, pp. 6824–6828, 2011.

[24] C. Ren, B. Yang, M. Wu et al., "Synthesis of Ag/ZnO nanorods array with enhanced photocatalytic performance," *Journal of Hazardous Materials*, vol. 182, no. 1–3, pp. 123–129, 2010.

[25] Y. Lai, M. Meng, and Y. Yu, "One-step synthesis, characterizations and mechanistic study of nanosheets-constructed fluffy ZnO and Ag/ZnO spheres used for Rhodamine B photodegradation," *Applied Catalysis B*, vol. 100, no. 3-4, pp. 491–501, 2010.

[26] M. A. Barakat, H. Schaeffer, G. Hayes, and S. Ismat-Shah, "Photocatalytic degradation of 2-chlorophenol by Co-doped TiO_2 nanoparticles," *Applied Catalysis B*, vol. 57, no. 1, pp. 23–30, 2005.

[27] M. A. Barakat, J. M. Tseng, and C. P. Huang, "Hydrogen peroxide-assisted photocatalytic oxidation of phenolic compounds," *Applied Catalysis B*, vol. 59, no. 1-2, pp. 99–104, 2005.

[28] A. Abdel Aal, M. A. Barakat, and R. M. Mohamed, "Electrophoreted Zn-TiO2-ZnO nanocomposite coating films for photocatalytic degradation of 2-chlorophenol," *Applied Surface Science*, vol. 254, no. 15, pp. 4577–4583, 2008.

[29] M. Nomura and A. Koyama, "Design of an XAFS beamline at the photon factory: possibilities of bent conical mirrors," *Journal of Synchrotron Radiation*, vol. 6, no. 3, pp. 182–184, 1999.

[30] M. A. Barakat, Y. T. Chen, and C. P. Huang, "Removal of toxic cyanide and Cu(II) Ions from water by illuminated TiO_2 catalyst," *Applied Catalysis B*, vol. 53, no. 1, pp. 13–20, 2004.

[31] J. R. Pemberton, "Retention of preservative levels of formaldehyde in desiccated biological products," *Journal of Clinical Microbiology*, vol. 2, no. 2, pp. 144–146, 1975.

[32] A. Caballero, F. Villain, H. Dexpert, F. Lepeltier, B. Didillon, and J. Lynch, "In situ EXAFS studies of modifications to supported metallic catalysts under reactive atmospheres," *Catalysis Letters*, vol. 20, no. 1-2, pp. 1–13, 1993.

[33] R. J. Davis and Z. Liu, "Titania-silica: a model binary oxide catalyst system," *Chemistry of Materials*, vol. 9, no. 11, pp. 2311–2324, 1997.

[34] H. Yoshida, T. Shimizu, C. Murata, and T. Hattori, "Highly dispersed zinc oxide species on silica as active sites for photoepoxidation of propene by molecular oxygen," *Journal of Catalysis*, vol. 220, no. 1, pp. 226–232, 2003.

[35] M. Huang, P. E. J. Rivera-Díaz-Del-Castillo, O. Bouaziz, and S. Van Der Zwaag, "Irreversible thermodynamics modelling of plastic deformation of metals," *Materials Science and Technology*, vol. 24, no. 4, pp. 495–500, 2008.

[36] G. D. Mihai, V. Meynen, M. Mertens, N. Bilba, P. Cool, and E. F. Vansant, "ZnO nanoparticles supported on mesoporous MCM-41 and SBA-15: a comparative physicochemical and photocatalytic study," *Journal of Materials Science*, vol. 45, no. 21, pp. 5786–5794, 2010.

[37] M. Anpo and M. Che, "Applications of photoluminescence techniques to the characterization of solid surfaces in relation to adsorption, catalysis, and photocatalysis," *Advances in Catalysis*, vol. 44, pp. 119–257, 1999.

[38] G. Lassaletta, A. Fernández, J. P. Espinós, and A. R. González-Elipe, "Spectroscopic characterization of quantum-sized TiO_2 supported on silica: influence of size and TiO_2-SiO_2 interface composition," *Journal of Physical Chemistry*, vol. 99, no. 5, pp. 1484–1490, 1995.

[39] J. F. Rivadulla, M. C. Vergara, M. C. Blanco, M. A. López-Quintela, and J. Rivas, "Optical properties of platinum particles synthesized in microemulsions," *Journal of Physical Chemistry B*, vol. 101, no. 44, pp. 8997–9004, 1997.

[40] N. A. M. Barakat, K. D. Woo, M. A. Kanjwal, K. E. Choi, M. S. Khil, and H. Y. Kim, "Surface plasmon resonances, optical properties, and electrical conductivity thermal hystersis of silver nanofibers produced by the electrospinning technique," *Langmuir*, vol. 24, no. 20, pp. 11982–11987, 2008.

[41] D. Zhang, "Visible light-induced photocatalysis through surface plasmon excitation of platinum-metallized titania for photocatalytic bleaching of rhodamine B," *Monatshefte für Chemie*, vol. 143, no. 5, pp. 729–738, 2012.

Hindawi Publishing Corporation
International Journal of Photoenergy
Volume 2012, Article ID 624270, 7 pages
doi:10.1155/2012/624270

Research Article

Degradation of Antibiotics in Wastewater during Sonolysis, Ozonation, and Their Simultaneous Application: Operating Conditions Effects and Processes Evaluation

Vincenzo Naddeo, Daniele Ricco, Davide Scannapieco, and Vincenzo Belgiorno

Department of Civil Engineering, University of Salerno, V. Ponte don Melillo, 84084 Fisciano, Italy

Correspondence should be addressed to Vincenzo Naddeo, vnaddeo@unisa.it

Received 20 March 2012; Accepted 16 May 2012

Academic Editor: Manickavachagam Muruganandham

Pharmaceutical drugs frequently found in treated effluents, lakes and rivers, can exhibit adverse effects on aquatic organisms. The present study focuses on the application of advanced oxidation processes as ozonation (O_3), sonolysis (US), and their combined application (US+O_3) for the degradation of diclofenac in wastewater. Under the applied conditions, all three systems proved to be able to induce diclofenac oxidation, leading to 22% of mineralization for O_3 and 36% for US process after 40 min of treatment. The synergy observed in the combined schemes, mainly due to the effects of US in enhancing the O_3 decomposition, led to a higher mineralization (about 40%) for 40-minute treatment and to a significantly higher mineralization level for shorter treatment duration.

1. Introduction

The widespread occurrence of pharmaceuticals and personal care products in the aquatic environment is a recognized problem of unknown consequences [1–3]. Different sources may cause the appearance of pharmaceuticals in water and soils. The main one is represented by wastewater treatment plants (WWTPs) effluents [4, 5]. Other sources include direct applications in aqua farming, manure run-off [1], via hospital effluent [6], or finally, via landfill leaching [7]. In the aquatic environment, diclofenac (DCF) is one of the most frequently detected pharmaceuticals [8]. Its presence in urban wastewater treatment plants (UWTPs) effluents has been often documented [3, 9–12], with a usual concentration ranging from 2 to 10 μg/L [1, 3, 5, 6].

Recent studies revealed that conventional water treatment processes cannot completely remove DCF from source waters [13–17], so the adoption of advanced oxidation processes (AOPs) in the tertiary treatment section of existing UWTPs can significantly represent a tool for this reduction [12, 17–21].

Several AOPs have been evaluated for the degradation of diclofenac. A number of studies indicated a high reactivity of DCF towards ozonation [12, 13, 17, 21, 22]. In [22], Authors also noted a positive effect of hydrogen peroxide addition on the diclofenac conversion by ozone.

In a different work [20], the H_2O_2/UV treatment of DCF has been investigated, and the obtained results have been compared with ozonation and direct photolysis. At an initial DCF concentration of 296 mg/L, direct photolysis ensured a drug removal up to 45% for a treatment time of 1.5 h using a 17-W low-pressure Hg lamp that emitted UV light at 254 nm with an intensity of $2.7 \cdot 10^{-6}$ Einstein/s.

The DCF degradation was strongly enhanced by the addition of hydrogen peroxide (170 mg/L; H_2O_2/UV AOP) to more than 90% conversion. The Fenton-type process has had an apparent disadvantage during the DCF degradation because the drug (pKa = 4.15) precipitated in an acidic medium, which is required to keep iron dissolved [23, 24]. Titanium dioxide photocatalysis induced by UV-A [25, 26] or artificial solar irradiation [24, 27] was also evaluated for the DCF degradation.

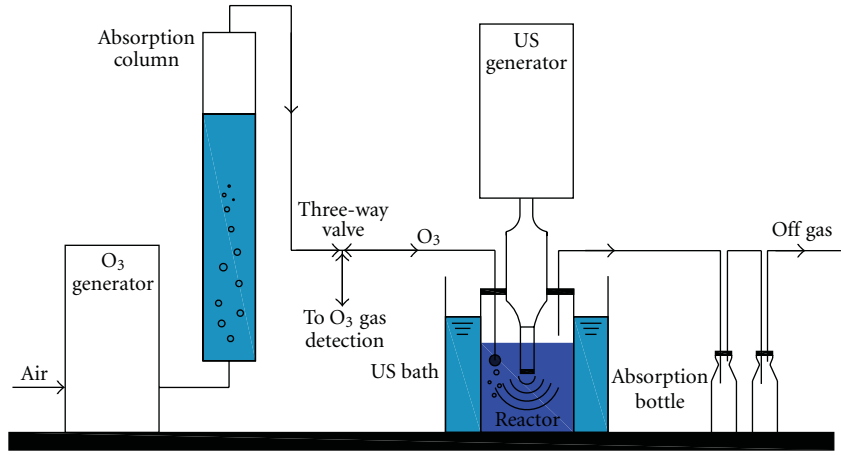

Figure 1: Laboratory-scale experimental setup for the degradation of diclofenac through ozonation/sonolysis.

DCF sonochemical degradation in synthetic water has been analyzed only in recent times [28–30].

Among the mentioned processes, sonolysis, ozonation, and their combined application have been investigated in this study as suitable tools for pharmaceutical degradation from UWTPs effluents.

The application of ultrasound technology to wastewater treatment has been developed in recent times [28, 31–36]. The sonolysis of aqueous solutions, based on cavitation with high temperatures and pressures, leads to the formation of highly reactive hydroxyl radicals ($^{\bullet}OH$).

The main objective was to investigate and compare the effects of ultrasound (US), ozone (O_3), and their combination (US+O_3) on DCF degradation, with the analysis of operating parameters such as pH, temperature, US power density, and O_3 dose.

2. Materials and Methods

2.1. Reagents. DCF (crystalline sodium salt of [2-(2,6-dichlorophenylamino)-phenyl]-acetic acid), characterized by a solubility in water of 237 mg/L at 25°C and a melting point of 275–277°C, was provided by Sigma-Aldrich.

Tests were performed on urban wastewater samples (Table 1), in which a known concentration of DCF was spiked.

According to reported concentration levels in drug industry wastewater, the spiked concentrations were considerably higher than DCF occurrence levels in the environment, but these concentrations were intentionally selected so as to be able to better monitor the removal and mineralization potential with available analytical techniques [6, 17, 26, 29, 34].

2.2. Experimental Setup. Ozone was generated onsite by an O_3 supply system (Microlab, Aeraque, Italy) using ultrapure air. The air flow rate to the ozone generator was monitored with a rotameter. Ozone flow was controlled using an absorption column containing deionised water. Surplus ozone was passed into gas absorption bottles containing 2% (w/v) KI solution.

Table 1: Physicochemical characterization of sampled wastewater (WWTP effluent).

Parameter	Average value
pH	8.10 ± 0.98
DO (mg/L)	5.30 ± 1.03
Electrical conductivity (μS/cm)	1696 ± 182
Turbidity (NTU)	0.827 ± 0.158
BOD_5 (mg/L)	7 ± 2
COD (mg/L)	8.6 ± 3
TOC (mg/L)	4.51 ± 1.62

The US tests were carried out with a Sonics Vibracell VCX-750 (Sonics & Materials Inc., USA) ultrasonic transducer, equipped with a 20 kHz converter and a titanium horn with a 1.3 cm in diameter tip. During the tests, the probe was partially immersed in the liquid for about 4 cm, fixed at the centre of the reactor, and plugged with a polyethylene cap during the operation. The ultrasonic process was performed into an ultrasonic bath in order to keep the temperature constant over time. In Figure 1, a scheme of the experimental setup at laboratory scale is provided.

Combined US+O_3 tests were carried out using a combined ozonation and sonolysis experimental setup as detailed in [29]. In all tested conditions, a spiked wastewater solution (150 mL), contained in a 250 mL cylindrical Pyrex glass reactor (Schott Duran, Germany), was used.

2.3. Experimental Conditions. The ozonation tests were conducted at different treatment duration (i.e., 5, 10, 20, and 40 min), using two different ozone flows (2.4 and 31 g/h), which were able to keep dissolved ozone concentrations in the 5–15 mg/L range, similar to those already used for disinfection and other compounds removal [17, 37, 38].

Ozone was generated onsite by an O_3 supply system (Microlab, Aeraque) using ultrapure air. The air flow-rate to

the ozone generator was monitored with a rotameter. Ozone flow was controlled using an absorption column containing bidistilled water. Surplus ozone was passed into gas absorption bottles containing 2% (w/v) KI solution.

The US tests were carried out with (TC) and without (NTC) temperature control, under varying treatment duration (i.e., 15, 30, 45, and 60 minutes), using power densities of 100, 200, and 400 W/L. In TC tests, sample temperature was maintained constant at 20 ± 3°C using an appropriate ultrasonic bath. To compare the experimental results obtained with O_3 and combined US+O_3 processes, tests were also repeated at the same treatment duration (i.e., 5, 10, 20, and 40 min), using the optimum investigated sonolysis conditions (NTC, 400 W/L).

The combined US+O_3 tests were also carried out at varying duration (i.e., 5, 10, 20, 40 min), using an ozone flow of 31 g/h and a 400 W/L power density according to the best ozonation and sonolysis results in distinct applications.

2.4. Analytical Methods. DCF conversion was assessed in terms of TOC and UV absorbance. A UV-Vis spectrophotometer equipped with a 1 cm quartz cell (Lambda 12, Perkin Elmer) was used for the absorbance measurements and the determination of the DCF spectrum with a characteristic peak at 276 nm (UV276), which is the wavelength that corresponds to the maximum absorbance and gives a sufficient indication of each drug's concentration [26]. The assumption that some of the by-products formed during the oxidation could also absorb at the same wavelength should of course be considered. However, in that case, the conversion of the parent compounds obtained in this study would have been even higher. Therefore, despite this assumption, UV absorption measurements provide a quick and indicative determination of the conversion.

These measurements were used as a fast and preliminary assessment of the compound behaviour [26, 29, 34]. TOC values were detected by a TOC analyzer (Shimadzu TOC-5000A). Water parameters such as pH, turbidity, conductivity, dissolved oxygen, and temperature were also detected before and after treatment in each test by a multiparameter equipment (HANNA Instrument, USA). Dissolved ozone concentrations in water and ozone flows were measured according to procedures described in AWWA-APHA-WEF Standard Methods 4500-O_3 and 2350-E. The off-gas ozone was trapped in a KI solution scrubber to quench ozone. DCF mineralization was due to oxidation reactions that involved the original compound at first, and then its by-products that had been gradually formed.

3. Results and Discussion

3.1. Ozonation. During ozonation tests, its effect on various physicochemical properties of the solutions was investigated. In all tested conditions, electrical conductivity increased versus treatment duration (initial DCF concentration = 40 mg/L, ranging from 10 to 157 mg/L for 40 min treatment time), while pH was reduced to low values (pH = 3-4). Figure 2 shows the DCF concentration decrease, in terms of absorbance (UV_{276}), in relation to both ozonation time and initial concentration of DCF. For the highest O_3 flow (31 g/h), DCF degradation is approximately exponential versus ozonation time, with an almost complete DCF removal after 40 minutes, even at high initial DCF concentrations. Reducing the ozone flow, the DCF degradation versus time was reduced, this being even more evident when the DCF concentration was increased. The DCF degradation was certainly not due to its stripping by the ozone flow because of its Henry coefficient low value, equal to $3 \cdot 10^{-3}$ Pa·m^3/mol at 25°C [39]; instead, it was probably due to hydrogen peroxide formation, because of the direct reactions of ozone with DCF and its aromatic and unsaturated organic intermediates formed during the initial stage of the process [17].

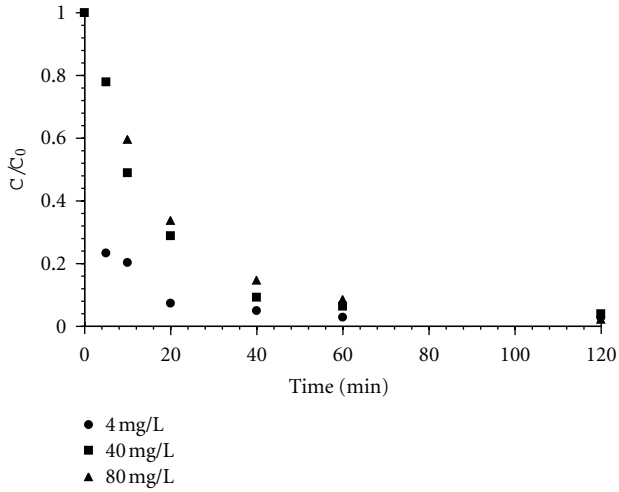

Figure 2: Comparative rates of diclofenac decay, in terms of absorbance, by ozonation (ozone flow = 31 g/h).

Table 2: Ozonation: degradation rate constants (k, K) for three different DCF concentrations.

Spiked DCF (mg/L)	Absorbance		TOC	
	k (L/(mg·min))	R^2	K (mg/(L·min))	R^2
4	2.652	0.789	0.006	0.961
40	0.166	0.977	0.106	0.960
80	0.126	0.879	0.293	0.794

At higher DCF concentrations (40 and 80 mg/L), ozonation followed a second-order kinetic. Depending on the pharmaceutical initial dose, the apparent rate constants (k, K) are reported in Table 2. The removal rate significantly increased when the DCF initial concentration was reduced. At DCF initial concentration of 4 mg/L, a significant pharmaceutical reduction was achieved at very short treatment durations (10 min).

The initial degradation rate was approximately linear versus initial DCF concentration. Reducing the ozone flow, the pharmaceutical degradation was decreased versus time, so different runs were compared using the initial conversion rate (ICR) referred to the first 20 minutes (Figure 3).

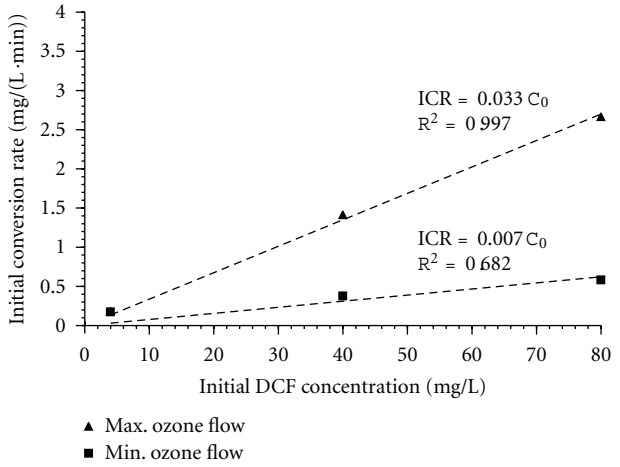

Figure 3: Initial DCF conversion rates, in terms of absorbance, by ozonation (ozone flow = 31 g/h).

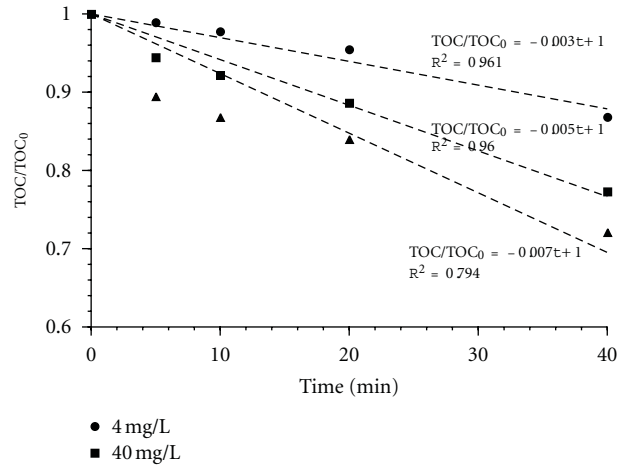

Figure 4: Comparative rates of diclofenac organic carbon decay in terms of TOC by ozonation (ozone flow = 31 g/h).

The fact that the compound reacts so fast with ozone makes more necessary the process analysis in terms of TOC reduction that represents in a better way the real capacity of ozone to deal with DCF and its by-products mineralization. TOC removal behaviour was linear in relation to the ozonation duration and increased with initial DCF concentration (Figure 4). Although UV absorbance measurements indicated complete drug removal after 40 minutes, the maximum TOC reduction achieved was only 30% for an initial DCF concentration of 80 mg/L.

This result, as documented in the literature about organic compound ozonation [17, 40, 41], can be probably attributed to the formation of secondary organic by-products (carboxylic acids such as maleic, malonic, pyruvic, and oxalic acids), with some polar character, which did not react with ozone and showed a different UV absorbance profile than that of the parent compound [29, 30, 34].

3.2. Sonolysis. During sonication tests, the effect on the treatment efficiency of physicochemical properties of tested solutions has been investigated. In all analyzed conditions, electrical conductivity was increased, while pH and redox potential were reduced by the sonication treatment duration. However, the behaviour of these parameters was strongly influenced by the ultrasonic power dose [33].

The DCF concentration decline, in terms of TOC, is shown in relation to irradiation time and US density in Figure 5.

Since the DCF salt is considerably soluble in water and nonvolatile, degradation inside the cavitation bubble was insignificant, and therefore, hydroxyl radical-induced reactions were likely to be the main DCF degradation mechanism. Hydroxyl radicals, formed through water sonolysis, can partly recombine yielding hydrogen peroxide which in turn reacts with hydrogen to regenerate hydroxyl radicals. Therefore, the showed results (Figure 5) are, perhaps, directly connected to the hydroxyl radicals action, which increased when high ultrasound densities were applied. A higher

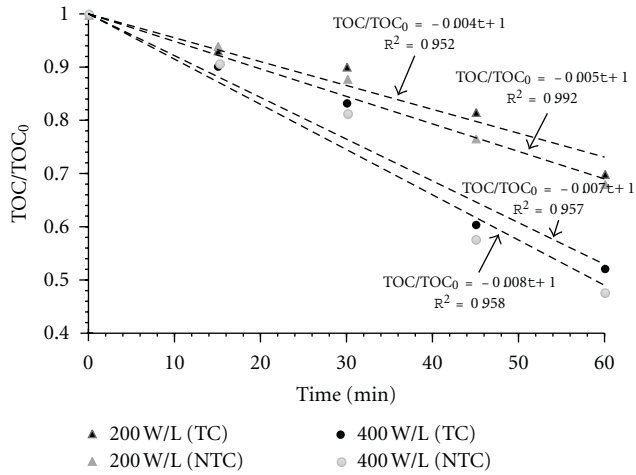

Figure 5: DCF degradation in terms of TOC in relation to ultrasound power densities and bulk temperature conditions (20 kHz, C_0 = 40 mg/L).

US density results in higher supply energy that leads to an enhanced formation of cavitation bubbles. Hence, the degradation rate of DCF increased with the power density.

In NTC conditions, a gradual temperature increase of the liquid bulk solution was recorded due to heat dissipation. For the experiments performed at 400 W/L, temperature increased from 25°C at t = 0 to 71°C at 30 min and finally to 76°C at 60 min; the corresponding values at 200 W/L were 66 and 71°C. Consequently, increased temperatures favour DCF conversion: in NTC tests, more than 55% of DCF was degraded by a 400 W/L power density within 60 min, at initial concentration of 80 mg/L.

At 100 W/L, the DCF degradation rate was quite low, whereas only small differences between the degradation rate at 200 and 400 W/L were observed. Since the maximum temperature obtained during the bubble collapse is proportional to the liquid bulk temperature, increased temperatures are expected to enhance reaction rates. Nevertheless, this effect

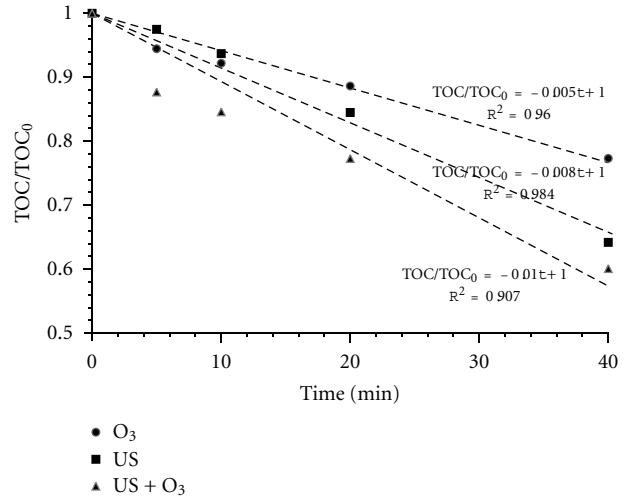

Figure 6: Comparative rates of diclofenac (C_0 = 40 mg/L) organic carbon decay in terms of TOC in 40 min by sonolysis (20 kHz, 400 W/L, NTC), ozonation (31 g/h), and their simultaneous application (US+O_3).

can be counterbalanced or even overcome by the fact that bubbles contain more vapour, which moderates implosion and consequently reduces reaction rates. However, in NTC conditions, the increase in liquid bulk temperature resulted in an increase in DCF conversion; therefore, during TC tests, the pharmaceutical degradation was always lower.

3.3. Combined US+O_3 Treatment. The US+O_3 tests were carried out through the combination of the sonolysis and ozonation optimized removal conditions, which were obtained through the former experimental runs (31 g/h O_3 flow, at 400 W/L ultrasonic power density, without temperature control). During US+O_3 tests, the initial solution temperature and electrical conductivity increased versus treatment time. As for sonolysis and ozonation, pH was instead reduced from a nearly neutral to acidic values (pH = 3-4).

In terms of absorbance, DCF degradation can be described by a first order reaction kinetic. The removal rate increased significantly when comparing the ozonation treatment efficiency to the combined US+O_3 process. In terms of absorbance measurements, the final DCF concentration in solution is probably the same (about 3 mg/L) for 40 minutes, in both cases, but for 5 to 20 minutes the combined US+O_3 action induced much higher degradation.

TOC measurements showed linear trends (Table 3). For 40-minute treatment, DCF reduction was up to 39%, greater than the degradation attributable to ozonation (22%), and comparable with those due to sonolysis (36%). During the first 20 minutes of the experiment, the combined US+O_3 action induced significantly higher TOC removal (Figure 6).

4. Conclusions

The persistence in the environment of DCF and its oxidative degradation by means of ozone, ultrasound, and their simultaneous application has been studied in the present work. The ozonation has been demonstrated to be a suitable tool for pharmaceuticals degradation in wastewater samples even at process conditions usually adopted in drinking water facilities. Sonolysis is more efficient than ozonation for the mineralization of DCF. Results show that there is a synergistic effect when sonolysis and ozonation are applied jointly, and this is attributed to the enhanced O_3 degradation by collapsing bubbles that may yield additional free radicals. The degradation pattern of high concentrations of DCF in wastewater is similar for all tested processes.

The results obtained through this research work can be further enhanced through the investigation of the by-products formation by chromatographic techniques, in order to better determine and assess the removal kinetics of the formed compounds. In addition, toxicity bioassays can help in the evaluation of the potential impact that these by-products may exhibit. It is also necessary to implement the combined processes at a pilot scale to better assess the pharmaceuticals degradation in real wastewater samples.

Table 3: DCF degradation rate constants (K) in terms of TOC referred to sonolysis (20 kHz, 400 W/L, NTC), ozonation (31 g/h), and their combination (US + O_3) for an initial DCF concentration of 40 mg/L.

Treatment process	TOC	
	K (mg/(L·min))	R^2
US	0.169	0.984
O_3	0.106	0.960
US + O_3	0.211	0.907

Acknowledgment

The authors wish to thank P. Napodano and M. Landi for the technical support provided. The study was partly funded by the University of Salerno (FARB-ex 60%, 2009).

References

[1] B. Halling-Sørensen, S. Nors Nielsen, P. F. Lanzky, F. Ingerslev, H. C. Holten Lützhøft, and S. E. Jørgensen, "Occurrence, fate and effects of pharmaceutical substances in the environment-A review," *Chemosphere*, vol. 36, no. 2, pp. 357–393, 1998.

[2] D. W. Kolpin, E. T. Furlong, M. T. Meyer et al., "Pharmaceuticals, hormones, and other organic wastewater contaminants in U.S. streams, 1999-2000: a national reconnaissance," *Environmental Science and Technology*, vol. 36, no. 6, pp. 1202–1211, 2002.

[3] T. Heberer, "Occurrence, fate, and removal of pharmaceutical residues in the aquatic environment: a review of recent research data," *Toxicology Letters*, vol. 131, no. 1-2, pp. 5–17, 2002.

[4] C. G. Daughton and T. A. Ternes, "Pharmaceuticals and personal care products in the environment: agents of subtle change?" *Environmental Health Perspectives*, vol. 107, no. 6, pp. 907–938, 1999.

[5] B. Kasprzyk-Hordern, R. M. Dinsdale, and A. J. Guwy, "The occurrence of pharmaceuticals, personal care products,

endocrine disruptors and illicit drugs in surface water in South Wales, UK," *Water Research*, vol. 42, no. 13, pp. 3498–3518, 2008.

[6] K. Kümmerer, "Drugs in the environment: emission of drugs, diagnostic aids and disinfectants into wastewater by hospitals in relation to other sources—a review," *Chemosphere*, vol. 45, no. 6-7, pp. 957–969, 2001.

[7] M. L. Richardson and J. M. Bowron, "The fate of pharmaceutical chemicals in the aquatic environment," *Journal of Pharmacy and Pharmacology*, vol. 37, no. 1, pp. 1–12, 1985.

[8] R. Triebskorn, H. Casper, A. Heyd, R. Eikemper, H. R. Köhler, and J. Schwaiger, "Toxic effects of the non-steroidal anti-inflammatory drug diclofenac: part II. Cytological effects in liver, kidney, gills and intestine of rainbow trout (*Oncorhynchus mykiss*)," *Aquatic Toxicology*, vol. 68, no. 2, pp. 151–166, 2004.

[9] B. Soulet, A. Tauxe, and J. Tarradellas, "Analysis of acidic drugs in Swiss wastewaters," *International Journal of Environmental Analytical Chemistry*, vol. 82, no. 10, pp. 659–667, 2002.

[10] C. Tixier, H. P. Singer, S. Oellers, and S. R. Müller, "Occurrence and fate of carbamazepine, clofibric acid, diclofenac, ibuprofen, ketoprofen, and naproxen in surface waters," *Environmental Science and Technology*, vol. 37, no. 6, pp. 1061–1068, 2003.

[11] R. Andreozzi, V. Caprio, C. Ciniglia et al., "Antibiotics in the environment: occurrence in Italian STPs, fate, and preliminary assessment on algal toxicity of amoxicillin," *Environmental Science and Technology*, vol. 38, no. 24, pp. 6832–6838, 2004.

[12] M. M. Sein, M. Zedda, J. Tuerk, T. C. Schmidt, A. Golloch, and C. Von Sonntag, "Oxidation of diclofenac with ozone in aqueous solution," *Environmental Science and Technology*, vol. 42, no. 17, pp. 6656–6662, 2008.

[13] T. A. Ternes, M. Meisenheimer, D. McDowell et al., "Removal of pharmaceuticals during drinking water treatment," *Environmental Science and Technology*, vol. 36, no. 17, pp. 3855–3863, 2002.

[14] P. E. Stackelberg, E. T. Furlong, M. T. Meyer, S. D. Zaugg, A. K. Henderson, and D. B. Reissman, "Persistence of pharmaceutical compounds and other organic wastewater contaminants in a conventional drinking-water-treatment plant," *Science of the Total Environment*, vol. 329, no. 1–3, pp. 99–113, 2004.

[15] O. A. Jones, J. N. Lester, and N. Voulvoulis, "Pharmaceuticals: a threat to drinking water?" *Trends in Biotechnology*, vol. 23, no. 4, pp. 163–167, 2005.

[16] O. A. H. Jones, N. Voulvoulis, and J. N. Lester, "Aquatic environmental assessment of the top 25 English prescription pharmaceuticals," *Water Research*, vol. 36, no. 20, pp. 5013–5022, 2002.

[17] F. J. Beltrán, P. Pocostales, P. Alvarez, and A. Oropesa, "Diclofenac removal from water with ozone and activated carbon," *Journal of Hazardous Materials*, vol. 163, no. 2-3, pp. 768–776, 2009.

[18] M. Ernst and M. Jekel, *Advanced Treatment Combination for Groundwater Recharge of Municipal Wastewater by Nanofiltration and Ozonation*, Pergamon-Elsevier Science, 1999.

[19] A. Lopez, A. Bozzi, G. Mascolo, and J. Kiwi, "Kinetic investigation on UV and UV/H_2O_2 degradations of pharmaceutical intermediates in aqueous solution," *Journal of Photochemistry and Photobiology A*, vol. 156, no. 1–3, pp. 121–126, 2003.

[20] D. Vogna, R. Marotta, R. Andreozzi, A. Napolitano, and M. D'Ischia, "Kinetic and chemical assessment of the UV/H_2O_2 treatment of antiepileptic drug carbamazepine," *Chemosphere*, vol. 54, no. 4, pp. 497–505, 2004.

[21] M. M. Huber, A. Göbel, A. Joss et al., "Oxidation of pharmaceuticals during ozonation of municipal wastewater effluents: a pilot study," *Environmental Science and Technology*, vol. 39, no. 11, pp. 4290–4299, 2005.

[22] C. Zwiener and F. H. Frimmel, "Oxidative treatment of pharmaceuticals in water," *Water Research*, vol. 34, no. 6, pp. 1881–1885, 2000.

[23] J. L. Packer, J. J. Werner, D. E. Latch, K. McNeill, and W. A. Arnold, "Photochemical fate of pharmaceuticals in the environment: naproxen, diclofenac, clofibric acid, and ibuprofen," *Aquatic Sciences*, vol. 65, no. 4, pp. 342–351, 2003.

[24] L. A. Pérez-Estrada, M. I. Maldonado, W. Gernjak et al., "Decomposition of diclofenac by solar driven photocatalysis at pilot plant scale," *Catalysis Today*, vol. 101, no. 3-4, pp. 219–226, 2005.

[25] A. A. Cavalheiro, J. C. Bruno, M. J. Saeki, J. P. S. Valente, and A. O. Florentino, "Photocatalytic decomposition of diclofenac potassium using silver-modified TiO_2 thin films," *Thin Solid Films*, vol. 516, no. 18, pp. 6240–6244, 2008.

[26] L. Rizzo, S. Meric, D. Kassinos, M. Guida, F. Russo, and V. Belgiorno, "Degradation of diclofenac by TiO_2 photocatalysis: UV absorbance kinetics and process evaluation through a set of toxicity bioassays," *Water Research*, vol. 43, no. 4, pp. 979–988, 2009.

[27] F. Méndez-Arriaga, S. Esplugas, and J. Giménez, "Photocatalytic degradation of non-steroidal anti-inflammatory drugs with TiO_2 and simulated solar irradiation," *Water Research*, vol. 42, no. 3, pp. 585–594, 2008.

[28] J. Hartmann, P. Bartels, U. Mau et al., "Degradation of the drug diclofenac in water by sonolysis in presence of catalysts," *Chemosphere*, vol. 70, no. 3, pp. 453–461, 2008.

[29] V. Naddeo, V. Belgiorno, D. Ricco, and D. Kassinos, "Degradation of diclofenac during sonolysis, ozonation and their simultaneous application," *Ultrasonics Sonochemistry*, vol. 16, no. 6, pp. 790–794, 2009.

[30] V. Naddeo, V. Belgiorno, D. Kassinos, D. Mantzavinos, and S. Meric, "Ultrasonic degradation, mineralization and detoxification of diclofenac in water: optimization of operating parameters," *Ultrasonics Sonochemistry*, vol. 17, no. 1, pp. 179–185, 2010.

[31] V. Belgiorno, L. Rizzo, D. Fatta et al., "Review on endocrine disrupting-emerging compounds in urban wastewater: occurrence and removal by photocatalysis and ultrasonic irradiation for wastewater reuse," *Desalination*, vol. 215, no. 1–3, pp. 166–176, 2007.

[32] A. Antoniadis, I. Poulios, E. Nikolakaki, and D. Mantzavinos, "Sonochemical disinfection of municipal wastewater," *Journal of Hazardous Materials*, vol. 146, no. 3, pp. 492–495, 2007.

[33] V. Naddeo, V. Belgiorno, and R. M. A. Napoli, *Behaviour of natural organic matter during ultrasonic irradiation*, Elsevier Science, 2007.

[34] V. Naddeo, S. Meriç, D. Kassinos, V. Belgiorno, and M. Guida, "Fate of pharmaceuticals in contaminated urban wastewater effluent under ultrasonic irradiation," *Water Research*, vol. 43, no. 16, pp. 4019–4027, 2009.

[35] V. Naddeo, M. Landi, V. Belgiorno, and R. M. A. Napoli, "Wastewater disinfection by combination of ultrasound and ultraviolet irradiation," *Journal of Hazardous Materials*, vol. 168, no. 2-3, pp. 925–929, 2009.

[36] V. Naddeo, V. Belgiorno, M. Landi, T. Zarra, and R. M. A. Napoli, "Effect of sonolysis on waste activated sludge solubilisation and anaerobic biodegradability," *Desalination*, vol. 249, no. 2, pp. 762–767, 2009.

[37] P. Xu, M. L. Janex, P. Savoye, A. Cockx, and V. Lazarova, "Wastewater disinfection by ozone: main parameters for

process design," *Water Research*, vol. 36, no. 4, pp. 1043–1055, 2002.

[38] R. Chand, D. H. Bremner, K. C. Namkung, P. J. Collier, and P. R. Gogate, "Water disinfection using the novel approach of ozone and a liquid whistle reactor," *Biochemical Engineering Journal*, vol. 35, no. 3, pp. 357–364, 2007.

[39] Y. Zhang, S. U. Geißen, and C. Gal, "Carbamazepine and diclofenac: removal in wastewater treatment plants and occurrence in water bodies," *Chemosphere*, vol. 73, no. 8, pp. 1151–1161, 2008.

[40] H. Hoigne and H. Bader, "Rate constants of reactions of ozone with organic and inorganic compounds in water. II. Dissociating organic compounds," *Water Research*, vol. 17, no. 2, pp. 185–194, 1983.

[41] D. Vogna, R. Marotta, A. Napolitano, R. Andreozzi, and M. D'Ischia, "Advanced oxidation of the pharmaceutical drug diclofenac with UV/H_2O_2 and ozone," *Water Research*, vol. 38, no. 2, pp. 414–422, 2004.

Hindawi Publishing Corporation
International Journal of Photoenergy
Volume 2012, Article ID 305989, 6 pages
doi:10.1155/2012/305989

Research Article

Contribution of Dissolved Oxygen to Methylene Blue Decomposition by Hybrid Advanced Oxidation Processes System

Heon Lee,[1] Sung Hoon Park,[1] Byung Hoon Kim,[2] Sun-Jae Kim,[3] Sang-Chai Kim,[4] Seong-Gyu Seo,[5] and Sang-Chul Jung[1]

[1] *Department of Environmental Engineering, Suncheon National University, Suncheon, Jeonnam 540-742, Republic of Korea*
[2] *Department of Dental Materials, School of Dentistry, Chosun University, Gwangju 501-759, Republic of Korea*
[3] *Faculty of Nanotechnology and Advanced Materials Engineering, Sejong University, Seoul 143-747, Republic of Korea*
[4] *Department of Environmental Education, Mokpo National University, Muan, Jeonnam 534-729, Republic of Korea*
[5] *Department of Civil & Environmental Engineering, Chonnam National University, Yeosu, Jeonnam 550-749, Republic of Korea*

Correspondence should be addressed to Sang-Chul Jung, jsc@sunchon.ac.kr

Received 1 March 2012; Revised 3 May 2012; Accepted 17 May 2012

Academic Editor: Manickavachagam Muruganandham

Experimental results of photocatalysis under high dissolved oxygen (DO) concentration conditions are reported. Methylene blue was used as the organic pollutant to be degraded by a novel microwave/UV/DO/TiO_2 photocatalyst hybrid system. The degradation rate increased with TiO_2 nanoparticle dosages and DO concentration. However, inhibition of photocatalysis due to bubbles produced by DO generator was also observed. When the DO generator was used to increase the DO concentration in the pollutant solution treated by the microwave-assisted UV-TiO_2 photocatalysis, the decomposition rate constant was highest among all the experimental conditions tested in this study. This result demonstrated that high concentration of DO can enhance the photocatalytic reaction rate by causing a synergistic effect of constituent techniques.

1. Introduction

Conventional wastewater treatment technologies have limitations hence demanding advanced research to tackle complex wastewater treatment. One of the promising technologies could be the more effective destruction by the use of advanced oxidation processes (AOPs) [1]. Application of photocatalyst in AOP industry effluents treatment has been investigated widely [2].

TiO_2, a representative photocatalyst, has been successfully applied to the various photocatalytic reactions in a gas phase as well as in an aqueous phase [3]. Owing to its relatively high photocatalytic activity, biological and chemical stability, low cost, nontoxic nature, and long-term stability, TiO_2 has been widely used as a photocatalyst [4–6].

Application of TiO_2 photocatalyst in water treatment has recently been investigated widely [7]. There are still many problems yet to be solved, however, in application of TiO_2 photocatalyst in the treatment of non-biodegradable materials. First, photocatalysis has usually been used in air pollutants treatment because it is suitable for treatment of low-concentration pollutants. Concentrations of water pollutants, however, are much higher than those of air pollutants. Thus, their treatment by photocatalysis is difficult compared to that of air pollutants. Second, polluted water often contains mixture of hydrophilic and hydrophobic materials. Therefore, it is not easy for the pollutants to be adsorbed on the photocatalyst surface. Third, polluted water has high turbidity, hence, low transparency, hindering activation of photocatalysts by ultraviolet (UV) rays. Fourth, some materials are not easily degraded by photocatalysis only. Fifth, the amount of oxygen available for photocatalytic oxidation is very low in water compared to that in air. Due to these reasons, photocatalytic oxidation of water pollutants has not received large attention thus far. Recently, researches have been conducted actively to improve oxidative

degradation performance by adding microwave irradiation as an effort to utilize TiO_2 photocatalyst in water treatment more efficiently [8, 9].

On decomposition and mineralization, TiO_2 photocatalysis consumes O_2. In an earlier study on photocatalysis, this O_2 consumption was found to be "photo-adsorption" of O_2. The photoadsorption of O_2 has been a general term of the consumption of O_2 by photocatalytic reaction. Actually, photocatalytic reaction should proceed simultaneously by reduction and oxidation. In general photocatalysis, O_2 in air is reduced to give O_2^-, while organic compounds are oxidized to form organic radicals which consume O_2 as well for further oxidation [10–12].

In this study, the effect of dissolved oxygen (DO) on photocatalysis was investigated using a novel microwave/UV/DO/photocatalyst hybrid system. A microwave-assisted electrodeless lamp is used as the UV source. The effect of microwave irradiation on photocatalytic reaction efficiency is investigated. To improve the pollutant removal rate, further O_2 gas is added to the reaction and its effects on the reaction efficiency is investigated based on the experimental results. The role of each element technique and interaction among them are discussed.

2. Experimental Procedure

Figure 1 shows the schematic of the Microwave/UV-TiO_2 experimental apparatus used in this study. Microwave radiation was emitted from a microwave system manufactured by Korea microwave instrument Co. Ltd. It consisted of a microwave generator (frequency, 2.45 GHz; maximal power, 1 kW), a three-stub tuner, a power monitor, and a reaction cavity. Microwave radiation (actual power used, 200 ~ 600 W) used to irradiate the organic dye aqueous solution containing TiO_2 particles was delivered through a waveguide. Microwave irradiation was continuous and its intensity was adjusted by connection to a power monitor. Optimal low reflection of the microwave radiation was achieved using the three-stub tuner. A stirrer was installed on the back side in the reaction cavity (Figure 1) to enhance the transfer of microwave. As the microwave-irradiated reactant solution is heated steadily, it was not possible to carry out experiments at constant temperature without a cooling system. In this study, the reactant solution was stored in a stainless steel beaker installed in a constant-temperature equipment. A pump in the DO generator was used to circulate the heated reactant solution through a cooling system to keep the reaction temperature constant at 298 K.

In order to assess the effect of DO on TiO_2 photocatalysis, DO concentration in the reaction solution was varied between 30 and 70 ppm using a DO generator (OxyLife Co.). O_2 microbubbles were generated into the reaction solution inflow using a helix-type bubble generator installed in the DO generator tank. The DO concentration in the solution increased further while the solution passed devices with inner diameters smaller than that of the circulation pipe in the generator, due to increased flow velocity and friction coefficient. DO concentration was adjusted by using different combinations of the devices through which the solution passed.

Table 1: Comparing the UV intensities radiated at different microwave intensities.

Microwave intensity (kW)	UV intensity (W/m^2)		
	UV-A	UV-B	UV-C
0.2	0.221	0.364	3.750
0.4	0.577	0.922	5.570
0.6	1.213	1.845	5.930

TiO_2 photocatalysts are excited by UV light, producing strong oxidants that can degrade organic compounds. Therefore, provision of UV is essential for a use of TiO_2 photocatalysts. Typical UV lamps, however, have metal electrodes, which prevent them from being used in the microwave-irradiation equipment. Therefore, a double-tube-type microwave discharge electrodeless lamp (170 mm length, 44 mm inner diameter, 60 mm outer diameter, hereafter MDEL) which emits UV upon the irradiation of microwave was developed in this study. It was made of quartz to maximize the reaction efficiency. Small amount of mercury was doped between the tubes inside the double-tube UV lamp that was kept vacuumed. The lamp used in this study is UV-C-type lamp although little amount of UV-A and UV-B wavelength lights are emitted as well. Figure 2 shows the MDEL emitting UV light upon microwave irradiation in the microwave cavity. Another measurement made in this study was the irradiance (W/m^2) measured at three different UV wavelength ranges that are called UV-A, UV-B, and UV-C with the wavelength range of 315 ~ 400 nm, 280 ~ 315 nm, and 220 ~ 280 nm, respectively. A UV radiometer (HD2102-2, Delta OHM) was used to measure the irradiance. Table 1 summarizes the UV irradiance measured with three different microwave intensities. The UV irradiances at all three wavelength ranges were shown to increase with the microwave intensity.

The photocatalyst was Degussa P-25 TiO_2 (specific surface area 53 $m^2\ g^{-1}$ measured by the BET method, particle size 20 ~ 30 nm by TEM, composition 83% anatase and 17% rutile by X-ray diffraction). In this study, the photocatalytic activity of TiO_2 particle was investigated with the photocatalytic decomposition of methylene blue (referred to as MB hereafter) in its aqueous solution. High-purity-grade MB was purchased from Jin Chem. Co. Ltd. Initial concentration of MB was about 3.0×10^{-5} mol/liter, and 3,000 mL of solution was circulated into the quartz reactor tube (230 mm length, 40 mm diameter) with a flow rate of 500 cc/min.

The solution contained in a stainless steel beaker located in a cooling bath was circulated through the reactor and DO generator for 60 minutes to maintain the initial reactant concentration at constant. P25 (0.1 ~ 0.3 g) was injected into the beaker, and then the solution was circulated for another 5 minutes to disperse P25 throughout the entire system. TiO_2 photocatalysis was performed by irradiating microwave and UV using the microwave generator (0.2/0.4/0.6 Kw). The

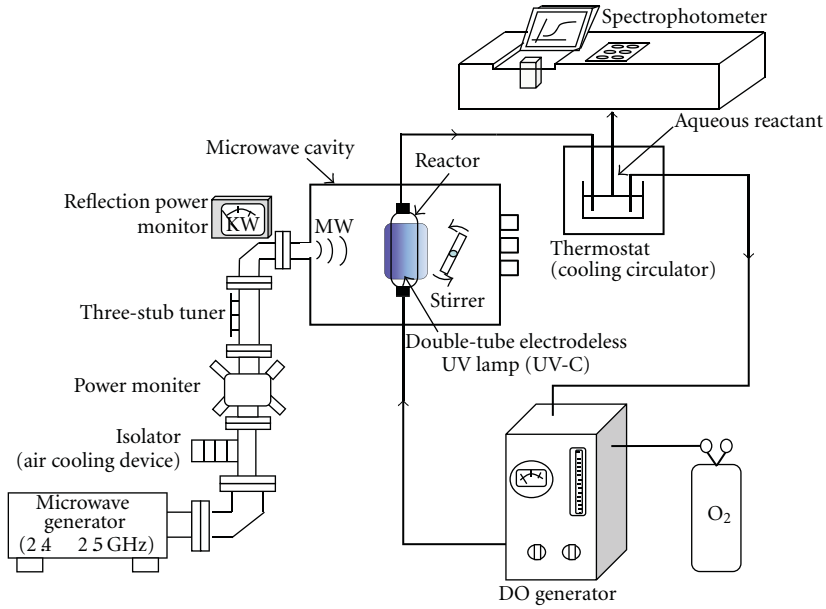

Figure 1: Schematics of the microwave/UV/DO TiO_2 photocatalytic degradation system.

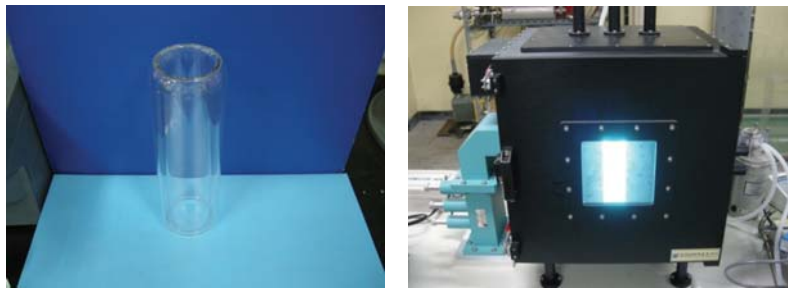

(a) (b)

Figure 2: Snapshot of the double-tube-type MDEL (a) and microwave-discharged lamp set in the microwave oven (b).

solution samples taken at predefined time steps were centrifuged at 2,000 rpm for 30 minutes. Then, the absorbance of supernatant was measured using a spectrophotometer (UV-1601, Shimadzu) at 665 nm to obtain the reaction rate. The solution samples used for absorbance measurements were injected back into the reaction system.

3. Result and Discussion

3.1. Effect of TiO_2 Particle Dosages. Figure 3 shows the results of decomposition experiments of MB obtained at different TiO_2 particle dosages. The microwave intensity was 0.4 kW, and the DO concentration was 70 ppm. Addition of a larger amount of TiO_2 particle resulted in a higher decomposition rate. Certain amount of MB was shown to be decomposed by MDEL and high concentration of DO without the aid of TiO_2 photocatalytic reaction. The plots for the four cases were all fitted well by linear line, which indicates that decomposition of MB in the presence of TiO_2 catalyst can be approximated by a pseudo-first-order reaction model:

$$\frac{C}{C_0} = \exp(-Kt), \tag{1}$$

where C is the MB concentration at time t, C_0 the initial concentration, and K the overall rate constant. The overall rate constant K is determined as the slope of the line in Figure 3 by regression analysis. It is clearly shown in this figure that the degradation rate increases with the amount of TiO_2 particle dosages.

3.2. Relationship between the Degradation Rate and DO Levels. The rates of MB degradation by TiO_2 photocatalytic reaction

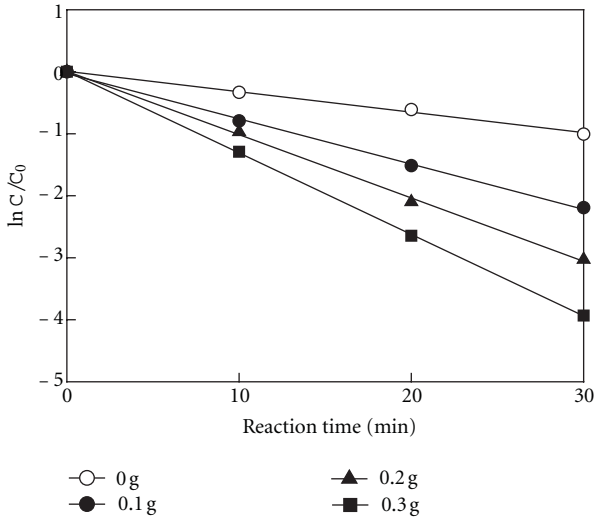

Figure 3: Effect of TiO_2 particle dosages for decomposition of methylene blue in aqueous solutions.

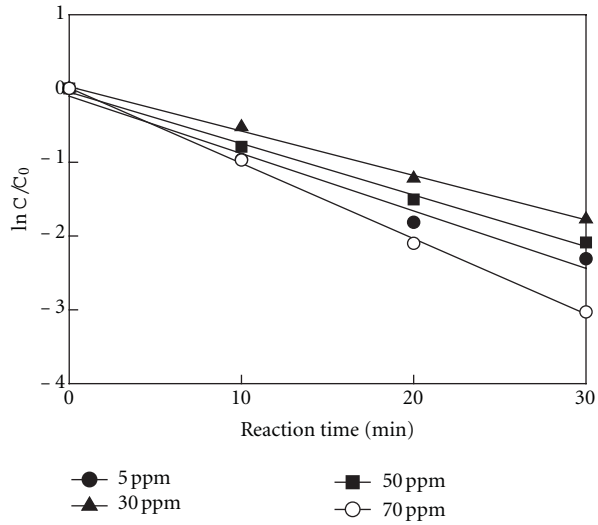

Figure 4: Degradation rate of methylene blue measured at various dissolved oxygen levels.

measured at different DO concentration levels (5 ~ 70 ppm) are shown in Figure 4. The average DO concentration of the as-prepared MB solution without using DO generator was about 5 ppm. All experiments were carried out under the microwave intensity of 0.4 kW and the TiO_2 particle dosage of 0.2 g. When the DO generator was used to adjust the DO concentration between 30 and 70 ppm, the degradation rate was shown to increase with DO concentration. However, the degradation rates measured at 30 ppm and 50 ppm were lower than that measured without using the DO generator (at 5 ppm). This result may be attributed to the inhibition effect of the bubbles. In this study, high-pressure oxygen gas was injected into the DO generator in which the oxygen bubbles were produced by the helix-type bubble generator. In general, photocatalysis is a surface reaction. Bubbles produced by the DO generator may be attached on the photocatalyst surface inhibiting the surface reaction. Nevertheless, when DO concentration was high enough (70 ppm), the degradation rate was higher than that measured without using the DO generator. Moreover, a higher DO concentration resulted in a higher degradation rate among the experiments in which a DO generator was used. This result indicates that dissolved oxygen promotes the photocatalytic decomposition of MB.

The effect of dissolved oxygen can be explained as follows. UV irradiated on TiO_2 photocatalysts causes excitation, leading to movement of electrons in the valance band towards the conduction band. If the reaction does not follow immediately, recombination occurs. By playing a role as electron capturers, oxygen molecules can slow down the recombination rate and help produce peroxide and hydroperoxy radicals and therefore enhance the degradation reaction rate [13].

The results of this study showed that the use of a DO generator may result in inhibition of photocatalysis due to attachment of bubbles on the catalyst surface. Therefore, when a DO generator is applied for enhancing the photocatalysis rate, high concentration of DO, enough to compensate the side effect of bubble attachment, is required.

3.3. Microwave Effects in Photocatalytic Oxidation Reactions. MB decomposition experiments were carried out at different microwave intensity levels to evaluate the effect of microwave intensity on photocatalysis. The results are shown in Figure 5 as a function of microwave intensity. The experiments were carried out with the 0.2 g TiO_2 particle at 70 ppm DO concentration. Three different microwave powers were used: 0.2, 0.4, and 0.6 kW. It is clearly shown in this figure that the degradation rate increases with microwave intensity. Microwave causes polar reactant molecules to vibrate million times a second. Microwave has thermal and nonthermal effects. The thermal effect denotes the increase in the chemical reaction rate due to selective, fast, uniform increase of temperature by microwave radiation. The nonthermal effect represents the promotion of the chemical reaction resulting from increased molecular movement and collision frequency. In this study, temperature was controlled at constant to exclude the thermal effect. Therefore, the increase in the degradation rate by the microwave irradiation is believed to result from the resulting UV radiation and the non-thermal effect of microwave.

In this study, a short wavelength electromagnetic wave UV is emitted by MDEL upon the irradiation of microwave. Therefore, the intensity of UV increases with the microwave power. UV, which carries intense energy, is used for exciting photocatalyst. It can also contribute to degrading MB directly. It was not possible to figure out the detailed mechanism how microwave took part in the degradation of MB. Nevertheless, it can be inferred from the experimental result, which showed higher degradation efficiency at higher

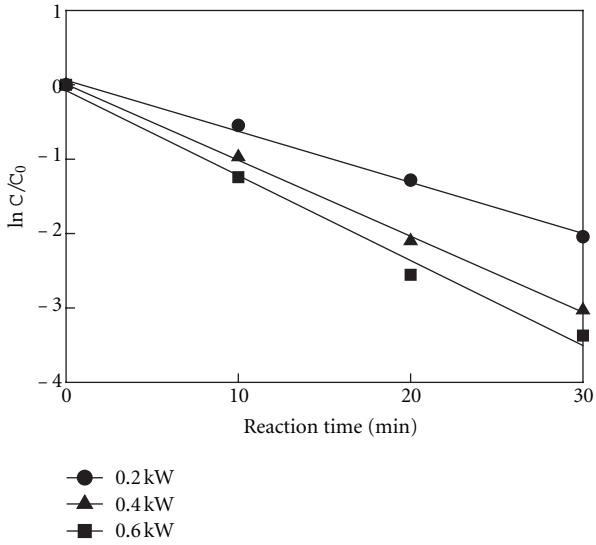

Figure 5: Effect of microwave intensity for decomposition of methylene blue in aqueous solution.

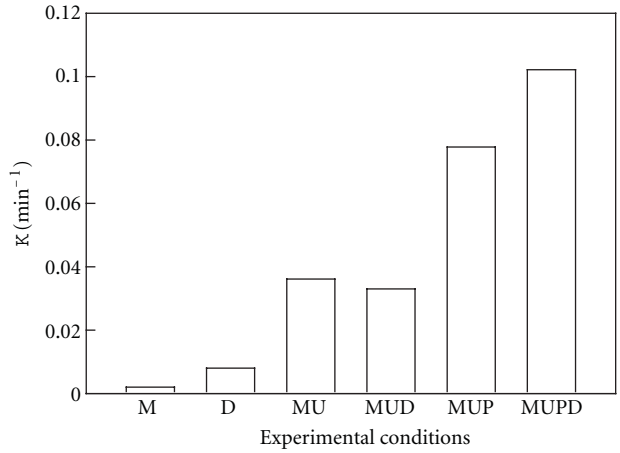

Figure 6: Rate constants obtained under different experimental conditions.

microwave intensity, that microwave contributed to degradation of MB indirectly by increasing UV intensity. The thermal and non-thermal effects of microwave are also presumed to have contributed directly to the degradation reaction.

3.4. Comparison of the Effects of the Constituent Techniques. This study was aimed at enhancing the photocatalytic degradation rate of MB by adding microwave and high-concentration DO. To evaluate the effect of each constituent technique, different sets of combinations of microwave, DO, UV, and photocatalyst were used for degradation of organic dye. Figure 6 shows the degradation rate constants obtained at different conditions of the microwave/UV/DO/photocatalyst hybrid process system. The amount of reaction solution of 3,000 mL, DO concentration of 70 ppm, and the microwave intensity of 0.4 kW were used for all experiments. The results of six different experiments are compared in Figure 6: microwave irradiation only (M), DO generator only (D), microwave irradiation on top of the use of MDEL (MU), addition of DO generator to MU (MUD), microwave-assisted UV-TiO_2 photocatalysis by MDEL (MUP), and addition of DO generator to MUP (MUPD).

When only microwave was applied (M), MB was seldom degraded because the thermal effect was excluded in this study by maintaining the temperature of the solution at 298 K. On the other hand, when only DO generator was used (D) to adjust the DO concentration at 70 ppm, certain level of degradation reaction was detected. When microwave and MDEL were used together (MU), the degradation rate was significantly higher. As the DO generator was added to MU (MUD) to increase the DO concentration, the degradation rate was reduced. This result can be attributed to the inhibition effect of the bubbles produced by DO generator as was explained above. For the microwave-assisted UV-TiO_2 photocatalysis (MUP), the decomposition rate constant was very high. When the DO generator was added to MUP (MUPD), the rate constant was even higher. This result demonstrates that high concentration of DO can enhance the photocatalytic reaction rate by causing a synergistic effect of constituent techniques.

The results of this study show that combining elemental techniques, which are not very efficient when they are used exclusively, induce a synergistic effect. The objective of this study was to promote the photocatalytic reaction by adding microwave irradiation, which was expected to activate pollutant and photocatalyst, and high-concentration DO, as an auxiliary oxidant, to the conventional photocatalysis system. According to the experimental results of this study, the influence of microwave on organic dye and photocatalyst was minimal, whereas high-concentration DO was shown to contribute to production of activation species that participate in the degradation reaction. Inhibition of photocatalysis due to bubbles produced by DO generator was also observed, indicating that care should be taken to find an optimal hybrid process for practical use.

The above-mentioned explanations, however, cannot be proven with the limited experimental data obtained in this study. More precise and quantitative analyses on the elemental techniques tested in this study are required in the future for more reliable evaluation and application of them.

4. Conclusions

The following conclusions were inferred from the results of advanced oxidation of MB by novel microwave/UV/DO/TiO_2 photocatalysts hybrid process system.

(1) The degradation rate increased with TiO_2 particle dosages, microwave intensity and DO concentration.

(2) When a DO generator was used to adjust the DO concentration between 30 and 70 ppm, the degradation

rate was shown to increase with DO concentration. However, the degradation rates measured at 30 ppm and 50 ppm were lower than that measured without using the DO generator (at 5 ppm).

(3) The result demonstrates that high concentration of DO can enhance the photocatalytic reaction rate by causing a synergistic effect of constituent techniques.

(4) The results of this study showed that the use of a DO generator may result in inhibition of photocatalysis due to attachment of bubbles on the catalyst surface. Therefore, when a DO generator is applied for enhancing the photocatalysis rate, high concentration of DO, enough to compensate the side effect of bubble attachment, is required.

Acknowledgment

This research was supported by the Basic Science Research Program through the National Research Foundation of Korea (NRF) funded by the Ministry of Education, Science and Technology (2010-0007412 and 2011-0016699).

References

[1] W. F. Jardim, S. G. Moraes, and M. M. K. Takiyama, "Photocatalytic degradation of aromatic chlorinated compounds using TiO_2: toxicity of intermediates," *Water Research*, vol. 31, no. 7, pp. 1728–1732, 1997.

[2] P. Saritha, C. Aparna, V. Himabindu, and Y. Anjaneyulu, "Comparison of various advanced oxidation processes for the degradation of 4-chloro-2 nitrophenol," *Journal of Hazardous Materials*, vol. 149, no. 3, pp. 609–614, 2007.

[3] R. W. Matthews, "Photo-oxidation of organic material in aqueous suspensions of titanium dioxide," *Water Research*, vol. 20, no. 5, pp. 569–578, 1986.

[4] A. Dixit, A. J. Tirpude, A. K. Mungray, and M. Chakraborty, "Degradation of 2, 4 DCP by sequential biological-advanced oxidation process using UASB and UV/TiO_2/H_2O_2," *Desalination*, vol. 272, no. 1–3, pp. 265–269, 2011.

[5] S. C. Jung, S. J. Kim, N. Imaishi, and Y. I. Cho, "Effect of TiO_2 thin film thickness and specific surface area by low-pressure metal-organic chemical vapor deposition on photocatalytic activities," *Applied Catalysis B*, vol. 55, no. 4, pp. 253–257, 2005.

[6] S. C. Jung, "Photocatalytic activities and specific surface area of TiO_2 films prepared by CVD and sol-gel method," *Korean Journal of Chemical Engineering*, vol. 25, no. 2, pp. 364–367, 2008.

[7] M. Harir, A. Gaspar, B. Kanawati et al., "Photocatalytic reactions of imazamox at TiO_2, H_2O_2 and TiO_2/H_2O_2 in water interfaces: kinetic and photoproducts study," *Applied Catalysis B*, vol. 84, no. 3-4, pp. 524–532, 2008.

[8] G. Zhanqi, Y. Shaogui, T. Na, and S. Cheng, "Microwave assisted rapid and complete degradation of atrazine using TiO_2 nanotube photocatalyst suspensions," *Journal of Hazardous Materials*, vol. 145, no. 3, pp. 424–430, 2007.

[9] S. C. Jung, "The microwave-assisted photo-catalytic degradation of organic dyes," *Water Science and Technology*, vol. 63, no. 7, pp. 1491–1498, 2011.

[10] T. Hirakawa, C. Koga, N. Negishi, K. Takeuchi, and S. Matsuzawa, "An approach to elucidating photocatalytic reaction mechanisms by monitoring dissolved oxygen: effect of H_2O_2 on photocatalysis," *Applied Catalysis B*, vol. 87, no. 1-2, pp. 46–55, 2009.

[11] H. C. Liang, X. Z. Li, Y. H. Yang, and K. H. Sze, "Effects of dissolved oxygen, pH, and anions on the 2,3-dichlorophenol degradation by photocatalytic reaction with anodic TiO_2 nanotube films," *Chemosphere*, vol. 73, no. 5, pp. 805–812, 2008.

[12] C. C. Lo, C. W. Huang, C. H. Liao, and J. C. S. Wu, "Novel twin reactor for separate evolution of hydrogen and oxygen in photocatalytic water splitting," *International Journal of Hydrogen Energy*, vol. 35, no. 4, pp. 1523–1529, 2010.

[13] M. R. Hoffmann, S. T. Martin, W. Choi, and D. W. Bahnemann, "Environmental applications of semiconductor photocatalysis," *Chemical Reviews*, vol. 95, no. 1, pp. 69–96, 1995.

Hindawi Publishing Corporation
International Journal of Photoenergy
Volume 2012, Article ID 398787, 7 pages
doi:10.1155/2012/398787

Research Article

Rapid Photocatalytic Degradation of Methylene Blue under High Photon Flux UV Irradiation: Characteristics and Comparison with Routine Low Photon Flux

Qian Zhang, Chaolin Li, and Ting Li

Environmental Science & Engineering Research Center, Shenzhen Graduate School, Harbin Institute of Technology, Shenzhen 518055, China

Correspondence should be addressed to Chaolin Li, lichaolinhit@gmail.com

Received 9 January 2012; Accepted 29 February 2012

Academic Editor: Manickavachagam Muruganandham

This study examined the photocatalytic degradation efficiency under high UV photon flux (intensity normalized by photon energy) irradiation; the incident UV photon flux was 1.71×10^{-6}–3.13×10^{-6} einstein $cm^{-2}\,s^{-1}$ made by a super high-intensity UV apparatus. A comparative study between high photon flux photocatalytic process and routine low photon flux photocatalytic process for methylene blue degradation has been made in aqueous solution. The experimental results showed that under the best conditions of high UV photocatalytic reaction 99% decolorization and 95% TOC removal of 20 mg L^{-1} methylene blue could be achieved in 30 s and 120 s of UV irradiation time, respectively. To the best of our knowledge, photocatalytic decolorization and photocatalytic degradation of dyes in such a short time has not been reported. Aiming at the low photonic efficiency in high photon flux photocatalytic process, we found that reducing the density of excited electron-hole appropriately could improve initial apparent photonic efficiency effectively. The TOC experiments under high UV photon flux showed a faster mineralization rate and a different mineralization process compared to that under low UV photon flux.

1. Introduction

Heterogeneous photocatalytic oxidation has potential applications for the treatment of waste water with dilute concentration of organic compounds because it effectively oxidizes a large number of chemical pollutants [1]. Among the most popular semiconductors studied, TiO_2 is one of the best candidates [2]. However, the commercial application of this method for the treatment of aqueous solutions is limited by both the long time of the process and the low efficiency in the use of the radiation [3]. If TiO_2 photocatalysis is to have a commercial future as a method for water purification, reaction time must compare favorably with those of its competitors (UV/H_2O_2, UV/O_3, photo Fenton, etc.). On this basis, many studies have been conducted to improve the photocatalytic reaction rate such as the doping of some elements or compounds into TiO_2 [4], increasing the external surface area [5], improving photocatalytic reactor design [6], and so forth. Light photon flux (intensity normalized by photon energy) is one of the most parameters in photocatalytic reaction, and high UV intensity could compensate for the low photocatalytic efficiency of TiO_2 itself [7]. Ollis et al. [8] observed that the relationship between UV intensity and degradation rate changed from first order ($K \propto I$) to half order ($K \propto I^{0.5}$) when the UV intensity increased beyond a certain value (approximately 25 mW cm^{-2}), and then changed from half order ($K \propto I^{0.5}$) to zero order ($K \propto I^{0}$) when the UV intensity reached a high level. Many similar studies have confirmed this finding [9–11]. Because the efficiency of photocatalytic reaction declines under extremely high UV intensity, the application of improving photocatalytic reaction rate by increasing UV intensity is not fully developed. However, the high photon flux UV irradiation can effectively lessen the photocatalytic reaction time [12]; therefore, it is important to improve the understanding of the high UV intensity photocatalytic reaction and to increase UV light efficiency of the reaction.

The aim of this paper was to determine the effectiveness of photocatalytic processes based on high photon flux irradiation ranging from 1.71×10^{-6} to 3.13×10^{-6} einstein $cm^{-2}\,s^{-1}$ (approximately UV intensity from 550 to 1000 $mW\,cm^{-2}$) in the photocatalytic degradation of a typical basic dye, methylene blue (MB), from aqueous solution. The operating conditions were adjusted to permit a comparison between high UV photon flux photocatalytic process (HUP) and routine low UV photon flux photocatalytic process (LUP) (photon flux ranging 0.667×10^{-9} to 3.07×10^{-9} einstein $cm^{-2}\,s^{-1}$ approximately equal to UV intensity from 0.4 to 2 $mW\,cm^{-2}$). Three different criteria were used to contrast both processes: (i) reaction rate and reaction time, (ii) the initial apparent photonic efficiency, and (iii) mineralization rate and mineralization degree.

2. Material and Methods

2.1. Materials and Reagents. The photocatalyst was titania Degussa P-25 (anatase/rutile = 7/3, surface area = 50 $m^2\,g^{-1}$, nonporous particles, mean size = 30 nm). MB was obtained from Hongyan chemical Co., Ltd., (≥99%). Potassium ferrioxalate was obtained from Hefei Asialon chemical Co., Ltd., (≥99%). Solutions were prepared using water from a Millipore Waters Milli-Q purification unit.

2.2. Light Source and Photoreactor. Two kinds of UV lamp were used: (a) a 250 W UV high pressure mercury lamp (Ushio Inc, Japan) with a quartz reflector were used as a high photon flux light source. The incident photon flux entering the photoreactor was varied from 1.71×10^{-6} to 3.13×10^{-6} einstein $cm^{-2}\,s^{-1}$. (b) An 8 W black light lamp (Philips TL 6W/08) was used as a low photon flux light source. The incident photon flux entering the photoreactor was varying from 0.667×10^{-9} to 3.07×10^{-9} einstein $cm^{-2}\,s^{-1}$. The spectral distributions of both lamps are shown in Figure 1.

The schematic diagram of the photoreactor apparatus is shown in Figure 2. All the irradiation experiments were conducted in a glass cylinder of 35.6 mm diameter and 45 mm height. The top of the glass cylinder was open to the atmosphere. The lamp was placed at the focal axis of the quartz reflector and an optical filter was inserted to cut off the long wavelength components ($\lambda > 425$ nm) for avoiding heating the aqueous solution (no quartz reflector and optical filter for the black light lamp). A sliding shutter with electronic time switch was used to determine exactly the moment at which the photocatalytic reaction started or ended. Between the lamp and the reactor, there are neutral density filters of different transmissions to change the photon flux of the incident irradiation on the reactor. Different photon fluxes were measured inside the reactor cylinder using potassium ferrioxalate method [13]. A magnetic stirrer located at the bottom of the glass cylinder kept the TiO_2 particles suspended during the irradiation. The photoreactor, the reflector, and the lamp were enclosed in a box to ensure safe operation and to prevent the entrance of extraneous light.

2.3. Experiments Procedure. All experiments were in the following range of the experimental variables: the incident photon flux of the high photon flux light source was between 1.71×10^{-6} and 3.13×10^{-6} einstein $cm^{-2}\,s^{-1}$; the incident photon flux of the low photon flux light source was between 0.667×10^{-9} and 3.07×10^{-9} einstein $cm^{-2}\,s^{-1}$; temperature 25°C (room temperature); MB initial concentration 20 $mg\,L^{-1}$; TiO_2 concentration between 0.25 $g\,L^{-1}$ and 1.5 $g\,L^{-1}$.

Each run adhered to the following protocol: (i) the lamp was turned on, allowing for 40 min to stabilizing their operation, and a suspension of TiO_2 and MB was mixed well in the dark at least 60 min for reaching an equilibrated adsorption as steady-state concentrations. (ii) 10 mL of MB solution was injected in the photoreactor. (iii) The solution was then irradiated by UV light and sample was collected at specific time to measure the MB concentration. (iv) Simple suspensions were filtered by a 0.45 μm membrane filter to remove the TiO_2 powder. Samples at different reaction time were obtained by repeating steps (ii), (iii), and (iv). The decolorization efficiency was tested in terms of the changes of the UV-vis absorbance of MB. The absorbance intensity of MB was determined by an UV-vis spectrophotometer (UV-2450 SHIMADZU) with a 1 cm path length spectrometric quartz cell. Total organic carbon (TOC) was analyzed with a total organic carbon analyzer (Analytik Jena multi-N/C 3100).

3. Results and Discussion

3.1. Preliminary Tests. Preliminary tests using different experimental conditions were carried out to make sure that the dye degradation was mainly due to the photocatalytic reaction. The results are as follows. The MB concentration decreased about 4% in the darkness in the presence of TiO_2. This suggests a weak adsorption of the dye molecules on TiO_2. In the absence of TiO_2, the MB concentration decreased about 1% under low photon flux irradiation (3.07×10^{-9} einstein $cm^{-2}\,s^{-1}$) after 1 h and the MB concentration almost remained unchanged at high photon flux irradiation (3.13×10^{-6} einstein $cm^{-2}\,s^{-1}$) after 60 s. This indicates that the dye degradation by the direct photolysis only is unimportant. Therefore, the reduction of dye concentration is primarily caused by the photocatalytic reaction.

3.2. UV Irradiation Intensity and Irradiation Time. In order to compare different UV irradiation intensities and irradiation times on the rate of photocatalytic decolourization, a set of tests was carried out in both HUP and LUP, and the results are shown in Figures 3(a) and 3(b). In all cases, MB was removed rapidly from the beginning and as time elapsed the decolorization rate decreased. The decolorization percentage of MB was >90% in reaction time 15 s and >99% in 30 s in HUP with a UV photon flux 3.13×10^{-6} einstein $cm^{-2}\,s^{-1}$ (Figure 3(a)), whereas the decolorization percentage of MB was >90% in 40 min and >96% in 60 min in LUP with a UV photon flux 3.07×10^{-9} einstein $cm^{-2}\,s^{-1}$ (Figure 3(b)). It is clear that increasing the UV photon flux enhances the rate of decolorization remarkably.

Figures 3(a) and 3(b) also show that the plots of $\ln(C/C_0)$ versus irradiation time for HUP and LUP were linear, which suggest that both the photocatalytic processes approximately

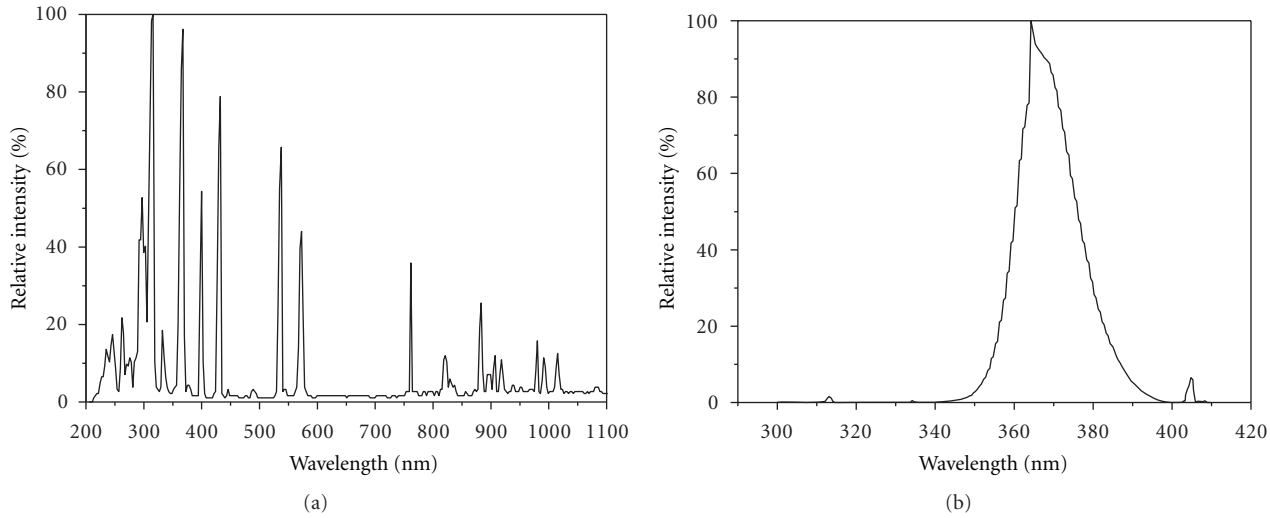

Figure 1: UV spectra of 250 W UV high pressure mercury lamp (a) and 8 W black light lamp (b).

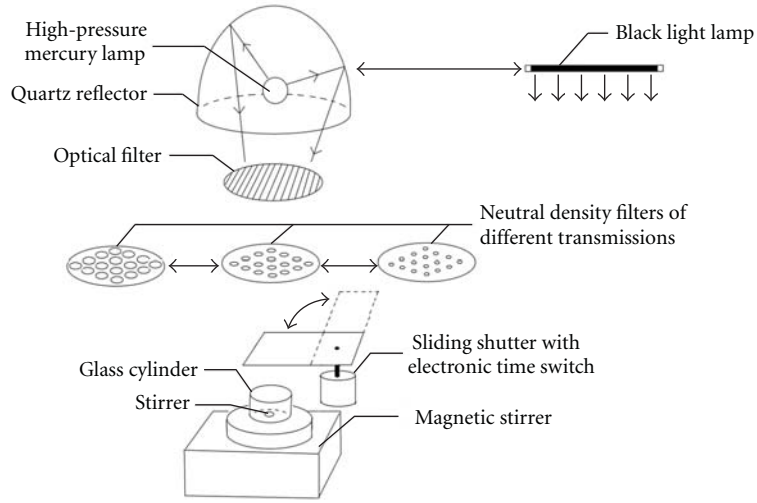

Figure 2: Schematic diagram of the photoreactor apparatus.

follow pseudo-first-order kinetics. Rate constants were estimated from the slopes of $\ln(C/C_0)$ versus time. The pseudo-first-order constants for HUP with photon fluxes 1.71×10^{-6}, 1.99×10^{-6}, 2.28×10^{-6}, 2.56×10^{-6}, 2.85×10^{-6}, and 3.13×10^{-6} einstein $cm^{-2}\,s^{-1}$ were 0.1103, 0.1182, 0.1245, 0.1334, 0.1421, and $0.1513\,s^{-1}$, and for LUP with photon fluxes 0.667×10^{-9}, 1.03×10^{-9}, 1.33×10^{-9}, 1.71×10^{-9}, 2.28×10^{-9}, 3.07×10^{-9} einstein $cm^{-2}\,s^{-1}$ were 2.5×10^{-4}, 3.8×10^{-4}, 5.1×10^{-4}, 6.6×10^{-4}, 8.5×10^{-4}, $1.1 \times 10^{-3}\,s^{-1}$, respectively. We suggest that the significant improvement in MB decolorization is mainly due to the more hydroxyl radicals that are produced by more radiations falling on the catalyst surface [14].

There were two different reaction rate regimes as a function of UV photon flux by different UV lamps. It is found that the reaction rate depends on photon flux of UV light I in a power law [8] such as

$$r = r'' I^{\alpha}, \tag{1}$$

where r' is the reaction constant independent of photon flux. The exponent value (α) could be estimated from the reaction rates and photon fluxes. The value (α) is 0.512 for HUP and 0.9813 for LUP. Both of the values (α) show good fits with the data and the correlation coefficients are $R^2 = 0.9906$ $R^2 = 0.9977$, respectively. These results indicate that in our experiment the photocatalytic decolorization rate increases with the square root of photon flux under high photon flux in the range from 1.71×10^{-6} to 3.13×10^{-6} einstein $cm^{-2}\,s^{-1}$and the photocatalytic degradation rate increase linearly with photon flux under low photon

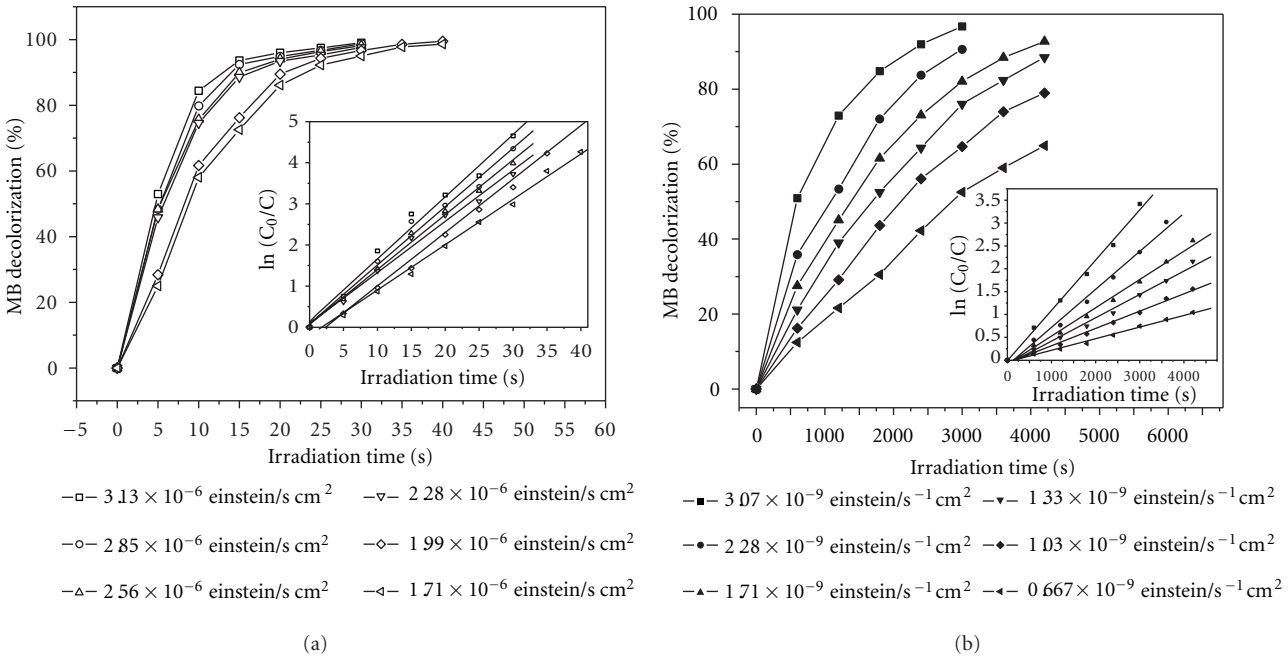

Figure 3: Photocatalytic decolorization of MB versus irradiation time by (a) HUP and (b) LUP. (Experimental conditions: TiO_2, 1 g L^{-1}; MB initial concentration 20 mg L^{-1}).

flux in the range from 0.667×10^{-9} to 3.07×10^{-9} einstein $cm^{-2}\,s^{-1}$. The tendency of the effect by photon flux is in agreement with some studies, and in these reports the authors attributed this to electron-hole recombination [9–11]. The rate of electron-hole formation exceeds the rate photocatalytic oxidation under high photon flux, resulting in electron-hole recombination [9–11, 14].

3.3. Initial Apparent Photonic E ciency. The photonic efficiency (ξ) describing the effectiveness of light conversion to product in heterogeneous, light scattering systems, is directly proportional to the quantum yield and may be considered to be the lower limit of this more commonly used measure of light [15].

In our case, the initial apparent photonic efficiency was calculated from the ratio of the initial reaction rate of photooxidation (mol $L^{-1}\,s^{-1}$) to the rate of incident photons reaching the reactor as obtained by chemical actinometry (einstein $L^{-1}\,s^{-1}$) [16].

Table 1 summarizes initial apparent photonic efficiencies of photocatalytic decolorization of MB for HUP and LUP. The initial apparent photonic efficiencies at high photon fluxes were lower than the case of low photon fluxes, which illustrated that high photon fluxes photocatalytic processes had lower light energy utilization efficiency. This result satisfies the law that the initial apparent photonic efficiency decreases as the light intensity increases, and this is in agreement with other authors [17, 18].

The explanation of the lower initial apparent photonic efficiencies is that high photon flux causes lower effect on reaction rate (from first order ($r \propto I$) to half order ($r \propto I^{0.5}$) in Section 3.2), and therefore decreases the initial apparent photonic efficiency. At low light intensity reactions involving electron-hole separation were predominant and electron-hole recombination was negligible, whereas at increased light intensity electron-hole pair separation competed with recombination, thereby causing lower influence on initial apparent photonic efficiency [9–11, 14]. Based on this theory, we infer that the decreasing of the TiO_2 concentration properly may decrease the density of excited electron-hole pairs, and thereby ease the electron-hole recombination in high photon flux photocatalytic reaction. As a test of the hypothesis, we examined the relationship between the TiO_2 concentration and the initial apparent photonic efficiency under both low and high photon flux. And we kept constant the product of TiO_2 concentration and the optical path length in different volume sample in order to modify

Table 1: Relative photonic efficiencies of photocatalytic degradation of MB under different photon fluxes.

High photon flux photocatalytic process		Low photon flux photocatalytic process	
Photon flux (10^{-6} einstein $cm^{-2}\,s^{-1}$)	Relative photonic efficiencies (%)	Photon flux (10^{-9} einstein $cm^{-2}\,s^{-1}$)	Relative photonic efficiencies (%)
3.13	0.302	3.07	2.23
2.85	0.311	2.28	2.33
2.56	0.325	1.71	2.41
2.28	0.341	1.33	2.40
1.99	0.371	1.03	2.37
1.71	0.403	0.667	2.43

the TiO_2 concentration without changing the total amount of TiO_2.

Series of experiments were designed as follows: (i) sample optical path length 0.67 cm, sample volume 6.7 mL, TiO_2 concentration 1.5 g L^{-1}, MB concentration 20 mg L^{-1}; (ii) sample optical path length 1 cm, sample volume 10 mL, TiO_2 concentration 1 g L^{-1}, MB concentration 20 mg L^{-1}; (iii) sample optical path length 2 cm, sample volume 20 mL, TiO_2 concentration 0.5 g L^{-1}, MB concentration 20 mg L^{-1}; (iv) sample optical path length 3 cm, sample volume 30 mL, TiO_2 concentration 0.33 g L^{-1}, MB concentration 20 mg L^{-1}; (v) sample optical path length 4 cm, sample volume 40 mL, TiO_2 concentration 0.25 g L^{-1}, MB concentration 20 mg L^{-1}; (vi) sample optical path length 5 cm, sample volume 50 mL, TiO_2 concentration 0.20 g L^{-1}, MB concentration 20 mg L^{-1}; (vii) sample optical path length 6 cm, sample volume 60 mL, TiO_2 concentration 0.17 g L^{-1}, MB concentration 20 mg L^{-1}; (viii) sample optical path length 7 cm, sample volume 70 mL, TiO_2 concentration 0.14 g L^{-1}, MB concentration 20 mg L^{-1}. As optical path length changed, adjusted the height of photoreactor to keep a constant distance between light source and the solution surface, which maintained a constant photon flux in each experiment. Experiments were carried out under both high and low photon flux. The initial apparent photonic efficiencies under these conditions are summarized in Table 2. It could be clearly observed that under low photon flux the initial apparent photonic efficiency steadily decreased with optical path length. On the contrary, under high photon flux, initial apparent photonic efficiency firstly increased with the increase of optical path length from 0.67 to 3 cm. When the optical path length increased further than 3 cm, the initial apparent photonic efficiency decreased. The results in low photon flux experiments are mainly due to the fact that long path lengths will promote absorbance of light by MB and other solution chemicals, as the Lambert-Beer law states. And this is in agreement with other reports [19]. In high photon flux experiments, as the optical path length increased from 0.67 to 3 cm, the absorption of UV by MB and other solution chemicals also increased with the optical length path. However, instead of decreasing, the initial apparent photonic efficiency increased. We deduce that the increase of initial apparent photonic efficiency is probably due to the decrease of electron-hole recombination. It means that under high photon flux decreasing TiO_2 concentration could decrease the density of excited electron-hole pairs and reduce the electron-hole recombination. As optical path length above 3 cm, the decline in initial apparent photonic efficiency was due to the increased incident photons beings absorbed by a longer path length of the suspension in excess of the decrease of electron-hole recombination. The results in this study clearly prove our hypothesis and indicate that the reduction in the density of excited electron-hole could actually improve the photonic efficiency in high photon flux photocatalytic reaction.

3.4. Mineralization. It is well known that complete decolorization of MB does not mean that the dye is completely mineralized into CO_2 and H_2O. Hence, it is necessary to simultaneously investigate the mineralized process. TOC values have been related to the total concentration of organic in the solution and the decrease of TOC reflects the degree of mineralization at the end of the photocatalytic process. Mineralization of MB was studied by monitoring TOC loss in the dye solution.

Table 2: Relative photonic efficiencies of photocatalytic degradation of MB with different optical path length and TiO_2 concentration.

Optical path length (cm)	Initial apparent photonic efficiency (%)	
	Photon flux 3.13×10^{-6} einstein cm^{-2} s^{-1}	Photon flux 3.07×10^{-9} einstein cm^{-2} s^{-1}
(i) 0.67	0.235	2.25
(ii) 1	0.302	2.23
(iii) 2	0.329	2.01
(iv) 3	0.335	1.82
(v) 4	0.319	1.52
(vi) 5	0.298	1.36
(vii) 6	0.264	1.18
(viii) 7	0.242	1.09

The TOC removal and decolorization efficiencies with irradiation time are shown in Figure 5 the TOC removal and decolorization efficiencies with irradiation time in LUP. At the beginning of the reaction, an initial period of constant or slowly decreasing TOC values occurred. The inflect point corresponded to a reaction time of 60 min, which was equal to the decolorization time of MB. After the complete decolorization of the solution, the TOC values decreased, and then reached a plateau at the reaction time of 300 min. The results demonstrate that in LUP mineralization step starts only when decolorization is almost complete. The initial period of constant or slowly decreasing TOC values could correspond to the fact that MB molecules are decomposed to lower-molecular-weight compounds and the intermediates still contribute to the TOC of solution. The emergence of mineralization plateau indicates that the total oxidation is nearing completion, corresponding to the oxidation of most stable products. The tendency of the mineralization process is similar to the previous results [20].

However, the photocatalytic mineralization of MB solution in HUP had a different mineralization procedure than the LUP. As shown in Figure 4(a), the TOC values decreased approximately exponentially with reaction time from the beginning of the reaction. The continuous decay of TOC value confirmed the progressive mineralization of MB under high photon flux. This pattern meant that during the decolorization step (irradiation time 0–30 s) there was obvious decrease of the TOC value, which was due to the fact that MB molecules were decomposed to intermediate product and further oxidized to the intermediate product simultaneously.

UV photon flux determines the amount of photons injected into the solution. Under high photon flux irradiation, the photocatalyst could absorb more photons, leading to more electron-hole pairs on the photocatalyst surface. We

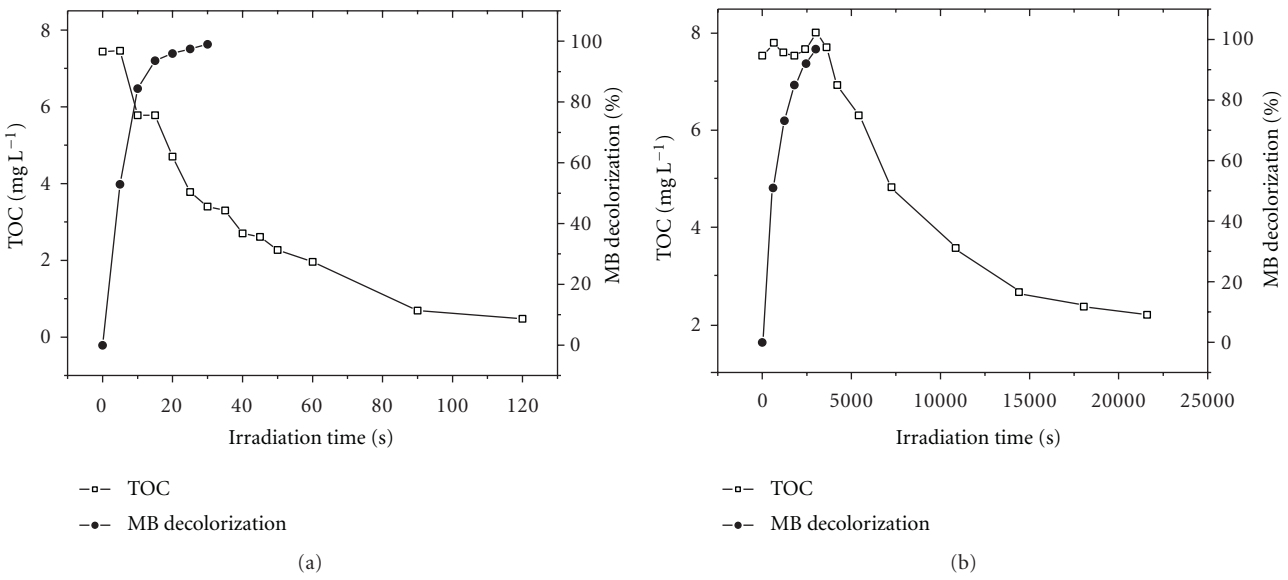

Figure 4: The TOC removal and decolorization efficiencies versus irradiation time by (a) HUP and (b) LUP. (Experimental conditions: photon flux (a) 3.13×10^{-6} einstein cm^{-2} s^{-1} (b) 3.07×10^{-9} einstein cm^{-2} s^{-1}; TiO_2, 1 g L^{-1}; MB initial concentration 20 mg L^{-1}).

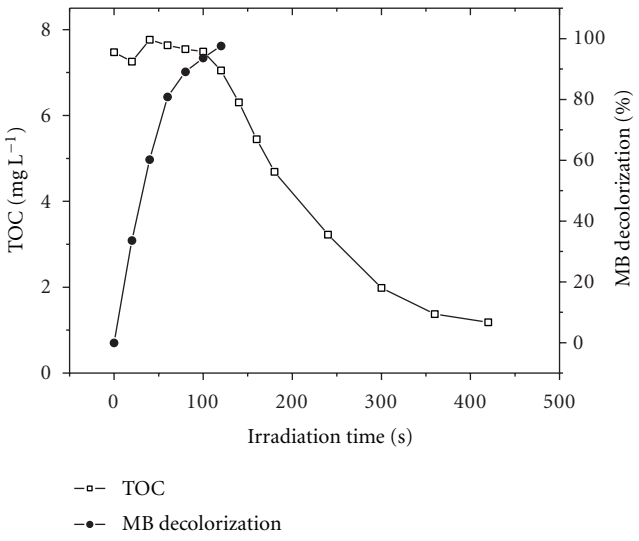

Figure 5: The TOC removal and decolorization efficiencies versus irradiation time. (Experimental conditions: photon flux 3.13×10^{-6} einstein cm^{-2} s^{-1}; TiO_2, 0.01 g L^{-1}; MB initial concentration 20 mg L^{-1}).

infer that in HUP while MB molecules are being decomposed to lower-molecular-weight compounds, there are still enough electron-hole pairs and $^{\bullet}$OH radicals to mineralize the intermediates of MB, which provides a higher efficiency in photocatalytic mineralization. In addition, the mineralization plateau observed (about 0.6 mg L^{-1}) near 100 s was much lower than that in LUP (about 3 mg L^{-1}), and the comparison of the two constant level of TOC values suggested that the stable products could be oxidized more easily in HUP than in LUP. It indicates that large numbers of electron-hole pairs and $^{\bullet}$OH radicals can also increase the rate of oxidation of stable products, dramatically enhancing the degree of mineralization in the photocatalytic reaction.

To further investigate the effect of the amount of excited electron-hole pairs on the photocatalytic mineralization procedure, we reduced excited electron-hole pairs by reducing the TiO_2 concentration by two orders of magnitude to 0.01 g L^{-1} and maintaining the photon flux constant. The TOC removal and decolorization efficiencies with irradiation time are shown in Figure 5. During the decolorization time (0–120 s), there was only a small decrease of TOC. After the decolorization of the solution, TOC decreased sharply, reaching a terminal value of about TOC 1.2 mg L^{-1}. Obviously, the mineralization procedure of this experiment is similar with LUP (Figure 4(b)). The two mineralization procedures have both been designed by two different methods of reducing excited electron-hole pairs. These results confirm the speculation, indicating that the amount of excited electron-hole pairs is truly the main reason for the different photocatalytic mineralization procedures.

4. Conclusion

The photocatalytic degradation of MB was investigated in HUP and LUP. Three criteria have been selected to compare both processes: (i) reaction rate and reaction time, (ii) the initial apparent photonic efficiency, and (iii) mineralization rate and mineralization degree. It was found that high UV photon flux is effective for accelerating the photocatalysis rate. Under optimal operational conditions, 99% decolorization of MB solution could be achieved within 30 s of UV irradiation time or more than 90% decolorization within 15 s, and 95% removal of 9.75 mg L^{-1} TOC could be achieved within 120 s. The analysis of initial apparent photonic efficiency shows the initial apparent photonic efficiency decreases with the increase of photon flux. Furthermore, we

have established that a high density of electron-hole pairs is one of reasons that caused decline of initial apparent photonic efficiency at high photon flux photocatalytic reaction, and the reduction in the density of excited electron-hole could actually improve the initial apparent photonic efficiency in high photon flux photocatalytic reaction. The obtained results in mineralization processes showed that high photon flux could dramatically improve the mineralization rate and enhance the degree of mineralization in the photocatalytic reaction, which is attributed to the large numbers of electron-hole pairs and $^{\bullet}$OH radicals.

References

[1] C. A. Martínez-Huitle and E. Brillas, "Decontamination of wastewaters containing synthetic organic dyes by electrochemical methods: a general review," *Applied Catalysis B*, vol. 87, no. 3-4, pp. 105–145, 2009.

[2] Z. Wang, W. Ma, C. Chen, H. Ji, and J. Zhao, "Probing paramagnetic species in titania-based heterogeneous photocatalysis by electron spin resonance (ESR) spectroscopy—a mini review," *Chemical Engineering Journal*, vol. 170, no. 2-3, pp. 353–362, 2011.

[3] U. I. Gaya and A. H. Abdullah, "Heterogeneous photocatalytic degradation of organic contaminants over titanium dioxide: a review of fundamentals, progress and problems," *Journal of Photochemistry and Photobiology C*, vol. 9, no. 1, pp. 1–12, 2008.

[4] C. Quiñones, J. Ayala, and W. Vallejo, "Methylene blue photoelectrodegradation under UV irradiation on Au/Pd-modified TiO_2 films," *Applied Surface Science*, vol. 257, no. 2, pp. 367–371, 2010.

[5] A. L. Linsebigler, G. Lu, and J. T. Yates, "Photocatalysis on TiO_2 surfaces: principles, mechanisms, and selected results," *Chemical Reviews*, vol. 95, no. 3, pp. 735–758, 1995.

[6] S. M. Meunier, J. Gamage, Z. Duvnjak, and Z. Zhang, "Design and characterization of a novel rotating corrugated drum reactor for wastewater treatment," *International Journal of Photoenergy*, vol. 2010, Article ID 146743, 10 pages, 2010.

[7] L. Elsellami, F. Vocanson, F. Dappozze et al., "Kinetic of adsorption and of photocatalytic degradation of phenylalanine effect of pH and light intensity," *Applied Catalysis A*, vol. 380, no. 1-2, pp. 142–148, 2010.

[8] D. F. Ollis, E. Pelizzetti, and N. Serpone, "Photocatalyzed destruction of water contaminants," *Environmental Science and Technology*, vol. 25, no. 9, pp. 1522–1529, 1991.

[9] K. Okamoto, Y. Yamamoto, H. Tanaka, and A. Itaya, "Kinetics of heterogeneous photocatalytic decomposition of phenol over anatase TiO_2 powder," *Bulletin of the Chemical Society of Japan*, vol. 58, no. 7, pp. 2023–2028, 1985.

[10] S. B. Kim and S. C. Hong, "Kinetic study for photocatalytic degradation of volatile organic compounds in air using thin film TiO_2 photocatalyst," *Applied Catalysis B*, vol. 35, no. 4, pp. 305–315, 2002.

[11] J. T. Carneiro, R. Berger, J. A. Moulijn, and G. Mul, "An internally illuminated monolith reactor: pros and cons relative to a slurry reactor," *Catalysis Today*, vol. 147, pp. S324–S329, 2009.

[12] S. Ahmed, M. G. Rasul, R. Brown, and M. A. Hashib, "Influence of parameters on the heterogeneous photocatalytic degradation of pesticides and phenolic contaminants in wastewater: a short review," *Journal of Environmental Management*, vol. 92, no. 3, pp. 311–330, 2011.

[13] C. G. Hatchard and C. A. Parker, "A new sensitive chemical actinometer II potassium ferrioxalate as a standard chemical actinometer," *Proceedings of the Royal Society of London. Series A*, vol. 235, no. 1203, pp. 518–536, 1956.

[14] I. K. Konstantinou and T. A. Albanis, "TiO_2-assisted photocatalytic degradation of azo dyes in aqueous solution: kinetic and mechanistic investigations: a review," *Applied Catalysis B*, vol. 49, no. 1, pp. 1–14, 2004.

[15] A. Chatzitakis, C. Berberidou, I. Paspaltsis, G. Kyriakou, T. Sklaviadis, and I. Poulios, "Photocatalytic degradation and drug activity reduction of chloramphenicol," *Water Research*, vol. 42, no. 1-2, pp. 386–394, 2008.

[16] M. Muneer and D. Bahnemann, "Semiconductor-mediated photocatalyzed degradation of two selected pesticide derivatives, terbacil and 2,4,5-tribromoimidazole, in aqueous suspension," *Applied Catalysis B*, vol. 36, no. 2, pp. 95–111, 2002.

[17] L. Zhang, W. A. Anderson, and Z. Zhang, "Development and modeling of a rotating disc photocatalytic reactor for wastewater treatment," *Chemical Engineering Journal*, vol. 121, no. 2-3, pp. 125–134, 2006.

[18] O. K. Dalrymple, D. H. Yeh, and M. A. Trotz, "Removing pharmaceuticals and endocrine-disrupting compounds from wastewater by photocatalysis," *Journal of Chemical Technology and Biotechnology*, vol. 82, no. 2, pp. 121–134, 2007.

[19] E. E. Coyle and M. Oelgemöller, "Micro-photochemistry: photochemistry in microstructured reactors. The new photochemistry of the future?" *Photochemical and Photobiological Sciences*, vol. 7, no. 11, pp. 1313–1322, 2008.

[20] A. Houas, H. Lachheb, M. Ksibi, E. Elaloui, C. Guillard, and J. M. Herrmann, "Photocatalytic degradation pathway of methylene blue in water," *Applied Catalysis B*, vol. 31, no. 2, pp. 145–157, 2001.